
Calendar of forthcoming meetings

10–16 May 2008

Baltimore, MD, USA

HPLC 2008: 32nd International Symposium on High Performance Liquid Phase Separations and Related Techniques.

Contact: Janet Cunningham, Barr Enterprises, PO Box 279, Walkersville, MD 21793, USA.

Tel.: (+1-301) 668-6001;

Fax: (+1-301) 668-4312;

E-mail: Janetbarr@aol.com;

URL: <http://www.hplc2008.com>

11–15 May 2008

Gdansk, Poland

PBA 2008: 18th International Symposium on Pharmaceutical and Biomedical Analysis.

Contact: Symposium Secretariat, Department of Biopharmaceutics and Pharmacodynamics, Medical University of Gdansk, Gen. J. Hallera 107, 80-416 Gdansk, Poland.

Tel. (+48-58) 349-3260;

Fax: (+48-58) 349-3262;

E-mail: pba2008@amg.gda.pl

13–16 May 2008

La Grande Motte, Montpellier, France

SBCN 2008: 11th International Symposium on Biochromatography and Nanoseparations.

Contact: Professor Xavier Santarelli, Tel. +33 5 5757 1713;

E-Mail: Xavier.santarelli@estbb.u-bordeaux2.fr

14–16 May 2008

Shanghai, China

Biosensors 2008: The Tenth World Congress on Biosensors. URL: www.biosensors-congress.elsevier.com

19–21 May 2008

Egmond aan Zee, The Netherlands

EuroResidue VI Conference on Residues of Veterinary Drugs in Food. Contact: EuroResidue, PO Box 18, 5298 ZG Liempde, The Netherlands.

Tel. (+31-411) 611-199;

E-mail: euroresidue@congressservice.nl;

URL: www.euroresidue.nl

25–29 May 2008

Neuherberg, Germany

4th International Conference on Trace Element Speciation in Biomedical, Nutritional and Environmental Sciences.

URL: <http://www.gsf.de/spec>

30 June – 4 July 2008

Montpellier, France

CAC 2008: 11th Conference on Chemometrics in Analytical Chemistry. Contact: Dr Jean-Michel Roger, Cemagraf, 361 rue J.F. Breton, BP 5095, F-34196 Montpellier, France.

Tel. (+33-4) 6704-6383;

Fax: (+33-4) 6704-6306;

E-mail: contact@cac2008.org;

URL: <http://cac2008.teledetection.fr>

27 July – 1 August 2008

Quebec City, PQ, Canada

CPT 2008: IXth World Conference on Clinical Pharmacology and Therapeutics. URL: <http://www.cpt2008.org>

7–11 September 2008

Bologna, Italy

ISLS 2008: XIIIth International Symposium on Luminescence Spectrometry. Contact: Professor Aldo Roda, Department of Pharmaceutical Sciences, Faculty of Pharmacy, University of Bologna, Italy.

Tel. (+39-051) 343-398;

Fax: (+39-051) 343-398;

E-mail: isls2008@unibo.it;

URL: <http://www.isls2008.unibo.it>

14–16 September 2008

Muenster, Germany

SIMS Europe 2008: 6th European Workshop on Secondary Ion Mass Spectrometry.

URL: <http://www.sims-europe.uni-muenster.de>

5–10 October 2008

Dobogokö, Hungary

Matrafüred '08: International Conference on Electrochemical Sensors.

URL: www.matrafured-08.ethz.ch

16–17 October 2008

Lisbon, Portugal

European Biomarkers Summit 2008.

URL: <https://selectbiosciences.com/conferences/EBS2008>

16–17 October 2008

Lisbon, Portugal

Proteomics Europe 2008.

URL: <https://selectbiosciences.com/conferences/PE2008>

16–17 October 2008

Lisbon, Portugal

Advances in Metabolic Profiling.

URL: <https://selectbiosciences.com/conferences/AMP2008>

2–5 November 2008

Kaohsiung, Taiwan

APCE 2008: 8th Asia-Pacific International Symposium on Microscale Separations and Analysis.

URL: <http://www.tl.ntu.edu.tw/apce2008>

11–15 May 2009

Frankfurt am Main, Germany

Achema 2009: 29th International Exhibition-Congress on Chemical Engineering, Environmental Protection and Biotechnology.

URL: <http://www.achema.de>

6–10 September 2009

Innsbruck, Austria

Euroanalysis 2009.

Contact: Euroanalysis 2009 Symposium Office, PCO Tyrol Congress, c/o Ina Kaehler, Rennweg 3, 6020 Innsbruck, Austria.

Tel. (+43-512) 575-600;

Fax: (+43-512) 575-607;

E-mail: euroanalysis09@come-innbruck.at;

URL: www.euroanalysis2009.at

Talanta

The International Journal of Pure and Applied Analytical Chemistry

Editors-in-Chief

Professor G.D. Christian, University of Washington, Department of Chemistry, 36 Bagely Hall, P.O. Box 351700, Seattle, WA 98195-1700, U.S.A.

Professor J.-M. Kauffmann, Université Libre de Bruxelles, Institut de Pharmacie, Campus de la Plaine, C.P. 205/6, Boulevard du Triomphe, B-1050 Bruxelles, Belgium

Associate Editors

Professor J.-H. Wang, Research Center for Analytical Sciences, Northeastern University, Box 332, Shenyang 110004, China

Professor J.L. Burguera, Los Andes University, IVAQUIM, Faculty of Sciences, P.O. Box 542, 5101-A Mérida, Venezuela.

Assistant Editors

Dr R.E. Synovec, Department of Chemistry, University of Washington, Box 351700, Seattle, WA 98195-1700, U.S.A.

Professor J.-C. Vire, Université Libre de Bruxelles, Institut de Pharmacie, Campus de la Plaine, C.P. 205/6, Boulevard du Triomphe, B-1050 Bruxelles, Belgium

Talanta

R. Apak (Istanbul, Turkey)
E. Bakker (Auburn, AL, U.S.A.)
D. Barceló (Barcelona, Spain)
B. Birch (Luton, UK)
K. S. Booksh (Tempe, AZ, U.S.A.)
J.-L. Capelo-Martinez (Caparica, Portugal)
Z. Cai (Kowloon, Hong Kong)
O. Chailapakul (Thailand)
S. Cosnier (Grenoble, France)
D. Diamond (Dublin, Ireland)
W. Frenzel (Berlin, Germany)
A.G. Gonzales (Seville, Spain)
E.H. Hansen (Lyngby, Denmark)
P. de B. Harrington (OH, U.S.A.)

A. Ho (Hsin-chu, Taiwan)
P. Hubert (Liège, Belgium)
J. Kalivas (Pocatella, ID, U.S.A.)
B. Karlberg (Stockholm, Sweden)
J.-M. Lin (Beijing, China)
Y. Lin (Richland, WA, U.S.A.)
M.D. Luque de Caastro (Cordoba, Spain)
I.D. McKelvie (Victoria, Australia)
S. Motomizu (Okayama, Japan)
D. Nacapricha (Bangkok, Thailand)
J.-M. Pingarron (Madrid, Spain)
E. Pretsch (Zürich, Switzerland)
W. Schuhmann (Bochum, Germany)
M. Shamsipur (Kermanshah, Iran)

M. Silva (Porto Alegre, Brazil)
P. Solich (Hradec Králové, Czech Republic)
K. Suzuki (Yokohama, Japan)
D.G. Themelis (Thessaloniki, Greece)
D.L. Tsalev (Sofia, Bulgaria)
Y. van der Heyden (Belgium)
B. Walczak (Katowice, Poland)
J. Wang (Tempe, AZ, U.S.A.)
J.D. Winefordner (Gainesville, U.S.A.)
Xiu-Ping Yan (Tianjin, China)
E.A.G. Zagatto (Piracicaba, SP, Brazil)
X. Zhang (China)

Copyright © 2008 Elsevier B.V. All rights reserved

Publication information: *Talanta* (ISSN 0039-9140). For 2008, volumes 74–76 are scheduled for publication. Subscription prices are available upon request from the Publisher or from the Regional Sales Office nearest you or from this journal's website (<http://www.elsevier.com/locate/talanta>). Further information is available on this journal and other Elsevier products through Elsevier's website: (<http://www.elsevier.com>). Subscriptions are accepted on a prepaid basis only and are entered on a calendar year basis. Issues are sent by standard mail (surface within Europe, air delivery outside Europe). Priority rates are available upon request. Claims for missing issues should be made within six months of the date of dispatch.

Orders, claims, and journal enquiries: please contact the Customer Service Department at the Regional Sales Office nearest you:

Orlando: Elsevier, Customer Service Department, 6277 Sea Harbor Drive, Orlando, FL 32887-480 USA; phone: (+1) (877) 8397126 [toll free number for US customers], or (+1) (407) 3454020 [customers outside US]; fax: (+1) (407) 3631354; e-mail: usjcs@elsevier.com

Amsterdam: Elsevier, Customer Service Department, PO Box 211, 1000 AE Amsterdam, The Netherlands; phone: (+31) (20) 4853757; fax: (+31) (20) 4853432; e-mail: nlinfo-f@elsevier.com

Tokyo: Elsevier, Customer Service Department, 4F Higashi-Azabu, 1-Chome Bldg, 1-9-15 Higashi-Azabu, Minato-ku, Tokyo 106-0044, Japan; phone: (+81) (3) 5561 5037; fax: (+81) (3) 5561 5047; e-mail: jp.info@elsevier.com

Singapore: Elsevier, Customer Service Department, 3 Killiney Road, #08-01 Winsland House I, Singapore 239519; phone: (+65) 63490222; fax: (+65) 67331510; e-mail: asiainfo@elsevier.com

USA mailing notice: *Talanta* (ISSN 0039-9140) is published monthly by Elsevier B.V. (P.O. Box 211, 1000 AE Amsterdam, The Netherlands). Annual subscription price in the USA US\$ 4,085 (valid in North, Central and South America), including air speed delivery. Application to mail at periodical postage rate is paid at Rathway, NJ and additional mailing offices.

USA POSTMASTER: Send address changes to *Talanta*, Publications Expediting Inc., 200 Meacham Avenue, Elmont, NY 11003.

AIRFREIGHT AND MAILING in the USA by Publications Expediting Inc., 200 Meacham Avenue, Elmont, NY 11003.

Ultrasound-assisted extraction of capsaicinoids from peppers

G.F. Barbero, A. Liazid, M. Palma*, C.G. Barroso

Departamento de Química Analítica, Facultad de Ciencias, Universidad de Cádiz, P.O. Box 40, 11510 Puerto Real, Cádiz, Spain

Received 15 June 2007; received in revised form 20 January 2008; accepted 24 January 2008

Available online 2 February 2008

Abstract

The development of a rapid, reproducible and simple method of extraction of the majority capsaicinoids (nordihydrocapsaicin, capsaicin, dihydrocapsaicin, homocapsaicin and homodihydrocapsaicin) present in hot peppers by the employment of ultrasound-assisted extraction is reported. The study has covered four possible solvents for the extraction (acetonitrile, methanol, ethanol and water), the optimum temperature for extraction (10–60 °C), the extraction time (2–25 min), the quantity of sample (0.2–2 g), and the volume of solvent (15–50 mL). Under the optimum conditions of the method developed, methanol is employed as solvent, at a temperature of 50 °C and an extraction time of 10 min. The repeatability and reproducibility of the method (R.S.D. < 3%) have been determined. The capsaicinoids extracted have been analysed by HPLC with fluorescence detection and using monolithic columns for the chromatographic separation. The method developed has been employed for the quantification of the various capsaicinoids present in different varieties of hot peppers cultivated in Spain.

© 2008 Elsevier B.V. All rights reserved.

Keywords: Capsaicinoids; Ultrasound-assisted extraction; Peppers

1. Introduction

Capsaicinoids are the compounds responsible for the hot, spicy flavour presented by many varieties of peppers. Among the many natural capsaicinoids found in hot chilli peppers, two compounds are predominant: capsaicin (*trans*-8-methyl-*N*-vanillyl-6-nonenamide) and dihydrocapsaicin (8-methyl-*N*-vanillylnonanamide) [1]; they represent around 90% of the total capsaicinoids present in the hot spicy varieties of peppers. In addition to these two major capsaicinoids, other minor capsaicinoids are found in hot peppers, including nordihydrocapsaicin, norcapsaicin, homocapsaicin I and II, homodihydrocapsaicin I and II, nornorcapsaicin, nornornorcapsaicin, and nonivamide, among others [2,3]. The structural characteristic of capsaicinoids that determines their spicy properties is associated with the presence of an amide bond connecting a vanillyl ring and an acyl chain [4].

Hot peppers are one of the most important species cultivated widely around the world. The properties of colour, aroma, flavour and pungency presented by these peppers account for their extensive usage. In addition to these culinary properties,

capsaicinoids present many biological activities. Among these activities, capsaicinoids act as powerful antioxidants [5], present anti-mutagenic and anti-tumoral properties [6,7], function as topical analgesics against pain [8], have anti-inflammatory properties [9] and stimulate the cardiovascular and respiratory systems [10].

Many different techniques have been employed for the extraction of capsaicinoids from pepper, such as maceration [11], magnetic stirring [12], enzymatic extraction [13], ultrasound-assisted extraction [14], Soxhlet [15], extraction by supercritical fluids [16], extraction by pressurized liquids [17] and microwave-assisted extraction [18,19]. The conventional extraction methods, like Soxhlet extraction, which have been employed for decades, need long extraction times and require relatively large quantities of solvent [20]. Recent years have seen increasing demand for extraction techniques that shorten extraction times and reduce the consumption of organic solvents. Among these more efficient extraction techniques are ultrasound-assisted extraction (UAE), microwave-assisted extraction, supercritical fluid extraction and accelerated solvent extraction. The UAE technique is particularly attractive because of its simplicity and low equipment cost; it is based on the employment of the energy derived from ultrasounds (sound waves with frequencies higher than 20 kHz) to facilitate the extraction of analytes from the solid sample by the organic

* Corresponding author. Tel.: +34 956 016775; fax: +34 956 016460.

E-mail address: miguel.palma@uca.es (M. Palma).

solvent, which is selected in function of the nature of the solutes to be extracted [21]. This technique has been employed to extract various organic compounds from different matrices, including phenolics in cosmetic creams [22], chlorinated pesticides in bird livers [23], organic acids in grapes [24], phenolic compounds from strawberries [25] or isoflavones from soybeans [26].

The enhancement of extraction efficiency of organic compounds by ultrasound is attributed to the phenomenon of cavitation produced in the solvent by the passage of an ultrasonic wave. Cavitation bubbles are produced and compressed during the application of ultrasound. The increase in the pressure and temperature caused by the compression leads to the collapse of the bubble. With the collapse of bubble, a resultant “shock wave” passes through the solvent enhancing the mixing [27].

Ultrasound also exerts a mechanical effect, allowing greater penetration of solvent into the sample matrix, increasing the contact surface area between solid and liquid phase. This, coupled with the enhanced mass transfer and significant disruption of cells, via cavitation bubble collapse, increases the release of intracellular product into the bulk medium. The use of higher temperatures in UAE can increase the efficiency of the extraction process due to the increase in the number of cavitation bubbles formed [27–29].

Although studies have been published on the employment of UAE for the recovery of capsaicinoids from peppers [14], these not have evaluated the influence of the extraction variables nor has a systematic study for the optimisation of the method been carried out; therefore no specific protocol for the UAE of capsaicinoids in peppers has been produced. Thus, the object of the work reported here is to perform the optimisation of the various extraction parameters, particularly the appropriate solvent, temperature, extraction time, quantity of sample, etc. It is also intended to utilise the method developed to quantify the capsaicinoids present in several varieties of hot peppers cultivated in Spain.

2. Experimental

2.1. Chemical and reagents

The solvents utilised: ethanol (Panreac, Barcelona, Spain), methanol, acetonitrile and glacial acetic acid (Merck, Darmstadt, Germany), are of HPLC grade. The water was obtained by a Milli-Q water purification system, from Millipore (Bedford, MA, USA). The capsaicinoid standards: capsaicin (97%) and dihydrocapsaicin (90%), and the internal standard 2.5 dihydroxybenzaldehyde utilised were obtained from Sigma–Aldrich (Steinheim, Germany).

2.2. Plant material

The hot Cayenne pepper (*Capsicum frutescens* L.) was employed for the development of the ultrasound-assisted extraction method. They were obtained from local markets. The peppers were peeled, and the peduncle and seeds were separated. Only the pericarp and the placenta of the pepper were

studied. Both the pericarp and the placenta were triturated with a conventional beater, until a homogeneous sample was obtained for the analysis. The triturated sample obtained was conserved in a freezer at -20°C until its analysis.

2.3. Extraction procedure

The extraction of capsaicinoids originating from peppers by means of ultrasound was performed employing various different extraction conditions—solvents: methanol, ethanol, acetonitrile and water; percentage of water in methanol: 0–100%; temperature: $10\text{--}60^{\circ}\text{C}$; volume of solvent: 15–50 mL; quantity of sample: 0.2–2 g; extraction time: 2–25 min. A volume of 0.5 mL of internal standard was added to the extracts obtained (1300 ppm). The extracts were filtered through a $0.45\ \mu\text{m}$ nylon syringe filter (Millex-HN, Ireland) before the chromatographic analysis.

The extraction by ultrasound was performed in an ultrasonic bath of 360 W (J.P. Selecta, Barcelona, Spain) coupled to a temperature controller, which allowed the water in the bath to be renewed.

2.4. HPLC-fluorescence analysis

The HPLC-fluorescence analysis was carried out in a Dionex chromatographic system (Sunnyvale, CA, USA), consisting of an automated sample injector (ASI-100), pump (P680), thermostated column compartment (TCC-100), a photodiode array detector (PDA-100), a fluorescence detector (RF 2000), a universal chromatography interface (UCI-50) and Chromeleon 6.60 software. Capsaicinoids were separated using a Chromolith Performance PR-18e (100 mm \times 4.6 mm) monolithic column (Merck).

The chromatographic separation was performed with extracts of the hot Cayenne pepper (*C. frutescens* L.). The wavelengths employed for the detection were 278 nm (excitation) and 310 nm (emission).

The method of chromatographic separation utilised a gradient of two solvents: acidified water (0.1% acetic acid, solvent A) and acidified methanol (0.1% acetic acid, solvent B), working at a flowrate of 6 mL/min. The gradient method utilised is the following: 0 min, 10% B; 2 min, 50% B; 4 min, 50% B; 4.5 min, 55% B; 5.5 min, 55% B; 6 min, 60% B; 7 min, 60% B; 9 min, 70% B; 10 min, 100% B; 15 min, 100% B. The temperature of the column was held constant at 30°C . The chromatogram obtained by utilising this separation method is represented in Fig. 1.

2.5. Calibration

Using the method developed, calibration curves were prepared for capsaicin and dihydrocapsaicin, which are the two capsaicinoid standards commercially available. The results obtained are presented in Table 1. The limits of detection and quantification were calculated using the ALAMIN software [30].

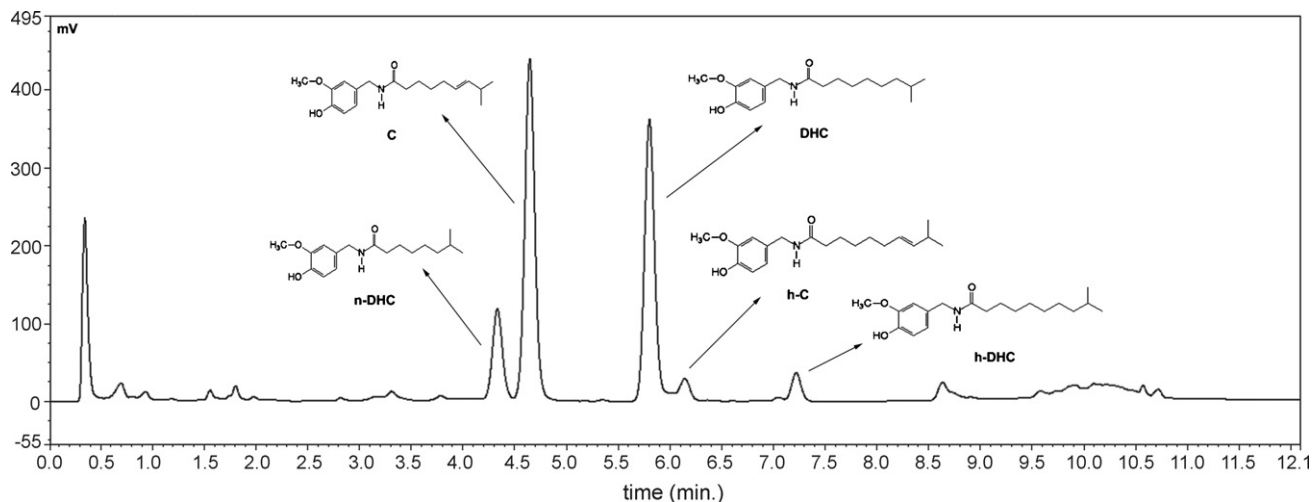


Fig. 1. Chromatogram of separation of the capsaicinoids extracted from hot Cayenne pepper. n-DHC: nordihydrocapsaicin, C: capsaicin, DHC: dihydrocapsaicin, h-C: homocapsaicin and h-DHC: homodihydrocapsaicin.

3. Results and discussion

3.1. Selection of the solvent

The selection of the most appropriate solvent for extracting the analytes of interest from the matrix of the sample is a basic step in the development of any method of extraction. First, the effectiveness of the ultrasound-assisted extraction is going to depend on the extraction solvent's capacity for absorbing and transmitting the energy of the ultrasounds. Second, the capsaicinoids should be soluble in the solvent that is employed for the extraction.

The four solvents that have been studied for extracting capsaicinoids from the matrix of the sample are methanol, ethanol, acetonitrile and water. Methanol [11,14], ethanol [13,17], and acetonitrile [12,31] are solvents that are normally employed for the extraction of capsaicinoids in various extraction techniques, such as Soxhlet extraction, maceration, and extraction by magnetic stirring. Water is not a good solvent for extracting capsaicinoids, but it has been observed that sometimes the addition of small percentages of water to the extraction solvent helps to increase the effectiveness of extraction of the analytes of interest from the sample [26].

The extractions have been performed with a quantity of triturated hot Cayenne pepper of about 1 g of the sample, in 25 mL of solvent, at a temperature of 50 °C for an extraction period of 20 min. All the assays were performed in triplicate.

Table 1
Analytical properties ($n=3$) of the calibration curve of capsaicin and dihydrocapsaicin

	Capsaicin	DHC
Equation	$y = 112,901x + 187$	$y = 151,770x + 4589$
r^2	0.9995	0.9995
LD (mg/L)	0.008	0.011
LQ (mg/L)	0.028	0.036

Relative recoveries were calculated by calculating the relative area to the area found for each compound in the extraction showing the highest amount. The relative areas of the different capsaicinoids extracted with the four solvents studied, in the extraction conditions previously described, are represented in Fig. 2.

In the light of Fig. 2, it can be observed that both methanol and ethanol extract similar quantities of capsaicinoids; no significant differences ($p > 0.05$) are observed in the recoveries obtained with these two solvents, in the extraction conditions studied. Acetonitrile is a fairly efficacious solvent for extracting the capsaicinoids present in samples of hot peppers, but is less efficacious than ethanol and methanol, and in these extraction conditions it gives recoveries of only about 80% of those obtained with methanol and ethanol. It was decided to employ methanol as solvent for the development of the extraction method, since this solvent is more compatible with the solvents employed in the chromatographic method.

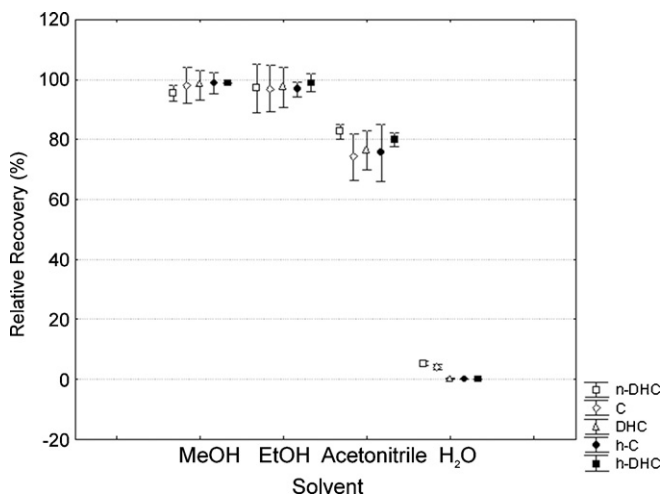


Fig. 2. Relative recoveries of capsaicinoids from hot Cayenne pepper employing different pure solvents.

Table 2

Relative recovery of capsaicinoids extracted from hot Cayenne pepper employing as solvents different mixtures of methanol and water (0, 10, 25, 50 and 100% of water)

Solvent	n-DHC	C	DHC	h-C	h-DHC
0% methanol	5.71	4.20	0.21	0	0
50% methanol	71.66	71.00	67.46	65.01	63.10
75% methanol	79.34	79.52	79.36	79.37	79.19
90% methanol	86.61	86.81	87.14	86.98	87.23
100% methanol	100	100	100	100	100

In Fig. 2 it can also be observed that water, which is a very polar solvent, has a poor capacity of extraction of capsaicinoids. This reduced effectiveness is accentuated in the case of the less polar capsaicinoids such as dihydrocapsaicin, homocapsaicin and homodihydrocapsaicin, where it extracts a lower percentage of these capsaicinoids than of the other more polar capsaicinoids like nordihydrocapsaicin and capsaicin.

On the other hand, in many instances, it has been shown that the addition of differing percentages of water to other extraction solvents improves their extractant properties. For this reason, our study has included the addition of particular percentages of water (0, 10, 25, 50 and 100%) to methanol, as the optimum solvent for extraction, to evaluate how the properties of extraction of this solvent are modified. The extraction conditions were the same as those employed for the selection of the optimum extraction solvent. Similarly, all the assays were performed in triplicate.

The relative recoveries of capsaicinoids extracted from hot Cayenne pepper employing as solvents different mixtures of methanol and water (0, 10, 25, 50 and 100% of water) are represented in Table 2.

It was found that the addition of varying quantities of water to the methanol did not produce any improvement in extracting the capsaicinoids present in the fresh samples of peppers. An addition of water, such as 10% of water in the methanol, in these extraction conditions, has the effect of reducing the recoveries obtained to around 87% of those obtained with undiluted methanol. Higher percentages of water, such as 25%, reduce even further the recoveries obtained, to around 79% of those with undiluted methanol; and the recoveries obtained continue to decline in line with increases in the percentage of water added to the methanol. Therefore, the development of the method was continued based on employing undiluted methanol as the extraction solvent.

3.2. Extraction temperature

Temperature is a fundamental parameter in extracting compounds. Generally speaking, the higher the extraction temperature, the higher the velocity and the efficacy of the extraction process. However some degradation processes can occur at high temperature, then lower recoveries can be obtained. In this study the aim was to evaluate temperatures ranging from 10 to 60 °C (10, 20, 30, 40, 50 and 60 °C). It was not proposed to perform extractions at higher temperatures because 64.7 °C is the boiling point of methanol, working at atmospheric pressure.

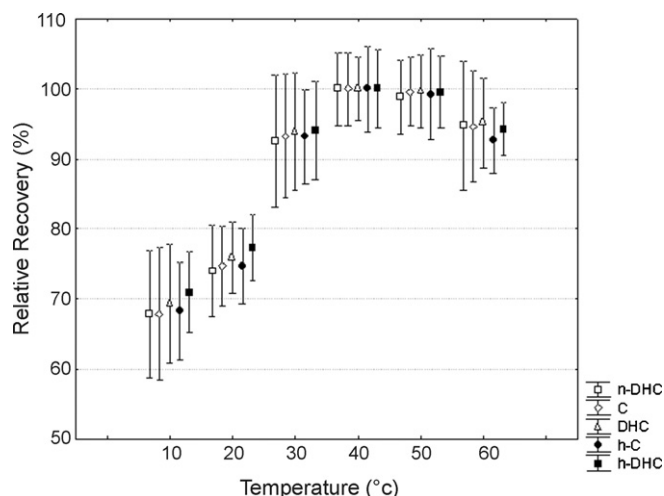


Fig. 3. Relative area of the capsaicinoids extracted at the different temperatures of the assay.

The following were the extraction conditions employed in this study—extraction solvent: methanol; extraction time: 20 min; volume of solvent: 25 mL; quantity of sample: approximately 1 g. All the assays have been carried out in triplicate.

The relative area of the capsaicinoids extracted at the different temperatures of the assay is represented in Fig. 3.

From Fig. 3 it can be observed that, in these extraction conditions, the highest recoveries are obtained at 40 and 50 °C, although the differences are not significant ($p > 0.05$) between 30 and 60 °C. At temperatures lower than 30 °C, the method is not able to extract the same quantity of capsaicinoids as are extracted at higher temperatures, probably because the extraction kinetics take place more slowly the lower the temperature.

The optimum temperature can be considered to be between 30 and 60 °C, at this range of temperatures no degradation of capsaicinoids is observed, in the extraction conditions studied. For later experiments, 50 °C was used as extraction temperature.

3.3. Extraction time

Until saturation, by increasing the extraction time, the quantity of analytes extracted is increased, although there is the risk that degradation may occur. To determine the time needed to obtain complete extractions, extractions from samples of peppers were performed for different lengths of time. Extraction times of 2, 5, 10, 15, 20 and 25 min were evaluated. The rest of the variables employed were: temperature of 50 °C, methanol as extraction solvent, 25 mL of solvent and approximately 1 g of sample. All the assays were performed in triplicate.

The results obtained are given in Fig. 4, in which the relative quantities of capsaicinoids extracted with different times of extraction (2, 5, 10, 15, 20 and 25 min), in the extraction conditions previously indicated, are represented.

It can be observed that, at extraction times longer than 5 min, there are no significant differences ($p > 0.05$) in the recoveries of the capsaicinoids, and quantitative recoveries are obtained. However, a considerable increase in the variability of the recovery is observed by employing as few as 5 and as many as 25 min;

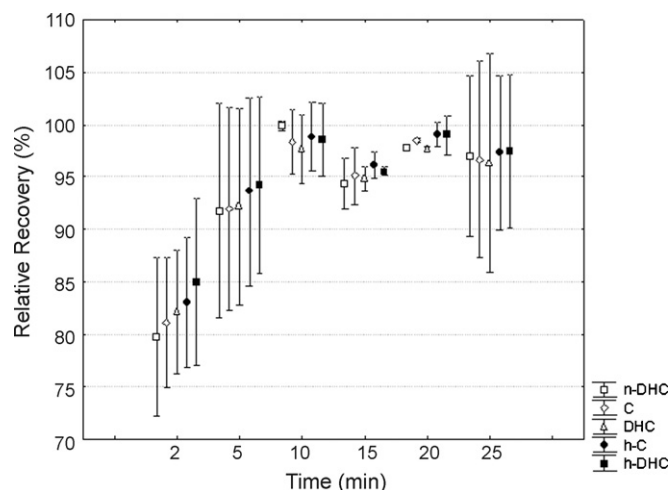


Fig. 4. Relative recoveries of capsaicinoids from hot Cayenne pepper employing different times of extraction.

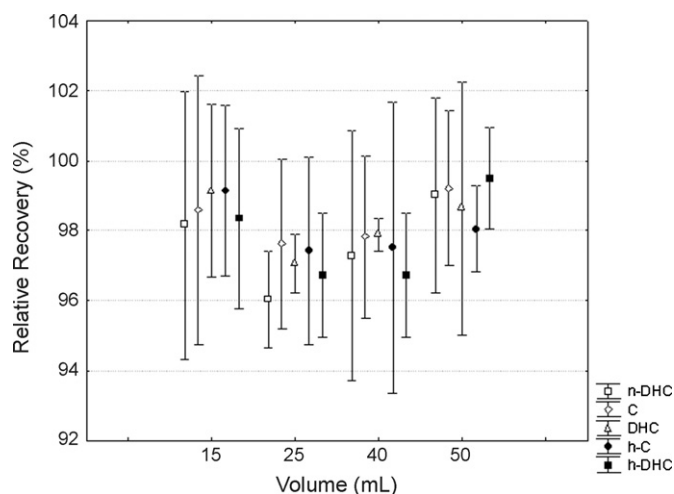


Fig. 5. Relative quantities of capsaicinoids extracted with different volumes of methanol.

therefore it is considered that an adequate time of extraction should fall between 10 and 20 min.

3.4. Volume of solvent

The mass/volume ratio of solvent is a factor that must be studied to increase the efficacy of extraction of capsaicinoids employing ultrasound-assisted extraction. For the conventional techniques of solid–liquid extraction, the tendency is to reduce the ratio of mass/volume of solvent, and in many instances this increases the extraction volume obtained. When this happens, the improvement is due to there being a greater volume of solvent to extract the same quantity of solute.

To evaluate the effect of the volume of the solvent on the extraction, a series of extractions were carried out with different volumes of solvent (15, 25, 40 and 50 mL). The rest of the extraction conditions were: temperature of 50 °C, approximately 1 g of sample, 10 min of extraction and methanol as solvent. All the assays were performed in triplicate.

The relative quantities of capsaicinoids extracted with different volumes of solvent are represented in Fig. 5.

In Fig. 5 it can be observed that there are no significant differences ($p > 0.05$) when the volume of the extraction solvent is varied. Therefore, the variable of solvent volume will not be a determining factor when extracting capsaicinoids in these conditions. It was decided to work with a volume of 25 mL since this enables compounds to be found in levels higher than the LOQ of the chromatographic method.

3.5. Quantity of sample

Once the volume of extraction solvent had been optimised, the next step was to optimise the quantity of sample, the other factor influencing the ratio of mass/volume of solvent previously mentioned. In general, by reducing the quantity of sample while holding the volume constant, the quantities of analytes extracted are increased, since the ratio of mass/volume of solvent is dimin-

ished; but the disadvantage of this practice is the decrease of the signal in the subsequent chromatographic system.

In this study sample quantities of 0.2, 0.5, 1, 1.5 and 2 g of peppers have been employed while maintaining the solvent volume constant at 25 mL of methanol. The rest of the extraction parameters utilised were: temperature of 50 °C, 25 mL of methanol as extraction solvent, and 10 min of extraction time. All the assays were performed in triplicate.

The results obtained are given in Fig. 6, in which the relative quantities of capsaicinoids extracted with different sample quantities (0.2, 0.5, 1, 1.5 and 2 g), in the extraction conditions previously indicated, are represented.

In the light of Fig. 6 it can be observed that the quantity of sample is not a relevant parameter. Thus, it was decided to employ 1 g, since this quantity of sample produces compounds found in levels higher than the LOQ of the chromatographic method.

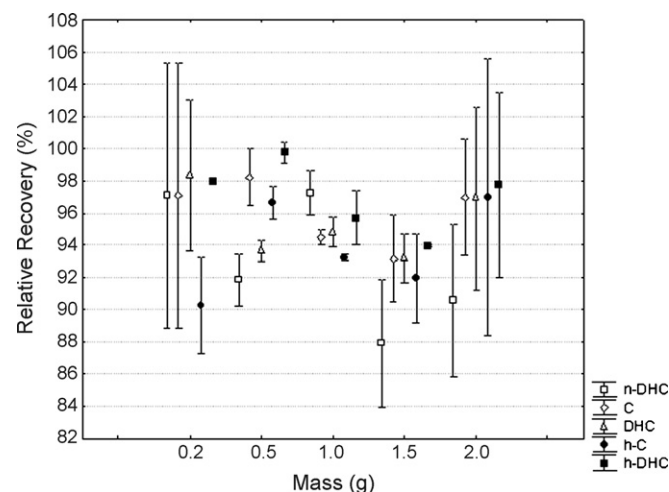


Fig. 6. Recoveries of capsaicinoids from hot Cayenne pepper employing different quantities of sample.

Table 3

Repeatability ($n=9$) and reproducibility ($n=18$) of the method developed for the capsaicinoids analysed

	n-DHC	C	DHC	h-C	h-DHC
R.S.D. (%) intraday	1.97	1.72	1.84	2.35	1.83
R.S.D. (%) interday	2.42	2.46	2.56	2.37	2.58

Table 4

μmol of capsaicinoid per kilogram of fresh pepper in the samples analysed

Pepper	n-DHC	C	DHC	h-C	h-DHC
Cayenne	94 \pm 6	448 \pm 28	265 \pm 15	30 \pm 1	47 \pm 2
BTR	40 \pm 3	370 \pm 23	190 \pm 11	n.d.	20 \pm 1
BTL	25 \pm 2	275 \pm 17	122 \pm 7	n.d.	14 \pm 1

n.d.: not detected. BTR: Bolilla Redondo pepper and BTL: Bolilla Largo pepper.

3.6. Repeatability and reproducibility of the method

The repeatability and reproducibility of the method developed have been studied. For this a total of 21 extractions were performed, distributed as follows: 9 extractions performed on the first day of the study, and 6 more extractions on each of the two consecutive days. The resulting R.S.D.s are given in Table 3. Similar results were found for all capsaicinoids, all of them lower than 3%.

3.7. Quantification of the capsaicinoids present in different samples of peppers

The amounts of capsaicinoids (nordihydrocapsaicin, capsaicin, dihydrocapsaicin, homocapsaicin and homodihydrocapsaicin) present in three varieties of peppers have been quantified using this method. Samples of hot Cayenne pepper (*C. frutescens*), Bolilla Largo pepper (*Capsicum annuum*) and Bolilla Redondo pepper (*C. annuum*) were employed. Capsaicin and dihydrocapsaicin were quantified from the calibration curves obtained from the standard solutions. Since there are no commercial standards of nordihydrocapsaicin, homocapsaicin and homodihydrocapsaicin, these were quantified from the calibration curve of dihydrocapsaicin (for nordihydrocapsaicin and for homodihydrocapsaicin) and from the calibration curve of capsaicin (for homocapsaicin), given the structural similarities between these molecules. Table 4 gives the quantities of capsaicinoids present in the different varieties of peppers studied.

It can be observed that, of the three varieties of peppers studied, it is hot Cayenne pepper that contains the largest amount of capsaicinoids, followed by the Bolilla Redondo pepper, and lastly by the Bolilla Largo pepper. Homocapsaicin was only found in hot Cayenne pepper; neither of the other two varieties studied (Bolilla Redondo and Bolilla Largo) contained this compound.

4. Conclusions

Ultrasound-assisted extraction, by means of the method developed, allows the quantitative and reproducible (R.S.D.

<3%) extraction of the capsaicinoids present in peppers, in a short time (10 min), employing methanol as extractant solvent. Given its low instrumental requirement, its simplicity and its analytical capabilities, the method developed can be applied for the routine analysis of capsaicinoids in peppers.

Acknowledgements

G.F. Barbero is grateful to the Ministerio de Educación y Ciencia for a doctoral scholarship. This study was supported by the Consejería de Innovación, Ciencia y Empresa of the Junta de Andalucía under the project FQM-01282/2005.

References

- [1] K. Iwai, T. Suzuki, H. Fujiwaka, *Agric. Biol. Chem.* 43 (1979) 2493.
- [2] H.L. Constant, G.A. Cordell, *J. Nat. Prod.* 58 (1995) 1925.
- [3] Y. Zewdie, P.W. Bosland, *Biochem. Syst. Ecol.* 29 (2001) 161.
- [4] J. Szolcsanyi, *Neuropeptides* 38 (2004) 377.
- [5] D.E. Henderson, A.M. Slickman, *J. Agric. Food Chem.* 47 (1999) 2563.
- [6] B. Toth, P. Gannett, *In Vivo* 6 (1992) 59.
- [7] Y.J. Surh, C.R.J. Lee, K.K. Park, S.T. Mayne, A. Liem, J.A. Miller, *Carcinogenesis* 16 (1995) 2467.
- [8] G.C. Morris, S.J. Gibson, R.D. Helme, *Pain* 63 (1995) 93.
- [9] R. Sancho, C. Lucena, A. Macho, M.A. Calzado, M. Blanco-Molina, A. Mináis, G. Appendino, E. Muñoz, *Eur. J. Immunol.* 32 (2002) 1753.
- [10] V.S. Govindarajan, M.N. Sathyanarayana, *Crit. Rev. Food Sci. Nutr.* 29 (1991) 435.
- [11] P. Kirschbaum-Titze, C. Hiepler, E. Mueller-Seitz, M. Petz, *J. Agric. Food Chem.* 50 (2002) 1260.
- [12] M. Contreras-Padilla, E.M. Yahia, *J. Agric. Food Chem.* 46 (1998) 2075.
- [13] R.I. Santamaría, M.D. Reyes-Duarte, E. Bárzana, D. Fernández, F.M. Gama, M. Mota, A. López-Munguía, *J. Agric. Food Chem.* 48 (2000) 3063.
- [14] R. Karnka, M. Rayanakorn, S. Watanek, Y. Vaneesorn, *Anal. Sci.* 18 (2002) 661.
- [15] F. Korel, N. Bagdatlioglu, M.O. Balaban, Y. Hisil, *J. Agric. Food Chem.* 50 (2002) 3257.
- [16] H.G. Daood, V. Illés, M.H. Gnayfeed, B. Mészáros, G. Horváth, P.A. Biacs, *J. Supercrit. Fluids* 23 (2002) 143.
- [17] G.F. Barbero, M. Palma, C.G. Barroso, *J. Agric. Food Chem.* 54 (2006) 3231.
- [18] O.J. Williams, G.S. Viyaya-Raghavan, V. Orsat, J. Dai, *J. Food Biochem.* 28 (2004) 113.
- [19] G.F. Barbero, M. Palma, C.G. Barroso, *Anal. Chim. Acta* 578 (2006) 227.
- [20] M.D. Luque de Castro, L.E. García-Ayuso, *Anal. Chim. Acta* 369 (1998) 1.
- [21] L. Wang, C.L. Weller, *Trends Food Sci. Technol.* 17 (2006) 300.
- [22] M. Padilla, M. Palma, C.G. Barroso, *J. Chromatogr. A* 1091 (2005) 83.
- [23] D.A. Lambropoulou, I.K. Konstantinou, T.A. Albanis, *Anal. Chim. Acta* 573–574 (2006) 223.
- [24] M. Palma, C.G. Barroso, *Anal. Chim. Acta* 458 (2002) 119.
- [25] M.C. Herrera, M.D. Luque de Castro, *J. Chromatogr. A* 1100 (2005) 1.
- [26] M.A. Rostagno, M. Palma, C.G. Barroso, *J. Chromatogr. A* 1012 (2003) 119.
- [27] L. Paniwnyk, E. Beaufoy, J.P. Lorimer, T.J. Mason, *Ultrason. Sonochem.* 8 (2001) 299.
- [28] J. Wu, L. Lin, F. Chau, *Ultrason. Sonochem.* 8 (2001) 347.
- [29] D.A. Lambropoulou, I.K. Konstantinou, T.A. Albanis, *J. Chromatogr. A* 1124 (2006) 97.
- [30] A.M.G. Campana, L.C. Rodriguez, F.A. Barrero, M.R. Ceba, J.L.S. Fernández, *Trends Anal. Chem.* 16 (1997) 381.
- [31] B. Estrada, M.A. Bernal, J. Díaz, F. Pomar, F. Merino, *J. Agric. Food Chem.* 48 (2000) 6234.

Selective extraction/isolation of hemoglobin with ionic liquid 1-butyl-3-trimethylsilylimidazolium hexafluorophosphate (BtmsimPF₆)

De-Hong Cheng, Xu-Wei Chen, Yang Shu, Jian-Hua Wang*

Research Center for Analytical Sciences, Box 332, Northeastern University, Shenyang 110004, China

Received 27 November 2007; received in revised form 14 January 2008; accepted 15 January 2008

Available online 1 February 2008

Abstract

Ionic liquid was for the first time employed for selective isolation of heme-protein species. Direct extraction of hemoglobin into ionic liquid without using any concomitant reagent or extractant was carried out. Hemoglobin at the level of 100 ng μL^{-1} could readily be quantitatively extracted into ionic liquid (IL) 1-butyl-3-trimethylsilylimidazolium hexafluorophosphate (BtmsimPF₆) in the absence of any co-existing extractants/additives at pH 7, at the same time; however, the other protein species do not interfere and remain in the aqueous phase. A back extraction efficiency of ca. 80% for 20 ng μL^{-1} hemoglobin in ionic liquid phase was achieved with sodium dodecyl sulfate (SDS) solution as stripping reagent. ⁵⁷Fe Mossbauer spectra and circular dichroism (CD) spectra indicated that the penta-coordinated ferrous atom in hemoglobin provide a vacant or free coordinating position, which could be occupied by the cationic Btmsim⁺ moiety. The interaction/coordination reaction between the iron atom in the heme group of hemoglobin and the cationic ionic liquid moiety furnishes the driving force for facilitating fast transfer of hemoglobin into BtmsimPF₆. The present system was applied for selective isolation of heme-protein, i.e., hemoglobin from human whole blood without any pretreatment, giving rise to satisfactory results.

© 2008 Elsevier B.V. All rights reserved.

Keywords: 1-Butyl-3-trimethylsilylimidazolium hexafluorophosphate; Heme-proteins; Hemoglobin; Ionic liquid; Extraction

1. Introduction

Termed as green solvents, the ionic liquids (ILs) have attracted extensive attention because of their unique properties characterized by low or virtually no volatility, negligible vapor pressure and ease of handling, which have shown great promise as an attractive alternative or replacement to conventional volatile organic solvents and exhibit bio-compatibility when employed in bio-science. In the past decade, room temperature ionic liquids have successfully been applied in the fields of organic synthesis, [1–4] biocatalysts [5] and extraction/separation, [6–8] the latter case includes isolation of various species from complex matrices, e.g., metal species, [9–12] organic compounds [13] and biological molecules [14,15].

The heme proteins including hemoglobin, cytochrome *c* and myoglobin play important roles in numerous biological pro-

cesses, particularly those involving transport of oxygen and electron transfer in life activities. Life science investigations including proteomic analysis require high purity of these proteins free of a broad range of impurities coexisting in biological sample matrices. Therefore, separation and purification of specific protein species from real-world sample matrices is among the most critical procedures for life science studies. A range of extraction/separation procedures for protein isolation can be located in the literature, [16–21] yet it is frequently problematic when adopting conventional organic solvents as extraction medium due to their natural toxicity to biological molecules and life processes. In this respect, the employment of ionic liquids as green solvents in analytical and biological sciences provide a promising alternative, which has drawn considerable and increasing interest [22].

Extraction of proteins by using ionic liquid with the assistance of a concomitant extractant has been investigated [23]. So far, however, there is no report about the direct extraction of proteins with ionic liquid in the absence of concomitant extractants, this might be attributed to the very limited solubility of proteins in ionic liquids [24]. A few studies have been directed

* Corresponding author. Tel.: +86 83688944; fax: +86 83676698.

E-mail address: jianhua@jz@mail.neu.edu.cn (J.-H. Wang).

to the activities and stabilities of protein or enzyme species in ionic liquid phase, [25,26] while investigations about the conformation, activity and stability of proteins in ionic liquids were blocked due to their low solubilities.

In the present paper, we report for the first time that heme-protein (hemoglobin, myoglobin) can readily be extracted into ionic liquid 1-butyl-3-trimethylsilylimidazolium hexafluorophosphate (BtmsimPF₆), without using any concomitant reagent or extractant. It has been demonstrated that the ferrous atom in heme group of heme-proteins provides a vacant coordinating position, which offers possibilities for covalent coordination or interaction between the ferrous atom and the cationic Btmsim⁺ moiety in the ionic liquid used, which in turn facilitates the transfer of heme-protein into the ionic liquid phase.

2. Experimental

2.1. Chemicals

Proteins used in the present study were acquired from Sigma (Louis, MO, USA), including bovine hemoglobin (H2500), cytochrome *c* from horse heart (C7752), myoglobin (0630), apo-myoglobin (A8673), transferrin (T3309), and bovine serum albumin (A3311). Protein Molecular Weight Marker (Broad) (TaKaRa Biotechnology Co., Ltd., Dalian, China) was used as purchased. Hexafluorophosphoric acid (Kunshan Fine Chemicals, Jiang-Su, China), 1-chlorobutane (Beijing Chemicals, China), 1-methylimidazole and 1-trimethylsilylimidazole (Kaile Chemicals, Jiang-Su, China) were used as received. Other chemicals employed were at least of analytical reagent grade and were used without further purification. 18 MΩ cm deionized water was used throughout.

2.2. Apparatus and measurements

Proteins were quantified by measuring their Soret peaks using a UV–vis spectrophotometer (Purkinje General Instruments, Beijing, China). ¹H NMR spectra of the prepared ionic liquids were recorded in (CD₃)₂CO at 293 K on a Bruker Avance 500 spectrometer, with chemical shifts referenced to tetramethylsilane (TMS). The circular dichroism (CD) spectra were recorded on a Jasco J-810 spectropolarimeter (JASCO, Japan) in the range of 200–550 nm. The spectra were acquired every 0.5 nm with a bandwidth setting of 1 nm at a scanning speed of 100 nm/min, with a response time of 1 s and averaged for 3 scans. The fluorescence spectra were recorded on an F-7000 fluorimeter (Hitachi, Japan) with the excitation wavelength at 344 nm and the slit widths for excitation and emission set at 10 nm. Room temperature ⁵⁷Fe Mossbauer spectra were measured by using an FH-1918 Mossbauer spectrometer (Beijing Nuclear Instrument Factory, China), with a room temperature palladium matrix cobalt-57 source and was calibrated with a natural α-iron foil. The spectra were fitted with symmetric quadrupole doublets by using a standard least squares fitting procedure.

2.3. Preparation of ionic liquids

1-Butyl-3-trimethylsilylimidazolium hexafluorophosphate (BtmsimPF₆) was prepared by adopting a documented pathway with minor modifications [27].

1-Butyl-3-trimethylsilylimidazolium chloride (BtmsimCl) was first prepared by the reaction of 0.5 mol 1-trimethylsilylimidazole and 0.5 mol chlorobutane in 50 mL of toluene in a nitrogen atmosphere at 90 °C for 72 h with stirring and refluxing. The obtained transparent viscous BtmsimCl was cooled and then washed with 50 mL of ethyl acetate for three times, followed by drying at 80 °C.

0.5 mol of BtmsimCl was mixed with 100 mL of water in a flask, to which 100 mL of hexafluorophosphoric acid (63%) was added drop-wise in order to control the temperature not to exceed 50 °C. After the mixture was stirred vigorously for 1 h, the ionic liquid phase in the bottom of the flask was separated and washed with a sufficient amount of water until a neutral wash out solution was obtained, i.e., pH 6.5. The BtmsimPF₆ was finally dried at 80 °C under vacuum for 24 h. The yield at this stage, i.e., the conversion of chloride to hexafluorophosphate ionic liquid, was 85%. The ¹H NMR data of the product were listed in the following: 0.46 (s, 9H), 0.889 (t, 3H), 1.324 (m, 2H), 1.868 (m, 2H), 4.34 (m, 2H), 7.512 (d, 1H), 7.674 (d, 1H), 8.71 (d, 1H).

1,3-Dibutylimidazolium hexafluorophosphate (BBimPF₆) was prepared employing the following procedure: [28] 1,3-dibutylimidazolium chloride (BBimCl) was first obtained by the reaction of 0.5 mol 1-trimethylsilylimidazole and 1.0 mol chlorobutane at 90 °C for 72 h. The viscous BBimCl was cooled and then washed with 50 mL of ethyl acetate for three times followed by drying at 80 °C.

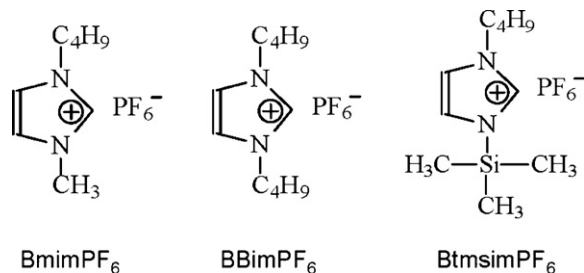
0.5 mol of BBimCl was mixed with 100 mL of water in a flask, to which 100 mL of hexafluorophosphoric acid (63%) was added drop-wise in order to control the temperature and not exceed 50 °C. Afterwards, similar operations as those for the preparation of BtmsimPF₆ were adopted. A 75% yield at this stage was achieved. The ¹H NMR data of the product: 0.963 (s, 6H), 1.394 (m, 4H), 1.938 (m, 4H), 4.371 (m, 4H), 7.768 (d, 1H), 7.770 (d, 1H), 9.03 (d, 1H).

1-Butyl-3-methylimidazolium hexafluorophosphate (BmimPF₆) was prepared adopting a documented pathway by modification, [15,29] as detailed previously [14].

2.4. Extraction and back extraction processes

An appropriate amount of ionic liquid, 50–1000 μL, was taken into a 5 mL centrifuge tube with 3 mL of protein aqueous solution within a concentration range of 20–200 ng μL⁻¹. The mixture was shaken vigorously in an oscillator for 30 min to facilitate the transfer of proteins into the ionic liquid phase. After extraction, the concentrations of proteins in both phases were determined by the absorbance of the Soret band peak using a UV–vis spectrophotometer, and the extraction efficiencies (*E*) of proteins were calculated as described in the following equation:

$$E = \frac{V_{\text{IL}} C_{\text{IL}}}{V_{\text{aq}} C_{\text{aq}}} \times 100\% \quad (1)$$



Scheme 1. The molecular structures of ionic liquids: BmimPF₆, BBimPF₆ and BtmsimPF₆.

where C_{aq}^0 and C_{IL} represent the concentrations of proteins in aqueous and ionic liquid phases, while V_{aq} and V_{IL} denote the volumes of the two phases, respectively.

The back extraction of proteins from the ionic liquid phase into aqueous phase was performed in the presence of sodium dodecyl sulfate (SDS) as a stripping reagent, by shaking the reaction mixture in a 5-mL cuvette for 30 min, and the back extraction efficiency was derived accordingly.

3. Results and discussion

3.1. Direct extraction of proteins into ionic liquids without any concomitant extractant

The three ionic liquids prepared in Section 2 have been investigated for the extraction of proteins. The molecular structures of the ionic liquids are illustrated in Scheme 1. It is obvious that they have a common counter anion of PF₆⁻, while the different cationic moieties exhibit various hydrophobicities according to the length of the alkyl side chains, i.e., the hydrophobicities of the three ionic liquids are increased in the line of BmimPF₆ < BBimPF₆ < BtmsimPF₆.

The investigations have showed that except for hemoglobin and myoglobin, the other protein species employed in the present study, i.e., cytochrome *c*, apo-myoglobin, BSA and transferrin,

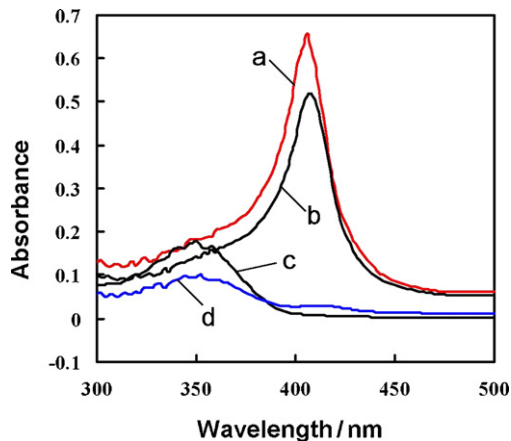


Fig. 2. UV-vis spectra recorded in aqueous solution: (a) before extraction; (b) after extraction with BmimPF₆; (c) after extraction with BBimPF₆; (d) after extraction with BtmsimPF₆. 100 ng μL⁻¹ of hemoglobin in 3 mL aqueous solution was extracted with 400 μL of ionic liquids for 30 min.

could not be extracted into BmimPF₆, BBimPF₆ and BtmsimPF₆ in the absence of coexisting extractants/additives. Fig. 1 illustrates the photographs of an aqueous-BtmsimPF₆ two-phase system containing hemoglobin in a 5-mL cuvette before and after extraction. It is obvious that the aqueous phase was turbid before extraction because of the existence of high concentration of hemoglobin, while after extraction the hemoglobin was virtually completely transferred into the ionic liquid phase, which resulted in a clear and transparent aqueous phase.

3.2. Selective extraction of hemoglobin into BtmsimPF₆

Fig. 2 shows that when 3.0 mL of hemoglobin solution (100 ng μL⁻¹, pH 7) was extracted by employing 400 μL of the three kinds of ionic liquids, a quantitative transfer of hemoglobin into the BtmsimPF₆ phase was achieved without employing any coexisting extractants/additives, indicated by the complete disappearance of the absorption band at 406 nm attributed to

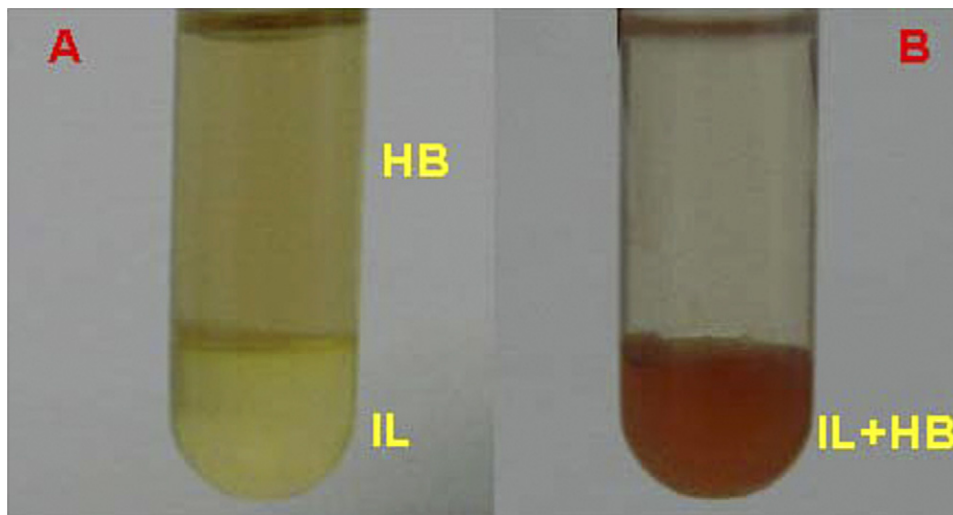


Fig. 1. The photographs of an aqueous-BtmsimPF₆ two-phase system containing 400 ng μL⁻¹ hemoglobin in a 5-mL cuvette: (A) before extraction; (B) after extraction.

hemoglobin in the aqueous phase. On the other hand, extraction efficiencies of ca. 93% and ca. 20% were achieved by using BBmimPF₆ and BmimPF₆ respectively at identical experimental conditions. This observation obviously indicated that hemoglobin inclines to dissolve into a more hydrophobic ionic liquid phase, and thus an enhancement of the hydrophobicity of the adopted ionic liquid tends to result in a favorable extraction of hemoglobin. More details about this issue will be given in Section 3.4. In the present case, BtmsimPF₆ facilitates quantitative extraction of hemoglobin, which offers a promising approach for its isolation from complex matrix in the presence of other protein species and complex sample matrices.

For a certain amount of protein in a fixed volume of aqueous solution (50 ng μL^{-1} hemoglobin in 3 mL), a significant increment of the extraction efficiency was observed with the increase of the BtmsimPF₆ volume, and virtually quantitative extraction was achieved with an ionic liquid volume of 400 μL , and thereafter a plateau was encountered. For the ensuing experiments, 400 μL of BtmsimPF₆ was used. Further experiments also indicated that a rapid increase of the extraction efficiency for hemoglobin was observed with the increase of extraction time up to 20 min, while afterwards a quantitative extraction was obtained and thus there is no need to further extend the extraction time. In the present investigations, an extraction time of 30 min was adopted.

There is an argument that the disappearance of hemoglobin from the aqueous phase might be attributed to not only its transfer into the ionic liquid phase, but also the concentration of hemoglobin at the interface of aqueous–ionic liquid phase, and the dissociation of heme-group because hemoglobin has a noncovalently protein-bound heme group, which is readily dissociated from the hydrophobic core of the polypeptide chain.

Our experiments have showed that the UV–vis spectra recorded in ionic liquid phase clearly showed the characteristic absorption bands of hemoglobin at 406 nm, 535 nm and 560 nm, indicating the presence of polypeptide chain in the ionic liquid phase. CD spectra were also measured to provide information about the secondary structure of hemoglobin in ionic liquid. However, the interfering effects of ionic liquid on the CD spectrum of the α -helix region of hemoglobin provided no accurate information. On the other hand, fair agreements were achieved between the concentrations of hemoglobin in ionic liquid phase and those obtained by measuring in aqueous phase by spectrophotometry. These observations illustrated the transfer of hemoglobin into the ionic liquid phase, and there is no obvious concentration of hemoglobin at the interface of aqueous–ionic phase.

3.3. Back extraction of hemoglobin from ionic liquid into aqueous solution

Back extraction of hemoglobin from ionic liquid into aqueous phase is necessary to fulfill the requirements for further biological investigations. Thus, SDS, sodium chloride, EDTA, hydrochloride and acetonitrile as stripping reagents were investigated. A back extraction efficiency of 80% for 20 ng μL^{-1} hemoglobin was achieved by using SDS, while the others were

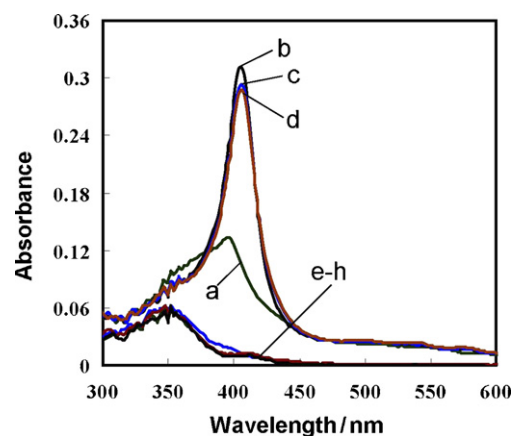


Fig. 3. UV–vis spectra of 50 ng μL^{-1} hemoglobin aqueous solution. Before extraction: (a) pH 2; (b) pH 4; (c) pH 7; (d) pH 9; after 50 ng μL^{-1} hemoglobin in 3 mL aqueous solution was extracted with 400 μL BtmsimPF₆ for 30 min: (e)–(h), pH 2, 4, 7, 9.

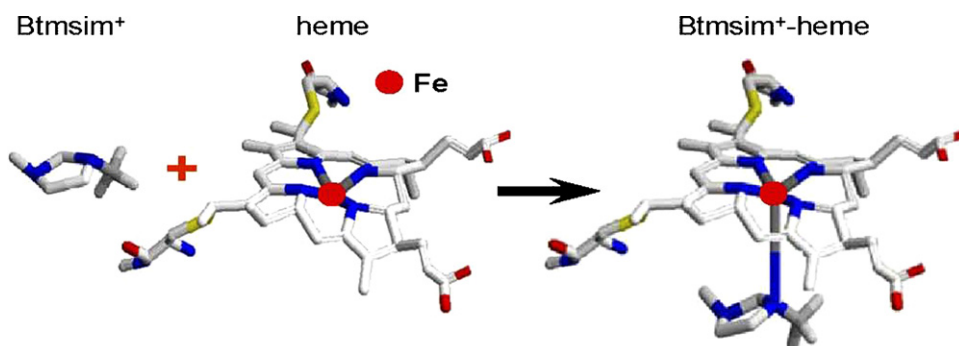
proved to be not suitable to be stripping reagents. The possible mechanism of back-extraction is supposed as such that SDS provides anionic moiety to replace the heme-group in the Btmsim⁺–heme complex in ionic liquid phase and form ion-pair with cationic Btmsim⁺, the hemoglobin was thus released and transferred into the aqueous phase.

The back extraction of hemoglobin from ionic liquid into aqueous phase was thus performed in the presence of SDS as a stripping reagent. Hemoglobin aqueous solution was mixed with 400 μL of BtmsimPF₆ to facilitate its extraction into the ionic liquid phase. Afterwards, the ionic liquid phase was separated and taken into a 5-mL cuvette with 3 mL of SDS aqueous solution, and the back extraction of hemoglobin was facilitated by shaking the mixture in an oscillator for 30 min.

3.4. Extraction mechanism

3.4.1. Electrostatic interaction

The isoelectric point of 6.8 for hemoglobin results in an overall positive charge in acidic medium while gives rise to a negative charge in basic medium [19]. In the present study, the effects of surface charge and the conformation of hemoglobin on its extraction property were exploited in the range of pH 2–9, with the variations of UV–vis spectra of hemoglobin in aqueous solution illustrated in Fig. 3. It can be seen that a maximum absorbance at ca. 406 nm was encountered at a pH value close to the isoelectric point of hemoglobin, while a decrement of the absorbance was observed as pH of the aqueous solution depart from the isoelectric point of hemoglobin, i.e., at pH < 4 or pH > 9. This observation is very likely related to the variation of the surface charge and the conformation of hemoglobin. On the other hand, it is obvious that the absorption spectra of the aqueous phase remained virtually unchanged after extraction, regardless the variation of pH. This phenomenon illustrated that the variations of surface charge or the configuration of the protein do not interfere with the extraction of hemoglobin, which further indicated that the electrostatic interaction between hemoglobin and



Scheme 2. The extraction mechanism of heme-protein by BtmsimPF₆ incorporating covalent coordination of ferrous atom with the cationic Btmsim⁺ moiety.

the ionic liquid moiety is not the driving force for the extraction process.

3.4.2. Covalent coordination between the cationic Btmsim⁺ and iron atom in heme group

Generally, the hydrophilic nature of hemoglobin should prohibit its distribution into the hydrophobic ionic liquid, BtmsimPF₆. However, Fig. 2 shows that hemoglobin inclines to transfer into a hydrophobic ionic liquid phase, and an increase of the hydrophobicity of the ionic liquid tends to result in a favorable extraction of hemoglobin. In fact, the length of the alkyl side chain in the imidazole entity dominates the hydrophobicity of the ionic liquid, an increase of the alkyl side chain length results in an increase of hydrophobicity of the ionic liquid and a decrease of electron density in the nitrogen atom, which improved the coordination capability of the cationic imidazole group (Btmsim⁺), i.e., its coordination with the iron atom in the heme-group in this particular case, and thus facilitates the direct extraction of hemoglobin into the BtmsimPF₆ phase.

The above observations illustrated that variation on the configuration of the cationic Btmsim⁺ plays a very important rule in the extraction of hemoglobin.

The experiments have indicated that the extraction of BSA, transferrin and apo-myoglobin by using BtmsimPF₆ was not observed at all, while hemoglobin and myoglobin could be readily extracted in the absence of any coexisting extrac-

tants/additives, and the transfer of a part of cytochrome *c* into BtmsimPF₆ was achieved at pH 1. The most important structural difference of hemoglobin, myoglobin and cytochrome *c* with BSA, transferrin and apo-myoglobin is that there are heme groups in the former category of proteins, while there are not in the latter group. Therefore, these observations clearly suggested that the extraction of protein species by BtmsimPF₆ was significantly facilitated probably by the existence of heme group.

Iron-nitrogen bondings in heme group have been reported previously [30–32]. In the case of hemoglobin, the iron atom is coordinated with four pyrrole nitrogen atoms of protoporphyrin IX and nitrogen atom in imidazole of histidine [33]. The iron atom also provides a sixth vacant coordinating position, which offers a potential to coordinate with one extra nitrogen atom of imidazole [34]. Previous investigations have proved that imidazole is a strong covalent coordinating ligand with iron atom in heme group [34–36]. For the heme proteins such as hemoglobin and myoglobin, the sixth vacant coordinating position of iron atom is available to bind with other small molecules [37].

Therefore, the extraction mechanism of heme-protein into BtmsimPF₆ was assumed as such that the cationic Btmsim⁺ moiety was covalently bond to the iron atom in the heme group, as illustrated in Scheme 2, and the Btmsim⁺-heme complex facilitates the transfer of heme-proteins into the ionic liquid phase.

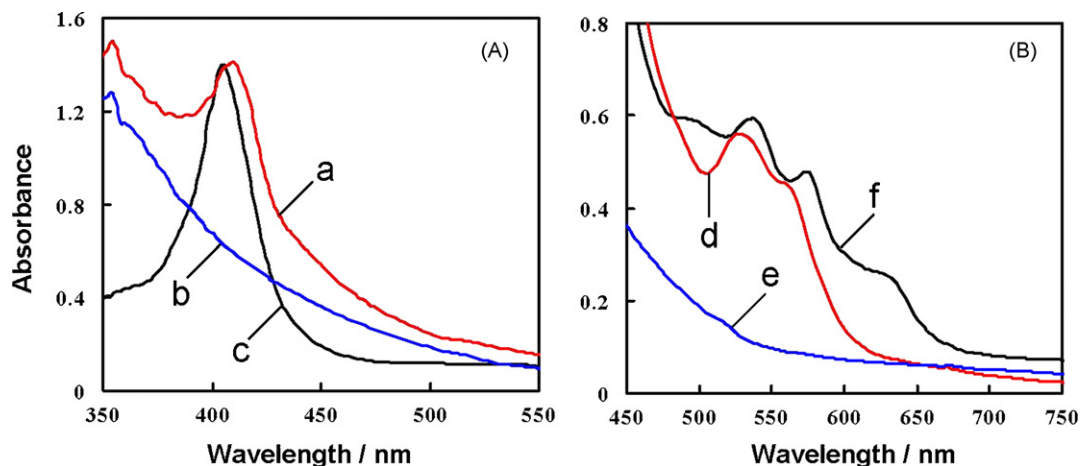


Fig. 4. UV-vis spectra of hemoglobin in aqueous solution and BtmsimPF₆ at two concentration levels. (A) 250 ng μL⁻¹ hemoglobin: (a) in aqueous solution; (b) pure ionic liquid; (c) in ionic liquid; (B) 1.5 μg μL⁻¹ hemoglobin: (d) in aqueous solution; (e) pure ionic liquid; (f) in ionic liquid.

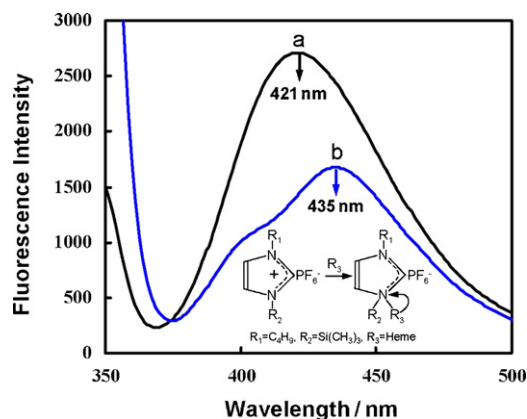


Fig. 5. Fluorescence spectra of BtmsimPF₆: (a) saturated ionic liquid in aqueous solution; (b) saturated ionic liquid in aqueous solution with 100 ng μL^{-1} hemoglobin.

3.4.3. Evidence from the UV–vis and fluorescence spectra

Fig. 4 illustrates UV–vis spectra of hemoglobin at two concentration levels in both aqueous solution and ionic liquid phase. In aqueous solution, the spectra show a sharp Soret band at 406 nm, a broad Q-band at 538 nm and two characteristic bands at 574 nm and 630 nm. While in the ionic liquid phase, a slight red shift for the Soret band from 406 nm to 410 nm, blue shifts for the Q-band from 538 nm to 530 nm and the characteristic band from 574 nm to 556 nm were obtained, and particularly, the band at 630 nm was completely disappeared. The shifts of absorption bands can be attributed to the change of coordinating sphere of the iron atom in heme group. In aqueous phase, a H₂O molecule serves as the sixth ligand coordinating with iron atom [38]. After transferred into the ionic liquid phase, however, the cationic Btmsim⁺ moiety was covalently coordinated with the iron atom by replacing the H₂O molecule, which gave rise to obvious changes in the absorption bands.

Fig. 5 shows that the fluorescence spectra of BtmsimPF₆ in the absence and presence of hemoglobin. BtmsimPF₆ has an obvious emission at 421 nm with an excitation wavelength at 344 nm, because of the π – π^* conjugate N–C–N of bonds. In the presence of hemoglobin, however, a red shift of its emission

wavelength from 421 nm to 435 nm was observed, indicating the variation of the π – π^* conjugate of the N–C–N bonds of the cationic Btmsim⁺ group, i.e., covalent coordination between the cationic Btmsim⁺ and the iron atom in heme resulted in the change of the π – π^* conjugate configuration, as illustrated in the insert.

3.4.4. Evidence from ⁵⁷Fe Mossbauer spectra

To identify that the cationic Btmsim⁺ group was covalently bond to the iron atom in heme group, ⁵⁷Fe Mossbauer spectra of hemoglobin and Btmsim⁺–heme adduct/complex were measured at room temperature (Fig. 6). The parameters of hemoglobin related to α -Fe were calculated as (IS, isomer shift) = 0.2348 mm s⁻¹, (QS, quadrupole split) = 0 mm s⁻¹, with a half-line width of the spectra of 0.9442 mm s⁻¹. On the other hand, the corresponding parameters of Btmsim⁺–heme complex were obtained as IS = 0.2161 mm s⁻¹, QS = -0.055 mm s⁻¹ with a half-line width of 0.7694 mm s⁻¹. The error limits of IS and QS were 0.001 mm s⁻¹ and 0.002 mm s⁻¹, respectively.

Although the recorded ⁵⁷Fe Mossbauer spectra for hemoglobin and Btmsim⁺–heme complex at room temperature both exhibit singlet states, an obvious decrease on the IS value of the Btmsim⁺–heme complex was observed as compared to that of hemoglobin. The decline of IS value could be attributed to indirectly decrement in the d-electron density of the iron atom [39,40]. When nitrogen atom in the cationic Btmsim⁺ was bond to iron atom in the heme group, the cationic Btmsim⁺ ligand tends to serve as an electron acceptor because the empty orbital of nitrogen in cationic Btmsim⁺ was lack of electron, thus transfer of electron density occurred from a filled d-orbital of iron atom into an empty orbital of nitrogen in the cationic Btmsim⁺, which resulted in an decrement of electron density of iron atom in the heme group. In addition, a slight quadrupole split was also encountered in the Btmsim⁺–heme complex, which showed a variation of the symmetry of electron density in the iron atom with respect to that in hemoglobin. Furthermore, the negative QS value indicated that the doubly occupied orbital of iron and nitrogen atom in the Btmsim⁺–heme complex was perpendicular to the heme plane [41,42]. As a summary, the ⁵⁷Fe Mossbauer spectra provided an overall picture of the bond char-

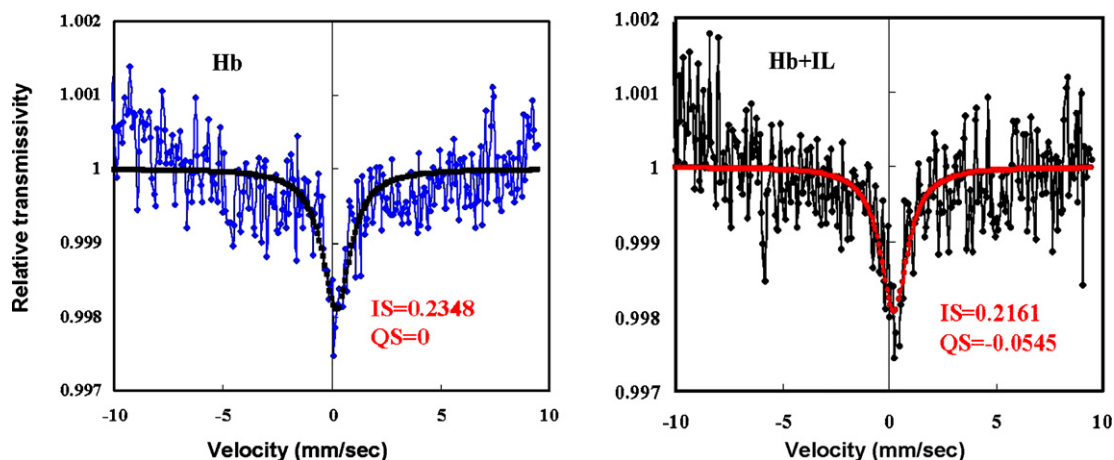


Fig. 6. ⁵⁷Fe Mossbauer spectra of hemoglobin and Btmsim⁺–heme adduct/complex.

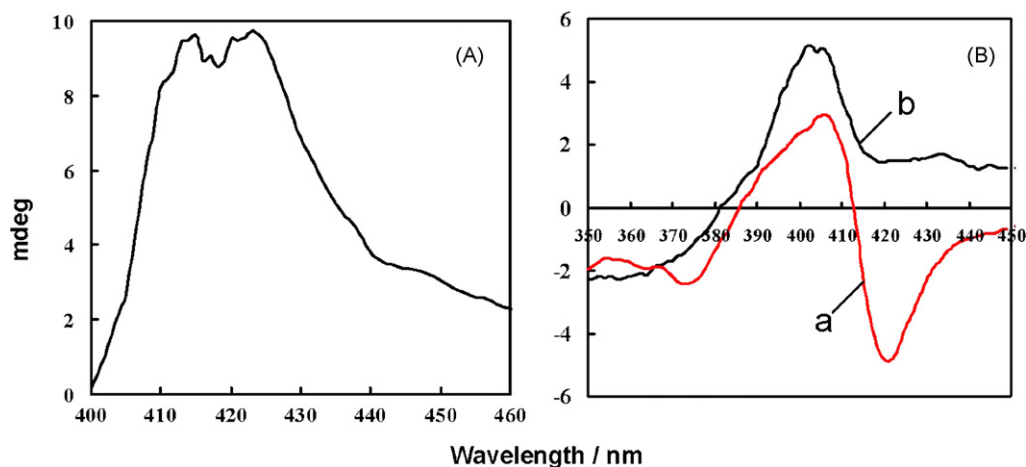


Fig. 7. (A) CD spectra of hemoglobin at the level of $200 \text{ ng } \mu\text{L}^{-1}$. (B) CD spectra of cytochrome *c* at the level of $200 \text{ ng } \mu\text{L}^{-1}$. (a) pH 7; (b) pH 1.

acter between the cationic Btmsim⁺ ligand and the iron atom, that is, the Btmsim⁺ ligand was perpendicularly bond to iron atom during the extraction process.

3.4.5. The importance of the sixth coordinating position of iron atom in heme group

It has been demonstrated that hemoglobin can be quantitatively extracted into BtmsimPF₆ via covalent coordination between Btmsim⁺ and iron atom in heme group. However, when treating cytochrome *c* similarly, a direct extraction efficiency of only ca. 10% was achieved under identical experimental conditions. An obvious difference between hemoglobin and cytochrome *c* is that in the former case the ferrous iron in heme group provides a sixth vacant coordinating position for binding other small molecules, while in the case of cytochrome *c*, the ferric iron coordinates with two strong-field protein ligands, i.e., histidyl-18 and methionyl-80 [43], which provides no vacant coordinating positions for external molecules. The circular dichroism (CD) spectra of hemoglobin and native cytochrome *c* showed clearly the difference of the oxidation states of iron. Fig. 7A and B illustrates the Soret region CD spectra of hemoglobin and cytochrome *c* in aqueous solution. A positive peak at 420 nm was observed from hemoglobin, while a negative peak at 420 nm along with a positive peak at 404 nm were recorded for cytochrome *c*.

According to the extraction mechanism if a coordinating position in cytochrome *c* is available for binding other molecules, e.g., Btmsim⁺, the extraction of cytochrome *c* into BtmsimPF₆ will be feasible. Further experiments indicated that an extraction efficiency of 85% was obtained for cytochrome *c* at the level of $5 \text{ ng } \mu\text{L}^{-1}$ by adjusting the aqueous solution to pH 1. In this case, as illustrated in Fig. 7B, the CD spectrum is characterized by the complete disappearance of the negative Cotton effect and a concomitant increase in the intensity of the positive Cotton effect at 404 nm. These changes indicate the cleavage of the sixth coordinating bond between iron and the methionyl-80 occurred, [24,43] which facilitate the formation of coordinating bond between iron and the Btmsim⁺ moiety of the ionic liquid, and thus the transfer of cytochrome *c* into BtmsimPF₆.

At this stage, the effect of the solubility of ionic liquid in water and vice versa on the extraction of hemoglobin should be clarified. BtmsimPF₆ is highly hydrophobic and has a very limited solubility, so far there is no evidence showing the effect of the dissolved ionic liquid. On the other hand, there is only minute amount of water incorporated in the ionic liquid phase. Although the water molecules tend to covalently coordinate with the iron atom in heme-group, the very strong coordinating power of the cationic Btmsim⁺ dominates the interaction between the ligands and the iron atom. Thus, there is no risk to neglect the effect of the minute amount of water in ionic liquid and vice versa.

3.5. Extraction and separation of hemoglobin from human whole blood

The present study provided potentials for the selective isolation/separation of hemoglobin from other protein species in biological sample matrices. Hemoglobin in human whole blood was separated by direct extraction with BtmsimPF₆ to demonstrate the practical applicability of the procedure.

10 μL human whole blood was directly diluted with 20 mL of deionized water without any further pretreatment. 3.0 mL of the diluted sample was then used to mix with 600 μL of BtmsimPF₆ for facilitating the extraction by shaking vigorously in an oscillator for 30 min, and thereafter the two phases were separated by centrifugation. Afterwards, the ionic liquid phase was taken into a 5-mL cuvette with 3 mL of SDS aqueous solution of 6% (m/v) to undergo the back extraction process as described in the Experimental section. The aqueous solution after back extraction was employed to perform standard SDS-PAGE, in order to evaluate the efficiency of the entire extraction process.

The standard SDS-PAGE (in 12% gels) obtained were illustrated in Fig. 8, including those for human whole blood, hemoglobin isolated from human whole blood employing the present procedure, standard hemoglobin solutions before and after undergoing the extraction process. It is obvious that quite a few bands were recorded within the range of ca. 6.5–116 kDa for human whole blood without treatment, which might be attributed

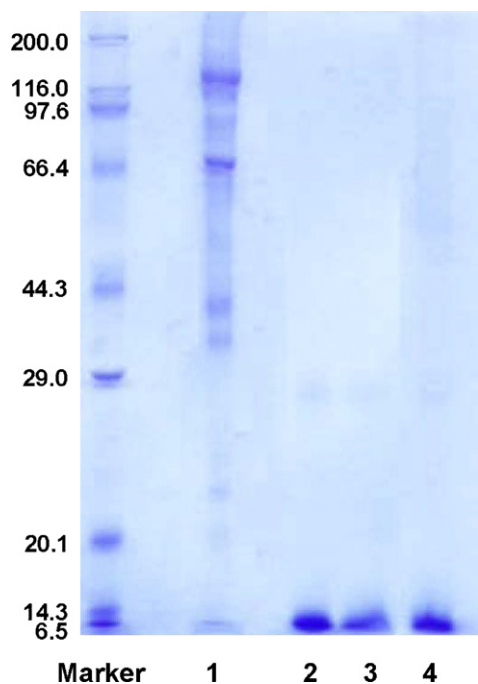


Fig. 8. The standard SDS-PAGE. 1, human whole blood without treatment; 2, hemoglobin isolated from human whole blood with the present extraction/back extraction procedure; 3, 250 ng μL^{-1} standard hemoglobin solution; 4, 250 ng μL^{-1} standard hemoglobin solution undergoing the present extraction/back extraction procedure.

mainly to albumin, transferrin, heme proteins and ceruloplasmin. After extraction by BtmsimPF₆ and back extraction into aqueous phase, it is clearly showed that there is only a single band of hemoglobin left at ca. 14 kDa, indicating that selective separation of hemoglobin from human whole blood was achieved.

4. Conclusions

The selective extraction/separation of hemoglobin by employing ionic liquid BtmsimPF₆ was reported for the first time. A quantitative extraction of hemoglobin at the level of 100 ng μL^{-1} or less could readily be achieved without any coexisting additives/extractants. The extraction of hemoglobin was facilitated by the coordination of the cationic Btmsim⁺ moiety of ionic liquid and the iron atom in the heme group. The present observation provides a potential procedure for direct isolation of heme-proteins from complex biological sample matrix, while the avoidance of toxic organic solvents tends to offer bio-compatibility of the procedure. The selective separation of hemoglobin from human whole blood demonstrated the practical applicability of the present procedure.

Acknowledgments

The authors are indebted to the financial support from the National Natural Science Foundation of China (NSFC-20635010, 20725517).

References

- [1] Y.S. Vygodskii, E.I. Lozinskaya, A.S. Shaplov, K.A. Lyssenko, M.Y. Antipin, Y.G. Urman, *Polymer* 45 (2004) 5031.
- [2] C.E. Song, E.J. Roh, *Chem. Commun.* 10 (2000) 837.
- [3] F. Favre, H. Olivier-Bourbigou, D. Commereuc, L. Saussine, *Chem. Commun.* 15 (2001) 1360.
- [4] M.J. Earle, P.B. McCormac, K.R. Seddon, *Chem. Commun.* 20 (1998) 2245.
- [5] S. Shah, M.N. Gupta, *Bioorg. Med. Chem. Lett.* 17 (2007) 921.
- [6] J.G. Huddleston, H.D. Willauer, R.P. Swatloski, A.E. Visser, R.D. Rogers, *Chem. Commun.* 16 (1998) 765.
- [7] G.T. Wei, Z.S. Yang, C.J. Chen, *Anal. Chim. Acta.* 488 (2003) 183.
- [8] M. Matsumoto, K. Mochiduki, K. Fukunishi, K. Kondo, *Sep. Purif. Technol.* 40 (2004) 97.
- [9] M.L. Dietz, *Sep. Sci. Technol.* 41 (2006) 2047.
- [10] K. Shimojo, M. Goto, *Anal. Chem.* 76 (2004) 5039.
- [11] E. Visser, R.P. Swatloski, W.M. Reichert, R. Mayton, S. Sheff, A. Wierzbicki, J.H. Davis, R.D. Rogers, *Chem. Commun.* 1 (2001) 135.
- [12] H.M. Luo, S. Dai, P.V. Bonnesen, *Anal. Chem.* 76 (2004) 2773.
- [13] J.F. Liu, G.B. Jiang, Y.G. Chi, Y.Q. Cai, Q.X. Zhou, J.T. Hu, *Anal. Chem.* 75 (2003) 5870.
- [14] J.H. Wang, D.H. Cheng, X.W. Chen, Z. Du, Z.L. Fang, *Anal. Chem.* 79 (2007) 620.
- [15] S.V. Smirnova, I.I. Torocheshnikova, A.A. Formanovsky, I.V. Pletnev, *Anal. Bioanal. Chem.* 378 (2004) 1369.
- [16] W.J. Hurkman, C.K. Tanaka, *Plant Physiol.* 81 (1986) 802.
- [17] Y. Meyer, J. Grosset, Y. Chartier, J.C. Cleyet-Marel, *Electrophoresis* 9 (1988) 704.
- [18] W. Wang, R. Vignani, M. Scali, E. Sensi, *Anal. Biochem.* 329 (2004) 139.
- [19] T. Ono, M. Goto, F. Nakashio, T.A. Hatton, *Biotechnol. Prog.* 12 (1996) 793.
- [20] M.G. Roper, M.L. Frisk, J.P. Oberlander, J.P. Ferrance, B.J. McGrory, J.P. Landers, *Anal. Chim. Acta* 569 (2006) 195.
- [21] M. Vasudevan, J.M. Wienczek, *Ind. Eng. Chem. Res.* 35 (1996) 1085.
- [22] J.L. Anderson, D.W. Armstrong, G.T. Wei, *Anal. Chem.* 78 (2006) 2892.
- [23] K. Shimojo, K. Nakashima, N. Kamiya, M. Goto, *Biomacromolecules* 7 (2006) 2.
- [24] K. Shimojo, N. Kamiya, F. Tani, H. Naganawa, Y. Naruta, M. Goto, *Anal. Chem.* 78 (2006) 7735.
- [25] C.A. Summers, R.A. Flowers II, *Protein Sci.* 9 (2000) 2001.
- [26] J.L. Kaar, A.M. Jesionowski, J.A. Berberich, R. Moulton, A.J. Russell, *J. Am. Chem. Soc.* 125 (2003) 4125.
- [27] Z.J. Li, Q. Wei, R. Yuan, X. Zhou, H.Z. Liu, H.X. Shan, Q.J. Song, *Talanta* 71 (2007) 68.
- [28] Y.S. Vygodskii, E.L. Lozinskaya, A.S. Shaplov, K.A. Lyssenko, M.Y. Antipin, Y.G. Urman, *Polymer* 45 (2004) 5031.
- [29] B.S. Carda, A. Berthod, D.W. Armstrong, *Anal. Bioanal. Chem.* 375 (2003) 191.
- [30] G. Smulevich, F. Neri, O. Willemsen, K. Choudhury, M.P. Marzocchi, T.L. Poulos, *Biochemistry* 34 (1995) 13485.
- [31] K. Nagai, C. Welborn, D. Dolphin, T. Kitagawa, *Biochemistry* 19 (1980) 4755.
- [32] M.M. Fitzgerald, M.J. Churchill, D.E. McRee, D.B. Goodin, *Biochemistry* 33 (1994) 3807.
- [33] K.D. Egeberg, B.A. Springer, S.A. Martinis, S.G. Sligar, *Biochemistry* 29 (1990) 9783.
- [34] D. Barrick, *Biochemistry* 33 (1994) 6546.
- [35] J. Hirst, S.K. Wilcox, P.A. Williams, J.D. Blankenship, E. McRee, D.B. Goodin, *Biochemistry* 40 (2001) 1265.
- [36] W.F. Reynolds, I.R. Peat, M.H. Freedman, J.R. Lyerla, *J. Am. Chem. Soc.* 95 (1973) 328.
- [37] C.M. DiCarlo, D.L. Compton, K.O. Evans, J.A. Laszlo, *Bioelectrochemistry* 68 (2006) 134.
- [38] T. Itoh, T. Yamada, Y. Kodera, A. Matsushima, M. Hiroto, K. Sakurai, H. Nishimura, Y. Inada, *Bioconjugate. Chem.* 12 (2001) 3.

- [39] H. Nakazawa, S. Ichimura, Y. Nishihara, K. Miyoshi, S. Nakashima, H. Sakai, *Organometallics* 17 (1998) 5061.
- [40] B.H. Goodreau, L.R. Orlando, G.J. Long, J.T. Spencer, *Inorg. Chem.* 35 (1996) 6579.
- [41] C.J. Hu, B.C. Noll, C.E. Schulz, W.R. Scheidt, *J. Am. Chem. Soc.* 127 (2005) 15018.
- [42] C. Hu, A. Roth, M.K. Ellison, J. An, C.M. Ellis, C.E. Schulz, W.R. Scheidt, *J. Am. Chem. Soc.* 127 (2005) 5675.
- [43] T.Y. Tsong, *Biochemistry* 14 (1975) 1542.

Development of an anodic stripping voltammetric assay, using a disposable mercury-free screen-printed carbon electrode, for the determination of zinc in human sweat

A. Crew, D.C. Cowell, J.P. Hart *

Centre for Research in Analytical Materials & Sensor Science, Faculty of Health & Life Sciences, University of the West of England, Coldharbour Lane, Bristol BS16 1QY, UK

Received 23 October 2007; received in revised form 4 January 2008; accepted 9 January 2008

Available online 1 February 2008

Abstract

This paper reports on the development of a novel electrochemical assay for Zn^{2+} in human sweat, which involves the use of disposable screen-printed carbon electrodes (SPCEs). Initially, SPCEs were used in conjunction with cyclic voltammetry to study the redox characteristics of Zn^{2+} in a selection of supporting electrolytes. The best defined cathodic and anodic peaks were obtained with 0.1 M NaCl/0.1 M acetate buffer pH 6.0. The anodic peak was sharp and symmetrical which is typical for the oxidation of a thin metal film on the electrode surface. This behaviour was exploited in the development of a differential pulse anodic stripping voltammetric (DPASV) assay for zinc. It was shown that a deposition potential of -1.6 V versus Ag/AgCl and deposition time of 60 s with stirring (10 s equilibration) produced a well-defined stripping peak with $E_{pa} = -1.2$ V versus Ag/AgCl. Using these conditions, the calibration plot was linear over the range 1×10^{-8} to 5×10^{-6} M Zn^{2+} . The precision was examined by carrying out six replicate measurements at a concentration of 2×10^{-6} M; the coefficient of variation was calculated to be 5.6%. The method was applied to the determination of the analyte in sweat from 10 human volunteers. The concentrations were between 0.39 and 1.56 $\mu\text{g/mL}$, which agrees well with previously reported values. This simple, low-cost sensitive assay should have application in biomedical studies and for stress and fatigue in sports studies.

© 2008 Elsevier B.V. All rights reserved.

Keywords: Zinc; Chloride; Differential pulse anodic stripping voltammetry (DPASV); Disposable; Screen-printed carbon electrode (SPCE); Sweat

1. Introduction

Changes in the concentration of zinc in biological fluids may be used as wide-ranging marker for a range of medical conditions from physical fatigue to immunosuppression [1]. Zinc is involved in cellular respiration, DNA replication, maintenance of cell membrane integrity and free radical scavenging. It is involved in the structure and activity of over 300 enzymes within the human body [2] and has a significant role in reducing apoptosis [3]. Zinc concentrations in plasma and saliva have been the subject of extensive research. However, has been reported that intrusive methods, e.g. using hyperdermic syringes for the collection of a biological fluids may cause significant interference to the analyte [4,5]. In order to avoid this problem, the use of sweat as the sample may offer the possibility of using non-

invasive methods for the measurement of zinc in human samples. We considered that it should be possible to collect sweat by using a suitably constructed sweat patch. As electrochemical methods have been successfully applied to zinc determinations in a variety of matrices, we considered that this approach might offer advantages in the current investigation.

The feasibility of using anodic stripping voltammetry (ASV) for the determination of zinc concentrations in the analysis of biological fluids has been demonstrated using mercury-based electrodes [6]. However, the toxic nature of mercury precludes its use for wide-scale routine analysis [7]. Disposable screen-printed carbon electrodes (SPCEs) are inexpensive and reproducible and may provide a viable and practical system for rapid measurements. Such electrodes have previously been used in other applications involving the electrochemical determination of trace metals in varied media including biological fluids [8]. Modified and unmodified SPCEs have been successfully used for the determination of copper in serum [9] and lead in potable and pond water [10,11] using ASV techniques.

* Corresponding author. Tel.: +44 117 3282469; fax: +44 117 3282904.
E-mail address: John.Hart@uwe.ac.uk (J.P. Hart).

The purpose of the present study was to explore the possibility of developing a stripping voltammetric assay for zinc ions (Zn^{2+}) in human sweat using a disposable screen-printed carbon electrode. However, it has been reported that zinc is difficult to measure due to its very negative reduction potential [12]. Consequently, cyclic voltammetry (CV) was initially used to investigate the electrochemical behaviour of Zn^{2+} in a wide range of supporting electrolytes using a bare SPCE. The supporting electrolyte significantly alters the redox characteristics of zinc in solution [13]. The most suitable electrolyte was selected on the basis of the most sensitive anodic signal produced on the reverse scan. The optimum instrumental conditions for the differential pulse anodic stripping voltammetry (DPASV) measurement of zinc were then deduced. The zinc concentrations of sweat patch extracts were successfully determined using the optimised conditions. This paper describes the results of these studies.

2. Experimental

2.1. Reagents and materials

All reagents were of analytical grade. The zinc nitrate, sodium acetate, acetic acid, hydrochloric acid, potassium chloride, nitric acid, potassium nitrate were supplied by Sigma (Dorset, UK). Sodium dihydrogen orthophosphate, di-sodium hydrogen orthophosphate and tri-sodium orthophosphate was supplied by VWR International (Lutterworth, UK). Deionised water was obtained from a Purite Select Analyst 80 System (Purite, Oxfordshire, UK). Screen-printed carbon electrodes were comprised of working electrodes based on carbon D14 ink with an area of 4 mm^2 (C10903D14) and were obtained from Gwent Electronic Materials Ltd. (GEM, Pontypool, UK) on a PVC support with an Ag/AgCl counter/reference electrode.

CV was carried out with an EG&G Polarographic Analyzer 265A (EG&G Princeton Applied Research, Princeton, USA) in conjunction with a Hewlett-Packard 7047A chart recorder (Hewlett-Packard, London, UK). CV was performed between an initial potential of -1.60 V and a switching potential of $+0.00\text{ V}$ with a scan rate of 50 mV s^{-1} . Optimisation studies were completed to select the most appropriate electrolyte using 4 mL aliquots of 0.1 M solutions of each electrolyte for each study. SPCEs were used for single measurements only. DPASV was performed with a Pstat10 potentiostat (Autolab, Slough, UK) interfaced to a PC for data acquisition via the General Purpose Electrochemical System Software Package (GPES) version 3.4 (Eco Chemie B.V., Netherlands). DPASV was performed with an initial potential of -1.60 V and a final potential of $+0.00\text{ V}$. The optimum initial potential and deposition time were determined with an equilibration time of 15 s and a scan rate of 50 mV s^{-1} . Optimisation, calibration and recovery measurements were taken in triplicate using a fresh SPCE for each measurement. The solution was stirred during deposition using a magnetic stirrer (Barloworld Scientific Ltd., Staffordshire, UK). The influence of the potential interfering compounds was also studied.

2.2. Sweat zinc collection

55 mm diameter Whatman 540 cellulose filter papers (Whatman International Ltd., Kent, UK) were used for the collection of sweat. A stack of four filter papers were used in each patch adjacent to the skin. The filter papers were covered by laboratory sealing film (Duraseal, Diversified Biotech, Boston, USA) with approximately a 2 cm overlap on each side. The patch was held in place with a 7.5 cm cohesive bandage (General Medical, Aldershot, UK). Sweat patches were placed on the front of the forearm of each participant approximately 2 cm below the elbow immediately prior to the exercise period. The individuals cycled on a Cateye Ergociser EC 1200 (CatEye Co., Inc., Osaka, Japan) at a constant cadence of 60 rpm . The calculated target pulse was measured with an integral photo-optic pulsimeter and maintained automatically by adjustment of the work required to turn the pedals. The target pulse was estimated at 70% or 80% of the optimum pulse. Resistance was automatically adjusted to maintain pulse at the target pulse $\pm 3\text{ bpm}$ for the duration of the exercise. The exercise period lasted for 20 min in total after which the sweat patches were removed.

The filter papers from each sweat patch were immediately weighed and dried at $4\text{ }^\circ\text{C}$ in a desiccator. A 3 cm^2 sub-sample of each sweat patch was then extracted by agitating in 4 mL of the supporting electrolyte, for 60 min . The extracts were then placed in an ultrasonic water bath for 1 min , shaken and then returned to the ultrasonic water bath for one additional minute. The filter paper was then removed from the extract and the extract analysed. The extract was placed in a 10 mL beaker that had previously been cleaned with concentrated nitric acid and rinsed thoroughly with deionised water before drying. The DPASV measurement was then taken with a SPCE in conjunction with an Ag/AgCl counter/reference electrode.

3. Results and discussion

3.1. Cyclic voltammetric behaviour of zinc at bare SPCEs

The redox characteristics of Zn^{2+} , at bare SPCEs, was investigated in various supporting electrolytes using cyclic voltammetry. Fig. 1 shows a selection of the cyclic voltammograms (CVs) obtained in several buffers, KCl and HCl. It can be seen that the CV obtained with 0.1 M acetate pH 6.0 shows clearly visible reduction and oxidation peaks; the latter is sharp and symmetrical which is typical for the oxidation of a thin metal film on an electrode surface. Such behaviour is a pre-requisite for the development of sensitive anodic stripping voltammetric methods. The cyclic voltammograms obtained with the remaining buffers did not show such a well-defined anodic peak, whereas that obtained with HCl was quite sharp but the i_{pa} was difficult to measure. The magnitudes of the anodic peaks obtained with a total of nine supporting electrolytes are summarised in Fig. 2. While the largest i_{pa} for zinc was obtained with 0.1 M HCl the precision (coefficient of variation) with which this peak could be measured was 32.8% ; however, the precision of the i_{pa} values obtained with acetate buffer was 6.1% . Therefore, we initially considered that the latter would offer the

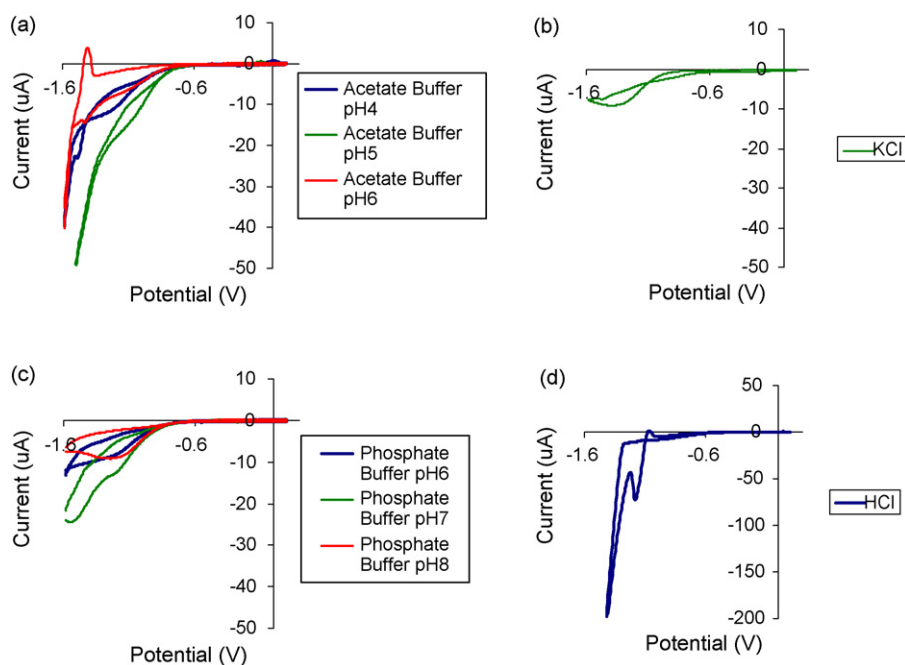


Fig. 1. Cyclic voltammograms for a selection of electrolytes containing 1 mM Zn^{2+} : (a) 0.1 M acetate buffers pH 4–6, (b) 0.1 M KCl, (c) 0.1 M phosphate buffers pH 6–8 and (d) 0.1 M HCl.

best compromise between sensitivity and reproducibility in the development of an anodic stripping voltammetric procedure for the target metal ion.

3.2. Effect of NaCl addition and voltammetric waveform on the oxidation peak of zinc

During our optimisation studies, it occurred to us that, following the collection and processing of sweat samples (discussed later), the final solutions subjected to ASV would contain chloride ions. Therefore, we decided to investigate the effect of this anion, added to acetate buffer pH 6.0, on the voltammetric behaviour of Zn^{2+} .

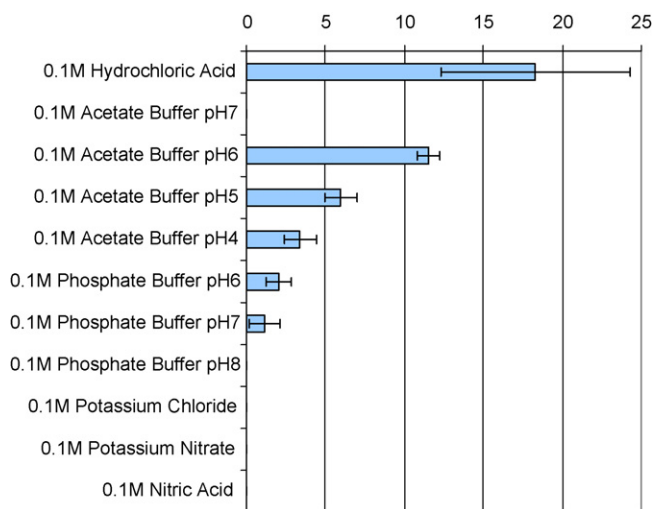


Fig. 2. Magnitudes of anodic peaks obtained by cyclic voltammetry in nine electrolytes containing 1 mM Zn^{2+} .

Fig. 3a shows the CV obtained with 10^{-6} M Zn^{2+} in a supporting electrolyte comprising 0.1 M NaCl/0.1 M acetate buffer pH 6.0, and for comparison Fig. 3b shows the same concentration of Zn^{2+} in acetate buffer pH 6.0 only. Clearly, the former now shows a well-defined cathodic peak with a greater current magnitude than the latter; the oxidation peak also shows a significant enhancement in current magnitude as a result of the greater deposition of Zn atoms. One explanation for the improvement in the definition and size of the cathodic peak is that the reduction of Zn^{2+} is facilitated when this cation forms weak complexes with both acetate and Cl^{-} ions. Other workers [13] have suggested that Zn^{2+} can form complexes with Cl^{-} and Ac^{-} with equilibrium constants of $10^{0.96}$ and $10^{0.66}$, respectively. In our study, we did not observe a well-defined cathodic or anodic peak in KCl only (Fig. 1) which suggests that both ions are required to give an improvement in redox behaviour at our SPCEs. We considered that this phenomenon could be very beneficial in improving the sensitivity of our proposed assay. However, we wondered whether phosphate buffer pH 6.0 with added Cl^{-} , might also produce improved cyclic voltammetric behaviour for Zn^{2+} . Fig. 3c shows that the anodic peak current had increased in magnitude compared to the same phosphate buffer without added Cl^{-} (Fig. 3d), but it was considerably smaller than the i_{pa} shown in Fig. 3a (0.1 M NaCl/0.1 M acetate buffer pH 6.0). Consequently, we considered that a supporting electrolyte comprising acetate buffer pH 6.0 with added Cl^{-} would produce well-defined stripping voltammetric peaks in our proposed assay.

At this stage, we decided to investigate the differential pulse waveform with anodic stripping voltammetry as it often offers better sensitivity and resolution than the linear sweep waveform. Fig. 4b shows a differential pulse stripping voltammogram (DPASV) obtained with 10^{-6} M Zn^{2+} in 0.1 M NaCl/0.1 M

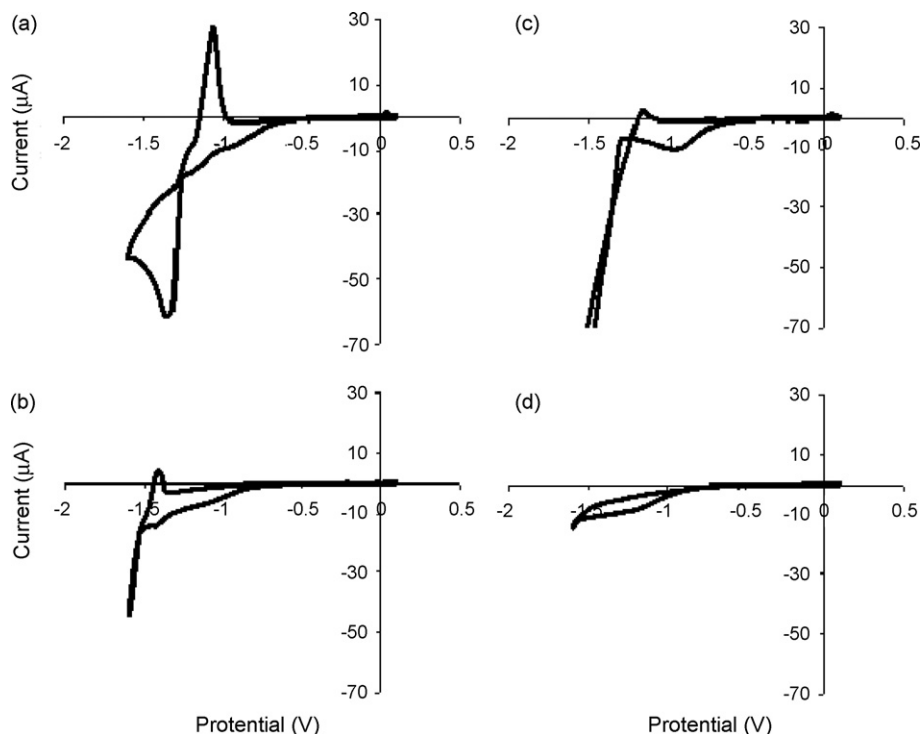


Fig. 3. Cyclic voltammograms obtained in electrolyte solutions containing 1 mM: (a) 0.1 M NaCl/0.1 M acetate buffer pH 6.0, (b) 0.1 M acetate buffer pH 6.0, (c) 0.1 M NaCl/0.1 M phosphate buffer pH 6.0 and (d) 0.1 M phosphate buffer pH 6.0.

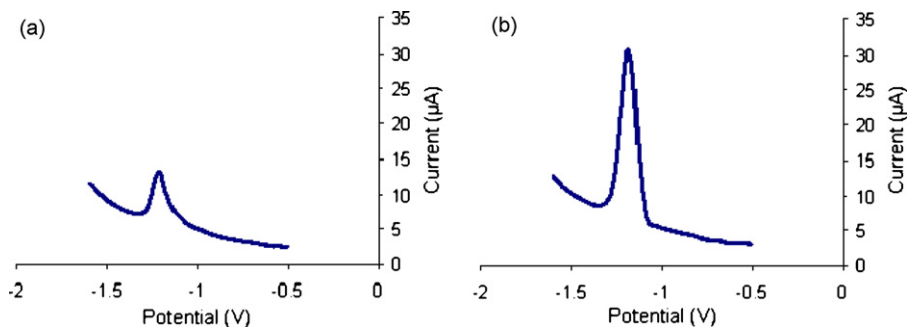


Fig. 4. DPASV of electrolytes containing 10^{-6} M Zn^{2+} : (a) 0.1 M acetate buffer pH 6.0 and (b) 0.1 M NaCl/0.1 M acetate buffer pH 6.0.

acetate buffer pH 6.0. Clearly, one well-defined anodic stripping peak was obtained under the conditions described in Section 2. For comparison, Fig. 4a shows a DPASV obtained under the same conditions as for Fig. 4b except that NaCl was omitted; it is readily apparent that the addition of Cl^- significantly enhances the magnitude of the Zn oxidation peak.

In order to deduce the optimum concentration of chloride ions to be added to the acetate buffer, a DPASV study was performed with different NaCl concentrations. Fig. 5 shows a plot of the DPASV peak currents versus the added Cl^- concentration. From this we considered that 0.1 M Cl^- would be appropriate for our proposed assay.

3.3. Optimisation of DPASV conditions and calibration study

The effect of the deposition potential (E_d) on the magnitude of the DPASV peak current was studied using a solution con-

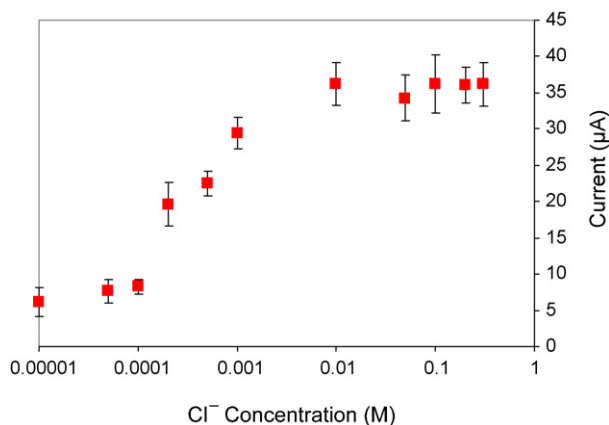


Fig. 5. Effect of Cl^- ions on the DPASV peak currents for 0.1 M NaCl/0.1 M acetate buffer pH 6.0 solution containing 2×10^{-5} M Zn^{2+} .

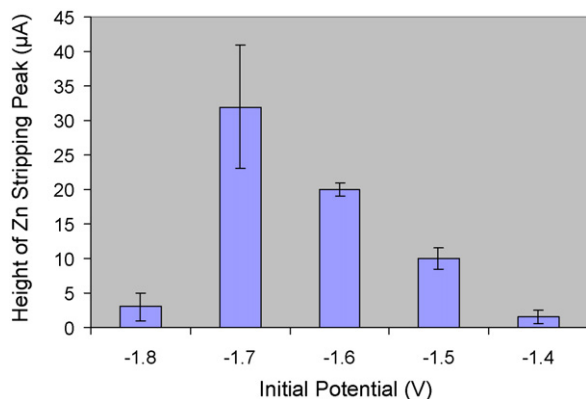
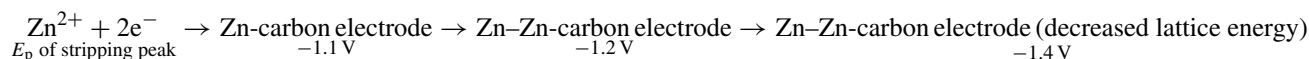


Fig. 6. Effect of deposition potential on the magnitude of DPASV peak currents in solutions containing 2×10^{-6} M Zn^{2+} in 0.1 M NaCl/0.1 M acetate buffer pH 6.0 solution.

taining 2×10^{-6} M Zn^{2+} in 0.1 M NaCl/0.1 M acetate buffer pH 6.0. Fig. 6 shows a plot of the resulting i_{pa} of the Zn stripping peak, with $E_p = -1.2$ V, using a deposition time (t_d) of 60 s. The magnitude of the peak obtained using an E_d value of -1.7 V was



the largest; however, the precision obtained with separate SPCEs was calculated to be 28.1% ($n=3$). Consequently, we selected a deposition potential of -1.6 V for further studies as the i_{pa} was only slightly smaller but the precision was much better (5.0%, $n=3$), than that obtained with $E_d = -1.7$ V.

The effect of deposition time (t_d) on the magnitude of the DPASV peak current was examined using a solution with the same composition as described above. Fig. 7 shows a selection of the DPASVs obtained at different t_d values and fixed E_d value of -1.6 V. The magnitude of the peak current, with $E_{pa} = 1.2$ V can be seen to increase with deposition time; the inset shows that the peak current becomes constant above a t_d value of about 250 s. We decided to select a t_d of 60 s for further studies as this was on the linear portion of the i_p versus t_d plot; consequently, for concentrations of Zn^{2+} below 10^{-6} M the currents should be linearly dependent on Zn^{2+} concentration. It should also be possible to use the standard addition method, which requires a linear relationship between i_p and concentration for our later studies involving sweat. It should be mentioned that at a deposition time of 300 s a small oxidation peak begins to appear at -1.4 V and a small shoulder at -1.1 V. One explanation for the appearance of the more negative peak is that this arises as a result of stripping zinc atoms from a monolayer deposited onto the carbon electrode; therefore, these atoms require higher energy for the oxidation process to occur. The peak occurring at -1.4 V is probably the result of the oxidation of a zinc layer with a slightly smaller lattice energy. Such behaviour has been previously reported by

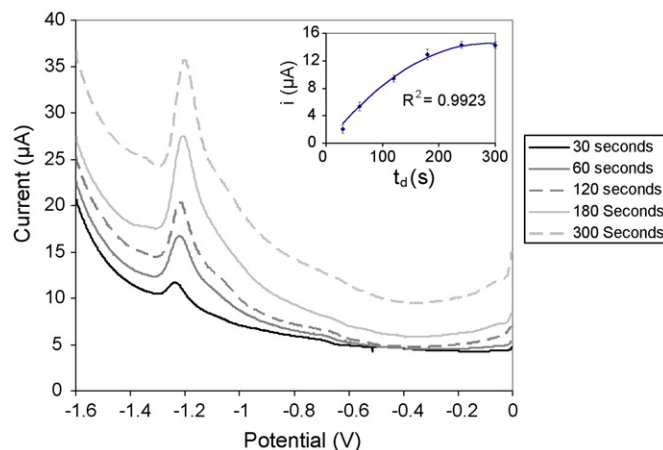


Fig. 7. Effect of deposition time on the magnitude of DPASV peak currents in solutions containing 2×10^{-6} M Zn^{2+} in 0.1 M NaCl/0.1 M acetate buffer pH 6.0 solution.

our group in an investigation involving stripping voltammetric behaviour of lead [10]. This may be summarised in the following scheme:

A calibration study was carried out using Zn^{2+} standards prepared in 0.1 M NaCl/0.1 M acetate buffer pH 6.0. These standards were subjected to DPASV using the optimised t_d and E_d values and a fresh SPCE for each measurement. Fig. 8 shows a calibration plot obtained for Zn^{2+} between 0.5 and 10 μM and inset between 10 nM and 0.5 μM . From these plots, we deduced that the linear range was between 10 nM and 5 μM . The detection limit calculated as the noise multiplied by three was 6.67 nM with a confidence limit of 2.26 nM ($n=6$). This study demonstrated the possibility of applying DPASV to the analysis of Zn^{2+} in human sweat.

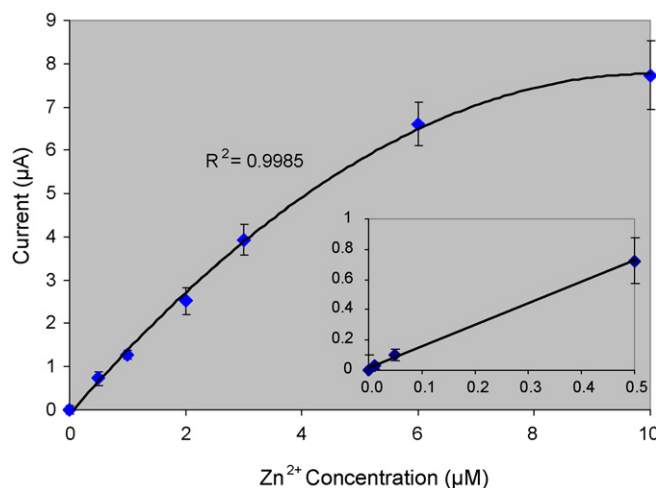


Fig. 8. Calibration plot for Zn^{2+} analysis in 0.1 M NaCl/0.1 M acetate buffer pH 6.0 by DPASV; $E_d = -1.6$ V, $t_d = 60$ s.

Table 1
Recovery of Zn^{2+} from dried sweat patches extracted using a variety of extractants

Extractant	Zn^{2+} recovery (%)
Deionised water	8.0
0.1 M HCl	49.7
0.1 M acetate buffer pH 6.0	86.8
0.1 M acetate buffer pH 5.0	71.2
0.1 M acetate buffer pH 4.0	67.4
0.1 M acetate buffered saline pH 6.0	95.0
0.1 M acetate buffered saline pH 5.0	80.0
0.1 M acetate buffered saline pH 4.0	75.0

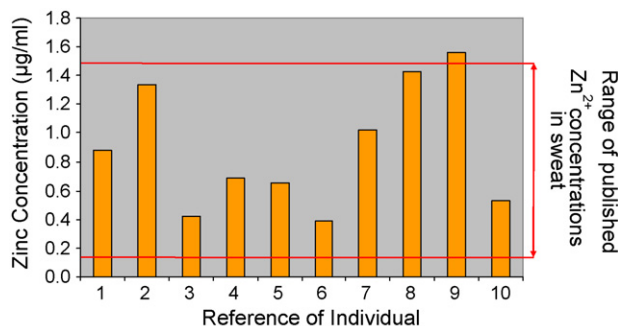


Fig. 9. Concentration of Zn^{2+} in the sweat of 10 individuals extracted from dried sweat patches following controlled exercise.

3.4. Recovery of Zn^{2+} from sweat patches and analysis of human sweat by DPASV

In order to determine the optimum solution for the extraction of Zn^{2+} from the sweat patches, a fixed volume of 0.25 mL of 10^{-4} M $Zn(NO_3)_2$ was deposited on to sweat patches and allowed to dry. These were then extracted with 4 mL of the chosen electrolyte as described earlier, and the resulting solution subjected to DPASV; the concentration of Zn^{2+} was determined by reference to calibration graphs. Table 1 summarises the recoveries calculated for each solution, and from this data it was concluded that 0.1 M NaCl/0.1 M acetate buffer pH 6.0 provided the highest recovery; consequently, this was used for the assay of human sweat.

Human volunteers (5 males and 5 females) were involved in our study to determine the endogenous level of Zn^{2+} in sweat. The protocol is described in detail in Section 2. Fig. 9 shows the calculated concentration of Zn^{2+} in the sweat of 10 individuals involved in the study. It should be added that apart from one subject these concentrations fall within the range reported in the literature [14,15]. This data indicates that our proposed DPASV assay using disposable SPCEs holds promise for the measurement of Zn^{2+} in sweat of human subjects and may find wide application in sports science as well as biomedical studies.

Although, we used an exercise protocol to obtain sweat samples, it should be feasible to use other methods, e.g. iontophoresis or sauna [6] depending on the purpose of the analysis.

4. Conclusions

We have investigated the redox characteristics of zinc at SPCEs prepared from a commercial ink preparation (C10903D14) and found that well-defined oxidation peaks could be obtained in 0.1 M NaCl/0.1 M acetate buffer pH 6.0. It was shown that one well-defined anodic stripping peak could be obtained at a potential of -1.2 V versus Ag/AgCl, using a deposition potential of -1.6 V versus Ag/AgCl. We believe that this peak results from the oxidation of a multilayer of zinc atoms, which are deposited onto a monolayer of zinc atoms, previously deposited onto the carbon electrode surface. It should be mentioned that, in an earlier report it was stated that zinc is a notoriously difficult metal to determine because it deposits and strips with hydrogen evolution [12]. However, our investigation into the effects of chloride ions revealed that greatly improved reduction and oxidation peaks are obtained when this anion is incorporated into the acetate buffer; this behaviour could be exploited for the determination of low-levels of zinc using DPASV.

We have shown that the DPASV assay could be readily applied to the measurement of Zn^{2+} in human sweat samples. The collection of sweat was performed using a novel sweat patch attached to the subject's forearm, then removed and extracted using the optimised electrolyte; DPASV was carried out directly on this extraction solution. A deposition time of only 60 s was required in the determination of zinc in all of these samples. The zinc levels found using our new DPASV assay was found to fall within the range of values reported in the literature [14,15].

References

- [1] A. Cordova, M. Alvarez-Mon, *Neurosci. Biobehav. R* 19 (1995) 439.
- [2] A. Micheletti, R. Rossi, S. Rufini, *Sports Med.* 31 (2001) 577.
- [3] M. Seve, F. Chimienti, A. Favier, *Pathol. Biol.* 50 (2002) 212.
- [4] K. Mitsubayashi, M. Suzuki, E. Tamiya, I. Karube, *Anal. Chim. Acta* 289 (1994) 27.
- [5] L. Rivier, *Baillieres Clin. Endocr.* 14 (2000) 147.
- [6] J.L. Stauber, T.M. Florence, *Sci. Total Environ.* 74 (1988) 235.
- [7] J. Wang, B. Tian, *Anal. Chem.* 65 (1993) 1529.
- [8] K.C. Honeychurch, J.P. Hart, *Trends Anal. Chem.* 22 (2003) 456.
- [9] K.C. Honeychurch, D.M. Hawkins, J.P. Hart, D.C. Cowell, *Talanta* 57 (2002) 565.
- [10] K.C. Honeychurch, J.P. Hart, D.C. Cowell, *Electroanalysis* 12 (2000) 171.
- [11] K.C. Honeychurch, J.P. Hart, D.C. Cowell, *Anal. Chim. Acta* 431 (2001) 89.
- [12] N. van Dijk, S. Fletcher, C.E. Madden, F. Marken, *Analyst* 126 (2001) 1878.
- [13] J. Yu, H. Yang, X. Ai, Y. Chen, *Russ. J. Electrochem.* 38 (2002) 321.
- [14] F.O. Omokhodion, J.M. Howard, *Clin. Chim. Acta* 231 (1994) 23.
- [15] J.L. Stauber, T.M. Florence, *Sci. Total Environ.* 60 (1987) 263.

Response of a copper(II) and iron(III) ion-selective electrode bielectrode array in saline media

Roland De Marco*, Jay Martizano¹

*Nanochemistry Research Institute, Department of Applied Chemistry, Curtin University of Technology,
GPO Box U1987, Perth, Western Australia 6845, Australia*

Received 25 September 2007; received in revised form 10 January 2008; accepted 10 January 2008
Available online 19 January 2008

Abstract

A bielectrode array comprising a jalpaite membrane (i.e., $\text{Ag}_{1.5}\text{Cu}_{0.5}\text{S}$) copper(II) ion-selective electrode (ISE) and chalcogenide glass membrane (i.e., $\text{Fe}_{2.5}(\text{Se}_{60}\text{Ge}_{28}\text{Sb}_{12})_{97.5}$) iron(III) ISE has been assembled by individually wiring each solid-state sensor into a single electrode body. Furthermore, a dual metal ion buffer calibration standard incorporating copper(II) and iron(III) coordinating ligands to regulate the levels of free copper(II) and iron(III) in the buffer has been developed to enable simultaneous calibration of the bielectrode ISE array. In this work, the bielectrode ISE array has been employed in the continuous flow analysis (CFA) of free copper(II) and iron(III) in seawater media. It is shown that the individual electrodes displayed Nernstian response in the metal ion buffer calibration standard over a wide dynamic range (viz., 10^{-15} to 10^{-5} M αCu^{2+} and 10^{-21} to 10^{-11} M αFe^{3+}), and the results of repetitive CFA analyses of free copper(II) and iron(III) in seawater are commensurate with the typical values found in coastal seawater samples. Clearly, the bielectrode ISE array may be used in the simultaneous analysis of free copper(II) and iron(III) in seawater without fear of cross-interference between the solid-state sensors.

© 2008 Elsevier B.V. All rights reserved.

Keywords: Ion-selective electrode; Trace metals; Metal speciation; Copper and iron; Seawater

1. Introduction

Despite the possibility of using ion-selective electrodes (ISEs) in the analysis of environmentally important trace metals such as copper(II) and iron(III), a past misconception has been that ISE devices lack the sensitivity and selectivity needed for the analysis of trace analytes in complex and challenging samples such as seawater.

Notwithstanding, there were several excellent papers in the 1970s and 1980s [1–4] demonstrating that it is possible to use a crystalline membrane copper ISE in the analysis of nanomolar levels of copper in natural waters, as long as the ISE is handled correctly, so as to minimize the dissolution of the ISE and the concomitant carry-over of copper from sample to sample. Clearly, these seminal papers laid the foundations for the use of solid-state membrane ISEs in environmental analysis.

The great virtue of ISEs in environmental analysis is their ability to sense the free metal ion activity, which is widely recognized as a master variable governing the uptake and toxicity of metals by biota [5], thereby providing an analytical technique capable of monitoring the impact of trace metal inputs in the environment. Notably, the free metal content of environmental waters is regulated by the metal buffering ability of the natural water [5], as dictated by the inorganic and organic speciation of metals in the sample, and this is a critical factor in determining the fates of trace metals in the marine environment.

Copper is a major trace metal in the environment due to its extensive use in antifouling paints, and poses a serious environmental threat at high levels due to its toxicity [6]. Essentially, copper is an essential trace metal nutrient at ambient levels [7,8], and it has been demonstrated on a variety of aquatic organisms [7–11] that the toxicity of copper on marine biota is related to free copper(II) or Cu^{2+} , not the concentration of total dissolved copper. This is the single most important feature that makes the copper ISE so attractive in environmental science leading to considerable research in the development of copper ISE methods for the analysis of natural samples (i.e., seawater, lakes, rivers, soils, etc.) [1–4,6–9,12–24].

* Corresponding author. Tel.: +61 8 9266 7322; fax: +61 8 9266 2602.
E-mail address: r.demarco@curtin.edu.au (R. De Marco).

¹ Present address: University of the Philippines in the Visayas, Miag-ao, Iloilo 5023, Philippines.

Iron is an important limiting trace metal nutrient in marine waters [25–27], as it limits the growth of phytoplankton and biomass production in the ocean. Since iron finds its way into marine environments by atmospheric dust deposition and by upwelling of water, it is present at very low levels in isolated areas such as Antarctica, and this was demonstrated clearly in an iron fertilization event in The Southern Ocean that led to a phytoplankton bloom in the fertilization zone [28,29].

A seminal paper by Zirino et al. [13] has demonstrated the positive influence of hydrodynamic flow [either at a rotating disc electrode or in a continuous flow analysis (CFA) flow-cell] in lowering the detection limit of the jalpaite membrane copper(II) ISE [13] to nanomolar levels, and this led to the conclusion that ISE determinations of trace metals in seawater are undertaken ideally in a flow-injection analysis (FIA) or CFA analysis mode. Accordingly, Eriksen et al. [20] developed a CFA method for the analysis of free and total copper in Pacific Ocean seawater, and found that the total copper levels obtained by ISE potentiometry in acidified seawater compared favourably with those determined using graphite furnace atomic absorption spectrometry (GFAAS). Furthermore, De Marco et al. [30] developed a chalcogenide glass membrane iron(III) ISE CFA method for the determination of free iron(III) in acidified and UV photo-oxidized Southern Ocean or open ocean seawater, and found that the CFA ISE method yielded a $\log(a\text{Fe}^{3+})$ value for 10 repetitive injections of seawater that correlated brilliantly with the expected iron(III) speciation calculated using an inorganic speciation model for seawater. Clearly, the results of these previous studies have demonstrated the power of CFA in the ISE analysis of free copper(II) and iron(III) in seawater.

The present study integrates the aforesaid copper(II) and iron(III) ISE-CFA analysis techniques into a single “all solid-state” bielelectrode array method including conventional copper(II) and iron(III) ISEs, so as to enable the simultaneous analysis of free copper(II) and iron(III) in seawater. This technique is likely to appeal to environmental analytical scientists since copper(II) is a potent environmental threat due to its extensive use in antifouling paints [6], while iron(III) is a limiting nutrient that regulates the growth of phytoplankton and biomass production in the ocean [25–27]. This represents a significant improvement in methodology since it will enable simultaneous and rapid determinations of these environmentally important analytes in marine waters within approximately a minute, as opposed to lengthy analyses of >10 min duration while each analyte is assayed separately using single electrodes (i.e., >20 min for copper(II) and iron(III) or n analytes $X > 20$ min), especially if a tested and proven extrapolation method is used to estimate the steady-state CFA signals of the ISEs using the first minute of simultaneously recorded potential time transients in a sample [20,30]. In this context, we have used the previously published electrode array approach of Shatkin et al. [31] in the fabrication of a bielelectrode ISE array [see Fig. 1 for a schematic diagram of the copper(II) and iron(III) bielelectrode array]. Clearly, this study has necessitated the development of a combined copper(II) and iron(III) calibration buffer, and a study of the CFA potentiometric response characteristics of the bielelectrode array in the calibration buffer was deemed necessary to ascertain if there are

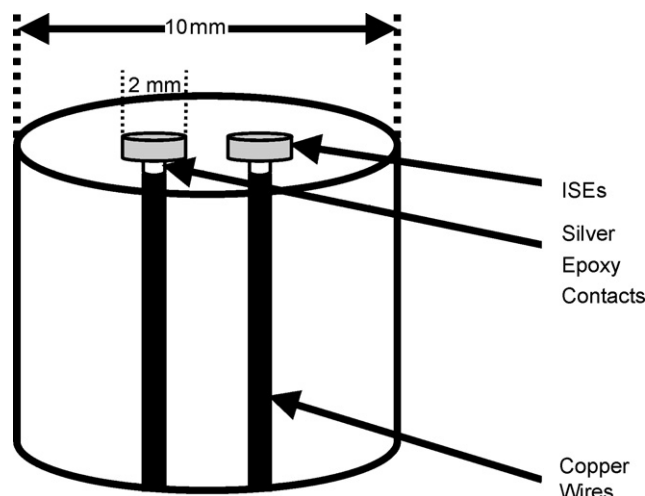


Fig. 1. A schematic diagram showing the independent wiring of copper(II) and iron(III) ISEs into a single solid-state ISE array.

any cross-interference and cross-contamination effects from one electrode to the other in a combined metal ion buffer solution. Last, a CFA analysis of raw seawater was undertaken to ascertain the suitability of the new bielelectrode array for the simultaneous determination of free copper(II) and iron(III) in seawater.

2. Experimental

2.1. Copper(II) and Iron(III) ISE membranes

The Cu(II) ISE membrane was prepared according to the procedure described elsewhere by Heijne et al. [32]. This procedure involves the slow addition of a solution consisting of 0.02 mole of $\text{Cu}(\text{NO}_3)_2$ and 0.04 mole AgNO_3 (50 mL) drop wise to 1 M Na_2S (72 mL) to produce jalpaite ($\text{Cu}_{0.5}\text{Ag}_{1.5}\text{S}$) powder. The above-mentioned solutions were cooled to 2°C before addition, and the resultant precipitate and supernatant were gradually heated to $70\text{--}75^\circ\text{C}$ for 40 min and maintained at that temperature for an additional 30 min. The precipitate was washed four times with deionized water (200 mL) at 70°C followed by one time in 0.1 M nitric acid (100 mL) at 70°C . The precipitate was rinsed with Milli-Q water at room temperature to remove any acid from the precipitate, and the filtered powder was rinsed with acetone prior to drying at 80°C . A pressed disk was prepared from the jalpaite powder by applying a pressure of 7600 kg cm^{-2} , and it was fashioned into a small disk that is suitable for use in the bielelectrode ISE array using emery paper.

The chalcogenide glass membrane Fe(III) ISE with a composition $\text{Fe}_{2.5}(\text{Se}_{60}\text{Ge}_{28}\text{Sb}_{12})_{97.5}$ [33] was prepared by mixing appropriate amounts of the pure metallic powders [viz., iron (96% purity, Ajax Chemical Co.), selenium (99.5% purity, Aldrich), germanium (99.99% purity, Aldrich) and antimony (99.999% purity, Aldrich)] in a Vycor ampoule (6-cm long, 13-cm diameter, 1-mm thickness). A total weight of 3 g was used, and the evacuated ampoule was sealed prior to heating. The ampoule was heated for 24 h at 1030°C followed by cooling to room temperature in air [33]. The resultant glass was annealed at 240°C for 2 h to remove any stress in the glass [33]. The

glass was shaped into a small disk for use in the bielectrode ISE array.

2.2. Assembly of the bielectrode ISE

The bielectrode ISE was assembled by incorporating both the jalpaite membrane copper(II) ISE and chalcogenide glass membrane ISE into a single electrode body (see Fig. 1). The individual membranes were attached to separate copper wires using silver epoxy contacts, noting that the electrode configuration could accommodate several additional electrodes [mercury(II) and cadmium(II) ISEs] if desired, thereby making this electrode array a potentially powerful research tool in environmental science. The contacts were allowed to dry for 24 h at room temperature prior to sealing both electrodes into a cylindrical Perspex electrode housing by using epoxy cement taking great care to ensure that the ISEs were isolated electrically. Note, the epoxy resin was allowed to cure for 48 h, and the bielectrode tip was polished on 500 grit silicon carbide paper to expose the membrane surface of the electrode followed by mechanical polishing sequentially on 1000 grit silicon carbide paper and on Stuers™ 1 μm diamond spray in conjunction with Stuers™ red lubricant and a Stuers™ polishing cloth until a mirror finish was obtained.

2.3. Ethylenediamine–salicylate–EDTA dual buffer for copper(II) and iron(III)

A combined copper–iron buffer was prepared using 10^{-4} M FeCl_3 , 10^{-3} M $\text{Cu}(\text{NO}_3)_2$, 10^{-2} M sodium salicylate, 1.50×10^{-2} M ethylenediamine (en), 10^{-4} M EDTA and 0.600 M NaNO_3 in Milli-Q high-purity water (>18 M Ω resistivity). The pH was adjusted between pH 5 and 9.5 to give a pFe range of 11–21 and pCu range of 5–15 (encompassing the typical pCu and pFe values of seawater) using analytical grade reagent sodium hydroxide and/or hydrochloric acid and the solutions were equilibrated at each pH for at least 30 min, with the free copper(II) and iron(III) levels at the equilibrium pH values calculated using the MINTEQA2 V3.11 software obtained from the Scientific Software Group (USA).

2.4. CFA analysis with the bielectrode ISE

In CFA with the bielectrode ISE, a flow-cell obtained from Chem Flow Devices (Melbourne, Australia) was utilized (see Fig. 2 [30,34]). This flow-cell has a wall jet design that could take a standard size, flat-ended ISE. The reference electrode, which was prepared by anodizing silver wire in chloride media, was built into the device. An Autoclude™ Model VIL peristaltic pump was used to transport two streams of solution into the flow-cell at a flow-rate of 5 ml/min. The calibration buffer solution and the sample stream passed directly below the ISE, while that of the reference solution (0.60 M KCl) went through the side of the device where it came into contact with the Ag/AgCl reference electrode. The two solution streams merged into one before leaving the device as waste. All connections in the CFA manifold were made using Tygon™ tubing (0.0449 in. i.d. and 0.1124 in. o.d.) with the fitting of 3-stop silicon tubing (2.54 mm i.d.) to

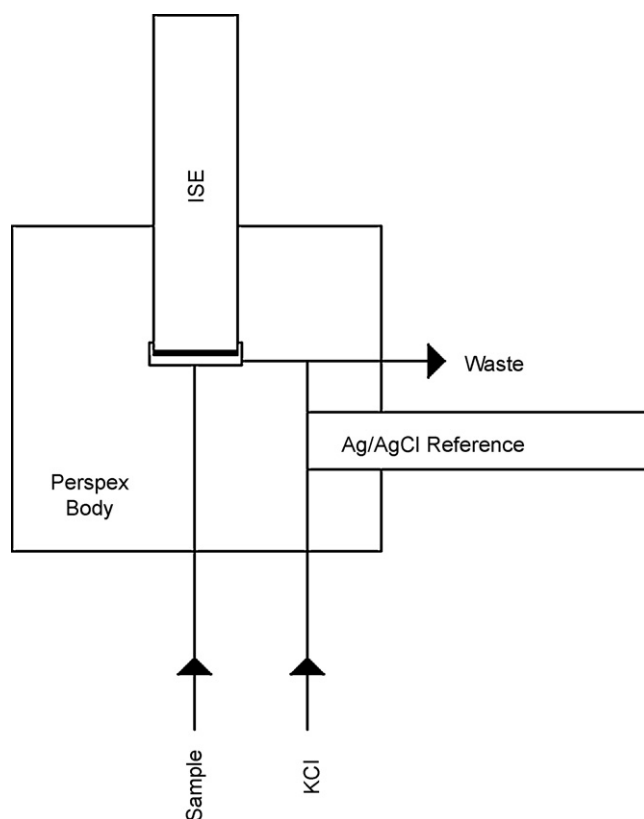


Fig. 2. A schematic diagram of the wall jet flow-cell used in this CFA-ISE study.

the peristaltic pump. The CFA manifold [30,34] is presented in Fig. 3.

A freshly polished and newly calibrated ISE was employed in all cases. Solutions were stored in polyethylene containers that had been soaked in 10 wt.% nitric acid for 2 days prior to rinsing with copious amounts of Milli-Q high-purity water (>18 M Ω resistivity). The electrode was equilibrated with a sacrificial pCu ≈ 15 and pFe ≈ 22 prior to the analysis of each seawater sample, thereby minimizing the electrode carry-

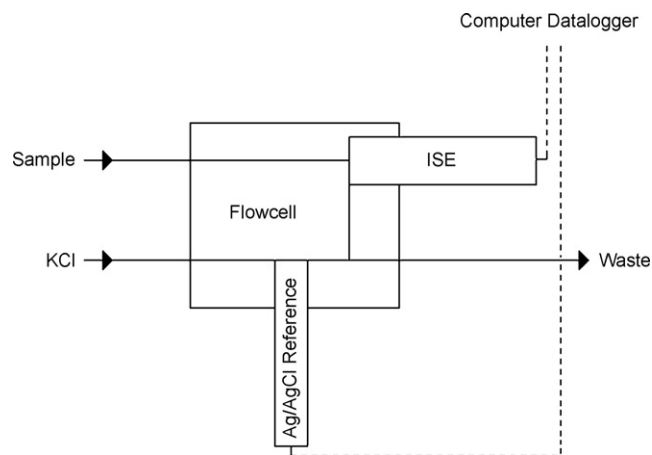


Fig. 3. A schematic diagram of the CFA manifold used in this study noting that all connections in the CFA manifold were made using Tygon™ tubing (0.0449 in. i.d. and 0.1124 in. o.d.) with the fitting of 3-stop silicon tubing (2.54 mm i.d.) to the peristaltic pump, and a flow-rate of 5 ml/min was used.

over of adsorbed Cu^{2+} and Fe^{3+} . A seawater sample (several 100 mL) was collected from The Aquaculture Laboratory at the Muresk Institute of Agriculture at Curtin University, and the unfiltered and unadulterated sample (at pH 8) was used in the ISE analysis of free copper(II) and iron(III) in seawater using CFA.

3. Results and discussion

3.1. Copper(II) and iron(III) speciation in the calibration buffer

Recent work by De Marco et al. [35] used electrochemical impedance spectroscopy (EIS)/synchrotron radiation-grazing incidence X-ray diffraction (SR-GIXRD) to monitor in situ the surface chemistry of the iron(III) ISE in artificial and real seawater showing that the surface crystalline phases of this sensor (i.e., metal selenides) are attacked aggressively by chloride and hydroxide in organic-free or artificial seawater, but this deleterious process is suppressed significantly by the natural organic ligands in seawater. The EIS/SR-GIXRD data revealed a destruction of the surface layer of the ISE in organic-free or artificial seawater due to a complete removal of all surface crystalline phases, while raw seawater comprising natural organic ligands and a seawater ligand mimetic system containing en, salicylate, EDTA along with millimolar and sub-millimolar amounts of iron and copper is capable of protecting the iron(III) ISE's surface against this destructive dissolution process. In later research by De Marco and Martizano [34], it was demonstrated that this seawater ligand mimetic was capable of averting the seawater ligand interference on the chalcogenide glass membrane iron(III) ISE allowing reliable determinations of free iron(III) in seawater, and this is the reason for its selection as the calibration buffer in the present study.

Table 1 lists the equilibria and major species that are implicated in the MINTEQA2 V3.11 calculations of the metal speciation in the calibration buffer system. The MINTEQA2 V3.11 software uses its database of equilibrium constants, K , at zero ionic strength, I , and utilizes a so-called ion association model to correct to $K(I)$ taking account of the variation in activity coefficients, γ , as a function of I , viz.

$$\log K(I) = \log K + \sum v \log \gamma$$

and

$$\log \gamma = \frac{-0.511Z^2\sqrt{I}}{1 + B\sqrt{I}} + CI + DI^{3/2}$$

where $\sum v \log \gamma$ represents the sum of multiples of $v \log \gamma$ for reactants minus the sum of $v \log \gamma$ for products, v denotes the reaction stoichiometric coefficients, Z is the charge carried by each individual ion, and B , C and D are constants for each individual ion. Ultimately, the inherent algorithm in MINTEQA2 V3.11 establishes and solves the appropriate mass and charge balances associated with equilibration of all of the species presented in Table 1.

Table 1
MINTEQA2 V3.11 equilibria used to solve for pCu and pFe in the calibration buffer used in this study

Species	Solution reaction
$[\text{Cu}(\text{en})]^{2+}$	$\text{Cu}^{2+} + \text{en} \rightleftharpoons [\text{Cu}(\text{en})]^{2+}$
$[\text{Cu}(\text{en})_2]^{2+}$	$\text{Cu}^{2+} + 2\text{en} \rightleftharpoons [\text{Cu}(\text{en})_2]^{2+}$
$[\text{Fe}(\text{salicylate})]^+$	$\text{Fe}^{3+} + \text{salicylate}^{2-} \rightleftharpoons [\text{Fe}(\text{salicylate})]^+$
$[\text{Fe}(\text{salicylate})_2]^-$	$\text{Fe}^{3+} + 2\text{salicylate}^{2-} \rightleftharpoons [\text{Fe}(\text{salicylate})_2]^-$
$[\text{Fe}(\text{EDTA})]^-$	$\text{Fe}^{3+} + \text{EDTA}^{4-} \rightleftharpoons [\text{FeEDTA}]^-$
$\text{Fe}(\text{HEDTA})$	$\text{Fe}^{3+} + \text{HEDTA}^{3-} \rightleftharpoons \text{Fe}(\text{HEDTA})$
$[\text{Fe}(\text{OH})\text{EDTA}]^{2-}$	$\text{Fe}^{3+} + \text{H}_2\text{O} + \text{EDTA}^{4-} \rightleftharpoons [\text{Fe}(\text{OH})\text{EDTA}]^{2-} + \text{H}^+$
$[\text{Fe}(\text{OH})_2\text{EDTA}]^{3-}$	$\text{Fe}^{3+} + 2\text{H}_2\text{O} + \text{EDTA}^{4-} \rightleftharpoons [\text{Fe}(\text{OH})_2\text{EDTA}]^{3-} + 2\text{H}^+$
$[\text{Fe}(\text{OH})]^{2+}$	$\text{Fe}^{3+} + \text{H}_2\text{O} \rightleftharpoons [\text{Fe}(\text{OH})]^{2+} + \text{H}^+$
$[\text{Fe}(\text{OH})_2]^+$	$\text{Fe}^{3+} + 2\text{H}_2\text{O} \rightleftharpoons [\text{Fe}(\text{OH})_2]^+ + 2\text{H}^+$
$\text{Fe}(\text{OH})_3$	$\text{Fe}^{3+} + 3\text{H}_2\text{O} \rightleftharpoons \text{Fe}(\text{OH})_3 + 3\text{H}^+$
$[\text{Fe}(\text{OH})_4]^-$	$\text{Fe}^{3+} + 4\text{H}_2\text{O} \rightleftharpoons [\text{Fe}(\text{OH})_4]^- + 4\text{H}^+$
$[\text{Fe}_2(\text{OH})_2]^{4+}$	$2\text{Fe}^{3+} + 2\text{H}_2\text{O} \rightleftharpoons [\text{Fe}_2(\text{OH})_2]^{4+} + 2\text{H}^+$
Hen^+	$\text{Hen}^+ \rightleftharpoons \text{en} + \text{H}^+$
H_2en^{2+}	$\text{H}_2\text{en}^{2+} \rightleftharpoons \text{en} + 2\text{H}^+$
Hsalicylate^-	$\text{Hsalicylate}^- \rightleftharpoons \text{salicylate}^{2-} + \text{H}^+$
$\text{H}_2\text{salicylate}$	$\text{H}_2\text{salicylate} \rightleftharpoons \text{salicylate}^{2-} + 2\text{H}^+$
HEDTA^{3-}	$\text{HEDTA}^{3-} \rightleftharpoons \text{EDTA}^{4-} + \text{H}^+$
$\text{H}_2\text{EDTA}^{2-}$	$\text{H}_2\text{EDTA}^{2-} \rightleftharpoons \text{EDTA}^{4-} + 2\text{H}^+$
H_3EDTA^-	$\text{H}_3\text{EDTA}^- \rightleftharpoons \text{EDTA}^{4-} + 3\text{H}^+$
H_4EDTA	$\text{H}_4\text{EDTA} \rightleftharpoons \text{EDTA}^{4-} + 4\text{H}^+$

The free copper(II) and iron(III) levels at the equilibrium pH values in the calibration buffer were calculated using the MINTEQA2 V3.11 software obtained from the Scientific Software Group (USA). In this medium, it is evident that an adjustment of the pH leads to deprotonation/protonation of the copper(II) and iron(III) binding ligands (i.e., ethylenediamine, salicylic acid and EDTA) in the buffer solution influencing the speciation of copper(II) and iron(III) in the buffer, and this behaviour is exemplified by the MINTEQA2 V3.11 speciation data for the calibration buffer that are presented in Fig. 4.

An examination of Fig. 4 shows that the pCu and pFe values in the buffer in the pH range of 5–9 are pFe = 10–21 and pCu = 5–15, respectively. Given that free and total levels of copper(II) and iron(III) in seawater generally fall within the

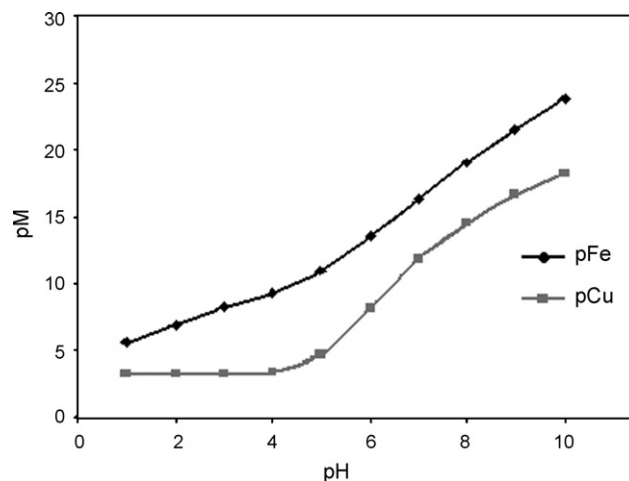


Fig. 4. The MINTEQA2 V3.11 derived speciation data in the calibration buffer as depicted by the pCu and pFe vs. pH curves.

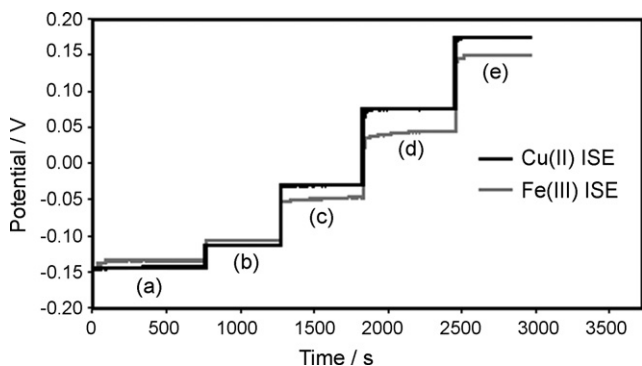


Fig. 5. CFA response curves for the bielectrode ISE array in the combination buffer to stepwise changes in pCu and pFe: (a) pCu = 15.8 and pFe = 20.4; (b) pCu = 14.7 and pFe = 19.2; (c) pCu = 11.9 and pFe = 16.4; (d) pCu = 8.3 and pFe = 13.5; (e) pCu = 4.8 and pFe = 11.2.

ranges, $pCu_{total} = 8-10$ and $pCu_{free} = 11-13$ [7–11,23] as well as $pFe_{total} = 9.0-10.7$ and $pFe_{free} = 19.5-21.2$ [25–27,36,37], a pH range of 5–9 is ideally suited to provide a calibration range applicable to the analysis of free copper(II) and iron(III) in raw seawater, as well as total copper(II) and iron(III) in acidified seawater that breaks down all of the copper(II) and iron(III) complexes in seawater yielding the level of total dissolved metal [12,20].

3.2. CFA response of the bielectrode ISE in the calibration buffer

Fig. 5 presents the CFA response curves for the bielectrode ISE array over the pCu range of 5–15 and pFe range of 10–21, and it is clearly evident that the monotonic response of the copper(II) ISE in the bielectrode array reaches a steady-state value within seconds of a stepwise change in the activity of Cu^{2+} in the different buffers, while the iron(III) ISE response is slightly slower needing about 10–100 s to achieve a steady-state potential. Notwithstanding, a 10–100 s response time, especially considering that the bielectrode ISE is simultaneously detecting both copper(II) and iron(III) in the sample, is excellent and permits an entire calibration of the bielectrode ISE within minutes.

Fig. 6(a) and (b) presents the CFA potentiometric response curves for the copper(II) and iron(III) ISEs of the bielectrode in the combined calibration buffer. It is evident that both ISEs in the bielectrode yielded the theoretical Nernstian response obtainable with these sensors, i.e., about 29 mV per decade change in the activity of M^{n+} . Obviously, the combined calibration buffer is not inducing any electrode errors on the copper(II) and iron(III) ISEs, and there is no evidence of any cross-interference or cross-contamination between the copper(II) and iron(III) ISEs in the bielectrode array.

3.3. CFA analysis of seawater

It is important to note that quadruplicate CFA measurements of free Cu(II) and Fe(III) concentrations in seawater using the bielectrode ISE and the combined buffer yielded val-

ues of $pCu = 12.16 \pm 0.21$ and $pFe = 20.2 \pm 0.32$, noting that the copper(II) and iron(III) ISE techniques have been validated previously [12,20,23,30,38] and that the present values compare favourably with recent data obtained by Millero et al. [27] as well as Eriksen et al. [20,23] for free copper(II) and iron(III) in seawater, respectively. It is worth noting that the CFA response curves of the copper(II) ISE in seawater (not shown) required about 10 min to achieve a steady-state value, and this is consistent with previous reports by Eriksen et al. [20]. Nevertheless, Eriksen et al. [20] demonstrated that it is possible to employ an electrode kinetic model describing the response characteristics of the ISE to extrapolate reliably the steady-state potential of the copper(II) ISE using the first couple of minutes of the potential time transient following a switch to seawater, and De Marco et al. [30] showed that this extrapolation method is also applicable to the iron(III) ISE. Clearly, simultaneous measurements of analyte concentrations using the bielectrode ISE array in conjunction with an extrapolation method to predict the steady-state potentials of the individual ISEs following a switch into a seawater sample will provide a powerful method for the rapid and reliable analysis of copper(II) and iron(III) in seawater.

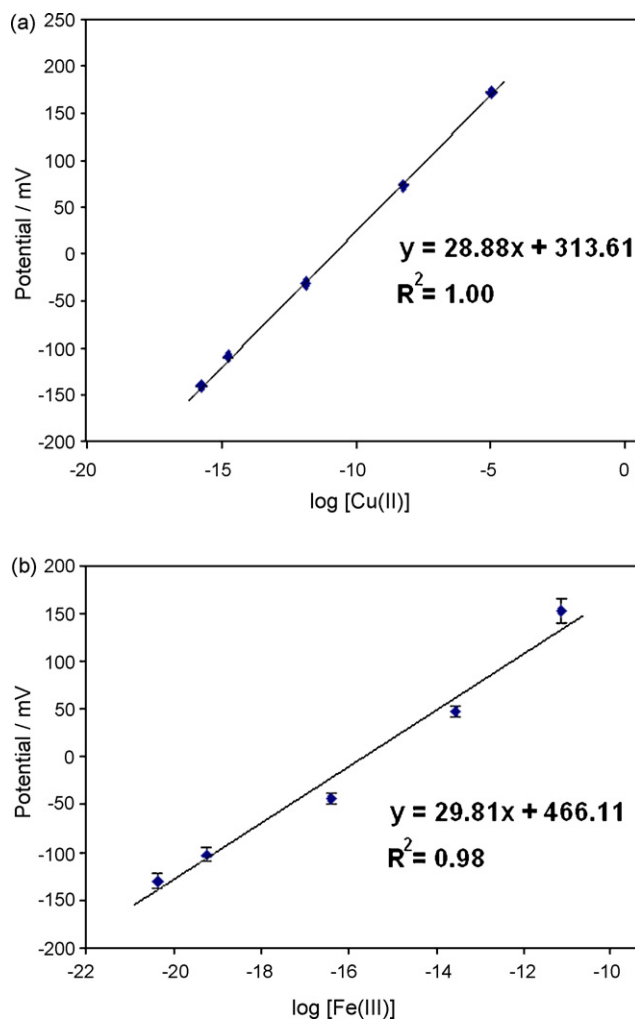


Fig. 6. CFA Nernstian response curves obtained using the bielectrode ISE array: (a) copper(II) ISE and (b) iron(III) ISE.

4. Conclusions

The results of this study demonstrate that a copper(II) and iron(III) bielelectrode ISE array and a combined copper(II) and iron(III) calibration buffer can be used in the rapid and reliable calibration of a CFA system within minutes. Accordingly, it is possible to employ the calibrated bielelectrode ISE array in the CFA electroanalysis of free copper(II) and iron(III) in raw seawater.

The sluggish response of the copper(II) ISE in seawater (with over 10 min equilibration times) may be averted by using an extrapolation method to predict reliably the steady-state potential using the initial data (first minute or so) in the potential time transient of a seawater sample, and this provides scope for sample throughputs of 30–60 samples per hour.

Acknowledgments

The Australian Research Council (ARC) and Australian Institute of Nuclear Science and Engineering (AINSE) are acknowledged for financial support.

References

- [1] A. Zirino, P.F. Seligman, *Mar. Chem.* 10 (1981) 249.
- [2] M.J. Smith, S.E. Manahan, *Anal. Chem.* 45 (1973) 836.
- [3] R. Jasinski, I. Trachtenberg, D. Andrychuk, *Anal. Chem.* 46 (1974) 364.
- [4] A. Zirino, C. Clavell, P.F. Seligman, *Mar. Chem.* 12 (1983) 25.
- [5] J. Buffle, R.S. Altman, M. Filella, A. Tessier, *Geochim. Cosmochim. Acta* 54 (1990) 1535.
- [6] S.L. Belli, A. Zirino, *Anal. Chem.* 65 (1993) 2583.
- [7] W.G. Sunda, P.A. Gillespie, *J. Mar. Res.* 37 (1979) 761.
- [8] W. Sunda, R.L. Guillard, *J. Mar. Res.* 34 (1976) 511.
- [9] W.G. Sunda, A.M. Lewis, *Limnol. Oceanogr.* 23 (1978) 870.
- [10] K.H. Coale, K.W. Bruland, *Limnol. Oceanogr.* 33 (1988) 1084.
- [11] K.W. Bruland, E.L. Rue, J.R. Donat, S.A. Skrabal, J.W. Moffett, *Anal. Chim. Acta* 405 (2000) 99.
- [12] R. De Marco, D.J. Mackey, A. Zirino, *Electroanalysis* 9 (1997) 330.
- [13] A. Zirino, R. De Marco, I. Rivera, B. Pejčić, *Electroanalysis* 14 (2002) 493.
- [14] M. Camusso, G. Tartari, A. Zirino, *Environ. Sci. Technol.* 25 (1991) 678.
- [15] R. De Marco, *Anal. Chem.* 66 (1994) 3202.
- [16] M.T. Neshkova, *Anal. Chim. Acta* 273 (1993) 255.
- [17] A. Zirino, S.L. Belli, D.A. van der Weele, *Electroanalysis* 10 (1998) 423.
- [18] A. Zirino, D.A. VanderWeele, S.L. Belli, R. De Marco, D.J. Mackey, *Mar. Chem.* 61 (1998) 173.
- [19] R. Stella, M.T. Ganzerli-Valentini, *Anal. Chem.* 51 (1979) 2148.
- [20] R.S. Eriksen, D.J. Mackey, P. Alexander, R. De Marco, X.D. Wang, *J. Environ. Monit.* 1 (1999) 483.
- [21] I. Rivera-Duarte, A. Zirino, *Environ. Sci. Technol.* 38 (2004) 3139.
- [22] I. Rivera-Duarte, G. Rosen, D. Lapota, D.B. Chadwick, L. Kear-Padilla, A. Zirino, *Environ. Sci. Technol.* 39 (2005) 1542.
- [23] R.S. Eriksen, D.J. Mackey, R. van Dam, B. Nowak, *Mar. Chem.* 74 (2001) 99.
- [24] D.J. Mackey, A. Zirino, *Anal. Chim. Acta* 284 (1994) 635.
- [25] M. Gledhill, C.M.G. van den Berg, *Mar. Chem.* 47 (1994) 41.
- [26] E.L. Rue, K.W. Bruland, *Mar. Chem.* 50 (1995) 117.
- [27] F.J. Millero, W. Yao, J. Aicher, *Mar. Chem.* 50 (1995) 21.
- [28] E.R. Abraham, C.S. Law, P.W. Boyd, S.J. Lavender, M.T. Maldonado, A.R. Bowie, *Nature* 407 (2000) 727.
- [29] A.J. Watson, D.C.E. Bakker, A.J. Ridgwell, P.W. Boyd, C.S. Law, *Nature* 407 (2000) 730.
- [30] R. De Marco, B. Pejčić, X.D. Wang, *Lab. Robotics Automat.* 11 (1999) 284.
- [31] J.A. Shatkin, H.S. Brown, S. Licht, *Anal. Chem.* 67 (1995) 1147.
- [32] G.J.M. Heijne, W.E. van Der Linden, D.G. Boef, *Anal. Chim. Acta* 89 (1977) 287.
- [33] C.E. Koenig, E.W. Grabner, *Electroanalysis* 7 (1995).
- [34] R. De Marco, J. Martizano, *Electroanalysis* 19 (2007) 2513.
- [35] R. De Marco, Z.-T. Jiang, J. Martizano, A. Lowe, B. Pejčić, A. van Riessen, *Electrochim. Acta* 51 (2006) 5920.
- [36] M. Gledhill, C.M.G. van den Berg, *Mar. Chem.* 50 (1995) 51.
- [37] J. Wu, G.W. Luther III, *Mar. Chem.* 50 (1995) 159.
- [38] R. De Marco, D.J. Mackey, *Mar. Chem.* 68 (2000) 283.

Principal components of phenolics to characterize red *Vinho Verde* grapes: Anthocyanins or non-coloured compounds?

M.S. Dopico-García^a, A. Figue^a, L. Guerra^a, J.M. Afonso^b,
O. Pereira^b, P. Valentão^a, P.B. Andrade^a, R.M. Seabra^{a,*}

^a *REQUIMTE - Serviço de Farmacognosia, Faculdade de Farmácia, Universidade do Porto,
R. Aníbal Cunha 164, 4050-047 Porto, Portugal*

^b *Direcção Regional de Agricultura de Entre-Douro-e-Minho, Portugal*

Received 17 September 2007; received in revised form 4 January 2008; accepted 9 January 2008

Available online 17 January 2008

Abstract

Phenolic profile of 10 different varieties of red “Vinho Verde” grapes (Azal Tinto, Borraçal, Brancelho, Doçal, Espadeiro, Padeiro de Basto, Pedral, Rabo de ovelha, Verdelho and Vinhão), from Minho (Portugal) were studied. Nine Flavonols, four phenolic acids, three flavan-3-ols, one stilben and eight anthocyanins were determined. Malvidin-3-*O*-glucoside was the most abundant anthocyanin while the main non-coloured compound was much more heterogeneous: catechin, epicatechin, myricetin-3-*O*-glucoside, quercetin-3-*O*-glucoside or syringetin-3-*O*-glucoside. Anthocyanin contents ranged from 42 to 97%. Principal component analysis (PCA) was applied to analyse the date and study the relations between the samples and their phenolic profiles. Anthocyanin profile proved to be a good marker to characterize the varieties even considering different origin and harvest. “Vinhão” grapes showed anthocyanins levels until twenty four times higher than the rest of the samples, with 97% of these compounds.

© 2008 Elsevier B.V. All rights reserved.

Keywords: Anthocyanins; Non-coloured phenolics; Multivariate analysis; “Vinho Verde” red grapes

1. Introduction

Characterization of phenolic compounds in red grapes, considering both non-coloured compounds (flavan-3-ols, flavonols, phenolic acids and stilbens) and anthocyanins, have attracted much interest for different reasons: these substances have demonstrated to have potential beneficial effects for health [1,2], they contribute strongly to the organoleptic characteristics of grapes and therefore of the wine obtained from them [3], and they have showed to be good chemical markers to characterize different varieties of grapes, specially anthocyanins [4,5].

Additionally, the simultaneous characterization of the both types of compounds in grapes is important due to their joint effect in the colour of wine: during the aging process of wines new and more stable pigments are formed [6] from the reaction between anthocyanins and flavanols [7–11]. Besides, the levels of several specific non-coloured components (including flavonols, phenolic acids and flavan-3-ols) influence the copigmentation that can account for between 30 and 50% of the colour in young wines [12].

Although several works have been focused on the determination, in red grapes, of either anthocyanins [4,5,13–15] or non-coloured compounds [16–19], their simultaneously determination is not so common. Determination of non-coloured compounds presents the difficulty of the possible interferences caused by anthocyanins, since these also absorb at the same wavelengths, whereas anthocyanins can be more easily determined at a more specific wavelength, around 500 nm, without interferences. In other hand, the anthocyanin profile has demonstrated to be a good chemical marker for classifying red grapes cultivars [4,5] since anthocyanin profile seems to be

Abbreviations: PCA, principal component analysis; SLDA, stepwise linear discriminant analysis; SPE, solid-phase extraction; MeOH, methanol; HCl, hydrochloric acid; NaOH, sodium hydroxide; C18, octadecylsilane; HPLC, high-performance liquid chromatography; DAD, diode array detector; SL, solid-liquid; ODS, octadecylsilane; UV-vis, ultraviolet-visible.

* Corresponding author. Tel.: +351 222 078 934; fax: +351 222 003 977.

E-mail address: rseabra@ff.up.pt (R.M. Seabra).

characteristic of the cultivar and independent of the production area. Non-genetic factors, such as environmental conditions or viticultural practices have a greater effect on the concentration of anthocyanins rather than on their qualitative/quantitative profile [5]. Different studies have shown that anthocyanin profiles were rather stable during ripening [4,5,15] and different vintages [4,5], allowing the proper classification of grapes using multivariate analysis of different cultivars, including grapes of different year and maturation grade [5]. The non-coloured phenolics profile has been less used to characterize red grapes, although some authors have used it like Mattivi et al. [17] and Castillo-Muñoz [19].

The determination of some non-coloured phenolics and total anthocyanins was reported by Pastrana-Bonilla et al. [20] and Oszmianski et al. [21]. In a few studies the individual identification of the both types of compounds was carried out employing two different options: either the direct chromatographic analysis of the extract without any other pre-treatment [22,23] or the analysis of two fractions, one for anthocyanins analysis and another for the analysis of non-coloured phenolics obtained after the separation and purification of the initial extract [17,24]. The advantage of the first methodology is its simplicity, although a lower number of compounds are usually determined. For example, Cantos et al. [22] directly analysed the extract of red grapes quantifying 16 compounds including phenolic acids, flavonols and anthocyanins, but the analytical method did not allow the individual quantification of the identified flavan-3-ols. However, the methodology reported by Kammerer et al. [24], after modifying a method previously reported by Osmianski et al. [25], allowed the quantification of 39 phenolic compounds. This methodology used a first solid/liquid extraction step to extract all the phenolic compounds and two more steps of separation and cleaning up of the non-coloured phenolics extract with liquid/liquid extraction followed by solid-phase extraction.

“Vinho Verde” is considered a QWPSR (quality wine produced in a specified region) and is confined to the north-west region of Portugal. Characterization of phenolic compounds of white “Vinho Verde” grapes has been previously reported [26,27] but as far as we know it has not been determined yet for the red varieties, although some studies on Vinhão wine were published [28,29].

The work herein aimed, at first, the selection of the most suitable analytical method to determine phenolic compounds, both anthocyanins and non-coloured phenolics, from red grapes. The target compounds were determined using high-performance liquid chromatography (HPLC) coupled to a diode array detector (DAD). Afterwards, samples of all the red grape varieties of the “Vinho Verde” recommended by “Comissão de viticultura da região dos Vinhos Verdes” [30] (i.e. Azal Tinto, Borraçal, Brancelho, Espadeiro, Padeiro de Basto, Pedral, Rabo de ovelha and Vinhão) and two authorized varieties (Doçal and Verdelho) were analyzed to characterize their phenolic profile. Samples came from three different locations in Minho (Portugal) and were harvested in two different years. Afterwards, principal components analysis (PCA) was employed in order to analyse the obtained data.

2. Experimental

2.1. Standards and reagents

Acetic acid, acetonitrile, methanol (MeOH), ethyl acetate, formic acid and sodium hydroxide were obtained from Merck (Darmstadt, Germany), hydrochloric acid from Pronalab (Lisboa, Portugal). The water was treated in a Milli-Q water purification system (Millipore, Bedford, MA). The ultrasonic bath was from Bandelin (Berlin, Germany).

The phenolic compounds used as references were obtained from the following sources:

Caffeic acid, ferulic acid, gallic acid, 5-(hydroxymethyl)furfural, myricetin-3-*O*-rhamnoside, *p*-coumaric acid, quercetin-3-*O*-glucoside, resveratrol and syringic acid from Sigma-Aldrich (Steinheim, Germany); catechin, cyanidin-3-*O*-glucoside, delphinidin-3-*O*-glucoside, (–)-epicatechin, epicatechin gallate, isorhamnetin-3-*O*-glucoside, kaempferol-3-*O*-glucoside, kaempferol-3-*O*-rutoside, malvidin-3-*O*-glucoside, peonidin-3-*O*-glucoside, quercetin-3-*O*-galactoside, quercetin-3-*O*-rutoside and syringetin-3-*O*-glucoside from Extrasynthèse (Genay, France).

2.2. Grape samples

Twenty-nine samples of different varieties of red “Vinho Verde” grapes were collected in September of 2005 and 2006, in three different vineyards, one located in Famalicão and two located in Ponte de Lima: Quinta de Barreiros and Quinta da Facha. The varieties under study were: Azal Tinto, Borraçal, Brancelho, Doçal, Espadeiro, Padeiro de Basto, Pedral, Rabo de ovelha, Verdelho, Vinhão (Table 1). After harvest, the entire grapes were stored at -20°C and freeze-dried in a Labconco 4.5 apparatus (Kansas City, MO).

2.3. Extraction and solid-phase extraction (SPE)

The solid-phase extraction (SPE) columns used were Chromabond C18 non-end-capped (NEC) columns (50 μm particle size, 60 Å porosity; 10 g sorbent mass/70 mL reservoir volume) from Macherey-Nagel (Düren, Germany).

Two experimental procedures described in the literature were tested, with small modifications:

2.3.1. Procedure described by Oszmianski et al. [21]

Aliquots of 5 g of pulverized sample were accurately weighed and extracted with 100 mL of 80% MeOH for 2 h under stirring after flushing with nitrogen in order to prevent oxidations during extraction. The extract was centrifuged (10 min, 4000 rpm) and the material was re-extracted with 100 mL of 80% MeOH (15 min). The combined supernatants were evaporated to dryness under reduced pressure at 30°C . The residue was dissolved in 50 mL of deionised water and applied to the SPE cartridge preconditioned with 20 mL of ethyl acetate, 20 mL of methanol and 20 mL of 0.01N HCl. The loaded cartridge was washed with 3 mL of HCl 0.01N. Non-coloured phenolics were eluted with 20 mL of ethyl acetate (fraction I). Anthocyanins were

Table 1
Vintage, variety and origin of the “Vinho Verde” red grape samples studied

Observation	Identification	Year	Variety	Geographical origin ^a
1	EspFam5	2005	Espadeiro	Famalicão
2	PadFam5	2005	Padeiro de Basto	Famalicão
3	VinFam5	2005	Vinhão	Famalicão
4	AzBa5	2005	Azal tinto	Ponte da Lima (Quinta Barreiros)
5	BorBa5	2005	Borraçal	Ponte da Lima (Quinta Barreiros)
6	BraBa5	2005	Brancelho	Ponte da Lima (Quinta Barreiros)
7	DoBa5	2005	Doçal	Ponte da Lima (Quinta Barreiros)
8	EspBa5	2005	Espadeiro	Ponte da Lima (Quinta Barreiros)
9	PadBa5	2005	Padeiro de Basto	Ponte da Lima (Quinta Barreiros)
10	PedBa5	2005	Pedral	Ponte da Lima (Quinta Barreiros)
11	RabBa5	2005	Rabo de ovelha	Ponte da Lima (Quinta Barreiros)
12	VerBa5	2005	Verdelho	Ponte da Lima (Quinta Barreiros)
13	VinBa5	2005	Vinhão	Ponte da Lima (Quinta Barreiros)
14	BorrFa5	2005	Borraçal	Ponte da Lima (Quinta Facha)
15	VerFa5	2005	Verdelho	Ponte da Lima (Quinta Facha)
16	VinFa5	2005	Vinhão	Ponte da Lima (Quinta Facha)
17	EspFam6	2006	Espadeiro	Famalicão
18	PadFam6	2006	Padeiro de Basto	Famalicão
19	VinFam6	2006	Vinhão	Famalicão
20	AzBa6	2006	Azal tinto	Ponte da Lima (Quinta Barreiros)
21	BorBa6	2006	Borraçal	Ponte da Lima (Quinta Barreiros)
22	BraBa6	2006	Brancelho	Ponte da Lima (Quinta Barreiros)
23	DoBa6	2006	Doçal	Ponte da Lima (Quinta Barreiros)
24	EspBa6	2006	Espadeiro	Ponte da Lima (Quinta Barreiros)
25	PadBa6	2006	Padeiro de Basto	Ponte da Lima (Quinta Barreiros)
26	PedBa6	2006	Pedral	Ponte da Lima (Quinta Barreiros)
27	RabBa6	2006	Rabo de ovelha	Ponte da Lima (Quinta Barreiros)
28	VerBa6	2006	Verdelho	Ponte da Lima (Quinta Barreiros)
29	VinBa6	2006	Vinhão	Ponte da Lima (Quinta Barreiros)

^a When grapes come from different locations in the same geographical origin, it is noted in parentheses.

eluted with 40 mL of methanol containing 0.1% HCl (fraction II).

The eluates were concentrated under reduced pressure, and the residues obtained were dissolved in 1 mL of methanol (fraction I) and in 20 mL of acidified water, pH 3.0 (fraction II), respectively, membrane-filtered (0.45 µm) and analyzed by HPLC-DAD.

2.3.2. Procedure described by Kammerer et al. [24]

Aliquots of 5 g of pulverized sample were accurately weighed and extracted with 100 mL of methanol/0.1% HCl (v/v) for 2 h under stirring after flushing with nitrogen in order to prevent oxidations during extraction. The extract was centrifuged (10 min, 4000 rpm) and the material was re-extracted with 100 mL of the same solvent (15 min). The combined supernatants were evaporated to dryness under reduced pressure at 30 °C, and the residue was dissolved in 20 mL of acidified water (pH 3.0). Anthocyanins were analyzed by direct injection of this solution (fraction I). To analyse the non-coloured phenolics the following procedure was used: the pH of the aqueous solution was adjusted to 1.5 and extracted four times with 50 mL of ethyl acetate each. The combined extracts were evaporated to dryness, dissolved in water and applied to the SPE cartridges after the pH had been adjusted to 7.0. SPE cartridges were previously activated with 20 mL of methanol and 20 mL of water. Phenolic acids were eluted with 10 mL of deionised water and 10 mL of 0.01% HCl (fraction II); anthoxantins and stilbenes were eluted

with 20 mL of ethyl acetate (fraction III). The eluates (fractions II and III) were concentrated under reduced pressure, sequentially in the same Erlenmeyer flask and the residue was dissolved in 2 mL of methanol, membrane-filtered (0.45 µm) and analyzed by HPLC-DAD.

2.4. Alkaline hydrolysis of the non-coloured phenolics extract

Three millilitres of 2N NaOH were added to 300 µL of dried methanolic extract obtained as previously mentioned. The solution was kept in the dark for 4 h, acidified with HCl and passed through a C18 Bond Elut cartridge, preconditioned with MeOH and 2N HCl. The phenolic compounds were eluted with MeOH. This solution was taken to dryness under reduced pressure (30 °C), dissolved in MeOH, and 20 µL were analyzed by HPLC-DAD.

2.5. Acid hydrolysis of the anthocyanin extract obtained

1 mL of HCl 2N was added to 900 µL of anthocyanin extract obtained by SL-SPE, and boiled with reflux during 30 min. The obtained solution was passed through a C18 Bond Elut cartridge, preconditioned with MeOH and 2N HCl. The retained anthocyanins were eluted with MeOH. This solution was taken to dryness under reduced pressure (30 °C), dissolved in acid water (pH 3), and 20 µL were analyzed by HPLC-DAD.

2.6. HPLC-DAD analysis of phenolic compounds

The extracts were analyzed on an analytical HPLC unit (Gilson), using a Spherisorb ODS2 column (25.0 cm × 0.46 cm; 5 µm particle size Waters, Milford, MA, USA) with a C18 ODS guard column.

2.6.1. System I (anthocyanins)

The conditions described by Kammerer et al. [24] were employed. The mobile phase consisted of water/formic acid/acetonitrile (87:10:3, v/v/v; eluent A) and water/formic acid/acetonitrile (40:10:50, v/v/v; eluent B) using a gradient program as follows: from 10 to 25% B (10 min), from 25 to 31% B (5 min), from 31 to 40% (5 min), from 40 to 50% B (10 min), from 50 to 100% B (10 min), from 100 to 10% B (5 min). Total run time was 50 min. Flow rate of 0.8 mL min⁻¹. The injection volume was 20 µL.

2.6.2. System II (non-coloured phenolics)

The conditions described by Kammerer et al. [24] for analysing phenolic acids and anthoxanthins and stilbenes were modified to analyse all these compounds in the same analysis. The mobile phase consisted of 2% (v/v) acetic acid in water (eluent A) and 0.5% (v/v) acetic acid in water and acetonitrile (50:50, v/v, eluent B) using a gradient program as follows: from 10 to 24% B (20 min), from 24 to 30% B (20 min), from 30 to 55% B (20 min), from 55 to 70% B (5 min), from 70 to 80% B (5 min), from 80 to 100% (5 min), 100% B isocratic (5 min), from 100 to 10% B (2 min). Flow rate of 1.0 mL min⁻¹. The injection volume was 20 µL.

Detection was done using a Gilson diode array detector. The compounds quantified in each sample were identified comparing their retention times and UV–vis spectra in the 200–600 nm range with individual standards.

Phenolic compounds quantification was achieved using a calibration plot of external standard at 350 nm for quercetin-3-*O*-glucoside, quercetin-3-*O*-rutinoside, myricetin-3-*O*-rhamnoside, isorhamnetin-3-*O*-glucoside and kaempferol-3-*O*-glucoside; at 320 nm for *p*-coumaric acid, caffeic acid and resveratrol; at 280 for catechin, (–) epicatechin, epicatechin gallate, gallic acid and syringic acid; at 500 nm for cyanidin-3-*O*-glucoside, delphinidin-3-*O*-glucoside, peonidin-3-*O*-glucoside and malvidin-3-*O*-glucoside. The correlation coefficient for the standard curves invariably exceeded 0.99 for all studied compounds.

Caftaric and coumaric acids were quantified as caffeic and *p*-coumaric acids, respectively. Quercetin-3-*O*-glucuronide, quercetin-3-*O*-galactoside and quercetin-3-*O*-rutinoside were quantified together as quercetin-3-*O*-rutinoside. Myricetin-3-*O*-glucoside, laricitrin-3-*O*-glucoside and syringetin-3-*O*-glucoside were quantified as myricetin-3-*O*-rhamnoside. Polydatin was quantified as resveratrol. Petunidin-3-*O*-glucoside, petunidin 3-*O*-*p*-coumaroylglucoside and malvidin 3-*O*-*p*-coumaroylglucoside were quantified as malvidin-3-*O*-glucoside. Peonidin-*O*-*p*-coumaroylglucoside was quantified as peonidin-3-*O*-glucoside.

The repeatability and reproducibility of the chromatographic method was evaluated by measuring the peak chromatographic area of each compound six times on the same standard solution in the same day and in different days, respectively. The chromatographic methods are precise: the repeatability study showed relative standard deviation (R.S.D.) between 2.8 and 4.7% for anthocyanins, and between 0.73 and 5.6% for non-coloured phenolics. The reproducibility study showed that R.S.D. ranged from 7.7 and 9.7% for anthocyanins and from 1.0 and 7.1 for non-coloured phenolics.

2.7. Statistical analysis

ANOVA and principal component analysis (PCA) were performed by SPSS Program (version 14.0). Levene's test for homogeneity of variance was used to assess the validity of the ANOVA analysis. When variance homogeneity was not acceptable, the Welch test, a one-way robust test of equality of means, was employed instead of ANOVA. PCA was performed separately for each studied chemical parameter and expressed as percentage (weight), for both non-coloured phenolics and anthocyanin profiles and also for the global data. Expression in percentages was used because it is expected to diminish the variability due to the environment [5].

3. Results and discussion

3.1. Identification of compounds

Red “Vinho Verde” grapes showed a phenolic profile composed by 25 identified phenolics.

3.1.1. Non-coloured phenolics

17 non-coloured phenolics were identified and quantified in most part of the samples. The identified phenolic acids were: gallic acid, caftaric acid, coumaric acid and syringic acid; the flavan-3-ols were: catechin, epicatechin and epicatechin gallate; and the flavonols were: myricetin-3-*O*-glucoside, quercetin-3-*O*-galactoside, quercetin-3-*O*-glucuronide and quercetin-3-*O*-rutinoside, quercetin-3-*O*-glucoside, laricitrin-3-*O*-glucoside, kaempferol-3-*O*-glucoside, isorhamnetin-3-*O*-glucoside and syringetin-3-*O*-glucoside together with polydatin (resveratrol-3-*O*-glucoside). Other compounds as kaempferol-3-*O*-rutinoside and *p*-coumaric acid were found in some samples at trace levels. A non-phenolic compound, 5-(hydroxymethyl)furfural, already reported by Kammerer et al. [24], was also identified. The HPLC-DAD chromatograms obtained for a sample at 280, 320 and 350 nm are shown in Fig. 1.

In a general way, the compounds were identified by comparing their retention times and UV–vis spectra in the 200–400 nm range with individual standards. When standards were not available, the phenolics identification was carried out as follows:

Phenolic acids: caftaric and coumaric acids were identified considering their retention time and UV spectrum [24]. Alkaline hydrolysis of a methanolic extract of red “Vinho Verde” grapes showed the absence of the chromatographic peaks correspond-

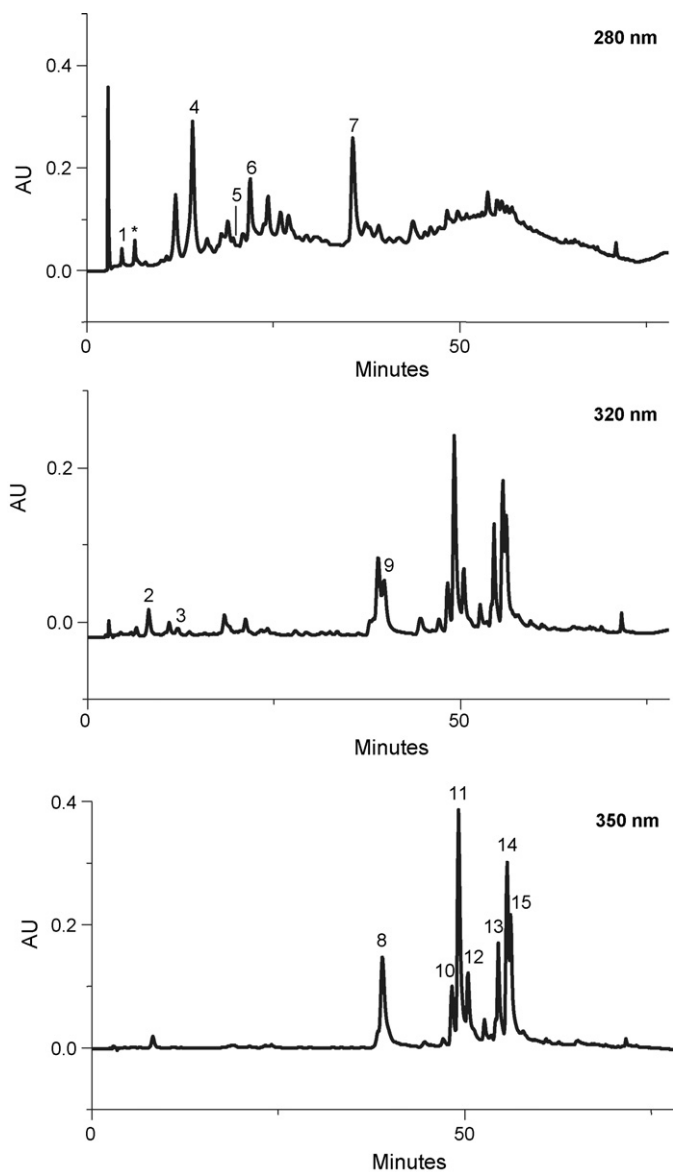


Fig. 1. Non-coloured phenolics profile of Verdelho (280 nm) and Padeiro de Basto, (320, 350 nm) red “Vinho Verde” grape samples from Quinta Barreiros, harvested in 2006. Identification of the peaks according to Table 1.

ing to coumaric and caffeic and the presence of *p*-coumaric and caffeic acids, which confirmed the identity of these compounds.

Stilben: polydatin was identified considering its retention time [24] and UV spectrum [31].

Flavonols: myricetin-3-*O*-glucoside and laricitrin-3-*O*-glucoside were identified after a HPLC-DAD analysis of a methanolic extract of red “Vinho Verde” grapes, under the conditions previously used in our laboratory [16], and described by Castillo-Muñoz et al. [19], respectively, both considering their retention time and UV-vis spectrum.

While derivatives of quercetin, kaempferol and isorhamnetin had been detected in many *V. vinifera* both red and white grapes cultivars, the determination of derivatives of laricitrin and syringetin is not so common. Laricitrin-3-*O*-glucoside [32] and syringetin-3-*O*-glucoside [33] have been reported as minor compounds in grapes. In the study carried out by Mattivi et al. [17]

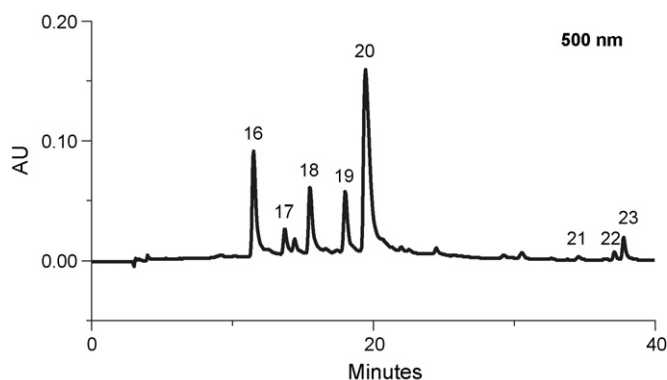


Fig. 2. Anthocyanin profile (500 nm) from Vinhão red “Vinho Verde” grapes samples from Quinta Barreiros, harvested in 2006. Identification of the peaks according to Table 1.

both glucosides were determined co-eluting with their respective galactosides suggesting that this last form was the main derivative. But in a later study [19] both derivatives, glucoside and galactoside, were separated under the chromatographic conditions used and the glucoside assigned as the main compound, therefore we can suppose that the grape samples under analysis contain laricitrin-3-*O*-glucoside and syringetin 3-*O*-glucoside. It is noted that these last two flavonols together with myricetin-3-*O*-glucoside [16,18,20,32,34,35] have been only found in red varieties of grapes.

3.1.2. Anthocyanins

Eight anthocyanins were identified and quantified in most part of the samples: delphinidin-3-*O*-glucoside, cyanidin-3-*O*-glucoside, petunidin-3-*O*-glucoside, peonidin-3-*O*-glucoside, malvidin-3-*O*-glucoside, petunidin-3-*O*-*p*-coumaroylglucoside, peonidin-3-*O*-*p*-coumaroylglucoside and malvidin-3-*O*-*p*-coumaroylglucoside. The HPLC-DAD chromatogram obtained for an analysed sample at 500 nm is shown in Fig. 2.

Delphinidin-3-*O*-glucoside, cyanidin-3-*O*-glucoside, peonidin-3-*O*-glucoside and malvidin-3-*O*-glucoside were identified by comparing their retention times and UV-vis spectra in the 200–600 nm range with individual standards. Petunidin-3-*O*-glucoside, petunidin-3-*O*-*p*-coumaroylglucoside, peonidin-3-*O*-*p*-coumaroylglucoside and malvidin-3-*O*-*p*-coumaroylglucoside were identified considering their retention time [24] and UV-vis spectrum. Spectra of *p*-coumaroyl derivatives showed the characteristic shoulder of cinnamoyl derivatives around 313–315 nm [14,36]. Additionally, acid hydrolysis of an acidic extract of red “Vinho Verde” grapes showed the absence of the chromatographic peaks corresponding to those glucoside derivatives and the presence of delphinidin, cyanidin, peonidin, petunidin and malvidin, which confirmed the identity of these compounds.

3.2. Comparison of the two extractive methodologies

Two experimental procedures described in the literature by Kammerer et al. [24] and Oszmianski et al. [21] were tested to extract the phenolic compounds from red “Vinho Verde” grapes.

Both methodologies consisted of a first step of solid–liquid extraction and a SPE step to purify the extract and separate the non-coloured phenolics from the anthocyanins that can cause interferences in their determination. The method described by Kammerer et al. [24] has also an additional step of liquid–liquid extraction previously to the SPE, to improve the purity of the extract of non-coloured phenolics due to the presence of anthocyanins in this extract can cause errors in their determination.

Considering that the objective of this work is the characterization of the phenolic profile of *Vinho Verde* grapes, the method described by Kammerer et al. [24] was selected in order to quantify the highest possible number of compounds individually. It was compared with the pre-treatment described by Oszmianski et al. [21] that could simplify the experimental procedure. Other procedures consulted in the references employ simpler methodologies but they quantify total amount of compounds [20] or the aglycons after hydrolysis of the glycoside derivatives [17,20]. Some of them even do not use any pre-treatment of the sample previously to the chromatographic analysis [22,23] but the number of compounds determined is quite lower.

Both methodologies were applied to a Verdelho grapes sample from Quinta da Facha (2005). Table 2 shows the obtained results, as a mean of three replicates. To guarantee the completeness of the extraction of phenolic compounds, after the performance of the all extractive method, the extracted matrix

was subjected to another full extraction procedure and metabolites were all below the quantification limit.

First, mean recoveries obtained for each compound using both methods were compared using ANOVA or Welch test if the variance homogeneity was not acceptable. Only 12 compounds (Table 2) showed significant differences ($p < 0.05$): the most polar compounds, which are first eluted in the C18 chromatography column, such as phenolic acids, catechin, and the glucoside anthocyanins, were recovered in higher levels using the method described by Oszmianski et al. [21] that employ an aqueous solvent (methanol:water 80:20). However, the highest recovery of flavonols, less polar compounds which are later eluted, was achieved with the method reported by Kammerer et al. [24] using an organic solvent (acidic methanol).

The results obtained for the rest of the compounds did not show significant differences, probably due to the high variability showed for the results obtained using the method described by Oszmianski et al. [21], with R.S.D. ranged from 3.0 to 24% whereas that the method described by Kammerer et al. [24] showed better reproducibility, with R.S.D. between 1.3 and 13%.

Regarding to the non-coloured extract, the additional liquid/liquid extraction included in the method reported by Kammerer et al. [24] let to obtain extracts of higher purity.

Considering these results, the method reported by Kammerer et al. [24] showed to be a good compromise solution to extract

Table 2

Comparison between the methods described by Kammerer et al. [24] and Oszmianski et al. [21] for the extraction of phenolic compounds from a sample of Verdelho red “Vinho Verde” grapes from Quinta Barreiros, harvested in 2005 ($n = 3$)

Compound	Retention time (min)	Method described by Oszmianski et al. [21]		Method described by Kammerer et al. [24]	
		Mean	R.S.D.	Mean	R.S.D.
1 Gallic acid	4.7	21	15	4.6	6.6
2 Caftaric acid	8.9	40**	7.5	3.2**	6.9
3 Coumaric acid	12.8	19**	6.1	1.3**	2.1
4 Catechin	14.2	844**	24	303**	13
5 Syringic acid	19.6	nd		nq	
6 Epicatechin	21.9	313	23	145	1.3
7 Epicatechin gallate	35.6	44	24	64	12
8 Myricetin 3- <i>O</i> -glucoside	37.8	36	6.6	56	8.7
9 Polydatin	40.2	4.5**	4.1	9.0**	6.1
10 Quercetin 3- <i>O</i> -galactoside/quercetin 3- <i>O</i> -glucuronide/quercetin 3- <i>O</i> -rutinoside	47.2	11	3.0	17	11
11 Quercetin 3- <i>O</i> -glucoside	48.2	30**	16	58**	7.7
12 Laricitrin 3- <i>O</i> -glucoside	49.7	12**	12	22**	3.3
13 Kaempferol 3- <i>O</i> -glucoside	53.9	5.4**	20	11**	11
14 Isorhamnetin 3- <i>O</i> -glucoside	55.0	2.4**	6.5	13**	6.9
15 Syringetin 3- <i>O</i> -glucoside	55.7	23**	13	31**	6.3
16 Delphinidin 3- <i>O</i> -glucoside	11.5	524**	12	347**	13
17 Cyanidin 3- <i>O</i> -glucoside	13.6	43	7.1	28	3.6
18 Petunidin 3- <i>O</i> -glucoside	15.4	512**	15	361**	11
19 Peonidin 3- <i>O</i> -glucoside	17.9	200	8.1	134	3.3
20 Malvidin 3- <i>O</i> -glucoside	19.4	2087**	9.4	1507**	10
21 Petunidin 3- <i>O</i> - <i>p</i> -coumaroylglucoside	34.3	47	22	55	4.1
22 Peonidin 3- <i>O</i> - <i>p</i> -coumaroylglucoside	36.9	49	24	61	4.5
23 Malvidin 3- <i>O</i> - <i>p</i> -coumaroylglucoside	37.2	182	23	252	4.4
* 5-(Hydroxymethyl)furfural	6.4				

Concentration of compounds in mg kg^{-1} of lyophilized sample.

** Significant differences were found between the means using ANOVA or Welch test ($p < 0.05$).

Table 3
Anthocyanin contents (mg kg⁻¹ of lyophilized sample) of red “Vinho Verde” grape samples

			Del 3- <i>O</i> -gluc	Cya 3- <i>O</i> -gluc	Pet 3- <i>O</i> -gluc	Peo 3- <i>O</i> -gluc	Mal 3- <i>O</i> -gluc	Pet 3- <i>O</i> - p-cmgluc	Peo 3- <i>O</i> - p-cmgluc	Mal 3- <i>O</i> - p-cmgluc	Total AC content
1	EspFam5	Mean	32	nd	39	nq	275	36	23	186	592
		S	2.7		0.71		27	2.0	1.4	16	
2	PadFam5	Mean	138	21	176	112	1520	30	15	154	2165
		S	12	0.87	8.0	8.0	96	0.93	2.0	11	
3	VinFam5	Mean	1467	162	1195	536	3927	72	55	252	7664
		S	39	3.8	35	17	14	6.6	0.30	3.4	
4	AzBa5	Mean	268	48	242	337	767	24	30	60	1777
		S	7.9	0.86	7.5	3.3	11	0.31	0.75	4.2	
5	BorBa5	Mean	101	20	108	130	646	30	21	102	1158
		S	5.5	0.54	1.5	4.5	11	0.15	0.47	0.9	
6	BraBa5	Mean	nq	nq	nq	76	64	nq	nq	21	160
		S				2.5	2.0			2.8	
7	DoBa5	Mean	157	29	141	136	751	39	31	166	1449
		S	2.7	0.93	4.6	2.0	11.1	0.92	1.1	13	
8	EspBa5	Mean	46	nq	49	56	414	43	40	245	892
		S	1.7		1.1	2.9	16	1.6	1.3	5.5	
9	PadBa5	Mean	91	nq	92	114	1172	26	16	142	1654
		S	0.05		7.3	1.4	12	0.6	1.1	4.1	
10	PedBa5	Mean	74	24	90	123	666	48	41	241	1307
		S	0.47	0.49	2.3	1.1	12	0.94	0.58	4.3	
11	RabBa5	Mean	242	25	209	116	1178	32	15	86	1904
		S	9.9	0.74	12	1.5	11	0.20	0.92	5.7	
12	VerBa5	Mean	329	21	306	77	1298	48	16	200	2295
		S	3.8	0.23	4.1	2.2	13	1.9	0.22	0.7	
13	VinBa5	Mean	3653	409	2054	623	4736	106	29	233	11842
		S	155	34	58	32	48	1.2	0.40	1.1	
14	BorFa5	Mean	481	55	513	259	1469	42	26	122	2966
		S	20	0.50	8.6	7.3	20	0.39	1.5	1.7	
15	VerFa5	Mean	318	28	320	145	1486	56	32	260	2645
		S	3.1	0.51	6.3	0.8	45	0.71	0.34	16	
16	VinFa5	Mean	2320	228	1570	410	2524	65	17	140	7274
		S	37	0.25	102	11	54	0.69	0.35	0.80	
17	EspFam6	Mean	37	nq	51	63	346	34	35	162	727
		S	0.6		0.79	1.2	4.2	0.47	2.5	6.2	
18	PadFam6	Mean	108	nq	135	88	1575	33	19	218	2176
		S	1.1		2.5	4.4	24	0.8	0.40	4.6	
19	VinFam6	Mean	1428	212	1146	682	4028	63	47	244	7850
		S	34	2.0	42	12	76	2.2	1.1	4.9	
20	AzBa6	Mean	111	41	129	391	901	28	43	114	1757
		S	0.5	0.11	0.78	5.1	8.8	0.67	0.11	0.73	
21	BorBa6	Mean	151	31	161	164	809	38	30	139	1521
		S	1.5	0.30	1.2	2.0	3.8	0.75	0.52	3.6	
22	BraBa6	Mean	32	21	44	148	219	nd	40	53	557
		S	0.42	0.63	1.6	4.6	4.0		0.76	0.87	
23	DoBa6	Mean	210	26	220	168	1409	44	41	234	2353
		S	5.2	0.69	4.6	3.6	24	0.24	0.55	4.6	
24	EspBa6	Mean	31	nd	35	nq	246	38	23	172	546
		S	0.65		2.2		5.1	0.44	0.81	1.7	
25	PadBa6	Mean	378	48	387	292	2230	40	35	189	3598
		S	14	0.26	0.51	3.3	17	0.56	2.9	4.3	
26	PedBa6	Mean	71	24	102	128	528	49	47	228	1178
		S	0.12	1.5	1.5	2.0	6.8	0.57	1.3	4.1	
27	RabBa6	Mean	175	24	199	135	1284	42	33	208	2099
		S	5.9	1.2	11.5	6.8	71	1.9	2.2	12.7	
28	VerBa6	Mean	76	nq	96	59	916	43	30	322	1543
		S	3.3		3.1	0.86	35	1.3	1.9	20.6	
29	VinBa6	Mean	1124	134	983	549	4358	59	45	267	7520
		S	30	2.8	44	11	132	1.0	1.9	14.2	

Abbreviations—del: delphinidin; cya: cyaninidin; pet: petunidin; peo: peonidin; mal: malvidin; glc: glucoside; pcm: *p*-coumaroyl; AC: anthocyanin; nd: not detected (concentration sample < detection limit); nq: not quantified (detection limit < concentration sample < quantification limit).

the wide range of phenolic compounds determined with high purity and good reproducibility in red “Vinho Verde” grapes.

3.3. Analysis of red “Vinho Verde” grapes

3.3.1. Anthocyanins

Eight anthocyanins were quantified in red “Vinho Verde” grapes (Table 3) which total concentration ranged from 160 mg kg⁻¹ of Brancelho to 11842 mg kg⁻¹ of Vinhão, both from Quinta de Barreiros (2005). ANOVA analysis and Tukey comparison test showed significant differences between the total concentration of anthocyanins of the variety Vinhão and the rest of the varieties ($p < 0.05$).

The most abundant anthocyanin was malvidin-3-*O*-glucoside (35–72%) for all the analysed grapes samples except for the variety Brancelho, in which the major compounds were malvidin-3-*O*-glucoside (39%) or peonidin-3-*O*-glucoside (47%).

The second most abundant compound was more heterogeneous: peonidin-3-*O*-glucoside (<47%), delphinidin-3-*O*-glucoside (<32%), malvidin-3-*O*-*p*-coumaroylglucoside (<32%) or petunidin-3-*O*-glucoside (<22%) while the rest of the compounds were found in amounts lower than 7.1%.

These results agree with those previously described by other authors: the major anthocyanin group is usually that of the 3-*O*-glucoside derivatives (of delphinidin, cyanidin, petunidin and peonidin) especially malvidin [5,10,14,17,22,24,32] or peonidin [14,17,22] because they are the final products of anthocyanin pathway biosynthesis [37]. However, the second major compound determined in red grapes by other authors was also more heterogeneous: peonidin-3-*O*-glucoside, malvidin-3-*O*-glucoside or malvidin-3-*O*-*p*-coumaroylglucoside [5,14,17,22,24,32], and less commonly the glucoside derivatives of cyanidin, petunidin and delphinidin [5,14,17,22].

To study the relation between the varieties and their anthocyanin profiles, principal component analysis was applied to the percentage (in weight) of each compound in relation with the total content of anthocyanins. PCA yields three principal components (with eigenvalue higher than 1) explaining 91% of the total variance in the data although only the two first were retained (explaining 70.4% of the total variance) considering the scree plot to simplify the analysis of the results [38].

Fig. 3 shows the corresponding loading plots that establish the relative importance of each variable. The first PC, which explains 48.3% of the variance, correlates positively with the glucoside derivatives of delphinidin, cyanidin and petunidin and negatively with the *p*-coumaroyl derivatives while peonidin-3-*O*-glucoside and malvidin-3-*O*-glucoside did not have high weight in this component. The second PC (22.1%) correlates positively with all the compounds except malvidin-3-*O*-glucoside that is the compound with higher weight in this component.

As can be seen in Fig. 4 anthocyanin profile was related to the variety of the grapes more than harvest and origin. Three groups could be clearly distinguished: the grapes of the variety Vinhão appeared in the positive part of the PC1, due to their highest content in delphinidin-3-*O*-glucoside (15–32%), cyanidin-3-*O*-glucoside (1.8–3.5%) and petunidin-3-*O*-glucoside (13–22%)

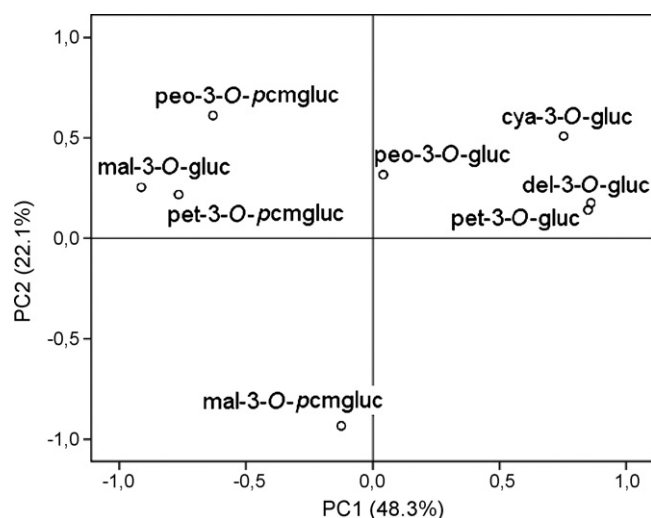


Fig. 3. Principal component analysis of anthocyanins in red “Vinho Verde” grapes: loadings plot.

and low content in the *p*-coumaroyl derivatives. Padeiro grapes appeared in the positive part of the PC2 due to their highest content in malvidin-3-*O*-glucoside (62–72%) and low content in the rest of the anthocyanins. The third group, on the left, contains Espadeiro, Pedral and Brancelho grapes with high contents in *p*-coumaroyl derivatives. Espadeiro grapes showed the highest contents in these compounds (32–43%) followed by Pedral (25–27%) and Brancelho (13–17%) that showed the highest percentage of peonidin-3-*O*-glucoside of all the samples (27–47%). The rest of the varieties (Azal Tinto, Borraçal, Doçal, Verdelho and Rabo de Ovelha) showed more similar anthocyanin profiles, with higher contents in peonidin-3-*O*-glucoside for Azal Tinto (19–22%) and Borraçal (9.4–11%).

3.3.2. Non-coloured phenolics

17 compounds were quantified in most part of the analysed red “Vinho Verde” grapes (Table 4): four phenolic acids, three

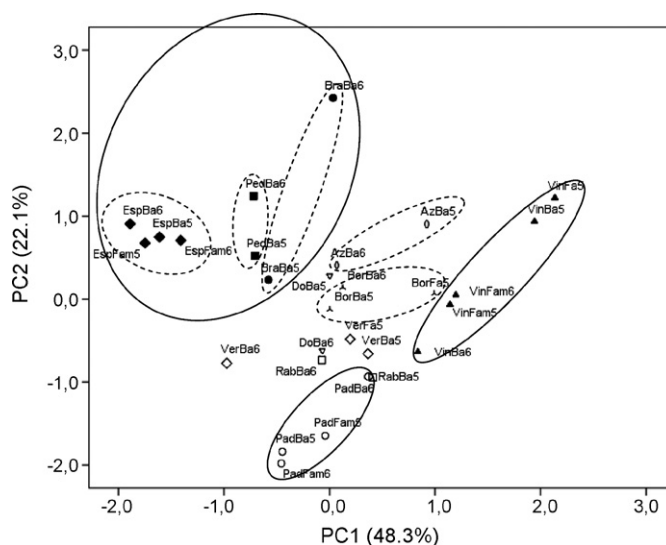


Fig. 4. Principal component analysis of anthocyanins in red “Vinho Verde” grapes: scores plot.

Table 4
Non-coloured phenolics composition of red “Vinho Verde” grape samples (mg kg⁻¹ of lyophilized sample)

			Gal	Caft	Cout	Syr	Cat	Epicat	Epicatgal	Myr gluc	Polyd	q 3-O-gal/glucur/rut	q 3-O-gluc	Lar 3-O-gluc	Kaemp 3-O-gluc	Isorhm 3-O-gluc	Syr 3-O-gluc	Total
1	EspFam5	Mean	7.5	9.1	2.5	nd	152	117	85	13	nq	46	27	9.2	1.7	44	25	541
		S	0.68	0.11	0.14		9.1	1.1	1.3	0.61			1.1	0.71	0.21	0.02	1.2	1.1
2	PadFam5	Mean	4.7	3.8	1.0	31	16	12	11	52	6	28	67	32	19	37	48.9	370
		S	0.31	0.05	0.05	0.19	0.25	0.65	0.93	0.30	0.11	0.47	1.0	0.38	0.47	0.52	3.09	
3	VinFam5	Mean	3.3	4.1	2.4	13	11	12	9.3	59	11	7.8	12	23	1.6	13	43	227
		S	0.34	0.06	0.17	0.33	0.31	1.30	0.37	1.6	0.23	0.76	0.33	0.46	0.06	1.4	0.7	
4	AzBa5	Mean	3.4	11	5.5	2.5	94	124	49	21	31	46	27	15	2.9	26	21	480
		S	0.23	0.35	0.12	0.22	5.5	7.3	1.0	1.9	1.3	0.90	1.4	0.05	0.14	1.3	2.7	
5	BorBa5	Mean	2.4	4.5	1.1	9.0	445	336	139	22	28	46	32	16	3.2	22	22	1128
		S	0.10	0.20	0.03	0.36	21	18	5.3	0.58	1.4	1.7	0.71	0.17	0.28	1.1	1.3	
6	BraBa5	Mean	nq	10	4.1	4.0	7.0	24	nd	14	13	32	32	28	6.5	14	32	221
		S	0.09	0.42	0.04	0.05	0.45			0.85	0.73	2.5	0.23	2.60	0.20	0.38	2.80	
7	DoBa5	Mean	4.5	4.4	nd	6.3	478	265	61	18	6.4	33	22	8.9	nd	18	10	934
		S	0.19	0.12		0.20		21	3	0.07	0.51	0.63	0.36	0.49		0.12	0.40	
8	EspBa5	Mean	5.1	44	8.9	nd	203	155	136	33	nd	163	93	45	23	48	38	996
		S	0.33	0.30	0.52		3.3	6.7	9.8	1.5		7.8	4.1	3.0	0.73	3.3	3.8	
9	PadBa5	Mean	3.1	7.2	3.1	18	107	113	56	7.8	18	72	80	29	3.3	19	20	557
		S	0.03	0.09	0.22	2.6	2.3	0.8	2.1	0.24	0.33	1.5	1.4	1.8	0.16	1.5	0.60	
10	PedBa5	Mean	2.2	17	3.3	nd	70	117	45	11	38	22	13	6.2	3.3	4.7	15	368
		S	0.12	0.05	0.35		0.69	7.7	3.7	0.44	1.0	1.3	0.08	0.48	0.07	0.18	0.23	
11	RabBa5	Mean	nd	20	6.3	5.6	176	85	84	76	2.6	92	78	40	15	33	38	751
		S		0.19	0.09	0.71	18	10	3.8	4.4	0.28	2.0	1.3	0.26	1.2	1.5	4.5	
12	VerBa5	Mean	5.6	2.2	0.80	3.4	32	42	17	47	4	5.8	11.3	14	7.9	3.7	19	216
		S	0.08	0.04	0.04	0.23	2.0	2.0	0.90	4.5	0.04	0.16	0.50	0.26	0.20	0.44	2.6	
13	VinBa5	Mean	2.7	11	5.3	8.9	90	35	35	163	9.1	10	13	21	1.6	7.6	26	440
		S	0.14	0.21	0.13	0.51	4.4	3.5	2.2	14	0.17	0.17	0.17	1.1	0.13	0.52	1.1	
14	BorFa5	Mean	4.6	13	3.5	13	700	333	142	32	24	12	40	11	4.4	22	24	1378
		S	0.25	0.11	0.06	0.1	41	21	3.0	1.1	0.79	0.60	1.1	0.39	0.43	1.2	1.7	
15	VerFa5	Mean	4.6	3.2	1.3	nd	303	145	64	56	9.0	16.9	58	22	11	13	31	738
		S	0.30	0.2	0.03		40	1.9	8.0	4.9	0.5	1.8	4.4	0.72	1.3	0.91	1.9	
16	VinFa5	Mean	15	11	5.0	25	72	59	41	208	13	14	37	40	5.3	16	63	626
		S	1.6	0.41	0.22	0.76	3.5	1.5	2.0	5.1	0.32	0.39	0.75	1.4	0.55	0.10	3.0	
17	EspFam6	Mean	2.7	19	3	3.7	45	48	32	38	4.6	10	58	19	11	34	26	355
		S	0.19	0.12	0.10	0.47	5.9	2.7	2.4	1.6	0.21	1.2	1.4	2.4	0.18	0.38	0.17	
18	PadFam6	Mean	nq	7.4	4.7	3.7	22	3.9	9.8	20	7.1	11	38	22	9.0	19	38	214
		S		0.25	0.41	0.27	1.9	0.60	0.14	1.5	0.16	0.07	0.66	1.3	0.38	0.19	0.83	
19	VinFam6	Mean	2.5	2.7	1.6	22	nd	nd	nd	67	9.5	18	27	32	3.4	25	59	270
		S	0.10	0.02	0.05	0.83				0.92	0.61	0.50	1.1	1.2	0.12	0.57	1.7	
20	AzBa6	Mean	nq	4.1	0.73	7.3	150	77	75	19	33	12	45	20	6.2	27	24	501
		S		0.24	0.02	1.8	11	6.7	3.1	0.42	0.75	0.56	0.86	0.75	0.04	0.30	0.97	
21	BorBa6	Mean	3.9	3.3	nq	5.5	113	80	49	21	12	7.2	19	13	6.7	21	18	372
		S	0.28	0.05		0.1	1.4	0.29	3.2	0.66	0.03	0.65	0.49	0.09	0.48	1.6	1.0	
22	BraBa6	Mean	2.2	2.6	0.73	2.2	21	26	29	8.4	2.8	8.3	30	8.0	5.1	24	15	184
		S	0.18	0.13	0.04	0.16	0.67	0.74	1.1	1.0	0.05	0.16	0.22	0.06	0.33	0.26	1.6	
23	DoBa6	Mean	2.1	3.9	0.75	7.3	293	134	70	41	3.7	10	25	20	3.4	15	27	656
		S	0.10	0.04	0.02	0.61	3.6	15	2	1.1	0.28	0.13	0.53	0.50	0.30	0.89	2.6	

24	EspBa6	Mean	1.9	7.2	1.4	7.9	36	22	21	18	4.2	12	15	22	23	17	61	270
		S	0.14	0.12	0.02	0.81	3.8	0.51	0.66	0.43	0.52	0.37	0.49	0.72	1.3	0.84	3.9	
25	PadBa6	Mean	2.1	5.1	1.1	8.9	24	8.4	9.8	93	12	43	132	56	39	72	92	598
		S	0.18	0.06	0.02	0.26	0.40	0.95	0.80	4.8	0.18	0.56	1.7	4.7	0.67	1.2	7.4	
26	PedBa6	Mean	2.8	8.3	0.90	1.9	nd	19	24	4.5	19	7.1	42	10	4.7	34	19	197
		S	0.22	0.63	0.03	0.08	nd	1.72	0.94	0.55	0.32	0.43	0.99	0.76	0.07	1.6	1.6	
27	RabBa6	Mean	2.6	3.2	0.62	7.0	69	32	22	40	4.6	23	26	19	3.0	15	28	296
		S	0.24	0.06	0.03	0.40	1.4	2.9	1.1	1.4	0.18	1.5	0.39	1.9	0.04	0.64	0.58	
28	VerBa6	Mean	5.7	nq	nd	11	505	245	126	22	3.7	7.0	23	12	8.2	17	26	1011
		S	0.37			0.15	32	17	4	0.34	0.18	0.64	0.97	0.70	0.34	0.12	2.9	
29	VinBa6	Mean	1.3	3.1	0.95	5.1	39	21	25	17	3.4	7.3	33	12	6.1	30	23	227
		S	0.12	0.07	0.01	0.20	1.4	2.8	1.4	1.0	0.33	0.21	1.3	0.55	0.01	0.09	0.28	

Abbreviations—gal: gallic acid; caft: caffeic acid; cout: coumaric acid; epicat: epicatechin; epicatgal: epicatechin gallate; myr gluc: myricetin-3-O-glucoside; polyd: polydatin; q 3-O-gal/glucur/rut: quercetin 3-O-galactoside/quercetin 3-O-glucuronide/quercetin 3-O-galactoside; q 3-O-gluc: quercetin 3-O-glucoside; lar 3-O-gluc: laricitrin 3-O-glucoside; kaemp 3-O-gluc: kaempferol 3-O-glucoside; isorhm 3-O-gluc: isorhamnetin 3-O-glucoside; syr 3-O-gluc: syringetin-3-O-glucoside; nd: not detected (concentration sample < detection limit); nq: not quantified (detection limit < concentration sample < quantification limit).

flavan-3-ols, 9 flavonols and polydatin. Their total concentration ranged from 184 mg kg⁻¹ of Brancelho (Quinta Barreiros, 2006) to 1378 mg kg⁻¹ of Borraçal (Quinta da Facha, 2005), both from Ponte de Lima.

The major non-coloured phenolic determined in the samples showed higher variability than anthocyanins in relation with the variety, origin and harvest; although for some varieties it was independent of the harvest such as Borraçal, Brancelho, Doçal and Rabo de Ovelha. The major compounds were: catechin (<51%), myricetin-3-O-glucoside (<37%), epicatechin (<32%), syringetin-3-O-glucoside (<23%) or quercetin-3-O-glucoside (<22%). The rest of the compounds were found in lower levels of 17%. If the different classes of compounds are considered, flavonols (11–88%) or flavan-3-ols (0–87%) were the most represented groups while phenolic acids were the minor ones (1.2–11%).

The major compounds described in the references were also different according to the variety of grape studied and even the part of the grape (pomace, skin, complete grape) analysed: epicatechin [20], quercetin-3-O-glucuronide [19,22], quercetin-3-O-glucoside [19,32], the mixture quercetin-3-O-glucoside/quercetin-3-O-rutinoside [22] or myricetin-3-O-glucoside [19]. Flavan-3-ols or flavonols were also the most abundant group depending on the type of grape studied [22].

PCA for non-coloured compounds yields four principal components with eigenvalues greater than 1 accounting for 78.2% of the total variance in the data (Table 4). Considering the scree plot only two components were retained, that account for 58.3% of the total variance. The first PC (41.5% of the variance) was correlated positively with all the compounds except the flavan-3-ols, being flavan-3-ols and the flavonols syringetin-3-O-glucoside and laricitrin-3-O-glucoside the compounds of highest weight. PC2 (16.8%) was correlated positively with the flavan-3-ols epicatechin and epicatechin gallate, caftaric and coumaric acids, polydatin and the flavonols derivatives of quercetin, kaempferol and isorhamnetin and negatively with the rest (Fig. 5).

Samples appeared grouped due to their different phenolic profile (Fig. 6): on the left of the PC1 appeared the samples with the

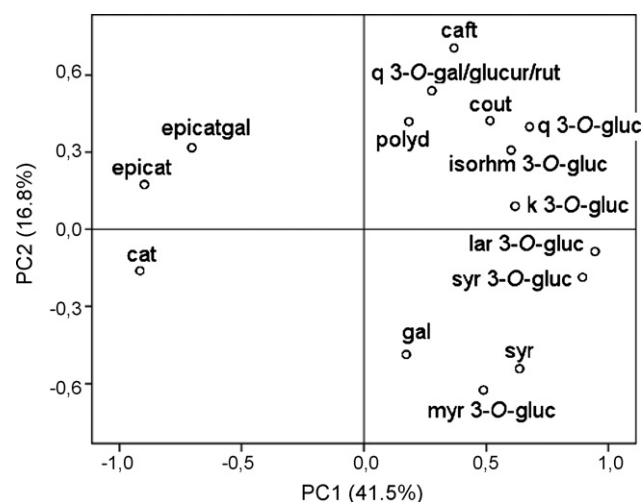


Fig. 5. Principal component analysis of non-coloured phenolics in red “Vinho Verde” grapes: loadings plot.

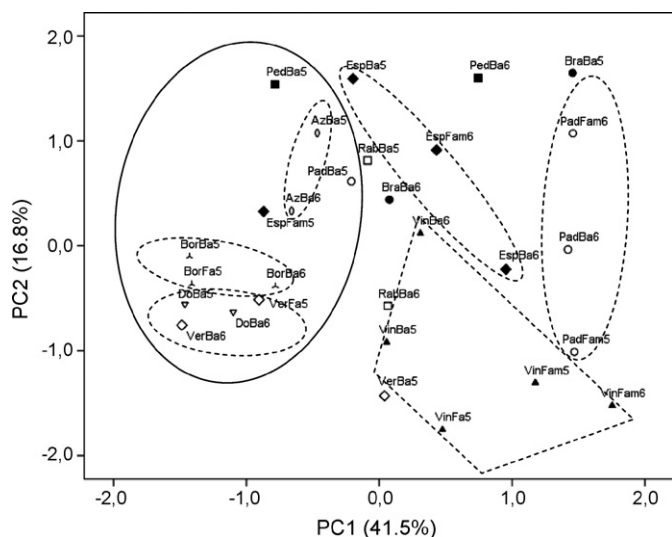


Fig. 6. Principal component analysis of non-coloured phenolics in red "Vinho Verde" grapes: scores plot.

highest percentages of flavan-3-ols, Doçal (76–86%), Verdelho (69–87%), Borraçal (65–85%) and Azal Tinto (56–60%), and on the right the samples with lower percentages of flavan-3-ols: Padeiro de Basto with the highest percentages of flavonols (73–88%), especially of quercetin; Vinhão with the highest values of myricetin-3-*O*-glucoside (7.3–37%) and Espadeiro, Rabo de Ovelha, and Brancelho. In general, samples harvested in 2006 showed higher percentages of flavonols than those harvested in 2005. It is noted that samples that show the highest values of myricetin-3-*O*-glucoside are also rich in laricitrin-3-*O*-glucoside and syringetin-3-*O*-glucoside what can be explained because the last two compounds are obtained from the first one (laricitrin and syringetin are, respectively, the 3'-methoxy and 3',4'-dimethoxy derivatives of myricetin) [17].

Although anthocyanin profile has shown to be more useful to characterize the varieties of the red "Vinho Verde" grapes, some relationships between the different varieties and their composition could be observed for both non-coloured phenolics and anthocyanin profiles that are interesting because the character-

istics of the wine depend strongly on the composition of the grapes.

3.3.3. Global analysis

Fig. 7 shows the concentration of total phenolics and the percentage of non-coloured compounds and anthocyanins found for each grapes sample. Total concentration of phenolics ranged from 381 mg kg⁻¹ of the sample Brancelho to 12282 mg kg⁻¹ of the sample Vinhão, both from Quinta do Barreiro (2005). The percentage of anthocyanins was between 42% of Brancelho and 97% of Vinhão. Usually the samples with lower contents in total phenolics showed also lower percentages of anthocyanins and the samples with higher content in total phenolics were also richer in anthocyanins. So, the highest contents in phenolic compounds and percentages of anthocyanins were shown by Vinhão samples whereas that the lowest ones were shown by Brancelho, Espadeiro, Borraçal and Pedral varieties.

PCA was applied to the global data set, both anthocyanin and non-coloured compound, expressed as percentage in weight regarding the sum of total phenolics. Although the analysis yields five PCs (84.5%) only two PCs (58.9%) were retained into the model after checking the scree plot: PC1 39.7% and PC2 19.2%. PC1 was correlated positively with all the non-coloured phenolics and with the anthocyanins peonidin-3-*O*-glucoside and the *p*-coumaroyl derivatives and negatively with the rest of anthocyanins. PC2 was correlated positively with all the compounds, except syringic acid, the flavan-3-ols and the *p*-coumaroyl derivatives (Fig. 8).

Two groups of samples appeared clearly differentiated of the rest (Fig. 9): Vinhão and Espadeiro. Vinhão grapes showed the highest content in anthocyanins (92–97%) and the lowest content in non-coloured phenolics, while Espadeiro grapes showed the highest contents in *p*-coumaroyl derivatives (17–29%) and flavan-3-ols (10–31%). Between these two groups, the rest of the samples appeared distributed according to their composition, being closer the samples of the same variety. So, for example, Padeiro, Rabo de Ovelha and Azal Tinto were rich in glucoside anthocyanins but with higher contents in flavonols and flavan-3-ols than Vinhão.

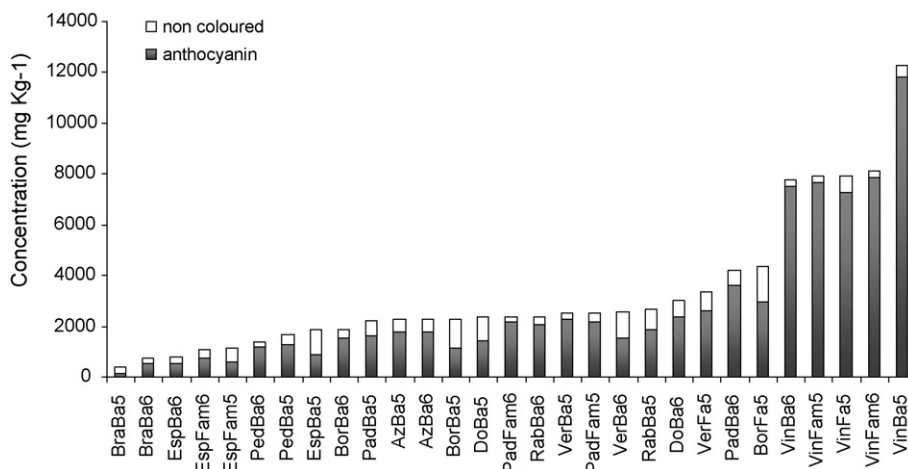


Fig. 7. Total concentration of phenolic compounds expressed as the sum of anthocyanin and non-coloured phenolics (mg kg⁻¹) in the red "Vinho Verde" grapes.

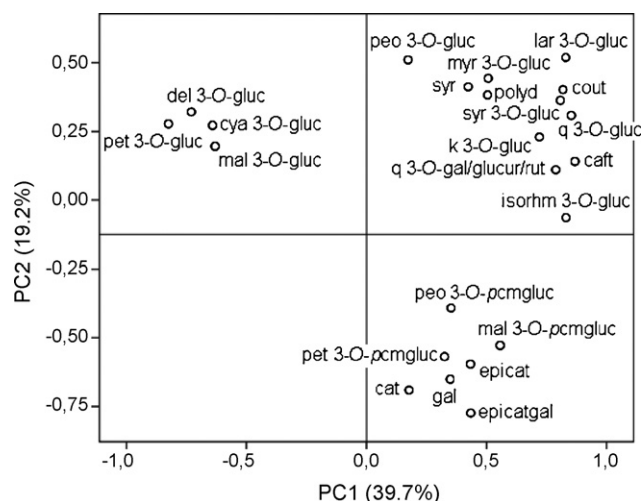


Fig. 8. Principal component analysis of all analysed phenolic compounds in red “Vinho Verde” grapes: loadings plot.

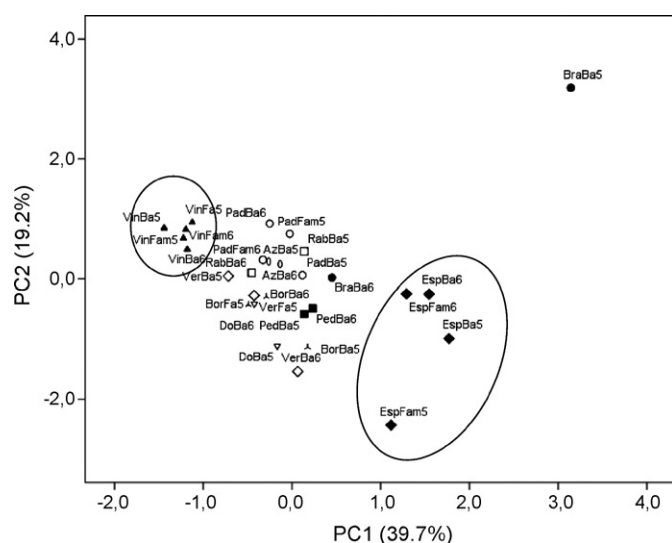


Fig. 9. Principal component analysis of all analysed phenolic compounds in red “Vinho Verde” grapes: scores plot.

If the PCA is applied to the phenolics distribution (flavonols, flavan-3-ol, phenolic acids, polydatin, glucoside anthocyanin and *p*-coumaroylglucoside anthocyanin) instead of the individual compounds, a similar plot is obtained (data not shown), with two PCs that account for 76.5% of the variance explained, which suggest that groups of compounds are also suitable to characterize the varieties of samples although they do not show so detailed information.

4. Conclusions

In summary, two extractive methods previously described in the bibliography were compared to choose which was able to determine the highest number of phenolic compounds, both coloured and non-coloured, from red “Vinho Verde” grapes, and the selected method was that described by Kammerer et al. [14]. Besides, the described chromatographic method was

slightly modified in order to simplify the analytic conditions for the non-coloured fraction.

Phenolic profiles of both non-coloured phenolics and anthocyanins were obtained for red “Vinho Verde” grapes of 10 different varieties, grown in 3 different geographical locations and harvested in two consecutive years. The most abundant compounds found were malvidin-3-*O*-glucoside for anthocyanins, and the flavan-3-ols catechin and epicatechin or the flavonols myricetin-3-*O*-glucoside, syringetin-3-*O*-glucoside and quercetin-3-*O*-glucoside for non-coloured phenolics. Proportion of anthocyanins ranged from 42 to 97%.

Analysis of the results by using multivariate techniques showed that anthocyanin profile was more independent of origin and harvest than non-coloured phenolics profile. PCA of anthocyanin compounds accounted for higher variability (70.4% with two PCs determining eight compounds) than the PCA of non-coloured compounds (58.9% determining 15 compounds). Besides, these analyses showed more clearly the relationship among the samples and their composition to carry out the characterization of the different varieties according to their higher content in flavan-3-ols, flavonols, glucoside anthocyanins or *p*-coumaroyl anthocyanins: Vinhão grapes were clearly differentiated by their high content in anthocyanins (97%) with levels of phenolic compounds until 16 times higher than the rest of the samples. Espadheiro grapes showed the highest content in *p*-coumaroyl derivatives of anthocyanins and flavan-3-ols.

Acknowledgments

M.S. Dopico-García is indebted to the Fundação para a Ciência e a Tecnologia (SFRH/BPD/21757/2005) for her grant. L. Guerra is indebted to the Fundação para a Ciência e a Tecnologia for his BIC grant (POCI/AGR/57399/2004).

References

- [1] B. Halliwell, in: C. Rice-Evans (Ed.), *Wake up to flavonoids*. International Congress and symposium Series, 226, Royal Society of Medicine Press, UK, 2000, pp. 13–23.
- [2] A. Van de Wiel, P.H.M. Van Golde, H.Ch. Hart, *Eur. J. Int. Med.* 12 (2001) 484.
- [3] R.S. Jackson, *Wine Science—Principles, Practice, Perception*, 2nd ed., Academic Press, New York, 1994, pp. 544–577.
- [4] E. Revilla, E. García-Beneytez, G. Martín-Ortega, J.M. Ryan, *J. Chromatogr. A* 915 (2001) 53.
- [5] F. Pomar, M. Novo, A. Masa, *J. Chromatogr. A* 1094 (2005) 34.
- [6] C.A. Williams, R.J. Grayer, *Nat. Prod. Rep.* 21 (2004) 539.
- [7] J.C. Rivas-Gonzalo, S. Bravo-Haro, C. Santos-Buelga, *J. Agric. Food Chem.* 43 (1995) 1444.
- [8] E.M. Francia-Aracha, M.T. Guerra, J.C. Rivas-Gonzalo, C. Santos-Buelga, *J. Agric. Food Chem.* 45 (1997) 2262.
- [9] I. Revilla, S. Pérez-Magariño, M.L. González-SanJosé, S. Beltrán, *J. Chromatogr. A* 847 (1999) 83.
- [10] T. Escribano-Baylón, M. Álvarez-García, J.C. Rivas-Gonzalo, F.J. Heredia, C. Santos-Buelga, *J. Agric. Food Chem.* 49 (2001) 1213.
- [11] N. Mateus, A.M.S. Silva, J.C. Rivas-Gonzalo, C. Santos-Buelga, V. De Freitas, *J. Agric. Food Chem.* 51 (2003) 1919.
- [12] R. Boulton, *Am. J. Enol. Vitic.* 52 (2001) 67.
- [13] V. Núñez, M. Monagas, M.C. Gomez-Cordovés, B. Bartolomé, *Postharvest Biol. Technol.* 31 (2004) 69.

- [14] E. García-Beneytez, F. Cabello, E. Revilla, *J. Agric. Food Chem.* 51 (2003) 5622.
- [15] J.M. Ryan, E. Revilla, *J. Agric. Food Chem.* 51 (2001) 3372.
- [16] P.B. Andrade, G. Mendes, V. Falco, P. Valentão, R.M. Seabra, *Food Chem.* 73 (2001) 397.
- [17] F. Mattivi, R. Guzzon, U. Vrhovsek, M. Stefanini, R. Velasco, *J. Agric. Food Chem.* 54 (2006) 7692.
- [18] R. Rodríguez Montealegre, R. Romero Peces, J.L. Chacón Vozmediano, J. Martínez Gascueña, E. García Romero, *J. Food Comp. Anal.* 19 (2006) 687.
- [19] N. Castillo-Muñoz, S. Gómez-Alonso, E. García-Romero, I. Hermosín-Gutiérrez, *J. Agric. Food Chem.* 55 (2007) 992.
- [20] E. Pastrana-Bonilla, C.C. Akoh, S. Sellappan, G. Krewer, *J. Agric. Food Chem.* 51 (2003) 5497.
- [21] J. Oszmianski, J.Y. Lee, *Am. J. Enol. Vitic.* 41 (1990) 204.
- [22] E. Cantos, J.C. Espín, F.A. Tomás-Barberán, *J. Agric. Food Chem.* 50 (2002) 5691.
- [23] E. Revilla, J.M. Ryan, *J. Chromatogr. A* 881 (2000) 461.
- [24] D. Kammerer, A. Claus, R. Carle, A. Schieber, *J. Agric. Food Chem.* 52 (2004) 4360.
- [25] J. Oszmianski, T. Ramos, M. Bourzeix, *Am. J. Enol. Vitic.* 39 (1998) 259.
- [26] M.S. Dopico-García, P. Valentão, L. Guerra, P.B. Andrade, R.M. Seabra, *Anal. Chim. Acta* 583 (2007) 15.
- [27] M.S. Dopico-García, P. Valentão, A. Jagodzińska, J. Klepczyńska, L. Guerra, P.B. Andrade, R.M. Seabra, *Talanta* 74 (2007) 20–31.
- [28] J.J. Castillo-Sánchez, J.C. Mejuto, J. Garrido, S. García-Falcón, *Food Chem.* 97 (2006) 130.
- [29] J.X. Castillo-Sánchez, M.S. García-Falcón, J. Garrido, E. Martínez-Carballo, L.R. Martins-Dias, X.C. Mejuto, *Food Chem.* 106 (2008) 18.
- [30] Comissão de viticultura da região dos Vinhos Verdes <http://www.vinhoverde.pt/>.
- [31] J. Sun, F. Liang, Y. Bin, P. Li, C. Duan, *Molecules* 12 (2007) 679.
- [32] V. Amico, E.M. Napoli, A. Renda, G. Ruberto, C. Spatafora, C. Tringali, *Food Chem.* 88 (2004) 599.
- [33] H. Wang, E.J. Race, A.J. Shrikhande, *J. Agric. Food Chem.* 51 (2003) 7989.
- [34] J. Burns, P.T. Gardner, D. Matthews, G.G. Duthie, M.E.J. Lean, A. Crozier, *J. Agric. Food Chem.* 49 (2001) 5797.
- [35] G.E. Pereira, J.P. Gaudillere, P. Pieri, G. Hilbert, M. Maucourt, C. Deborde, A. Moing, D. Rolin, *J. Agric. Food Chem.* 54 (2006) 6765.
- [36] P. Ribéreau-Gayon, *Les composés phénoliques des végétaux*, Dunod, Paris, 1968, pp. 142–172.
- [37] J.P. Roggero, S. Coen, B. Ragonnet, *Am. J. Enol. Vitic.* 37 (1986) 77.
- [38] G. Ramis Ramos and M.C. García Álvarez-Coque, *Quimiometría para Química Analítica, Síntesis*, Madrid, 2001, pp. 157–197.

Resonance Rayleigh scattering, second-order scattering and frequency doubling scattering methods for the indirect determination of penicillin antibiotics based on the formation of $\text{Fe}_3[\text{Fe}(\text{CN})_6]_2$ nanoparticles

Hui Duan, Zhongfang Liu, Shaopu Liu*, Aoer Yi

School of Chemistry and Chemical Engineering, Southwest University, Chongqing 400715, China

Received 25 October 2007; received in revised form 15 January 2008; accepted 15 January 2008

Available online 20 January 2008

Abstract

Under the HCl solution and heating condition, penicillin antibiotics such as amoxicillin (AMO), ampicillin (AMP), sodium cloxacillin (CLO), sodium carbenicillin (CAR) and sodium benzylpenicillin (BEN) could react with Fe(III) to produce Fe(II) which further reacted with $\text{Fe}(\text{CN})_6^{3-}$ to form a $\text{Fe}_3[\text{Fe}(\text{CN})_6]_2$ complex. By virtue of hydrophobic force and Van der Waals force, the complex aggregated to form $\text{Fe}_3[\text{Fe}(\text{CN})_6]_2$ nanoparticles with an average diameter of 45 nm. This resulted in a significant enhancement of resonance Rayleigh scattering (RRS) and non-linear scattering such as second-order scattering (SOS) and frequency doubling scattering (FDS). The increments of scattering intensity (ΔI) were directly proportional to the concentrations of the antibiotics in a certain range. The detection limits for the five penicillin antibiotics were 2.9–6.1 ng ml^{-1} for RRS method, 4.0–6.8 ng ml^{-1} for SOS method and 7.4–16.2 ng ml^{-1} for FDS method, respectively. Among them, the RRS method exhibited the highest sensitivity and the AMO system was more sensitive than other antibiotics systems. Based on the above researches, a new highly sensitive and simple method for the indirect determination of penicillin antibiotics has been developed. It can be applied to the determination of penicillin antibiotics in capsule, tablet, human serum and urine samples. In this work, the spectral characteristics of absorption, RRS, SOS and FDS spectra, the optimum conditions of the reaction and the influencing factors were investigated. In addition, the reaction mechanism was discussed. © 2008 Elsevier B.V. All rights reserved.

Keywords: Resonance Rayleigh scattering; Second-order scattering; Frequency doubling scattering; Penicillin antibiotics; $\text{Fe}_3[\text{Fe}(\text{CN})_6]_2$ nanoparticles

1. Introduction

Penicillins developed from benzylpenicillin belong to 6-aminopenicillanic acid (6-APA) derivatives of the β -lactam antibiotics. They kill bacteria by restraining the formation of cell wall via inhibiting mucopeptide transpeptidase [1,2]. The drugs have high selectivity and low toxicity because they are adiphorous to human cells which do not have cell wall. Owing to the extensive application of these drugs in clinic [3], it is significant for pharmaceutical analysis and clinical control to further develop a new method for the determination of penicillin antibiotics.

Various methods such as high-performance liquid chromatography (HPLC) [4], spectrophotometry [5–7], fluorescence

method [8,9], chemiluminescence [10] and capillary electrophoresis [11], etc. were reported for the determination of penicillin antibiotics. Among them, HPLC was very useful for the determination of trace penicillin antibiotics in some complicated samples [12,13], but it needed complex pretreatments. Spectrophotometric methods have been applied in the determination of penicillin antibiotics because of its simplicity. However, the sensitivities were not high enough to determine the antibiotics for trace analysis. Some other reported methods such as fluorescence [8] and chemiluminescence [10] methods also have some deficiencies in the sensitivity, selectivity or simplicity. So, it is necessary to develop a more sensitive, simple and selective method for the determination of penicillin antibiotics.

In recent years, resonance Rayleigh scattering (RRS), as a new analytical technique, has drawn much more attention. It has been applied to the analysis of biomacromolecules, organic compounds, pharmaceuticals and inorganic ions [14–16]. In studying RRS of the systems, the strong scattering of light is

* Corresponding author. Tel.: +86 23 68252748; fax: +86 23 68254000.
E-mail address: liusp@swu.edu.cn (S. Liu).

observed at double and half wavelength of the incident light. The former is well known very much and is named as “second-order scattering (SOS)”. As it may interfere with fluorimetric measurements, SOS is always eliminated as a harmful phenomenon. For the latter, because the frequency of this radiation is double that of the incident light, this radiation can be named “frequency doubling scattering (FDS)” or “hyper Rayleigh scattering (HRS)”. As its wavelength is far shorter than that of the incident light, this radiation was seldom noticed and studied in analytical chemistry for a long time. Recent researches indicated that the two kinds of scattering were the non-linear optical phenomena [17,18] produced by some substances (e.g. nanoparticles). Early in 1995, we already studied them as a new spectroscopic phenomenon [19], which showed that they could be applied successfully to the study of nanoparticles [20], and determination of inorganic ions [21], biological macromolecules [22] and some physical chemistry parameters as a new analytical technique [23].

Amoxicillin (AMO), ampicillin (AMP), sodium cloxacillin (CLO), sodium carbenicillin (CAR) and sodium benzylpenicillin (BEN) were penicillin antibiotics that applied extensively in clinic. Our experiment found that under the HCl solution and heating condition, they could react with Fe(III) to produce Fe(II) which further reacted with $\text{Fe}(\text{CN})_6^{3-}$ to form a $\text{Fe}_3[\text{Fe}(\text{CN})_6]_2$ complex. By virtue of hydrophobic force and Van der Waals force, the complex aggregated to form nanoparticles with an average diameter of 45 nm, which not only resulted in a change of absorption spectra, but also led to a significant enhancement of resonance Rayleigh scattering, second-order scattering and frequency doubling scattering. In this work, the spectral characteristics of absorption, RRS, SOS and FDS spectra and the reaction conditions and the influencing factors were investigated. The results indicated that the three scattering methods exhibited high sensitivities and the RRS method had the lowest detection limit of 2.9–6.1 ng ml^{-1} for the determination of the five antibiotics. The sensitivities of the scattering methods are higher than those of common spectrophotometry [7], fluorescence method [9], HPLC [4] and chemiluminescence [10]. A new highly sensitive and simple method for the indirect determination of penicillin antibiotics has been developed based on the above studies. It can be applied to the determination of penicillin antibiotics in capsule, tablet, human serum and urine samples.

2. Experimental

2.1. Apparatus

A Hitachi F-2500 spectrofluorophotometer (Tokyo) was used for measuring the scattering intensities with the slits (EX/EM) of 2.5/2.5 nm (RRS) and 5.0/5.0 nm (SOS and FDS). A UV-8500 spectrophotometer (Shanghai) was used for recording the absorption spectra. The DHT type miniature mixing electrothermal set (Shandong) was used for heating. HITACHI-600 transmission electron microscopy (TEM, Electronic Company of Japan) was used to observe the appearance and size of nanoparticles.

2.2. Materials and reagents

200 $\mu\text{g ml}^{-1}$ stock solution of penicillins such as amoxicillin (Huamei Biology Technique Co.), ampicillin (Huamei Biology Technique Co.), sodium cloxacillin (Huabei Pharmacy), sodium carbenicillin (Huamei Biology Technique Co.) and sodium benzylpenicillin (Huabei Pharmacy) were prepared. The working solution of 20 $\mu\text{g ml}^{-1}$ was prepared by diluting the stock solution. $3.0 \times 10^{-3} \text{ mol l}^{-1}$ of Fe(III) was prepared by dissolving 0.1446 g $\text{NH}_4\text{Fe}(\text{SO}_4)_2 \cdot 12\text{H}_2\text{O}$ in 1 ml concentrated H_2SO_4 and diluting it to 100 ml. $3.0 \times 10^{-3} \text{ mol l}^{-1}$ of $\text{Fe}(\text{CN})_6^{3-}$ was prepared by dissolving 0.2468 g $\text{K}_3\text{Fe}(\text{CN})_6$ in 250 ml distilled water. The concentration of HCl was 0.1 mol l^{-1} . All the reagents used were of analytical reagent (A.R.) grade and doubly distilled water was used throughout.

2.3. General procedure

Into a 10.0 ml calibrated flask were added certain amount of penicillin antibiotics, 1.0 ml of HCl solution (0.01 mol l^{-1} for AMO and CAR, 0.0125 mol l^{-1} for CLO, 0.015 mol l^{-1} for AMP and BEN, respectively) and 0.4 ml $3.0 \times 10^{-3} \text{ mol l}^{-1}$ Fe(III). The solution was heated in a boiling water bath for 25 min and cooled to room temperature, then added 0.2 ml $3.0 \times 10^{-3} \text{ mol l}^{-1}$ $\text{Fe}(\text{CN})_6^{3-}$. Finally, it was diluted to the mark and mixed thoroughly. In 15 min, the RRS spectra were recorded with synchronous scanning at $\lambda_{\text{ex}} = \lambda_{\text{em}}$, and the SOS and FDS spectra were recorded by scanning at $\lambda_{\text{ex}} = 1/2\lambda_{\text{em}}$ and $\lambda_{\text{ex}} = 2\lambda_{\text{em}}$, respectively. The scattering intensity I_{RRS} , I_{SOS} and I_{FDS} for the reaction product and I_{RRS}^0 , I_{SOS}^0 and I_{FDS}^0 for the reagent blank at their maximum wavelengths were measured, $\Delta I = I - I_0$, the absorption spectra were recorded simultaneously.

3. Results and discussion

3.1. The absorption spectra

Fe(III) could be reduced by penicillin antibiotics to produce Fe(II) [24] which further reacted with $\text{Fe}(\text{CN})_6^{3-}$ to form $\text{Fe}_3[\text{Fe}(\text{CN})_6]_2$ [25] resulting in a change of absorption spectra. From Fig. 1a, it shows that the absorption of reaction products of the five penicillin antibiotics with Fe(III) could not be observed in visible light region and its maximum absorption wavelength was located at 255–350 nm of ultraviolet region, and the maximum absorption wavelength of $\text{Fe}(\text{CN})_6^{3-}$ under experimental condition was 303 nm. When the reduced product Fe(II) reacted with $\text{Fe}(\text{CN})_6^{3-}$, a new absorption peak at 738 nm was observed (Fig. 1b) and the spectral characteristic was consistent with that of $\text{Fe}_3[\text{Fe}(\text{CN})_6]_2$. At 738 nm, the molar absorptivities (ϵ) are $2.3 \times 10^4 \text{ l mol}^{-1} \text{ cm}^{-1}$ (AMO), $1.6 \times 10^4 \text{ l mol}^{-1} \text{ cm}^{-1}$ (CAR), $1.4 \times 10^4 \text{ l mol}^{-1} \text{ cm}^{-1}$ (AMP and BEN), $1.0 \times 10^4 \text{ l mol}^{-1} \text{ cm}^{-1}$ (CLO), respectively. So, this reaction was useful as a basis for the determination of penicillin antibiotics by visible spectrophotometry with the sensitivity of four times higher than that of spectrophotometric method based on the oxidization of Fe(III) [24].

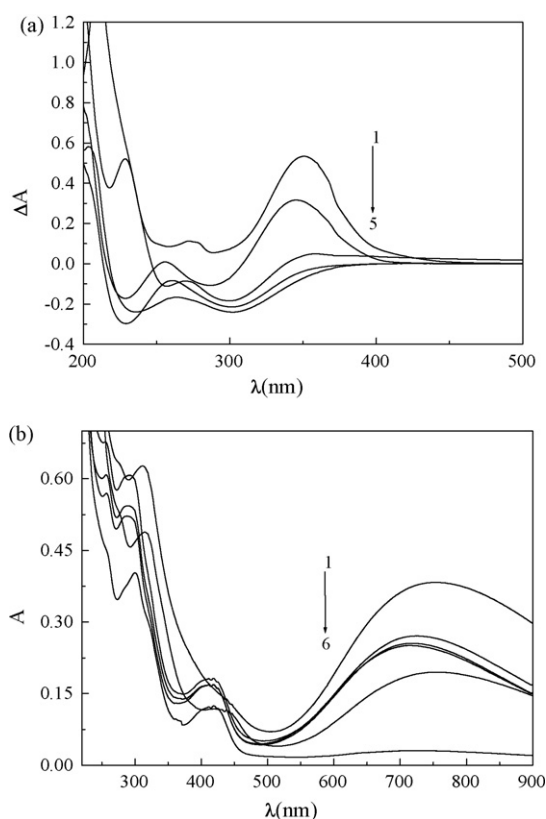


Fig. 1. Absorption spectra. (a) Absorption spectra of penicillins–Fe(III) (measured against the reagent blank). 1, AMO; 2, AMP; 3, CLO; 4, BEN; 5, CAR. (b) Absorption spectra of penicillins–Fe(III)–Fe(CN) $_6^{3-}$ (measured against water blank). 1, AMO; 2, CAR; 3, AMP; 4, BEN; 5, CLO; 6, Fe(III)–Fe(CN) $_6^{3-}$. All concentrations of the antibiotics: $6.0 \mu\text{g ml}^{-1}$; concentration of Fe(III): $1.2 \times 10^{-4} \text{ mol l}^{-1}$; concentration of Fe(CN) $_6^{3-}$: $0.6 \times 10^{-4} \text{ mol l}^{-1}$.

3.2. RRS spectra

The RRS spectra of the five systems are shown in Fig. 2a. It can be seen that Fe(III)–Fe(CN) $_6^{3-}$ and the five penicillin antibiotics have faint RRS peaks under the optimum conditions. When Fe(III) was reduced by the antibiotics to produce Fe(II) in a HCl medium and Fe(II) further reacted with Fe(CN) $_6^{3-}$ to form Fe $_3$ [Fe(CN) $_6$] $_2$, RRS intensities were enhanced greatly. The reaction products have similar spectral characteristics, and the maximum peaks are located at about 341 nm. The RRS intensity of AMO–Fe(III)–Fe(CN) $_6^{3-}$ is the highest among the five systems. From Fig. 2b, it is clear that the RRS intensity (ΔI_{RRS}) is directly proportional to the concentrations of antibiotics. So, the RRS method can be applied to the determination of penicillin antibiotics.

3.3. Second-order scattering and frequency double scattering (FDS) spectra

Fig. 3A and B shows the spectra of SOS and FDS for the investigated antibiotics–Fe(III)–Fe(CN) $_6^{3-}$ systems, respectively. Here, λ_1 was the incident wavelength and λ_s was the scattering wavelength. The intensities of SOS and FDS changed with the difference of incident wavelengths. When λ_1/λ_s was

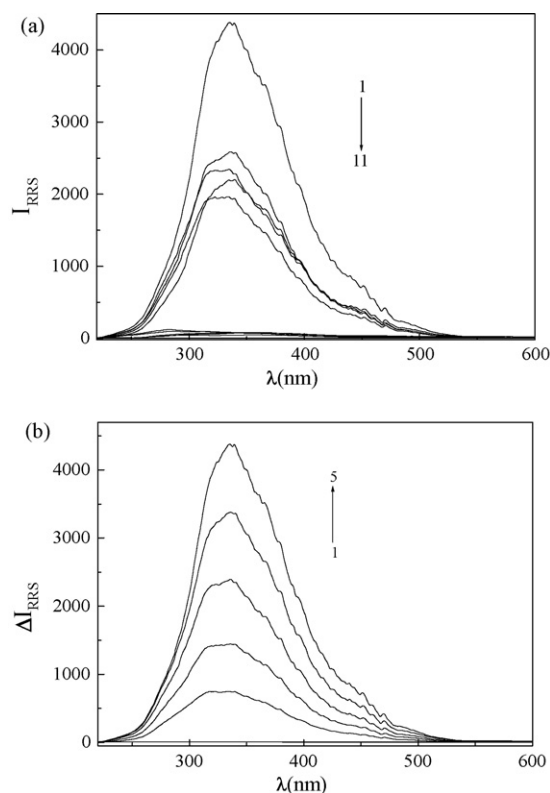


Fig. 2. Resonance Rayleigh scattering spectra. (a) Fe(III)–Fe(CN) $_6^{3-}$ –penicillins system. 1, AMO–Fe(III)–Fe(CN) $_6^{3-}$; 2, CAR–Fe(III)–Fe(CN) $_6^{3-}$; 3, AMP–Fe(III)–Fe(CN) $_6^{3-}$; 4, BEN–Fe(III)–Fe(CN) $_6^{3-}$; 5, CLO–Fe(III)–Fe(CN) $_6^{3-}$; 6, Fe(III)–Fe(CN) $_6^{3-}$; 7, AMP; 8, AMO; 9, CLO; 10, CAR; 11, BEN. All concentrations of the antibiotics: $2.0 \mu\text{g ml}^{-1}$; concentration of Fe(III): $1.2 \times 10^{-4} \text{ mol l}^{-1}$; concentration of Fe(CN) $_6^{3-}$: $0.6 \times 10^{-4} \text{ mol l}^{-1}$. (b) Fe(III)–Fe(CN) $_6^{3-}$ –amoxicillin system. Concentrations of AMO (from 1 to 5): $0.4 \mu\text{g ml}^{-1}$, $0.8 \mu\text{g ml}^{-1}$, $1.2 \mu\text{g ml}^{-1}$, $1.6 \mu\text{g ml}^{-1}$, $2.0 \mu\text{g ml}^{-1}$, respectively. Concentration of Fe(III): $1.2 \times 10^{-4} \text{ mol l}^{-1}$; concentration of Fe(CN) $_6^{3-}$: $0.6 \times 10^{-4} \text{ mol l}^{-1}$.

$320/640 \text{ nm}$, the intensity of SOS reached the highest, and when λ_1/λ_s was $780/390 \text{ nm}$ the intensity of FDS reached the highest. In this condition, the two kinds of scattering intensities (ΔI_{SOS} and ΔI_{FDS}) were directly proportional to the concentrations of the antibiotics in a certain range. Therefore, the SOS and FDS method can be applied to the determination of the investigated antibiotics.

3.4. Sensitivity of the method

Through constructing the calibration graphs of ΔI versus the concentrations of the antibiotics, the linear ranges, correlation coefficients and detection limits of RRS, SOS and FDS methods for the determination of the five penicillin antibiotics were investigated. The results showed that the linear ranges were $0.010\text{--}2.4 \mu\text{g ml}^{-1}$ for the RRS method, $0.013\text{--}3.6 \mu\text{g ml}^{-1}$ for the SOS method and $0.024\text{--}3.6 \mu\text{g ml}^{-1}$ for the FDS method (as shown in Table 1). The detection limits (3σ) were $2.9\text{--}6.1 \text{ ng ml}^{-1}$ for the RRS method, $4.0\text{--}6.8 \text{ ng ml}^{-1}$ for the SOS method and $7.4\text{--}16.2 \text{ ng ml}^{-1}$ for the FDS method, respectively. Among them, the RRS method

Table 1
Parameters of calibration graphs for the determination of penicillin antibiotics

Method	System	Regression equation, C ($\mu\text{g ml}^{-1}$)	Correlation coefficient, r	Detect limits (ng ml $^{-1}$)	Linear range ($\mu\text{g ml}^{-1}$)
RRS	Amoxicillin–Fe(III)–Fe(CN) $_6^{3-}$	$\Delta I = -287.2 + 2372.5c$	0.9981	2.9	0.010–2.0
	Ampicillin–Fe(III)–Fe(CN) $_6^{3-}$	$\Delta I = 247.1 + 1255.4c$	0.9928	5.5	0.018–2.1
	Cloxacillin–Fe(III)–Fe(CN) $_6^{3-}$	$\Delta I = 165.7 + 1135.8c$	0.9957	6.1	0.021–2.3
	Benzylpenicillin–Fe(III)–Fe(CN) $_6^{3-}$	$\Delta I = 130.3 + 1188.7c$	0.9952	5.8	0.019–1.9
	Carbenicillin–Fe(III)–Fe(CN) $_6^{3-}$	$\Delta I = 158.2 + 1274.3c$	0.9961	5.4	0.018–2.4
SOS	Amoxicillin–Fe(III)–Fe(CN) $_6^{3-}$	$\Delta I = 48.8 + 150.7c$	0.9991	4.0	0.013–3.2
	Ampicillin–Fe(III)–Fe(CN) $_6^{3-}$	$\Delta I = -15.4 + 105.7c$	0.9998	5.6	0.019–3.0
	Cloxacillin–Fe(III)–Fe(CN) $_6^{3-}$	$\Delta I = 13.6 + 88.1c$	0.9991	6.8	0.023–3.6
	Benzylpenicillin–Fe(III)–Fe(CN) $_6^{3-}$	$\Delta I = -13.6 + 100.2c$	0.9982	6.0	0.020–2.8
	Carbenicillin–Fe(III)–Fe(CN) $_6^{3-}$	$\Delta I = -26.1 + 112.1c$	0.9992	5.4	0.018–3.4
FDS	Amoxicillin–Fe(III)–Fe(CN) $_6^{3-}$	$\Delta I = 15.2 + 68.6c$	0.9993	7.4	0.024–3.2
	Ampicillin–Fe(III)–Fe(CN) $_6^{3-}$	$\Delta I = -8.4 + 36.6c$	0.9988	13.9	0.046–3.0
	Cloxacillin–Fe(III)–Fe(CN) $_6^{3-}$	$\Delta I = 2.8 + 31.4c$	0.9996	16.2	0.054–3.6
	Benzylpenicillin–Fe(III)–Fe(CN) $_6^{3-}$	$\Delta I = 1.89 + 35.8c$	0.9992	14.2	0.047–2.8
	Carbenicillin–Fe(III)–Fe(CN) $_6^{3-}$	$\Delta I = 7.5 + 53.1c$	0.9993	9.6	0.032–3.4

had the highest sensitivity, which was not only 1–3 orders of magnitude higher than that of common spectrophotometry, but also higher than those of some fluorescence and chemiluminescence methods and even higher than that of HPLC with electrochemical detector by means of solid-phase extraction (see Table 2).

Therefore, the RRS method was taken as an example for the following studies including optimum conditions, influencing factors, effects of coexisted substances and analytical applications. The reaction mechanism was also discussed.

3.5. Optimum conditions for the reaction

3.5.1. Effect of heating time

The effects of temperature on the reaction were tested. The results showed that the redox reaction of investigated antibiotics with Fe(III) was slow, whereas elevation of temperature could accelerate the process of reaction, and the intensities of

scattering (ΔI_{RRS}) reached the maximum in 25 min in a boiling water bath.

3.5.2. Effect of acidity

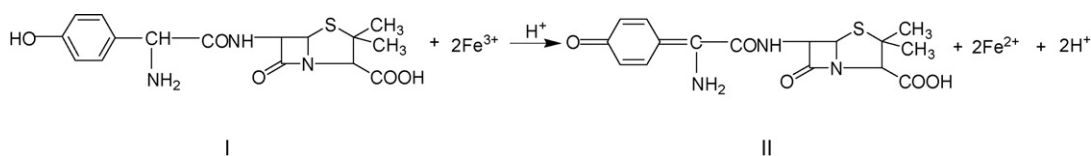
The effects of HCl concentrations on the RRS of five systems were investigated. The results shown in Fig. 4 revealed that the optimum concentrations of HCl were about 0.010 mol l $^{-1}$ (AMO and CAR systems), 0.015 mol l $^{-1}$ (AMP and BEN systems) and 0.0125 mol l $^{-1}$ (CLO system). So, the corresponding concentration of HCl was chosen as a reaction medium.

3.5.3. Effect of reagent's concentration

The results of Fe(III) and Fe(CN) $_6^{3-}$ concentration variation indicated that the maximum intensities of scattering would be obtained when the Fe(III) concentration was in a range of 0.9–1.5 $\times 10^{-4}$ mol l $^{-1}$. Therefore, 1.2 $\times 10^{-4}$ mol l $^{-1}$ Fe(III)

Table 2
Comparison of sensitivities for the determination of penicillin antibiotics between present methods and some other common methods

Method	Drug	Reagent	λ_{max} (nm)	Detection limit (ng ml $^{-1}$)	Reference
Spectrophotometry	Ampicillin	Mo(V)-thiocyanate	467	450	[5]
	Cloxacillin	Pyrocatechol violet	604	60	[6]
	Ampicillin	1,2-Naphthoquinone-4-sulfonic	463	1500	[26]
	Flucloxacillin	<i>p</i> -Nitrophenol	446	550	[27]
	Amoxicillin	Diazotized benzocaine	455	600	[7]
HPLC	Cloxacillin	Electrochemical detection		8	[4]
	Amoxicillin	UV detection	220	19	[28]
Fluorimetry	Ampicillin	Cu(II)	343/420 ($\lambda_{\text{ex}}/\lambda_{\text{em}}$)	148.6	[8]
	Amoxicillin	Ce(IV)	256/351 ($\lambda_{\text{ex}}/\lambda_{\text{em}}$)	288	[9]
Chemiluminescence	Amoxicillin	Ce(IV)-rhodamine 6G		10	[10]
	Amoxicillin	Fe(III)–Fe(CN) $_6^{3-}$	341/341 ($\lambda_{\text{ex}}/\lambda_{\text{em}}$)	2.9	This work
	Ampicillin	Fe(III)–Fe(CN) $_6^{3-}$	341/341 ($\lambda_{\text{ex}}/\lambda_{\text{em}}$)	5.5	This work
RRS method	Cloxacillin	Fe(III)–Fe(CN) $_6^{3-}$	341/341 ($\lambda_{\text{ex}}/\lambda_{\text{em}}$)	6.1	This work
	Carbenicillin	Fe(III)–Fe(CN) $_6^{3-}$	341/341 ($\lambda_{\text{ex}}/\lambda_{\text{em}}$)	5.8	This work
	Benzylpenicillin	Fe(III)–Fe(CN) $_6^{3-}$	341/341 ($\lambda_{\text{ex}}/\lambda_{\text{em}}$)	5.4	This work



Scheme 1.

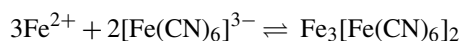
was chosen as the experimental concentration for the five systems. And the optimum concentration of $\text{Fe}(\text{CN})_6^{3-}$ was about $0.6 \times 10^{-4} \text{ mol l}^{-1}$. The ΔI_{RRS} decreased when the reagent concentrations were too low resulting in incomplete reaction, but the reagent concentrations were too high ΔI_{RRS} also decreased slightly due to the reagent blank I_0 increased.

3.6. The complexation and formation of nanoparticles

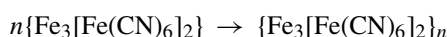
Taking the most sensitive AMO as an example, the interaction of investigated antibiotics with $\text{Fe}(\text{III})$ and $\text{Fe}(\text{CN})_6^{3-}$ and the structure of the products were studied.

In a acidic medium, $\text{Fe}(\text{III})$ was reduced by AMO(I) to give $\text{Fe}(\text{II})$ and the corresponding oxidized product of AMO [24] (Scheme 1).

$\text{Fe}(\text{II})$ further reacted with $\text{Fe}(\text{CN})_6^{3-}$ to form a $\text{Fe}_3[\text{Fe}(\text{CN})_6]_2$ complex:



$\text{Fe}_3[\text{Fe}(\text{CN})_6]_2$ as a charge neutralization complex has strong hydrophobicity. Under the extrusion action of water, they drew close to each other and further aggregated to form larger nanoparticles by Van der Waals force:



The diameter and shape of the formed nanoparticles were observed by transmission electron microscopy, and it was found that $\text{Fe}_3[\text{Fe}(\text{CN})_6]_2$ had already aggregated to form $\{\text{Fe}_3[\text{Fe}(\text{CN})_6]_2\}_n$ nanoparticles with an average diameter of 45 nm (see Fig. 5). Hence, it might be deduced that the formation of $\{\text{Fe}_3[\text{Fe}(\text{CN})_6]_2\}_n$ nanoparticles was the main reason for the enhancement of RRS, SOS and FDS.

3.7. Selectivity and analytical application of the method

3.7.1. Selectivity of the method

Under the optimum conditions, the effects of some coexisting substances on the determination of AMO ($1.0 \mu\text{g ml}^{-1}$) were investigated and the results were given in Table 3. As shown, when the relative error was $\leq \pm 5\%$, the large amounts of amino acids, saccharides, some vitamins, common inorganic ions (NH_4^+ , NO_3^- , Cl^- and SO_4^{2-}), metal ions (K^+ , Na^+ , Mn^{2+} , Mg^{2+} , Ca^{2+} , Zn^{2+} and Al^{3+}) and HSA do not interfere with the determination.

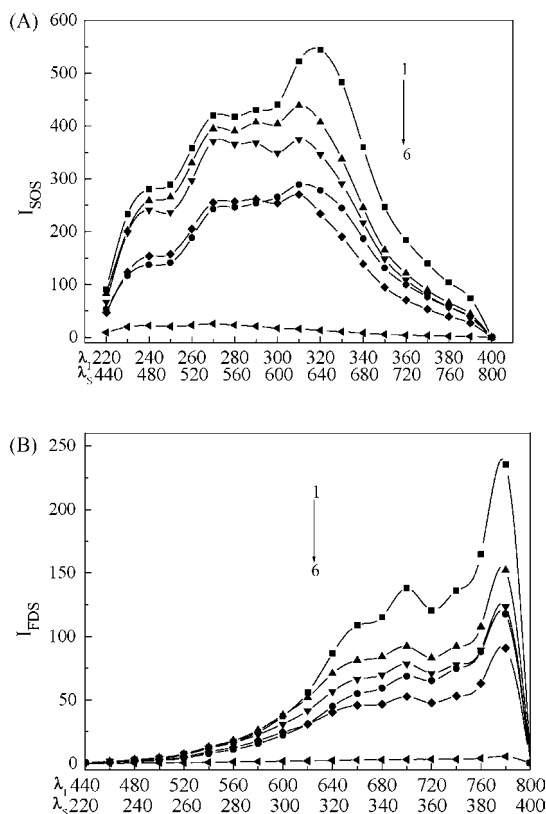


Fig. 3. SOS and FDS spectra. (A) SOS spectra of $\text{Fe}(\text{III})\text{--Fe}(\text{CN})_6^{3-}$ –penicillins; (B) FDS spectra of $\text{Fe}(\text{III})\text{--Fe}(\text{CN})_6^{3-}$ –penicillins; 1, AMO– $\text{Fe}(\text{III})\text{--Fe}(\text{CN})_6^{3-}$; 2, CAR– $\text{Fe}(\text{III})\text{--Fe}(\text{CN})_6^{3-}$; 3, AMP– $\text{Fe}(\text{III})\text{--Fe}(\text{CN})_6^{3-}$; 4, BEN– $\text{Fe}(\text{III})\text{--Fe}(\text{CN})_6^{3-}$; 5, CLO– $\text{Fe}(\text{III})\text{--Fe}(\text{CN})_6^{3-}$; 6, $\text{Fe}(\text{III})\text{--Fe}(\text{CN})_6^{3-}$; 7, AMP; 8, AMO; 9, CLO; 10, CAR; 11, BEN. All concentrations of the antibiotics: $2.0 \mu\text{g ml}^{-1}$; concentration of $\text{Fe}(\text{III})$: $1.2 \times 10^{-4} \text{ mol l}^{-1}$; concentration of $\text{Fe}(\text{CN})_6^{3-}$: $0.6 \times 10^{-4} \text{ mol l}^{-1}$.

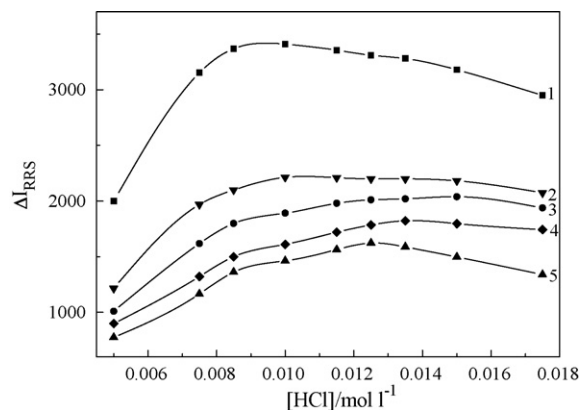


Fig. 4. Effect of HCl concentration on ΔI_{RRS} . 1, AMO– $\text{Fe}(\text{III})\text{--Fe}(\text{CN})_6^{3-}$; 2, CAR– $\text{Fe}(\text{III})\text{--Fe}(\text{CN})_6^{3-}$; 3, AMP– $\text{Fe}(\text{III})\text{--Fe}(\text{CN})_6^{3-}$; 4, BEN– $\text{Fe}(\text{III})\text{--Fe}(\text{CN})_6^{3-}$; 5, CLO– $\text{Fe}(\text{III})\text{--Fe}(\text{CN})_6^{3-}$. All concentrations of the antibiotics: $2.0 \mu\text{g ml}^{-1}$.

Table 3
Results for the determination of amoxicillin in capsules and tablets

Method	Sample	Label claim (g per capsule or tablet)	Found (g per capsule or tablet)	Mean (g per capsule or tablet)	R.S.D (%)	Recovery (%)
RRS	Capsules	0.250	0.248, 0.253, 0.252, 0.248, 0.257	0.252	1.6	100.8
	Tablets	0.250	0.263, 0.258, 0.256, 0.247, 0.252	0.255	2.4	102.0
SOS	Capsules	0.250	0.243, 0.241, 0.254, 0.257, 0.252	0.249	2.8	99.6
	Tablets	0.250	0.263, 0.242, 0.245, 0.263, 0.255	0.254	3.8	101.6
FDS	Capsules	0.250	0.247, 0.249, 0.252, 0.256, 0.253	0.251	1.4	100.4
	Tablets	0.250	0.269, 0.253, 0.246, 0.243, 0.261	0.254	3.9	101.6
Pharmacopoeia [29]	Capsules	0.250	0.236, 0.241, 0.246	0.241	2.0	96.4
	Tablets	0.250	0.256, 0.250, 0.247	0.251	1.8	100.4

Table 4
Results for the determination of amoxicillin in urine and serum samples

Method	Sample	Found ($\mu\text{g ml}^{-1}$)	Added ($\mu\text{g ml}^{-1}$)	Mean, $n=5$ ($\mu\text{g ml}^{-1}$)	R.S.D, $n=5$ (%)	Recovery, $n=5$ (%)
RRS	Urine 1	ND	1.50	1.50	2.5	100.0
	Urine 2	2.52	0.50	3.00	1.3	99.3
SOS	Urine 1	ND	1.50	1.51	3.5	100.7
	Urine 2	2.49	0.50	2.99	1.1	100.0
FDS	Urine 1	ND	1.50	1.52	2.0	101.3
	Urine 2	2.48	0.50	3.01	0.8	101.0
RRS	Serum 1	ND	0.60	0.59	4.0	98.3
	Serum 2	ND	1.20	1.20	3.2	100.0
SOS	Serum 1	ND	0.60	0.61	2.8	101.7
	Serum 2	ND	1.20	1.21	3.2	100.8
FDS	Serum 1	ND	0.60	0.60	3.7	100.0
	Serum 2	ND	1.20	1.19	2.0	99.2

ND: not detected. Urine 2: Fresh urine samples taken from healthy people who had oral administration of amoxicillin capsules 3 h before.

3.7.2. Analytical application

Determination of AMO in capsule and tablet. The contents of five capsules (250 mg per capsule) were emptied and weighed carefully. Suitable amount of the powder (containing about 16 mg of the drug) was dissolved and transferred into a 100.0 ml

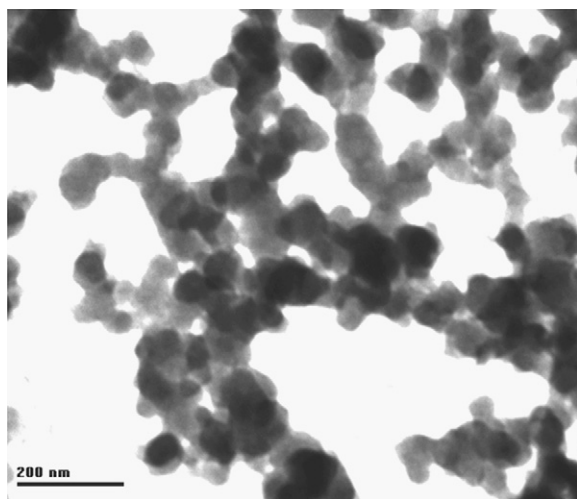


Fig. 5. TEM image of $\{\text{Fe}_3[\text{Fe}(\text{CN})_6]_2\}_n$ nanoparticles. Concentration of AMO: $2.0 \mu\text{g ml}^{-1}$; concentration of Fe(III): $1.2 \times 10^{-3} \text{ mol l}^{-1}$; concentration of $\text{Fe}(\text{CN})_6^{3-}$: $6.0 \times 10^{-4} \text{ mol l}^{-1}$.

volumetric flask. In addition, five tablets (250 mg per tablet) were powdered and a quantity of the powder (containing about 16 mg of the drug) was dissolved, filtrated and transferred into another 100.0 ml volumetric flask. The two flasks were diluted to the mark and mixed thoroughly, respectively. Then, the above solutions were diluted to the working solution. The concentration of AMO in the working solutions was determined according to the general procedure under the optimum conditions by RRS, SOS and FDS method. The results for the determination of capsules and tablets were listed in Table 3 and were in good agreement with those obtained by the standard method of The Pharmacopoeia of People's Republic of China (HPLC) [29].

Determination of AMO in human urine. Two kinds of fresh urine samples were taken. The one was taken from healthy people who took AMO capsules, and the other was taken from the healthy people without taking AMO capsules. Deproteinization was achieved by adding certain amounts of 10% trichloroacetic acid and centrifuging the mixture at 4500 rpm for 20 min. Then 5.0 ml aliquot of the supernatant fluid was taken into a 10.0 ml of calibrated flask for determining AMO concentration according to the general procedure. The accuracy was tested by a standard addition method. The recovery was 99.3–101.3% (see Table 4).

Determination of AMO in human serum. A 2.0 ml aliquot of fresh serum sample (healthy people) was treated with 0.5 ml 10% of trichloroacetic acid and was centrifuged at 4500 rpm for

20 min to eliminate proteins. Then 1.0 ml supernatant fluid was transferred into a 10.0 ml of calibrated flask for determining AMO concentration according to the general procedure. The accuracy was tested by a standard addition method. The recovery was 98.3–101.7% (see Table 4).

Acknowledgements

The work is supported by the National Natural Science Foundation of China (No. 20475045), and all authors here express their deep thanks.

References

- [1] National Medicine Supervisory Bureau of Ministry of Personnel in China, The Pharmaceutical Chemistry, Chinese Pharmaceutical Technique Press, Beijing, 2004, p. 165.
- [2] Q.D. You, The Pharmaceutical Chemistry, Chemical Industry Press, Beijing, 2004, p. 457.
- [3] R.L. Wang, Z.P. Yuan, Handbook of Chemical Products. Medicine, 3rd ed., Chemical Industry Press, Beijing, 1999, p. 3.
- [4] W.R. LaCourse, C.O. Dasenbrock, J. Pharm. Biomed. Anal. 19 (1999) 239.
- [5] G.G. Mohamed, J. Pharm. Biomed. Anal. 24 (2001) 561.
- [6] A.S. Amin, Farmaco 56 (2001) 211.
- [7] S.M. El-Ashry, F. Belal, M.M. El-Kerdawy, D.R. El Wasseef, Mikrochim. Acta 135 (2000) 191.
- [8] A. Fernández-González, R. Badía, M.E. Díaz-García, Anal. Chim. Acta 484 (2003) 223.
- [9] A. Muñoz de la Peña, M.I. Acedo-Valenzuela, A. Espinosa-Mansilla, R. Sánchez-Maqueda, Talanta 56 (2002) 635.
- [10] S.L. Fan, L. Zhang, W.M. Mai, Z.H. Wu, Phys. Test. Chem. Anal. B: Chem. Anal. 39 (2003) 257.
- [11] S.M. Santos, M. Henriques, A.C. Duarte, V.I. Esteves, Talanta 71 (2007) 731.
- [12] L.K. Sørensen, L.K. Snor, Chromatographia 53 (2001) 367.
- [13] G. Valentina, D. Gyglielmo, Anal. Chim. Acta 483 (2003) 69.
- [14] R.F. Pasternack, P.J. Collings, Science 269 (1995) 935.
- [15] E.K. Wang, Advances in Analytical Chemistry, Science Press of China, Beijing, 2002, p. 280.
- [16] W. Lu, B.S. Fernández Band, Y. Yu, Q.G. Li, J.C. Shang, C. Wang, Y. Fang, R. Tian, L.P. Zhou, L.L. Sun, Y. Tang, S.H. Jing, W. Huang, J.P. Zhang, Microchim. Acta 158 (2007) 29.
- [17] M. Jacobsohn, U. Banin, J. Phys. Chem. 104 (2000) 1.
- [18] Y. Zhang, X. Wang, M. Ma, D.G. Fu, J.Z. Liu, M. Gu, Z.H. Lu, L. Xu, K.J. Chen, Chin. J. Inorg. Chem. 18 (2002) 1177.
- [19] S.P. Liu, Z.F. Liu, M. Li, Acta Chim. Sinica 53 (1995) 1178–1185.
- [20] Y.Q. He, S.P. Liu, L. Kong, Z.F. Liu, Spectrochim. Acta A 61 (2005) 2861.
- [21] S.P. Liu, Z.F. Liu, Z.L. Jiang, M. Li, X.F. Long, Acta Chim. Sinica 59 (2001) 1864.
- [22] S.P. Liu, Z. Yang, Z.F. Liu, L. Kong, Anal. Biochem. 353 (2006) 108.
- [23] N.B. Li, S.P. Liu, H.Q. Luo, Anal. Chim. Acta 472 (2002) 89.
- [24] H. Salem, G.A. Saleh, J. Pharm. Biomed. Anal. 28 (2002) 1205.
- [25] S.C. Chen, Important Inorganic Chemical Reactions, Shanghai Science Technique Press, Shanghai, 1982, p. 1019.
- [26] L.X. Xu, H.Y. Wang, Y. Xiao, Spectrochim. Acta A 60 (2004) 3007.
- [27] M.Y. El-Mamml, Spectrochim. Acta A 59 (2003) 771.
- [28] G. Hoizey, D. Lamiable, C. Frances, T. Trenque, M. Kaltenbach, J. Denis, H. Millart, J. Pharm. Biomed. Anal. 30 (2002) 661.
- [29] Editorial Committee of the Pharmacopeia of People's Republic of China, Pharmacopeia of People's Republic of China (Part II), Chemical Industry Press, Beijing, 2005, p. 297.

Investigation of biosensor signal bioamplification: Comparison of direct electrochemistry phenomena of individual Laccase, and dual Laccase-Tyrosinase copper enzymes, at a Sonogel-Carbon electrode

Mohammed ElKaoutit^a, Ignacio Naranjo-Rodriguez^a, Khalid Riffi Tamsamani^b, Manuel Domínguez^c, Jose Luis Hidalgo-Hidalgo de Cisneros^{a,*}

^a *Departamento de Química Analítica, Facultad de Ciencias, Universidad de Cádiz, Apdo. 40, 11510 Puerto Real, Cádiz, Spain*

^b *Departement de Chimie, Equipe de Recherche Electrochimie et Systèmes Interfaciaux, Faculté des Sciences de Tétouan, Université Abdelmalek Essaâdi, B.P. 2121, M'Hannech II-93002, Morocco*

^c *Departamento de Física de la Materia Condensada, Facultad de Ciencias, Universidad de Cádiz, Spain*

Received 31 July 2007; received in revised form 23 January 2008; accepted 24 January 2008

Available online 6 February 2008

Abstract

Direct electrochemistry of *Trametes versicolor* Laccase (LAC) was found at a Sonogel-Carbon electrode. The bioamplification, performed by dual immobilization of this enzyme and *Mushroom* Tyrosinase (TYR), of the bio-electrocatalytic reduction of O₂ was investigated. The calculated α transfer coefficients were 0.64 and 0.67, and the heterogeneous electron-transfer rate constants were 6.19 and 8.52 s⁻¹, respectively, for the individual LAC and dual LAC-TYR-based Nafion/Sonogel-Carbon bio-electrodes. The responses of the dual enzymes electrode to polyphenols were stronger than those of the individual LAC or TYR biosensors. Hypotheses are offered about the mechanism of bioamplification. The surfaces of the biosensors were also characterized by AFM.

© 2008 Elsevier B.V. All rights reserved.

Keywords: Dual enzymes based biosensor; Direct electrochemistry; Signal bioamplification; Sonogel-Carbon electrode

1. Introduction

To improve the sensitivity of biosensors based on polyphenoloxidase enzymes, several research groups have described different signal amplification approaches. Among these the addition of reducing, pre-concentrating molecules and/or the integration of pairs of enzymes on a single transducer are particularly notable. This last strategy is very interesting because it permits the sensitivity to be enhanced and the range of substrates detected to be increased [1–6]. Nevertheless, the mechanism of signal bioamplification underlying this strategy is not fully elucidated in the bibliography. One of the aims of this work is to contribute to the better understanding of this phenomenon.

Further, in addition to the study of the redox activity of proteins, investigation of the direct electron transfer (DET) between an electrode and a metalloenzyme is considered to be a highly attractive research area in the biosensors field. This is because of its potential application in the research and development of highly sensitive biosensors, effective biofuel cells, and selective routes of biosynthesis. Therefore, since the first reports on the DET between cytochrome *c* and bipyridyl-modified gold [7] or tin doped indium oxide [8] electrodes were communicated in 1977, a number of papers have been published giving detailed information on electrochemical reaction mechanisms of redox proteins and enzyme film at various types of electrode [9–13]. The electrode material may play a vital role in the production of a bio-electrochemical device able to access the desired information.

The carbon-based electrodes have been used widely as materials for studying metalloenzyme bio-electrocatalysis [13–20]. This preference possibly began from the fact that carbon can act as a primary electron donor to native electroactive site of

* Corresponding author. Tel.: +34 956 016355; fax: +34 956 016460.

E-mail address: jluishidalgo@uca.es (J.L. Hidalgo-Hidalgo de Cisneros).

enzymes [11]. Ceramic-carbon composite electrodes, made by mixing organic–inorganic sol–gel material and carbon powder, represent a new kind of carbon electrode. These composites are rigid, porous, and easily modifiable by chemical and biological recognition components [21,22].

Our group has made a significant contribution to this subject; we have devised a new method for fabricating these composites by applying high energy ultrasounds. The materials we have developed have been termed Sonogel-Carbon [23]. This matrix offers an alternative route for developing new composite sensors and biosensors with a wide variety of structures and shapes. It presents favourable electroanalytical properties when used for amperometric sensors and biosensors, as well as an excellent sensitivity compared to classical electrodes [24–26]. In this context, we report here the use of Sonogel-Carbon as a transducer for the investigation of the very interesting phenomenon of DET. Cyclic voltammograms of two biosensors based on enzymes with copper centres and Sonogel-Carbon are discussed in detail. The first biosensor is based on modification by Laccase, while the second is based on a dual Laccase and Tyrosinase enzymatic modification. Our research into signal bioamplification by mixing these enzymes in the same biosensor has demonstrated that this strategy cannot only affect the selectivity of the resulting bioprobe, but can also improve its sensitivity compared to that achieved with biosensors made from individual enzymes. This phenomenon has been demonstrated not only in the case when the analyte is typically a substrate of two enzymes, but also when the substrate is especially reactive with only one of them [27]. In the present paper, we try to give an explanation using the information obtained from the direct electrochemistry of the two biosensors; the anticipation of an explanatory mechanism is also provided.

2. Experimental

2.1. Reagents

Methyltrimethoxysilane (MTMOS) was obtained from Merck (Darmstadt, Germany) and HCl was obtained from Pan-reac (Barcelona, Spain). Graphite powder (spectroscopic grade RBW) was obtained from SGL Carbon (Ringsdorff, Germany). *Mushroom* Tyrosinase (E.C. 1.14.18.1, 3000 U mg⁻¹) and *Trametes versicolor* Laccase (E. C. 1. 10. 3. 2, 23.3 U mg⁻¹) were obtained from Fluka (Steinheim, Germany). KH₂PO₄/K₂HPO₄ and acetic acid/sodium acetate for phosphate or acetate buffer were acquired from Fluka (Buchs, Switzerland) and Merck (Darmstadt, Germany), respectively. Nafion-perfluorinated ion-exchange resin (Cat. No. 27, 470-4) 5% (w/v) in a mixture of lower aliphatic alcohols and water, and Glutaricdialdehyde, 25 wt% solution in water, were obtained from Aldrich (Steinheim, Germany). Pure water was obtained by passing twice-distilled water through a Milli-Q system (18 MΩ cm, Millipore, Bedford, MA). Phenolic compounds were of analytical grade and obtained from Merck, Sigma or Pan-reac.

Stock solutions of the phenolic compounds (0.1 mol L⁻¹) were prepared daily by dissolving the appropriate amount in

ethanol. Glass capillary tubes, i.d. 1.15 mm, were used as the bodies for the composite electrodes.

2.2. Apparatus

Electrochemical measurements were performed with an Autolab PGSTAT20 (Ecochemie, Utrecht, The Netherlands) potentiostat/galvanostat interfaced with a personal computer, using the AutoLab GPES software for waveform generation and data acquisition and elaboration.

A 600-W model, 20 kHz ultrasonic processor (Misonix Inc., Farmingdale, NY) equipped with a 13 mm titanium tip was used.

Surface topological studies were performed using an atomic force microscope (AFM) Veeco Nanoscope IIIa, in tapping mode. Phosphorus (*n*) doped silicon cantilevers, with spring constants in the range 20–80 N m⁻¹, were used. Calibration of the microscope was achieved by imaging calibration gratings supplied by the manufacturer. AFM images were examined for artifacts, and reproducibility was checked in the usual way, i.e. by changing the AFM cantilever and by either moving (during the experiment) the sample in the *X*- or *Y*-directions or by varying the scanning angle and frequency.

2.3. Methods

2.3.1. Electrochemical transducer preparation

The unmodified Sonogel-Carbon electrode was prepared as described previously [23,24]. Before modification, the electrodes were polished with emery paper No. 1200 to remove extra composite material, gently wiped with weighing paper, and electrochemically pre-treated by dipping them in 0.05 mol L⁻¹ sulphuric acid. Finally, they were polarized in the three-electrodes cell by voltage cycling from –0.5 to 1.5 V (five cycles). The electrodes with similar current background were selected, carefully washed with MilliQ water and let to dry at ambient temperature after their biological modification.

2.3.2. Biosensors fabrication

The dual LAC-TYR Sonogel-Carbon-based biosensor was fabricated as follows: adequate quantities of the enzymes LAC and TYR were dissolved in 30 μL of 0.2 mol L⁻¹ pH 6 phosphate buffer solutions. At this enzymatic solution, 1.25 μL of glutaricdialdehyde were added, set to polymerize in ultrasonic bath for 3 min, and modified by adding 3.5 μL of Nafion 5%. From the resulting solution, adequate quantities were deposited on the top of the Sonogel-Carbon electrodes with a μ-syringe and allowed to dry under ambient conditions. Finally, the resulting biosensors had 23–100 Units/Electrode of LAC and TYR, respectively, ≈ 0.9% of glutaricdialdehyde and 0.5% of Nafion. The same method was used to prepare individual LAC and TYR-based biosensors and the resulting bio-probes have 23 U and 100 Units/Electrode of LAC and TYR, respectively, and the same quantities of Nafion and glutaricdialdehyde as the dual bi-enzymatic biosensor. Before their use, all biosensors were dipped in stirred buffer solution for 15 min, to eliminate the

excess of non-absorbed enzymes, rinsed with the same buffered solution and stored immersed in the buffered solution at 4 °C when not in use.

2.4. Measurements

Cyclic voltammetry were carried out in an electrochemical cell containing 25 mL of an aerated 0.05 molL⁻¹ acetate buffer solution at pH 5; the three-electrodes system consisted of a enzyme-modified Sonogel-Carbon electrode as working electrode, and a Ag/AgCl (3 M KCl) and a platinum wire as reference and auxiliary electrodes, respectively. Potential range and scan rate are shown in the respective figures.

Tapping mode AFM measurements were performed over different regions of all samples to check for sample surface homogeneity. All AFM images selected to be shown here are representative of the sample's surface topology. For comparison, the scanned area is always 500 × 500 nm².

3. Results and discussion

3.1. Morphologies

As shown in Fig. 1, tapping mode AFM was used to evaluate the structure of the silica-based Sonogel material (a), the composite Sonogel-Carbon electrode (b), and the modification with Nafion alone (c) or with the mixtures of Nafion and individual

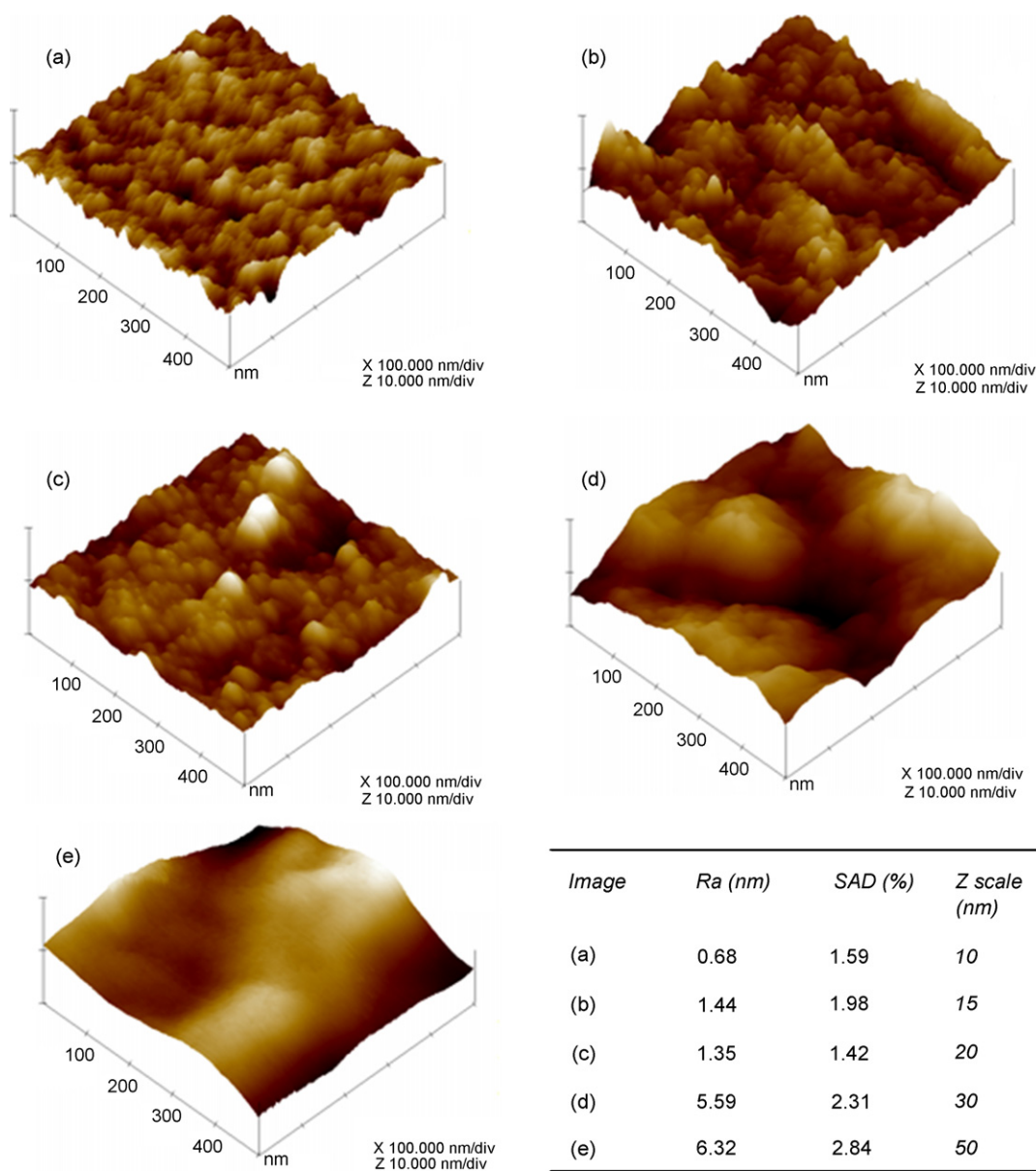


Fig. 1. FM images of (a) Sonogel; (b) Sonogel-Carbon Composite; (c) Sonogel-Carbon coated with 0.5% Nafion; (d) individual LAC-Nafion/Sonogel-Carbon; and (e) dual LAC-TYR-Nafion/Sonogel-Carbon biosensors. Note that the value of one Z-axis division increases from (a) to (e) and is always lower than in X and Y-axes (100 nm).

LAC (d) or dual LAC-TYR (e). The table in Fig. 1 shows the roughness (R_a) values for each of the images. This parameter is calculated by the AFM analysis software as the arithmetic average of the absolute values of the surface height deviations measured from the mean plane within the scanned area:

$$R_a = \frac{1}{n} \sum_{j=1}^n |z_j|$$

Additionally, the table shows the percentage of *surface area difference* (S.A.D.) between the three-dimensional area of the image and its projected two-dimensional area, expressed as:

$$\text{S.A.D.} = \left(\frac{\Sigma(\text{surface area})_i}{\Sigma(\text{projected area})_i} - 1 \right) \times 100$$

As seen in Fig. 1, films of the silica Sonogel (a) were dense, with pore sizes around 10 nm. Since the pores were of smaller size than the carbon particles, this result implies that, during the formation of the Sonogel-Carbon composite, the graphite particles do not get inside the silica pore; instead, the gel is formed around the graphite particles, and the conductivity of the final formed composite is promoted by a percolation mechanism between these particles. When Nafion was deposited (c) on the surface of the Sonogel-Carbon electrode (b), a slight decrease in the roughness and in surface area difference of the composite can be observed, but the same porous structure is conserved and a new granular aspect is generated for the composite. Bio-modification of the composite Sonogel-Carbon by a mixture of enzyme and Nafion produces a significant increase in the roughness, as well as a considerable gain in the surface area difference from 1.42% to 2.3–2.84%, while preserving the granular aspect due to Nafion, as shown in Fig. 1 (c–e). In addition, the AFM phase detection technique, applied to these three samples, does not show any significant differences over the entire surface, i.e., it must be homogeneous in composition. These results lead us to think that the enzyme may possibly be introduced inside the ionic cluster region of the Nafion.

3.2. Electrochemistry of dual LAC-TYR and individual LAC-based enzyme electrodes

Fig. 2 shows the current–potential curves firstly for bare and Nafion-coated Sonogel-Carbon, and lastly for LAC, TYR and dual LAC-TYR-based Sonogel-Carbon biosensors. As can be seen, the voltammogram of the TYR-based biosensor is similar to that of the Nafion-coated electrode; furthermore, when the scan rate is varied between 25 and 500 mV s^{-1} , this latter biosensor does not show any Faradaic current. For these reasons, we focussed all the studies on the individual LAC and dual LAC-TYR-based biosensors. The curves of the non bio-modified Sonogel-Carbon electrodes are almost flat, indicative of purely capacitive behaviour. The curves (voltammograms) of the LAC and LAC-TYR-based biosensors are different and manifest redox waves with a proportional increase in the capacitive current due to the enzymatic modification of the electrode. Reversible double-layer capacitance can be obtained from the relationship $C_{DL} = j/\nu$, where j is the current density in the

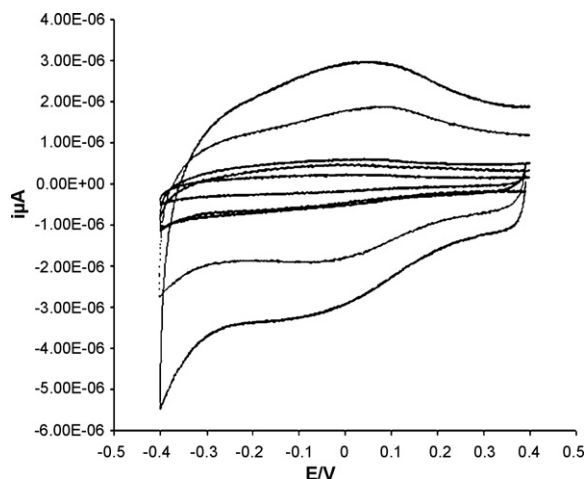


Fig. 2. Cyclic voltammograms of five electrodes (from inner to outer curves): Sonogel-Carbon, Nafion/Sonogel-Carbon, TYR-Nafion/Sonogel-Carbon, LAC-Nafion/Sonogel-Carbon, and LAC-TYR-Nafion/Sonogel-Carbon, respectively. Medium: aerated acetate pH 5 buffer solution. Scan rate: 200 mV s^{-1} .

plateau current regions and ν is the scan rate [28]. We have varied the scan rate from 50 to 500 mV s^{-1} for these four electrodes, and no current corresponding to Faradaic process has been found in the case of non bio-modified electrodes, contrary to the case of the biosensors. Furthermore, to calculate C_{DL} in the case of the biosensors, the Faradaic current was eliminated using a linear correction from the peak's beginning to its end. From the slope of the linear curve representing a limiting current density (for the same absolute cathodic and anodic values) versus scan rate, capacitance values were obtained for all cases as summarised in Table 1. An increase of capacitance with the degree of modification can be seen. So, the unmodified electrode shows the lowest capacitance and the electrodes modified with Nafion and the two enzymes show the highest capacitance value (i.e. 10 times higher than that of the unmodified electrode). These results are in accordance with the morphology study, and can be attributed to the limitation of charge movement through the modification layers, and to the changes in the active surface exposed to the electrolyte, as seen in the AFM studies.

3.3. Cyclic voltammetry behaviour in the absence of organic mediators

Laccase and Tyrosinase belong to the same family of oxidase enzymes with active copper centres. Laccase contains four copper atoms with different electron paramagnetic resonances: Type 1 or blue (T_1), Type 2 or normal (T_2), and Type

Table 1
Double-layer capacitances of Sonogel-Carbon and enzyme/Sonogel-Carbon electrodes

Electrodes	C_{DL} (mF cm^{-2})
Sonogel-Carbon	0.083 ± 0.06
Nafion/Sonogel-Carbon	0.236 ± 0.019
LAC-Nafion/Sonogel-Carbon	0.565 ± 0.102
LAC-TYR-Nafion/Sonogel-Carbon	0.959 ± 0.106

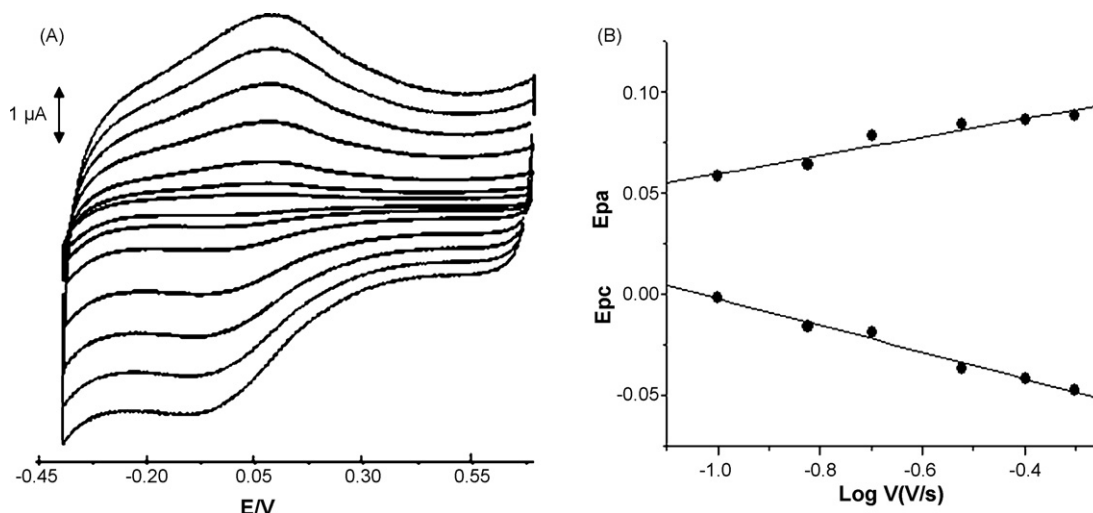


Fig. 3. (A) Effect of scan rate on the cyclic voltammograms (from inner to outer curves) of the LAC-Nafion/Sonogel-Carbon biosensor, from 100 to 500 mV s^{-1} . (B) Dependence of peak potentials versus scan rate in logarithmic scale. Conditions as in Fig. 1.

3 or coupled binuclear copper site (T_3), that catalyze the oxidation of hydrogen atom from the hydroxyl group of various aromatics, mainly the large number of phenolic compounds, polyamines, lignins and aryl diamines, as well as some inorganic ions, coupled to the reduction of molecular dioxygen to water [29]. It can be assumed that the donor substrates react initially near the T_1 and one electron is transferred to a T_2/T_3 cluster site where oxygen is reduced via four electrons exchange. Tyrosinase (monophenol monooxygenase) contains two copper T_3 type centres, and therefore catalyzes two different oxygen-dependent reactions: the *o*-hydroxylation of monophenols to *o*-diphenols (cresolase activity), and the successive oxidation of *o*-diphenols to *o*-quinones (catecholase activity) [30]. For special kinds of immobilization and electrode, LAC (of different origin) and TYR (from *Mushroom*) have demonstrated electrochemical activities without any mediator [11]. This electron transfer can be described as a tunnelling process between the enzyme catalytic centre and the electrode.

In this study, cyclic voltammetry was applied to illustrate the electron transfer between these multicopper enzymes and the surface of the Sonogel-Carbon electrode. Two biosensors have been compared in this respect, individual LAC/Sonogel-Carbon and a dual LAC-TYR/Sonogel-Carbon. As can be seen in the voltammograms of Fig. 2, redox processes were not observed for the uncoated or the Nafion-coated Sonogel-Carbon electrodes. In contrast, two redox peaks can be seen for the LAC/Sonogel-Carbon and LAC-TYR/Sonogel-Carbon bio-electrodes: the reduction/oxidation potential peaks are around -14 and 86 mV (vs. Ag/AgCl), with $\Delta E_p = 100$ mV and $E_m = 36$ mV, for the LAC-based biosensor, while the peaks are -131 and 3 mV, with $\Delta E_p = 116$ mV and $E_m = -64$ mV, for the dual LAC-TYR-based biosensor. The separation of peak values, much larger than 60 mV/n, prove the quasi reversible behaviour in the two electrocatalytic biosensors [28]. On the other hand, it can also be observed that the reduction currents start at 300 and 330 mV for LAC, and LAC-TYR-based biosensors, respectively; these val-

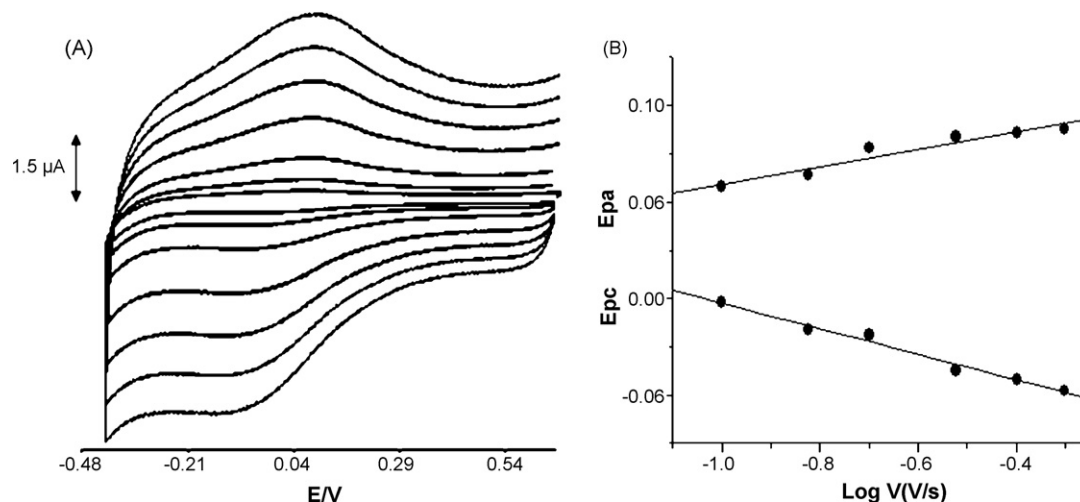


Fig. 4. (A) Effect of scan rate on the cyclic voltammograms (from inner to outer curves) of the dual LAC-TYR-Nafion/Sonogel-Carbon biosensor, from 50 to 500 mV s^{-1} . (B) Dependence of peak potentials versus scan rate in logarithmic scale. Condition as in Fig. 1.

ues are more negative than others reported for similar Laccase: around 550 mV at pH 3.5 for *Trametes Ochrasera*, and *Trametes Hirsuta* Laccases entrapped at a HOPG electrode surface [31], and around 450 mV at pH 5.5 for *Polyperous versicolor* Laccase adsorbed on the surface of a pyrolytic graphite electrode [16]. Moreover, the quasi-reversible couple that appears for our two biosensors is similar to that reported by Lee et al. [16], when 2,9-dimethylphenanthroline was added to the supporting electrolyte, and also similar to that shown for Laccase, from *Trametes Hirsuta*, immobilized on a bare gold electrode in aerated citrate–phosphate buffer at pH 4 [32].

Figs. 3(A) and 4(A), show, respectively, the cyclic voltammograms of the two biosensors at different scan rates, from 0.05 to 0.5 V s⁻¹. The anodic and cathodic peaks show linear increase in current intensity with scan rate, thus indicating a surface control electrode process (data not shown). The average covered surface can be calculated from the Faraday's law as follows: $Q = nFA\Gamma_m$; where Q is the integrated peak value, A is the surface electrode (0.0103 cm²), and n is the number of transferred electrons assumed equal to 4, so this is the number of electrons necessary to reduce the molecular oxygen near the T_2/T_3 cluster site of active enzymes. From the cathodic peaks recorded at a scan rate of 0.5 V s⁻¹, values of 1.7×10^{-10} and 1.9×10^{-10} mol cm⁻² for LAC and dual LAC-TYR-based Sonogel-Carbon biosensors, respectively, were obtained. These values are much higher than that obtained by a saturated pyrolytic graphite electrode surface with *Polyperous versicolor* Laccase [16], which indicates the performance of our immobilization matrix and electrode, taking into account the similar mass for the two Laccase enzymes (about 70 kDa).

The most important parameter for use as a criterion in investigating the bioamplification procedure is the electron-transfer rate constant k_{ET} , which quantifies the direct electron-transfer efficiency in the two cases. Laviron's model [33] for a diffusionless electrochemical system has been used to determine this parameter, which makes it possible to deduce the transfer coefficient and the rate constant of an electrochemical reaction from the experimental study of the variation of the potential peak as a function of the scan rate. Figs. 3(B) and 4(B), show the linear dependence of the anodic and cathodic potential peaks on scan rate in logarithmic scale. According to the Laviron's criterion, when $n\Delta E_p > 200$ mV, the transfer coefficient α can be determined from the slope of the representation $E_p = f(\log(\nu))$ which equals $-2.3RT/\alpha nF$ and $2.3RT/(1-\alpha)nF$ for the cathodic and anodic peaks, respectively, and k_{ET} can be obtained from the following equation:

$$\log(k_{ET}) = \alpha \log(1 - \alpha) + (1 - \alpha) \log(\alpha) - \log\left(\frac{RT}{nF\nu}\right) - \alpha(1 - \alpha) \frac{nF\Delta E_p}{2.3RT}$$

From these, we calculated $\alpha = 0.64$ and $k_{ET} 6.19 \text{ s}^{-1}$ for the Laccase biosensor, and 0.67 and 8.52 s^{-1} for the dual enzymes biosensor. As expected, the bioamplification does not affect the transfer coefficient and possibly reflects that the active sites present in the dual enzymes layer and in the individual enzyme

layer do not differ qualitatively between the two cases. In addition, the k_{ET} values reported here for both cases are close to those obtained with *Coriolus versicolor* Laccase monolayer covering a pyrocarbon surface electrode [15], and lower than that obtained with Laccase, from the same origin, immobilized on highly dispersed colloidal graphite or carbon black [19].

3.4. Effect of organic mediator

Fig. 5(A), shows the voltammograms of the two biosensors when a 0.5 mM concentration of gallic acid was added in the electrochemical cell. As expected, the shape of the voltammograms changes completely from the unmediated voltammograms: the change can be summarised as the shift of the oxido-reduction peaks to positive potentials, and the appearance of the catalytic wave at a potential beyond -50 mV. The current collected in the catalytic wave, the origin of which is the reduction of the enzymatic product, is larger in the case of the dual enzymes modification than that obtained for the individual Laccase modification, and indicative of the signal bioamplification. Moreover, it is important to note that gallic acid is not an ideal substrate for Tyrosinase. Thus, in our investigation in this context, we found that the sensitivity of the LAC-based biosensor to gallic acid is 100 times stronger than that shown by the TYR-based biosensor and the response of the dual electrode is stronger than the sum of the responses of individual LAC and TYR-based biosensors [27].

Although this amplification has already been reported, the mechanism has not yet been adequately elucidated. Our results, especially the E_m potential, the average of covered surface and the calculated k_s for the two biosensors, may demonstrate that this amplification can also be manifested in catalytic bioelectroreduction of oxygen as well as in the DET manifested in all cases.

In the catalytic cycle of the two enzymes, oxygen is reduced to water without the intermediate formation of hydrogen peroxide [32]. Furthermore, it has been demonstrated that the presence of H₂O₂ increases the oxy-Tyrosinase content for Tyrosinase and the peroxide-level intermediate for Laccase [29]. Based on these findings, a speculative explanation of this signal amplification has been reported, in the generation of H₂O₂ between the two enzymes [2,6]. To check this assumption, we added peroxide to the solution in the case of TYR and LAC-based individual enzyme electrodes. In the presence of gallic acid no significant changes in the current was observed in the voltammogram for the individual TYR-based biosensor, because of the low sensitivity of this enzyme to gallate, although in the presence of catechol, as prototype substrate of this enzyme, the current registered at potential of -200 mV was amplified by approximately 30% compared with that without peroxide, and the irreversible peak was not changed, as seen in Fig. 5(B). On the other hand, the voltammograms for the individual LAC biosensor in the presence of gallic acid and peroxide displayed significant changes, as shown in Fig. 5(C). These changes are an amplification of the current of the peaks, the displacement of their potentials, and the variation in the waveform with an increase in the catalytic current up to the potential of about -200 mV.

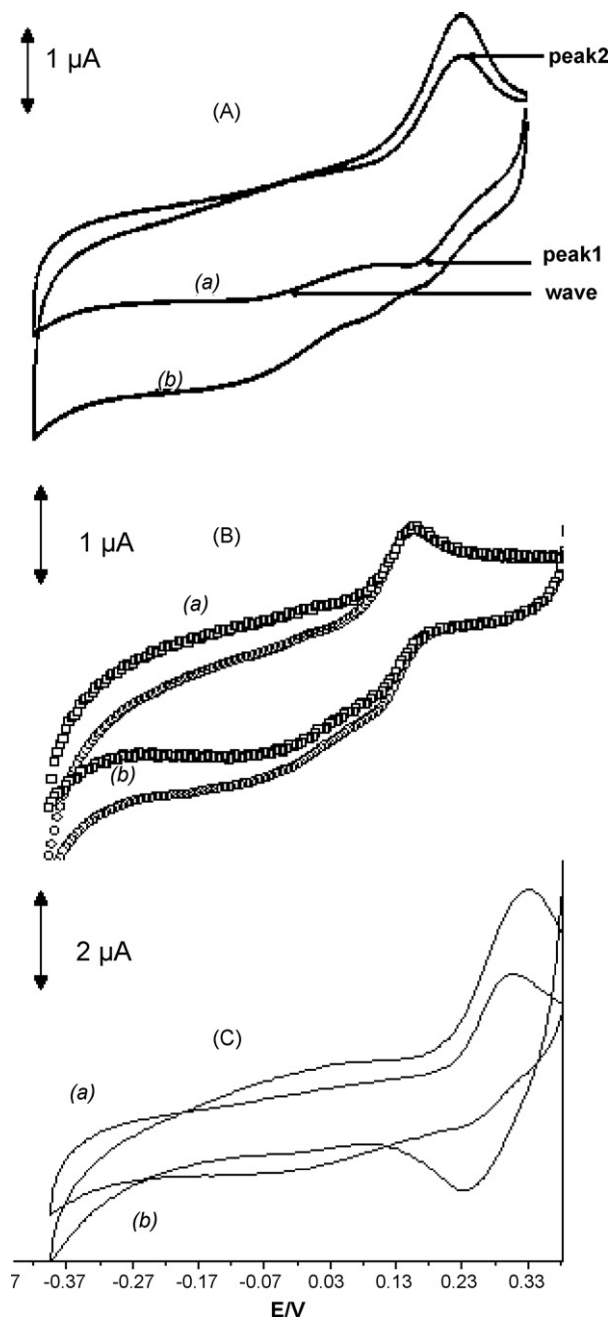


Fig. 5. Cyclic voltammograms of: [A] LAC-Nafion/Sonogel-Carbon (a), dual LAC-TYR-Nafion/Sonogel-Carbon (b) in absence of peroxide, [B] TYR-Nafion/Sonogel-Carbon in absence (a) and presence (b) of peroxide, and [C] LAC-Nafion/Sonogel-Carbon in absence (a) and presence (b) of peroxide. Condition: aerated acetate pH 5 buffer solution, 0.01 mM of peroxide for [B] and [C], 0.5 mM gallic acid for [A] and [C], and 0.5 mM of catechol for [B], scan rate 100 mV s^{-1} .

These results confirm a relative favourable effect on the catalytic cycle of the two enzymes, depending on the nature of the substrate, although this is not sufficient to give a clear response to the question: At what stage of the catalytic cycles of the enzymes does the peroxide have this effect? Nor do the results illustrate unequivocally the mechanism of the signal amplification in the case of dual enzymes electrode.

However, considering all the collective results accumulated in this research, we can postulate three hypotheses. The first hypothesis is that the generation of peroxide, which is also observed in the catalyzed TYR system, increases the intermediate peroxide-level in the LAC cycle, and this promotes a reduction of oxygen by this enzyme; the amplification of the parameter in the DET and the increase in the current of the peaks observed in Fig. 5(C) serve as the basis for this hypothesis. The second hypothesis is that the effectiveness of the TYR biocatalysis is promoted by a radical phenol, as well as by the peroxide generated by LAC; the relatively favourable effect of H_2O_2 on the catalytic wave in Fig. 5(B) is proof of that. Finally, simple explanations could be based on the data obtained in the characterization study of the surface and/or the use of the crosslinkage procedure to immobilize the enzymes in both biosensors. The increase in the protein quantity in the dual biosensor compared to that used for the individual one conserving the same percentage of glutaraldehyde can protect the enzymes from the undesirable desnaturation caused by inter-crosslinkage phenomena and also increase the sensitivity of the resulting biosensor. The roughness, together with the considerable gain in the surface area, demonstrated for the dual enzyme-based sensor (see table in Fig. 1) might be advantageous for mass transfer or for redox cycle-based amplification. In an attempt to confirm this third possible explanation, amperometric measurements were performed with three biosensors (TYR, LAC, and dual enzyme-based biosensors) in the presence of Ferulic acid. No response was obtained for the TYR-based biosensor, as a consequence of the ortho-occupation in this substrate; nevertheless, bioamplification phenomenon was observed in the case of the dual enzymes based biosensor, with an increase in the sensitivity and a decrease in the apparent Michaelis–Menten constant, when compared with the response of the individual Laccase biosensor.

Although the definitive confirmation of one of these mechanisms is not easy, the use of a multi-transducer could help to elucidate it, especially by proving the two first explanations, but this strategy is considerably limited by the distance between the active centres of the two different enzyme-based biosensors [6].

Acknowledgements

The authors are grateful to the FEDER (Fondo Europeo de Desarrollo Económico y Regional) and the Ministerio de Educación y Ciencia of Spain (Project CTQ2007-6753/BQU), to the Junta de Andalucía for financial support, and to the Agencia Española de Cooperación Internacional (AECI) for a grant to Mohammed ElKaoutit.

References

- [1] A.I. Yaropolov, A.N. Kharybin, J. Emnéus, G. Marko-Varga, L. Gorton, *Anal. Chim. Acta* 308 (1995) 137.
- [2] S. Cosnier, I.C. Popescu, *Anal. Chim. Acta* 319 (1996) 145.
- [3] S.C. Chang, K. Rawson, C.J. McNeil, *Biosens. Bioelectron.* 17 (2002) 1015.
- [4] R.S. Freire, S. Thongngamdee, N. Durán, J. Wang, L.T. Kubota, *Analyst* 127 (2002) 258.
- [5] D. Quan, Y. Kim, W. Shin, *Bull. Korean. Chem. Soc.* 25 (2004) 1195.

- [6] H. Notsu, T. Tatsuma, *J. Electroanal. Chem.* 566 (2004) 379.
- [7] M.J. Eddowes, H.A.O. Hill, *J. Chem. Soc. Chem. Commun.* (1977) 771.
- [8] P. Yeh, T. Kuwama, *Chem. Lett.* (1977) 1145–1148.
- [9] L. Gordon (Ed.), *Biosensors and Modern Biospecific Analytical Techniques*, Elsevier, Amsterdam, 2005, Ch. 5.
- [10] F.A. Armstrong, H.A.O. Hill, N.J. Walton, *Acc. Chem. Res.* 21 (1988) 407.
- [11] S. Shleev, J. Tkac, A. Christenson, T. Ruzgas, A.I. Yaropolov, T.W. Whitaker, L. Gorton, *Biosens. Bioelectron.* 20 (2005) 2517.
- [12] A. Christenson, N. Dimcheva, E.F. Ferapontova, L. Gorton, T. Ruzgas, L. Stoica, S. Shleev, A.I. Yaropolov, D. Haltrich, R.N.F. Thornely, S.D. Aust, *Electroanalysis* 16 (2004) 1074.
- [13] E.E. Ferapontova, *Electroanalysis* 16 (2004) 1101.
- [14] M.R. Tarasevich, Y.G. Chirkov, V.B. Bogdanovskaya, A.V. Kapustin, *Electrochem. Acta* 51 (2005) 418.
- [15] M.A. Osina, V.A. Bogdanovskaya, B.N. Efremov, *Russ. J. Electrochem.* 38 (2002) 1082.
- [16] C.W. Lee, H.B. Gray, F.C. Anson, B.G. Malmström, *J. Electroanal. Chem.* 172 (1984) 289.
- [17] I.V. Berezin, V.A. Bogdanovskaya, S.D. Varfolomeev, M.R. Tarasevich, A.I. Yaropolov, *Dokl. Akad. Nauk SSSR* 240 (1978) 615.
- [18] M.R. Tarasevich, A.I. Yaropolov, V.A. Bogdanovskaya, S.D. Varfolomeev, *Bioelectrochem. Bioenerg.* 6 (1979) 393.
- [19] M.R. Tarasevich, V.A. Bogdanovskaya, L.N. Kuznetsova, *Russ. J. Electrochem* 37 (2001) 833.
- [20] C.E.W. Hahn, H.A.O. Hill, M.D. Ritchie, J.W. Sear, *J. Chem. Soc., Chem. Commun* (1990) 125.
- [21] M. Tsionsky, G. Gun, V. Glezer, O. Lev, *Anal. Chem.* 66 (1994) 1747.
- [22] G. Oskan, P.C. Searson, *J. Phys. Chem. B* 102 (1998) 2464.
- [23] J.L. Hidalgo-Hidalgo de Cisneros, M.M. Cordero-Rando, I. Naranjo-Rodríguez, O.E. Blanco, F.L. Esquivias, Patent P200100556, Spain, March 2001.
- [24] M.M. Cordero-Rando, J.L. Hidalgo-Hidalgo de Cisneros, E. Blanco, I. Naranjo-Rodríguez, *Anal. Chem.* 74 (2002) 2423.
- [25] M.M. Cordero-Rando, I. Naranjo-Rodríguez, J.M. Palacios-Santander, L.M. Cubillana-Aguilera, J.L. Hidalgo-Hidalgo de Cisneros, *Electroanalysis* 17 (2005) 806.
- [26] M. El Kaoutit, I. Naranjo-Rodríguez, K.R. Tamsamani, J.L. Hidalgo-Hidalgo de Cisneros, *Biosens. Bioelectron.* 22 (2007) 2958.
- [27] M. ElKaoutit, I. Naranjo-Rodríguez, K.R. Tamsamani, M.D. De la Vega, J.L. Hidalgo-Hidalgo de Cisneros, *J. Food. Agric. Chem* 55 (2007) 8011.
- [28] A.J. Bard, L.R. Faulkner, *Electrochemical methods fundamentals and applications*, second ed., John Wiley & Sons, Inc., New York, 2001.
- [29] E.I. Solomon, U.M. Sundaram, T.E. Machonkin, *Chem. Rev.* 96 (1996) 2563.
- [30] J.N. Rodriguez-Lopez, J. Tudela, R. Varon, F. Garcia-Carmona, F. Garcia-Canovas, *J. Biol. Chem.* 267 (1992) 3801.
- [31] S. Shleev, A. Jarros-Wilkolazka, A. Khalumina, O. Morozova, A. Yaropolov, T. Ruzgas, L. Gorton, *Bioelectrochemistry* 67 (2005) 115.
- [32] S. Shleev, M. Pita, A. Yaropolov, T. Ruzgas, L. Gorton, *Electroanalysis* 18 (2006) 1901.
- [33] E. Laviron, *J. Electroanal. Chem.* 101 (1979) 19–28.

Phthalates determination in physiological saline solutions by HPLC–ES–MS

C. Pérez Feás, M.C. Barciela Alonso, E. Peña-Vázquez,
P. Herbello Hermelo, P. Bermejo-Barrera *

*Department of Analytical Chemistry, Nutrition and Bromatology, University of Santiago de Compostela,
Santiago de Compostela 15782, Spain*

Received 14 September 2007; received in revised form 2 January 2008; accepted 9 January 2008
Available online 19 January 2008

Abstract

Phthalates are a group of chemical compounds with increasing interest from the analytical point of view. The risks for human health associated with some of these compounds have unleashed the necessity to develop analytical methods with great sensitivity that allow us to detect their presence at trace levels in order to assure protection for the population.

A simple and rapid method for determining a group of phthalate esters in aqueous samples was developed. The method was based on high-performance liquid chromatography–(electrospray)–mass spectrometry (HPLC–ES–MS), working in positive ionisation (PI) mode. A gradient elution was performed with acetonitrile–ultrapure water starting from 5 to 75% acetonitrile in 5 min followed by isocratic elution during 5 min. Standard calibration curves were linear for all the analytes over the concentration range 10–500 ng mL⁻¹. The LOD values found for DMP, DEP, BBP and DBP were 0.8, 3.4, 0.6 and 1.2 ng mL⁻¹ respectively. The relative standard deviation ranged from 0.8 to 1.7%, which indicated good method precision.

The proposed analytical method has been applied to the analysis of commercial physiological saline solutions in order to check the presence of phthalates and to determine their concentration.

© 2008 Published by Elsevier B.V.

Keywords: Phthalates; HPLC–ES–MS; Physiological saline solutions

1. Introduction

Diesters of phthalic acid, commonly referred to as phthalates, are a group of chemical compounds widely used in industry and commerce due to their large variety of uses. Because of their properties to improve softness and flexibility to the plastics they are used mainly as plasticizers to give products to consumer and industry versatile, durables and accessibles such as medical devices, children's toys and all kind of packaging. Furthermore, phthalates are also used as industrial solvents and lubricants, as additives in textile industry and pesticides and also in personal care products such as deodorants, lotions and perfumes, to retain the colour and fragrance [1–4].

Approximately 93% of all plasticizers are phthalates, the remaining 7% corresponding to esters and polyesters based

on adipate, phosphoric acid, sebacic acid, etc. [1]. The world production of these compounds is estimated at several million tonnes per year. Phthalates are not chemically bound in the plastics; therefore, they can be lost from plastic and released to the environment [5].

Consistent toxicological evidence indicates association between several of these phthalate esters and risks for human health and the environment. In particular, dibutyl phthalate (DBP), butyl benzyl phthalate (BBP), and di-(2-ethylhexyl) phthalate (DEHP) are in the list of the proposed substances suspected to produce endocrine alterations published by European Union (EU) [6].

Section 307 of the US Clean Water Act establishes that dimethyl phthalate (DMP), diethyl phthalate (DEP), butyl benzyl phthalate, dibutyl phthalate, di-(2-ethylhexyl) phthalate and dioctyl phthalate (DOP) must be considered priority toxic pollutants [7]. These concerns have been further aggravated by recent analysis of human blood and urine samples, where traces of various phthalates (or their metabolites) have been found [8,9]. For

* Corresponding author.

E-mail address: pbermejo@usc.es (P. Bermejo-Barrera).

these reasons, the interest in the study of this type of chemical substances has increased during the last few years, and therefore it is essential to develop a reliable and sensible analytical method that allows us to determine and quantify this group of compounds at trace levels.

Several methods have been developed for their determination in different matrices, including water (drinking water, surface water, wastewater), soil, sediment, sludge, dust, air and biota (vegetation, milk, fish, etc.) [2,10–12].

The analysis of phthalic acid esters is mostly performed by gas chromatography (GC) [13–17]. Generally, GC methods present better sensibility than HPLC methods, although depend on the pre-treatment step, the instrumental conditions and the sample matrix [6]. High-performance liquid chromatography (HPLC) can be used as an alternative technique and is especially useful for analysis of isomeric mixtures and metabolites of phthalates without derivatisation [18].

Phthalates can be detected using UV detection [8,19–21], flame ionisation detection (FID) [22,23], electron capture detection (ECD) [24] or mass spectrometry (MS) [10,11,25,26]. Some official methods (US EPA methods 606 and 8060) describe the use of ECD for the phthalate determination. Although ECD detectors are relative sensitive for phthalates, the specificity is restricted. The most important detector for phthalate analysis is mass spectrometric detection. All types of MS analysers, including quadrupole analysers, triple quadrupole analysers, ion traps and magnetic sector instruments have been used for phthalates determination [27].

The major problem in phthalate analysis is the contamination, resulting in false positive results or over-estimated concentrations. The risk of contamination is present in the whole analytical scheme, including sampling, sample preparation and chromatographic analysis. Due to the fact that phthalates are widely used, they are present in air, water, and organic solvents and plastic and adsorbed on glass or other materials [27].

A recent study carried out by Reid et al. [28] shows significant quantities of phthalates from various components commonly found in the environmental of analytical laboratory. Consequently, plastic syringes, pipette tips, plastic filters and all type of plastic material must be avoided, and glass material must be used instead. Once plastic materials containing phthalates are avoided, the main source of contamination are phthalates present as vapours or part of the particulate matter in air, contaminating all surfaces, particularly glassware, plastic objects and our skin [29].

As a result of the contribution of all these sources of contamination, the experiments to reduce its produce confusing results because, the sources of contamination vary from one laboratory to another and depend on factors such as season, weather and ventilation of the laboratory [29].

Different cleaning methods have been proposed to avoid the contamination problems due to the phthalates from the material used in the laboratory. In all of them glass material is rinsed with organic solvents after a rigorous washing [11,30–35].

The aim of this work is to develop a method for phthalates determination presents in trace levels in physiological saline solutions, using HPLC–ES-MS.

2. Experimental

2.1. Reagents and standards

All reagents used were of analytical reagent-grade. Dimethyl phthalate and butyl benzyl phthalate were obtained from Supelco (Bellefonte, PA, USA). Diethyl phthalate and dibutyl phthalate were obtained from Riedel-de Haën (Seelze, Germany). The purity of these reagents was over 98%.

Lichrosolv gradient grade acetonitrile and methanol were purchased from Merck (Darmstadt, Germany). Technical-grade acetone and acetic acid glacial (HPLC) for instrumental analysis were purchased from Panreac (Barcelona, Spain). Ultrapure (resi-analyzed) water for environmental inorganic and organic trace analysis was supplied by J.T. Baker (Phillipsburg, NJ, USA).

Individual standard solutions of each phthalate ester at a concentration of 1000 mg L⁻¹ were prepared in methanol, preserved of light and stored at 4 °C in a Teflon-capped glass vial. From these solutions, a working mixture in methanol was prepared weekly containing all standards of concentration 100 mg L⁻¹ each. All the working solutions were prepared daily by diluting this solution.

Special care was taken to avoid the contact of reagents and solvents with plastic materials. In order to reduce background contamination, all glassware was cleaned prior to the analysis according to the recommendations specified in EPA method 506. All material was washed with hot water and soap, rinsed with tap and ultrapure water and finally thorough rinsed with technical-grade acetone. Then, glassware was sealed with aluminium foil and stored in a clean environment to avoid adsorption of phthalates from the air.

2.2. Instrumentation

Phthalates separation and quantification was carried out using liquid chromatography/electrospray ionisation-mass spectrometry system.

The HPLC system used was an 1100 Series equipped with an automatic injector (Agilent Technologies, Waldbronn, Germany) that is coupled to an API 150 EX single quadrupole mass spectrometer equipped with a Turboionspray interface (PE Biosystems, Concord, Canada).

The analytical column was a ZORBAX Eclipse XDB-C₈ of 50 mm length and 2.1 mm internal diameter (particle size 3.5 μm) supplied by Agilent Technologies.

2.3. Chromatographic and mass spectrometry conditions

The binary mobile phase consisted of ultrapure water and acetonitrile, both solvents containing 0.1% (v/v) acetic acid. The elution gradient started with 95% of ultrapure water, which was reduced linearly to 25% in 5 min. Then, this composition was maintained for 5 min before returning to the initial conditions. The column was equilibrated for 10 min.

The flow rate and the injection volume were 200 μL min⁻¹ and 10 μL, respectively and the chromato-

Table 1
Optimal values of the compound parameters for the four phthalates studied

Compound	Acronym	<i>m/z</i>	Potentials		
			DP	FP	EP
Dimethyl phthalate	DMP	163.25	40.38	73.87	8
Butyl benzyl phthalate	BBP	91.15	25	225	6
Diethyl phthalate, dibutyl phthalate	DEP, DBP	149.05	25	290	8.5

graphic separation was carried out at room temperature. Under these conditions the separation time was less than 10 min.

Electrospray ionisation was performed in positive ion mode. The operational parameters were the same for all of analytes with an ionspray voltage of 5500 V; nitrogen was used as nebulizer and curtain gas at a pressure of 14 psi in both cases; air current at 450 °C and 7000 cc min⁻¹ was used as turbo heater gas.

The compound parameters such as declustering potential (DP), focusing potential (FP) and entrance potential (EP) were optimized for each analyte. The optimal conditions are shown in the Table 1.

2.4. Sample preparation

Samples were injected directly in the chromatograph, it wasn't necessary any sample preparation process.

3. Results and discussion

3.1. ES-MS optimization

Four phthalate esters (DMP, DEP, BBP and DBP) were selected for this study.

To evaluate the mass spectral fragmentation pattern of each compound and to optimize the set of parameters used, a standard solution (100 mg L⁻¹) of each compound was analyzed by direct injection in the spectrometer. For these experiments, a KD Scientific, model 100, syringe pump (New Hope, MN, USA) at 15 μL min⁻¹, was used.

Full-scan data acquisition was performed from 80 to 400 *m/z*, with the target mass fixed to the following *m/z* values: 91.15 for BBP, 149.05 for DEP and DBP and 163.25 for DMP. The spectral data provided ions in accordance with previous studies reported in literature [2,15,16,36,37]. The selected ions were chosen to attain the best response in the SIM mode acquisition. Characteristics as molecular weight, identification ions and retention time corresponding to these compounds are given in Table 2.

Table 2
Molecular weight, selected ions and retention time to the analysis of the target phthalates

Phthalate	Molecular weight	SIM ion	Identification ions	RT (min)
Dimethyl phthalate	194	163	149, 163, 181	6.90
Diethyl phthalate	222.24	149	149, 177, 195	7.59
Butyl benzyl phthalate	312.40	91	91, 149, 205, 223, 247	9.18
Dibutyl phthalate	278.35	149	149, 205, 223	9.44

3.2. Optimization of HPLC separation

After optimizing the detection conditions, the following experiments were conducted to optimize the chromatographic separation of the analytes.

Experiments were carried out using different mobile phases reported in the literature (methanol:water [38], acetonitrile:water [20], acetonitrile (1% methanol):water [21]), working in isocratic mode. The best resolution was obtained using acetonitrile:water as a mobile phase. These results agree with the experiments developed by López-Jiménez et al. [10]. In order to improve the resolution and to decrease the time of analysis, different experiments were carried out working in gradient mode. The best results were obtained started with 95% of ultrapure water and decreasing this percentage to 25% in 5 min. Then, this composition was maintained for 5 min before returning to the initial conditions. Finally, the column was equilibrated during 10 min before each injection. Other parameters optimized were the percentage of acetic acid and the flow rate of the mobile phase. The optimal conditions were 0.1% (v/v) acetic acid and a flow rate of 200 μL min⁻¹.

The chromatogram obtained for a mixed of these compounds under the optimized conditions is shown in the Fig. 1.

3.3. Analytical performance

To evaluate the linearity of the method, a direct calibration curve was realized. Ten microliters of standard solutions in ultrapure water with concentrations ranging from 10 to 500 ng mL⁻¹ were injected by triplicate. Detector signals, measured in arbitrary units (peak areas), were plotted versus the amount of analyte injected, expressed in ng mL⁻¹ and background levels were subtracted from the results. The equations obtained for each compound were as follows:

$$\text{DMP : } Q_A = 46399 C + 377217 \quad r = 0.9964$$

$$\text{DEP : } Q_A = 1784 C + 16643 \quad r = 0.9987$$

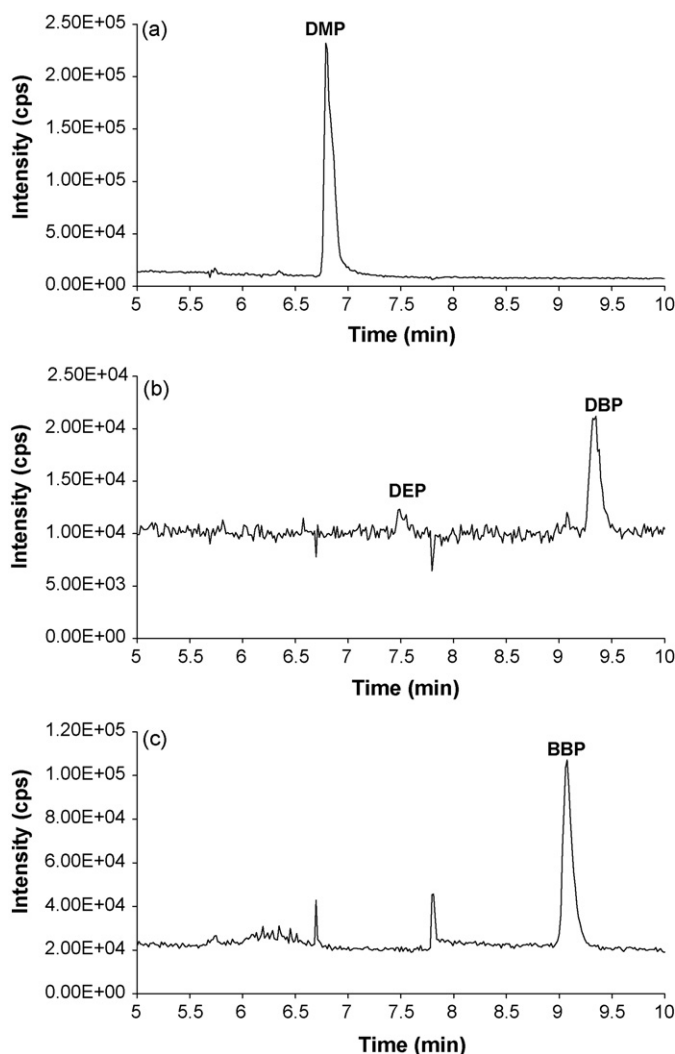


Fig. 1. LC/MS extracted ion chromatogram obtained from a standards solution (100 ng mL^{-1}) in a physiological saline sample purchased in a glass bottle to the following m/z values: (a) 163.25 for DMP, (b) 149.05 for DEP and DBP, and (c) 91.15 for BBP.

$$\text{BBP: } Q_A = 18218 C + 153056 \quad r = 0.9978$$

$$\text{DBP: } Q_A = 5166 C + 66474 \quad r = 0.9963$$

where Q_A is the peak area and C is the concentration in ng mL^{-1} .

Standard addition method was applied over the same range of concentrations using a commercial physiological saline solution purchased in a glass bottle. The equations obtained for each compound were as follows:

$$\text{DMP: } Q_A = 12334 C + 12308 \quad r = 0.9998$$

$$\text{DEP: } Q_A = 114 C + 1686 \quad r = 0.9979$$

$$\text{BBP: } Q_A = 5319 C - 20441 \quad r = 0.9988$$

$$\text{DBP: } Q_A = 639 C - 8128 \quad r = 0.9985$$

Table 3

Linear range, correlation coefficients, LODs and LOQs values obtained from the standard addition method in physiological saline solutions

Phthalate	Linear range (ng mL^{-1})	Correlation coefficient (r)	LODs (ng mL^{-1})	LOQs (ng mL^{-1})
DMP	10–500	0.9998	0.99	3.29
DEP	10–500	0.9979	22.13	73.78
BBP	10–500	0.9988	5.32	17.73
DBP	10–500	0.9985	24.07	80.23

To compare slopes of the calibration and addition graphs for the four compounds, the t -test (95% significance levels) [39] was applied and differences were observed for all compounds. This means that the sample matrix had influence in the sensitivity of the method, so, standard addition graphs had been used to analyze these samples.

The limit of detection (LOD) and limit of quantification (LOQ) for the method were calculated according with the equations:

$$\text{LOD} = \frac{3\text{S.D.}}{m}; \quad \text{LOQ} = \frac{10\text{S.D.}}{m}$$

where S.D. is the standard deviation of 11 measurements of a blank and m is the slope of the addition graph. The commercial physiological saline solution purchased in a glass bottle was used as a blank. The results obtained for LODs and LOQs are shown in the Table 3. As can be seen in the Table 3, LODs are between 0.99 and 24.07 ng mL^{-1} for all compounds, and the highest levels obtained were for DEP and DBP.

To check the precision an interday assay was developed. A physiological saline solution sample purchased in a glass bottle and spiked with three concentration levels (50 , 100 and 300 ng mL^{-1}) were analyzed during different days (six determinations per concentration each day) for all compounds studied. The results obtained are shown in the Table 4. The R.S.D. values were between 1.9 and 10.9% so, the method is precise for all studied compounds.

The recovery of the method was evaluated by injection of the physiological saline solution purchased in a glass bottle spiked with three different concentrations of these compounds. The solutions were injected by triplicate and the recovery calculated using the standard addition graph. The results obtained are shown in Table 5. The average recoveries were 101.5%, 94.7%, 108.3% and 101.4% for DMP, DEP, BBP and DBP, respectively.

Table 4

Relative standard deviation (%) obtained for three concentration levels (based on six determinations) in interday assay

Phthalate	R.S.D. (%)		
	50 ng mL^{-1}	100 ng mL^{-1}	300 ng mL^{-1}
DMP	10.9	3.5	3.6
DEP	8.0	4.5	4.1
BBP	5.6	6.2	2.2
DBP	5.1	7.5	1.9

Table 5
Recovery percentage for physiological saline solutions \pm standard deviation

Phthalate	% Recovery		
	50 ng mL ⁻¹	100 ng mL ⁻¹	300 ng mL ⁻¹
DMP	103.7 \pm 1.4	105.4 \pm 1.0	95.0 \pm 1.2
DEP	89.7 \pm 3.3	99.5 \pm 3.5	95.1 \pm 3.1
BBP	111.3 \pm 9.5	104.2 \pm 2.0	109.5 \pm 1.5
DBP	105.8 \pm 2.7	89.8 \pm 2.1	108.7 \pm 3.5

Table 6
Concentrations (ng mL⁻¹) \pm standard deviation (based on three replicates) found in different physiological saline solutions

Physiological saline solutions	DMP	DEP	BBP	DBP
Brand A	5 \pm 1	335 \pm 5	<LOD	50 \pm 2
Brand B	<LOD	<LOD	<LOD	<LOD
Brand C	<LOD	<LOD	5 \pm 1	<LOD
Brand D	153 \pm 2	<LOD	<LOD	<LOD

<LOD: lower than the detection limit.

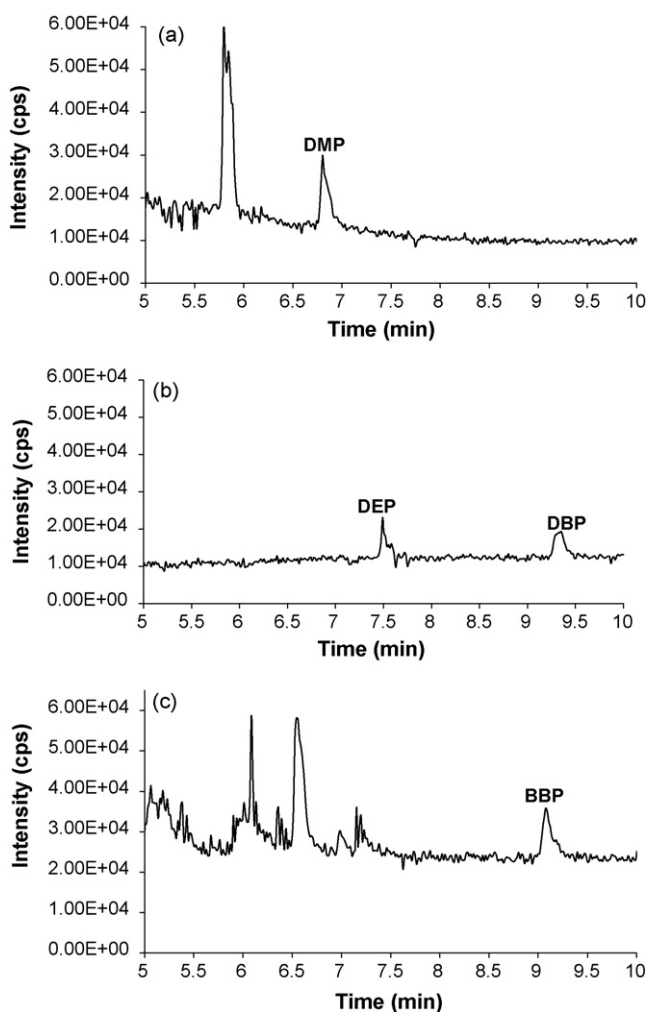


Fig. 2. LC/MS extracted ion chromatogram obtained from brand A physiological saline solution to the following m/z values: (a) 163.25 for DMP, (b) 149.05 for DEP and DBP, and (c) 91.15 for BBP.

3.4. Application to physiological saline solutions

The proposed analytical method has been applied to the analysis of four commercial physiological saline solutions in order to check the presence of these phthalates and to determine their concentration. Samples were injected directly in the chromatograph, it wasn't necessary any sample preparation process.

The original recipients containing three of these physiological saline solutions were made from plastic material. The other one was in a glass bottle. The phthalate esters are used in the manufacture of the plastic recipients, so the influence of the material on the concentration of the phthalates has been evaluated.

Physiological saline solutions were analyzed in order to verify the presence of different peaks at the same retention time as the compounds studied. Some peaks appeared at the retention times corresponding to DMP, DEP, BBP and DBP. The spectra of these peaks confirmed that they correspond to these four phthalates.

The results obtained for these phthalates in the four samples are given in the Table 6. The levels of these compounds in the brand B, was less than the LODs of the method. The absence of these compounds in this sample can be attributed to that this sample is distributed in a glass bottle. Fig. 2 shows the LC/MS ion chromatograms obtained from brand A of physiological saline solution.

4. Conclusions

A method for the determination of different phthalates by HPLC–ES–MS was developed. The method is rapid (the separation and determination was realized in less than 10 min), precise and accurate.

Four commercial physiological saline solutions from different brands were analyzed using the proposed method. The results shown, that these compounds are present only in the samples distributed in plastic bottles. In physiological saline solution distributed in glass bottle, these compounds were not detected (<LODs).

Acknowledgement

C. Pérez Feás wishes to thank Ministerio de Educacion y Ciencia for her FPU grant.

References

- [1] H.M. Koch, L.M. Gonzalez-Reche, J. Angerer, J. Chromatogr. B 784 (2003) 169.
- [2] P. Serodio, J.M.F. Nogueira, Water Res. 40 (2006) 2572.
- [3] K. Kato, T. Yamauchi, K. Higashimaya, H. Nakazawa, J. Liq. Chromatogr. Relat. Technol. 26 (2003) 2167.
- [4] T. Jones-Lepp, C.L. Gerlach, E.J. Cooter, Trends Anal. Chem. 19 (2000) 286.
- [5] A. Gómez-Hens, M.P. Aguilar-Caballos, Trends Anal. Chem. 22 (2003) 847.
- [6] Communication from the Commission to the Council and the European Parliament on the implementation of the community strategy for endocrine disrupters—a range of substances suspected of interfering with the hormone

- systems of humans and wildlife, COM (1999) 706; COM (2001) 262 final, Brussels, 2001.
- [7] US Environmental Protection Agency (EPA), Protection Agency, Introduction to Water Policy Standards, Office of Water, Washington, DC, 1999.
- [8] D. De Orsi, L. Gagliardi, R. Porrá, S. Berri, P. Chimenti, A. Granese, I. Carpani, D. Tonelli, *Anal. Chim. Acta* 555 (2006) 238.
- [9] K. Kato, S. Shoda, M. Takahashi, N. Doi, Y. Yoshimura, H. Nakazawa, *J. Chromatogr. B* 788 (2003) 407.
- [10] F.J. López-Jiménez, S. Rubio, D. Pérez-Bendito, *Anal. Chim. Acta* 551 (2005) 142.
- [11] R.A. Gimeno, R.M. Marcé, F. Borrull, *Chromatographia* 58 (2003) 37.
- [12] G.K. Mortensen, K.M. Main, A.M. Andersson, H. Leffers, N.E. Skakkebaek, *Anal. Bioanal. Chem.* 382 (2005) 1084.
- [13] A. Peñalver, E. Pocurull, F. Borrull, R.M. Marcé, *J. Chromatogr. A* 872 (2000) 191.
- [14] L. Brossa, R.M. Marcé, F. Borrull, E. Pocurull, *Chromatographia* 61 (2005) 61.
- [15] K. Luks-Betlej, P. Popp, B. Janozska, H. Paschke, *J. Chromatogr. A* 938 (2001) 93.
- [16] M. Polo, M. Llompart, C. García-Jares, R. Cela, *J. Chromatogr. A* 1072 (2005) 63.
- [17] L. Brossa, R.M. Marcé, F. Borrull, E. Pocurull, *Environ. Toxicol. Chem.* 24 (2005) 261.
- [18] M.J. Silva, A.R. Slakman, J.A. Reidy, J.L. Preau Jr., A.R. Herbert, E. Samandar, L.L. Needham, A.M. Calafat, *J. Chromatogr. B* 805 (2004) 161.
- [19] K. Mitani, F. Izushi, H. Kataoka, *J. Anal. Toxicol.* 28 (7) (2004) 575.
- [20] N. Hata, E. Yuwatini, K. Ando, M. Yamada, I. Kasahara, S. Taguchi, *Anal. Sci.* 20 (2004) 149.
- [21] S. Jara, C. Lysebo, T. Greibrokk, E. Lundanes, *Anal. Chim. Acta* 407 (2000) 165.
- [22] O.S. Fatoki, A. Noma, *J. Chem.* 54 (2001) 69.
- [23] U. Kotowska, K. Garbowska, V.A. Isidorov, *Anal. Chim. Acta* 560 (2006) 110.
- [24] G. Prokupková, K. Holadová, J. Poustka, J. Hajslová, *Anal. Chim. Acta* 457 (2002) 211.
- [25] M. Castillo, A. Oubiña, D. Barceló, *Environ. Sci. Technol.* 32 (1998) 2180.
- [26] K. Kato, M.J. Silva, L.L. Needham, A.M. Calafat, *Anal. Chem.* 77 (2005) 2985.
- [27] F. David, P. Sandra, B. Tienpont, F. Vanwallegem, in: C.A. Staples (Ed.), *The Handbook of Environmental Chemistry. Part Q. Phthalate Esters*, vol. 3, Springer, Berlin, 2003, p. 15.
- [28] A.M. Reid, C.A. Brougham, A.M. Fogarty, J.J. Roche, *Int. J. Environ. Anal. Chem.* 87 (2007) 125.
- [29] A. Fankhauser-Noti, K. Grob, *Anal. Chim. Acta* 582 (2007) 353.
- [30] W.A.C. Anderson, K.A. Barnes, L. Castle, A.P. Damant, M.J. Scotter, *Analyst* 127 (2002) 1193.
- [31] S. Jonsson, J. Ejlertsson, A. Ledin, I. Mersiowsky, B.H. Svensson, *Water Res.* 37 (2003) 609.
- [32] M.A. Faouzi, F. Khalfi, T. Dine, M. Luyckx, C. Brunet, B. Gressier, F. Goudaliez, M. Cazin, A. Belabed, J.C. Cazin, *J. Pharm. Biomed. Anal.* 21 (1999) 923.
- [33] S. Takatori, Y. Kitagawa, M. Kitagawa, H. Nakazawa, S. Hori, *J. Chromatogr. B* 804 (2004) 397.
- [34] T. Hanawa, E. Muramatsu, K. Asakama, M. Suzuki, M. Tanaka, K. Kawano, T. Seki, K. Juni, S. Nakajima, *Int. J. Pharm.* 210 (2000) 109.
- [35] Y.Q. Cai, G.B. Jiang, J.F. Liu, Q.X. Zhou, *Anal. Chim. Acta* 494 (2003) 149.
- [36] R. Kumar, *A Mass Spectral Guide for Quick Identification of Phthalate Esters*, American Laboratory, 1999, p. 32.
- [37] E. Psillakis, N. Kalogerakis, *J. Chromatogr. A* 999 (2003) 145.
- [38] Y. Saito, Y. Nakao, M. Imaizumi, Y. Morishima, Y. Kiso, K. Jinno, *Anal. Bioanal. Chem.* 373 (2002) 81.
- [39] R. Cela (Ed.), *Avances en Quimiometría práctica*, Universidad de Santiago de Compostela, Santiago de Compostela, Spain, 1994, p. 171.

Preparation and characterization of a novel pyrrole-benzophenone copolymerized silica nanocomposite as a reagent in a visual immunologic-agglutination test

Pola Goldberg-Oppeneheimer^a, Serge Cosnier^b, Robert S. Marks^{c,d}, Oren Regev^{a,c,*}

^a Department of Chemical Engineering, Ben-Gurion University of the Negev, 84105 Beer-Sheva, Israel

^b Département de Chimie Moléculaire UMR-5250, ICMG FR-2607, CNRS Université Joseph Fourier, BP-53, 38041 Grenoble, Cedex 9, France

^c The Ilse Katz Center for Meso and Nanoscale Science and Technology, Ben-Gurion University of the Negev, 84105 Beer-Sheva, Israel

^d The National Institute for Biotechnology in the Negev, The Department of Biotechnology Engineering, Ben-Gurion University of the Negev, 84105 Beer-Sheva, Israel

Received 28 October 2007; received in revised form 20 January 2008; accepted 23 January 2008

Available online 8 February 2008

Abstract

Biological sensing is explored through novel stable colloidal dispersions of pyrrole-benzophenone and pyrrole copolymerized silica (PPy-SiO₂-PPyBPh) nanocomposites, which allow covalent linking of biological molecules through light mediation. The mechanism of nanocomposite attachment to a model protein is studied by gold labeled cholera toxin B (CTB) to enhance the contrast in electron microscopy imaging. The biological test itself is carried out without gold labeling, i.e., using CTB only. The protein is shown to be covalently bound through the benzophenone groups. When the reactive PPy-SiO₂-PPyBPh-CTB nanocomposite is exposed to specific recognition anti-CTB immunoglobulins, a qualitative visual agglutination assay occurs spontaneously, producing as a positive test, PPy-SiO₂-PPyBPh-CTB-*anti-CTB*, in less than 1 h, while the control solution of the PPy-SiO₂-PPyBPh-CTB alone remained well-dispersed during the same period. These dispersions were characterized by cryogenic transmission microscopy (cryo-TEM), scanning electron microscopy (SEM), FTIR and X-ray photoelectron spectroscopy (XPS).

© 2008 Elsevier B.V. All rights reserved.

Keywords: Gold labeling; Silica; Nanocomposites; Immunodiagnostics; Cryo-TEM; XPS

1. Introduction

Immunodiagnostics are testing methods that harness an antigen–antibody binding reaction to measure, or simply identify the presence of one of these naturally occurring components within a physiological fluid or cytologic/histologic specimen. Such procedures have become an essential tool in the identification of metabolic and disease markers.

Methods such as radioimmunoassays (RIA) [1], enzyme immuno assays (EIA) and enzyme-linked immunosorbent assays (ELISA) [2,3] are widely used for immunoassay diagnostics, but require handling radioactive materials or sophisticated equipment such as a scintillation counter, UV–vis spectrometers

or sophisticated luminometers or fluorometers. Another immunodiagnostic tool in development is the immunosensor, which usually couples immobilized biospecific recognition entities to the surface of a transducer. The latter transduces a molecular recognition event into a measurable electric signal [4] such as in the case of fiber-optic or amperometric [5] immunosensors. However, in the preparation of biosensors the immobilization of biospecific entities onto the transducer [6], be it an electrode, a piezoelectric crystal or optical fiber, is a key feature requiring improvement by way of better characterization methods such as those proposed here in devising an alternative immunoassay device.

Polypyrrole-coated polystyrene latex and particularly silica particles were extensively studied in the last years as they are potentially useful in immunodiagnostics. Latex agglutination tests [7] and hemagglutination [8] are very popular in clinical laboratories. These tests have been applied to the detection of over 100 infectious diseases, and many other applications are

* Corresponding author at: Department of Chemical Engineering, Ben-Gurion University of the Negev, 84105 Beer-Sheva, Israel.

E-mail address: oregev@bgu.ac.il (O. Regev).

currently available. In agglutination assays, the visible phase of the reaction is enhanced by binding one of the reactants to a solid phase such as latex beads [9–11], red blood cells, or as will be demonstrated here, to an alternative medium PPy-SiO₂-PPyBPh “raspberries”. Particle immunoassays add sensitivity by enhancing surface area and visibility. By linking several antigens to the particle, the particle is able to bind many antibody molecules simultaneously. This greatly accelerates the speed of the visible reaction, and allows rapid and sensitive detection of antibodies (markers of diseases).

Molecular recognition receptors are usually prepared by immobilizing antigens or antibodies onto a substrate material, by either physical adsorption or covalent binding. Since physical adsorption is weak it is desirable to immobilize biomolecules of interest by covalent binding to the carrier surface. Additionally, the specific activity of these nanocomposites-based immuno reagents can be enhanced by binding ligands through intervening spacer molecule, especially to regions isolated from the binding site [12].

There are many methods to covalently bind bioreceptors to particles via surface treatment of the particles through chemical functionalization so as to facilitate analyte attachment and to increase binding stability. Functional treatments include carboxylation, amidation, amination, hydroxylation and even magnetization. Recently, novel ester-functionalized polypyrrole-silica particles were used for the covalent attach-

ment of proteins [13]. A photoreactive benzophenone (BPh) derivative is bound to silica surfaces via a silane anchor. Fig. 1A describes the elementary steps in the radical photo-attachment process of benzophenone, which includes: (I) triplet state excitation, (II) H-abstraction and (III) radical recombination, thus allowing the formation of covalent binding with different substrates, such as nucleic acids or proteins, bearing amino acids with sterically accessible C–H bonds [14–16].

In this study, we utilize benzophenone derivatives to synthesize novel pyrrole copolymerized silica nanoparticles (PPy-SiO₂-PPyBPh). The combination of the two monomers, namely Py and PyBPh, allows efficient and strong covalent linking of biological molecules through light mediation (Fig. 1C and D), respectively. The immobilization of the receptor, (here cholera toxin B subunit (CTB) used as a model protein), to a PPy-SiO₂-PPyBPh nanocomposite is carried out by the photochemical linkage to photoreactive benzophenone derivatives that are bound to the SiO₂ surfaces (Fig. 1C and D). The immuno-conjugate is bound through C–H bonds in the spacer benzophenone molecule, without disruption of its biological activity. Since the protein molecules have low mass-thickness and diffraction contrast in electron microscopy, we labeled them by gold nanoparticles (GNP) having high mass-thickness contrast, which makes it then possible to follow the immobilization process at nanometric resolution.

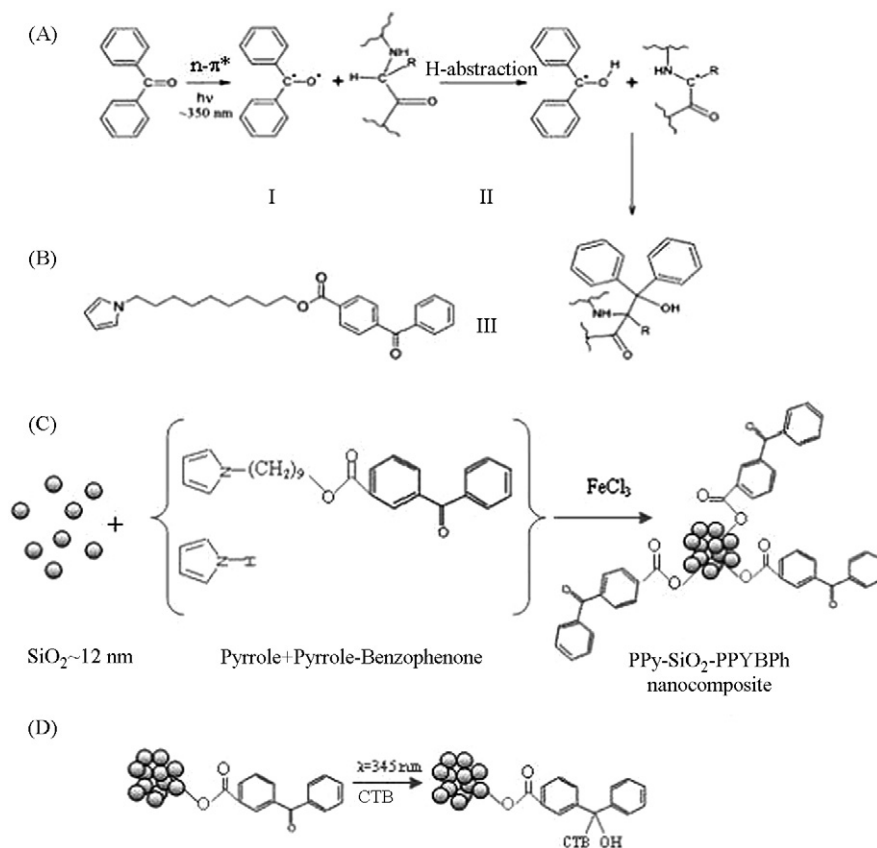


Fig. 1. (A) Mechanism for the photochemical reaction of benzophenone with a C–H bond of an amino acid side chain [40] (B) Structure of the pyrrole-benzophenone monomer. Schematic representation of the: (C) copolymerization process of silica beads with PPy and PPyBPh and (D) photochemical attachment of the CTB subunit to the polymerized silica bead surface by illumination through the pyrrole-benzophenone-coated silica beads immersed in the antigen solution.

The resulting nanocomposite dispersion is characterized by cryo-transmission electron microscopy (cryo-TEM) [17–20], its morphology is determined by scanning electron microscopy (SEM) and atomic force microscopy (AFM), while information about its structure is done by FTIR and its surface chemical composition by X-ray photoelectron spectroscopy (XPS). The reactive PPy-SiO₂-PPyBPh-CTB nanocomposites are then tested in a qualitative visual agglutination assay.

2. Experimental section

2.1. Materials

Cholera toxin B subunit (C9903, lyophilized powder), anti-cholera toxin antibody produced in rabbit (C-3062), pyrrole (131709, reagent grade, 98%), and Ludox colloidal silica sol (HS-30, 30% (w/v) water suspension) were purchased from Sigma, iron (III) chloride-6-hydrate (31232) and chloroauric acid (520918, ≥99.9%) from Aldrich, while sodium citrate dehydrate (S4641), was purchased from ACS. Tannic acid (Mallinckrodt Baker Inc.) was used as received. 3-(Cyclohexylamino)-1-propane sulfonic acid (CAPS) buffer solution with pH 10.5 (25 °C) was purchased from Bio-Chemika (82607, concentration: 20 mM CAPS). The pyrrole monomer, functionalized with a photoreactive benzophenone group (Fig. 1B) was prepared as previously described by the esterification of the 3-benzoylbenzoic acid with the 1-(3-hydroxypropyl) pyrrole using the carbodimide method [21].

2.2. Preparation

2.2.1. Synthesis of 8 nm colloidal gold nanoparticles and coupling of CTB to form a complex (CTB-Au₈)

Colloidal gold particles with a diameter of 8 nm ($\sigma = 1.2$ nm) were synthesized by the reduction of chloroauric acid with tri-sodium citrate and stabilized by tannic acid [22]. 79 ml distilled water and 1 ml 1% (w/v) aqueous gold chloride is added to solution consisting of 4 ml 1% (w/v) tri-sodium citrate-2H₂O, 0.08 ml of 1% (v/v) tannic acid and 16 ml distilled water. The mixed a solution was warmed to 60 °C on a hot plate. When a red color appeared, the mixture was heated up to 95 °C and finally cooled by ice. The diameters of GNPs were determined from digital electron micrographs using Digital Micrograph software/particles (Version 3.1). Zsigmondy's test [23] was used to determine the minimal concentration of protein required for stabilizing the sols (27 μg/ml). Thereafter, 1.5 times of the minimal concentration of CTB was bound to gold nanoparticles as previously described [24] to ensure that the GNPs are fully stabilized. The CTB-Au₈ complexes were first centrifuged at 70,000 × *g* for 1 h at 4 °C (Sorvall Discovery M120 ultracentrifuge, S120AT2 rotor). The supernatant was discarded, leaving a concentrated red precipitate, which was then re-suspended in double distilled water and centrifuged several times to wash out all possible traces of non-adsorbed CTB. Thereafter, the precipitate was re-suspended in double distilled water and kept at 4 °C.

2.2.2. Labeling confirmation

The samples were negatively stained and examined by TEM at room temperature to confirm that CTB was labeled with GNPs. Glow-discharged (under vacuum) carbon coated film on a copper EM grid was dipped for 2 min in a sample solution. The grid was then negatively stained with an aqueous solution of 2 wt% uranyl acetate for 1 min and washed clean from the uranyl residues.

2.2.3. Synthesis of poly(pyrrole-benzophenone)/poly(pyrrole)-coated silica nanocomposites (PPy-SiO₂-PPyBPh)

An aqueous dispersion of 100 μl of 12 nm silica particles was suspended in 1 ml double distilled water to which 0.5 g FeCl₃·6H₂O oxidant was added, with vigorous stirring into a two-neck 25 ml round-bottom flask with a rubber septum containing a magnetic stirrer. After degassing with nitrogen/argon, 10 μl Pyrrole monomer and 60 μl Pyrrole-benzophenone monomer (1:1 Pyrrole:Pyrrole-BPh feed ratio [25] for optimal copolymerization) were injected via a syringe to the stirred solution and the polymerization allowed to proceed for 3 h. The coated silica particles were then isolated and purified by repeated centrifugation–redispersion cycles (successive supernatants being replaced by deionized water) in order to remove the unwanted inorganic FeCl₂ and HCl, produced during the pyrrole polymerization. The pH of the solution was adjusted to 10.5 by using CAPS buffer solution before the photo-immobilization step.

Macroscopic stability is determined by visual inspection and, direct imaging of the dispersion is carried out via cryogenic-TEM. No aggregation and precipitation is observed upon a prolonged standing of 10 month.

2.2.4. Photo-immobilization of the gold labeled-antigen onto PPy-SiO₂-PPyBPh nanoparticles

To produce the desired activation radiation, we used a 100-W Xe lamp mount (Oriel 6271) connected to a light condenser (Oriel 66021). The light was reflected through a dichroic mirror (Oriel 66226). The large spectrum radiation was then condensed into the monochromator (Oriel 77250) using the appropriate lens (Oriel, plano-convex lens). Thereafter, a 345 nm wavelength light output, with a light intensity of 80 mW cm⁻², was projected for 10 min into the solution consisting of PPy-SiO₂-PPyBPh particles and gold labeled protein (CTB-Au_{8 nm}). The light intensity was measured by an Ophir Optronics power meter Nova reader, PD300-UV. The excited polymerized radicals could then bind to neighboring solvated cholera toxin B subunit, labeled with 8 nm colloidal gold particles.

2.2.5. Qualitative visual agglutination test

The new nanocomposites were tested in an immunodiagnostic assay: the CTB-coated PPy-SiO₂-PPyBPh particles were used to detect the presence of the corresponding antibodies by visual agglutination tests (precipitation indicated a positive test). CTB-decorated nanocomposites were incubated with anti-CTB. The agglutination test is performed by ocular observation. Therefore, TEM measurements were not performed and labeling was not required.

3. Characterization techniques

3.1. Transmission electron microscopy (TEM)

PPy-SiO₂-PPyBPh nanocomposites were imaged using TEM. Glow-discharged carbon coated film on a copper TEM grid (lacey carbon, 300 mesh, Ted Pella, Inc.) was dipped for 2 min in the PPy-SiO₂-PPyBPh solution and then dried via blotting. The samples were examined at room temperature using a FEI Tecnai 12 G² TWIN TEM, and the images recorded (Gatan model 794 charge-coupled device cameras) at 120 kV.

3.2. Cryogenic transmission electron microscopy

Aqueous dispersions of PPy-SiO₂-PPyBPh and PPy-SiO₂-PPyBPh-CTB-Au_{8nm} were imaged using the cryo-transmission electron microscopy technique. Sample preparation was carried out using a vitrobot [26] at room temperature and 100% RH. A drop of the solution is deposited on a TEM grid. The excess liquid is blotted, and the specimen vitrified by a rapid plunging into liquid ethane pre-cooled to its melting temperature by liquid nitrogen. The samples were examined at -178 °C using the TEM described above in low-dose mode.

3.3. Scanning electron microscopy

Scanning electron microscopy was used to obtain information about the surface morphology of the polymeric coatings. Samples for SEM imaging were prepared by placing a droplet of the PPy-SiO₂-PPyBPh dispersion on a lacey TEM grid, which was then dried. Scanning electron micrographs were obtained using a JEOL 7400F cold FEG. The accelerating voltage was set at 3.0 kV, and secondary electron images were recorded at various magnifications.

3.4. Atomic force microscopy

Atomic force microscopy images of PPy-SiO₂-PPyBPh were obtained by using a Nanoscope IV dimension 3100 multi-mode scanning probe microscope operated in the tapping mode. One drop of dispersed PPy-SiO₂-PPyBPh nanocomposite was deposited on the surface of a freshly cleaved silicon wafer, which was first cleaned by methanol, followed by a snow jet and then dried with nitrogen. A dry thin layer was accomplished by a spin coating procedure.

3.5. FTIR characterization of the PPy-SiO₂-PPyBPh nanoparticles

FTIR spectra (KBr disks) for bare silica nanoparticles, polypyrrole-coated silica and PPy-SiO₂-PPyBPh nanoparticles were obtained using a Nicolet Protégé 460 spectrometer. In the present study, FTIR spectra were recorded in the range of 800–2000 cm⁻¹.

3.6. Surface analysis by X-ray photoelectron spectroscopy

The surface composition of copolymerized nanocomposites of PPy-SiO₂-PPyBPh was examined by XPS using a Kratos HS spectrometer equipped with an Al K α X-ray source (1486.6 eV). Dried samples were mounted on a powder sample holder and a flood gun was used in order to minimize the static charging effects. The X-ray spot size was 500 μ m and the pass energy was set at 80 and 20 eV for survey and high resolution spectra, respectively. Peak fitting was carried out using a Casa XPS software. Spectral calibration was determined by setting the main C1s component at 285 eV. Sensitivity factors were provided by the manufacturer.

4. Results and discussion

4.1. Characterization of the PPy-SiO₂-PPyBPh nanocomposites

PPy-SiO₂-PPyBPh nanocomposites form macroscopically stable dispersions of homogeneous dark black solutions. Cryo-TEM micrographs show (Fig. 2) ~85 nm in diameter “raspberry-like” shaped particle morphology. These consist of copolymerized PPy-SiO₂-PPyBPh nanocomposites prepared from 12 nm silica particles, and trapped within the conducting pyrrole matrix, as has been previously shown with similar homopolypyrrole-silica nanostructures [27].

The dry form of PPy-SiO₂-PPyBPh particles is imaged by AFM and SEM (Fig. 3A and B). The average size of nanocomposites is found to be 93 \pm 18 nm, in good agreement with the cryo-TEM measurements (Fig. 2). AFM analysis of the PPy-

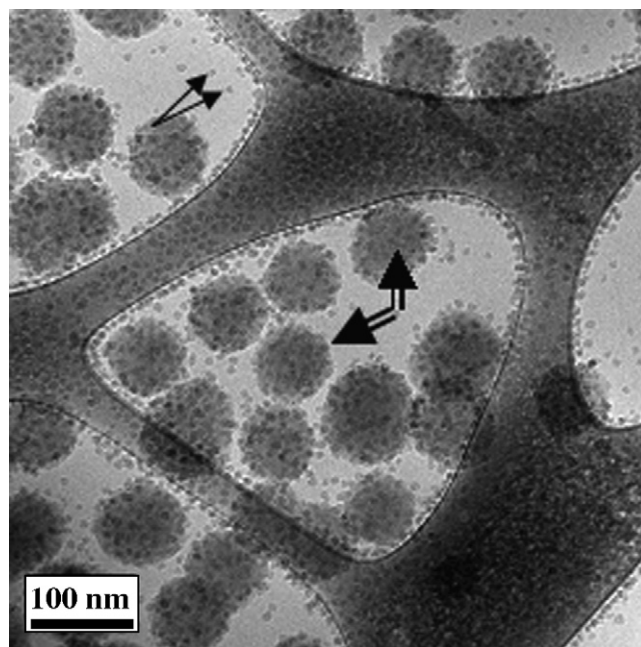


Fig. 2. Cryo-TEM micrograph of dispersion of the PPy-SiO₂-PPyBPh nanocomposites. Single arrows point at 12 nm silica particles and double arrows at ~80 nm “raspberry”-shaped nanocomposites.

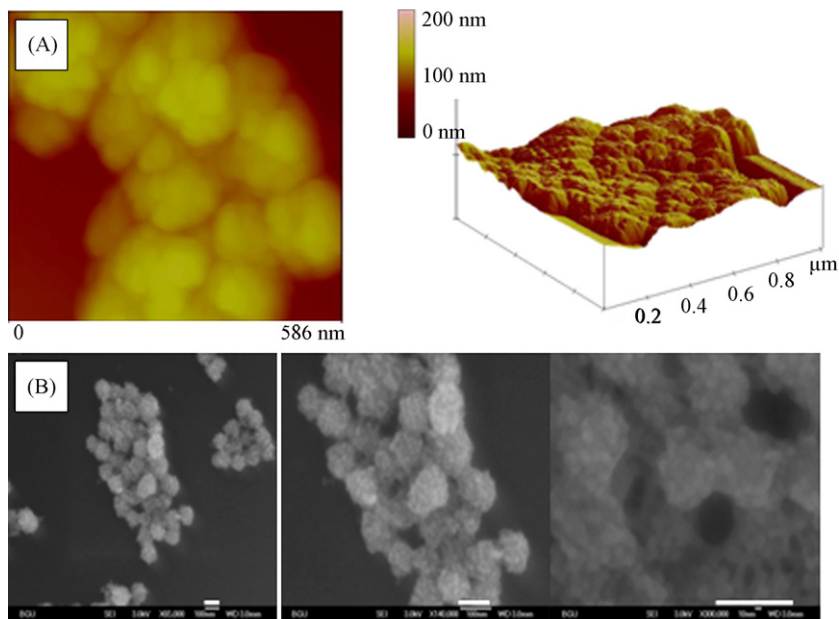


Fig. 3. (A) Two- and three-dimensional AFM images of conductive PPy-SiO₂-PPyBPh nanocomposites. (B) SEM micrographs of three different magnifications PPy-SiO₂-PPyBPh particles. Scale bar = 100 nm.

SiO₂-PPyBPh composites confirms the “raspberry-like” shape made by the silica nanoparticles.

FTIR spectra confirm the presence of benzophenone groups in the copolymerized particles. Spectra of silica, PPy-SiO₂ and PPy-SiO₂-PPyBPh particles are shown in Fig. 4. For the bare silica particles (Fig. 4A), the typical absorption bands found are: a shoulder peak near 1630 cm⁻¹ indicates -OH bending vibration, a strong and broad characteristic band near 1095 cm⁻¹ and a shoulder peak near 797 cm⁻¹ that corresponds to the asymmetric and symmetric stretching peaks of Si-O-Si [28] while a peak near 950 cm⁻¹ is due to the symmetric stretching peak of Si-OH.

Fig. 4B shows an FTIR spectrum of pure PPy with bands at 1547 (2,5-substituted pyrrole) and 1452 cm⁻¹ to be assigned to typical polypyrrole ring vibrations; a broad band at 1251 cm⁻¹ to be assigned to the N-C stretching band [29]. The IR peak observed at 889 cm⁻¹ may be assigned to the =C-H out of plane vibration indicating polymerization of pyrrole [30].

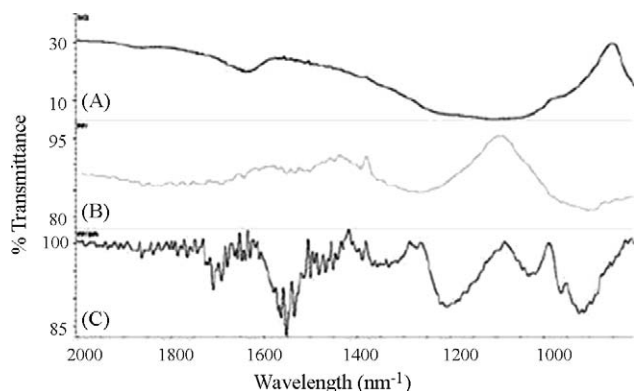


Fig. 4. Fourier transform infrared spectrum of: (A) SiO₂ nanoparticles (B) PPy-SiO₂ particles and (C) PPy-SiO₂-PPyBPh nanocomposites.

From the spectrum in 4C, α , β unsaturated ester stretching (Ar-COOR⁺) is observed at 1712.2 cm⁻¹. The recorded peak at 1694.4 cm⁻¹ is due to aromatic carbonyl (Ar-C=O) stretching. Skeletal vibrations of aromatic rings are observed at 1536.8, 1566 and 1572.4 cm⁻¹. The peaks at 1036, 1210.2, 1536.8, 1555.9, 1566 and 1572.4 cm⁻¹ are all due to in-plane bending of aromatic C-H bonds. The assignment of the observed frequencies is in full conformity with the characteristic transmission bands of benzophenone samples [31]. FTIR spectra provide a supporting evidence for the effective incorporation of benzophenone-pyrrole monomer into the conjugated copolymer.

X-ray photoelectron spectroscopy, XPS, is used for the characterization of the surface composition of PPyBPh (Fig. 5). In the XPS technique, the variations in the binding energy are used to differentiate between different chemical forms and the intensity of the peaks. The intensity (area under each peak) is proportional to the abundance of species after correction for the instrumental function and elemental photoemission cross-section. The low resolution survey spectrum (Fig. 5A) of PPyBPh/PPy copolymer consists of 5 peaks: Si2s around 103 eV and Si2p at 154 eV, Cls around 285 eV, N1s around 400 and O1s around 530. Peak fitting of the carbon 1s and oxygen 1s signals for PPy-SiO₂-PPyBPh are shown in Fig. 5B and C. The C1s signal has a roughly similar shape to that of frequently reported ones for a bulk polypyrrole [25,32].

Five peaks are used to curve-resolve the XPS carbon (1s) signal of the PPy-SiO₂-PPyBPh. These occurred at 284, 285, 286.5, 288.2 and 291.5 eV (Fig. 5B). The 284 eV peak represents contributions from both the aromatic and aliphatic carbons. The 285 eV peak contributions are mainly from carbons adjacent to carboxyl carbon (beta peak) and carbons bound to nitrogen (C-C and C-N, respectively), while the 286.5 eV peak are carbons bound to single oxygen through a single bond (C-O, C-O-C). The 288.2 eV corresponds to carbon bound to oxygen by either

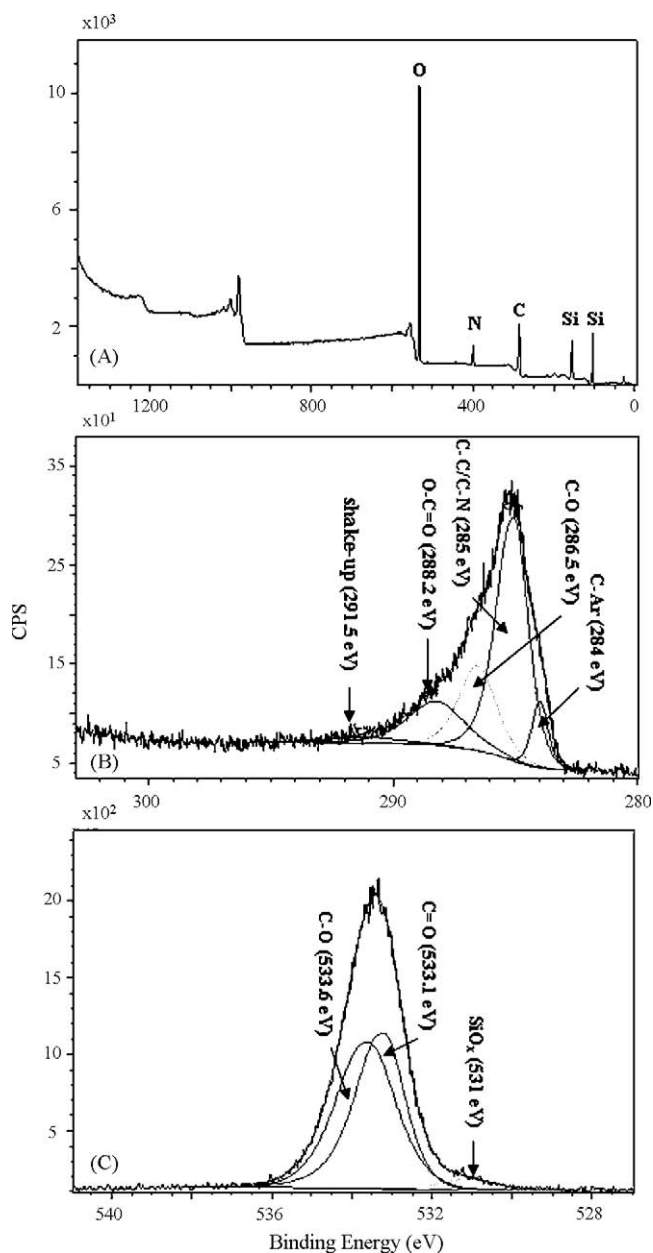


Fig. 5. XPS spectra of PPy-SiO₂-PPyBPh nanostructure: (A) survey scan, (B) C1s high resolution and (C) O1s high resolution spectra.

two or three oxygen bonds (C=O and O=C–O). In addition, there is a shake up at 291 eV arising from the aromatic rings, this is in contrast to the homopolypyrrole spectrum where no $\pi-\pi^*$ shake-up peak was observed, which is characteristic of aromatic carbon species [33]. The PPy-SiO₂-PPyBPh O1s signal was peak fitted with two components centered at 531 and 533.6 eV, which could be attributed to the carbonyl and C–O groups, respectively.

In order to quantify this effect, we determined the (C + O)/N atomic ratio in PPy/PPyBPh from the high resolution spectrum (Fig. 5B and C and Table 1). The $\sim 25\%$ increase in the (C + O)/N ratio copolymer in comparison to the PPy alone is indeed due to the addition of three oxygen and twenty three carbon atoms per pyrrole-benzophenone repeat unit from the conducting copolymer shell.

Table 1

Surface composition (atom%) of the PPy-SiO₂-PPyBPh nanostructure determined by XPS

Material	O	Si	C	N	(C + O)/N
PPy-SiO ₂	47.5%	17.1%	28.2%	7.2%	10.5%
PPy-SiO ₂ -PPyBPh	48.1%	16.9%	29.1%	5.9%	13.1%

The C_{BPh} fraction (determined by C1s peak fitting, Fig. 5B) increases from 15% to 19% ($\sim 24\%$ increase) upon copolymerization with PPyBPh while the O_{BPh} fraction (determined by O1s peak fitting) increases from 24% to 30%. These indicate incorporation of pyrrole-BPh repeat units in the copolymer over the layer surrounding the SiO₂ nanoparticles. The surface composition of PPy-SiO₂-PPyBPh and PPy-silica is presented in Table 1. The surface composition in atomic % of the nanocomposite, probed by XPS, is estimated to be: 65% silica, 30.5 \pm 4.7% pyrrole and 4.5 \pm 2.8% pyrrole-BPh [34].

4.2. Protein attachment studies with gold-labeled CTB immobilized onto PPy-SiO₂-PPyBPh nanocomposites

As mentioned, labeling CTB with 8 nm gold particles enhances the visualization of the protein attachment to the synthesized nanocomposites via electron microscopy [35]. The silica beads, coated by PPy-BPh, are further conjugated via photo-immobilization of the gold-labeled CTB subunits. The final composite (thereof PPy-SiO₂-PPyBPh-CTB-Au_{8nm}) is observed via TEM imaging (Fig. 6).

It can be clearly seen that gold labeled CTB conjugate molecules are attached to the PPy-SiO₂-PPyBPh nanocomposites but do not fully cover the surface. The main reactive sites found in CTB subunit polypeptides include the electron-rich tertiary centers, such as C γ -H of leucine (7.3% of the amino acid

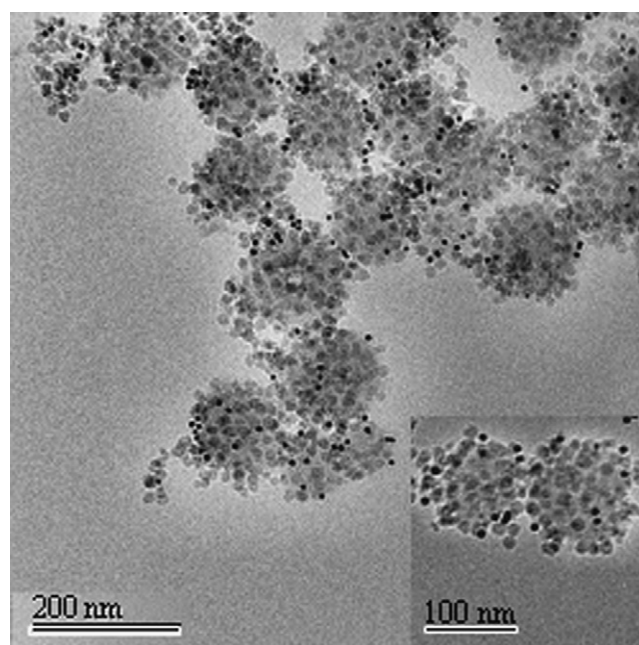


Fig. 6. TEM image of PPy-SiO₂-PPyBPh-CTB-Au_{8nm} nanocomposites.

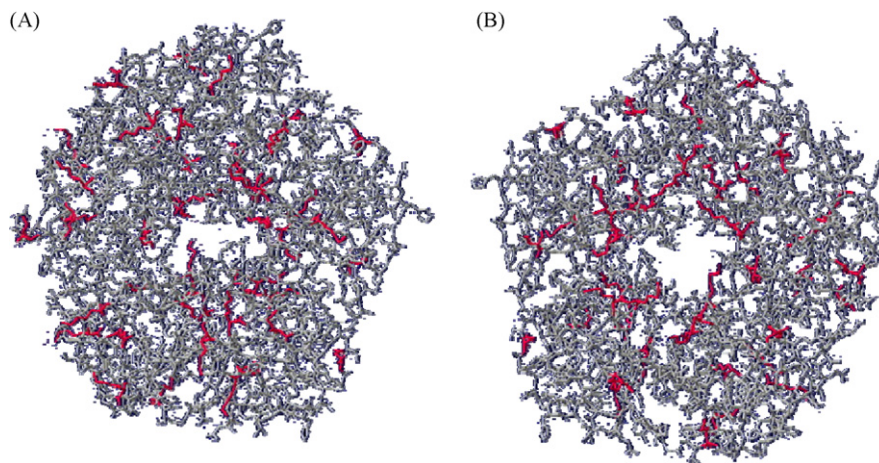


Fig. 7. Views of the three-dimensional structure of the CTB-pentamer: (A) front and (B) back view. The residues marked in red correspond to the lysine units (DeepView/Swiss PdbViewer [38]). (For interpretation of the references to color in this figure legend, the reader is referred to the web version of the article.)

composition), C_{β} -H of valine (4.8%) and CH_2 groups adjacent to heteroatoms in Lys (8.9%), Arg (2.4%) and Met (3.2%) [14]. The three-dimensional structure of the CTB pentamer subunit is presented in Fig. 7 [36].

Most aforementioned amino acids are buried inside the three-dimensional protein structure. Therefore, high steric hindrance will reduce their probabilities to participate in the photochemical binding of the CTB subunit. However, lysine amino acid residues (marked in red in Fig. 7) are located on the periphery of the protein molecule [37,38], which makes them accessible binding sites during the photochemical process. Therefore, the covalent attachment of the protein onto the benzophenone-functionalized PPy-SiO₂ nanocomposites is believed to take place due to the photochemical process between lysine amino acids in the CTB and the pendent benzophenone groups from the functionalized polypyrrole particles.

4.3. Qualitative visual agglutination test

We tested the new PPy-SiO₂-PPyBPh-CTB composite in an immunodiagnostic assay (here non-labeled CTB molecules are

used); the raspberry-like particles are used to detect the presence of the corresponding antibodies by visual agglutination test. The raspberry-like particles are incubated with anti-CTB. Visual agglutination (clumping together into visible composites) of positive PPy-SiO₂-PPyBPh-CTB-*anti-CTB* samples occurs in less than 1 h. The solution of the PPy-SiO₂-PPyBPh-CTB (control) remains well-dispersed during the same time period (Fig. 8A inset).

The visualized agglutination (clumping and precipitation) indicates that the test is positive. When clumping does not occur, the test is considered negative. Hence, simple macroscopic observation insinuates that a molecular recognition takes place.

The reaction of antibody with protein antigen is reported to consist of two-steps [39]. The first step results in the formation of an antibody-antigen complex. This reaction is followed by cross-linking of individual immune complexes forming a macromolecular aggregate, which eventually precipitates (Fig. 8A and B). Experimentally, we indeed found that upon addition of antibody the solution coagulates immediately (within a few seconds) and after about 1 h a complete phase separation is observed. The

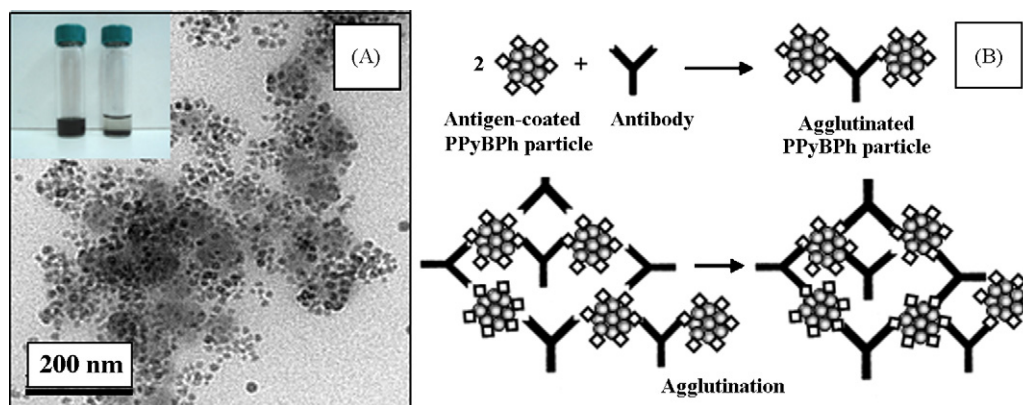


Fig. 8. (A) Clumping of the initially dispersed raspberry-shaped PPy-SiO₂-PPyBPh-CTB nanocomposites as visualized via cryo-TEM. Inset: vials containing black dispersion of SiO₂-PPyBPh-CTB nanocomposites only (left), and agglutination of the PPy-SiO₂-PPyBPh-CTB-*anti-CTB* complex. (B) Schematic illustration of the proposed agglutination process upon addition of anti-CTB to the dispersion of PPy-SiO₂-PPyBPh-CTB.

slow second reaction often requires some incubation to reach completion.

5. Conclusions

Novel PPy-SiO₂-PPyBPh composite nanoparticles are prepared and characterized in terms of size, dispersion stability, morphology and chemical structure. The reactivity of these nanocomposites is tested by model antigen (CTB), which is proved to be covalently bound to the particles through benzophenone groups. Moreover, the reactive PPy-SiO₂-PPyBPh-CTB nanocomposites are tested in a qualitative visual agglutination immunoassay. The agglutination reaction, i.e., formation of a precipitating PPy-SiO₂-PPyBPh-CTB-(anti-CTB) aggregate, macroscopically detects the presence of corresponding antibodies in the system. While a positive test includes composite clumping and precipitation, which can be ocularly detected, a negative test retains the PPy-SiO₂-PPyBPh-CTB nanocomposites in solution.

The successful development of a novel immunological agglutination route for a rapid and simple detection of diseases via human vision provides an improved tool to immunodiagnostics in laboratories or field tests for which sophisticated instrumentation is a problem.

Acknowledgements

Dr. Ayelet Vilan is kindly thanked for running the XPS experiments. Juergen Jopp is kindly acknowledged for running the AFM experiments and Dr. Dafna Frenkel for assisting in the negative staining procedure. Serge Cosnier and R.S. Marks thank NATO (Grant Award # 981086).

References

- [1] M. Cohen, L. Graves, P. Hayes, R. Gibson, J. Rasheed, J. Feeley, *J. Clin. Microbiol.* 18 (1983) 372.
- [2] J. Parsonnet, J. Mills, Z. Gillis, G. Pier, *J. Clin. Microbiol.* 22 (1985) 26.
- [3] V. Tsang, J. Brand, A. Boyer, *J. Infect. Dis.* 159 (1989) 50.
- [4] R.S. Marks, D. Cullen, C. Lowe, H.H. Weetall, I. Karube, *Handbook of Biosensors and Biochips*, John Wiley & Sons Ltd., 2007.
- [5] R.E. Ionescu, S. Cosnier, G. Herzog, K. Gorgy, B. Leshem, S. Herrmann, R.S. Marks, *Enzyme Microb. Technol.* 40 (2007) 403.
- [6] S. Cosnier, *Anal. Lett.* 40 (2007) 1260.
- [7] S. Rocha, L. Suzuki, A. Silva, G. Arruda, C. Rossi, *Rev. Inst. Med. Trop. S. Paulo* 44 (2002) 57.
- [8] A. Ferreira, A. Vaz, P. Nakamura, T. Sasaki, A. Ferreira, *J. Livramento, Rev. Inst. Med. Trop. S. Paulo* 39 (1997) 29.
- [9] R. Kesari, D.P. Mishra, G.K. Garg, A. Kumar, *Food Agric. Immunol.* 16 (2005) 73.
- [10] H.C. Koo, Y.H. Park, J. Ahn, W.R. Waters, M.J. Hamilton, G. Barrington, A.A. Mosaad, M.V. Palmer, S. Shin, W.C. Davis, *Clin. Diagn. Lab. Immunol.* 11 (2004) 1070.
- [11] J.P. McRedmond, N.T. Mulvihill, M. Kane, B. Burke, B. Aloul, T. Forde, M. Walsh, D.J. Fitzgerald, *Ir. J. Med. Sci.* 173 (2004) 204.
- [12] M.R. Pope, S.P. Armes, P.J. Tarcha, *Bioconjugate Chem.* 7 (1996) 436.
- [13] A. Azioune, A. Ben Slimane, L.A. Hamou, A. Pleuvy, M.M. Chehimi, C. Perruchot, S.P. Armes, *Langmuir* 20 (2004) 3350.
- [14] G. Dorman, G.D. Prestwich, *Biochemistry* 33 (1994) 5661.
- [15] S.A. Fleming, *Tetrahedron* 51 (1995) 12479.
- [16] C. Berens, P.J. Courtoy, E. Sonveaux, *Bioconjugate Chem.* 10 (1999) 56.
- [17] Y. Talmon, *Ber. Bunsen-Ges. Phys. Chem.* 100 (1996) 364.
- [18] N. Grossiord, O. Regev, J. Loos, J. Meuldijk, C.E. Koning, *Anal. Chem.* 77 (2005) 5135.
- [19] O. Medalia, I. Weber, A.S. Frangakis, D. Nicastro, G. Gerisch, W. Baumeister, *Science* 298 (2002) 1209.
- [20] O. Medalia, D. Tytke, R. Hegerl, M. Angenitzki, J. Sperling, R. Sperling, *J. Struct. Biol.* 138 (2002) 74.
- [21] G. Herzog, K. Gorgy, T. Gulon, S. Consier, *Electrochem. Commun.* 7 (2005) 808.
- [22] J.W. Slot, H.J. Geuze, *Eur. J. Cell Biol.* 38 (1985) 87.
- [23] K.T. Tokuyasu, *Histochem. J.* 12 (1980) 381.
- [24] W. Baschong, N.G. Wrigley, *J. Electron Microsc. Tech.* 14 (1990) 313.
- [25] G.P. McCarthy, S.P. Armes, S.J. Greaves, J.F. Watts, *Langmuir* 13 (1997) 3686.
- [26] P. Frederik, P. Bomans, <http://www.maastrichtinstruments.nl/projects/VR/DesignPhilosophy.html>, 2001.
- [27] S. Maeda, S.P. Armes, *J. Colloid Interface Sci.* 159 (1993) 257.
- [28] T. Uchino, A. Aboshi, S. Kohara, Y. Ohishi, M. Sakashita, K. Aoki, *Phys. Rev. B* 69 (2004).
- [29] M.E. Nicho, H. Hu, *Sol. Energy Mater.* 63 (2000) 423.
- [30] W. Chen, L. Xingwei, X. Gi, W. Zhaoquan, Z. Wenqing, *Appl. Surf. Sci.* 218 (2003) 216.
- [31] M. Arivanandhan, K. Sankaranarayanan, K. Ramamoorthy, C. Sanjeeviraja, P. Ramasamy, *Cryst. Res. Technol.* 39 (2004) 692.
- [32] C. Perruchot, M.M. Chehimi, D. Mordenti, M. Briand, M. Delamar, *J. Mater. Chem.* 8 (1998) 2185.
- [33] M.K. Ghosh, K.L. Mittal, *Polyimides: fundamentals and applications*, Marcel Dekker, Inc, New York, 1996, p. 222.
- [34] The C/N ratio is used to estimate the fraction of BPh in the PPy chain. It was calculated according to: $x/a = ([C]/[N] - 4)/23$, where x is the number of benzophenone units and a is the number of pyrrol rings, so x/a is the fraction. $[N]$ is the surface (XPS) concentration of nitrogen and it is proportional to a . $[C]$ is the surface (XPS) concentration of carbon and it equals to: $[C] = 4 \times a + 23 \times x$. $[C]/[N] = 4 + 23 \times x/a$.
- [35] To confirm CTB labeling by gold nanoparticles the solution is first negatively stained with 2% (w/v) uranyl acetate in order to reveal the occurrence and efficiency of the labeling (see supporting information).
- [36] E.A. Merrit, W.G.J. Hol, *PDBsum* (2000).
- [37] B. Leshem, G. Sarfati, A. Novoa, I. Breslav, R. Marks, *Luminescence* 19 (2004) 69.
- [38] <http://www.expasy.org/spdbv/>.
- [39] H. Nishizaki, Immunoassay method utilizing zeta potential and immunoassay kit, US patent 5686252 (1997) and PCT/IB1994/000039.
- [40] G.D. Prestwich, G. Dorman, J.T. Elliott, D.M. Marecak, A. Chaudhary, *Photochem. Photobiol.* 65 (1997) 222.

Low-temperature clean-up method for the determination of pyrethroids in milk using gas chromatography with electron capture detection

Simone Machado Goulart, Maria Eliana L.R. de Queiroz*, Antônio Augusto Neves, José Humberto de Queiroz

Departamento de Química, Universidade Federal de Viçosa, Av. P. H. Rolfs, s/n, 36570-000 Viçosa-MG, Brazil

Received 21 August 2007; received in revised form 22 January 2008; accepted 23 January 2008

Available online 8 February 2008

Abstract

This paper describes a new gas-chromatography with electron capture detection (GC-ECD) method for determination of some pyrethroids in milk samples. The extraction of the pyrethroids was carried out by liquid–liquid extraction with clean-up by precipitation at low temperature, without additional stages for removal of fat interferences. The method was efficient with recoveries of $93.0 \pm 0.1\%$ for cipermethrin and $84.0 \pm 0.3\%$ for deltamethrin. The quantification limits were $0.75 \mu\text{g L}^{-1}$ for both pyrethroids. The method was simple, of easy execution, and used only small quantities of organic solvent. After optimization and validation, the method was used for the determination of residues of the pyrethroids cipermethrin and deltamethrin in milk and in lactea drink commercialized in Viçosa (MG, Brazil). Some samples presented contamination with deltamethrin at levels below the maximum contamination limits established by the FAO.

© 2008 Published by Elsevier B.V.

Keywords: Pyrethroids; GC-ECD; Milk

1. Introduction

The pyrethroids deltamethrin and cipermethrin are widely used in dairy farming to kill ticks. The contamination of milk by pyrethroids is caused by the application of these products on the body of the cows, in the cow barn, or even in the milk processing areas [1,2]. The contamination of milk is an extremely preoccupying factor, because milk is an essential food for human health and is widely consumed in the initial stages of life. Therefore, the determination of residues of pyrethroids in milk is essential to assure the quality of milk consumed as food.

For the determination of pyrethroids in milk or other matrices, methods of extraction and quantification by chromatographic and electrophoretic techniques are normally used [3–9]. Normally, the conventional techniques of pesticide extraction from milk, for quantification by gas chromatography, require large amounts of solvent and involve a large number of steps, mainly for the cleaning of extracts, often resulting in loss of analytes

[10,11]. Moreover, the main difficulty for the determination of pyrethroids in both complex and fatty matrices, such as milk, is the co-extraction of fatty substances together with the pesticides [12], making quantification of residues of these pesticides in food impracticable.

An alternative liquid–liquid extraction technique was developed for extraction of organophosphorous insecticides in olive oil, in which the two phases are separated by freezing of the mixture. In this separation, the phase that contains the organic solvent and the pesticide residues remains liquid, whereas the other phase, composed mainly of the fatty matrix, is congealed. Insignificant amounts of fat materials are transferred to the liquid phase, so this technique does not require the use of additional stages for the purification of the extract [13].

The goal of the present work was the application of this new method for the extraction of deltamethrin and cipermethrin from milk, using gas-chromatography with electron capture detection (GC-ECD). This method was based on liquid–liquid extraction followed by precipitation at low temperature. The method was used to evaluate the presence of pyrethroid residues in milk and in lactea drinks commercialized in Viçosa—MG, Brazil.

* Corresponding author. Tel.: +55 31 3899 1430; fax: +55 31 3899 3065.
E-mail address: meliana@ufv.br (M.E.L.R. de Queiroz).

2. Experimental

2.1. Chemicals

All the reagents used were at least of analytical grade. Deltamethrin (99.0%) and cipermethrin (92.4%) were purchased from Chem Service (West Chester, PA, USA). Acetonitrile (Tedia/HPLC-spectro grade); anhydrous sodium sulphate (Merck), hexane (Tedia/Pesticide level), ethyl ether (Tedia/Pesticide level), and acetone (Tedia/Pesticide level) were used as received.

Standards were prepared as stock solutions of $500.0 \mu\text{g L}^{-1}$ in acetonitrile. Working solutions of $50.0 \mu\text{g L}^{-1}$ were prepared weekly by dilution of the stock solution with acetonitrile. The solutions were stored at -18°C .

2.2. Equipment

For the pyrethroid determinations, a Shimadzu gas chromatograph, model 17A, with electron capture detector was used. Separations were carried out with a HP-5 fused silica capillary column ($30.0 \text{ m} \times 0.25 \text{ mm I.D.}$; $1.00 \mu\text{m}$ film thickness). The chromatographic conditions were: Injector port temperature of 280°C ; detector temperature of 300°C , temperature program: 250°C , $10^\circ\text{C min}^{-1}$ to 280°C , held for 3 min. Nitrogen was used as carrier gas at 1.2 mL min^{-1} . The sample volume injected was $1.0 \mu\text{L}$ in the split mode (1:5).

2.3. Liquid–liquid extraction with clean up by precipitation at low temperature

To establish the best conditions for simultaneous extraction of pyrethroids, pasteurized milk samples (4.0 mL) were fortified with 0.1 mL of standard $50.0 \mu\text{g L}^{-1}$ and left standing for 24 h at 4°C . After this period the samples were submitted to the process of extraction with an organic solvent at a temperature of 25°C . The mixtures obtained in each assay were shaken on a shaking table (Tecnal TE - 420) at a rate of 175 rotations per minute and then left in freezer at -20°C for 12 h. After this period, the organic phase, having the organic solvent with the extracted compounds, remained liquid whereas the watery phase and the fatty fraction of milk were frozen. The liquid phase was passed through a previously cooled filter paper that contained anhydrous sodium sulfate (2.0 g). The extract obtained was adjusted to 10.0 mL with acetonitrile and analyzed by GC-ECD.

For the optimization of the milk pyrethroid extraction conditions, fortified milk samples (4.0 mL) were placed in contact with several different organic solvents (8.0 mL): hexane, ethyl acetate, acetone, acetonitrile and combinations of these. Using the optimized organic solvent, sample/organic solvent ratios (1:1, 1:2; 1:3 and 1:4 by volume) and the effect of agitation time (10, 20, 30, 40, 50 and 60 min) were evaluated to optimize the efficiency of the extraction of pyrethroids from milk.

2.4. Analytical curves

Quantification of extracts of milk containing deltamethrin and cipermethrin pyrethroids was carried out by the external standard method using analytical curves with seven concentration levels for each pyrethroid over the range of $0.75\text{--}10.0 \mu\text{g L}^{-1}$.

2.5. Method validation

Some analytical parameters of the liquid–liquid extraction technique with clean-up by precipitation at low temperature were evaluated, such as precision, accuracy, linearity, selectivity, limit of detection (LOD) and limit of quantitation (LOQ), as suggested by the protocols of the principal Brazilian regulatory agencies [14–17].

2.6. Application of the liquid–liquid extraction method with clean up by precipitation in low temperature

The validated method was applied for the determination of deltamethrin and cipermethrin in samples of type B milk, UHT whole milk, three different brands of pasteurized type C milk and two different brands of commercial lactea drink, purchased in local stores during January and February of 2004.

3. Results and discussion

The organic solvent, the effect of the ratios between the volumes of the sample and of the organic solvent and the time of agitation on the efficiency of the extraction were evaluated for the determination of pyrethroids. Of all solvents evaluated, the best results were with acetonitrile ($93.0 \pm 0.1\%$ for cipermethrin and $84.0 \pm 0.3\%$ for deltamethrin), and a mixture of acetonitrile and ethyl acetate in the ratio of 7:1 ($82.0 \pm 1.6\%$ for cipermethrin and $95.0 \pm 2.1\%$ for deltamethrin). Other solvents, such as hexane, ethyl ether, ethyl acetate, acetone and mixtures of those presented extractions below to 20% for the two pyrethroids. Although either acetonitrile or the mixture acetonitrile and ethyl acetate (7:1) could be used as organic solvent, pure acetonitrile was chosen. This solvent was also used by Rizoş et al. [13] in the extraction of organochloro pesticides from olive oil. In that study, acetonitrile, amongst all evaluated solvents, presented the highest recoveries of the compounds under study.

The ratio of the volume of acetonitrile to that of the sample that showed the best results was 2:1, giving recoveries superior to 80%. Moreover, this ratio between organic solvent and sample allowed an adequate separation of the frozen phase and the liquid organic phase. Other sample/organic solvent ratios resulted in recoveries lower than 63%. The time of contact between acetonitrile and the milk samples that resulted in the best recoveries of cipermethrin and deltamethrin was 20 min under low frequency agitation on the shaking table. Under these conditions, the percentage of recovery of pyrethroids in the milk sample was $93.0 \pm 0.1\%$ and $84.0 \pm 0.3\%$, for cipermethrin and deltamethrin, respectively.

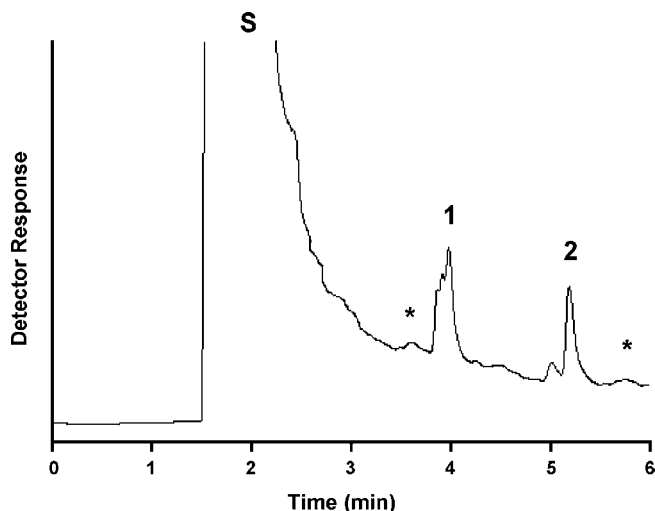


Fig. 1. Chromatogram of a milk extract fortified with $10 \mu\text{g L}^{-1}$ of deltamethrin and cipermethrin. Peaks identification: S—solvent, 1—cipermethrin, 2—deltamethrin, *—unknown.

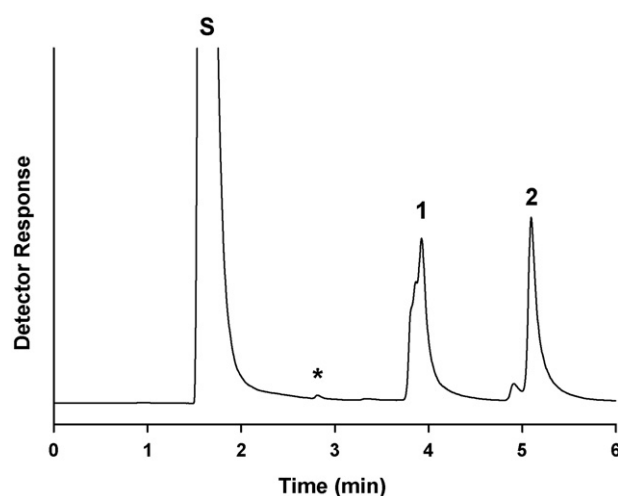


Fig. 2. Representative chromatogram of a standard solution of $100.00 \mu\text{g L}^{-1}$ of deltamethrin and cipermethrin. Peaks identification: S—solvent, 1—cipermethrin, 2—deltamethrin, *—unknown.

The optimized technique consists in adding 8.0 mL of acetonitrile to 4.0 mL of milk sample, the mixture being agitated for 20 min at 175 rpm. The extracts are frozen for approximately 12 h at -20°C and what stays in the liquid phase are the acetonitrile and the extracted material. On removal from the flask, the acetonitrile is passed through a pre-cooled filter that contains anhydrous sodium sulfate (2.0 g). The extracted volume is adjusted to 10.0 mL with acetonitrile and analyzed by GC-ECD.

An important advantage of this liquid–liquid extraction technique with clean-up by partition at low temperature is that the extract obtained is clear and relatively free of fat interference, as can be observed in the chromatogram of a milk extract obtained after extraction (Fig. 1). A chromatogram of a $100 \mu\text{g L}^{-1}$ standard solution of deltamethrin and cipermethrin is shown in Fig. 2. The presence of double peaks for pyrethroids is related with the presence of both isomeric forms produced during injection in the chromatograph [18]. The areas attributed to each pyrethroid are considered as the sum of the peak of areas of the isomers.

The quantification method, at optimized chromatographic conditions, showed good detectability, with a limit of detection of deltamethrin of $0.25 \mu\text{g L}^{-1}$, calculated from the detector response using a signal to noise ratio of 3 while the quantification limit was $0.75 \mu\text{g L}^{-1}$ using a signal to noise ratio of 10.

The detector response was linear over an ample range of concentrations, from 0.75 to $1000.0 \mu\text{g L}^{-1}$. Linearity expressed by the linear regression coefficient, was 0.999 for both compounds, which showed an acceptable adjustment of the linear regression data. The time of the chromatographic analysis was less than 7 min. Cipermethrin, with a retention time of 3.99 min, and deltamethrin, with a retention time of 5.22 min, could be simultaneously identified and quantified in the extracts.

Method repetitibility, expressed as the estimated coefficient of variation (%CV), was evaluated by applying the method to seven samples ($n=7$) that were fortified with deltamethrin and cipermethrin standard solutions of $1.25 \mu\text{g L}^{-1}$. Coefficients of variation of 3.8% for deltamethrin and 8.5% for cipermethrin were obtained, values that are relatively low, considering the sample complexity. In methods for impurity or trace analysis, the accepted coefficients of variation are up to 20%, taking into consideration the sample complexity [15].

The intermediate precision was evaluated on 3 different days, by the same analyst [14]. Assays with fortified milk samples were carried out at 1.25, 2.50 and $3.75 \mu\text{g L}^{-1}$. The coefficients of variation were inferior to 8.0%.

After optimization and validation, the liquid–liquid extraction technique with clean-up by precipitation at low temperature was applied to samples of milk and lactea drink commercialized

Table 1
Milk and lactea drinks analyzed for the presence of deltamethrin and cipermethrin

Samples	Deltamethrin ($\mu\text{g L}^{-1}$)	Cipermethrin ($\mu\text{g L}^{-1}$)
Pasteurized whole milk type B	<LOD	<LOD
Pasteurized whole milk type C, sample 1	1.45 ± 0.04	3.68 ± 0.54
Pasteurized whole milk type C, sample 2	<LOD	<LOD
Pasteurized whole milk type C, sample 3	0.98 ± 0.30	2.71 ± 0.02
Pasteurized skim milk type C	<LOD	<LOD
UHT whole Milk	0.25 ± 0.05	<LOD
Lactea Drink (UHT) 1	0.92 ± 0.40	1.51 ± 0.90
Lactea Drink (UHT) 2	<LOD	<LOD

The assays were carried out in triplicate.

in Viçosa (MG, Brazil). The residual levels of deltamethrin and cipermethrin found in these samples are presented in Table 1.

Considering that type C milk is a mixture having different origins and that the spraying of animals with pyrethroids is not the only method used by producers to control ticks, a dilution of pyrethroids in milk is observed. In this way, the amounts of pyrethroid residues found in the samples were below the limits demanded by international legislation [19,20], with values ranging from 1.0 to 5.0 $\mu\text{g L}^{-1}$. Similar results were observed in the lactea drink samples. For skim milk sample the pyrethroid residues were below the detection limit, because skim milk has less fat than whole milk.

4. Conclusions

The conventional techniques of pesticide analysis in milk have many steps and use large quantities of organic solvents. The method proposed here, based on liquid–liquid extraction with clean-up by precipitation at low temperature is simple, of easy execution and efficient, using reduced amounts of organic solvent, with few manipulation steps and no additional purification step. Moreover, the analytical methodology proposed for the determination of deltamethrin and cipermethrin residues in samples of different types of milk and lactea drink is sufficiently practical, allowing detection and quantification of residual levels of pyrethroids, below of the maximum limits suggested by CODEX Alimentarius (FAO/WHO) [19,20].

Acknowledgement

The authors acknowledge financial support and fellowships from the Fundação de Amparo à Pesquisa do Estado de Minas Gerais (FAPEMIG) and the Conselho Nacional de Desenvolvimento Científico e Tecnológico (CNPQ). They also

acknowledge Prof. Carol H. Collins for language assistance and Dr. Anízio M. Faria for discussions of results.

References

- [1] A. Venant, E.V. Neste, S. Borrel, J. Mallet, *Food Addit. Contam.* 7 (1990) 117.
- [2] M.H. Akhtar, K.E. Martin, H.L.C. Trebholm, *J. Agric. Food Chem.* 34 (1986) 753.
- [3] M. Anastassiades, S.J. Lehotay, D. Stajnbaher, F.J. Schenck, *J. AOAC Int.* 86 (2003) 412.
- [4] M.H. Akhtar, *J. Chromatogr.* 246 (1982) 81.
- [5] M. Zehringer, A. Herrmann, *Eur. Food Res. Technol.* 212 (2001) 247.
- [6] A. Sassine, S. Moura, V.M. Léo, O.V. Bustillos, *J. Anal. Toxicol.* 28 (2004) 238.
- [7] A. Di Muccio, P. Pelosi, D.A. Barbini, T. Generali, A. Ausili, F. Vergori, *J. Chromatogr. A* 765 (1997) 51.
- [8] L.M.R. Pérez, J.H. Borges, M.A.R. Delgado, *J. Sep. Sci.* 29 (2006) 2557.
- [9] F. Bordet, D. Inthavong, J.M. Fremy, *J. AOAC Int.* 85 (2002) 1398.
- [10] A.W. Chen, J.M. Fink, D.J. Letinski, *J. Agric. Food Chem.* 44 (1996) 3534.
- [11] D.Z. Bissacot, I. Vassilief, *J. Anal. Toxicol.* 21 (1997) 397.
- [12] A. Venant, E.V. Neste, S. Borrel, J. Mallet, *Food Addit. Contam.* 7 (1990) 535.
- [13] C.L. Rizos, E.J. Avramides, F. Cherasco, *J. Chromatogr. A* 912 (2001) 135.
- [14] ANVISA. Portaria No. 1.469/2000, of 29 December 2000. National Health Agency, Brasil.
- [15] M. Ribani, C.B.G. Bottoli, C.H. Collins, I.C.S.F. Jardim, L.F.C. Melo, *Quim. Nova* 27 (2004) 771.
- [16] F. M. Lanças, Validação de métodos cromatográficos de análise -Métodos Cromatográficos de Análise 6. Editora Rima, São Carlos, SP (2004).
- [17] INMETRO—Instituto Nacional de Metrologia, Normalização e Qualidade Industrial. Orientações sobre Validação de Métodos de Ensaio Químicos, DOQ-CGCRE-008 (2003).
- [18] K. Maštovska, S.J. Lehotay, *J. Chromatogr. A* 1040 (2004) 259.
- [19] WHO. Environmental Health Criteria. Cypermethrin. Who Technical Report Series (1989) N.82.
- [20] WHO. Environmental Health Criteria. Deltamethrin. Who Technical Report Series (1990) N.97.

Determination of perfluorooctanesulfonate and perfluorooctanoic acid in sewage sludge samples using liquid chromatography/quadrupole time-of-flight mass spectrometry

Rui Guo, Qunfang Zhou, Yaqi Cai, Guibin Jiang*

State Key Laboratory of Environmental Chemistry and Ecotoxicology, Research Center for Eco-Environmental Sciences, Chinese Academy of Sciences, Beijing 100085, China

Received 7 November 2007; received in revised form 22 January 2008; accepted 25 January 2008
Available online 3 February 2008

Abstract

A new method is developed for the determination of perfluorooctanesulfonate (PFOS) and perfluorooctanoic acid (PFOA) in sewage sludge samples. The analytes in sewage sludge samples are extracted by methanol and formic acid, cleaned by C18 solid-phase extraction, then separated, identified and quantitated by liquid chromatography/quadrupole time-of-flight mass spectrometry (LC-QTOF-MS). A C18 column (150 mm × 2.1 mm, 3.5 μm) with gradient elution of MeOH–H₂O (60:40) containing 5 mmol/L ammonium acetate and MeOH–H₂O (80:20) is used for the chromatographic separation. [M–K][–] ions at *m/z* 498.93 for PFOS and [M–COOH][–] ion at *m/z* 368.97 for PFOA are selected for QTOF-MS in the negative electrospray ionization mode. The detection limits for PFOS and PFOA in sewage sludge samples are 0.5 and 0.8 ng/g, respectively. The spiked recoveries are in the range of 85–114 and 71–98% for PFOS and PFOA, respectively. The proposed method is successfully applied to the analysis of PFOS and PFOA in 16 sewage sludge samples from China. PFOS and PFOA are detected in most sewage sludge samples and the concentrations of PFOS and PFOA are up to 5383 and 4780 ng/g (oven dry weight), respectively.

© 2008 Elsevier B.V. All rights reserved.

Keywords: PFOS; PFOA; Sewage sludge; HPLC-QTOF

1. Introduction

Perfluorinated surfactants perfluorooctanesulfonate (PFOS) and perfluorooctanoic acid (PFOA) are additives in a wide variety of industrial products and commodities, including protective coatings for carpets and apparel, paper coatings, insecticide formulations, and surfactants [1]. PFOS is also used as a surfactant in firefighting foams [2]. It spreads widely in the environment, wildlife, and humans [3–10]. Subchronic exposure to PFOS may lead to significant weight loss accompanied by hepatotoxicity and reductions of serum cholesterol and thyroid hormones. It has also been reported that PFOA can produce hepatotoxicity, anorexia, alteration of fatty acid metabolism, reduction of circulating thyroid hormones and androgen, bradycardia, and hypothermia in the rat [11]. The 3M Company, one of the most fluorochemical manufacturing companies, has claimed to cease

the manufacturing of perfluorooctanyl-related materials in 2000. Products made of perfluorooctanyl-related materials, however, are still widely available all over the world. Some publications have demonstrated widespread distribution of PFCs in China [12]. The distribution mode and the contamination levels of PFCs in some matrices such as sewage sludge are still not clear now and worthy of being studied in China.

High-performance liquid chromatography (HPLC) with triple quadrupole mass spectrometry in electrospray negative mode is the most extensively applied method for the analysis of PFCs in various environmental and biological matrices, because triple quadrupole mass spectrometry has high precision, wide linear range and high sensitivity for PFOS and PFOA determination in complicated matrices. It is able to determinate specific fragmentation of isolated precursor ions and eliminate background noise. More and more laboratories have HPLC coupled with triple quadrupole mass spectrometry, however, most of them have no ability to analysis PFOS and PFOA due to the high instrument blank. So auxiliary line fittings of LC/MS/MS should be stainless to avoid the contamination, which greatly

* Corresponding author. Tel.: +86 10 62849179; fax: +86 10 62849179.
E-mail address: gjbjiang@rcees.ac.cn (G. Jiang).

increases the experimental cost. Now only a few laboratories can afford it. The application of HPLC–MS in the selected ion monitoring (SIM) mode and HPLC-ion trap mass spectrometry has recently been reported as the attractive alternatives for the analysis of perfluorooctanesulfonate and related fluorochemicals [13–15]. However, when these methods are applied to detect low concentrations of PFCs in complicated matrix, the interference of matrix must be carefully gotten rid of. Other mass spectrometric techniques such as quadrupole time-of-flight mass spectrometry (QTOF-MS) are also applied in the environmental samples analysis for structure elucidation or confirmation purposes because it has high resolution and sensitivity. QTOF-MS has distinct advantages over other scanning instruments including the detection of a high percentage of ions, high mass resolution and accuracy, fast acquisition rates, high sensitivity, and large mass range. QTOF-MS technique is considered to be one of the attractive alterations for the unequivocal identification of unknown compounds using full-spectrum scan. However, it is seldom applied to quantitative analysis because of its relatively narrow linear range for most of the compounds. Recently, several papers have reported about liquid chromatography/quadrupole time-of-flight mass spectrometry (LC–QTOF-MS) being used to detect trace levels of organic pollutions [16,17]. It not only can record selected precursor ions, but also can offer high mass resolution and accuracy. Considering its specific advantage of high mass accuracy and sensitivity, we apply it to determine PFOS and PFOA in sewage sludge samples as there is no report on the application of LC–QTOF-MS in the analysis of PFCs in environmental samples. PFOS and PFOA can be confirmed by the retention time and the accurate mass spectrometry. The single MS mode is used for both qualitative and quantitative analysis. The MS/MS mode can be applied to identify PFOS and PFOA in more detail. The proposed method is applied to accurate and precise analysis of PFOS and PFOA in 16 sewage sludge samples.

2. Experimental

2.1. Chemicals and reagents

Potassium PFOS was purchased from Fluka (Milwaukee, MI, USA). PFOA and perfluoroheptanoic acid (PFHpA, as lock mass standard) were purchased from Aldrich (Milwaukee, MI, USA). HPLC-grade methanol was purchased from J.T. Baker (Philipsburg, NJ, USA). Ultra-pure water was prepared by Milli-Q system (Millipore, Milford, MA, USA). Ammonium acetate [$\text{CH}_3\text{COONH}_4$] and acetic acid (CH_3COOH) were of analytical reagent grade. The C18 SPE cartridge (500 mg, 6 mL) was bought from Alltech (Deerfield, IL, USA).

The nitrogen gas (N_2) was used as evaporation and nebulization gas. The argon was used as collision gas. All stock solutions were kept in polypropylene volumetric flasks at 4 °C in the dark.

2.2. Instrumentation

The analysis of PFOS and PFOA are carried out by the hyphenated system of HPLC with quadrupole time-of-flight

mass spectrometry. A model Alliance 2695 from Waters (Waters Corp., USA) is used to separate PFOS and PFOA. The separate column is XTerra C18 column (particle size of 3.5 μm , 2.1 mm i.d. \times 150 mm in length, Waters, Ireland) and the guard column is XTerra C18 2.1 mm \times 10 mm packed with particle size of 3.5 μm (Waters, Ireland). Optimum separation is achieved with a binary mobile phase at a flow rate of 300 $\mu\text{L}/\text{min}$. A deionized water solution containing 5 mmol/L ammonium acetate (pH 6.0) and methanol serve as mobile phase. According to previous studies, volatile buffer ammonium acetate in the mobile phase is essential to the ionization of PFOA and PFOS [18,19] because its suppressing effect on the signal is weak. Additionally, as a buffer compound, it is effective at pH 6.0, which is found to be the optimum value of pH for the separation of PFCs. The gradient starts at 60% methanol followed by 0.5 min ramp to 80% methanol, hold 9 min, and then reverting to initial conditions by 0.5 min ramp allowing 8 min stabilization time.

A quadrupole time-of-flight (QTOF micro) mass spectrometer (Micromass, Manchester, UK) with a Z-spray ESI source working in negative mode is used for the identification and quantitative analysis of PFOS and PFOA. Optimal ionization source working parameters are as follows: capillary and sample cone voltages, 2.5 kV and 35 V; source and desolvation temperatures, 120 and 250 °C; cone and desolvation gas flows (nitrogen), 100 and 650 L/h, respectively. The collision gas is argon at the pressure of 5.0×10^{-5} Torr and the collision energy is 35 V. Both the high- and low-resolution for mass filter are set at 10.0 V. The pressure in the TOF cell is lower than 5.0×10^{-7} Torr (1 Torr = 133.322 Pa). m/z 498.93 \pm 0.05 for PFOS and $[\text{M}-\text{COOH}]^-$ ion at m/z 368.97 \pm 0.05 for PFOA are monitored for their accurate identification and the selection of precursor ions.

The TOF analyzer is calibrated every day for the accurate mass analysis. The lock mass is utilized to guarantee the mass accuracy. Continuum mode TOF mass spectra are recorded using single MS modes from m/z 50 to 600 with a duty cycle of 1.0 s. The acquired data are converted to centroid (80% of the top peak area) to implement lock mass adjustment and to generate the accurate mass spectra. A window width of ± 0.05 Da is selected to obtain enough selectivity and to decrease the noise (i.e. better limits of detection). For MS/MS mode, the precursor ion is selected in the quadrupole analyzer and fragmented in the hexapole cell by applying collision cell offset voltages 35 V, depending on the compound. Product ion spectra are recorded in the TOF analyzer from m/z 50 to 600, too. Afterwards, the spectra are lock mass corrected using the m/z value of the precursor ion. Data are collected and processed by MassLynx v4.1 software.

2.3. Sample collection

Sewage sludge samples were collected in polypropylene bottles from 16 municipal waste water treatment plants in February 2004. They were transported in ice and frozen (-15 °C) until analysis. The sewage sludge samples were firstly grounded and homogenized in a methanol-rinsed carnelian mortar. Each sewage sludge sample was dried in oven at 103 °C overnight

to eliminate aliquots. The concentration of PFOS and PFOA in sewage sludge samples were calculated and expressed in the unit of ng/g (oven dry weight).

2.4. Sample preparation

A simple and efficient sample pretreatment method including extraction and cleanup steps used herein is similar to that described elsewhere [20], which offers satisfying quantitative recoveries of anionic PFCs in sewage sludge matrix. Briefly, approximate 0.1 g of oven dried sewage sludge samples are extracted by the mixture of 1% formic acid and methanol. In order to enrich the analytes and to remove the acetic acid, salts, and potential matrix interferences, the combined sludge extract is then loaded at a flow rate of 1–2 mL/min on a vacuum manifold onto a 500-mg C18 SPE cartridges which has been pre-conditioned with 10 mL of methanol followed by 10 mL of 1% acetic acid. The SPE cartridges are then rinsed with 10 mL of Milli-Q water, dried under vacuum for at least 2 h. PFCs are eluted from the cartridge with 4 mL of methanol and collected in 1:1 (v/v) methanol/acetone-washed graduated glass tubes. The eluent is then concentrated to 2 mL under nitrogen. In order to get rid of the deposited impurities, the analyte is transferred into a 10-mL glass vial. 800 μ L of methanol is used to rinse the graduated glass tubes for the complete transfer of the analytes and 1200 μ L of 0.01% aqueous ammonium hydroxide solution is added. To reduce matrix interferences and ensure the analyte's concentrations in the quantitative range of LC-QTOF-MS, sewage sludge extracts are further diluted to 5 mL by adding 1 mL of a 70:30 (v/v) methanol/aqueous ammonium hydroxide (0.01%) solution. The extracts are stored at 4 °C until analysis. A 500- μ L aliquot of extract is transferred to a 1.5-mL glass auto sampler vial.

2.5. Analytical procedure

A sample volume of 10 μ L is injected into the system of HPLC-QTOF-MS. After the base-lined separation by the C18 reversed column, PFOS and PFOA compounds are identified and further quantitatively analyzed by single mass mode using characteristic ions of $[M-K]^-$ at m/z 498.93 and $[M-COOH]^-$ at m/z 368.97 for the determination of PFOS and PFOA, respectively. Quantitative calculation is performed based on the ratio of the peak areas of the analytes to that of the standards. Three analysis replicates are performed for all the standards and samples.

In order to obtain the calibration curves of PFOS and PFOA, the matrix-matched calibration graphs for PFOS and PFOA are prepared by injecting extracted blank spiked with increasing amounts of standard ranging from 0 to 200 ng/g. The matrix-matched standards are then analyzed by the system of HPLC-QTOF-MS and the curves are drawn based on the average peak areas of PFOS and PFOA, which give an acceptable linearity ($\gamma^2 > 0.998$) over the test range.

For the confirmation of the feasibility of the proposed method in practical analysis of the sewage sludge samples, spiked recovery experiments are carried out by adding three levels of PFOS

(5, 80, 125 ng/g) and PFOA (8, 80, 160 ng/g) into a blank sewage sludge from Haikou and processed the pretreatment steps as described above, finally analyzed by HPLC-QTOF-MS. Five replicates are carried out to evaluate the precision of the analytical procedure.

3. Results and discussion

3.1. Optimization of buffer levels in mobile phase

According to previous reports, the volatile buffer ammonium acetate at pH 6.0 is found the optimum buffer for the ionization of PFOA and PFOS [18,19]. Additionally, the concentrations of the buffer may affect the intensity of signal to noise (S/N) ratio of the tested chemicals. Effects of concentration on the intensity of signal to noise (S/N) ratio are studied by adding different concentrations of ammonium acetate (0, 1, 5 and 10 mmol/L) to the inorganic phase. With the increase of the concentration of buffer, the intensities of PFOS and PFOA are enhanced. But 10 mmol/L ammonium acetate leads to less intensity both of PFOS and PFOA (data not shown). The highest S/N ratio of PFOS and PFOA are obtained using 5 mM ammonium acetate in water-methanol. The optimized mobile phase composition is applied to the following experiments.

3.2. Optimization of QTOF-MS parameters

The impacts of mass spectrometric parameters, such as cone, capillary and collision voltage, are investigated by the analysis of standard solution of PFOS (10 ng/mL) and PFOA (10 ng/mL). It is found that the intensity of PFOS and PFOA varies with the increasing of cone voltage from 20 to 60 V. With the increase of cone voltage, the response of PFOS and PFOA increase initially, and then they reach the maximum, followed by a fall trend. The curves of ion intensity versus cone voltage are obtained. As shown in Fig. 1, a sample cone voltage of 35 V is finally selected for further experiments. Under these experimental conditions, single MS spectra of PFCs obtained with the QTOF-MS instrument agree with those previously reported using quadrupole and ion trap mass spectrometry [21].

Capillary voltage is another important parameter greatly affecting the sensitivities. The responses of PFOS and PFOA significantly increase with capillary voltage varying from 1.0 to 2.5 kV, and then obtain stable state. As we all know, at relatively high voltages, the tip of the capillary can discharge, which would damage the ion source. So a 2.5 kV of capillary voltage is ultimately chosen.

With the enhancement of collision energy, the ratios of the intensities of specific fragment ions to those of the precursor ions increased significantly, whereas it is essential to maintain enough intensity of precursor ions to confirm the existence of PFOS and PFOA. In the proposed method, MS/MS mode is applied to confirm the feasibility and veracity of single mode. 35 V collision voltages are selected to produce specific fragmentation ions. In the determination of PFOS and PFOA in sewage sludge samples, single ms mode is used to confirm and calculate them. Individual analyte standard is directly infused to tune the

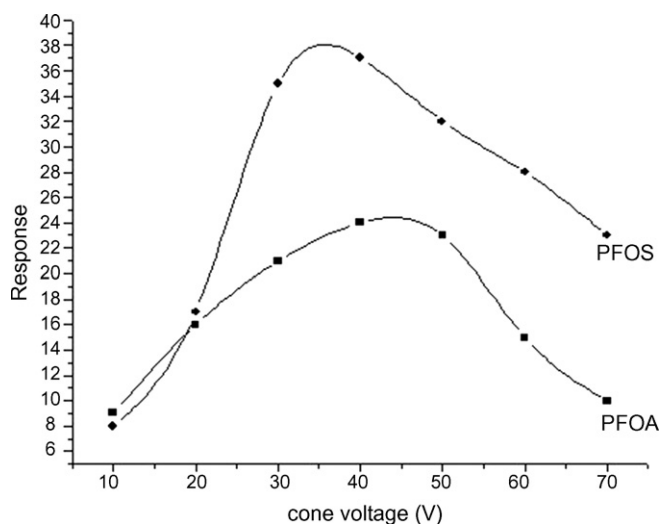


Fig. 1. The effect of sample cone voltage on the intensity of PFOS and PFOA (10 ng/mL for PFOS, 10 ng/mL for PFOA), flow rate is 10 μ L/min; capillary voltage is 2.5 kV; collision energy is 5 V; source and desolvation temperatures, 120 and 250 $^{\circ}$ C; cone and desolvation gas flows (nitrogen), 100 and 650 L/h, respectively.

instrument based on the parent ion and to determine the fragment ions of interest. All the optimal values achieved are used for the following analysis of the standards and the sewage sludge samples.

3.3. Fragmentation pathways of the PFOS and PFOA

Previous studies using triple quadrupole mass spectrometry have elucidated the structure of PFCs [20]. To obtain a more accurate assignment, the MS/MS spectra of PFOS and PFOA using the QTOF instrument are studied. Collision energies for all analytes are set at 35 V in order to obtain both the maximum signals for product ions and at least \sim 10% for the parent ion (optimal values are given in Section 3). In general, the MS/MS spectra of PFOS and PFOA are similar to those obtained previously with triple quadrupole mass spectrometry in terms of fragmentation patterns [20]. However, high-resolution makes it obtain more accurate mass. Fig. 2 shows the MS/MS spectrum obtained with the QTOF-MS instrument for PFOS, where the assignments with their corresponding mass accuracies are also indicated. For PFOS, the fragment at m/z 79.95 and 98.95 correspond to the SO_3^- and FSO_3^- , respectively [10]. For PFOA (Fig. 3), m/z 368.97, 168.98 and 118.99 correspond to the $\text{C}_7\text{F}_{15}^-$, C_3F_7^- and C_2F_5^- , respectively.

3.4. Method validation

Linear response range and the limits of quantitation of PFOS and PFOA using the LC-QTOF-MS system are studied to evaluate the feasibility and veracity of the proposed method in the application to analyzing sewage sludge sample. For sewage sludge samples, matrix-related ion interference may exist using LC-MS/MS analysis [20], which leads to the decrease in detector response. Using a matrix-matched standard can compensate for the interference. The analytical characteristics of the method,

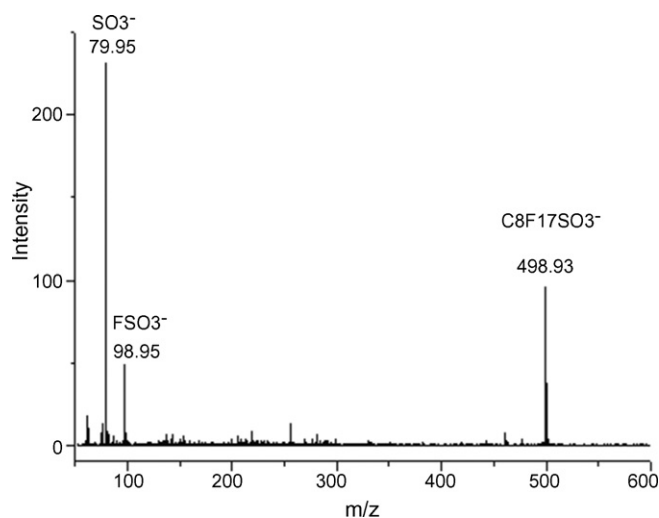


Fig. 2. The fragmentation ions of PFOS. The concentration of PFOS is 100 ng/mL; flow rate is 10 μ L/min. Capillary voltage and sample cone: 2.5 kV and 35 V; collision energy is 35 V; source and desolvation temperatures: 120 and 250 $^{\circ}$ C; cone and desolvation gas flows (nitrogen): 100 and 650 L/h, respectively. A window width of \pm 0.05 Da is selected.

such as linear response range, reproducibility and limits of quantitation are investigated and the results depicted in Table 1. The linearities of the PFOS and PFOA are calculated from the five-level calibration curve over the range from 5 to 125 ng/g for PFOS and 8 to 160 ng/g for PFOA, and an acceptable linearity ($\gamma^2 = 0.998$) in the test ranges are obtained. Quantification is based on the response of the external standards that bracketed the concentrations found in samples.

The limits of detection (LOD) based on three times of S/N ratio are 1.5 and 2.4 ng/g for PFOS and PFOA, separately. The limits of quantitation (LOQ), defined as S/N ratio of 10 are 5 and 8 ng/g for PFOS and PFOA in sewage sludge samples, respectively.

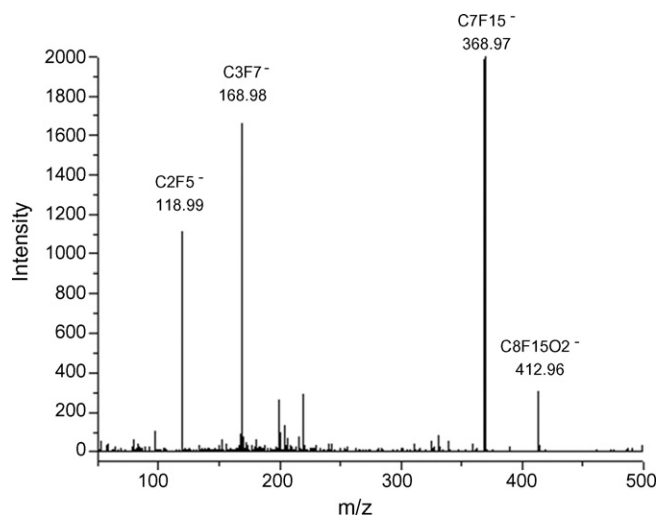


Fig. 3. The fragmentation ions of PFOA. The concentration of PFOA is 500 ng/mL; flow rate is 10 μ L/min. Capillary voltage and sample cone: 2.5 kV and 35 V; collision energy is 35 V; source and desolvation temperatures: 120 and 250 $^{\circ}$ C; cone and desolvation gas flows (nitrogen): 100 and 650 L/h, respectively. A window width of \pm 0.05 Da is selected.

Table 1
The standard curves of the analytical method

Analyte	Quantitation ions	Linear curve	γ^2	Linear range (ng/g)	LOD (ng/g)	LOQ (ng/g)
PFOS	$[M-K]^-$ m/z 498.93	$y = 0.9834x + 1.0869$	0.998	5–125	1.5	5
PFOA	$[M-COOH]^-$ m/z 368.97	$y = 1.0568x + 1.1667$	0.999	8–160	2.4	8

The accuracy, precision, and stability of the developed method are evaluated by the spiked recovery experiments at low-, middle- and high-spiked concentrations of PFOS and PFOA, respectively. The results shown in Table 2 indicate that the spiked recoveries are in the range of 85–114% for PFOS and 71–98% for PFOA. The relative standard deviations are less than 15%. The results are in compliance with those reported in the literature [20]. The results reveal that the method developed here could be applied to the analysis of PFOA and PFOS in sewage sludge samples.

3.5. Application

The proposed method is successfully used to analyze 16 sewage sludge samples from China. These samples collected from 16 cities, which distribute in large area of China, to some degree, could represent the contamination level of PFOS and PFOA in China. Fig. 4 shows the mass chromatogram comparison of the standards and the sewage sludge sample from Yinchuan. PFOS and PFOA are confirmed by comparing the mass spectrum and the corresponding retention time of samples with those of the standards. The concentrations are estimated by external standard method based on the matrix-matched standard calibration curves. Table 3 shows the contamination levels of PFOS and PFOA in sewage sludge samples. It could be found that PFOS and PFOA compounds are detected in most of the sewage sludge samples and the concentrations range from 278 to 5383 ng/g (dry weight), which is generally higher than the levels reported previously [20]. According to Table 3, it could be found that the contamination of PFOS and PFOA spreads widely in China, though there are no large production plants for PFCs. The values of PFOS and PFOA detected in Xiamen1 and Xiamen2 differ from each other greatly, it is might due to different waste water sources. According to previous reports, the waste water from industry plants, the concentrations of PFCs are high, while from domestic products, the concentrations of PFCs are low. The current contamination might come from the release

of PFC-containing products. The volatile precursors of PFOS and PFOA might be another potential source for the widespread contamination. PFOS may be present as unreacted residual in consumer products such as clothing and surface-treatment products. Previous study also suggests PFOS can be come from the biotransformation of *N*-ethyl-*N*-(2-hydroxyethyl) perfluorooctanesulfonamide [20]. PFOA, as the precursor of many surface materials, might remain in the product and be released when

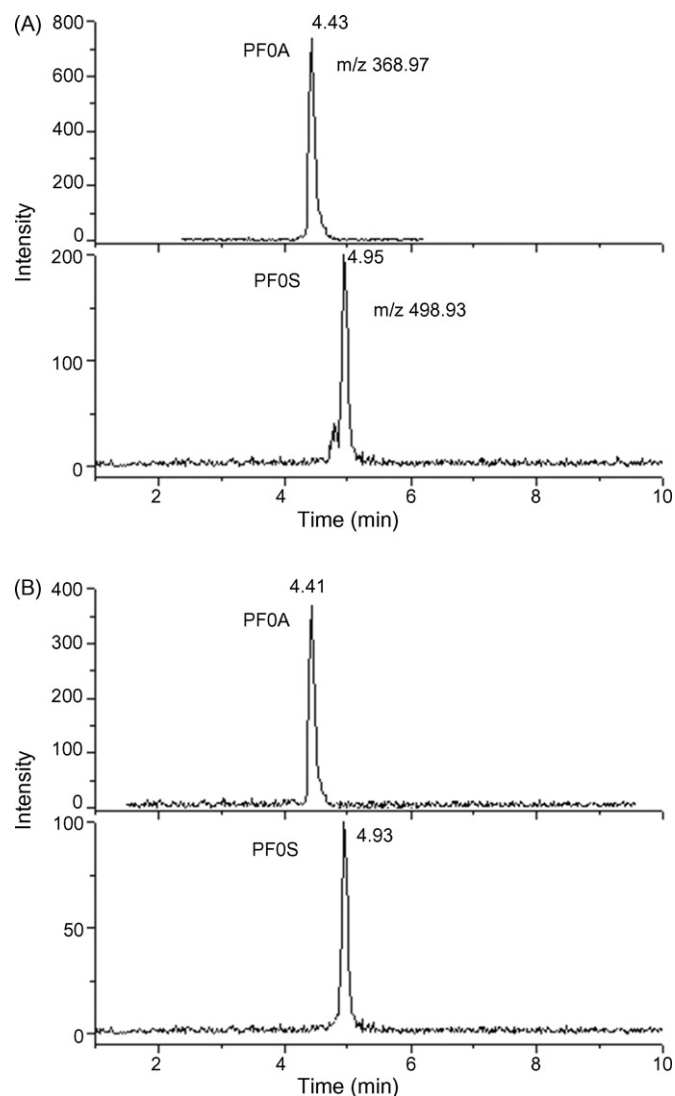


Fig. 4. The comparison of LC-MS ion chromatogram of PFOS and PFOA in standard mixture (45 ng/mL for PFOS, 100 ng/mL for PFOA) with a sample from Yinchuan (PFOS 2560 ng/g, PFOA 3259 ng/g). The condition of mass spectrometry is same as those in Fig. 2 except the collision energy is 5 V. The condition of separation is same with mentioned in Section 2.2, the injection volume is 10 μ L. (A) The chromatogram of standard. (B) The chromatogram of sample.

Table 2
Spiked recoveries of PFOS and PFOA in a Haikou sewage sludge sample^a ($n = 5$)

Analyte	Spiked level (ng/g)	Mean recovery \pm R.S.D. (%)
PFOS	5	99 \pm 15
	80	96 \pm 11
	125	105 \pm 9
PFOA	8	83 \pm 12
	80	88 \pm 10
	160	84 \pm 8

^a The Haikou sewage sludge sample served as the blank matrix. The experimental conditions are same as those in Fig. 4

Table 3
Concentrations of PFOS and PFOA (ng/g dry weight) in sewage sludge samples (average concentration \pm standard error) ($n = 3$)

Sample site	PFOS	PFOA
Baoding	N.D.	N.D.
Beixiaohe	280 \pm 34	492 \pm 69
Guangzhou1	5383 \pm 108	4591 \pm 89
Guangzhou2	1015 \pm 51	1680 \pm 118
Haerbin	N.D.	1650 \pm 82
Haikou	N.D.	N.D.
Hangzhou	N.D.	N.D.
Hefei	236 \pm 19	493 \pm 49
Linyi	N.D.	N.D.
Liuzhou	2522 \pm 76	1792 \pm 90
Shanghai	472 \pm 52	454 \pm 54
Shenyang	973 \pm 78	2159 \pm 86
Wulumuqi	1081 \pm 65	4780 \pm 143
Xiamen1	4257 \pm 85	2365 \pm 95
Xiamen2	278 \pm 25	563 \pm 62
Yinchuan	2560 \pm 77	3259 \pm 75

Note: N.D. = not detected. The experimental conditions are same as those in Fig. 4.

overheated. Other potential sources might include industrial sources, consumer products containing residuals, and releases of PFC-containing aqueous film-forming foam (AFFF) from firefighting activity and training, etc. It still needs further investigations on the potential sources of the PFOS and PFOA in China. There is not enough toxicological data affirming the safe levels of PFOA and PFOS for environmental organisms and human health. It should cause more concerns on the occurrence of these compounds in environment and organisms. More researches should be carried out for the further risk assessment of environmental contamination of PFCs.

4. Conclusion

LC-QTOF-MS is a powerful tool of yields full-scan mass spectrum about structure of the molecule to enable unequivocal confirmation of the presence of the PFOS and PFOA. The method using C18-SPE for sample pretreatment and LC-QTOF-MS system for the analysis of PFOS and PFOA in sewage sludge samples is firstly developed herein. The satisfying spiked recoveries and R.S.D.s confirm the reliability of the proposed method. The acceptable sensitivities endue it practical application to analyze PFOS and PFOA contamination in sewage sludge samples.

Acknowledgement

This research is supported by a grant from the Chinese Academy Sciences no. KZCX3-SW-431.

References

- [1] 3M, Health and Environmental Assessment of Perfluorooctane Sulfonic Acid and its Salts, EPA docket AR-226-1486, US Environmental Protection Agency, Washington, DC, 2003.
- [2] M.M. Schultz, D. Barofsky, J.A. Field, Environ. Sci. Technol. 38 (2004) 1828.
- [3] G.W. Olsen, T.R. Church, J.P. Miller, J.M. Burris, K.J. Hansen, J.K. Lundberg, J.B. Armitage, R.M. Herron, Z. Medhdizadehkashi, J.B. Nobiletti, E.M. O'Neill, J.H. Mandel, L.R. Zobel, Environ. Health Perspect. 111 (2003) 1892.
- [4] J.P. Giesy, K. Kannan, Environ. Sci. Technol. 35 (2001) 1339.
- [5] J.P. Giesy, K. Kannan, Environ. Sci. Technol. 36 (2002) 147A.
- [6] K. Kannan, J. Koistinen, K. Beckmen, T. Evans, J. Garzelany, K.J. Hansen, P.D. Jones, J.P. Giesy, Environ. Sci. Technol. 35 (2001) 1593.
- [7] K. Kannan, S.P. Hansen, C.J. Franson, W.W. Bowerman, K.J. Hansen, P.D. Jones, J.P. Giesy, Environ. Sci. Technol. 35 (2001) 3065.
- [8] K. Kannan, J.L. Newsted, R.S. Halbrook, J.P. Giesy, Environ. Sci. Technol. 36 (2002) 2566.
- [9] K. Kannan, S. Corsolini, J. Falandysz, G. Oehme, S. Focardi, J.P. Giesy, Environ. Sci. Technol. 36 (2002) 3210.
- [10] K. Kannan, J.W. Choi, N. Iseki, K. Senthilkumar, D.H. Kim, S. Masunaga, J.P. Giesy, Chemosphere 49 (2002) 225.
- [11] C. Lau, J.L. Butenhoff, J.M. Rogers, Toxicol. Appl. Pharmacol. 198 (2004) 231.
- [12] M.K. So, S. Taniyasu, N. Yamashita, J.P. Giesy, J. Zheng, Z. Fang, S.H. Im, P.K.S. Lam, Environ. Sci. Technol. 38 (2004) 4056.
- [13] C.L. Tseng, L.L. Liu, C.M. Chen, W.H. Ding, J. Chromatogr. A 1105 (2006) 119.
- [14] A. Karrman, B. van Bavel, U. Jarnberg, L. Hardell, G. Lindstrom, Anal. Chem. 77 (2005) 864.
- [15] B. Boulanger, J. Vargo, J.L. Schnoor, K.C. Hornbuckle, Environ. Sci. Technol. 38 (2004) 4064.
- [16] E. Barceli o-Barrachina, E. Moyano, M.T. Galceran, J. Chromatogr. A 1054 (2004) 409.
- [17] X. Fang, X. Fan, Y. Tang, J. Chen, J. Lu, J. Chromatogr. A 1036 (2004) 233.
- [18] C.A. Moody, W.C. Kwan, J.W. Martin, D.C.G. Muir, S.A. Mabury, Anal. Chem. 73 (2001) 2200.
- [19] J.W. Martin, S.A. Mabury, K. Kannan, U. Berger, P. de Voogt, J. Field, J. Franklin, J.P. Giesy, T. Harner, D.C.G. Muir, B. Scott, M. Kaiser, U. J arnberg, K.C. Jones, H. Schroeder, M. Simcik, C. Sottani, B. Van Bavel, A. K arrman, G. Lindstr om, S. van Leeuwen, Environ. Sci. Technol. 37 (2004) 248A.
- [20] C.P. Higgins, J.A. Field, C.S. Criddle, R.G. Luthy, Environ. Sci. Technol. 39 (2005) 3946.
- [21] C.Li. Tseng, L.L. Liu, C.M. Chen, W.H. Ding, J. Chromatogr. A 1105 (2006) 119.

PVC membrane electrode for the potentiometric determination of Ipratropium bromide using batch and flow injection techniques

M.E.M. Hassouna*, S.A.A. Elsuccary

Faculty of Science, Beni-Suef University, Beni-Suef, Egypt

Received 14 September 2007; received in revised form 7 January 2008; accepted 9 January 2008

Available online 17 January 2008

Abstract

Ipratropium (IP⁺) ion-selective electrode (ISE) has been constructed from poly(vinyl chloride) matrix membrane containing Ipratropium–tetraphenylborate (IP–TPB) as the electroactive component using 2-nitrophenyloctylether as plasticizer. The electrode exhibits near Nernstian response to Ipratropium bromide (IPBr) over the concentration range 10⁻⁵ to 10⁻² mol L⁻¹ and detection limit 5.1 × 10⁻⁶ mol L⁻¹. The electrode offers significant advantages including long lifetime (>2 months), excellent stability and reproducibility, fast response time (<10 s), wide pH working range (pH 2–9), high thermal stability (isothermal coefficient 0.37 mV/°C) and superior selectivity for IPBr over a large number of inorganic and organic substances. The electrode was successfully used as indicator electrode in the potentiometric titration of IPBr versus sodium tetraphenylborate (NaTPB) and in the determination of IPBr in Atrovent[®] vials and spiked urine samples applying batch and flow injection techniques, with satisfactory results.

© 2008 Elsevier B.V. All rights reserved.

Keywords: Ipratropium bromide; PVC membrane electrodes; Potentiometric determination; Flow injection analysis

1. Introduction

Ipratropium bromide (IPBr), chemically described as 8-azoniabicyclo [3,2,1]-octane-3-(3-hydroxy-1-oxo-2-phenylpropoxy)-8-methyl-8-(1-methylethyl) bromide monohydrate, is a synthetic quaternary ammonium antimuscarinic agent with peripheral effects similar to those of atropine. It is administered by inhalation as a bronchodilator in the treatment of chronic reversible airways obstruction, particularly in asthma and chronic bronchitis [1,2]. The structural formula is shown in Fig. 1.

HPLC [3–8], HPLC/MS [9], CE/MS [10], radio-receptor assay [11,12], non-aqueous titration [13], kinetic and first-derivative spectrophotometry [14] have been reported as suitable analytical methods for the determination of IPBr. However, most of these methods are generally involved in the use of more sophisticated instrumentation or more complex procedures, and some of them suffer from poor linearity of the calibration curve or from long response times.

Potentiometric detection based on ion-selective membrane electrodes (ISMES), as a simple method, offers several advantages such as speed and ease of preparation and procedures, simple instrumentation, relatively fast response, wide dynamic range, reasonable selectivity, application in colored and turbid solutions and low cost.

Although ion-selective membrane electrodes have been widely used in pharmaceutical analysis [15–22], no electrodes responsive to IPBr have so far been published.

Therefore, the aim of this work is the development of a polymeric ion-selective electrode (ISE) for IPBr. Studies on the determination of IPBr in pharmaceutical preparations (Atrovent[®] vials) and in spiked urine samples were carried out to illustrate the analytical utility of the proposed method in both batch and FI conditions.

2. Experimental

2.1. Reagents and materials

All reagents were of analytical grade and used without any further purification. Doubly distilled water was used throughout. IPBr·H₂O (95.8% as anhydrous IPBr) was kindly provided

* Corresponding author. Tel.: +20 123861504.

E-mail address: mhassouna47@yahoo.com (M.E.M. Hassouna).

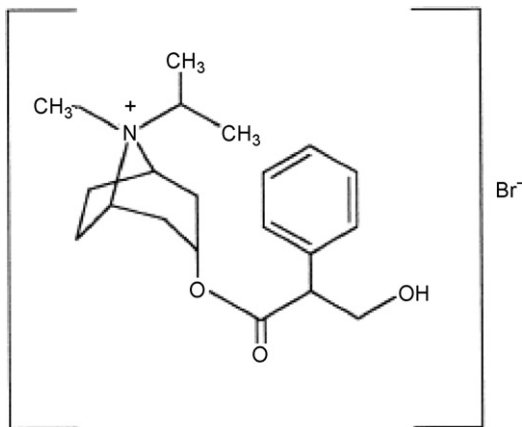


Fig. 1. Structure formula of Ipratropium bromide (IPBr).

by Boehringer Ingelheim, Germany. High relative molecular weight poly(vinyl chloride) (PVC), nitrobenzene (NB), benzyl acetate (BA), and tetrahydrofuran (THF) were from Aldrich. Dibutylphthalate (DBP) was from Riedel de Hein, dioctylphthalate (DOP) was from Merck, 2-nitrophenyl octyl ether (NPOE) was from (Fluka), sodium tetraphenylborate (NaTPB) was from Panreac. Atrovent[®] unit dose vials, labeled to contain 250 μg anhydrous IPBr per 2 mL, which were assayed for IPBr content in this study were purchased from a local pharmacy in Beni-Suef

Stock IPBr-H₂O solution 0.1 mol L⁻¹ was prepared by dissolving 2.246 g IPBr-H₂O in 50 mL of water. NaTPB was freshly prepared in hot water. Ionic strength adjustor buffer (ISAB), Composed of acetate buffer (pH 4.5; 0.5 mol L⁻¹) and 1.0 mol L⁻¹ NaCl, was prepared from acetic acid, sodium acetate and sodium chloride and was diluted as necessary.

2.2. Preparation of Ipratropium-tetraphenylborate (IP-TPB) ion pair

The IP-TPB ion pair was prepared by mixing 25 mL of 0.01 mol L⁻¹ solution of IPBr with 25 mL of 0.01 mol L⁻¹ solution of NaTPB. The formed white precipitate was filtered, and washed thoroughly with water until no bromide ion was detected in the washing solution. The white precipitate was then dried

under vacuum and finely powdered. The composition of the ion pair was found to be 1:1 as confirmed by elemental analysis done at the central laboratory unit (United Arab Emirates University, Al-Ain, UAE). The percentage values that were found are 80.94, 7.66, and 2.08 and the calculated values are 81.1, 7.73, and 2.15 for C, H, and N, respectively.

2.3. Preparation of membranes

The components listed in Table 1 were mixed and dissolved in 2 mL THF. The resulting solution was transferred into a 2.5-cm diameter glass ring placed on a glass Petri dish. After slow evaporation of THF at room temperature for 36 h, membranes with ~0.2 mm thickness were formed. These membranes were used for electrode construction in batch and FI modes.

2.4. Batch setup

2.4.1. Electrode construction

Electrodes were assembled by cutting 6-mm diameter disks from the prepared membranes and mounting them into the polished end of PVC tubing (4-mm i.d.) using 5% PVC-THF solution. The electrodes were then filled with a mixture of 0.1 mol L⁻¹ NaCl and 10⁻³ mol L⁻¹ IPBr as the internal filling solution and were conditioned in a solution of the same composition.

2.4.2. Electrochemical system

The electrochemical cell may be represented as follows: Ag/AgCl(s)/filling solution/membrane/sample solution/1.0 mol L⁻¹ CH₃COOLi salt bridge/44.0 mol L⁻¹ KCl/Ag/AgCl. The cell potential was measured using an Orion 420Aplus digital pH/mV meter (Thermo Electron Corporation, USA) and in some runs a four-channel high-input impedance module [23] attached to ADC-16 data acquisition card (purchased from Pico Technology Limited, London, UK) connected to a personal computer. The reference electrode was a Jenway Ag/AgCl double junction containing 1.0 mol L⁻¹ lithium acetate solution in the outer compartment.

Table 1
Influence of the membrane composition on the characteristics of the electrodes

Electrode no.	IP-TPB (mg)	PVC (mg)	Plasticizer (mg)	Slope (mV/decade)	Regression coefficient	Linear range (mol L ⁻¹)	LOD (mol L ⁻¹)	Response time (s)
1	3	61.1	DBP (121)	41.7	0.9999	7.9 × 10 ⁻⁵ to 10 ⁻²	1.0 × 10 ⁻⁵	<15
2	4	60.5	DBP (120.9)	57.53	0.9995	1.0 × 10 ⁻⁵ to 10 ⁻²	6.8 × 10 ⁻⁶	<10
3	5	60.0	DBP (120)	59.8	0.9991	1.0 × 10 ⁻⁵ to 10 ⁻²	5.6 × 10 ⁻⁶	<10
4	5	60.0	NB (120)	42.7	0.9993	9.8 × 10 ⁻⁵ to 10 ⁻²	1.3 × 10 ⁻⁵	<20
5	5	60.3	BA (121.1)	43.3	0.9991	2.4 × 10 ⁻⁵ to 10 ⁻²	5.5 × 10 ⁻⁶	<20
6	5	60.0	DOP (122)	60.2	0.9999	2.6 × 10 ⁻⁵ to 10 ⁻²	5.7 × 10 ⁻⁶	<15
7	5	60.0	2-NPOE (120)	59.4	0.9995	1.0 × 10 ⁻⁵ to 10 ⁻²	5.4 × 10 ⁻⁶	<10
8	4	60.3	2-NPOE (120.7)	61.4	0.9999	1.0 × 10 ⁻⁵ to 10 ⁻²	5.1 × 10 ⁻⁶	<10
9	4	91.3	DBP (91.1)	57.83	0.9993	1.0 × 10 ⁻⁵ to 10 ⁻²	6.8 × 10 ⁻⁶	<10
10	4	91.8	2-NPOE (91.5)	58.81	0.9998	1.0 × 10 ⁻⁵ to 10 ⁻²	5.1 × 10 ⁻⁶	<10

2.5. Flow injection setup

2.5.1. Construction of electrode unit

A laboratory-made tubular flow-through IP⁺-selective polymer membrane electrode was prepared as described by Meyerhoff et al. [24,25]. The polymer ISE-membrane casting solution was made by re-dissolving 6-mm diameter piece from the previously mentioned membrane in 0.5 mL of THF.

The tubular IP⁺-ISE was made by the following method. A 20-gauge syringe needle (1.5-in. long) with its tip rounded off was inserted into the bore of a small piece (50-mm) of PVC tubing (1.0-mm i.d.). A small part of the tubing wall near its midpoint was cut away using a razor blade. With the needle still in place, six drops of IP-TPB casting solution were added slowly, covering the hole. Between drops, the THF was allowed to evaporate. The final ISE-tube was allowed to dry completely for an additional 1–2 h. The tube was then mounted into an outer plastic jacket in which a hole slightly larger than the outer diameter of the electrode tube had been drilled. The tube was sealed in place with rubber glue (to prevent leakage of the internal reference solution) while the ISE-membrane was facing down. The syringe needle was removed after the glue had dried. The electrode assembly was completed by filling the inside of the jacket with the filling solution (sufficient to cover the tubular electrode) and inserting Ag/AgCl reference wire.

2.5.2. Setting up the IP⁺-ISE-FIA system

Fig. 2 shows a schematic diagram of the setup for the IP⁺-ISE-FIA system. The carrier stream reagent (acetate buffer (pH 4.5; 0.05 mol L⁻¹), NaCl 0.1 mol L⁻¹) was kept in a polyethylene bottle and delivered through the system by a four-channel variable speed peristaltic pump (Masterflex model 7519-20, Cole

Parmer Inc.). The outlet of the pump was connected to a rotary injection valve (Rheodyne, P/N 7125) which had a 100 μL sample injection loop with 30 cm polyethylene tubing coiled in 2.5-cm diameter reel. The outlet of the valve was connected to the IP⁺-ISE through 5-cm stainless steel tubing. The outlet of the IP⁺-ISE assembly was allowed to flow over the surface of a double junction Ag/AgCl reference electrode to complete the electrochemical cell, and then the sample solution was allowed to drip into a waste collector. Potentiometric measurements were made by connecting the IP⁺-ISE and reference electrode to the high-input impedance module and the ADC-16 data logger. The potential was continuously output to PC through the PicoLog recorder software.

2.6. Sensor calibration and selectivity

In batch measurements, the IP⁺-ISE and the reference electrode were immersed in 2.5 mL ISAB diluted to 25 mL with water, and suitable increments of standard IPBr solution were added, so as to span the concentration range 10⁻⁷ to 10⁻² mol L⁻¹ IPBr, while the solution was constantly stirred at ~25 °C. The EMF was continuously recorded using PicoLog recorder software. Additionally, a series of standard IPBr solutions covering the concentration range 10⁻⁷ to 10⁻² mol L⁻¹ were separately prepared and the EMF of each solution was measured using a pH/mV meter, under constant stirring. The EMF readings were plotted against pIPBr. The calibration process was repeated at 20, 30, 40, 50, 60 and 70 °C to study the effect of temperature.

In FI mode, a series of freshly prepared standard IPBr solutions in the concentration range of 10⁻⁶ to 10⁻² mol L⁻¹ were injected into the flow stream at room temperature, and the cal-

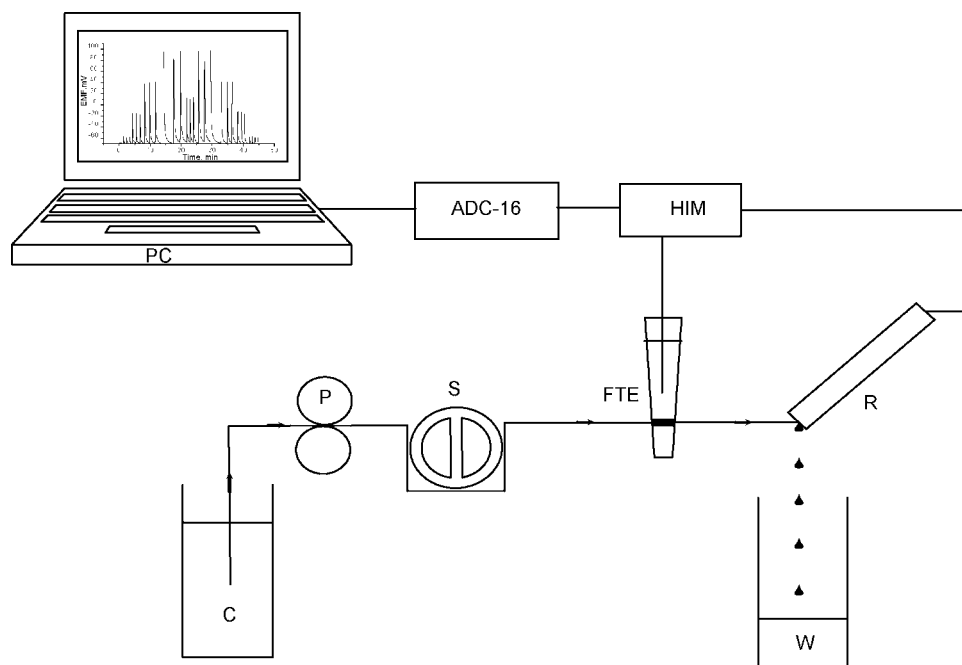


Fig. 2. Schematic diagram of the flow injection system: C, carrier stream reagent; P, peristaltic pump; S, sample injection valve; FTE, flow-through electrode; R, Ag/AgCl reference electrode; W, waste; HIM, high-input impedance module; ADC-16, ADC-16 data logger; PC, personal computer.

ibration curve was constructed by plotting the average peak potential of three signals for each standard versus pIPBr.

The selectivity coefficients $K_{IP,B}^{Pot}$ were evaluated by the separate solution method [26,27] in which the potential of a cell, comprising IP⁺-ISE and a Ag/AgCl reference electrode, was measured with each of two separate solutions: one is 10^{-4} mol L⁻¹ IP⁺, and the other is 10^{-4} mol L⁻¹ interferent B. The value of $K_{IP,B}^{Pot}$ was calculated from the equation:

$$\log K_{IP,B}^{Pot} = \frac{E_2 - E_1}{S} + \left(1 - \left(\frac{Z_{IP}}{Z_B} \right) \right) \log[1.0 \times 10^{-4}]$$

where E_1 and E_2 are the measured EMF values for the two solutions, respectively, and S is the slope of the calibration graph.

The selectivity coefficients in case of neutral and organic species were determined by the matched potential method (MPM) [27]. In this method, the potentiometric selectivity coefficient is defined as the activity ratio of primary and interfering ions that gives the same potential change under identical conditions. At first, a known activity (a_A') of IPBr solution is added into a reference solution that contains a fixed activity (a_A ; 1×10^{-6} mol L⁻¹) of IPBr, and the corresponding potential change (ΔE) is recorded. Next, a solution of an interfering ion is added to the reference solution until the same potential change (ΔE) is recorded. The change in potential produced at the constant background of the primary ion must be the same in both cases. The selectivity factor $K_{IP,B}^{MPM}$ for each interferent was calculated using the following equation:

$$K_{IP,B}^{MPM} = \frac{a_A' - a_A}{a_B}$$

2.7. Potentiometric determination of IPBr

2.7.1. Direct calibration method

ISAB (1 mL) was added to a 3 mL aliquot of the Atrovent[®] vials and the solution was diluted to 10 mL with water. The EMF values were measured using both batch and FI modes, and the IPBr concentration was calculated from their corresponding calibration curves.

2.7.2. Standard additions method

The standard additions method was applied as described elsewhere [39]. Atrovent[®] test solutions were prepared as previously described in the direct calibration method. The EMF values were recorded before and after addition of small increments (50–200 μ L) of standard IPBr solution (0.01 mol L⁻¹) using batch as well as FI modes.

The sample concentration was calculated using the equation:

$$C_x = \left(\frac{C_{st} V_{st}}{V_x} \right) \left(\frac{1}{10^{\Delta E/S} - 1} \right)$$

where C_x is the IPBr concentration of the test sample, C_{st} is the concentration of the standard solution, V_x and V_{st} are the corresponding volumes, S is the slope of the electrode response and ΔE is the difference in (mV) between EMF after and before addition of the standard solution.

2.7.3. Potentiometric titration of IPBr

Three solutions containing 10.7, 17.2, and 22.4 mg IPBr·H₂O were diluted to 20 mL with water, ISAB (2.5 mL) was added to each solution, and the solution was titrated with standard solution of 0.01 mol L⁻¹ NaTPB.

A 3 mL aliquot of Atrovent[®] sample adjusted with ISAB (2.5 mL) and diluted to 10 mL with distilled water was titrated against 0.001 mol L⁻¹ NaTPB. The volumes of titrant at the end points were obtained using the differential method.

2.7.4. Determination of IPBr in urine

Two series of solutions were prepared by adding varied quantities of IPBr·H₂O (5.0×10^{-4} to 1.0×10^{-2} mol) to urine sample (2.5 or 1.0 mL), the pH and the ionic strength were adjusted by adding ISAB (2.5 or 1 mL), and the volume is completed to 25 or 10 mL with distilled water to cover the concentration range 2×10^{-5} to 4×10^{-4} mol L⁻¹ and 5×10^{-5} to 1×10^{-3} mol L⁻¹, respectively. The IPBr contents in the first series were recovered by the batch mode, while those in the second one were recovered by the flow injection mode, using the direct calibration method. Appropriate aliquots of standard IPBr solution (0.01 mol L⁻¹) was then added to each solution of the above two series and the IPBr contents were recovered by the standard additions method as described in Section 2.7.2.

2.8. HPLC measurements

The measurements were carried out with isocratic conditions close to those reported in Ref. [8] using Agilent HPLC 1100 system, Agilent ZORBAX Eclipse XDB-C8 (4.6 mm \times 150 mm) column, acetonitrile/phosphate buffer (pH 4; 0.1 mol L⁻¹) (20:80) as a mobile phase with a flow rate of 1 mL min⁻¹ and UV detection at 210 nm at room temperature.

3. Results and discussion

3.1. Optimization of the membrane composition

The effect of the amount of ion pair in the membrane phase on the potentiometric response was investigated. The data shown in Table 1 clearly indicates that the electrode with small amount (1.6 wt%) of IP-TPB ion pair has a sub-Nernstian slope. In order to obtain Nernstian response, the electrode must have sufficient amount of lipophilic ion-pair. The electrodes with sufficient amounts (2.2–2.7 wt%) of IP-TPB exhibited improved sensitivity and working range. However, increasing the wt% above 2.7 turns the membrane turbid and the response deteriorates due to the membrane inhomogeneity.

Plasticizers play an important role in the behavior of ISEs. For the plasticizer to be adequate for its use in a polymeric ISE, it should gather certain properties and characteristics such as having high lipophilicity, high-molecular weight, low tendency for exudation from the polymeric matrix, low-vapor pressure and high capacity to dissolve the substrate and other additives present in the polymeric membrane. Additionally, its viscosity and dielectric constant should be adequate [28–30].

Five plasticizers namely BA, NB, DOP, DBP and 2-NPOE were evaluated. As shown in Table 1, the best performances, in terms of slopes, linear range and detection limit obtained have the following order: 2-NPOE \geq DBP > DOP > BA > NB. These results show that the plasticizer molecule should be sufficiently large as not to be lost to the aqueous solution; smaller molecules of very high polarity such as nitrobenzene ($\epsilon_r = 34.8$) are not suitable since they are readily lost from the membranes when it is contacted by an aqueous medium [31].

The best results were obtained for 2-NPOE ($\epsilon_r = 24$) and DBP ($\epsilon_r = 6.4$), being slightly better for 2-NPOE, since they have greater polarity, their lipophilicity is in principle high enough to avoid exudation. Membranes with DOP ($\epsilon_r = 5.1$) showed slightly higher LOQ and LOD, since it has a slightly higher lipophilicity and lower polarity compared with DBP and 2-NPOE.

Membranes constructed with BA ($\epsilon_r = 5.0$) had the worst results. This is due to the fact that the membrane does not reach the minimum polarity required for improving mobility and diffusion of the active centers, which is impeded, at the same time, as a result of high lipophilicity of the employed plasticizer.

These results seem to indicate a synergism between lipophilicity and polarity, where the best results were obtained when these properties reach an intermediate value [30]. Furthermore, the plasticizer/PVC ratios were examined; the results showed that 1:1 and 2:1 are comparable.

Based on the above-mentioned response characteristics of all the examined electrodes, electrode no. 8 was chosen for all subsequent studies.

3.2. The effect of the internal filling solution

Ionophore-based membranes are prone to suffer from electrolyte coextraction at the inner membrane side; as a result, the composition of the internal solution influences both the achievable lower detection limit and the shape of the response function [32–35].

With ionophore-free ion-exchanger-based membranes, no ionophore is present in the membrane that could lead to undesired coextraction of electrolyte at the inner membrane side, only a marginal influence of the inner solution composition on the detection limit is found [36].

To investigate the effect of the internal filling solution composition, different solutions of pure IPBr (10^{-4} to 10^{-2} mol L $^{-1}$) or mixed with NaCl (0.1 mol L $^{-1}$) were tested. The obtained results showed that the variation of the internal solution composition did not produce any significant difference in the potential response, except for an expected change in the intercept of the resulting Nernstian plots. Hence, a mixture of (10^{-3} mol L $^{-1}$ IPBr, 0.1 mol L $^{-1}$ NaCl) was chosen as internal solution in all subsequent studies.

3.3. Influence of pH and electrolyte concentration

The effect of pH on the electrode response was studied by measuring the electrode response at IPBr concentrations of 10^{-5} , 10^{-4} and 10^{-3} mol L $^{-1}$ over a wide pH range. The pH

of the solution was adjusted by adding small volumes of concentrated hydrochloric acid or concentrated sodium hydroxide to the test solution. The electrode response was found to be independent on the pH range from 2 to 9. At lower pH values, the potential increased probably due to the response of the membrane to H $_3$ O $^+$, while at high pH (pH > 9), the potential decreased due to the interference from OH $^-$. It should be noted, however, that such convenient working pH range of the electrode covers a wide range of samples that can be measured without prior pH adjustment.

The choice of a suitable ionic strength value at which the membrane electrode exhibits the best response is also of prime importance in quantitative analyses. Since the Atrovent $^{\text{®}}$ sample contains NaCl as additive, NaCl was chosen to adjust the ionic strength. The potential values of the membrane electrode at different electrolyte concentrations (0.02–0.2 mol L $^{-1}$ NaCl) were determined at pH 4.5. It was found that the electrode followed Nernstian behavior towards IPBr at all the examined ionic strength values.

The effect of NaCl on the electrode response was also examined by addition of NaCl to 10^{-4} mol L $^{-1}$ IPBr solution prepared in acetate buffer (pH 4.5; 0.05 mol L $^{-1}$). The electrode showed a slight anionic response (decrease in potential) towards chloride ion in the concentration range (0.02–0.08 mol L $^{-1}$). Increasing the NaCl concentration up to 0.2 mol L $^{-1}$ did not cause any further decrease in potential.

ISAB, composed of acetate buffer (pH 4.5; 0.05 mol L $^{-1}$) and 0.1 mol L $^{-1}$ NaCl, was chosen for further investigations.

3.4. Conditioning and storage

There was no significant difference in the response obtained whether fresh membranes or the soaked ones were used, though reproducible calibration graphs were obtained after soaking the electrodes in the internal filling solution for at least 30 min. The electrodes were rinsed with water between measurements and stored in the filling solution when not in use.

3.5. Effect of temperature

Calibration graphs (EMF vs. pIPBr) were constructed at test solution temperatures of 20, 25, 30, 40, 50, 60 and 70 °C. The slope, dynamic range, detection limits and the standard potential (E°) of the electrode were calculated at each temperature. For the determination of the isothermal coefficients (dE°/dt) of the cells, the standard electrode potentials E° , obtained from the calibration graphs as the intercepts at pIPBr = 0, were plotted versus ($t - 25$), where t is the temperature (°C) of the test solution. A straight-line plot was obtained according to the following equation [37]:

$$E^\circ = 0.37(t - 25) + 227.4$$

The slope of the line, which represents the isothermal coefficient of the cell (0.37 mV/°C), reveals a fairly high thermal stability of the cell within the investigated temperature range.

Table 2
Potentiometric selectivity coefficients for the IP⁺-ISE

Interferent	$-\log K_{IP,B}^{Pot\ a}$	Interferent	$-\log K_{IP,B}^{MPM\ b}$
KNO ₃	3.52	Glucose	5.25
NH ₄ Cl	3.62	Maltose	5.16
LiNO ₃	3.75	Fructose	5.08
MgCl ₂	2.96	Lactose	5.35
CaCl ₂	3.15	Starch	5.13
SrCl ₂	2.94	Caffeine	4.75
BaCl ₂	2.88	Ascorbic acid	5.12
CoCl ₂	3.56	Citric acid	4.94
NiSO ₄	3.67	Benzoic acid	4.85
Cu(NO ₃) ₂	3.36	Glycine	4.52
ZnCl ₂	3.18	Alanine	4.74
Al(NO ₃) ₃	3.42	Valine	4.55
Cr(NO ₃) ₃	3.53	Urea	4.67

^a Values obtained using the separate solution method (SSM).

^b Values obtained using the matched potential method (MPM).

3.6. Selectivity of the electrode

The selectivity of an ion-pair-based membrane electrode depends on the physico-chemical characteristics of the ion exchange process at the membrane–sample solution interface, the motilities of the respective ions in the membrane, and hydrophobic interactions between the primary ion and the organic membrane [38].

The response of the electrode to different substances has been investigated and the selectivity coefficient was used to evaluate the degree of interference. The selectivity coefficients obtained (Table 2) show that the proposed electrode is highly selective towards IP⁺ ion. The inorganic cations did not interfere due to the differences in their mobility and permeability, compared to IP⁺. In case of sugars and amino acids, the high selectivity is mainly attributed to the difference in polarity and to the moderately hydrophobic nature of their molecules relative to IP⁺ [18].

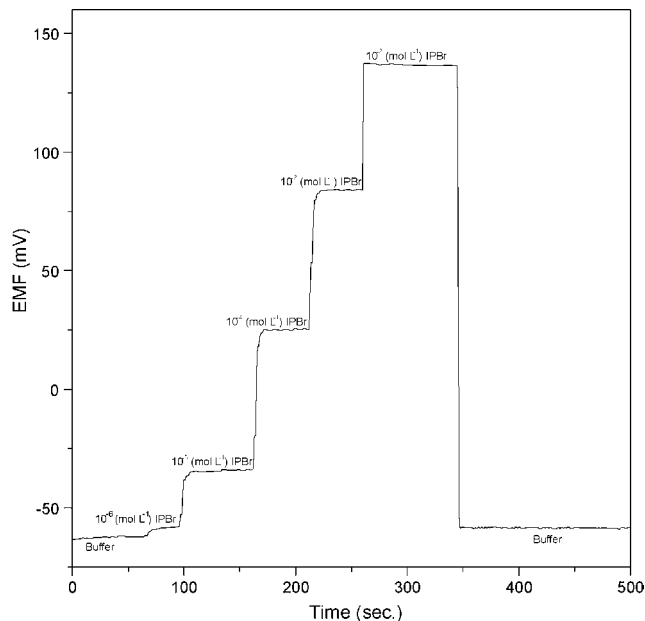


Fig. 3. Dynamic response and recovery time of IP⁺-ISE.

3.7. Lifetime, reproducibility and response time

The electrode lifetime was investigated by performing the calibration curve and the periodic testing of standard solutions (10^{-7} to 10^{-2} mol L⁻¹ IPBr) and calculating the response slope. It was observed that the investigated electrodes exhibit good stability in terms of slope in the linear domain of concentration and the electrodes can be used continuously for about 2 months without considerable decrease in its slope value.

The repeatability of the potential measurement for a 10^{-4} mol L⁻¹ standard IPBr solution for five replicate measurements gave a R.S.D. of 1.2%.

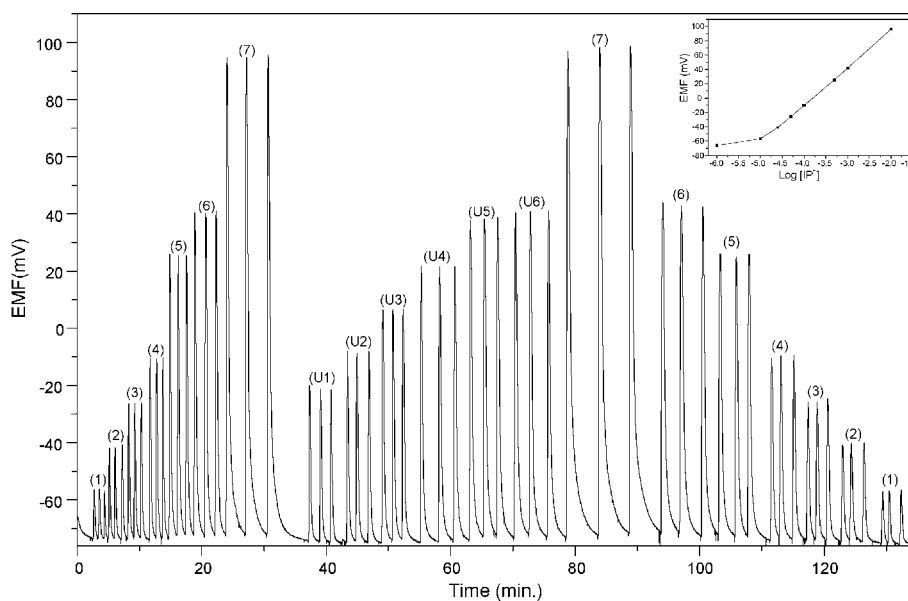


Fig. 4. FI output for injection of IPBr standards and spiked urine sample solutions: (1) 1×10^{-5} mol L⁻¹, (2) 2.5×10^{-5} mol L⁻¹, (3) 5×10^{-5} mol L⁻¹, (4) 1×10^{-4} mol L⁻¹, (5) 5×10^{-4} mol L⁻¹, (6) 1×10^{-3} mol L⁻¹ and (7) 1×10^{-2} mol L⁻¹ IPBr. Spiked urine sample solutions (U1–U6). Insert: corresponding calibration curve.

The dynamic response time [39,40], is defined as the time which elapses between the instant at which an ion-selective electrode and a reference electrode (ISE cell) are brought into contact with a sample solution, or at which the activity of the ion of interest in a solution is changed, and the first instant at which the EMF/time slope ($\Delta E/\Delta t$) becomes equal to a limiting value on the basis of the experimental conditions and/or requirements concerning the accuracy. This response time is measured by successive 10-fold increases in IPBr concentrations ranging between 10^{-6} and 10^{-2} mol L $^{-1}$ IPBr. The response time was fast, being nearly instantaneous (5–10 s), as shown in Fig. 3, and the potential readings remain constant for a prolonged period of time. A very short baseline recovery time was also observed when the electrode was washed with water. These characteristics assure the feasibility of using this electrode in flow measurements.

3.8. Flow injection

Flow injection analysis (FIA) is a simple, rapid, and versatile technique that is now firmly established, with widespread applications in quantitative chemical analysis. ISEs in flow injection potentiometry (FIP) have several advantages compared to steady-state measurements. They include, fast sample throughput, high precision, small sample volumes, economical use of reagents, correction of electrode drift by the measurement of peak heights and ease of computer automation [41–43].

Important variables of a single-line flow setup are confined to sampling volumes and flow-rates. The length of the tubing from injection valve port to electrochemical cell was made as small as possible to minimize dispersion and dilution. The optimization was carried out by measuring the analytical signals produced after injecting 20, 50, 100 and 200 μ L of 10^{-3} mol L $^{-1}$ IPBr, prepared in carrier solution, at flow rates of 1.5, 2.6, 4.5 and 6.5 mL min $^{-1}$.

A sample loop of size 100 μ L and flow rate of 2.6 mL min $^{-1}$ were found to give optimal peak height, low consumption of reagents, and a short base line recovery time. Under these conditions the electrode provides for a practical detection limit of 8.5×10^{-6} mol L $^{-1}$, a linear response in the range 2.5×10^{-5} to 10^{-2} mol L $^{-1}$ with slope of 52.7 mV/decade and correlation

coefficient of 0.9998, and a sampling frequency of about 40 samples/h that can be assayed with excellent precision in the concentration range of interest. The higher level of detection limits that observed in FI technique relative to batch one is due to the difference in dispersion coefficients between the two modes and the short time of contact between the sample and the electrode in case of FI [44]. A typical FI recording and its corresponding calibration graph are shown in Fig. 4.

3.9. Analytical applications and statistical evaluation of results

The electrode was utilized as an indicator electrode in the potentiometric titration of different concentrations of IPBr and Atrovent $^{\text{®}}$ vial samples with standardized NaTPB solution. Typical titration curves with sharp inflection breaks were obtained as found in Fig. 5. The signal change at the inflection breaks was found to be ~ 70 – 150 mV depending on the starting IPBr concentration.

Atrovent $^{\text{®}}$ vials were also analyzed by the direct potentiometry and standard addition methods applying both batch and FI conditions.

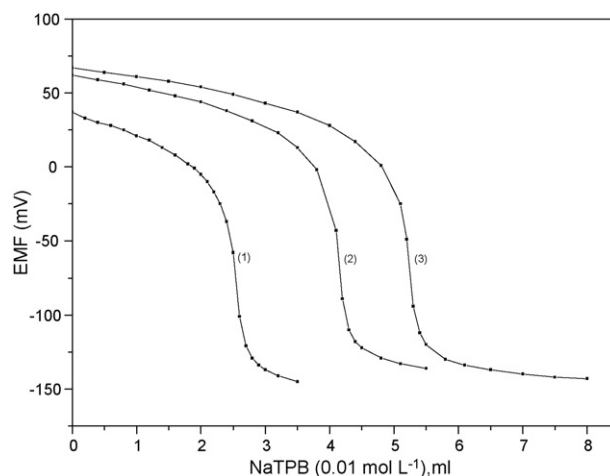


Fig. 5. Potentiometric titration curve of (1) 10.7 mg, (2) 17.2 mg and (3) 22.4 mg IPBr-H $_2$ O against 0.01 mol L $^{-1}$ NaTPB using IP $^+$ -ISE as indicator electrode.

Table 3
Determination of IPBr in Atrovent $^{\text{®}}$ vials

Method	Atrovent $^{\text{®}}$ (261 μ g/2 mL)		S.D.	R.S.D. (%)	<i>F</i> -Test ^a	<i>t</i> -Test ^b
	Found (μ g/2 mL)	Recovery ^c				
Batch technique						
Direct calibration	261.16	100.06	3.77	1.44	2.26	0.195
Standard additions	259.00	99.23	1.8	0.7	1.94	1.5
Potentiometric titration	261.13	100.05	2.84	1.09	1.28	0.25
FI technique						
Direct calibration	259.02	99.24	1.89	0.73	1.76	1.46
Standard additions	264.43	101.3	3.51	1.33	1.96	1.11
Reference method [8]	261.67	100.3	2.51	0.96		

^a The tabulated *F*-value at 95% confidence level, *F_c* (0.05, 3,3)=9.28.

^b The tabulated *t*-value at 95% confidence level, *t_c* (0.05, 4)=2.776.

^c % of the nominal values, average of three determinations.

Table 4
Determination of IPBr in spiked urine samples

Taken (mg)	Method							
	Batch Technique				FI Technique			
	Direct calibration		Standard additions		Direct calibration		Standard additions	
	Found (mg) ^a	Recovery ^b	Found (mg) ^a	Recovery ^b	Found (mg) ^a	Recovery ^b	Found (mg) ^a	Recovery ^b
0.215	0.302 (2.5)	140.5	0.32 (2.03)	148.9	0.27 (3.67)	125.4	0.276 (2.15)	128.4
0.43	0.497 (1.3)	115.5	0.5 (1.01)	116.7	0.465 (1.77)	108.1	0.461 (0.65)	107.2
0.861	0.93 (0.31)	107.8	0.873 (0.65)	101.4	0.89 (0.68)	103.3	0.89 (0.98)	103.1
1.722	1.79 (3.4)	104.2	1.673 (0.91)	97.2	1.717 (0.48)	99.7	1.786 (2.84)	103.8
3.44	3.53 (3.2)	102.4	3.26 (1.04)	94.5	3.54 (2.4)	102.7	3.35 (3.5)	97.4

^a Values in parentheses represent the percentage relative standard deviation of three determinations.

^b % of the taken values.

As shown in Table 3, good agreement between the recoveries is obtained by the proposed and the reported methods [8]. Statistical evaluation of the results [45] showed that there is no significant difference between the proposed and reported methods in terms of accuracy and precision.

The prepared electrode has been successfully used for the determination of IPBr in urine samples spiked with known amounts of IPBr, applying batch and FI conditions. As can be seen in Table 4, urine samples containing IPBr concentration down to 1×10^{-4} and 8×10^{-5} mol L⁻¹ could be determined with excellent recovery using batch and the FI modes, respectively.

4. Conclusion

The proposed electrode based on IP–TPB with PVC matrix, offers a valuable technique for the determination of IPBr in pure solutions, in urine and in pharmaceutical preparations. The inherent advantages of the proposed electrode are its rapid response, simple operation, precise results, low cost, direct application to the determination of IPBr in complex matrix without prior separation, high selectivity for IPBr, and the applicability in flow injection systems.

Acknowledgements

The authors gratefully acknowledge Beni-Suef University and UAE University for laboratory facilities and Boehringer Ingelheim Company for supply of the pure Ipratropium bromide. Sincere thanks are extended to Dr. Sayed Marzouk for providing the high impedance module.

References

- [1] J.E.F. Reynolds, Martindale, The Extra Pharmacopoeia, 20th ed., Pharmaceutical Press, London, 1989, p. 537.
- [2] F. Kässner, R. Hodder, E.D. Bateman, *Drugs* 64 (2004) 1671.
- [3] British Pharmacopoeia, HMSO, London, 1998, p. 1761.
- [4] V.G. Nayak, V.R. Bhate, S.N. Dhumal, V.R. Nururkar, S.M. Purandare, P.M. Dikshit, C.D. Gaitonde, *Drug Dev. Ind. Pharm.* 18 (1992) 1681.
- [5] G. Hopfgartner, T. Wachs, K. Bean, J. Henion, *Anal. Chem.* 65 (1993) 439.
- [6] J.L. Hopkins, K.A. Cohen, F.W. Hatch, T.P. Pitner, J.M. Stevenson, F.K. Hess, *Anal. Chem.* 59 (1987) 784A.
- [7] G.A. Jacobson, G.M. Peterson, *J. Pharm. Biomed. Anal.* 12 (1994) 825.
- [8] P.J. Simms, R.W. Towne, C.S. Gross, R.E. Miller, *J. Pharm. Biomed. Anal.* 17 (1998) 841.
- [9] J. Wang, Y. Jiang, Y. Wang, H. Li, J.P. Fawcett, J. Gu, *Rapid Commun. Mass Spectrom.* 21 (2007) 1755.
- [10] F.P.W. Tang, G.N.W. Leung, T.S.M. Wan, *Electrophoresis* 22 (2001) 2201.
- [11] H.A. Ensinger, D. Wahl, V. Brantl, *Eur. J. Clin. Pharmacol.* 33 (1987) 459.
- [12] K. Ensing, M. Pol, R.A. De-Zeeuw, *J. Pharm. Biomed. Anal.* 6 (1988) 433.
- [13] S. Nakazawa, K. Tanaka, *Bunseki Kagaku* 27 (1978) 100.
- [14] E.M. Hassan, *J. Pharm. Biomed. Anal.* 21 (2000) 1183.
- [15] H. Ibrahim, Y.M. Issa, H.M. Abu-Shawish, *J. Pharm. Biomed. Anal.* 44 (2007) 8.
- [16] Y.S. El-Saharty, F.H. Metwaly, M. Refaat, S.Z. El-Khateeb, *Talanta* 72 (2007) 675.
- [17] S.M. Ghoreishi, M. Behpour, M. Nabi, *Sens. Actuators B* 113 (2006) 963.
- [18] M.G.F. Sales, J.F.C. Tomás, S.R. Lavandeira, *J. Pharm. Biomed. Anal.* 41 (2006) 1280.
- [19] T. Kimbeni Malongo, B. Blankert, O. Kambu, K. Amighi, J. Nsangu, J.-M. Kauffmann, *J. Pharm. Biomed. Anal.* 41 (2006) 70.
- [20] H. Ibrahim, Y.M. Issa, H.M. Abu-Shawish, *J. Pharm. Biomed. Anal.* 36 (2005) 1053.
- [21] H. Ibrahim, Y.M. Issa, H.M. Abu-Shawish, *Anal. Chim. Acta* 532 (2005) 79.
- [22] Y.M. Issa, S.S. Badawy, A.A. Mutair, *Anal. Sci.* 21 (2005) 1443.
- [23] S.A. Marzouk, <http://www.picotech.com/experiments/ph-measurements>.
- [24] Y.M. Fraticelli, M.E. Meyerhoff, *Anal. Chem.* 53 (1981) 992.
- [25] M.E. Meyerhoff, P.M. Kofash, *J. Chem. Educ.* 60 (9) (1983) 766.
- [26] G.G. Guibault, R.A. Durst, M.S. Frant, H. Freiser, E.H. Hansen, T.S. Light, E. Pungor, G.A. Rechnitz, N.M. Rice, T.J. Rohm, W. Simon, J.D.R. Thomas, *Pure Appl. Chem.* 48 (1976) 127.
- [27] Y. Umezawa, P. Buhlmann, K. Umezawa, K. Tohda, S. Amemiyai, *Pure Appl. Chem.* 72 (2000) 1851.
- [28] R. Eugster, T. Rosatzin, B. Rusterholz, B. Aebbersold, U. Pedrazza, D. Rüegg, A. Schmid, U.E. Spichiger, W. Simon, *Anal. Chim. Acta* 289 (1994) 1.
- [29] I. Bedlechowicz, M. Maj-Zurawska, T. Sokalski, A. Hulanicki, *J. Electroanal. Chem.* 537 (2002) 111.
- [30] M. de los, A. Arada Pérez, L.P. Marín, J.C. Quintana, M. Yazdani-Pedram, *Sens. Actuators B* 89 (2003) 262.
- [31] R.D. Armstrong, G. Horvai, *Electrochim. Acta* 35 (1990) 1.
- [32] T. Sokalski, T. Zwickl, E. Bakker, E. Pretsch, *Anal. Chem.* 71 (1999) 1204.
- [33] T. Sokalski, A. Ceresa, M. Fibbioli, T. Zwickl, E. Bakker, E. Pretsch, *Anal. Chem.* 71 (1999) 1210.
- [34] A.C. Ion, E. Bakker, E. Pretsch, *Anal. Chim. Acta* 440 (2001) 71.
- [35] A. Ceresa, A. Radu, S. Peper, E. Bakker, E. Pretsch, *Anal. Chem.* 74 (2002) 4027.

- [36] A. Malon, A. Radu, W. Qin, Y. Qin, A. Ceresa, M. Maj-Zurawska, E. Bakker, E. Pretsch, *Anal. Chem.* 75 (2003) 3865.
- [37] L.I. Antropov, *Theoretical Electrochemistry*, Mir Publisher, Moscow, 1977.
- [38] V.V. Cosofret, R.P. Buck, *Analyst* 109 (1984) 1321.
- [39] R.P. Buck, E. Lendner, *Pure Appl. Chem.* 66 (1994) 2527.
- [40] C. Maccá, *Anal. Chim. Acta* 512 (2004) 183.
- [41] J. Ruzicka, E.H. Hansen, *Flow Injection Analysis*, 2nd ed., Wiley, New York, 1988.
- [42] J.M. Calatayud, *Flow Injection Analysis of Pharmaceuticals: Automation in the Laboratory*, Taylor & Francis, London, 1996.
- [43] M. Trojanowicz, *Flow Injection Analysis: Instrumentation and Applications*, World Scientific, London, 2000.
- [44] M. Trojanowicz, W. Matuszewski, *Anal. Chim. Acta* 138 (1982) 71.
- [45] P.C. Meier, R.E. Zünd, *Statistical Methods in Analytical Chemistry*, 2nd ed., John Wiley & Sons Inc., New York, 2000.

Encapsulation of glucose oxidase within poly(ethylene glycol) methyl ether methacrylate microparticles for developing an amperometric glucose biosensor

J.P. Hervás Pérez^a, E. López-Cabarcos^b, B. López-Ruiz^{a,*}

^a *Sección Departamental de Química Analítica, Facultad de Farmacia, Universidad Complutense de Madrid, Ciudad Universitaria s/n, 28040 Madrid, Spain*

^b *Departamento de Físico-Química Farmacéutica, Facultad de Farmacia, Universidad Complutense de Madrid, 28040 Madrid, Spain*

Received 18 September 2007; received in revised form 21 December 2007; accepted 7 January 2008

Available online 21 January 2008

Abstract

Poly(ethylene glycol) methyl ether methacrylate (PEGMEM) microparticles were synthesized and glucose oxidase (GOx) was immobilized within the microparticles. An amperometric biosensor was fabricated using the microparticles with GOx as biological component. The enzyme immobilization method was optimized by investigating the influence of monomer concentration and cross-linker content used in the preparation of the microparticles in the response of the biosensor. The best analytical results were obtained with the microparticles prepared with 0.21 M PEGMEM and 0.74% cross-linking. Furthermore, we have investigated the influence on the biosensor behaviour of parameters such as working potential, pH, temperature and enzymatic load. In addition, analytical properties such as sensitivity, linear range, response time and detection limit were determined. The biosensor was used to determine glucose in human serum samples and to avoid common interferences present in human serum such as uric and ascorbic acids. A Nafion layer was deposited on the electrode surface with satisfactory results. The useful lifetime of the biosensor was at least 520 days.

© 2008 Elsevier B.V. All rights reserved.

Keywords: Amperometric biosensor; PEGMEM; Glucose oxidase; Microparticles

1. Introduction

Glucose biosensors have attracted great interest because of the increasing incidence of diabetes in the population of developed countries [1,2]. The performance of a biosensor depends on the materials and fabrication techniques. The use of biocompatible materials will allow the monitorization *in vivo* of the different compounds such as glucose or cholesterol. Future progress and development in biosensor design will inevitably focus upon the technology of new materials that promise to solve the biocompatibility problems. Materials with hydrogel-like properties are generally biocompatible due to their high water content [3] and can be used to immobilize enzymes such as GOx. The immobilization of enzymes with complete reten-

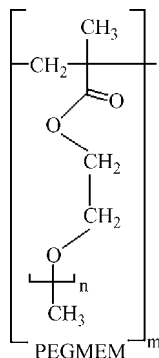
tion of its biological activity in matrices with good diffusion properties for substrates is a decisive factor for the development of biosensors. Various methods for enzyme immobilization have been reported, such as covalent binding [4,5], entrapment in a suitable matrix [6,7], adsorption onto insoluble materials [8], conjugation [9], ionic-covalent hybridization [10,11], etc.

Besides, GOx (EC 1.1.3.4) is a very robust enzyme that is often used as model for testing and developing new immobilization systems such as polymer films, polymer gels, conducting polymers, and methacrylate-based polymers that have been assayed for developing glucose biosensors [12–17].

After the pioneer work in the 1960s [18], the use of methacrylate hydrogels in biomedical applications has made remarkable progress in the field of biosensors, drug delivery systems, contact lenses and synthetic membranes [7,11,19–23].

PEGMEM (see Scheme 1) has been copolymerized with different cross-linkers to form comb-like copolymers with hydrogel

* Corresponding author. Tel.: +34 91 394 1756; fax: +34 91 394 1754.
E-mail address: bealopru@farm.ucm.es (B. López-Ruiz).



Scheme 1. Structure of PEGMEM.

properties because it is a non-cytotoxic, monofunctional and biocompatible polymer [24–26].

In this work we have prepared biocompatible microparticles of *p*-PEGMEM and we have used them as a new system of immobilization of GOx for application as biological component of an amperometric glucose sensor. The biosensor was optimized by studying the influence on the biosensor response of parameters used in microgel synthesis such as monomer concentration and cross-linking content as well as working conditions such as working potential, pH of the medium, temperature, and enzymatic load.

2. Experimental

2.1. Chemicals

PEGMEM, GOx (425 IU/mL) from *Aspergillus niger*, D+glucose, ascorbic acid, uric acid and Nafion 5 wt.% were purchased from Sigma (St. Louis, MO, USA). *N,N'*-Methylenebisacrylamide (BIS) from Aldrich (St. Louis, MO, USA), ammonium persulfate, *N,N,N',N'*-tetramethylethylenediamine (TEMED) and the surfactant Span 80 from Fluka (Buchs, Switzerland). Acetate/phosphate buffer solutions were prepared from stock solutions of sodium dihydrogen phosphate and sodium acetate (Panreac). The dialysis membrane (12,000–14,000 MWCO) was purchased from Spectrum Medical Industries. All reagents were used as received and the water was Milli Q quality (Millipore, Milford, MA, USA).

2.2. Apparatus and measurements

The microgel particles were examined using scanning electron microscopy (SEM) in a JEOL JSM-6400 microscope operating at an acceleration voltage of 20 kV and 5000 magnification. The grid with the microparticles was dried, and replicas were produced by shadowing with gold deposited with a Balzers Sputter Coater (SCD-004). Particle size measurements in the range 2–150 μm were performed with a Galai-Cis-1 particle analyzer system. The instrument consists of a laser-based analyzer which evaluates the particle diameter from the time it takes to cross a laser beam and a video-based analyser shows the shape of the microparticle. Amperometric measurements at constant potential were carried out at a

Metrohm Polarecord potentiostat, Model E-506. The pH of the buffer solution was adjusted using a Metler Toledo MP-230 pH-meter. Electrochemical measurements were performed in 0.05 M acetate/0.05 M phosphate buffer, in a three-electrode cell with a platinum electrode as working electrode, a SCE reference electrode and a platinum counter electrode.

2.3. Emulsion preparation

p-PEGMEM microgels with varying amounts of BIS were prepared using the concentrated emulsion polymerization method [27]. The immobilization of GOx was carried out by adding the enzyme (425 IU/mL) in the aqueous phase of the concentrated emulsion. The amount of cross-linking η (%) = $n_{\text{BIS}}/(n_{\text{BIS}} + n_{\text{monomer}})$ where n_{BIS} and n_{monomer} are the number of moles of BIS and monomer, respectively was varied between 0.34% and 5.82%. Since the time of synthesis is about 1.5 h, the temperature was controlled and kept below 25 °C to preserve the enzyme properties.

2.4. Overall reaction of the glucose biosensor

The electrode surface (diameter 3 mm) was polished with 0.05 μm alumina slurry paste. After polishing, any residual abrasive particles were removed ultrasonically in ethanol and subsequently in distilled water. An exactly weighed amount of microgel particles was placed on the electrode surface and fixed with a dialysis membrane. The resulting electrode was washed with phosphate buffer and overoxidized at +0.6 V versus SCE until the background current decreased to a constant level.

The biosensor response is based on an indirect measurement that correlates the amount of glucose with the concentration of hydrogen peroxide. Because the redox centres in GOx are insulated within the enzyme molecule, direct electron transport to the surface of the electrode does not occur to any measurable degree. GOx is first reduced by the substrate glucose and then reoxidized by oxygen. Oxygen behaves as electron acceptor for reduced GOx leading to the formation of hydrogen peroxide that is oxidized at the electrode and results in the current that is detected by amperometry.

3. Results and discussion

3.1. Characterization of the microparticles

Fig. 1 shows a micrograph of *p*-PEGMEM microparticles with entrapped GOx prepared with $\eta=0.74\%$. The microgels are spherical and polydisperse.

As Fig. 2 shows, the concentrated emulsion polymerization method produces microparticles with entrapped GOx whose diameters lie between 2 and 12 μm . The average size is 5.2 μm very close to the average size 5 μm of the microparticles without GOx and cross-linking $\eta=0.74\%$. As Fig. 2 illustrates, 50% of the microparticles present a size comprised between 2 and 4 μm .

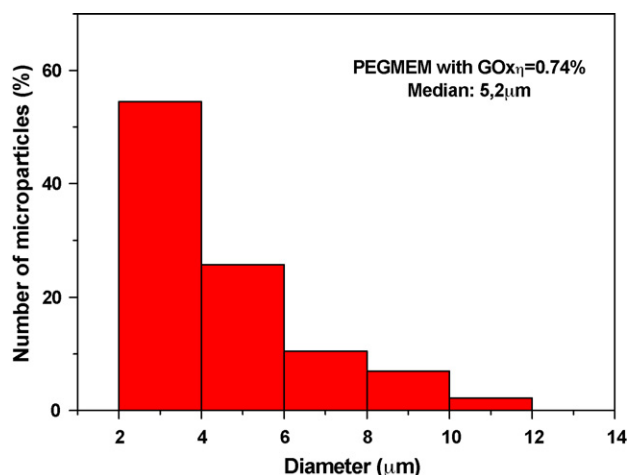


Fig. 1. SEM micrograph of freeze-dried *p*-PEGMEM microparticles with entrapped GOx.

3.2. Optimization of the synthesis method

3.2.1. Monomer concentration

The steady-state response curves, obtained at the platinum electrode with *p*-PEGMEM microparticles synthesized at pH 6.5, $\eta = 0.74\%$, containing 425 IU/mL of GOx and different proportions of monomer in the aqueous phase (0.10, 0.21, 0.83 and 1.17 M) are illustrated in Fig. 3a. The maximum current response was found when the monomer concentration was 0.21 M. A further increase in the monomer concentration decreases the current response and we attribute this behaviour to a higher diffusional barrier that hinders the motion of the substrate towards the enzyme catalytic site as well as the diffusion of the product of the enzymatic reaction towards the electrode. Decreasing the monomer concentration at 0.10 M also results in a decrease of the response, due to the loss of immobilized enzyme when small amount of monomer is used. The enzymatic activity observed in the supernatant liquid obtained after the synthesis of the microparticles when the monomer concentration is 0.10 M seems to support this interpretation.

3.2.2. Effect of the cross-linking contents

In order to find the optimum pore size of the polymer matrix, biosensors based on microparticles with different amount of

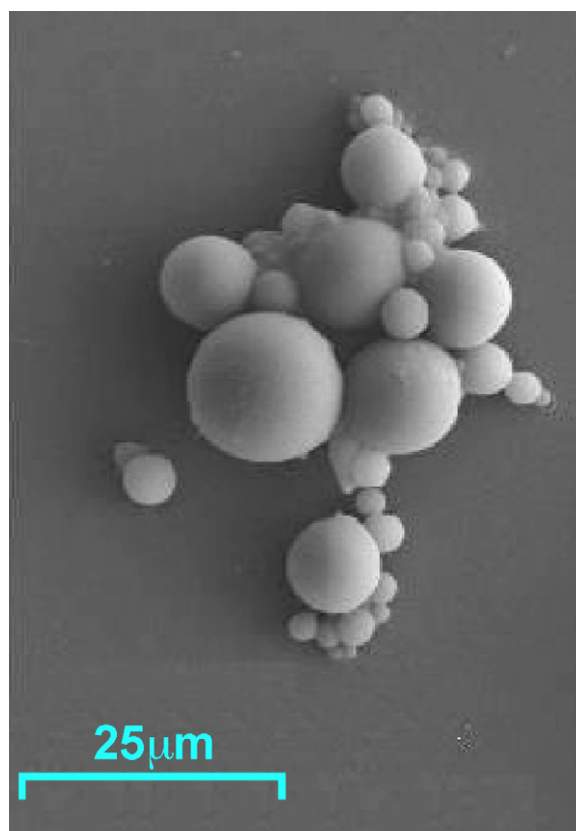


Fig. 2. Size distribution of the *p*-PEGMEM microparticles with entrapped GOx, in phosphate buffer pH 6.5 and 25 °C.

cross-linking (η) were prepared. Fig. 3b shows the calibration curves of the biosensor response versus glucose concentration for microparticles with cross-linking between 0.34% and 5.82%. The monomer concentration selected to obtain these curves was 0.21 M, and the amount of GOx 425 IU/mL.

The optimum response occurs in microgels with $\eta = 0.74\%$. Microparticles prepared with lower fractions of cross-linking present a pore size too large to efficiently retain the enzyme as it was confirmed by the enzymatic activity measured in the supernatant. The decrease of the response when the cross-linking fraction is higher than 0.74% is attributed to a higher substrate diffusional barrier imposed by the cross-linking. Accordingly

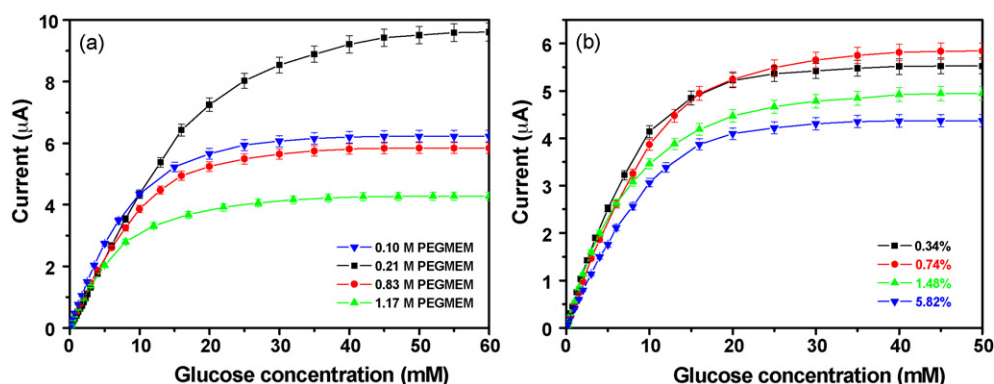


Fig. 3. Response of the glucose biosensor to different monomer concentrations (a) and to different cross-linking (b), by calibration plot for glucose in stirred 0.1 M phosphate buffer, pH 6.5, potential of +0.6 V vs. SCE and 25 °C.

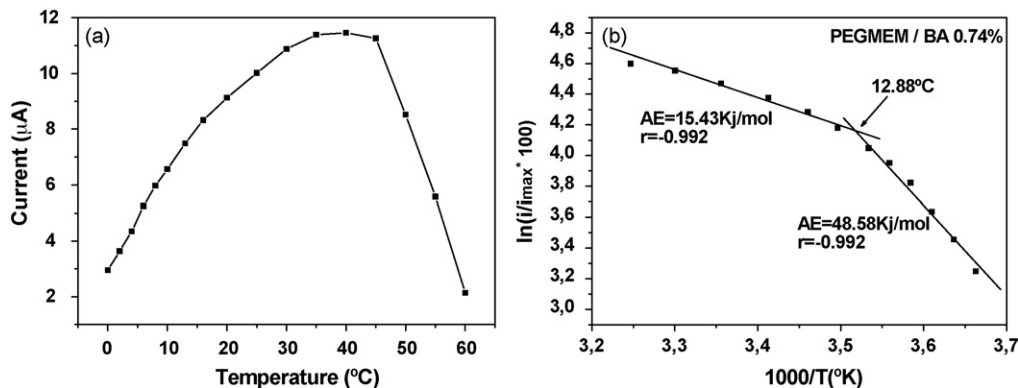


Fig. 4. Effect of working temperature (a) and Arrhenius plot (b) for GOx immobilized in *p*-PEGMEM $\eta=0.74\%$, on the biosensor response to 30 mM of glucose. Experimental conditions: 0.1 M phosphate buffer, pH 6.5 and +0.6 V vs. SCE.

microparticles with cross-linking 0.74% and monomer concentration 0.21 M were selected for subsequent measurements performed in this work.

3.3. Optimization of the biosensor response

3.3.1. Working potential

The dependency of the biosensor response (steady-state current at the electrode) on the applied potential was investigated in 0.1 M phosphate buffer solution, pH 6.5 containing 0.25 mM glucose. The response of the enzyme electrode increased with the applied potential up to a value of +0.60 V versus SCE and levels off after this value. The operating potential of +0.60 V versus SCE was used in all subsequent measurements.

3.3.2. Temperature

The effect of temperature on the biosensor response at 30 mM glucose was studied in the interval 0–60 °C performing all measurements under oxygen saturation condition and keeping the pH constant at 6.5.

As it can be seen in Fig. 4a, the optimum temperature for enzymatic activity is between 35 and 45 °C. The temperature of maximum activity of the free enzyme is 30 °C [28]. It seems that the immobilizing support slightly protects the enzyme. Although we have checked that the highest enzyme activity takes place between 35 and 45 °C, we wanted to verify that to these temperatures the enzyme was staying stable. To probe this, the kinetics of degradation to different temperatures that suffers the biosensors with 30 mM of glucose was studied, keeping constant the temperature for 1 h, verifying the intensity on time 0 and on 60 min (Table 1). When the temperature was overcoming 30 °C,

a decrease of the activity with time was observed, due to the enzyme denaturation.

The temperature of 30 °C was chosen as working temperature to all further experiments.

As Fig. 4b also illustrates, the Arrhenius plot for GOx immobilized in *p*-PEGMEM microparticles with $\eta=0.74\%$ presents two regions. The activation energies were calculated from the slopes and were found to be 15.43 and 48.58 kJ/mol, respectively. The activation energy observed in the low temperature region is significantly higher than the one reported for the free enzyme, which was found to be 14.6 kJ/mol [29]. The activation energies values reported by Rubio Retama et al. [30] when GOx was immobilized in polyacrylamide were found to be 26.60 and 50.46 kJ/mol, quite similar than we observed.

As we reported in previous articles, the temperature at which the slope changes is related with the volume phase transition of the microgel around the enzyme [30–32]. At a temperature higher than the temperature of the volume phase transition, the microgel is swollen, the enzyme is surrounded by water and its activation energy comes closer to that of the enzyme in solution. However, in the shrunk phase the amount of water retained inside the hydrogel decreases, hindering access of the substrate to the enzyme and the enzyme–substrate union so the activation energy is increased. These results, as the ones obtained in previous works [30–32], seem to indicate that the changes in the Arrhenius plots are not due to changes in enzyme, but to the medium around it.

3.3.3. pH

The influence of pH on the glucose biosensor response to 30 mM glucose was checked in 0.05 M acetate/0.05 M phosphate

Table 1
Kinetics of degradation of enzyme entrapped in microparticles with 0.74% cross-linking

Temperature (°C)	Current, $t=0$ s (nA)	Current, $t=60$ s (nA)	Percentage of degradation
25	120	120	0.00
30	145	145	0.00
35	175	150	14.29
40	205	165	19.51

Experimental conditions: 0.1 M phosphate buffer, pH 6.5 and +0.6 V vs. SCE.

buffer solutions from pH 4.0 to 8.0 at 25 °C. The optimal pH was found to be 6.5 coincident with the optimum pH reported to the free enzyme, which indicates that the catalytic function of the GOx does not seem to be affected by the immobilization process proposed in this work.

3.3.4. Loading

The glucose levels of diabetic patients are higher than 5 mM, therefore, we have extended the calibration range of the biosensor studying the effect of enzymatic load on the biosensor response. Based on previous works [31] we have chosen an enzymatic load of 425 IU/mL and we tested two methods of modifying the amount of enzyme in the surface of the electrode: varying the amount of microparticles placed on electrode surface, and changing the amount of enzyme immobilized within the microgel.

The linear range reaches to 8.0×10^{-3} M when the amount of GOx in aqueous phase goes from 255 to 765 IU/mL and is slightly increased when the microparticles placed on the electrode surface from 1 up to 3 mg. In both cases the sensitivity is increased when the amount of GOx in aqueous phase goes from 255 to 765 IU/mL and when the microparticles placed on the electrode surface from 1 up to 3 mg. In base of the above results we have selected for later experiments 3 mg of microparticles loaded with 765 IU/mL GOx. Table 2 shows the analytical properties of the biosensor prepared with *p*-PEGMEM microgels as a function of the amount of microparticles placed on electrode surface and the enzyme immobilized into the microgel.

Under all the optimal experimental conditions (0.74% cross-linking, potential +0.6 V, pH 6.5 and 30 °C), we realized a calibration curve in which the glucose biosensor presented a sensitivity of $17.78 \text{ mA M}^{-1} \text{ cm}^{-2}$, a maximum current density of $148.57 \mu\text{A cm}^{-2}$, a linear range between 2.0×10^{-6} and 7.6×10^{-3} M and a detection limit of $1 \mu\text{M}$. When comparing the results obtained with the proposed biosensors and that previously reported using a similar immobilization system (polymeric microparticles), an improvement is observed in the analytical properties as sensitivity, that was found to be $17.78 \text{ mA M}^{-1} \text{ cm}^{-2}$, and the maximum current density which increases from 114.3 to $148.57 \mu\text{A cm}^{-2}$ [30,31]. Also when this device was compared with others using different immobilization system as layer-by-layer self-assembly films or deposition on the electrode surface [33–36], it appears that the stability,

the detection limit and the linear range improved significantly. The detection limit decreased up to 10 times versus the reported devices, the linear range increased at least one order of magnitude and the stability changed from 30 and 150 days in the best of the case (microparticles) to 520 days observed with this biosensor.

3.4. Interference study

It is required that the enzymatic electrode operates at a potential of +0.6 V versus SCE for producing the oxidation of hydrogen peroxide. At this high potential, the H_2O_2 detection may be disturbed by the presence of interfering species such as uric acid (UA) and ascorbic acid (AA) when physiological samples are analyzed because these acids present a negative charge at the working pH (6.0–7.0). The interferences caused by electroactive molecules were reduced by the use of Nafion layer over the electrode surface. Nafion is a negatively charged polyelectrolyte whose effect on the negatively charged substrates is noticeable.

A layer of Nafion (50 μL) was applied on the electrode surface. The layer was dried in air for 15 min and, the electrode with Nafion film was kept at 80 °C for 45 min. Then microparticles of *p*-PEGMEM were placed over the Nafion film and subsequently covered with the dialysis membrane. For biosensor prepared without Nafion (GOx-biosensor), the interfering signals of 0.25 mM uric acid and ascorbic acid are significant (Fig. 5). On the contrary, when the GOx-Nafion-biosensor was used, the signals arising from interferents disappeared. However, current due to 0.25 mM of glucose was near constant, varying from 150 nm in the biosensor without Nafion to 145 nm in biosensor with Nafion.

3.5. Human serum sample analysis

The glucose concentration of five serum pools were analyzed by the GOx-biosensor and GOx-Nafion-biosensor. The glucose of these serums is analyzed also by the spectrophotometric method of hexokinase described by Young [37], which were used as reference method.

The result showed a good correlation with the reference methods, especially in the case of the biosensor prepared with Nafion. Measurements of glucose in serum samples

Table 2

Analytical properties of the *p*-PEGMEM biosensors as a function of the quantity of microparticles placed on electrode surface and the enzyme immobilized into the microparticles

Enzyme load		J_{max} ($\mu\text{A cm}^{-2}$)	Sensitivity ($\text{mA M}^{-1} \text{ cm}^{-2}$)	Linear range (M)	R^2 (n) ^a
Quantity of microparticles in the biosensors (mg)	Quantity of enzyme in the microparticles (IU/mL)				
1	425	62.58	4.09	1.0×10^{-5} to 1.0×10^{-2}	0.9949 (15)
2	425	77.71	6.63	1.1×10^{-5} to 4.0×10^{-3}	0.9944 (12)
3	425	83.49	6.78	1.0×10^{-5} to 4.0×10^{-3}	0.9963 (12)
3	255	54.36	6.13	1.0×10^{-5} to 3.0×10^{-3}	0.9962 (11)
3	765	148.57	17.78	2.0×10^{-6} to 7.6×10^{-3}	0.9985 (15)

^a Points of linear range in calibration curve.

Table 3

Quantitative results obtained from the analysis of the serum by the spectrophotometric method (reference), GOx-biosensor and GOx-Nafion-biosensor

Sample	Glucose (mg/dL) reference method	Glucose ^a (mg/dL) GOx-biosensor	R.S.D. (%)	GOx-biosensor deviations ^b (%)	Glucose ^a (mg/dL) GOx-Nafion-biosensor	R.S.D. (%)	GOx-Nafion-biosensor deviations ^b (%)
1	81	83 ± 1	1.7	+2.0	81 ± 1	1.3	−0.1
2	89	93 ± 2	2.3	+4.3	89 ± 2	2.2	−0.2
3	176	179 ± 1	1.2	+1.5	174 ± 1	1.9	−1.1
4	116	117 ± 1	1.2	+1.0	115 ± 1	1.8	−0.8
5	89	93 ± 1	2.0	+4.5	88 ± 1	1.3	−1.3

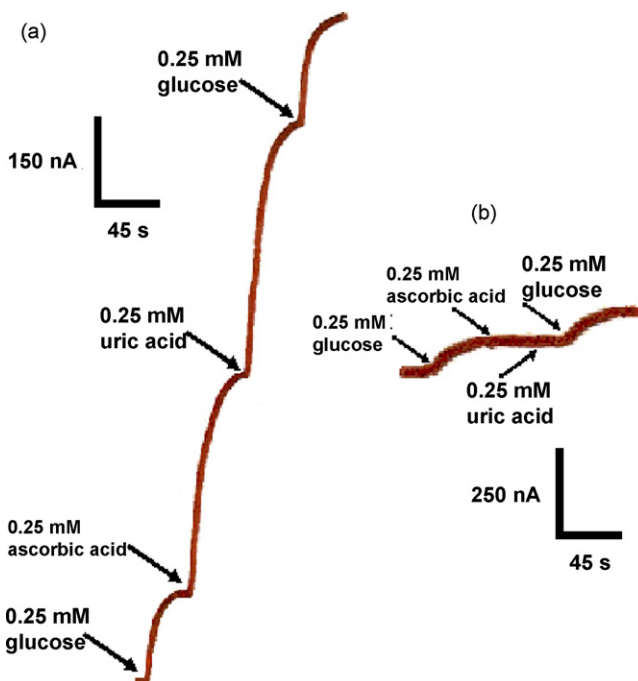
^a Average of the three measurements.^b Deviation between the reference method and the biosensor results.

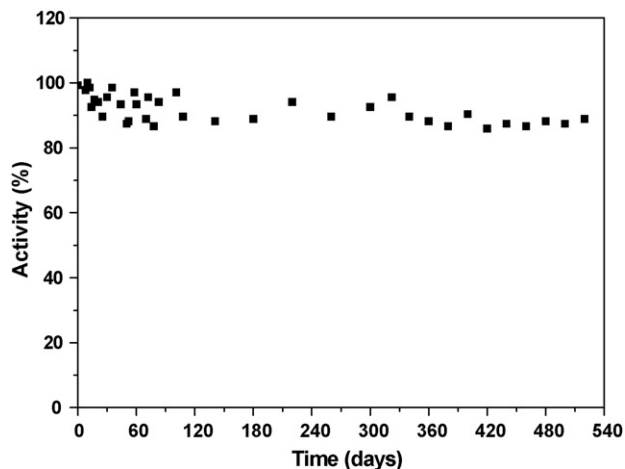
Fig. 5. GOx-biosensor response to 0.25 mM glucose, ascorbic and uric acids (a). GOx-Nafion-biosensor response to 0.25 mM glucose, ascorbic and uric acids (b).

obtained with GOx-Nafion-biosensor were similar with those of the reference method, and differences between them never overcame 1.3% and with good precision (R.S.D. < 2.3%) (Table 3). The GOx-biosensor gave values 1.0–4.5% higher than those obtained by the reference methods that confirm that the serum samples have interferences. The GOx-Nafion-biosensor gave values −0.1/−1.3% smaller than those obtained by the reference methods, possibly because the layer of Nafion prevents the step of the whole glucose. The recoveries obtained

Table 4

Recovery studies using both glucose oxidase biosensors^a

Sample	Glucose added (mg/dL)	GOx-biosensor		GOx-Nafion-biosensor	
		Glucose found ^a (mg/dL)	Recovery (%)	Glucose found ^a (mg/dL)	Recovery (%)
1	70	70 ± 1	100.2	71 ± 2	101.2
2	70	70 ± 1	100.1	71 ± 2	101.5
3	70	70 ± 1	97.5	70 ± 2	100.0
4	70	70 ± 1	94.8	70 ± 2	99.6
5	70	70 ± 1	99.3	70 ± 1	100.0

^a Average of the three measurements.Fig. 6. Storage stability profiles for *p*-PEGMEM biosensor. The biosensor was stored frozen in phosphate buffer at −4 °C when not in use.

with both biosensors are between about 94.8 and 101.5% (Table 4).

3.6. Stability

To characterize the electrode stability, they were stored in a frozen phosphate buffer solution pH 6.0 and, periodically, the response of the biosensor to 0.25 mM glucose solution, at potential +0.6 V versus SCE, 30 °C was measured. We have found that biosensor exhibits an 85% of the initial signal after 520 days. This study is still on course (Fig. 6).

3.7. Analytical properties

The repeatability and reproducibility of glucose biosensors based on *p*-PEGMEM microparticles were evaluated in buffer

solution. For the repeatability, 10 successive measurements of 0.25 mM glucose solution were performed. The relative standard deviation (R.S.D.) was 5.7%. The reproducibility of the analytical response obtained for three different electrodes when 5 mM of glucose was added (three measurements with each biosensor), obtained a R.S.D. of 0.88%.

4. Conclusions

Microparticles based on *p*-PEGMEM are presented as interesting matrix for GOx immobilization. We have demonstrated its application as enzyme immobilization support for an amperometric glucose biosensor. The optimal conditions of the synthesis medium were initiator's concentration of 10.96 mM, monomer concentration of 208.25 mM and 0.738% cross-linking content. Furthermore, the response of the biosensor was optimized for glucose detection. The optimal conditions of the biosensor response were: pH 6.5, 30 °C, 3 mg and 765 IU/mL. For eliminating the interferences caused by species with negative net charge, we have utilized a Nafion layer covering the electrode surface. The biosensor has been successfully applied to the determination of glucose in serum samples. The biosensor maintains 85% of the initial response 15 months later of the first use.

Acknowledgements

The authors acknowledge financial support from the Spanish Science and Education Ministry (MAT2006-13646-C03-01) from the CAM-UCM Program for "Consolidation of Research Groups" no. 950247 and no. 911033. We also thank M.E. Gil-Alegre (Department of Pharmacy and Pharmaceutical Technology, UCM) and A. Rodriguez (Electron Microscopy Centre, UCM) for valuable technical and professional assistance.

References

- [1] B.D. Malhotra, A. Chaubey, *Sens. Actuators B* 91 (2003) 117.
- [2] S. Chinnayelka, M.J. McShane, *Biomacromolecules* 5 (2004) 1657.
- [3] V. Kudela, *Encyclopaedia of Polymer Science and Engineering*, vol. 7, Wiley, New York, 1987, p.783.
- [4] L. Doretti, D. Ferrara, S. Lora, G. Palma, *Biotechnol. Appl. Biochem.* 29 (1999) 67.
- [5] S.H. Kim, S. Kim, V.K. Yadavalli, M.V. Pishko, *Anal. Chem.* 77 (2005) 6828.
- [6] S. Brahim, D. Narinesingh, A. Guiseppi-Elie, *Anal. Chim. Acta* 448 (2001) 27.
- [7] S. Brahim, D. Narinesingh, A. Guiseppi-Elie, *Biosens. Bioelectron.* 17 (2002) 53.
- [8] G. Bayramoğlu, E. Yalçın, M.Y. Arica, *Process Biochem.* 40 (2005) 3505.
- [9] T. Konno, J. Watanabe, K. Ishihara, *Biomacromolecules* 5 (2004) 342.
- [10] F.N. Kok, F. Bozuglu, V. Hasirci, *Biosens. Bioelectron.* 17 (2002) 531.
- [11] F.N. Kok, V. Hasirci, *Biosens. Bioelectron.* 19 (2004) 661.
- [12] M. Portaccio, M. El-Masry, N.R. Diano, A. De Maio, V. Grano, M. Lepore, P. Travascio, U. Bencivenga, N. Pagliuca, D.G. Mita, *J. Mol. Catal. B: Enzyme* 18 (2002) 49.
- [13] L. Cen, K.G. Neoh, E.T. Kang, *Biosens. Bioelectron.* 18 (2003) 363.
- [14] X. Liu, K.G. Neoh, L. Cen, E.T. Kang, *Biosens. Bioelectron.* 19 (2004) 823.
- [15] H. Suzuki, A. Kumagai, K. Ogawa, E. Kokufuta, *Biomacromolecules* 5 (2004) 486.
- [16] L.S. Bean, L.Y. Heng, B.M. Yamin, M. Ahmad, *Thin Solid Films* 477 (2005) 104.
- [17] L.S. Bean, L.Y. Heng, B.M. Yamin, M. Ahmad, *Bioelectrochemistry* 65 (2005) 157.
- [18] O. Wichterle, D. Lim, *Hydrophilic gels for biologic use*, in: Nature, St. Martin's Press Inc., NY, 1960, p. 117.
- [19] Y. Yang, S. Mu, H. Chen, *Synth. Metals* 92 (1998) 173.
- [20] P. Van der Wetering, E.E. Moret, N.M.E. Schuuemans-Nieuwenbrock, M.J. Van Steenberg, W.E. Hennik, *Bioconj. Chem.* 10 (1999) 589.
- [21] A. Blandino, M. Macias, D. Cantero, *Process Biochem.* 36 (2001) 601.
- [22] E.J. Calvo, R. Etchenique, L. Pietrasanta, A. Wolosiuk, C. Danilowicz, *Anal. Chem.* 73 (2001) 1161.
- [23] C.A. Marquette, L.J. Blum, *Sens. Actuators B* 90 (2003) 112.
- [24] M.A. Janney, O.O. Omatete, S.D. Walls, R.J. Nunn, R.J. Ogle, G. Westmoreland, *J. Am. Ceram. Soc.* 17 (1998) 581.
- [25] M. Potoczek, E. Zawadzak, *Ceram. Int.* 30 (2004) 793.
- [26] S.K. Mallapragada, B.C. Anderson, P.D. Bloom, V.V. Sheares-Ashby, *US Patent* 6,998,456 (2006) US 2002-357499P.
- [27] B.J. Rubio Retama, B. López-Ruiz, E.J. López-Cabarcos, *Biomaterials* 24 (2003) 2965.
- [28] L. Ying, E.T. Kang, K.G. Neoh, *J. Membr. Sci.* 208 (2002) 361.
- [29] S. Cosnier, S. Szunerits, R.S. Marks, A. Novoa, L. Puech, E. Perez, I. Rico-Lattes, *Talanta* 55 (2001) 889–897.
- [30] B.J. Rubio Retama, E.J. López-Cabarcos, B. López-Ruiz, *Talanta* 68 (2005) 99.
- [31] M. Sánchez-Paniagua López, D. Mecerreyes, E. López-Cabarcos, B. López-Ruiz, *Biosens. Bioelectron.* 21 (2006) 2320.
- [32] J.P. Hervás Pérez, M. Sánchez-Paniagua López, E. López-Cabarcos, B. López-Ruiz, *Biosens. Bioelectron.* 22 (2006) 429.
- [33] S.A. Miscordia, J. Desbrieres, G.D. Barrera, P. Labbé, G.A. Rivas, *Anal. Chim. Acta* 578 (2006) 137.
- [34] X. Chu, D. Duan, G. Shen, R. Yu, *Talanta* 71 (2007) 2040.
- [35] B.Y. Wu, S.H. Hou, F. Yin, Zi.X. Zhao, Y.Y. Wang, X.S. Wang, Q. Chen, *Biosens. Bioelectron.* 22 (2007) 2854.
- [36] L. Wu, X. Zhang, H. Ju, *Biosens. Bioelectron.* 23 (2007) 479.
- [37] D.S. Young, *Effects of Drug on Clinical Laboratory Test*, third edition, AACC Press, Washington, 1990.

Development of a portable biosensor for screening neurotoxic agents in water samples

Alain Hildebrandt^a, Jordi Ribas^a, Ramon Bragós^b,
Jean-Louis Marty^c, Màrius Tresànceh^a, Sílvia Lacorte^{a,*}

^a Department of Environmental Chemistry, IIQAB-CSIC, Jordi Girona 18-26, 08034 Barcelona, Spain

^b Departament d'Enginyeria Electrònica, Universitat Politècnica de Catalunya,
Gran Capità s/n, 08034 Barcelona, Spain

^c Centre de Phytopharmacie, Université de Perpignan, 52 Avenue Paul Alduy, 66860 Perpignan, France

Received 27 September 2007; received in revised form 8 January 2008; accepted 9 January 2008

Available online 21 January 2008

Abstract

A high sensitive portable biosensor system capable of determining the presence of neurotoxic agents in water has been developed. The system consists of (i) a screen-printed electrode with acetylcholinesterase (AChE) immobilized on it, (ii) a self-developed portable potentiostat with an analog to digital (A/D) converter and a serial interface for transferring data to a portable PC and (iii) an own designed software, developed with Lab-Windows CVI, used to record and process the measurements. The system has been developed to perform high precision amperometrical measurements with low drifts, low noise and a good reproducibility. In the configuration depicted, the percentage of AChE inhibition is proportional to the content of neurotoxic agents in a sample. This type of measurement is performed by the steady-state method from the first steady current (by a phosphate buffer solution) and the second steady current (by an enzymatic reaction produced by the addition of acetylthiocholine chloride to the solution). Validation was performed by analyzing spiked water samples containing pesticides. The design is specially suited for screening purposes, does not need sample preconcentration, is totally autonomous and suitable for the field detection of neurotoxic agents in water.

© 2008 Elsevier B.V. All rights reserved.

Keywords: Environmental analysis; Enzyme biosensor; Pesticide; Portable

1. Introduction

Pesticides are neurotoxic agents used in agriculture, industry, housework and as war gases. Neurotoxic pesticides mainly kill by the inhibition of acetylcholinesterase enzymes (AChE) [1], an essential enzyme that permits the transmission of electrical signals in the nervous system of most animal beings. Most common types are organophosphorus, but also carbamates, which are considered less toxic since the reversibility of their coupling with AChE. Due to their high acute toxicity and risk towards the population, some neurotoxic pesticides are included in Directives 76/464/CEE and in 60/2000/EU or in food regulations [2]. However, in the recent years there is a fear towards the poisoning of water tanks and drinking water

reservoirs by neurotoxic agents which at very low concentration can produce acute poisoning to the general population, being then a great need to have tools to quickly determine with high reliability and preferably at low cost the presence of compounds which can affect the nervous transmission in humans or fauna.

Several analytical methods are used to detect neurotoxic pesticides in water matrices. Routine methods are based on extraction, clean up and analysis normally performed by gas chromatography (GC) or liquid chromatography (LC) coupled to sensitive and specific detectors such as nitrogen–phosphorus detectors (NPD) [3–5], flame ionization detectors (FID) [4,5], ultraviolet detectors (UV) or diode array detectors (DAD) [6–8], although recently most methods involve the use of mass spectrometry (MS) as detector to provide ultimate confirmation [9,10]. These methods are highly sensitive and are capable to determine a large number of compounds but they are costly, long and/or complex.

* Corresponding author. Tel.: +34 934006169; fax: +34 932045904.
E-mail address: slbqam@iiqab.csic.es (S. Lacorte).

Biosensors are alternative methods capable to monitor the total concentration of a chemical family in terms of neurotoxicity and if properly designed, are very helpful tools for environmental/food monitoring [11,12]. AChE biosensors permit to detect the concentration of total neurotoxic agents by measuring the inhibition of AChE [13–15]. By performing an adequate calibration, biosensors can quantify the concentration of total neurotoxic compounds in a sample. The main advantage of AChE-based biosensor is that above a threshold value, they can discern between positive and negative samples with high precision, thus reducing the number of samples to be monitored by analytical tools to determine the exact composition or concentration.

Among different configurations, basically AChE biosensors consist in the enzyme immobilized on a graphite working electrode, and the measurement is performed with 2-electrode amperometry using a potentiostat. Commercial potentiostats are able to perform a wide range of measurements [16] but the main inconvenient is that they are bulky, expensive and cannot be transported to the field/facility for *in situ* measurements. Laboratory biosensors permit to determine neurotoxic agents at the ppb level with reproducibility below 10% and high precision [17]. Their main problem, for early warning stages, is that the sample has to be transported to the laboratory and thus, in an alarm situation, decisions cannot be established with enough effectiveness.

Portable biosensors for pesticide analysis have already been reported in the literatures [18,19] with similar analytical characteristics but with fiber-optics technology or expensive multi-parametric features which would increase the price of the instrument. Also, some portable potentiostats have been developed using electrochemical detection [20,21]. The biosensor herein reported is tailored in such a way that it has the advantage that the system is simplified and analyte specific, while still fulfils the specifications of high-quality commercial potentiostats. Therefore, the goal of this study was to develop a tailored portable biosensor, which permits the measurement of neurotoxic agents in water with high sensitivity. The own designed potentiostat only performs amperometric measurements with two- or three-electrode sensor and has user friendly features like the adjustment of the applied voltage between the electrodes and an internal calibration system. In this study we describe the design and performance of the biosensor in terms of noise, sensitivity, reproducibility, portability and validation.

2. Experimental

2.1. Chemicals and reagents

The pesticides carbaryl (CA), chlorpyrifos (OP) and chlorfenvinphos (OP) (99% purity pesticides from Sigma–Aldrich, St. Louis, U.S.A.) were used as model AChE toxic compounds belonging to the carbamate (CA) and organophosphorus (OP) family. Stock standard solutions at 1000 $\mu\text{g}/\text{mL}$ were prepared in methanol and kept at $-20\text{ }^\circ\text{C}$. Chlorpyrifos oxo-derivative was prepared by oxidizing the parental compound with *N*-bromosuccinimide, which rendered chlorpyrifos-oxon of 99%

purity. Chlorpyrifos is applied in the environment in the sulfured form ($\text{C}_9\text{H}_{11}\text{Cl}_3\text{NO}_3\text{P}=\text{S}$) but its oxidation is very fast giving the more active and toxic metabolite chlorpyrifos-oxon ($\text{C}_9\text{H}_{11}\text{Cl}_3\text{NO}_3\text{P}=\text{O}$) [22]. Working standard solutions were prepared daily by successive dilutions in HPLC grade water. A 0.05-M phosphate buffer solution with 0.1 M KCl (reagents from Merck, Darmstadt, Germany) at pH 8.0 was used to give a stable aqueous medium for enzymatic reaction. Acetylthiocholine chloride (substrate of AChE) was obtained from Sigma–Aldrich.

2.2. System description

The developed portable amperometric biosensor consists of a recognition element, in this case a sensor strip or screen-printed electrode where AChE has been immobilized, a transducer based in a thiol oxidation at a potential of 100 mV and a detection element which measures the total circulating current. The system is formed by three parts:

- (i) A screen-printed electrode, with a graphite working electrode and an Ag/AgCl reference electrode. The sensor strip was manufactured by successive screen-printing of six layers upon a polyvinyl chloride (PVC) sheet. The first layer is a silver track used as the conductor. The second layer is a graphite film used to isolate the silver conducting track from solution. The reference electrode (RE), made of Ag/AgCl, is printed in the third layer. The working electrode (WE) is printed in the fourth layer; it is made of graphite and 7,7,8,8-tetracyanoquinodimethane as a mediator. The fifth layer is an insulating ink to fix the working surface. The sixth and last layers are manually deposited on the WE; it is *Drosophila melanogaster* acetylcholinesterase enzyme entrapped in a polyvinyl alcohol photopolymer – named PVA-SbQ – with a polymerization degree of 2300 from Toyo Gosei Kogyo Co., Ltd. Photopolymers are easy to handle and have shown excellent performance when immobilizing enzymes over screen-printed electrodes; the procedure used is based with that described previously [23]. The electrodes are designed for single use.
- (ii) Potentiostat: the potentiostat is a circuit designed in such a way that it ensures that the voltage between the working and reference electrodes of the sensor is set at a predetermined value, and also gives a path for electron flow around the sensor. The potentiostat includes a current to voltage converter that yields an output voltage proportional to the sensor current. This output voltage is converted to a digital format using an analog to digital converter (A/D). Data is transmitted to a PC via a serial port and displayed with a customized software.
- (iii) The circuitry needed for analog to digital conversion and serial port interface with a personal computer (PC) and a program in C for Virtual Instrumentation (Lab-Windows), designed to control the biosensor: the user can have a graph of the current plotted, autoscale the graph, make calibrations and store data and information about current waveforms in files.

2.3. Experimental setup

The system has been characterized by testing the noise (both electronic and overall), drift, temperature dependence and repeatability of the measurements. Calibration curve has been constructed using hydrogen peroxide. Only the simple and common 2-electrode configuration has been tested.

2.3.1. Electronic noise

There are two main sources of noise: the electronics and the biosensor. Electronic noise has been measured for three different full-scale ranges (5 μA , 500 nA and 50 nA, which correspond to $R_{\text{feedback}} = 1 \text{ M}\Omega$, 10 $\text{M}\Omega$ and 100 $\text{M}\Omega$, respectively). To perform the measurements, the sensor was replaced with a resistance equal to R_{feedback} placed between auxiliary and working electrodes. The applied voltage was 600 mV. Measurement of the noise was performed without any further processing.

2.3.2. Overall system noise and drifts

The overall system noise included the noise generated by the electronics and the biosensor. The measurements were performed by dipping the sensor into 500 mL of phosphate buffer kept at constant 25 °C with stirring. Full-scale range was set to 5 μA . Data was analyzed in raw and filtered with a moving average to demonstrate the benefits of this signal processing technique. Low frequency noise, which includes drifts, was measured for 400 sample points.

2.3.3. Temperature dependence

Temperature coefficient of the biosensor has been calculated measuring the steady-state current by dipping the sensor into 500 mL of phosphate buffer with a small temperature change between 22.6 °C and 25.1 °C. This range has been chosen because only small changes in temperature should be expected between consecutive measurements.

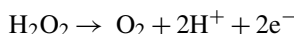
2.3.4. Repeatability and repetitivity of the measurements

To certify the reliability of the self-made electrodes, repeatability tests were carried out during three consecutive days with hydrogen peroxide. Additions of 10 μL of hydrogen peroxide solutions into 10 mL of fresh phosphate buffer were performed for a final concentration of $7.5 \times 10^{-4} \text{ M}$ using the same electrode without an enzyme. Four measurements were as well completed to check the repetitivity of the biosensor to 10 μL substrate addition into 10 mL of fresh phosphate buffer, using the same electrode with 5 mU of AChE enzyme. The temperature remained mainly constant during these experiments.

2.3.5. Calibration

Calibration curve has been done using hydrogen peroxide with nine calibration points from 7.50×10^{-4} to $6.75 \times 10^{-3} \text{ M}$ using electrodes without an enzyme. Hydrogen peroxide was added to the biosensor's reaction cell and a potential of 600 mV (increasing this value to 1 V which corresponds to the maximum response of hydrogen peroxide at electrode based on carbon would represent extra power consumption from (limited) batteries and besides, extra noise) was applied for its oxidation into

oxygen following the reaction:



This reaction is usually used to determine the efficiency of electrodes in amperometrical analysis.

To investigate the dynamic range of the AChE electrodes, HPLC grade water was spiked at different levels from 0 $\mu\text{g/L}$ to 16 $\mu\text{g/L}$ with chlorpyrifos-oxon, known to be one of the most toxic compounds to *D. melanogaster* AChE [24]. Experimental was conducted as depicted in Section 2.4.

2.4. Experimental procedure

Measurement of neurotoxic agent is achieved in a two-step ratiometric measurement. In the first step the amperometric response of the biosensor is measured as the current increases in relation with the base current when the substrate is added to the buffer ($\Delta I_1 = I_{\text{buffer with substrate}} - I_{\text{buffer}}$). After that, the biosensor is placed for 10 min in contact with the sample containing the neurotoxic agents, which inhibit the AChE and the same measurement is repeated (ΔI_2). The relative inhibition is calculated as follows:

$$\text{Inhibition (\%)} = \frac{\Delta I_1 - \Delta I_2}{\Delta I_1} \times 100$$

Concentration of neurotoxic agents is proportional to the inhibition of AChE and, if quantification is required, it can be measured using linear regression calibration.

Samples with inhibition lower than 10% are considered free of neurotoxic agents. If the inhibition is greater than 90%, the concentration of neurotoxic agents cannot be measured because of the sensor saturation and thus sample should be diluted.

2.5. Application to water samples

The biosensor was used to determine total neurotoxic agents from waters. Carbaryl, chlorpyrifos and chlorfenvinphos were used as inhibitors. Four wastewater samples from different wastewater treatment plants were collected using amber glass bottles. These samples were filtered and spiked with carbaryl to concentrations from 0 $\mu\text{g/L}$ to 4.1 $\mu\text{g/L}$. Electrodes with 1 mU of enzyme were used for this experiment. Four other samples of groundwater and bottled water were tested spiked with chlorpyrifos, chlorfenvinphos or a mix of organophosphorus and carbamate pesticides. As these pesticides are the greater inhibitors of AChE, electrodes with 10 mU of enzyme were used allowing a greater linear range. Spiked concentrations are shown in Table 1.

3. Results and discussion

3.1. Performance of the portable potentiostat

A portable potentiostat was designed and tested to determine neurotoxic agents at the low microgram/liter levels, which are the lowest limits imposed for individual pesticides in water and food. The initial requirement was to develop a portable,

Table 1
Matrix and pesticides studied, concentrations spiked and inhibitions measured with the biosensor

Matrix	Compound	Units of AChE (mU)	Concentration spiked (in $\mu\text{g/L}$)	Biosensor inhibition (%)
Wastewater 1	None	1	0.0	0
Wastewater 2	Carbaryl	1	0.3	11
Wastewater 3	Carbaryl	1	3.4	60
Wastewater 4	Carbaryl	1	4.1	72
Groundwater	Chlorfenvinphos	10	34.0	29
Groundwater	Chlorpyrifos-oxon	10	10.0	44
Bottled water	None	10	0.0	3
Bottled water	Mix of OP and CA	10	100.0	96

autonomous system capable to be used in the field. The first step was then to reduce the size of the potentiostat and the weight, which by the present design is kept at only 45 g, making it light enough for field use. A picture of the developed potentiostat is shown in Fig. 1.

The main requirement of the potentiostat for low level pesticide measurements was to achieve high sensitivity. This can only be obtained with a wide dynamic range, which in turn calls for a low noise system. The voltage applied between electrodes is obtained from a low noise voltage source integrated circuit and can be adjusted between -1.2 V and 1.2 V . The current-to-voltage converter uses a low-noise operational amplifier (OA) combined with a single high-quality, high-value, R_{feedback} resistor in the feedback loop of the current-to-voltage converter. Increasing the value of R_{feedback} increases the signal and the noise. Signal is increased proportionally to the value of R_{feedback} . Noise can be split into two main sources: thermal noise, which increases with the square root of R_{feedback} and the noise of the OA which in turn can be split into voltage and current noise. Both noises are independent of the resistance, but current noise is converted into voltage in R_{feedback} and therefore it also increases linearly with its value. The aggregated signal-to-noise ratio increases with R_{feedback} up to a certain value, which

is mainly given by the noise figures of the OA. The use of a low-noise OA allows the use of very high-value resistors, which permits low level measurements. Power supply is obtained from two batteries, which also helps to lower the overall noise of the system. With $\pm 7.2\text{ V}$ and 1500 mA batteries, an autonomy of 3 weeks was achieved using it daily.

In order to process the response of the biosensor the voltage signal is digitized using a 24-bit A/D delta-sigma converter. This A/D was chosen because of its very high resolution and low noise permitting to obtain a very wide dynamic range.

The software was designed to collect real-time data. In order to record the response of the biosensor, the digitized signal is transmitted to a PC via an RS-232 serial port. The signal is plot in a strip-chart by means of a customized software made with Lab-Windows CVI. This program permits to select several parameters like sampling rate, number of samples averaged in each time slice and value of the feedback resistance. A 3-point calibration algorithm [25] can be applied to reduce linear and non-linear errors. Data can be filtered with a user-selectable moving average to further reduce the noise. Raw data can be saved in ASCII files and retrieved for display.

3.2. Electronic noise

The electronic noise measurements for the tested ranges are shown in Table 2. In each case, the noise was approximately gaussian. As it can be seen, there is a noise reduction as R_{feedback} increases, which permits us to conclude that noise is mainly due to voltage sources and theoretically higher resolution could be achieved by further increasing the R_{feedback} . In practice, this is not feasible as will be shown in the following section.

3.3. Overall system noise, drifts and temperature dependence

Overall system noise was found to be around 160 pA and followed a gaussian distribution as shown in Fig. 2. This overall

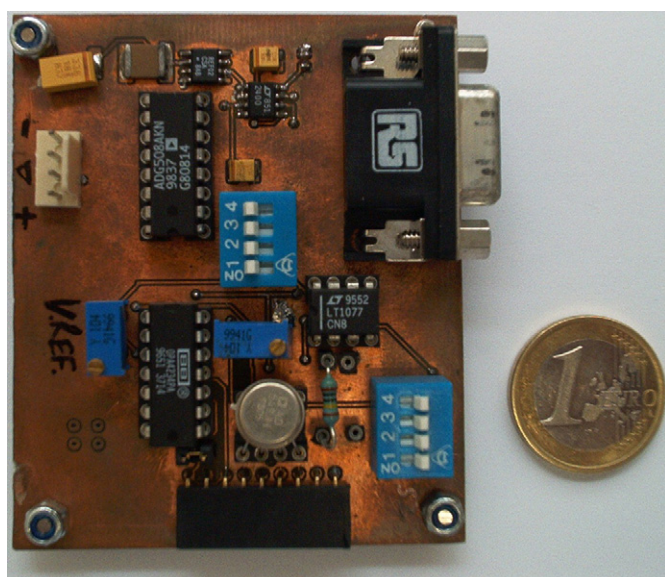


Fig. 1. Picture of the miniaturized electronic plate that functions as a potentiostat.

Table 2
Electronic noise for different R_{feedback} tested

R_{feedback} ($\text{M}\Omega$)	Range (nA)	I (mean) (nA)	σ_I (pA)
1	5000	603.99	31
10	500	60.921	1.4
100	50	6.0866	0.19

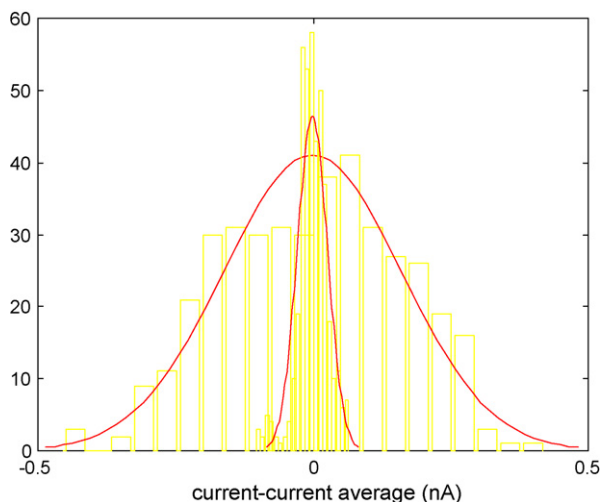


Fig. 2. System noise and its reduction with a moving average. Noise in a steady segment ($n = 400$ samples) $s = 0.16$ nA and 0.5 nA resolution. Applying a moving average $t_f = 10$ s, $s = 0.03$ nA and 0.1 nA resolution.

noise is much higher than the electronic noise and therefore it is due to the biosensor noise, it is the one which determines the resolution of the system. Averaging the output signal it is possible to reduce the noise to 30 pA, which is close to the limit posed by the electronics. It should be noted that averaging reduces electronic noise to 5 pA, so we can still affirm that biosensor is, by far, the main source of noise.

The temperature dependence has been established in $5\% \text{ } ^\circ\text{C}^{-1}$. Fig. 3 shows the drift of the current intensity with the temperature. The values indicated in Fig. 3 correspond to the amperometric response of the first step before inhibition. Biosensor measurements were performed at laboratory temperature ($23\text{--}24$ $^\circ\text{C}$).

3.4. Calibration and quality parameters of the measurements for AChE electrodes

As a first approach, calibration points were performed with hydrogen peroxide, which showed a good linearity with $R^2 = 0.997$ in the chosen range of 7.50×10^{-4} M to

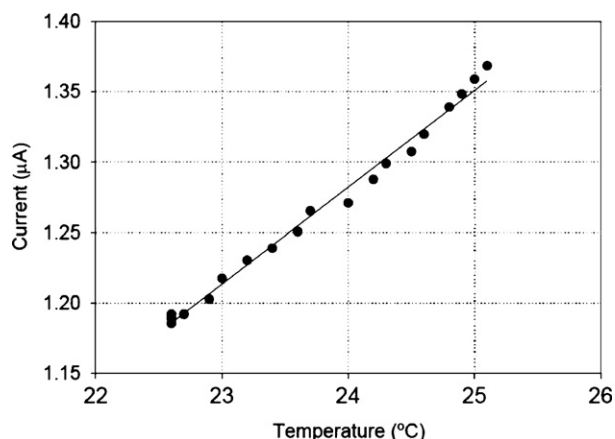


Fig. 3. Temperature dependence on the biosensor's current.

6.75×10^{-3} M. This performance proves the good proportional response of the electronic system *versus* different analyte concentrations. Moreover different quality parameters tested showed a good performance of the method:

- *Low drifts*: once the reactions have reached the stationary state, the intensity current is constant. The maximum derivative of the averaged intensity is $0.001\% \text{ s}^{-1}$.
- *Low noise*: when measuring currents of mean μ (in nA), equivalent noise due to the electronic components present a gaussian distribution with a standard deviation $\sigma < 0.002\mu$.
- *Wide dynamic range*: the dynamic range is higher than four orders of magnitude, specifically from 1 to $50,000$, equivalent to a resolution of 15.7 bits.
- *Repeatability*: differences between measurements performed in different days under the same conditions are below 5% .

In a second step, the neurotoxic agent chlorpyrifos-oxon was used as a test compound. With such, the following parameters were measured:

- *Narrow dynamic range*: concentrations between 0 $\mu\text{g/L}$ and 16 $\mu\text{g/L}$ were tested in HPLC grade water with the analysis of six calibration points with five replicates. Four calibration points showed linearity at a narrow concentration range from 2 $\mu\text{g/L}$ to 8 $\mu\text{g/L}$ for electrodes with 10 mU of AChE. Linear regression in this interval gave the following equation:

$$y = 9.646x + 9.576, \quad r^2 = 0.9969$$

- *Detection limits*: the system permitted to detect selected pesticide below 2 $\mu\text{g/L}$ using a 10 -mU enzyme screen-printed electrode. The limit was achieved by successive tests at different concentrations with replicates searching for the lower concentration that would give a significant inhibition over blank values (over 10% as described in Section 2.4).
- *Repetitivity*: the repetitivity of the amperometric response was better than 5% for both 1 mU and 10 mU electrodes. The addition of 10 μL of substrate to both types of biosensors was repeated four times washing the sensor before each addition. This performance certifies the correct setup of the electrodes and the efficient entrapment of the enzyme on their surfaces.

3.5. Application to water samples

The level of saturation of the enzyme immobilized in the screen-printed electrode (and then, the linear working range) will depend on the toxicity of the pesticide but it would be generally very short (a range of some $\mu\text{g/L}$ for the most toxic pesticides). So, the use of the biosensor to determine neurotoxic agents permitted to discern between positive (spiked) and negative samples, being an appropriate measurement to discriminate between contaminated and non-contaminated samples. Table 1 reports the samples tested, the type of compound tested, the concentration spiked and the percentage of inhibition determined.

According to Table 1, a high inhibition was observed in “wastewater 3” and “wastewater 4” what was in agreement with the spiked concentrations of carbaryl. 3–4 $\mu\text{g/L}$ of concentration gave an inhibition close to the saturation point (near 85–90%). The low enzyme charge immobilized on the electrode (1 mU) was easily inhibited by carbaryl even though it is a weak inhibitor of the AChE [26]. For other compounds like chlorpyrifos and chlorfenvinphos, a very significant difference was observed in groundwater: 10 $\mu\text{g/L}$ of spiked chlorpyrifos-oxon gave higher inhibition (44%) than 34 $\mu\text{g/L}$ of spiked chlorfenvinphos (29%). In those experiments, the enzymatic charge was of 10 mU to obtain a greater linear range when working with more toxic compounds. The explanation of the different inhibition rates is found in the toxicity of each compound, being the oxidized form of chlorpyrifos much more toxic towards AChE than chlorfenvinphos [22]. Finally, two samples of bottled water were tested without and with 100 $\mu\text{g/L}$ of a mix of pesticides (sum of all) to demonstrate the biosensor capacity to discern between non-contaminated and contaminated samples. The bottled water sample spiked with a high level of pesticides (100 $\mu\text{g/L}$) gave a complete AChE inhibition while the unspiked sample gave no inhibition at all (lower than 10%).

Sample measurements can be performed *in situ* with a total analysis time of 20 min per sample, no need of sample preparation or processing and thus, a high sample throughput can be envisaged. However, the results indicated in this study are only preliminary and ongoing studies are being performed to determine neurotoxic agents in water and food samples using the proposed biosensor.

4. Conclusions

The portable biosensor depicted in this study is capable to determine the presence of neurotoxic compounds *in situ*. The aim of this biosensors is to be used where high-speed analysis and excellent performance is needed to discern between positive (samples containing neurotoxic agents) and negative samples, without the need of transporting the sample to a laboratory. At this point it can be concluded that (i) the developed potentiostat produces low noise and low drift, (ii) the biosensor shows good amperometric response to buffer tests and the ability to detect low neurotoxic agents concentrations and (iii) the developed biosensor is totally autonomous and suitable for the field detection of pesticides, as has been demonstrated for different types of water samples where a good agreement was found between the biosensor response and pesticide concentration. However, the main feature of the developed biosensor is its versatility and possibility to increase the sensitivity and specificity by assembling

different screen-printed electrodes thus providing a multisensor system which has clear technical and competitive advantages in the food and environmental field. In addition, by changing the type of enzyme immobilized, different types of organic pollutants can be measured, thus, enlarging the future applicability of the biosensor.

Acknowledgement

This study has been financed by the Ministry of Education and Science of Spain.

References

- [1] M. Maroni, J. Jarvisalo, F. La Ferla, *Toxicol. Lett.* 33 (1986) 115.
- [2] I.S. Arvanitoyannis, S. Chorefaki, P. Tserkezou, *Int. J. Food Sci. Technol.* 40 (2005) 1021.
- [3] S. Lacorte, C. Molina, D. Barceló, *Anal. Chim. Acta* 281 (1993) 71.
- [4] Y. Pico, A.J. Louter, J.J. Vreuls, U.A. Brinkman, *Analyst* 119 (1994) 2025.
- [5] E. Ballesteros, M.J. Parrado, *J. Chromatogr. A* 1029 (2004) 267.
- [6] S. Lacorte, D. Barcelo, *J. Chromatogr. A* 725 (1996) 85.
- [7] J. Norberg, J. Slobodnik, R.J.J. Vreuls, U.A.T. Brinkman, *Anal. Methods Instrum.* 2 (1995) 266.
- [8] V. Pichon, M.C. Hennion, *J. Chromatogr. A* 665 (1994) 269.
- [9] R.B. Geerdink, W.M.A. Niessen, U.A.T. Brinkman, *J. Chromatogr. A* 970 (2002) 65.
- [10] M. Kuster, L.M. De Alda, D. Barcelo, *Mass Spectrom. Rev.* 25 (2006) 900.
- [11] M. Albareda-Sirvent, A. Merkoçi, S. Alegret, *Anal. Chim. Acta* 442 (2001) 35.
- [12] M.P. Marco, D. Barceló, *Meas. Sci. Technol.* 7 (1996) 1547.
- [13] T. Nogue, B. Leca, G. Jeanty, J.-L. Marty, *Field Anal. Chem. Technol.* 3 (1999) 171.
- [14] W. Russell Everett, G.A. Rechnitz, *Anal. Lett.* 32 (1999) 1.
- [15] F. Arduini, F. Ricci, C.S. Tuta, D. Moscone, A. Amine, G. Palleschi, *Anal. Chim. Acta* 580 (2006) 155.
- [16] A. Avramescu, S. Andrescu, T. Nogue, C. Bala, D. Andrescu, J.L. Marty, *Anal. Bioanal. Chem.* 374 (2002) 25.
- [17] S. Andrescu, A. Avramescu, C. Bala, V. Magearu, J.L. Marty, *Anal. Bioanal. Chem.* 374 (2002) 39.
- [18] V.G. Andreou, Y.D. Clonis, *Biosens. Bioelectron.* 17 (2002) 61.
- [19] F. Arduini, A. Amine, D. Moscone, F. Ricci, G. Palleschi, *Anal. Bioanal. Chem.* 388 (2007) 1049.
- [20] J.R. Blanco, F.J. Ferrero, J.C. Campo, J.C. Anton, J.M. Pingarron, A.J. Reviejo, J. Manso, in: *Conference Record—IEEE Instrumentation and Measurement Technology Conference*, 2006, p. 690.
- [21] M.D. Steinberg, *Sens. Actuator B: Chem.* 97 (2004) 284.
- [22] R.J. Richardson, *J. Toxicol. Environ. Health* 44 (1995) 135.
- [23] S. Andrescu, L. Barthelmebs, J.-L. Marty, *Anal. Chim. Acta* 464 (2002) 171.
- [24] G. Jeanty, A. Wojciechowska, J.L. Marty, M. Trojanowicz, *Anal. Bioanal. Chem.* 373 (2002) 691.
- [25] W.T. Bolk, *J. Phys. E: Sci. Instrum.* 18 (1985) 61.
- [26] C.D.S. Tomlin, *The Pesticide Manual: A World Compendium*, British Crop Protection Council, 2003.

A multicommuted flow system with solenoid micro-pumps for paraquat determination in natural waters

Carlos M.C. Infante^a, A. Morales-Rubio^b, M. de la Guardia^b, Fábio R.P. Rocha^{a,*}

^a Universidade de São Paulo, Instituto de Química, Av. Prof. Lineu Prestes 748, 05513-970 São Paulo, Brazil

^b Universidad de Valencia, Department of Analytical Chemistry, C/Dr. Moliner 50, 46100 Burjassot, Valencia, Spain

Received 25 October 2007; received in revised form 23 January 2008; accepted 24 January 2008

Available online 2 February 2008

Abstract

A flow system designed with solenoid micro-pumps is proposed for the determination of paraquat in natural waters. The procedure involves the reaction of paraquat with dehydroascorbic acid followed by spectrophotometric measurements. The proposed procedure minimizes the main drawbacks related to the standard chromatographic procedure and to flow analysis and manual methods with spectrophotometric detection based on the reaction with sodium dithionite, i.e. high solvent consumption and waste generation and low sampling rate for chromatography and high instability of the reagent in the spectrophotometric procedures. A home-made 10-cm optical-path flow cell was employed for improving sensitivity and detection limit. Linear response was observed for paraquat concentrations in the range 0.10–5.0 mg L⁻¹. The detection limit (99.7% confidence level), sampling rate and coefficient of variation ($n = 10$) were estimated as 22 µg L⁻¹, 63 measurements per hour and 1.0%, respectively. Results of determination of paraquat in natural water samples were in agreement with those achieved by the chromatographic reference procedure at the 95% confidence level.

© 2008 Elsevier B.V. All rights reserved.

Keywords: Flow analysis; Multi-pumping; Multicommutation; Spectrophotometry; Paraquat; Waters

1. Introduction

Paraquat (1,1'-dimethyl-4,4'-bipyridilium) is one of the most widely used herbicides in the world in several crops in view of its great efficiency and low cost. However, undesirable characteristics include high toxicity for plants and aquatic organisms [1] and several cases of accidental or intentional intoxication of humans have been reported [2]. Paraquat exposure can induce neuronal cell death, oxidative stress and stroke [3].

Several controversies are related to the use of paraquat, considering the effects in the environment and health of farmers [4,5]. Recently, the Environmental Protection Agency (EPA) of the United States [6] included paraquat as a possible human carcinogen, establishing the drink water equivalent level as 0.2 mg L⁻¹ and permitting the commercialization only in a restricted category. Diverse studies have shown that the cationic form of paraquat is strongly [7] and quickly [8] bonded to ground

molecules and mineral clays. Thus, risks of water contamination are reduced, but monitoring in natural waters is important because the mobility and bioavailability of the herbicide in the environment were not completely clarified [9].

The procedure for paraquat determination in waters recommended by the EPA is based on high performance liquid chromatography with spectrophotometric detection in the ultraviolet [10]. However, some spectrophotometric methods are available based on the classical reaction with sodium dithionite [11–13]. According to the most accepted reaction mechanism, dithionite in alkaline medium [14] reduces paraquat forming a blue free radical [15], which is measured at 600 nm.

Despite the extended use and application to different kind of samples [16,17], the aforementioned procedures present some drawbacks: large amounts of reagents, sample and organic solvents are generally required, also generating large amounts of wastes, specially in chromatographic procedures; severe matrix effects are caused by saturated ammonium chloride solution, typically used for elution in procedures involving solid-phase preconcentration. In the spectrophotometric determination of paraquat based on the reaction with sodium dithionite both,

* Corresponding author. Fax: +55 11 38155579.

E-mail address: frprocha@iq.usp.br (F.R.P. Rocha).

the reagent and the free radical formed, are very unstable. In chromatographic determinations, considering the ionic nature of paraquat, a separation procedure based on ion-pair formation is required [10,18], making difficult the determination, because the equilibrium between mobile and stationary phases is slow and the separation is susceptible to variations of temperature, pH and concentration of organic compounds in the mobile phase.

The multicommutation approach [19] provides interactive flow systems in which sample processing conditions can be changed by the control software as required by the analytical procedure. In recent years, multicommutation setups have incorporated solenoid micro-pumps [20,21] that can reproductively dispense micro-volumes of solutions. These devices can replace the injection and propulsion units, yielding compact manifolds that provide low reagent consumption and minimize waste generation. An additional advantage is the low power requirement of solenoid micro-pumps as compared with the conventional devices used in flow-based systems. The possibility of exploiting feedback mechanisms to change sample processing conditions makes this approach attractive to design flow systems for monitoring parameters of interest in the environment.

The aim of this work was to develop a flow system based on multicommutation for paraquat determination in natural waters. The flow system was designed with independently controlled solenoid micro-pumps and the dithionite reducing reagent was replaced by dehydroascorbic acid [22] in order to overcome the previously mentioned drawbacks. A home-made 10-cm optical-path flow cell was used to improve sensitivity and detection limit.

2. Experimental

2.1. Apparatus

The flow system was designed with four solenoid micro-pumps (Biochem, 090SP) with a nominal volume of $8\ \mu\text{L}$ per pulse and one three-way solenoid valve (NResearch, 161T031), 0.8-mm i.d. Teflon tubes and a Perspex connection (see Fig. 1). A parallel port of a Pentium III microcomputer was used for controlling the active devices through a power drive based

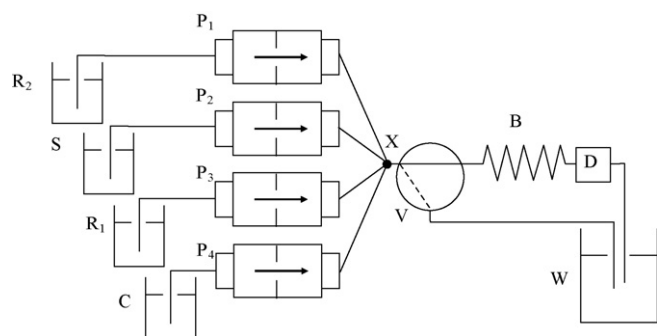


Fig. 1. Flow diagram of the system for paraquat determination. P₁–P₄: $8\text{-}\mu\text{L}$ solenoid micro-pumps; V: three-way solenoid valve; S: sample; C: carrier (H_2O); R₁: dehydroascorbic acid reagent; R₂: $1.0\ \text{mol L}^{-1}$ NaOH; B: 10-cm long reaction coil; D: diode-array spectrophotometer; X: confluence point; W: waste vessel.

on an ULN2803 integrated circuit [23]. Spectrophotometric measurements were carried out with a HP-8452A diode-array spectrophotometer (Waldbronn, Germany). The home-made flow cell was constructed from a glass tube of 10 cm length, 2 mm i.d. and ca. $300\text{-}\mu\text{L}$ internal volume. A quartz flow cell (Hellma) with 1-cm optical-path and ca. $50\ \mu\text{L}$ internal volume was also employed. The control software was developed in Visual Basic 6.0 (Microsoft) and the software furnished by the manufacturer of the diode-array spectrophotometer was employed for data acquisition.

A Dionex P680 liquid chromatograph (Sunny Valley, CA, USA) with an UV detector (UVD 170U), equipped with a C-18 reversed phase (Kromasil) column ($250\ \text{mm} \times 4.6\ \text{mm}$ i.d. and $5\text{-}\mu\text{m}$ particle diameter) was employed in the chromatographic reference procedure as described by the EPA [10].

2.2. Reagents and solutions

All solutions were prepared with analytical-grade chemicals and freshly distilled-deionized water. The chromogenic reagent (R₁) was prepared by dissolution of 0.25 g ascorbic acid, 0.10 g KIO_3 and 0.10 g EDTA (all reagents from Panreac, Barcelona, Spain), making the volume up to 100 mL with water. The R₂ reagent was a $1\ \text{mol L}^{-1}$ NaOH (Scharlau, Barcelona, Spain) solution. A $1000\ \text{mg L}^{-1}$ paraquat (Pq^{2+}) stock solution was prepared by dissolution of the dichloride salt (Riedel-de-Haën, Seelze, Germany) in water. Working solutions within 0.10 and $5.0\ \text{mg L}^{-1}$ were prepared by dilution of this stock in water.

Natural water samples were collected from rivers in the region of Valencia (Spain). Samples were filtered through a $0.22\text{-}\mu\text{m}$ Nylon membrane and preserved at $-4\ ^\circ\text{C}$. Drinking water was purchased from a local supermarket. Samples were stabilized at ambient temperature immediately before analysis.

2.3. Flow diagram and procedure

The flow system (Fig. 1) was designed with solenoid micro-pumps and one device was used for handling each solution. During actuation, the micro-pumps were operated at 5 Hz, thus providing a flow-rate of $2400\ \mu\text{L min}^{-1}$ (mean volume of each micro-pump = $8\ \mu\text{L}$ per pulse).

The switching course of the active devices for paraquat determination is shown in Table 1. The micro-pumps P₁–P₃ were simultaneously actuated to insert sample and reagent aliquots into the analytical path. This step was repeated 20 times (20 sampling cycles) for the 1-cm cell and 30 times (30 sampling cycles) for the 10-cm flow cell. The small sample and reagent aliquots undergo fast mixing, starting the chemical reactions. The effect of increasing the residence time was evaluated by processing aliquots of a $5.0\ \text{mg L}^{-1}$ Pq^{2+} solution in different stopping times (0–90 s). The sample zone was transported to the flow cell and the analytical signal was based on the difference between the absorbance values measured as peak height at 600 and 800 nm. It was verified that 220 pulses of P₄ (ca. 1.8 mL carrier) were enough to completely remove the sample zone from the manifold with the 1-cm flow cell and 250 pulses of P₄ were required for the 10-cm flow cell. The solenoid

Table 1
Switching course of the active devices for paraquat determination

Step	Description	P ₁	P ₂	P ₃	P ₄	V	Pulse number or time
1	Insertion of sample and reagents	1/0	1/0	1/0	0	0	20 or 30 ^a
2	Stopped flow	0	0	0	0	0	7 s
3	Signal measurement and system washing	0	0	0	1/0	0	220 or 250 ^b
4	Sample replacement	0	1/0	0	0	1	50
		0	0	0	1/0	1	20

Numbers 1 and 0 indicate that the pumps were switched on and off, respectively. Other symbols are defined in Fig. 1.

^a Twenty sampling cycles for the 1-cm flow cell and 30 sampling cycles for the 10-cm flow cell.

^b Two hundred and twenty pulses for the 1-cm flow cell and 250 pulses for the 10-cm flow cell.

valve V was employed for sample replacement. It was carried out by simultaneously actuating the micro-pump P₂ (50 pulses) and valve V, directing the solution towards the waste vessel. All measurements were carried out in triplicate.

For sample analysis by the HPLC reference procedure [10], the mobile phase was composed by 25:75 (v/v) acetonitrile–phosphate buffer (pH 3.2, 0.023 mol L⁻¹) with 10 mmol L⁻¹ 1-octanesulfonic acid. The flow-rate of the mobile phase was 1.5 mL min⁻¹. The UV detector was set at 254 nm and the injected sample volume was 20 μL. All chromatographic measurements were performed at ambient temperature and the running time was 8 min per sample.

3. Results and discussion

3.1. Experimental conditions

The reduction of the analyte by dehydroascorbic acid was carried out in alkaline medium forming a blue free radical. The spectra of the reaction product obtained with sodium dithionite, ascorbic acid and dehydroascorbic acid showed analogous bands, thus indicating the formation of the same species in the presence of different reducing agents. However, reaction kinetics was quite different, being faster in the presence of dithionite. Dehydroascorbic acid was preferred as reducing agent in view of its highest stability. A solution prepared from oxida-

tion of ascorbic acid by potassium iodate can be employed for up to a week against the 2-h stability of the dithionite solution.

As expected, when concentrated sodium hydroxide solutions were employed in the flow system, perturbations by Schlieren effect [24] were observed. This resulted in high blank signals (ca. $A = 0.200$) even when the lowest sodium hydroxide concentration required for product formation (1.0 mol L⁻¹) was employed. Measurements at two wavelengths, one at the absorption maximum of the reaction product (600 nm) and another selected as reference (800 nm) were exploited to compensate the perturbations by refractive index differences [24,25], thus reducing the blank signal to ca. $A = 0.002$.

The sample to reagent volumetric fraction was varied by adopting the binary sampling strategy [19], but sensitivity and repeatability were very poor. It was verified in an experiment carried out in batch conditions that when the mixture of the chromogenic reagent, sodium hydroxide and Pq²⁺ was shaken, the color disappeared, being re-established after few minutes. By considering this aspect, it is possible to suppose the presence of an oscillating reaction [26], in which the free radical Pq^{•+} is formed from the analyte and the reducing reagents. Thus, for improving the stability of the reaction product, the micro-pumps that handled reagents and sample solutions were simultaneously pulsed in the sampling step. Suitable mixing conditions were established in view of the merging zones approach, the small

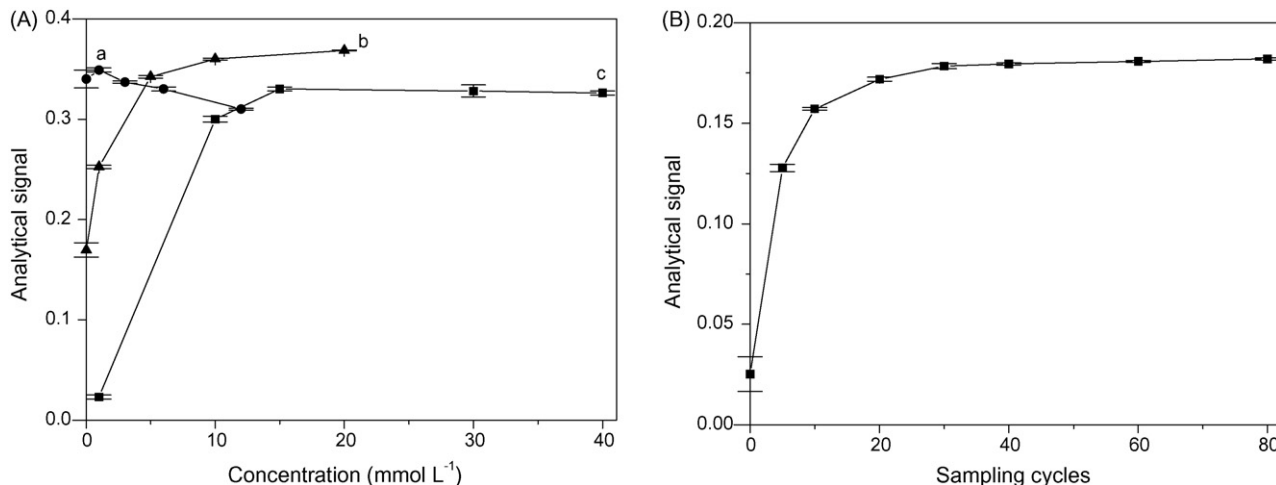


Fig. 2. Effect of experimental parameters: (A) reagents concentration: (a) EDTA; (b) potassium iodate, (c) ascorbic acid and (B) variation of the analytical signal with the number of sampling cycles. Paraquat concentration was maintained as 10 mg L⁻¹.

volume of the aliquots and the pulsed flow characteristic of fluid propulsion by solenoid micro-pumps.

The optimization of the experimental conditions was carried out by the univariate method, by changing the concentration of each solution while the number of pulses was maintained constant. Results shown in Fig. 2A indicate that the highest analytical signal was achieved with reagent concentrations of 15 mmol L^{-1} ascorbic acid, 5 mmol L^{-1} KIO_3 and 3 mmol L^{-1} EDTA (R_1), for a sodium hydroxide concentration of 1.0 mol L^{-1} (R_2). Under these conditions, the number of sampling cycles was varied, yielding the results in Fig. 2B. The analytical signal increased with the number of sampling cycles because the sample zone dispersion diminished. For 20 sampling cycles ($480\text{-}\mu\text{L}$ sample zone), the dispersion coefficient was 3.6 for the 1-cm flow cell and 4.1 for the 10-cm flow cell, which correspond to a medium dispersion [27]. These dispersion coefficients are slightly higher than the expected by considering the sample dilution caused by the addition of equal volumes of sample and reagents.

The variation of temperature did not cause any effect in the analytical signal as opposite to that found in previous works [22,28], in which variations of up to 700% were observed when temperature was increased to 60°C . It is probably due to the improved mixing conditions characteristic of the flow systems with solenoid micro-pumps [19].

The stopped-flow approach was adopted to investigate the effect of increasing the sample residence time. Significant variations were observed for stopping times up to 7 s (analytical signal 2.5-fold higher than those obtained without stopping the flow), being approximately constant for stopping times up to 90 s. These results confirm that the monitored reaction is relatively fast and the reaction product was stable when maintained without contact with oxygen. The efficient mixture of sample and reagents provided by the small volume of the aliquots and the simultaneous introduction of the solutions by a pulsed flow also contributed to improve the reaction rate.

3.2. Analytical figures of merit

For the 1-cm flow cell, linear response was observed for paraquat concentrations between 0.2 and 5.0 mg L^{-1} , described by the equation $A = (-0.0011 \pm 0.0001) + (0.0157 \pm 0.0001)C$, with a regression coefficient (r) of 0.999. The detection limit was estimated as $57 \mu\text{g L}^{-1}$ at the 99.7% confidence

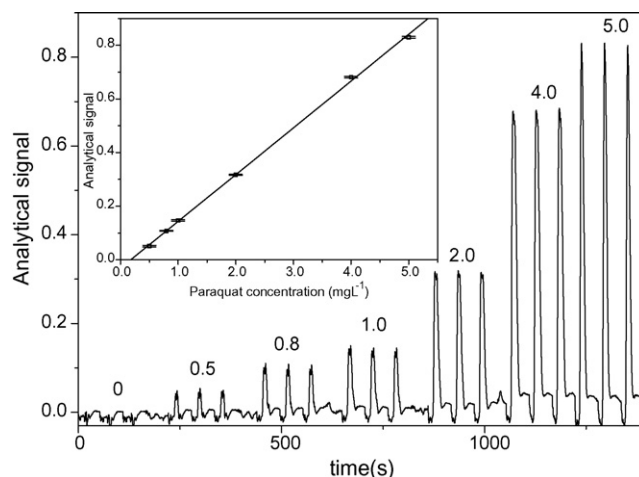


Fig. 3. Transient signals for paraquat measured with a 10-cm optical-path flow cell. Numbers indicate analyte concentrations in mg L^{-1} . The inset shows the corresponding calibration graph.

level. The sampling rate and coefficient of variation ($n=10$) were estimated as 63 measurements per hour and 1.0%, respectively. The proposed procedure consumed $400 \mu\text{g}$ ascorbic acid, $160 \mu\text{g}$ potassium iodate and $160 \mu\text{g}$ EDTA per determination, which was 12-times for ascorbic acid and 36-times for EDTA lower than the reagent consumption in the batch procedure [22]. The effluent volume was 2.0 mL per determination. By using the 10-cm optical-path flow cell, linear response was observed for paraquat concentrations in the range $0.10\text{--}5.0 \text{ mg L}^{-1}$ (Fig. 3), described by the equation: $A = (0.0010 \pm 0.0010) + (0.1670 \pm 0.0010)C$, with $r=0.997$. Sensitivity increased 10.4-fold using the 10-cm flow cell, and the detection limit (99.7% confidence level) was improved to $22 \mu\text{g L}^{-1}$, making feasible the application to the determination of paraquat in natural water samples [6]. Comparison of the reagent consumption with other flow-based procedures is difficult in view of the use of different reducing reagents [11–13]. However, the proposed procedure can be considered a greener alternative in view of the minimized consumption of low toxicity reagents. In addition, heating and strict temperature control was not required. In spite of this, as shown in Table 2, the analytical features are comparable with those attained by other flow procedures for paraquat determination [22,28].

Table 2
Analytical features of spectrophotometric procedures for paraquat determination

Analytical feature	Proposed system	Flow-injection [22]	Batch method [28]
Sampling rate (h^{-1})	63	120	–
Detection limit ($\mu\text{g L}^{-1}$)	22 ^a	20 ^b	1200
Linear range (mg L^{-1})	0.1–5.0	0.1–1.2	1.2–9.6
Coefficient of variation (%)	1.0 (9)	1.0 (6)	3.8
Effluent volume per determination (mL)	2.6	1	10
Reaction temperature ($^\circ\text{C}$)	25 ^c	60	20–30

^a Estimated according to the IUPAC recommendations at the 99.7% confidence level.

^b Calculated according to the criteria: $\text{LOD} = 3 \times \text{intercept of calibration curve/slope of calibration curve}$.

^c The procedure was carried out at ambient temperature.

Table 3
Effect of foreign species on paraquat determination

Added species ^a	Concentration (mg L ⁻¹)	Signal variation (%)
SO ₄ ²⁻	500	+3.6
NO ₃ ⁻	500	-1.1
Ca ²⁺	300	-2.0
CO ₃ ²⁻	300	-7.4
Glyphosate	200	+4.0
Cd ²⁺	140	-1.7
Fe ³⁺	80	+6.3
Mg ²⁺	80	+3.6

^a The paraquat concentration was fixed at 1 mg L⁻¹ and the concentration of the foreign species was varied from 10 to 500 mg L⁻¹.

3.3. Effect of foreign species

The effect of foreign species was evaluated in the range of 10–500 mg L⁻¹ in the presence of 1 mg L⁻¹ Pq²⁺ and the obtained results are presented in Table 3. Interference was considered when the analytical signal varied more than 5% in the presence of the foreign species. Selectivity was improved in the flow-based procedure in view of the lower residence time (ca. 20 s) than that used in batch, which minimizes the extension of side reactions. This aspect can be verified by the results obtained for glyphosate that interfered only when present in a 200-times excess. Glyphosate is largely utilized as herbicide and it is expected to be found in real samples. The main interference was caused by a species with a similar structure (Diquat), even at concentrations of the same order than paraquat, being in agreement with previous results [22]. Moreover, this interference can be avoided with a previous treatment with NaOH [29]. Additionally, it should be taken into account that the expected levels of the concomitant species in natural waters are lower than those considered in this study.

3.4. Analysis of water samples

The proposed procedure was applied to paraquat determination in natural waters from rivers and mineral sources, after spiking with 200 µg L⁻¹ (the drink water equivalent level established by EPA). Recoveries within 86 and 107% (mean value = 100.5%) were achieved, indicating the absence of matrix effects. In addition, results shown in Table 4 agreed with those achieved by the HPLC reference procedure [10] at the 95% con-

Table 4
Paraquat determination in spiked natural water samples

Sample	Proposed procedure		HPLC procedure	
	Concentration (µg L ⁻¹) ^a	R (%) ^b	Concentration (µg L ⁻¹) ^a	R (%) ^b
Jucar river	215 ± 3	107	208 ± 10	104
Turia river	204 ± 1	102	150 ± 13	75
Turia Dam	215 ± 3	107	184 ± 5	92
Mineral water	171 ± 4	86	200 ± 22	100

^a Concentration of herbicide added to the samples = 200 µg L⁻¹.

^b Recoveries of the analyte spiked in the samples.

fidence level, by considering a paired Student's *t*-test (*n* = 4). Another profitable characteristic is the improvement of precision in the mechanized procedure (coefficients of variation lower than 2% against to 8% found in the HPLC procedure) and reduction of the analyses time (ca. 1 and 8 min in the proposed and HPLC procedures, respectively).

4. Conclusions

The proposed procedure overcomes some drawbacks of procedures for paraquat determination. Sensitivity was improved by using a lab-made 10-cm optical-path flow cell yielding a linear response range compatible with the environmental requirements (e.g. the limits established by the EPA). Interferences were less pronounced, sampling throughput was improved (63 samples per hour) and reagent consumption was at least 12-fold reduced in relation to previous works. As a consequence, the proposed procedure can be considered as a clean alternative for fast paraquat determination in waters [30–32].

Acknowledgements

The authors acknowledge the fellowships and financial support from Conselho Nacional de Desenvolvimento Científico e Tecnológico (CNPq), Fundação de Amparo à Pesquisa do Estado de São Paulo (FAPESP), Programa Santander-Banespa, Universitat de Valencia (Acció Especial UV-AE-20070213) and Generalitat Valenciana (CTESIN/2004/051).

References

- [1] W.T. Tsai, M.F. Hsieh, H.F. Sun, S.F. Chien, H.P. Chen, *Bull. Environ. Contam. Toxicol.* 69 (2002) 189.
- [2] C. Bismut, A.H. Hall (Eds.), *Paraquat Poisoning, Prevention, Treatment*, Marcell Dekker, New York, 1995, pp. 1–16.
- [3] S. McCarthy, M. Somayajulu, M. Sikorska, H. Borowy-Borowski, S. Pandey, *Toxicol. Appl. Pharmacol.* 201 (2004) 21.
- [4] Richard Isenring, "Paraquat, unacceptable health risks for users", Pesticide Action Network, 2006, http://www.evb.ch/cm_data/EvB_Paraquat_E.pdf (accessed in July 2007).
- [5] Prasanna Srinivasan, "Paraquat, A unique contributor to agriculture and sustainable development", New Delhi, India, November 2003, <http://www.marshall.org/pdf/materials/183.pdf> (accessed in July 2007).
- [6] EPA 822-R-06-013, Office of Water United States, Environmental Protection Agency, Washington, 2006, <http://www.epa.gov/waterscience/criteria/drinking/dwstandards.pdf> accessed in June 2007.
- [7] Y. Seki, K. Yurdakoç, *J. Colloid Interface Sci.* 287 (2005) 1.
- [8] C.M.C. Infante, J.C. Masini, *Spectrosc. Lett.* 40 (2007) 3.
- [9] U.B. Cheah, R.C. Kirkwood, K.Y. Luma, *Pestic. Sci.* 50 (1997) 53.
- [10] J.W. Hodgeson, W.J. Bashe, J.W. Eichelberger, *Method 549.1, Revision 1.0*, Environmental Monitoring Systems Laboratory, Office of research and development, U.S. Environmental Protection Agency, 1992.
- [11] A. Calderbank, S.H. Yuen, *Analyst* 90 (1965) 99.
- [12] S.H. Yuen, J.E. Bangness, D. Myles, *Analyst* 92 (1967) 375.
- [13] C. Guijarro, E. Yáñez-Sedeño, L.M. Polo-Diéz, *Anal. Chim. Acta* 199 (1987) 203.
- [14] R.P. Mahoney, P.A. Fretwell, S.H. Demirdji, R.L. Mauldin, O. Benson Jr., T.H. Koch, *J. Anal. Chem. Soc.* 114 (1992) 186.
- [15] L. Michaelis, *Biochemistry* 2 (1932) 250.
- [16] I.S. Sellero, M. Lopezrivadulla, A. Cruz, A. Bermejo, P. Fernandez, *Anal. Lett.* 26 (1993) 1891.
- [17] T. Matsuoka, J. Okuda, *Forensic Sci. Int.* 62 (1993) 179.

- [18] R. Gill, S.C. Qua, A.C. Moffat, *J. Chromatogr. A* 255 (1983) 483.
- [19] F.R.P. Rocha, B.F. Reis, E.A.G. Zagatto, J.L.F.C. Lima, R.A.S. Lapa, J.L.M. Santos, *Anal. Chim. Acta* 468 (2002) 119.
- [20] R.A.S. Lapa, J.L.F.C. Lima, B.F. Reis, J.L.M. Santos, E.A.G. Zagatto, *Anal. Chim. Acta* 466 (2002) 125.
- [21] F.R.P. Rocha, C.M.C. Infante, W.R. Melchert, *Spectrosc. Lett.* 39 (2006) 651.
- [22] J. Archana, K.K. Verma, A. Townshend, *Anal. Chim. Acta* 284 (1993) 275.
- [23] E. Ródenas-Torralba, F.R.P. Rocha, B.F. Reis, A. Morales-Rubio, M. de la Guardia, *J. Autom. Methods Manage. Chem.* (2006) 1, Article ID 20384.
- [24] E.A.G. Zagatto, M.A.Z. Arruda, A.O. Jacintho, I.L. Mattos, *Anal. Chim. Acta* 234 (1990) 153.
- [25] F.R.P. Rocha, P.B. Martelli, B.F. Reis, *Anal. Chim. Acta* 438 (2001) 11.
- [26] R.D. Faria, *Quim. Nova* 18 (1995) 281.
- [27] J. Ruzicka, E.H. Hansen, *Flow Injection Analysis*, 2nd ed., Wiley Interscience, New York, 1988.
- [28] P. Shivhare, V.K. Gupta, *Analyst* 116 (1991) 391.
- [29] M. Ganesan, S. Natesan, V. Ranganathan, *Analyst* 104 (1979) 258.
- [30] F.R.P. Rocha, J.A. Nóbrega, O. Fatibello-Filho, *Green Chem.* 3 (2001) 216.
- [31] M. de la Guardia, J. Ruzicka, *Analyst* 120 (1995) 170.
- [32] M. de la Guardia, *J. Braz. Chem. Soc.* 10 (1999) 429.

Time-resolved XANES speciation studies of chromium on soils during simulated contamination

P. Kappen^{a,*}, E. Welter^b, P.H. Beck^c, J.M. McNamara^c,
K.A. Moroney^c, G.M. Roe^d, A. Read^c, P.J. Pigram^a

^a Centre for Materials and Surface Science and Department of Physics, La Trobe University,
Kingsbury Drive, Bundoora, Victoria 3086, Australia

^b Hamburger Synchrotronstrahlungslabor HASYLAB at Deutsches Elektronen-Synchrotron DESY,
Notkestrasse 85, Hamburg D-22607, Germany

^c Environmental Resources Management (ERM), 151 Clarendon Street,
South Melbourne, Victoria 3205, Australia

^d Department of Innovation, Industry and Regional Development (DIIRD), L17/80 Collins Street,
Melbourne, Victoria 3000, Australia

Received 30 October 2007; received in revised form 16 January 2008; accepted 16 January 2008
Available online 1 February 2008

Abstract

Time-resolved synchrotron X-ray absorption near edge structure (XANES) spectroscopy was used to study changes of chromium speciation in soils upon soil–water interaction. The time resolution was 30–45 min. In a flow-column apparatus operated near the synchrotron beamline, two different types of soil were treated with potassium-dichromate solution, and soil samples were taken and directly analysed by XANES. The results provide insight into different equilibrium times of a few hours, depending on the type of soil. The XANES speciation analyses, based on a model comprising insoluble Cr(III) and Cr(VI) compounds, show how the fate of Cr species on soils can be followed close to real-time. Since the method allowed the soils to be investigated close to real-time, sampling in the field and preservation before analysis were made redundant. This study benefits the development of corresponding *in situ* remediation techniques.

© 2008 Elsevier B.V. All rights reserved.

Keywords: Chromium; X-ray absorption spectroscopy; XANES; Speciation; *In situ*; Contamination; Soil; Remediation; Time-resolved

1. Background

The contamination of soil and water with hexavalent chromium is an important environmental issue affecting many sites around the world [1–6]. Hexavalent Cr is toxic, carcinogenic and can pose significant risks to human health. Management of chromium contamination, for example, Cr(VI) infused into soil, may require remediation treatments involving the addition of organic compounds to reduce Cr(VI) to the less hazardous Cr(III) [7,8]. In an ideal case, chromium-(III)-oxide precipitates are formed during the reduction, which are neither water soluble nor bioavailable and thus are less toxic.

Detailed information on the chemistry of the chromium in soils is a cornerstone in the development of successful and efficient remediation strategies. Without this information, remediation treatments may, for instance, impact the environment through pollution side effects such as altered soil pH or raised organic matter contents.

Many studies analysing the structure and chemistry of chromium in the environment employ laboratory methods such as chromatography, atomic absorption spectroscopy, colorimetry, ultra-violet spectroscopy, nuclear magnetic resonance, and others ([8–12] and references therein). Such investigations can be time consuming, requiring complex preparation and chemical-based Cr extraction methods with the risk of altering the Cr species before analysis. Laboratory methods also may not provide insight into the behaviour of particular chromium species in real time or close to real time, making estimation of reaction rates difficult.

* Corresponding author. Tel.: +61 3 9479 1329; fax: +61 3 9749 1552.
E-mail address: p.kappen@latrobe.edu.au (P. Kappen).

Synchrotron-based X-ray absorption near edge structure (XANES) has the potential to fill these gaps. XANES has proven to be a valuable tool for directly analysing the chemical speciation of heavy metals [13–15] such as chromium [1,8,16–21], lead [22], arsenic [23], copper [24,25], and others. XANES is element specific and probes the local atomic environment around the absorbing element, thus delivering chemical sensitivity. Since most XANES experiments are straightforward and do not require complex sample preparation procedures, chemical information can be accessed directly and within short time scales (often minutes to tens of minutes). Hence, this technique may be employed for time-resolved and *in situ* studies.

In situ investigations of heterogeneous systems have been reported routinely from a variety of fields including catalysis [26,27], fuel cell research [28], nanotechnology [29], and mineralogy [30]. In environmental research there have been a small number of reports of time resolved studies [25,31–34] dealing with Cu and As, for example, *in situ* studies of copper during electrokinetic remediation processes [25,31,33]. The advantage of *in situ* studies is that sample information can be obtained in real environments and in real time; these are critical factors when developing on-site remediation strategies.

Full *in situ* XANES measurements of Cr on soils, that is, acquisition of absorption spectra during a treatment, have not been reported previously. Such studies are likely to face significant technical challenges due to the comparably low photon energy of the Cr–K absorption edge (5989 eV). At this energy, soil-loaded flow cells may not be operated in transmission mode due to the high absorption level of most of the mineral phases comprising a soil. For example, about 63% (corresponds to absorption $\mu d = 1$) of the incoming photons would be absorbed by thin layers comprising grains of common minerals such as SiO₂ (50 μm) or Fe₂O₃ (10 μm). Some of the absorption issues can be overcome by measuring XANES in fluorescence mode, where a sample does not need to be X-ray transparent. While a corresponding *in situ* cell for gas treatment of a dry soil would be feasible (analogous to *in situ* fluorescence XANES set-ups in catalysis research), a liquid treatment cell would still pose absorption issues due to parasitic absorption by the liquid in a flow cell (for water: 63% per 350 μm). In addition, disentangling the contributions of liquid and solid phases to a XANES spectrum may not be possible without additional EXAFS analyses. However, acquiring full fluorescence mode EXAFS data of sufficient quality is time consuming, assuming that the element of interest (Cr) is present at realistically low concentrations. Thus, full EXAFS data collection is not suitable for *in situ* studies of Cr on soils in a treatment cell, and even *in situ* XANES studies on mixed solid–liquid systems are challenging and rare [9]. More work is needed to develop rapid Cr speciation techniques, capable of *in situ* implementation, to support the delivery of effective Cr remediation outcomes.

In this paper, we present time resolved XANES measurements of soils upon deliberate contamination with hexavalent chromium from solution. The soils were treated at the synchrotron facility in a flow column set-up and then prepared for

immediate XANES measurements. The typical time resolution of the experiments was 30–45 min.

2. Experimental

Experiments were conducted at the Hamburg Synchrotron Radiation Laboratory (HASYLAB) at Deutsches Elektronen Synchrotron (DESY) in Hamburg, Germany. Spill and contamination accidents were simulated by treating selected soils on-site. XANES scans were acquired from a range of reference samples, and from initially uncontaminated soils subjected to aqueous solutions of K₂Cr₂O₇.

The reference XANES spectra were used to evaluate chemical species via linear combination fitting (for details on the fit procedures see below). Reference samples, all insoluble or slightly soluble in H₂O, comprised PbCrO₄, CaCrO₄, Cr(OH)₃, Cr-acetylacetonate (Cr–(O₂C₅H₇)₃), and Cr₂O₃.¹ Water soluble chromium salts, such as chromium-(VI)-oxide, sodium and potassium chromates and dichromates, or chromium-(III)-nitrate are unlikely to precipitate from an aqueous solution and were thus disregarded. PbCrO₄ and CaCrO₄ were chosen, since both Pb and Ca were detected on the soils using XRF. Chromium-(III)-acetylacetonate was included to represent Cr embedded in an organic matrix. In Cr–(O₂C₅H₇)₃ the Cr is complexed by three organic ligands with the oxygen atoms forming the first coordination shell. This structure is similar to other Cr(III) materials, such as Cr in Cr(NO₃)₃ or Cr in humic acids. Cr(OH)₃ and Cr₂O₃ are further important, insoluble, trivalent Cr species in soils.

It should be noted that the reference materials used describe a model of the soils based on the available data. This model is intended to demonstrate the capabilities of our approach to time-resolved studies of Cr species. Choice of a different model using additional or different soil data may result in different outcomes with respect to the evolution of individual Cr species. Discussions of the behaviour of hexavalent and trivalent chromium in general (see below sections) are not affected by the choice of reference compounds.

Materials for XANES analyses were pressed to form free-standing discs (13 mm diameter), using a standard hydraulic pellet press ($p \sim 0.7 \text{ GN/m}^2$ for 60 s). Prior to pressing, the samples were dried on filter paper (if wet), ground and mixed with cellulose powder (Sigma–Aldrich, 20 μm particle size). The reproducibility of sample preparation protocols was verified by XANES analysis of three identically prepared pellets of Cr(NO₃)₃, using a total of 30 mg Cr(NO₃)₃ and 550 mg cellulose. After careful grinding and mixing, the resulting sample material was divided in three aliquots (193 mg each) and pressed to pellets.

Chromium treatment was performed on two initially uncontaminated soils: standard commercial potting mix (as a model for organic-rich soil), and natural soil sampled on-site at HASYLAB

¹ The spectrum of CaCrO₄ was kindly provided by Prof. Alojz Kodre, University of Ljubljana, Slovenia. It was acquired at beamline E4 at HASYLAB using a Si(1 1 1) double crystal monochromator.

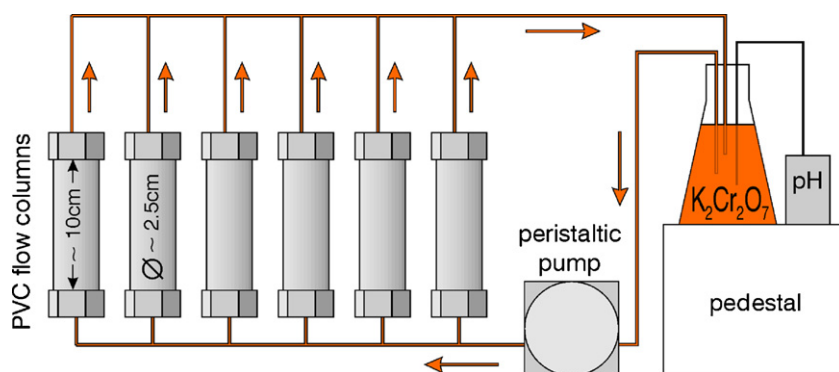


Fig. 1. Schematic representation of the flow column set-up used for contamination simulations. The reservoir holding the Cr containing solution was elevated, so that the columns did not drain when opened for sample excavation. The flow rate of the peristaltic pump was set to 100 mL/min.

containing visibly high concentrations of sand (from hereon referred to as “sand-rich soil”). Approximately, 100 g of potting mix and 200 g of sand-rich soil were used for the experiments (masses refer to dry weight). After removing larger stones (diameter few mm), the corresponding soil was loaded into up to six parallel flow columns connected to a peristaltic pump (Fig. 1). Potassium-dichromate ($K_2Cr_2O_7$) solution was cycled through the system from reservoir ($V = 1100$ mL, flow rate 100 mL/min). The concentration of the solution was $c = 14$ g/L, approximately corresponding to Cr levels used in, e.g., industrial leather tanning solutions [35].

After specific times, the treatment was paused, and small amounts of soil (ca 1 g) were sampled from any one of the flow columns. During sampling, the liquid level was kept high enough to cover the soils in the columns, avoiding direct air exposure. After a flow experiment, soil from one of the columns was drained on an unbleached paper filter. Approximately, 300–600 mg of material was used from each soil sample to prepare a pellet for XANES measurements. These scans were either acquired directly after sample preparation, or, if immediate measurements were not possible, samples were temporarily stored in a small vacuum chamber ($p < 10^{-2}$ mbar) to avoid prolonged exposure to air and minimise changes in chemical state.

The XANES experiments were carried out at bending magnet beamline A1 at HASYLAB. Scans were acquired at the Cr–K absorption edge using a channel cut Si(111) double crystal monochromator. The intensity of the monochromatic beam was monitored and controlled using an ionisation chamber (I_0 , filled with 1000 mbar N_2) and a digital monochromator stabiliser (D-MoStab). Higher harmonics suppression was achieved by detuning the monochromator to 50% of the peak intensity. XANES spectra were collected over a slightly extended range (5850–6250 eV) to enhance the reliability of background subtraction and normalisation. The acquisition time per scan, defining the experimental time resolution was about 30–45 min.

XANES scans of the reference samples were recorded in transmission mode using a second ionisation chamber (filled with 1000 mbar Ar); scans of soil samples were acquired in fluorescence mode using a seven-element Si(Li) solid state detector (custom made *Gresham Sirius*). Distortion of the fluorescence XANES spectra due to self-absorption effects could be ruled out due to the low Cr content on the soil ($\ll 10$ mg/g). Typi-

cal total count rates for entire fluorescence spectra were of the order of 20–30 kcps for the potting mix and 5–10 kcps for the sand-rich soil. The detector signals were pre-amplified within the experimental hutch. Further signal processing (outside the hutch) included seven digital signal processors (*Canberra DSP 2060*) feeding individual MCA cards linked to the beamline computer. For the fluorescence XAS scans, only Cr K_{α} fluorescence signals were selected (via software), thus resulting in least background and optimised signal-to-noise ratios in the XANES spectra.

After normalising to the incoming photon beam intensity (measured in the first ionisation chamber), the spectra were added using weight factors representing the statistical quality of the scans. The weight factors were calculated using the magnitude of the absorption edge jump and the intensity of the pre-edge absorption background. These steps were performed using self-developed software written in the programming language *IDL* [36]. Cr species were evaluated using the freeware *XANDA Dactyloscope* [37]. A linear fit routine was employed to approximate a given XANES scan using the Cr reference spectra. Principal components analysis and target transformation functions, as provided by the *XANDA Dactyloscope* software, were used to assist the linear combination. The fit routine yields relative species concentrations (as mol%).

3. Results and discussion

3.1. Reference spectra and fit routine verification

Fig. 2 shows spectra of the reference materials used for speciation. The scans of hexavalent Cr exhibit a distinct pre-edge feature at approximately 5993 eV. This feature is well known, characteristic of hexavalent chromium [38]. It is frequently used for differentiating between trivalent and hexavalent Cr [39–42]. In Cr(VI) compounds, Cr is generally co-ordinated tetrahedrally while it is octahedrally co-ordinated in Cr(III) compounds. Hence, in Cr(VI) the chromium is sitting on sites with no inversion symmetry. This lack of inversion symmetry permits dipole transitions from a 1 s level to unoccupied antibonding t_2^* orbitals ([43] and references therein), resulting in the distinct pre-edge peak.

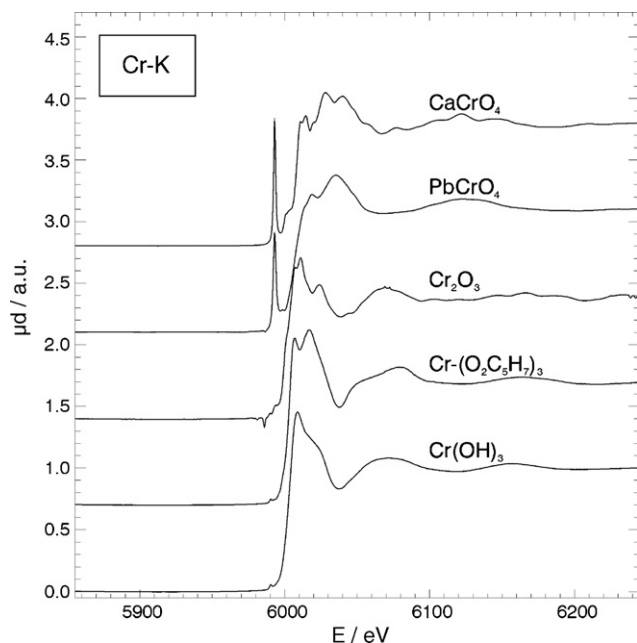


Fig. 2. XANES spectra of at the Cr–K absorption edge of chromium reference spectra. The spectra are presented as after background removal and normalisation. Note the distinct pre-edge feature by which Cr(VI) compounds can be distinguished from Cr(III) species.

Prior to speciation analyses of real systems, sample preparation and data processing tests were conducted using three identically prepared $\text{Cr}(\text{NO}_3)_3$ reference samples. For each sample, three XANES spectra were acquired at different sample positions. The resulting nine spectra are shown in Fig. 3. The variation of the spectra at the maximum intensity is of the order of 1%. This result demonstrates a good reliability of the sample preparation and data handling methods (in particular, background subtraction), thus introducing only a small error to the speciation process.

The fitting procedure to speciate Cr compound mixtures was tested using defined mixtures of powders of $\text{K}_2\text{Cr}_2\text{O}_7$ and Cr_2O_3 , and other reference materials. Some of the results are

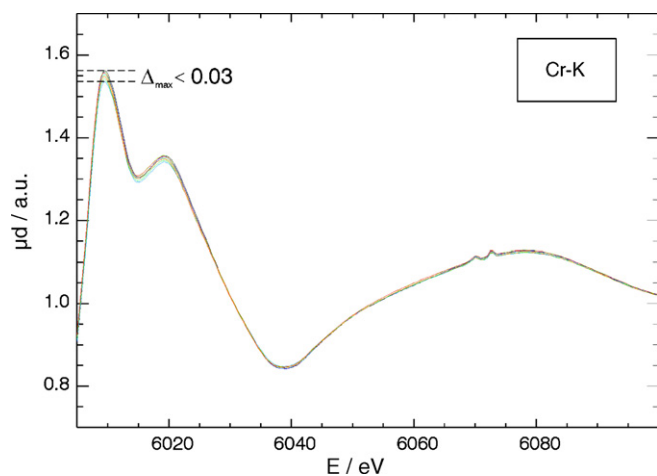


Fig. 3. Zoomed-in section of a set of nine spectra of $\text{Cr}(\text{NO}_3)_3$ to test the reproducibility of the sample preparation method (for details see text). Spectra were background subtracted and normalised.

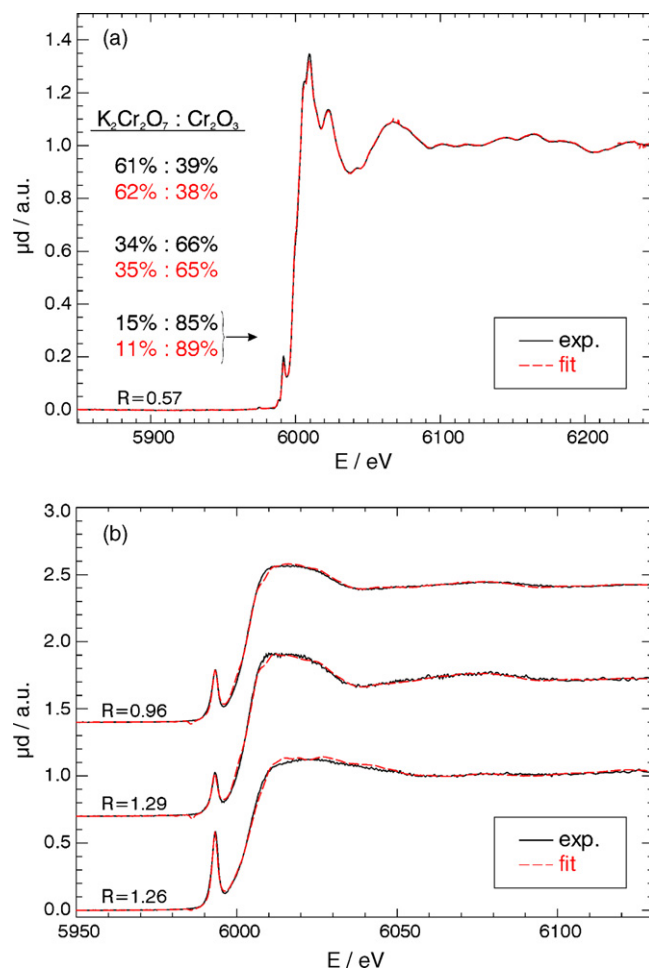


Fig. 4. (a) Linear combination fitting of XANES spectra of well defined mixtures of $\text{K}_2\text{Cr}_2\text{O}_7/\text{Cr}_2\text{O}_3$, showing very good agreements of fit results and expected values. (b) Typical linear combination results on real soil samples. The R -values give a measure for the goodness of the fit (perfect fit for $R=0$).

summarised in Fig. 4a, showing good agreement between actual and fitted relative concentrations. The spectra presented in the figure correspond to one of the fits as marked by the arrow. Only slight deviations between data and linear combination are observed, as reflected by the low R -value of 0.57. The deviations may partly be attributed to uncertainties from sample preparation (see also Fig. 3 and corresponding discussions). For two of the model mixtures, the fit routine was tested further by starting with additional reference spectra; Table 1 below summarises the results. The first data row per sample shows the speciation results with only the two expected references included. The results agree well with the targets (see first column). The following rows show the fit results upon addition of $\text{Cr}(\text{OH})_3$ and $\text{Cr}(\text{OH})_3$ plus CaCrO_4 reference spectra. In cases where concentration values of 0% are presented, the fit suggested a concentration of <2%, and the corresponding parameter was set to 0 to be not considered further in the fit.

The results in the table show that the fit procedure retrieved the correct results reliably. Only when using all four spectra on the XANES spectrum of the first sample (“15%:85%”), the fit wrongly suggests a 7% content of CaCrO_4 . Overall, the data

Table 1
Results of testing the linear combination fit routine

Test sample (%)	$c[\text{K}_2\text{Cr}_2\text{O}_7]$ (%)	$c[\text{Cr}_2\text{O}_3]$ (%)	$c[\text{Cr}(\text{OH})_3]$ (%)	$c[\text{CaCrO}_4]$ (%)	R
15:85	11	89	–	–	0.57
	8	88	4	–	0.57
	9	84	0 (<2)	7	0.57
35:65	35	65	–	–	0.75
	28	68	4	–	0.75
	28	68	4	0 (<2)	0.75

The XANES spectra of two defined mixtures of $\text{K}_2\text{Cr}_2\text{O}_7/\text{Cr}_2\text{O}_3$ were fitted starting from different sets of reference spectra (a dash means that this spectrum was not used).

discussed so far verify the reliability of the sample preparation and fitting method.

For fitting of soil related data, care was taken to reduce the number of reference spectra to a minimum. Each spectrum represents one degree of freedom. The use of many spectral components may result in a very good outcome; however, this result may then not be reliable due to the increased number of fit parameters. It should also be noted that chemical speciation analysis using XANES is not model free. While containing the full information on local atomic symmetry, each spectrum is one-dimensional only and disentangling the individual contributions has to be based on assumptions (choice of reference spectra for the fit). The results are considered in light of these assumptions.

3.2. Treatment of soils with Cr(VI) solution

Results of the treatment of the potting mix with potassium-dichromate solution are presented in Figs. 5 and 6. Fig. 5 summarises the speciation changes during one treatment (duration 22 h; only four flow columns were used for technical reasons). This experiment was repeated with fewer sampling intervals, but with subsequent draining of some of the soil material. Corresponding results of the speciation analyses are shown in Fig. 6. For the repeat experiment, all the six flow columns could be employed.

The XANES spectra in Fig. 5a (first treatment) show the presence of Cr(VI) species via the characteristic pre-edge feature. They also indicate some Cr(III) content via the shape of the XAS oscillations in the energy region between 6010 and 6050 eV. During the first 5 h of treatment, a high level of variability was observed in the relative concentrations of Cr species. This is reflected in the intensity of the pre-edge peak and the fine structure above the absorption edge. Beyond approximately 5 h treatment time, the conditions settled to a steady state as suggested by the spectra marked “B”.

The speciation results (Fig. 5b) confirm these observations. The total relative concentrations of Cr(III) and Cr(VI) species on the soil enter a steady state from approximately $t > 5$ h. This levelling may also be observed in the bottom graph in Fig. 5b, showing the evolution of the solution pH. From $t > 5$ h, the pH changes only marginally, indicating an equilibrium between soil and $\text{K}_2\text{Cr}_2\text{O}_7$ solution. Note that two different graphs for Cr(VI) are included in Fig. 5b. The dotted line represents the Cr(VI) as a result from the linear combination fit. The dash-dotted line

(Cr(VI)^{*}) was derived from the pre-peak intensity, that is independent of the fit process. For the Cr(VI)^{*} value of a spectrum, the onset of the absorption edge was modelled using a spline function, and the integral intensity of the pre-edge feature was

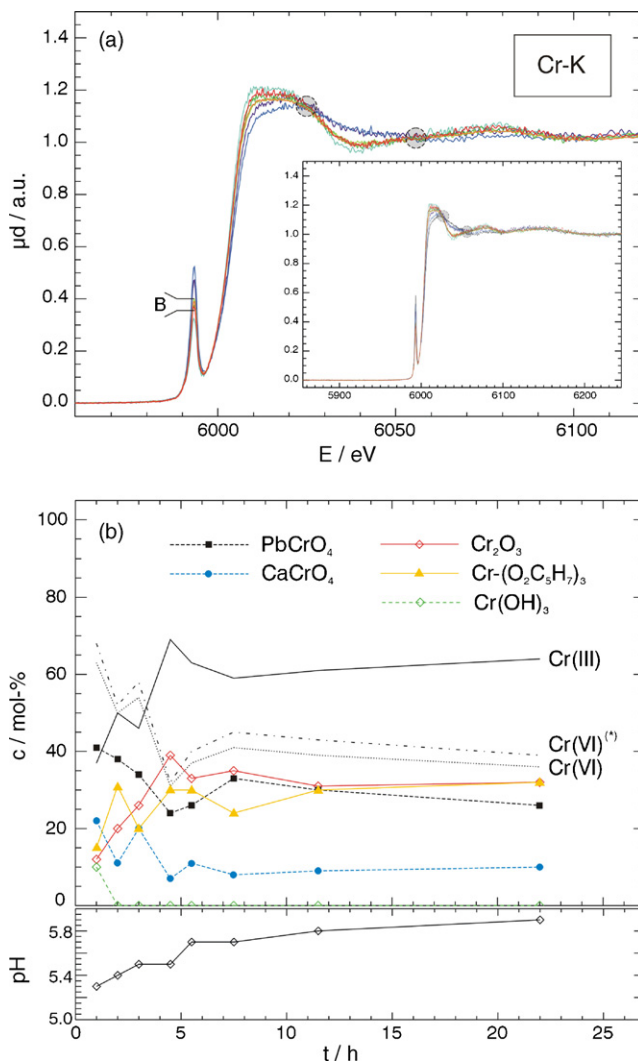


Fig. 5. XANES spectra (panel a) and speciation results (panel b) from a contamination simulation ($\text{K}_2\text{Cr}_2\text{O}_7$ (aq)/potting mix). Samples were taken from the flow column system at the times specified. In panel (a) isosbestic points are highlighted by dashed circles. The spectra marked “B” in panel (a) correspond to the last four data points in panel (b). The uncertainty for the data points in panel (b) is estimated to be ± 5 mol% (error bars omitted for presentation purposes).

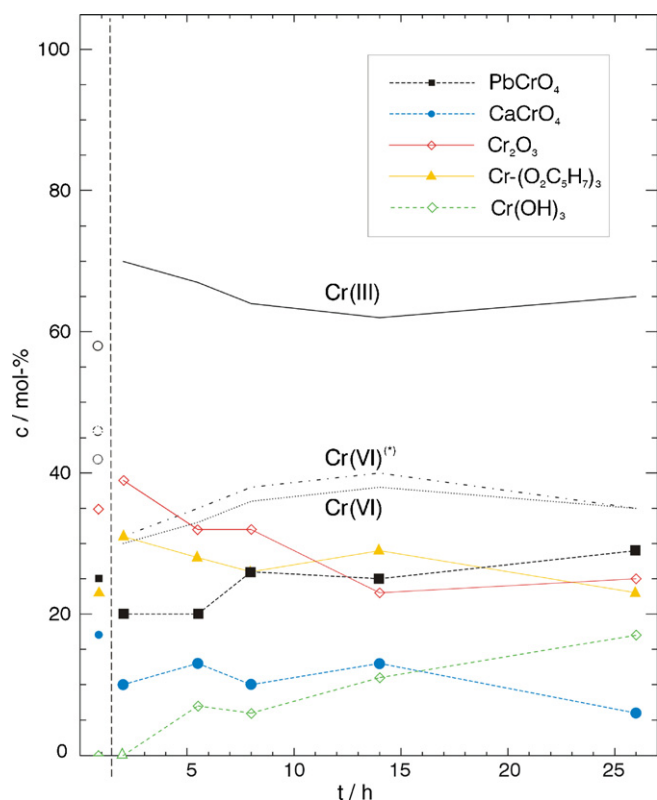


Fig. 6. Speciation results from a contamination simulation ($K_2Cr_2O_7$ (aq)/potting mix). Species evolutions are depicted for draining of treated soil in a filter. The individual symbols that are not connected by lines represent the species at the end of the preceding flow phase.

obtained after subtraction of the spline. In order to obtain a total relative concentration of hexavalent chromium, the resulting quantity was then normalised to the average of the integral pre-peak intensities of $PbCrO_4$ and $CaCrO_4$. As can be seen from Fig. 5b, the results for $Cr(VI)$ and $Cr(VI)^*$ are consistent within the uncertainty of ± 5 mol%. It is important to note that the results of $Cr(VI)^*$ were not used to constrain the linear combination fit. Thus, both measures of the concentration of hexavalent chromium are independent. The consistency of the data engenders confidence in the fit results.

Given the model reference spectra chosen for this study, the speciation data also show that the decrease in $Cr(VI)$ content on the soil is mainly due to a decrease in $PbCrO_4$ concentration, and the corresponding increase of $Cr(III)$ is a result of an increase of Cr_2O_3 content. The spectra of calcium chromate and chromium acetylacetonate also contribute to the speciation fit but the concentration values obtained do not exhibit clear trends during the first 5–6 h of the flow experiment. The speciation fits could also be performed without including $Cr(OH)_3$ (first data point excepted). This observation is consistent with the data, since during the experiment the pH was between 4 and 5, i.e. the chemical environment was acidic. In such environment the precipitation of basic $Cr(OH)_3$ is not favoured.

The normalised data in Fig. 5a also exhibit *isosbestic points* at 6025 and 6055 eV where all spectra meet (highlighted by dashed circles). At these points, the total absorbance of all chromium species remains constant. Thus there has to be a continuous

transition from one spectroscopic component to another, where a spectroscopic component may be a mixture of more than one chromium species. Note that the spectra are normalised to an edge jump of 1; hence, variations in the absolute concentrations of chromium do not need to be considered in this discussion. For the evolution of chromium species, the isosbestic points mean that no new Cr compound was created or consumed during the experiment (disregarding the initial phase before taking the first sample at $t = 1$ h). This result is consistent with the data presented in Fig. 5b.

Since the initial (uncontaminated) soil did not contain significant amounts of Cr (as verified by XRF), a rapid sorption of $K_2Cr_2O_7$ from solution with subsequent conversion must have occurred before the first sample was taken. With the potting mix being rich in organic content, it is likely that dichromate was reduced to $Cr(III)$ in the presence of organic matter. Such pathways have been reported previously (e.g. [7,8,44]). The speciation results are consistent with this mechanism, where in the corresponding fits the spectrum of Cr-acetylacetonate should be seen as a representative for Cr in organic matrices. As highlighted above, in Cr-acetylacetonate, the chromium is complexed by organic ligands with oxygen forming the first coordination sphere. The resulting structure is similar to Cr in organic matrices such as humic acids present in potting mix.

The data in Fig. 5b furthermore show a high relative concentration of $Cr(VI)$ on the soil (about 40% towards the end of the experiment). With an organic-rich soil, such as potting mix, one might expect a complete reduction of $Cr(VI)$ to $Cr(III)$ species. However, with the continuous supply of dichromate solution, it can be expected that reaction sites for the reduction of $Cr(VI)$ to $Cr(III)$ were saturated at some point, as reflected in the equilibrium observed. The redox reactions involved in these processes may be complicated in detail and may also have included other species such as $Fe(II)$ or $Mn(IV)$; both, Fe and Mn were detected in the soil using XRF. Detailed soil analyses and characterisation were beyond the scope of this study, which is to demonstrate the feasibility of time-resolved species analyses studies on complex systems (Cr in soils) using XANES. Detail clarification of the redox mechanisms involved will be a future step requiring comprehensive chemical and physical analyses (e.g. organic matter and other chromium reducing and oxidising species contents, Cr concentration in solution, redox potential, soil pH, and total soil surface area).

To study the effects of draining on the evolution of Cr species, a second soil treatment using $K_2Cr_2O_7$ solution and potting mix was conducted (again $V_{\text{solution}} = 1100$ mL, $c[K_2Cr_2O_7] = 14$ g/L). The speciation results are presented in Fig. 6; also included in this figure are concentrations for a sample taken at the end of the flow phase (see the symbols that are not connected by lines). These starting values are similar to the concentrations found in the preceding experiment for the individual species at $t = 22$ h. Some differences exist which are attributed to the different amounts of soil used in this experiment (six columns loaded, compared to four columns in the first experiment).

Upon draining the Cr species show some variability, and changes over time can be observed for all species. Cr_2O_3 exhibits

a large decrease in relative concentration (from 40 to 25%). Also Cr-acetylacetonate shows a decrease, which is a trend only due to the uncertainties (± 5 mol%) associated with the speciation procedure. In contrast to Cr_2O_3 and Cr-acetylacetonate, the relative concentration of PbCrO_4 increases from 20 to 30%. These results indicate that after the flow phase the soil system undergoes some further gradual changes with no clear equilibrium over 26 h of draining. During this time no further dichromate solution was delivered to the soil, and the material was exposed to ambient air. Further reactions on the soil as observed in Fig. 6 may have been promoted by these conditions.

The speciation results upon draining also show a steadily increasing contribution of $\text{Cr}(\text{OH})_3$. This species was newly formed during this experiment. In the corresponding XANES data, no well-defined isosbestic points can be observed. Consequently, the formation of a new species during the measurements can be justified. Chromium-(III)-hydroxide has been discussed previously in XANES speciation experiments of soils (e.g. [9,45–47]). For instance, Wei et al. [9] sorbed Cr(VI) on kitchen waste compost from solution (from CrO_3), and the corresponding speciation results indicated $\text{Cr}(\text{OH})_3$ contents in the order of 20%. The total relative concentrations of Cr(III) found were about 75% for sorption times of 0.5 and 12 h, respectively. These results are similar to the data presented in Fig. 6 (drain phase).

The results in Fig. 6 also show that the overall relative concentrations of Cr(III) and Cr(VI), respectively, changed only slightly within the 26 h of draining. Measurement of these quantities alone (for example via the integral intensity of the pre-edge peak) gives the impression that the soil system is almost stable during this period. However, reactions are occurring, leading to the formation of a new species, in our model, $\text{Cr}(\text{OH})_3$.

These results emphasise the importance of detailed analyses of the XANES spectra, sensible choice of reference spectra, and reliable background subtraction and normalisation procedures. Extending the scan range, beyond a typical XANES region, to a few hundred eV (e.g. up to 6250 eV as in this study) is beneficial for data treatment. The results also highlight that for XANES analysis of Cr or other pollutants in soil, simulations close to real conditions and close to the beamline are very valuable. Such experiments allow information to be gained almost in real-time.

Figs. 7 and 8 show XANES spectra and speciation results for the experiment subjecting a sand-rich soil to potassium-dichromate solution. The data show a sharp increase in the proportion of Cr(III) from 15 to 50% over the first 5–6 h of the experiment and some decrease (50–40%) towards the end of the flow phase. The individual model species reflect this behaviour moderately well. The contents of both, Cr_2O_3 and Cr-acetylacetonate increase over time. Inversely to Cr(III), the Cr(VI) concentration drops sharply first and increases towards the end of the flow experiment. These trends are well reflected by both Cr(VI) species, where the decrease and increase is more prominent for PbCrO_4 than for CaCrO_4 . As previously, the data for Cr(VI) and Cr(VI)* are consistent, thus supporting the fit results.

Overall it can be observed that the system moves towards an equilibrium after about 12 h. However, in contrast to the data of potting mix (see Fig. 5), this steady state is reflected only for

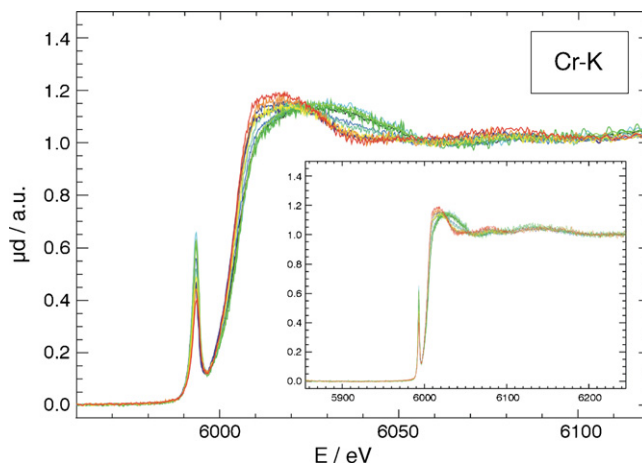


Fig. 7. XANES spectra from a contamination simulation ($\text{K}_2\text{Cr}_2\text{O}_7$ (aq)/sand-rich soil). Note that no clearly defined isosbestic points can be observed, as compared to Fig. 5.

Cr_2O_3 and PbCrO_4 . The data also show that on the sand-rich soil, the Cr(VI) content is higher during the entire flow phase as compared to the experiment on potting mix. Hence, the sand-rich soil provided fewer reactive sites for the reduction of Cr(VI) to Cr(III), which may be attributed to a lower content of reducing species (e.g. organic matter, Fe(II)) and/or a higher content of oxidising compounds (e.g. MnO_2).

It was observed that for the potting mix, the decrease in relative Cr(VI) content progressed more rapidly (ca 5 h) than on the sand-rich soil (ca 12 h). In the literature it has been described that reaction rates for $\text{Cr}(\text{VI}) \rightarrow \text{Cr}(\text{III})$ can be increased by amending a soil with organic matter [44,48,49]. Similar to the study by Bolan et al. [49], reaction time constants were modelled from

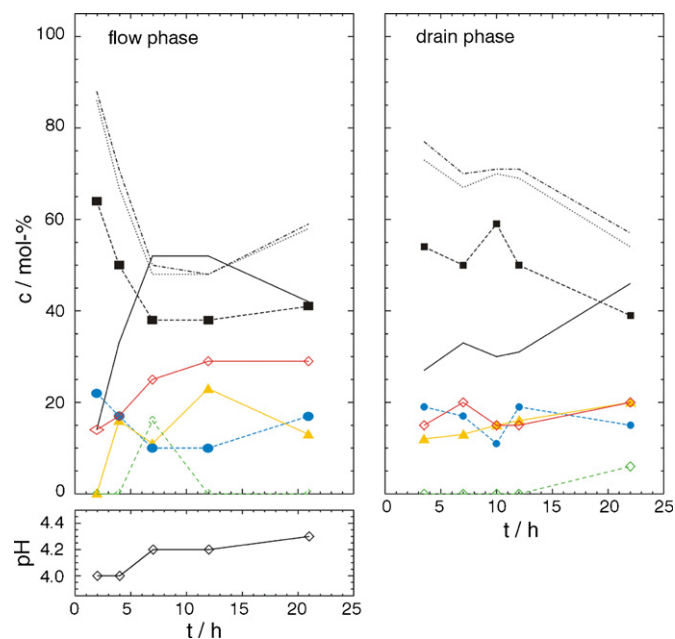


Fig. 8. Speciation results from a contamination simulation ($\text{K}_2\text{Cr}_2\text{O}_7$ (aq)/sand-rich soil). These results correspond to the spectra shown in Fig. 7. The experiment comprised two phases: flow treatment of the soil and draining in a filter. For explanation of the symbols refer to Figs. 5 or 6.

Table 2

Results from modelling reaction time constants for the reduction of Cr(VI) in the potting mix and sand-rich soils

Soil	$c_{\text{eq}} \times 100\%$	$\sigma(c_{\text{eq}}) \times 100\%$	τ (h ⁻¹)	$\sigma(\tau)$ (h ⁻¹)	χ^2
Potting mix	38	3	0.8	0.2	35
Sand-rich	50	7	0.3	0.1	71

The relative concentrations of hexavalent chromium used for the modelling were taken from the results of the linear combination processes. For explanations of the quantities c_{eq} and τ see the text; the σ -values are standard deviations of the fit, and χ^2 gives a measure of the goodness of the fits.

the data for Cr(VI) from Figs. 5 and 8. The expression used to fit the data was

$$y(t) = [1 - c_{\text{eq}}] e^{-\tau t} + c_{\text{eq}},$$

where y is the concentration of Cr(VI) as derived from the linear combination fit, t the reaction time in h, τ the reaction time constant in h⁻¹, and c_{eq} is the concentration of Cr(VI) upon reaching the equilibrium state. The factor $[1 - c_{\text{eq}}]$ ties the Cr(VI) concentration to 100% at the start of the experiment, i.e. when K₂Cr₂O₇ solution was introduced to the soil. Table 2 summarises the results from the modelling.

The fit results are good indicators for trends and a qualitative discussion; in a future experiment, more precise results could be obtained by repeating the flow experiments with more data points on the time scale. However, the results in Table 2 are consistent with the observations made so far. In case of the potting mix the equilibrium is reached faster than in case of the sand-rich soil ($\tau_{\text{pot}} > \tau_{\text{sand}}$), and the resulting relative concentration of hexavalent chromium was less on the potting mix ($c_{\text{eq,pot}} < c_{\text{eq,sand}}$). Also the initial estimates for flow durations until reaching an equilibrium are covered well by the simple reaction rate model. After 5 h flow experiment on the potting mix, the exponential function drops to $e^{-\tau t} = e^{-0.8/\text{h} \times 5\text{h}} = 0.02$. Thus the expected value for c_{eq} was almost reached after $t = 5$ h. For $t = 12$ h in the experiment on sand-rich soil one finds $e^{-\tau t} = e^{-0.3/\text{h} \times 12\text{h}} = 0.03$. Given the uncertainty of the fit and the respective standard deviations, these values are the same within the error margin.

Upon draining, only the concentration of PbCrO₄ exhibits strong variations, thus driving a decrease in the relative Cr(VI) content. In contrast to the experiment on potting mix, chromium hydroxide may only emerge as a species towards the end of the drain phase. The data in Fig. 8 also suggest that in a sand-rich soil, the relative Cr(III) and Cr(VI) contents are changing more dynamically upon draining than in the potting mix, which is also reflected in the concentration of PbCrO₄. This may be due to slower Cr(VI) reduction rates in organic poor media.

The results presented in this study demonstrate how near real-time XANES measurements can be used to analyse directly chromium species on soils upon contamination with Cr(VI) solution. The flow column set-up used could also be employed to treat soil from a contaminated site for remediation purposes. The advantages of the approach in this study are

- (I) samples can be analysed rapidly and on-site at the synchrotron, i.e. in a real scenario; remediation processes could be optimised on-line;
- (II) XANES allows information on the evolution of chemical species to be obtained directly and non-invasively.

Model reference materials for this study were chosen on the basis of elemental analyses using XRF data and water solubility. In future experiments, further soil chemical information (soil pH and Eh, organic matter content, absolute elemental concentrations, etc.) would be of advantage to build a model for XANES species analyses.

The time resolution of 30–45 min for evaluation of Cr species was achieved using a seven-element fluorescence detector at a bending magnet beamline. Shorter acquisition times would be feasible at a high-flux wiggler beamline in conjunction with a multi-element fluorescence detector with a large number of elements. The high beam intensity would sustain a sufficiently high count-rate for the larger number of detector pixels (assuming that their size decreases with increasing number). Such detector systems would require good energy resolution, high signal-to-noise ratio, and high count-rate capabilities. Commercial multi-element detector systems could be suitable; also current detector developments based on silicon or silicon-drift technology [50,51] are promising for the further development of *in situ* analyses of Cr species on soils.

Acknowledgements

The authors would like to thank Prof. Wolfgang Calmano, Technische Universität Harburg, Germany, for provision of Cr reference materials.

Mathias Herrmann, Ulf Brüggemann and Theo Cordes are gratefully acknowledged for their assistance during the beam-times at HASYLAB.

Parts of this work were funded by the Synchrotron Industry Access Program, State Government of Victoria, Australia. The authors also acknowledge financial support from the *Access to Major Research Facilities Programme* which is a component of the *International Science Linkages Programme* established under the Australian Government's innovation statement, *Backing Australia's Ability*.

References

- [1] P.A. O'Day, S.A. Carroll, S. Randall, R.E. Martinelli, S.L. Anderson, J. Jelinski, J.P. Knezovich, *Environ. Sci. Technol.* 34 (2000) 3665–3673.
- [2] F. Goodarzi, F.E. Huggins, *J. Environ. Monit.* 3 (2001) 1–6.
- [3] H. Akcay, A. Oguz, C. Karapire, *Water Res.* 37 (2003) 813–822.
- [4] M. Zhai, H.A.B. Kampunzu, M.P. Modisi, O. Totolo, *Environ. Geol.* 45 (2003) 171–180.
- [5] A.S. Chamon, M.H. Gerzabek, M.N. Mondol, S.M. Ullah, M. Rahman, W.E.H. Blum, *Commun. Soil Sci. Plant Anal.* 36 (2005) 907–924.
- [6] L.R. de Astudillo, I.C. Yen, I. Bekele, *Rev. Biol. Trop.* 53 (2005) 41–53.
- [7] T.K. Tokunaga, J.M. Wan, M.K. Firestone, T.C. Hazen, K.R. Olson, D.J. Herman, S.R. Sutton, A. Lanzirotti, *J. Environ. Qual.* 32 (2003) 1641–1649.
- [8] P.M. Jardine, S.E. Fendorf, M.A. Mayes, I.L. Larsen, S.C. Brooks, W.B. Bailey, *Environ. Sci. Technol.* 33 (1999) 2939–2944.
- [9] Y.L. Wei, Y.C. Lee, H.F. Hsieh, *Chemosphere* 61 (2005) 1051–1060.

- [10] S. Pamukcu, A. Weeks, J.K. Wittle, *Environ. Sci. Technol.* 38 (2004) 1236–1241.
- [11] W.P. Yang, Z.J. Zhang, W. Deng, *J. Chromatogr. A* 1014 (2003) 203–214.
- [12] M.J. Marques, A. Salvador, A.E. Moralesrubio, M. Delaguardia, *Fres. J. Anal. Chem.* 362 (1998) 239–248.
- [13] E. Welter, in: R. Cornelis (Ed.), *Handbook of Elemental Speciation*, Wiley, 2003, pp. 505–526.
- [14] A. Bernaus, X. Gaona, D. van Ree, M. Valiente, *Anal. Chim. Acta* 565 (2006) 73–80.
- [15] E. Welter, W. Calmano, S. Mangold, L. Troger, *Fres. J. Anal. Chem.* 364 (1999) 238–244.
- [16] J.F. Lee, S. Bajt, S.B. Clark, G.M. Lamble, C.A. Langton, L. Oji, *Phys. B* 209 (1995) 577–578.
- [17] R.R. Martin, S.J. Naftel, T.K. Sham, B. Hart, M.A. Powell, *Can. J. Chem.-Rev. Can. Chim.* 81 (2003) 193–196.
- [18] T.K. Tokunaga, J.M. Wan, M.K. Firestone, T.C. Hazen, E. Schwartz, S.R. Sutton, M. Newville, *Environ. Sci. Technol.* 35 (2001) 3169–3174.
- [19] E.C. Thornton, J.E. Amonette, *Environ. Sci. Technol.* 33 (1999) 4096–4101.
- [20] M.L. Peterson, G.E. Brown, G.A. Parks, C.L. Stein, *Geochim. Cosmochim. Acta* 61 (1997) 3399–3412.
- [21] R.W. Taylor, S.Y. Shen, W.F. Bleam, S.I. Tu, *Clay Clay Miner.* 48 (2000) 648–654.
- [22] W. Calmano, S. Mangold, E. Welter, *Fres. J. Anal. Chem.* 371 (2001) 823–830.
- [23] R. Kober, E. Welter, M. Ebert, A. Dahmke, *Environ. Sci. Technol.* 39 (2005) 8038–8044.
- [24] J.G. Parsons, M. Hejazi, K.J. Tiemann, J. Henning, J.L. Gardea-Torresdey, *Microchem. J.* 71 (2002) 211–219.
- [25] S.H. Liu, H.P. Wang, M.Y. Yu, Y.J. Huang, H.C. Wang, *J. Elect. Spectrosc. Rel. Phenom.* 144 (2005) 311–314.
- [26] J.D. Grunwaldt, M. Caravati, A. Baiker, *J. Phys. Chem. B* 110 (2006) 9916–9922.
- [27] P. Kappen, J.D. Grunwaldt, B.S. Hammershoi, L. Troger, B.S. Clausen, *J. Catal.* 198 (2001) 56–65.
- [28] E. Principi, A. Di Cicco, A. Witkowska, R. Marassi, *J. Synchron. Radiat.* 14 (2007) 276–281.
- [29] C.T. Meneses, W.H. Flores, J.M. Sasaki, *Chem. Mater.* 19 (2007) 1024–1027.
- [30] M. Wilke, F. Farges, G.M. Partzsch, C. Schmidt, H. Behrens, *Am. Mineral.* 92 (2007) 44–56.
- [31] S.H. Liu, H.P. Wang, *J. Environ. Qual.* 33 (2004) 1280–1287.
- [32] Y. Takahashi, R. Minamikawa, K.H. Hattori, K. Kurishima, N. Kihou, K. Yuita, *Environ. Sci. Technol.* 38 (2004) 1038–1044.
- [33] S.H. Liu, H.P. Wang, H.C. Wang, Y.W. Yang, *J. Synchron. Radiat.* 8 (2001) 919–921.
- [34] H.C. Wang, P.H. Wang, C.Y. Peng, S.H. Liu, Y.W. Wang, *J. Synchron. Radiat.* 8 (2001) 961–962.
- [35] A. Agrawal, V. Kumar, B.D. Pandey, *Miner. Process Extr. Metall. Rev.* 27 (2006) 99–130.
- [36] IDL, <http://www.itvis.com/index.asp>.
- [37] VIPER, <http://www.desy.de/~klmn/viper.html>.
- [38] A. Pantelouris, H. Modrow, M. Pantelouris, J. Hormes, D. Reinen, *Chem. Phys.* 300 (2004) 13–22.
- [39] F.E. Huggins, M. Najih, G.P. Huffman, *Fuel* 78 (1999) 233–242.
- [40] K. Nomura, N. Awaji, *Jpn. J. Appl. Phys. Part 2. Lett.* 45 (2006) L304–L306.
- [41] Y.L. Wei, W.J. Sun, H.C. Huang, Y.W. Yang, J.F. Lee, *J. Elect. Spectrosc. Rel. Phenom.* 144 (2005) 303–305.
- [42] N. Cheng, Y.L. Wei, L.H. Hsu, J.F. Lee, *J. Elect. Spectrosc. Rel. Phenom.* 144 (2005) 821–823.
- [43] I. Arcon, B. Mirtic, A. Kodre, *J. Am. Ceram. Soc.* 81 (1998) 222–224.
- [44] X.Q. Lu, W.D. Johnson, R.F. Howe, Y.Y. Chen, *Austr. J. Chem.* 50 (1997) 173–179.
- [45] M.A. Baig, M. Mir, S. Murtaza, Z.I. Bhatti, *J. Environ. Sci.* 15 (2003) 417–422.
- [46] C. Kim, Q.H. Zhou, B.L. Deng, E.C. Thornton, H.F. Xu, *Environ. Sci. Technol.* 35 (2001) 2219–2225.
- [47] M.J. Hu, Y.L. Wei, Y.W. Yang, J.F. Lee, *J. Phys. Condens. Matter* 16 (2004) S3473–S3478.
- [48] J.K. Song, T. Townsend, H. Solo-Gabriele, Y.C. Jang, *Soil. Sediment. Contam.* 15 (2006) 387–399.
- [49] N.S. Bolan, D.C. Adriano, R. Natesa, B.J. Koo, *J. Environ. Qual.* 32 (2003) 120–128.
- [50] A. Longoni, C. Fiorini, C. Guazzoni, S. Buzzetti, M. Bellini, L. Struder, P. Lechner, A. Bjeoumikhov, J. Kernmer, *IEEE Trans. Nucl. Sci.* 53 (2006) 641–647.
- [51] NSLS Science Highlights, <http://www.nsls.bnl.gov/newsroom/science/2007/04-Siddons.htm>, 2007.

Spectrophotometric determination of terfenadine in pharmaceutical preparations by charge-transfer reactions

Elmorsy Khaled*

Microanalysis Laboratory, Applied Organic Chemistry Department, National Research Centre, Dokki, Cairo, Egypt

Received 11 September 2007; received in revised form 8 January 2008; accepted 9 January 2008

Available online 21 January 2008

Abstract

A simple, rapid and accurate method for the spectrophotometric determination of terfenadine has been developed. The proposed method based on the charge-transfer reactions of terfenadine, as n -electron donor, with 7,7,8,8-tetracyanoquinodimethane (TCNQ), tetracyanoethylene (TCNE), 2,3-dichloro-5,6-dicyano-1,4-benzoquinone (DDQ) or 2,5-dichloro-3,6-dihydroxy-1,4-benzoquinone (chloranilic acid, *p*-CLA) as π -acceptors to give highly colored complexes. The experimental conditions such as reagent concentration, reaction solvent and time have been carefully optimized to achieve the highest sensitivity. Beer's law is obeyed over the concentration ranges of 3–72, 3–96, 12–168 and 24–240 $\mu\text{g mL}^{-1}$ terfenadine using TCNQ, TCNE, DDQ and *p*-CLA, respectively, with correlation coefficients 0.9999, 0.9974, 0.9997 and 0.9979 and detection limits 0.3, 0.4, 2.6 and 12.3 $\mu\text{g mL}^{-1}$, for the reagents in the same order. DDQ and *p*-CLA react spontaneously with terfenadine to give colored complexes that can be applied for the flow injection analysis of terfenadine in the concentration ranges 2.4–120 and 24–240 μg with correlation coefficients 0.9990 and 0.9985 and detection limits 0.8 and 2.7 μg for DDQ and *p*-CLA, respectively, in addition to the high sampling through output of 40 sample h^{-1} .

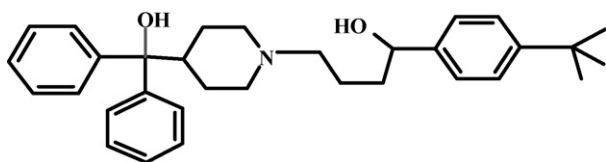
© 2008 Published by Elsevier B.V.

Keywords: Spectrophotometric; Terfenadine; Charge-transfer; Flow injection; Pharmaceutical preparations

1. Introduction

Drug quality control is a branch of analytical chemistry that has a wide impact on the public health, so the development of a reliable quick and accurate method for the active ingredient determination is welcomed.

Terfenadine (TFN) is a well-known selective histamine H_1 -receptor [1] with the following chemical structure:



Several methods have been reported for the determination of TFN in pharmaceutical dosage forms and biological fluids including HPLC [2,3], capillary electrophoresis [4], voltammetry [5], NIR and NMR spectroscopy [6,7], spectrofluorimetry

[8], AAS [9], UV–vis spectrophotometry [9–11] and non-aqueous potentiometric titration [12].

Molecular interactions between electron donors and acceptors are generally associated with the formation of intensely colored charge-transfer (CT) complexes which absorb radiation in the visible region [13,14]. These CT reactions were of particular interest in the analysis of many pharmaceutical compounds [15,16]. Formation of CT complexes between TFN and iodine, TCNQ [17] or picric acid [18] has been earlier reported for the batch spectrophotometric determination of TFN. Though the batch spectrophotometric methods allowed for the determination of TFN, they include the time as a variable to be strictly controlled with the exposure to the toxic organic solvents. However, flow-injection analysis (FIA) provides advantages of rapidity, easy assembly and efficient to control such serious experimental conditions as well as high sampling through output [19]. With respect to the CT spectrophotometric methods, only Uno et al. [20] reported a simple FIA system for monitoring the CT complexation reaction between iodine and tertiary alkylamines and no other investigations for CT reactions combined with FIA have been found in literature.

* Tel.: +20 1 0378 1777; fax: +20 2 3337 0931.

E-mail address: elmorsykhaled@yahoo.com.

Although some of the previously published methods are fairly specific, they tend to be lengthy and expensive [2–4], suffer from a narrow dynamic range [6,7], require the use of a highly toxic compound and solvents [5,9–11] or use less stable colored species with heating [17,18]. This paper describes a simple, direct, sensitive and precise spectrophotometric method for the determination of TFN via novel CT complexation reactions with different π -acceptors namely, *p*-CLA, DDQ and TCNE in addition to TCNQ. Application of FIA in terms of intermolecular CT complexes of TFN with either *p*-CLA or DDQ was also studied to avoid disadvantages of the batch methods and increase the sampling throughput in addition to minimizing the handling of the toxic organic solvent usually used in CT reactions. Stoichiometry, molar absorptivities, Sandell sensitivities, association constants and the free energy changes of the formed CT complexes were also determined.

2. Experimental

2.1. Reagents

All the reagents and chemicals used were of analytical grade. 7,7,8,8-Tetracyanoquinodimethane (TCNQ, Fluka 455372/1 with purity 98%), tetracyanoethylene (TCNE, Aldrich S28917-076 with purity 98%), 2,3-dichloro-5,6-dicyano-1,4-benzoquinone (DDQ, Fluka, 1335954 with purity 95%) and 2,5-dichloro-3,6-dihydroxy-1,4-benzoquinone (*p*-CLA Sigma, 98%) were used without further purification. 2,3,5,6-Tetrabromo-1,4-benzoquinone (bromanil), 2,3,5,6-tetrachloro-1,4-benzoquinone (chloranil) were purchased from BDH (Poole, UK, 0947000 purity 95%). All the reagent solutions were freshly prepared as 5 mg mL⁻¹ in acetonitrile.

2.2. Pharmaceutical preparations

Terfenadine (4-[4-(hydroxy-diphenylmethyl)-1-piperidyl]-1-(4-tert-butylphenyl)-butan-1-ol; C₃₂H₄₁NO₂) sample was obtained from the National Organization for Drug Control and Research (Egypt); the content of TFN was assigned according to the official method and found to be 98.1% [21]. Standard

solution (2.4 mg mL⁻¹ in acetonitrile) was stable at 4 °C for 1 week. Pharmaceutical preparations containing TFN (Histadine and Terfine, 120 and 60 mg TFN) were obtained from local drug stores. Five tablets were weighed and grinded to finally divided powder and an accurate weight of the powder containing 120 mg of TFN was dissolved in 50 mL acetonitrile; the solution was then filtered off and analyzed according to the proposed and the official methods.

2.3. Apparatus

A double beam spectrophotometer (V-570, Jasco) with 10 mm light path cells was used for the absorbance measurements.

FIA manifold: A schematic diagram of the flow-injection manifold is shown in (Fig. 1) which was composed of a four channel peristaltic pump (MCP Ismatec, Zurich, Switzerland) and a manual sample injection valve (ECOM, Ventil C, Czech Republic) with exchangeable sample loops (5–200 μ L). Solutions transferring were Tygon tubes (Cole-Parmer R-3603) with 0.7 and 0.5 mm i.d. for the reagent and the sample carrier streams, respectively. A homemade flow cell (10 mm quartz cell filled with Perspex having an input and output tubes with total volume 300 μ L) was used to detect the change in the absorbance of the effluents from the reaction coil.

2.4. Analytical procedures

2.4.1. Stoichiometry of the formed CT complexes

The stoichiometry of the formed complexes was determined by applying the molar ratio method. Successive aliquots (0.1–1 mL) of the standard TFN solutions (5×10^{-3} mol L⁻¹) were transferred into 10 mL measuring flasks followed by 0.5 mL of the reagent solution each 5×10^{-3} mol L⁻¹ and the volume was completed to 10 mL with acetonitrile. The absorbance of resultant CT complexes was measured at 520, 458, 412 and 842 nm for *p*-CLA, DDQ, TCNE and TCNQ, respectively, against the blank solution prepared without addition of the drug.

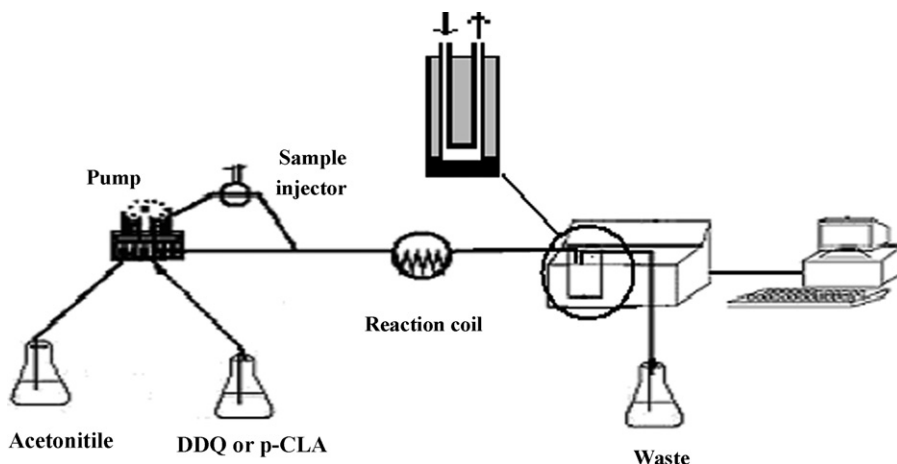


Fig. 1. Schematic diagram of the FIA system manifold used for the spectrophotometric determination of TFN.

2.4.2. Batch measurement

Aliquots containing different concentrations of TFN were transferred into 10 mL volumetric flask followed by 2 mL of different reagent solutions (each 5 mg mL⁻¹) and the volume was completed to the mark with acetonitrile. The colored species were generated immediately with *p*-CLA and DDQ and after 20 min for TCNE and TCNQ, respectively. The absorbance of the formed CT complexes was measured at the maximum absorbance corresponding to each reagent against the blank solution. Calibration graphs were constructed by plotting the absorbance of the formed CT complexes versus the final concentration of the drug (μg mL⁻¹).

2.4.3. FIA measurement

50 μL of TFN solutions with different concentrations was injected directly into the acetonitrile carrier stream (flow rate 2.2 mL min⁻¹) which was then mixed with the reagent stream (DDQ or *p*-CLA, 5 mg mL⁻¹ with a flow rate 3.3 mL min⁻¹) in the reaction coil where the colored CT complexes were formed. The colored CT complex was then sent to the homemade flow cell which detects the change in the absorbance of the effluents from the reaction coil at 458 and 520 nm for DDQ and *p*-CLA, respectively. The peak heights were proportional to the TFN concentrations and used for construction of the calibration curve, five replicate injections per sample were made in all instances.

3. Results and discussion

3.1. Spectral characteristics and reaction mechanism

TFN solution in acetonitrile showed negligible absorption band at 260 nm with low molar absorptivity (~700 L mol⁻¹ cm⁻¹) while upon addition of different π-acceptors (namely, TCNQ, TCNE, DDQ, *p*-CLA, chloranil or bromanil) to the drug solution, new characteristic bands at different absorption maxima were obtained due to the formation of CT complexes between TFN and these π-acceptors (Fig. 2).

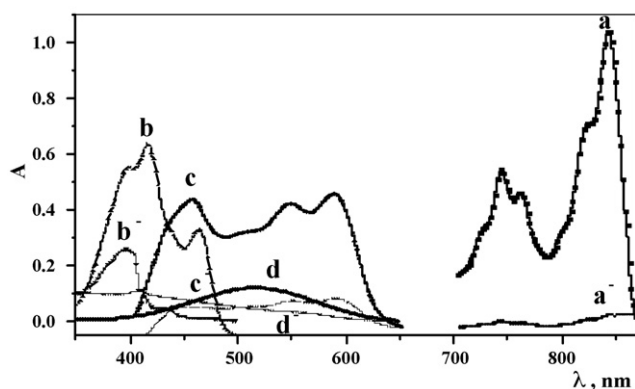
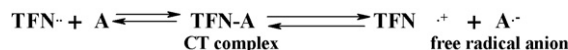


Fig. 2. Absorption spectra of the TFN CT complexes with TCNQ (a), TCNE (b), DDQ (c), *p*-CLA (d) and the correspondent reagents a⁻, b⁻, c⁻, and d⁻, respectively, against acetonitrile.

TFN, being an n-electron donor, reacts with π-acceptors giving CT complexes of the n-π type which dissociate to give the colored free radical anions of the acceptors according to the following equation.



Interaction of TFN with TCNQ gives a bluish-green chromogen which exhibits strong absorption maxima at 842 and 742 nm, the wavelength 842 nm is selected as it gives higher molar absorptivity with reproducible results. These bands may be attributed to the formation of the radical anion (TCNQ^{•-}), which was probably formed by the dissociation of an original (TFN-TCNQ) complex promoted by the high ionizing power of the acetonitrile solvent [17]. Similar mechanism can be suggested for TCNE as a yellow chromogen with triplet spectrum at 400, 412 and 464 nm was obtained, in quantitative analysis, the band at 412 was selected. The interaction of TFN with DDQ in acetonitrile at room temperature gave a red colored chromogen with a strong absorption maximum at 458, 546 and 588 nm due to the formation of the free radical anion [22] and the wavelength 458 was selected for the further studies. *p*-CLA acts as a π-acceptor in a manner similar to quinines and the TFN-*p*-CLA CT complex have intense absorption band at 520 nm due to the formation of the corresponding *p*-CLA free radical anion. The absorption maxima of TFN with bromanil and chloranil were at 413 and 425 nm with very low molar absorptivities which may be explained on the basis of insufficient ionization power of these relatively weak π acceptors which possess lower electron affinities than TCNQ, TCNE and DDQ, so they will be excluded from further investigations. Fig. 3 shows the suggested structures of the TFN CT complexes with different tested π-acceptors.

3.2. Optimization of reaction conditions

3.2.1. Effect of reagent concentration

To establish the optimum experimental conditions for TFN CT complexes formation, the drug (48 μg mL⁻¹) was allowed to react with different volumes of the reagents (DDQ, TCNE, TCNQ and *p*-CLA, respectively, each 5 mg mL⁻¹). The maximum absorbance was obtained with 1.5 mL of the reagent; higher concentrations of the reagents may be useful for rapidly reaching equilibrium, therefore, 2 mL was used as optimum value.

3.2.2. Effect of reaction solvent

In order to select the suitable solvent for CT complex formation, the reaction of TFN with *p*-CLA, DDQ, TCNE and TCNQ was made in different solvents. Acetonitrile showed super priority over chloroform, 2-propanol, dichloroethane, 1,4-dioxane, methanol and ethanol as the complex formed in these solvents either had low molar absorptivity or precipitated upon dilution. Further, acetonitrile, being a highly polar solvent (dielectric constant 37.5 [23]), facilitates the complete charge-transfer from donor to acceptor as well as the dissociation of such TFN CT complex to the free radical anion as the predominant chromogen.

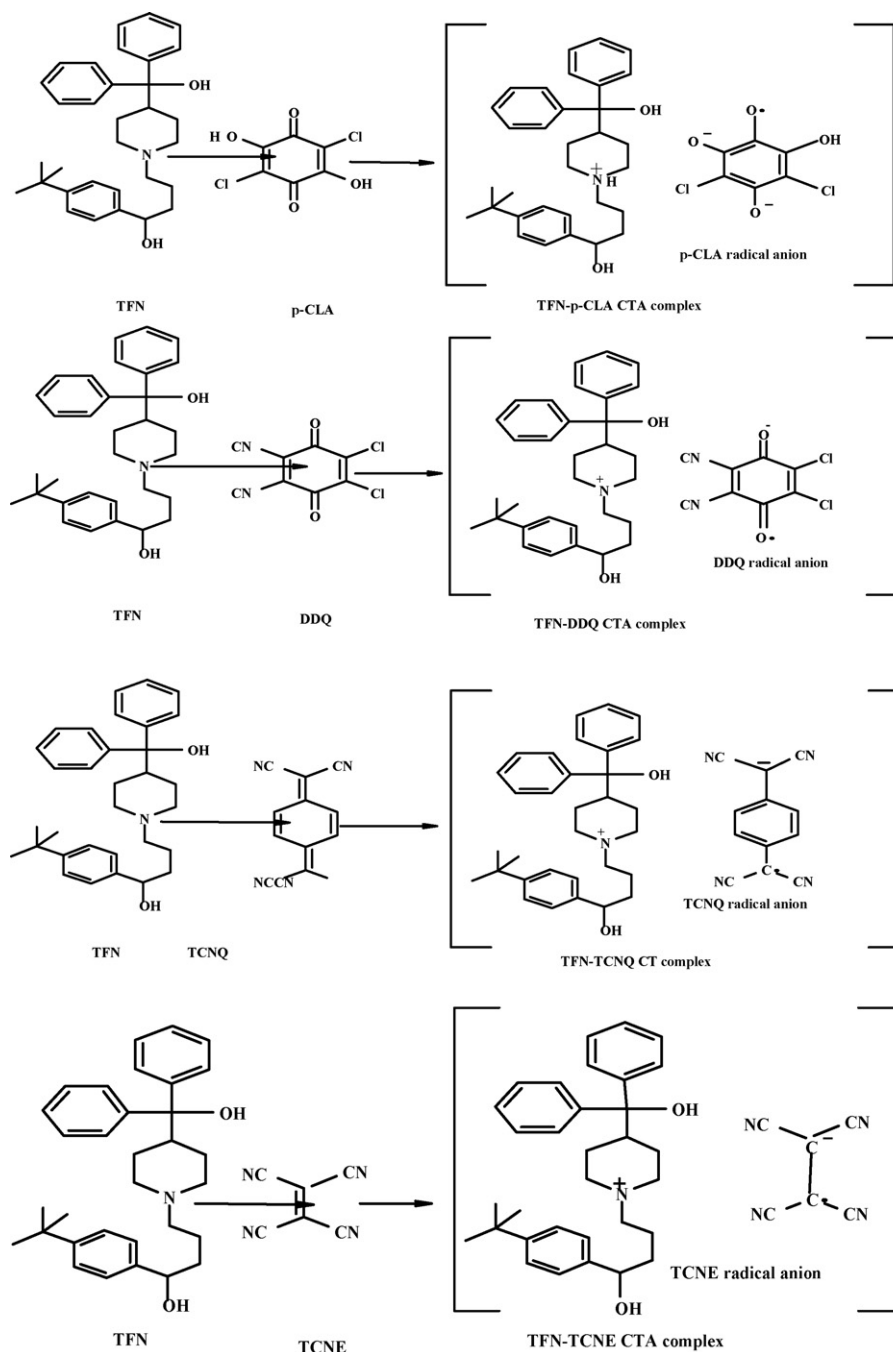


Fig. 3. Suggested structures of CT complexes of TFN with different π -acceptors.

3.2.3. Effect of reaction time

Reaction time was determined by following the color development upon the addition of TFN solution to the reagent solution at room temperature. The results obtained (Fig. 4) indicated that, complete color development was attained immediately with *p*-CLA and DDQ while TCNQ and TCNE form intense chromogen with a stable absorbance after 20 min. The absorbance of these complexes remains stable for at least 90, 60, 150 and 120 min for *p*-CLA, DDQ, TCNQ and TCNE, respectively, thus permitting quantitative determination of TFN

to be carried out with good reproducibility and indicating no side chemical reactions takes place.

3.2.4. Stoichiometry and association constants of the formed CT complexes

The stoichiometry of the formed CT complexes was determined by applying the molar ratio method and found to be about 1:1. This finding was anticipated by the presence of one basic electron-donating center (nitrogen atom) in the TFN structure (see Section 3.1, Fig. 3).

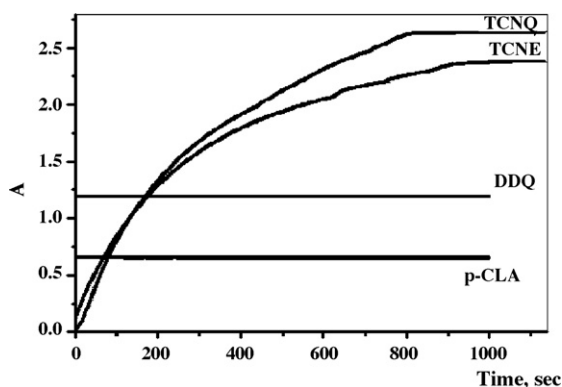


Fig. 4. Effect of time on the color intensity for TFN CT complexes.

The CT association constant is a measure of the complex stability and is given according to the Benesi–Hildebrand equation [24]:

$$\frac{[A]}{A_{CT}} = \frac{1}{K_{CT}\epsilon_{CT}[D]} + \frac{1}{\epsilon_{CT}}$$

where [D] is the molar concentration of the donor in the CT complex, [A] is the sum of the acceptor concentration in the CT complex and in the free state. A_{CT} , K_{CT} and ϵ_{CT} are the absorbance, association constant and the molar absorptivity of the formed complex, respectively.

Plotting $([A]/A_{CT})$ versus $1/[D]$ will give a linear curve whose slope equals to $(1/K_{CT}\epsilon_{CT})$ and intercept equals to $1/\epsilon_{CT}$. The values of the association constants (K_{CT}) obtained using Benesi–Hildebrand plots were found to be 0.44×10^3 , 1.43×10^3 , 0.98×10^3 and 1.31×10^3 L mol⁻¹ for TFN complexes with *p*-CLA, DDQ, TCNE and TCNQ, respectively (Fig. 5).

The standard free energy changes of complexation (ΔG°) were also calculated from the association constants (K_{CT}) using the following equation [25]:

$$\Delta G^\circ = -2.303 RT \log K_{CT}$$

The free energy changes were found to be -3.6 , -4.3 , -4.1 and -4.25 kJ mol⁻¹ for TFN complexes with *p*-CLA, DDQ, TCNE and TCNQ, respectively.

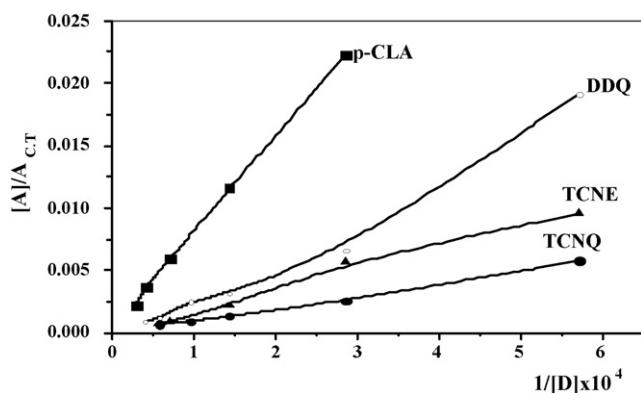


Fig. 5. Benesi–Hildebrand plots for determining the association constants of TFN CT complexes.

3.3. Flow injection variables

For the development of a new indicator reaction for practical applications in FIA measurements, attention should be paid to the reaction time to be short as possible to increase the sampling output and simplify the flow system. Though the reaction of TCNQ and TCNE with TFN gave CT complexes with higher molar absorptivities (see Fig. 2), these reagents were not suitable for FIA measurements as the reaction time was very long (20 min) which will require a very long reaction column and decrease the sampling output. On the other hand, DDQ and *p*-CLA spontaneously react with TFN to produce colored CT complexes which can be easily applied in FIA measurement.

The FIA conditions such as reagent concentration, flow rate, sample volume and the length of reaction coil were optimized in order to achieve the highest sensitivity. With injection of 60 μ g TFN in the flow system, the concentration of either DDQ or *p*-CLA was changed from 1 to 8 mg mL⁻¹ and 5 mg mL⁻¹ was selected as it gave the highest sensitivity and stable baseline.

The dependency of the peak height and residence time (time to recover the base line) on the flow rate was studied by applying different flow rates (0.66–6.6 mL min⁻¹). The flow rates of 3.3 and 2.2 mL min⁻¹ (for reagent and carrier streams, respectively) were selected as the slower flow rate gave broad peaks with long tail while the faster one depressed the peak height (Fig. 6). An increase in the injection volume from 5 to 200 μ l improved the peak height, though the sampling frequency decreased and the volume of 50 μ L was chosen as a compromise between the sensitivity and the sampling frequency.

The length of the reaction coil was changed from 5 to 30 cm; increasing of the coil length will reduce both the peak height and sharpness, which may be attributed from the dispersion of the produced colored complex. For the sake of high sensitivity and sampling frequency, a 5-cm reaction coil was employed. Typical FIA responses for the determination of TFN are shown in Fig. 7, the peaks were very sharp for all samples and the peak height was dependant on TFN injected. At these conditions, the reaction time was 60 s (from injection of the sample till measuring the absorbance of the colored complex in the flow cell) and the cycle run was 90 s, so more than 40 injections h⁻¹ can be measured.

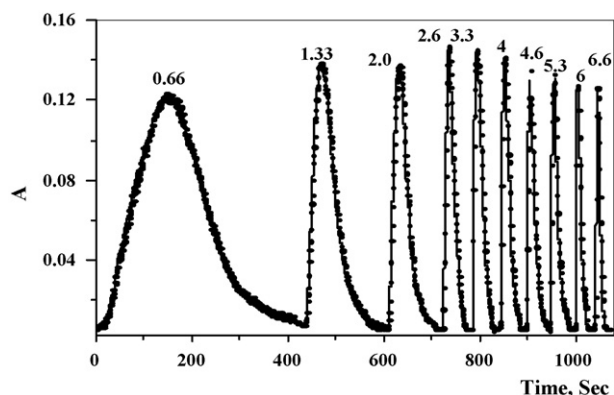


Fig. 6. Effect of the flow rate on the peak height and width of TFN-*p*-CLA complex.

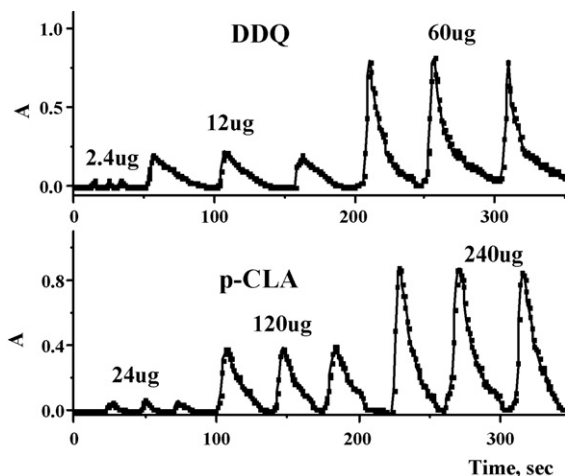


Fig. 7. Spectrophotometric flow injection determination of TFN using *p*-CLA and DDQ acceptors.

3.4. Validity of Beer's law

After selection of the suitable reaction conditions described above, calibration graphs were constructed for the investigated drug applying the four different reagents under either batch or FIA conditions (Fig. 8). The molar absorptivity (ϵ), Sandell sensitivity (S) and regression equation for each reagent were listed in Table 1. Beer's law was obeyed over the concentration ranges of 24–240, 12–168, 3–72, and 3–96 $\mu\text{g mL}^{-1}$ for *p*-CLA, DDQ, TCNQ and TCNE, respectively, with correlation coefficients 0.9979, 0.9997, 0.9999 and 0.9974 under the batch condition for the reagents with the same order. Calibration graphs under FIA conditions were obeyed in the concentration ranges 24–240 and 2.4–120 μg for *p*-CLA and DDQ with correlation coefficients of 0.9985 and 0.9990, respectively. The detection limits of the method were calculated as ($C_1 = 3.3\sigma/s$, where C_1 is the limit of detection, σ is the S.D. of the intercept, and s the slope of the standard curve) and found to be 0.3, 0.4, 2.6 and 12.3 $\mu\text{g mL}^{-1}$ for TCNQ, TCNE, DDQ and *p*-CLA under the batch measurement

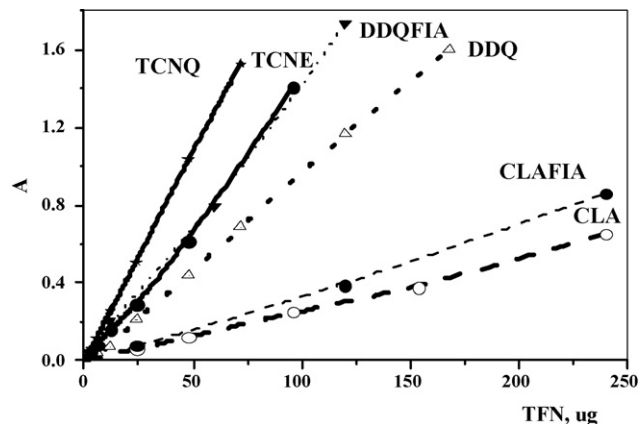


Fig. 8. Spectrophotometric determination of TFN applying different π -acceptors under the batch and FIA conditions.

while the corresponding values under the FIA conditions were 0.8 and 2.7 μg of TFN using DDQ and *p*-CLA, respectively.

The CT complex of TFN with TCNQ shows the highest molar absorptivity ($\epsilon = 10.40 \times 10^3 \text{ L mol}^{-1} \text{ cm}^{-1}$) with the smallest value of Sandell sensitivity (0.002) which indicates the high sensitivity of the proposed method in the determination of the drug under investigation. One can conclude that under the batch measurement, TCNQ is the most sensitive while DDQ is the most suitable for FIA measurements.

3.5. Between-day measurement

In order to prove the validity and applicability of the proposed method and the reproducibility of the results mentioned, four replicate experiments at different TFN concentrations were carried out using the four different reagents. Table 2 shows the values of between-day relative standard deviations for different concentrations of TFN from experiments carried out over a period of 4 days. It was found that the relative standard deviations were around 1% which indicates the high reproducibility of the method. The low R.S.D. values obtained with the FIA

Table 1
Characteristic parameters for the complexation of TFN with different π -acceptors

Item	<i>p</i> -CLA		DDQ		TCNQ	TCNE
	Batch	FIA	Batch	FIA		
A_{max} (nm)	520		458		412	842
Beer's law limits ($\mu\text{g mL}^{-1}$)	24–240	24–240	12–168	2.4–120	3–72	3–96
Molar absorptivity ($\text{L mol}^{-1} \text{ cm}^{-1}$)	1.26×10^3		4.30×10^3		10.40×10^3	7.01×10^3
Sandell sensitivity ($\mu\text{g cm}^{-2}$)	0.017		0.005		0.002	0.003
Detection limit ($\mu\text{g mL}^{-1}$)	12.3	2.7	2.6	0.8	0.3	0.4
Stability constant (L mol^{-1})	0.44×10^3		1.43×10^3		1.31×10^3	0.98×10^3
Reaction time (min)	Spontaneous	40 Sh ⁻¹	Spontaneous	40 Sh ⁻¹	20 min	20 min
Color stability (min)	90		60		150	120
Regression equation ^a						
Slope (b)	0.00268	0.00343	0.00972	0.01418	0.02134	0.01445
Intercept (a)	-0.00626	-0.00746	-0.01925	0.00104	-0.00108	-0.01794
S.D. of slope (S_b)	8.7×10^{-5}	2.0×10^{-4}	1.1×10^{-4}	3.1×10^{-4}	1.3×10^{-4}	4.7×10^{-4}
S.D. of intercept (S_a)	1.1×10^{-2}	3.1×10^{-3}	8.4×10^{-3}	3.8×10^{-3}	2.2×10^{-3}	2.0×10^{-3}
Correlation coefficient	0.9979	0.9985	0.9997	0.9990	0.9999	0.9974

^a $A = a + bC$, where A is the absorbance of the CT complex and C is the concentration of TFN in μg .

Table 2
Between-day precision of the determination of TFN using different π -acceptors

π -Acceptor	Taken ($\mu\text{g mL}^{-1}$)	Found ($\mu\text{g mL}^{-1}$)	Percentage recovery (%)	S.D. ^a	R.S.D. ^a
<i>p</i> -CLA					
Batch	120	121.8	101.5	0.33	0.27
FIA		119.6	99.6	0.19	0.16
DDQ					
Batch	60	59.5	99.1	0.38	0.64
FIA		60.2	100.3	0.26	0.42
TCNE	24	23.7	98.8	0.42	1.78
TCNQ	12	11.8	98.3	0.13	1.10

^a Means and relative standard deviations (R.S.D.) for four experiments carried out on 4 different days.

Table 3
Spectrophotometric determination of TFN in different pharmaceutical dosage using different π acceptors

	Drug						
	Taken (μg)	Histadine			Terfine		
		Found (μg)	Recovery (%)	R.S.D. ^a	Found (μg)	Recovery (%)	R.S.D. ^a
<i>p</i> -CLA							
Batch	164	158.7	96.8	0.54	160.3	97.7	0.84
FIA		159.4	97.2	0.37	162.0	98.7	0.53
							<i>DDQ</i>
Batch	72	70.7	97.9	0.87	71.2	98.8	1.15
FIA		71.5	99.3	0.35	71.8	99.7	0.47
TCNE	48	47.4	98.8	0.89	46.5	96.9	1.59
TCNQ	24	23.1	96.3	1.84	23.0	95.8	1.70
Official method	500	479.0	95.8	2.57	486.6	97.4	2.33

^a Average of five determination.

method compared with the batch method also indicate the high reproducibility of the FIA technique over the batch method.

3.6. Spectrophotometric determination of TFN in pharmaceutical preparations

The obtained high-intensity absorption bands and the very low reagent background make these procedures suitable for the routine quality control analysis of the investigated drug. It was found that the proposed method can be applied for the determination of TFN in the two pharmaceutical formulations under investigation without any analytical problems due to the tablet fillers usually present in pharmaceutical preparations such as glucose, lactose and starch. The results given in Table 3 reveal that the average recoveries were in the range 95.8–99.7% reflecting the high accuracy and precision of the proposed method as indicated by low values of R.S.D. comparing with the official method [21]. Further study will be carried out for the application of the proposed method in the stability assay of TFN which undergoes microbial oxidative degradation producing different products [26].

4. Conclusion

This paper demonstrated that CT reactions can be utilized as a useful method for the spectrophotometric determination of terfe-

nadine under both the batch and FIA conditions. Rapid and stable formation of the colored complexes with no need for extraction process is advantages of the developed method over the previously reported spectrophotometric method. The reported official method required high concentration of the drug to permit the titration process compared with the suggested methods which applied successfully for microgram levels without interference of excipients. Under the batch conditions, TCNQ showed the highest sensitivity, while DDQ is the most suitable reagent for the FIA conditions. The FIA technique has many advantages of permitting the simple, accurate and precise determination of TFN in pure and dosage formulations with average recoveries agreed with that of the official methods with the ability of analysis more than 40 sample h^{-1} .

References

- [1] V.K. Kulshrestha, P.P. Gupta, P. Turner, J. Wadsworth, Br. J. Clin. Pharmacol. 6 (1978) 25.
- [2] S. Emara, A. El-Gindy, K. Mesbah, G.M. Hadad, J. AOAC Int. 90 (2007) 384.
- [3] Y.Y. Lau, P.H. Anderson, R. Talaat, J. Liq. Chromatogr. Relat. Technol. 19 (1996) 2669.
- [4] M.A. Martinez-Gomez, M.M. Carril-Aviles, S. Sagrado, R.M. Villanueva-Camana, M.J. Medina-Hernandez, J. Chromatogr. A 1147 (2007) 261.
- [5] M. Ghoneim, R. Issa, A. Tawfik, J. Pharm. Biomed. Anal. 26 (2001) 593.
- [6] K. Terada, Y. Takada, Y. Yoshihashi, E. Yonemochi, Funtai Kogaku Kaishi 42 (2005) 632.

- [7] K. Masuda, Pharm. Tech. Jpn. 23 (2007) 1295.
- [8] A.A. Al-Majed, J. Al-Zehouri, F. Belal, J. Pharm. Biomed. Anal. 23 (2000) 281.
- [9] M. Ayad, H. Saleh, M. El-Maamli, M. El-Bolkiny, M. El-Henawee, Anal. Lett. 26 (1993) 913.
- [10] A.S. Amin, Y.M. Issa, Mikrochim. Acta 130 (1999) 173.
- [11] K. Kelani, L.I. Bebawy, L. Abdel-Fattah, J. Pharm. Biomed. Anal. 18 (1999) 985.
- [12] A.A. Badwan, A. Abu-Malooh, L. Owais, M.S. Salem, H. Al-Kaysi, Anal. Lett. 24 (1991) 217.
- [13] R.S. Mulliken, J. Am. Chem. Soc. 72 (1950) 600.
- [14] R. Foster, Organic Charge-Transfer Complexes, Academic Press, New York, 1969.
- [15] M. Krishnamurthy, U. Muralikrishna, Indian Drugs 22 (1985) 171.
- [16] M.S. Luo, Yaowu Fenxi Zazhi 15 (1995) 52.
- [17] M.E. Abdel-Hamid, M.A. Abuirjeie, Talanta 35 (1988) 242.
- [18] M.M. Abdel-Khalek, Bull. Fac. Pharm. (Cairo Univ.) 31 (1993) 45.
- [19] J. Ruzicka, E.H. Hansen, Flow Injection Analysis, 2nd ed., Wiley, New York, 1988.
- [20] B. Uno, K. Nakajima, S. Kawai, Bull. Chem. Soc. Jpn. 64 (1991) 2613.
- [21] K. Florey, Analytical Profiles of Drug Substances, vol. 19, Academic Press, New York, 1990, p. 627.
- [22] N. Rahman, Md.N. Hoda, J. Pharm. Biomed. Anal. 31 (2003) 381.
- [23] Vogel's, Textbook of Practical Organic Chemistry, 5th ed., Longman Group UK Ltd., England, 1989, pp. 1442–1444.
- [24] H.A. Benesi, J. Hidelbrand, J. Am. Chem. Soc. 71 (1949) 2703.
- [25] A.N. Martin, J. Swarbrick, A. Cammarata, Physical Pharmacy, 3rd ed., Lee and Febiger, Philadelphia, PA, 1969, p. 344.
- [26] C. Mazier, M. Jaouen, M. Sari, D. Buisson, Bioorg. Med. Chem. Lett. 14 (2004) 5423.

Determination of tetracyclines residues in honey by on-line solid-phase extraction high-performance liquid chromatography

Jiantao Li^a, Ligang Chen^a, Xiao Wang^{a,b}, Haiyan Jin^a,
Lan Ding^{a,*}, Kun Zhang^a, Hanqi Zhang^a

^a College of Chemistry, Jilin University, 2699 Qianjin Street, Changchun 130012, PR China

^b Jilin Province Product Quality Supervision Test Institute, 20 Weixing Road, Changchun 130022, PR China

Received 23 October 2007; received in revised form 14 January 2008; accepted 15 January 2008

Available online 20 January 2008

Abstract

An automated system using on-line solid-phase extraction (SPE) high-performance liquid chromatography (HPLC) with ultraviolet (UV) detection was developed for the determination of tetracyclines (TCs), such as tetracycline (TC), oxytetracycline (OTC), chlortetracycline (CTC), metacycline (MC), and doxycycline (DC) in honey. One milliliter diluted honey sample was injected into a conditioned C18 SPE column and the matrix was washed out with water for 3 min. By rotation of the switching valve, TCs were eluted and transferred to the analytical column by the chromatographic mobile phase. Chromatographic conditions were optimized. TCs were separated in less than 8 min with a gradient elution using a mixture of 0.8% formic acid and acetonitrile. The UV detection was performed at 365 nm. The conditions for on-line SPE, including solvent and total time for loading sample and washing matrix were also optimized. Time for extraction and separation decreased greatly. For the five kinds of TCs, the limits of detection (LODs) at a signal-to-noise of 3 ranged from 5 to 12 ng g⁻¹. The relative standard deviations (R.S.D.) for the determination of TCs ranged from 3.4 to 7.1% within a day and ranged from 3.2 to 8.9% in 3 days, respectively.

© 2008 Elsevier B.V. All rights reserved.

Keywords: On-line solid-phase extraction; HPLC; Honey; Tetracyclines

1. Introduction

Honey is a natural and wholesome product consumed by many people around the world. The addition of additives and preservatives is not allowed for honey [1]. A persistent problem for beekeepers is American and European foulbrood (AFB and EFB) disease of honeybees [2–4], caused by *Paenibacillus larvae* and *Melissococcus pluton*. For treating these infections, antibiotics belonging to the sulfonamide, tetracycline (TC) and amphenicol classes are often used. Moreover, tetracyclines (TCs) can be added directly to plants in the orchard environment during blossom. The contamination of the blossom with high concentrations of antibiotic implies the risk of a carry-over of residues into honey [5]. Hence, these antibiotics, especially TCs, persist as contaminants in honey and determination of these drugs in honey samples is considerably important.

TCs have a broad range of activity against gram-positive and gram-negative bacteria [6,7]. The basic structure of TCs consists of a hydronaphthacene framework containing four fused rings (Fig. 1) [8,9]. Because of their possible toxic or allergic reactions and the possibility that pathogenic organisms could become resistant to these drugs [10–12], much attention has paid to the TCs, recently.

Some countries do not have fixed maximum residue limits (MRLs) for honey because TCs are illegal for use with bees at any level. While some other countries make action limits in order to make the situation clearer. In Belgium, the action limit for the group of tetracycline was preliminarily set at 50 ng g⁻¹. Since July 1, 2002, this value has been fixed at 20 ng g⁻¹. France applies a nonconformity limits for tetracycline in honey of 15 ng g⁻¹, the reporting limit in Great Britain is 50 ng g⁻¹, while the tolerance levels in Switzerland are 20 ng g⁻¹ [13].

TCs have been successfully determined [2–7,14–21]. The most popular method for determination of TCs in honey was high-performance liquid chromatography (HPLC) in the reverse-phase mode, with different detection modes, such as

* Corresponding author. Tel.: +86 431 85168399; fax: +86 431 85112355.
E-mail address: dinglan@jlu.edu.cn (L. Ding).

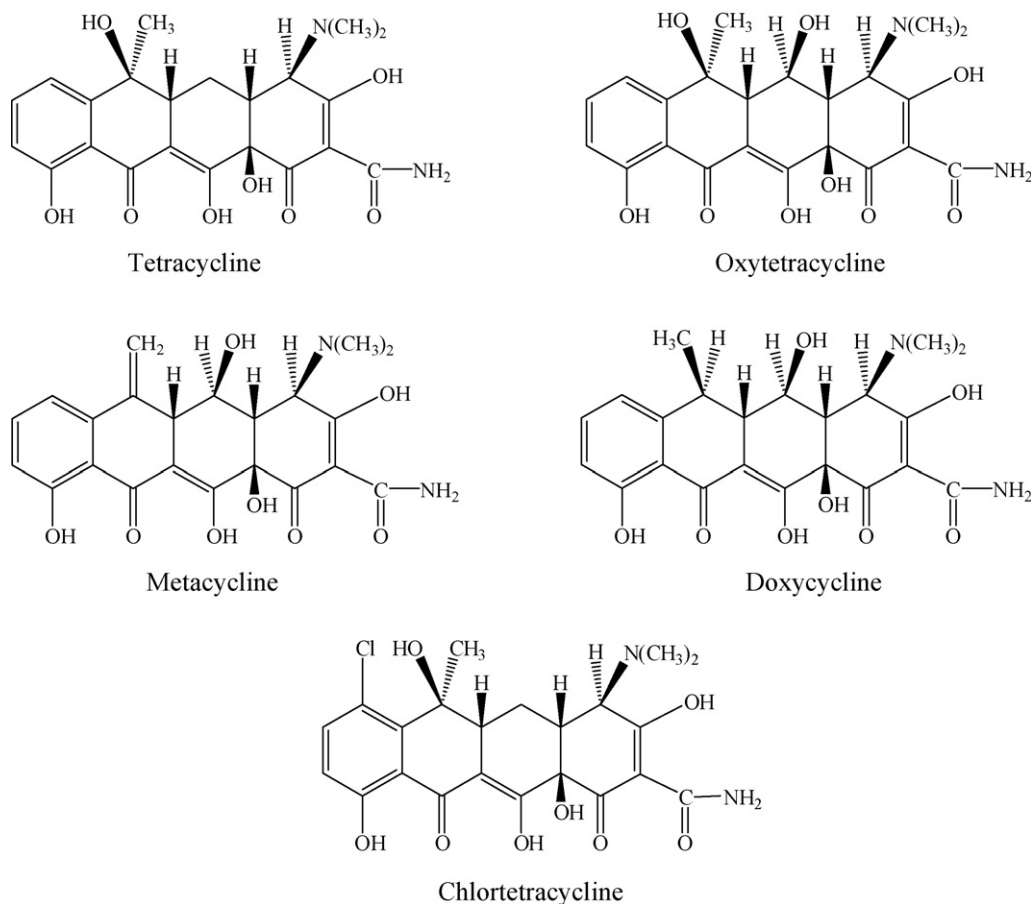


Fig. 1. The structures of tetracycline, oxytetracycline, metacycline, doxycycline and chlortetracycline.

fluorescence [3], chemiluminescence [5], ultraviolet [7] and mass spectrometry [8,15,16]. In these studies, sample preparation was performed by off-line solid-phase extraction (SPE) with sorbents of C18 [4,18], XAD-2 resin [5,14], DSC-phenyl [7] or Oasis HLB [2,3]. However, these methods involve tedious and laborious pre-treatment steps before the determination of TCs, such as the evaporation of the eluent from SPE in concentration procedure. Long et al. observed a loss near 80% in TC, oxytetracycline (OTC) and chlortetracycline (CTC) during solvent removal, performed in glass tubes. Careful consideration should be given before employing evaporation during method development [22]. It is the current trend to emphasize automation techniques that couple the sample pre-treatment using solid-phase extraction and the liquid chromatography separation on-line.

HPLC coupled with on-line solid-phase extraction (SPE) has been used in recent years [23–27]. The coupling technique offers several advantages, including reducing time and solvent volumes used, and many of the problems associated with more traditional approaches can be avoided. However, few on-line methods have been published for the determination of TCs in honey [28].

This study presents an efficient on-line technique by coupling SPE with HPLC for determination of five TCs in honey. The five TCs are TC, OTC, CTC, metacycline (MC), and doxycycline (DC), which are commonly used as veterinary medicines and feed additives [5]. The method allows sample extraction and the

subsequent analysis take place in a closed, automated system. The time is shortened in this way. The reliability and repeatability of the analysis method are improved, and the risks of sample loss and contamination are decreased as well.

2. Experimental

2.1. Instruments

An on-line SPE–HPLC system was assembled in our laboratory (Fig. 2). In the system, an Agilent 1100 two-dimensional liquid chromatograph (Palo Alto, CA, USA) was used, which was equipped with an automatic 10-port switching valve (valve 1), a 7725i injection valve (valve 2), a quaternary pump (Pump A), a heated column compartment, a sample loop (1.0 mL), a ultraviolet (UV) detector, a LC workstation and a Waters Symmetry[®] C18 reversed-phase column (150 mm × 4.6 mm i.d., 5 μm, Waters, Milford, MA, USA) used as analytical column. The Pump A was used for the establishment of the baseline and gradient elution. A guard column packed with C18 sorbent (4.6 mm × 12.5 mm i.d., 5 μm) was used as SPE column for cleanup and concentration of the analytes. A FI-2100 peristaltic pump (Pump B, Haiguang, Bingjing, China) and a P230 high-pressure pump (Pump C, Elite, Dalian, China) were used for completing injection of analytes and SPE, respectively.

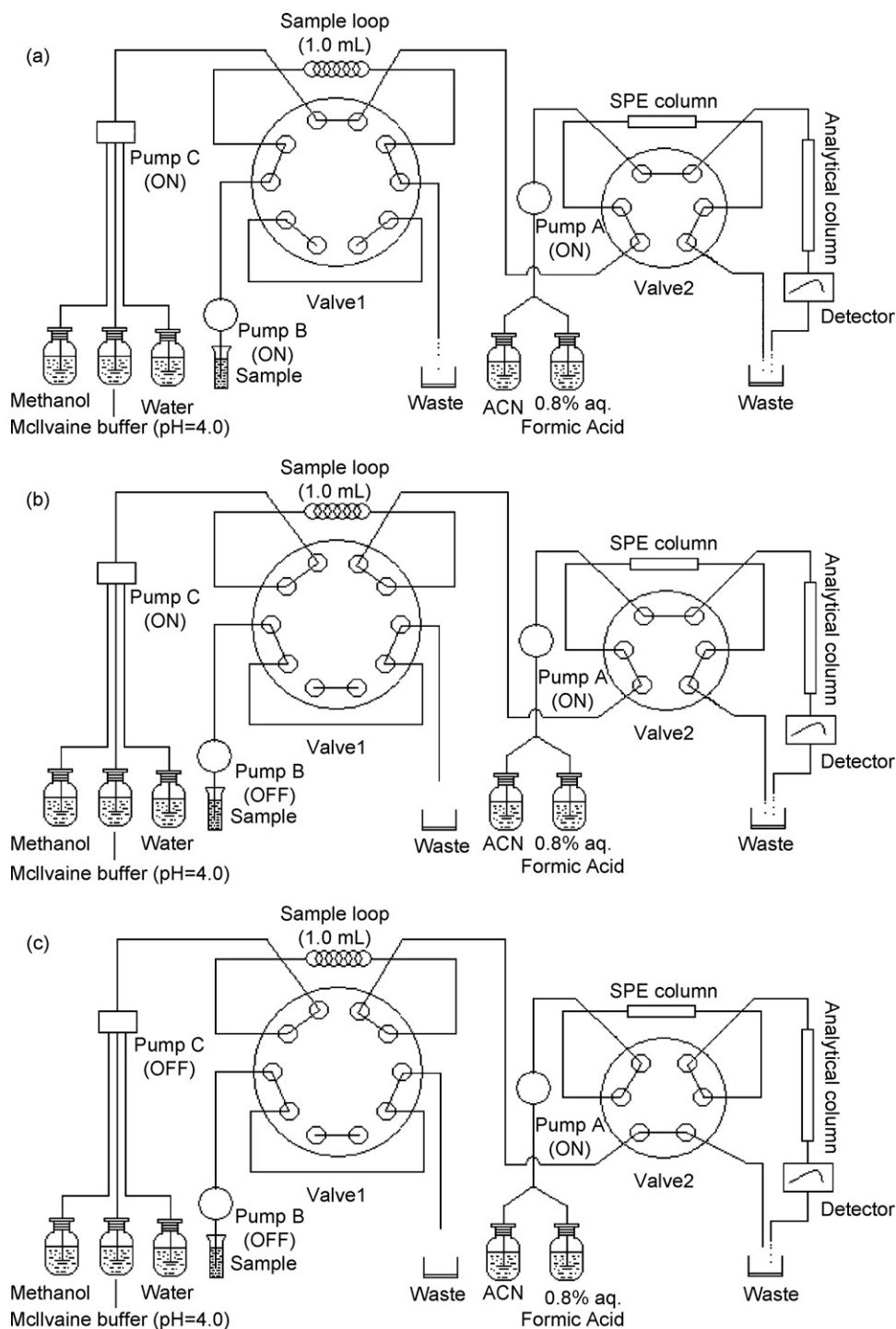


Fig. 2. The manifold diagram of on-line SPE-HPLC system. (a) Filling, conditioning the SPE column; (b) extraction, washing matrix; (c) separation, determination.

2.2. Reagents

HPLC grade formic acid, methanol and acetonitrile (ACN) were obtained from Fisher Corporation (Pittsburgh, PA, USA). All other chemicals used, such as citric acid monohydrate, ethylenediaminetetraacetic acid disodium salt dihydrate (Na_2EDTA) and disodium hydrogenphosphate dihydrate (Na_2HPO_4) were of analytical grade. High purity water was obtained from a Milli-Q water system (Millipore, Billerica,

MA, USA). 0.1 mol L^{-1} Na_2EDTA -McIlvaine buffer (pH 4.0) solution was prepared by dissolving 11.8 g of citric acid monohydrate, 13.72 g of Na_2HPO_4 , and 33.62 g of Na_2EDTA in 1 L of distilled water [29]. This solution was prepared weekly and stored in refrigerator until use.

Tetracycline, oxytetracycline, metacycline, doxycycline and chlortetracycline were purchased from National Institute for the Control of Pharmaceutical and Biological Products (Beijing, China). Each individual stock solution (1.0 mg mL^{-1}) was pre-

pared by dissolving 10 mg standard of TC in 50% methanol aqueous solution and stored in the refrigerator. A mixed standard solution of the target compounds was prepared by mixing the above solutions and diluting with 50% methanol aqueous solution to obtain analyte concentrations of 5, 10, 25, 50, and 100 $\mu\text{g mL}^{-1}$.

2.3. Chromatographic conditions

A gradient elution solvent containing 0.8% formic acid and ACN was applied. The gradient elution was carried out starting from 5 to 24% ACN in 4 min, held for 2 min, then to 40% ACN in 2 min and held for another 2 min. The flow-rate was 1 mL min^{-1} . The column temperature of 25 °C was maintained. The detection wavelength was 365 nm.

2.4. Analytical procedure

The honey samples were obtained from Wal-Mart located in Changchun, China. 5.0 g of the honey sample was accurately weighed and added into 25 mL volumetric flask, and then 0.1 mol L^{-1} Na_2EDTA –McIlvaine buffer (pH 4.0) was also added into the volumetric flask. The volumetric flask was shaken until all the honey dissolved in the buffer. Then the buffer was added into the mark and the volumetric flask was shaken for several minutes again. The solution obtained was further filtered through a 0.45 μm membrane before analysis by HPLC.

As shown in Fig. 2a, Pumps A, B and C were all activated at the same time. Pump A was used for establishing the baseline of detector with initial mobile phase (5% ACN). Pumps B and C were used for the injection of the sample and the conditioning of SPE, respectively. When the sample loop (1.0 mL) was filled with sample completely, the Pump B was stopped. The SPE column was conditioned by Pump C with 3 mL methanol and 3 mL Na_2EDTA –McIlvaine buffer successively at the flow-rate of 1 mL min^{-1} . After the conditioning of the SPE column, the valve 1 was turned to the extraction position (Fig. 2b). The sample in the loop was loaded into SPE column and the matrix was washed out by 3 mL water at a flow-rate of 1.0 mL min^{-1} . Finally (Fig. 2c), Pump C stopped and valve 2 was turned to the injection position. The analytes trapped on the SPE column were eluted into the analytical column by gradient elution. The eluate was monitored at 365 nm. The TCs were quantified according to the calibration curve, which was established based on the standard addition method.

3. Results and discussion

3.1. Optimization of the chromatographic conditions

The method proposed provides a simple and rapid procedure for the determination of TCs in honey samples. For all TCs, there are two maximum absorption wavelengths at 274 and 365 nm. Detection wavelengths of 274 and 365 nm were tested in our study to monitoring the extract. Though both of them have good sensitivity, less interfering compounds were observed at 365 nm. 365 nm was selected as the detection wavelength.

Due to the presence of two ketone groups, TCs form chelate complexes with metal ions and adsorb on the silanol group in a reversed-phase (RP) column, so that TCs are apt to appear as tailing peaks [9]. In order to avoid forming chelate complexes and their adsorption on RP columns, RP column chromatography using mobile phases containing various acids has been reported [30]. The acid acts as a simple ionization suppression agent to minimize the occurrence of mixed separation mechanisms. A most often used acid is formic acid, which is able to effectively mitigate the effect of residual silanols on the stationary phase, and perhaps even scavenge residual metals [22]. So, we chose the formic acid solution as the acidic solution. ACN–formic acid aqueous solution was confirmed as the combination of mobile phase. The gradient time-table was adopted from the literature [31,32], and was further adjusted for adapting to our experiment. The gradient elution was finally confirmed to carry out starting from 5 to 24% ACN in 4 min, held for 2 min, then to 40% ACN in 2 min and held for another 2 min.

TCs can be separated completely using C18 column (250 mm \times 4.6 mm i.d., 5 μm). But, peak tailings of CTC, MC and DC occurred with this type of column. In order to optimize the separation and get better signal of peaks, a shorter C18 column (150 mm \times 4.6 mm i.d., 5 μm) was tested. TCs were also separated completely. Besides, symmetrical, sharp peaks without tailings or overlaps were obtained using this shorter column.

3.2. The optimization of SPE

3.2.1. The choose of sorbent of SPE column

SPE is commonly employed to accomplish cleanup and concentration simultaneously. Due to their carbon backbone, aromatic region, and varied functional groups, TCs could theoretically be applied to wide range of SPEs [22]. The most commonly used sorbent is Oasis HLB. For performing on-line SPE–HPLC, it is important for direct desorption of analytes from preconcentration column to HPLC column by an eluent optimal for chromatographic separation. In other words, it is critical that the sorbent used in the SPE column be identical with the material packed in the analytical column to prevent broadening of the peak [33]. For this reason, C18 sorbent was chosen in this study because the sorbent of analytical column was C18.

3.2.2. The optimization of condition solvent

Saturated aqueous Na_2EDTA , water and Na_2EDTA –McIlvaine buffer (pH 4.0) were tested as the condition solvent of the C18 SPE [30] in this study. In this method, the extraction and cleanup are on-line (Fig. 2). When the saturated aqueous Na_2EDTA was used as condition solvent, the system, including valves and transition lines, was blocked after few samples were analyzed. When water was used as condition solvent, the recoveries of the analytes were decreased. It is because TCs adsorb onto silanols and form complexes with metal residues [22,30]. When Na_2EDTA –McIlvaine buffer (pH 4.0) was used, the system operated smoothly and satisfactory recoveries with good reproducibility were obtained. Another advantage was that the condition solvent was same to the extrac-

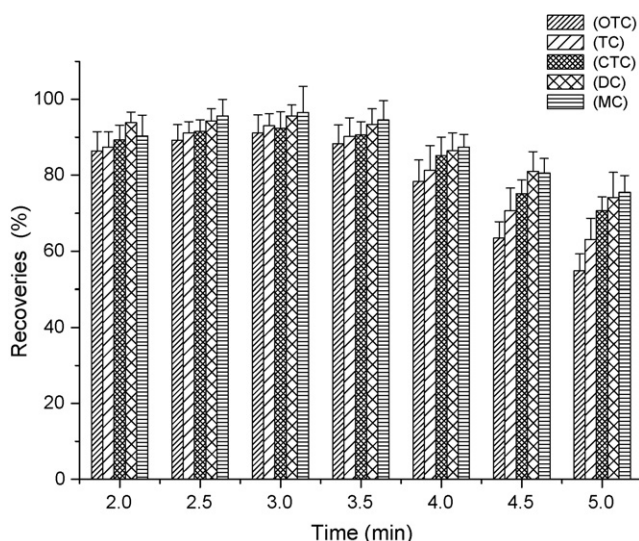


Fig. 3. The effect of washing time on the recoveries of TCs from honey samples.

tion solvent. So, before the Na_2EDTA – MClI vaine buffer (pH 4.0) containing TCs was injected into the SPE column, the column has been in an equilibrium state with the buffer. The equilibrium state was suitable for the adsorption of TCs. Therefore, Na_2EDTA – MClI vaine buffer (pH 4.0) was adopted as the condition solvent.

3.2.3. The optimization of time for loading sample and washing matrix

The washing time must be optimized for washing the matrix out and not washing the adsorbed analytes on the SPE column. The procedures of loading sample and washing matrix were successive and both of the solvents used were water in this study. Therefore, total time for loading sample and washing matrix was optimized. The total time in the range of 2.0–5.0 min was investigated when the washing flow-rate was fixed at 1.0 mL min^{-1} . When the time was longer than 3.5 min, the recoveries of TCs decreased (Fig. 3), because the TCs were washed away by the excess washing solvent. When the time was less than 3.0 min, more co-extracted matter retained on the SPE column. Total time of 3 min was chosen in the study.

3.3. Method validation

The method was validated by evaluation of the following parameters: specificity, calibration curve, sensitivity and intra-day and inter-day precisions.

3.3.1. Specificity

The components of honey are very complex. Except the basal components such as glucose and fructose which contributed about 75% of the total, there are other organic constituents including di/tri/oligo saccharides, aliphatic acids, vitamins, amino acids and proteins [16]. So not only the TCs but also some other components were extracted out during sample preparation. In order to prevent misidentification of analytes, relative retention time was checked for

all TCs. Additionally, typical chromatograms of blank honey sample and that of spiked sample were compared to confirm the specificity (Fig. 4). There were no interfering compounds observed in the retention time of TC, OTC, MC and DC. Although a small interfering peak was observed for CTC, it has no significant influence for the determination of CTC.

3.3.2. Calibration curve

Calibration curves were established based on the standard addition method. After the sample was weighed, $50 \mu\text{L}$ of different concentrations of mixed standard solution was spiked into the blank honey sample to prepare spiked samples at concentration of 50, 100, 250, 500 and 1000 ng g^{-1} , respectively. Calibration curves were obtained using the least squares regression procedure by plotting the peak-areas of the studied analytes versus their theoretical concentrations. All five standard curves were obtained (Table 1). The linearity for TCs, in the concentration range of 50– 1000 ng g^{-1} , was good, as shown by the fact that the determination of the correlation coefficients (r) is above 0.9930. The results showed that a good correlation exists between the peak-areas (Y) and the concentration (X) of TCs.

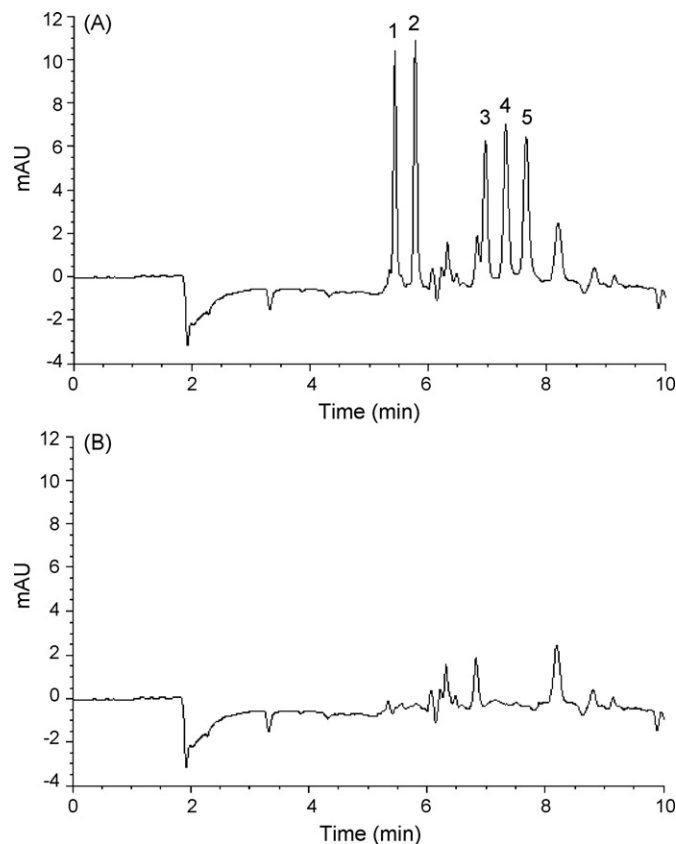


Fig. 4. Chromatograms of TCs with UV detection at 365 nm. TCs were separated using a gradient elution mode with a mixture of 0.8% formic acid and ACN. (A) Spiked honey sample containing 250 ng g^{-1} of each TCs. (B) Blank honey sample. The peaks correspond to: 1, OTC ($t_R = 5.5 \text{ min}$); 2, TC ($t_R = 5.8 \text{ min}$); 3, CTC ($t_R = 7.0 \text{ min}$); 4, MC ($t_R = 7.4 \text{ min}$) and 5, DC ($t_R = 7.8 \text{ min}$).

Table 1
Performance of the proposed LC method for the determination of TCs in honey matrix

Tetracycline	Regression equation	Correlation coefficient	LOD (ng g ⁻¹)	LOQ (ng g ⁻¹)	Linearity (ng g ⁻¹)
OTC	$Y=0.155X+0.603$	0.9981	12	40	50–1000
TC	$Y=0.204X+0.532$	0.9937	8	27	50–1000
CTC	$Y=0.127X+0.423$	0.9997	10	33	50–1000
MC	$Y=0.111X-0.180$	0.9941	5	17	50–1000
DC	$Y=0.157X-0.348$	0.9984	7	23	50–1000

3.3.3. Limits of detection (LODs) and limits of quantitation (LOQs)

The limits of detection (LODs) were determined by analyzing blank honey samples (Fig. 4B) at levels that provided signals at three times above the background noises. In a similar way, the limits of quantitation (LOQs) were identified at signal to noise ratios equaled to 10. LOD and LOQ were considered as the analyte minimum concentrations that can be confidently identified and quantified by the method, respectively. The LODs and LOQs obtained are in the range of 5–12 ng g⁻¹ and 17–40 ng g⁻¹ for oxytetracycline, tetracycline, chlortetracycline, metacycline and doxycycline (Table 1). It was sensitive enough to support this evaluation.

3.3.4. Precision

Precision was evaluated by measuring intra- and inter-day relative standard deviations (R.S.D.s). The intra-day precision was performed by analyzing spiked samples six times in 1 day at three different concentrations of 80, 250 and 800 ng g⁻¹. The inter-day precision was performed over 6 days by analyzing spiked samples at three different concentrations of 80, 250 and 800 ng g⁻¹. The results obtained were shown in Table 2. The R.S.D. of intra-day ranged from 3.4 to 7.1%. The inter-day R.S.D. ranged from 3.2 to 8.9% in 6 days. The precision of the proposed method were satisfactory.

Table 2
Within- and between-day precisions and recoveries of the assays ($n=6$)

Analyties	Theoretical concentration (ng g ⁻¹)	Within-day			Between-day		
		Concentration found (mean ± S.D.) (ng g ⁻¹)	R.S.D. (%)	Recovery (%)	Concentration found (mean ± S.D.) (ng g ⁻¹)	R.S.D. (%)	Recovery (%)
OTC	80	70 ± 3.7	5.3	87.5	72.3 ± 4.5	6.2	90.4
	250	226.2 ± 12.7	5.6	90.5	228.3 ± 16.2	7.1	91.3
	800	703.2 ± 24.6	3.4	90.4	726.4 ± 39.2	5.4	90.8
TC	80	70.9 ± 4.7	6.6	88.6	71.9 ± 5.2	7.2	89.9
	250	223.2 ± 9.6	4.3	89.3	221 ± 10.2	4.6	88.4
	800	728.8 ± 29.9	4.1	91.1	740.8 ± 23.7	3.2	92.6
CTC	80	70.1 ± 5.0	7.1	87.6	70.88 ± 4.8	6.8	88.6
	250	224.2 ± 11.2	5.0	89.7	226.2 ± 13.6	6.0	90.5
	800	722.4 ± 32.5	4.5	90.3	731.2 ± 38.8	5.3	91.4
MC	80	76.1 ± 5.1	6.7	95.1	79.4 ± 6.0	7.5	99.2
	250	268.2 ± 14.0	5.2	107.3	283.8 ± 19.6	6.9	113.5
	800	1000 ± 48.0	4.8	125.0	972.8 ± 54.5	8.9	121.6
DC	80	72.4 ± 3.3	4.6	90.5	71.8 ± 3.7	5.2	89.7
	250	233.5 ± 11.4	4.9	93.4	232.0 ± 14.6	6.3	92.8
	800	766.4 ± 29.1	3.8	95.8	781.6 ± 38.3	4.9	97.7

3.4. Application to real samples

Eight honey samples from different origins were purchased to evaluate the applicability of the present method. No contamination of TCs residues at detectable levels was found in the honey samples. If the positive samples can be obtained, the TCs in them could be detected using this method. The recovery study was then carried out by spiking honey samples with the TC standards at levels of 80, 250 and 800 ng g⁻¹. The recoveries (mean ± S.D.) ($n=3$), for the different TCs in the honey samples, were listed in Table 3. The recoveries from 84.2 ± 6.4 to 120.6 ± 4.3% were obtained for the five compounds. Therefore, the proposed method was applicable for the determination of TCs residues in honey.

3.5. Comparison of on-line SPE–HPLC method with existing reports

Several analytical methods for the determination of TCs have been published. In their studies, the sample preparation step was complicated. Viñas et al. developed a method for the determination of six TCs [7]. The mean recoveries of TCs in different honey samples are in the range of 92.1–96.1%. LODs are in the range of 15–30 ng g⁻¹. Pena et al. applied HPLC with fluorescence detection to determine TC and OTC in honey samples

Table 3
Recoveries of TCs in honey samples (% mean ± S.D.) (n = 3)

	OTC (ng g ⁻¹)			TC (ng g ⁻¹)			CTC (ng g ⁻¹)			MTC (ng g ⁻¹)			DTC (ng g ⁻¹)		
	80	250	800	80	250	800	80	250	800	80	250	800	80	250	800
Sample 1	90.1 ± 5.2	92.5 ± 3.5	93.2 ± 3.8	86.5 ± 6.7	87.6 ± 5.8	96.8 ± 4.6	86.5 ± 8.3	91.6 ± 5.6	89.5 ± 4.6	99.1 ± 9.5	110.5 ± 5.9	120.8 ± 4.6	90.5 ± 5.6	95.6 ± 5.6	98.6 ± 3.9
Sample 2	88.4 ± 4.3	91.3 ± 4.6	90.2 ± 4.9	87.6 ± 7.5	88.9 ± 6.4	89.7 ± 4.8	85.3 ± 6.8	90.3 ± 6.7	96.5 ± 3.6	92.3 ± 6.6	118.6 ± 6.1	110.5 ± 5.1	89.6 ± 4.6	90.5 ± 3.4	97.3 ± 5.6
Sample 3	86.3 ± 6.2	95.4 ± 5.1	89.6 ± 4.6	89.4 ± 8.3	90.5 ± 4.8	90.4 ± 5.2	86.4 ± 8.2	88.6 ± 5.8	88.4 ± 5.8	95.6 ± 7.1	120.6 ± 4.3	106.9 ± 4.8	88.4 ± 5.9	94.2 ± 4.6	90.6 ± 6.8
Sample 4	89.5 ± 5.8	88.6 ± 6.2	91.2 ± 3.8	90.5 ± 9.7	91.5 ± 4.6	89.0 ± 3.5	88.9 ± 7.4	89.6 ± 4.3	88.0 ± 4.6	92.1 ± 5.6	105.0 ± 5.8	95.6 ± 5.6	94.3 ± 6.3	92.4 ± 4.9	94.6 ± 4.0
Sample 5	90.4 ± 6.4	86.8 ± 4.3	91.4 ± 3.6	91.7 ± 5.6	92.8 ± 5.2	98.6 ± 3.8	90.5 ± 6.3	89.5 ± 7.8	90.6 ± 3.1	96.4 ± 8.4	96.8 ± 6.7	99.3 ± 6.1	92.1 ± 6.8	96.1 ± 6.2	95.6 ± 3.9
Sample 6	87.4 ± 4.6	89.4 ± 5.0	89.6 ± 5.0	84.3 ± 4.8	84.2 ± 6.4	91.3 ± 4.9	91.0 ± 5.6	92.5 ± 7.1	93.1 ± 4.9	100.8 ± 7.1	99.2 ± 4.9	112.5 ± 6.7	91.1 ± 5.8	94.1 ± 5.9	95.8 ± 4.5
Sample 7	88.5 ± 6.1	90.5 ± 3.5	89.4 ± 3.7	89.5 ± 5.9	86.9 ± 5.9	87.6 ± 6.1	88.2 ± 5.8	89.7 ± 6.5	94.6 ± 6.4	110.2 ± 5.3	90.5 ± 5.0	113.4 ± 4.2	90.5 ± 7.1	88.6 ± 6.7	89.6 ± 6.2
Sample 8	89.6 ± 7.4	89.6 ± 4.1	90.2 ± 3.2	89.4 ± 6.4	90.8 ± 4.9	92.5 ± 5.4	87.6 ± 6.9	86.9 ± 5.3	92.5 ± 5.8	90.6 ± 6.4	99.4 ± 4.6	106.5 ± 5.3	91.6 ± 4.2	93.6 ± 5.9	96.4 ± 5.7

[3]. The mean recoveries for OTC and TC were 90 and 93%, respectively. The LODs were 20 and 21 ng g⁻¹ for OTC and TC, respectively. The mean recoveries of TCs in different honey samples calculated from Table 3 range from 92.1 to 95.3% and LODs are in the range of 5–12 ng g⁻¹ in our study. The epimers of TCs have been studied in some literatures [8,10]. There were, however, no peaks of epimers of TCs observed in chromatogram under our experimental conditions. Five TCs were separated in less than 11 min in our research, which was shorter than those used in the work of Viñas for separating six TCs (22 min) and almost the same time in the work of Pena for separating two TCs (10 min). The off-line SPE was used in those studies which had to go through a time-consuming and arduous pre-treatment step. Bo et al. [28] have developed a column switching technique for the determination of three TCs in honey. In their study, when the matrix in the pre-column was washed out, the waste residues passed through the detector. The components of the waste residues are very complex. So, the detector was apt to be contaminated in this way. Besides, it is difficult to realized automatism for them. Whereas, an automatic 10-port switching valve (valve 1) was used in our study. The waste was discharged without passing through the detector. The detector was protected from contamination in this way. The on-line SPE–HPLC system used in the proposed method was easy and fast, reducing the reagents consumption and suitable for determination of TCs in honey.

4. Conclusions

In this paper, we have developed an on-line SPE–HPLC technique for the analysis of the TCs residues in honey samples. This method is highly reliable with few interfering peaks and avoids time-consuming treatment of samples before injection. Analysis time is greatly shortened in this way. Another advantage of the on-line method is the avoidance of the evaporation of samples. The TCs are thermo-labile substances. During the process of evaporation, the formation of epimers, which is a factor of sample loss, may occur. So the avoidance of the process improves the recoveries. It is the fundamental work to establish more convenient and simple method for the determination of TCs in honey.

Acknowledgement

This work was supported by the Development Program of the Ministry of Science and Technology of Jilin Province, China (grant number 20050560).

References

- [1] Ö. Erdoğrul, Food Control 18 (2007) 866.
- [2] S.P. Khong, Y.A. Hammel, P.A. Guy, Rapid Commun. Mass Spectrom. 19 (2005) 493.
- [3] A. Pena, N. Pelantova, C.M. Lino, M.I.N. Silveira, P. Solich, J. Agric. Food Chem. 53 (2005) 3784.
- [4] H. Oka, Y. Ikai, J. Hayakawa, K. Harada, H. Asukabe, M. Suzuki, R. Himei, M. Horie, H. Nakazawa, J.D. MacNeil, J. Agric. Food Chem. 42 (1994) 2215.

- [5] G.H. Wan, H. Cui, H.S. Zheng, J. Zhou, L.J. Liu, X.F. Yu, *J. Chromatogr. B* 824 (2005) 57.
- [6] S. Bogialli, R. Curini, A.D. Corcia, A. Lagana, G. Rizzuti, *J. Agric. Food Chem.* 54 (2006) 1564.
- [7] P. Viñas, N. Balsalobre, C. López-Erroz, M. Hernández-Córdoba, *J. Chromatogr. A* 1022 (2004) 125.
- [8] A.D. Corcia, M. Nazzari, *J. Chromatogr. A* 974 (2002) 53.
- [9] A.A.M. Stolker, U.A.T. Brinkman, *J. Chromatogr. A* 1067 (2005) 15.
- [10] W.C. Andersen, J.E. Roybal, S.A. Gonzales, S.B. Turnipseed, A.P. Pfening, L.R. Kuck, *Anal. Chim. Acta* 529 (2005) 145.
- [11] J.M. Traviesa-Alvarez, J.M. Costa-Fernández, R. Pereiro, A. Sanz-Medel, *Anal. Chim. Acta* 589 (2007) 51.
- [12] P. Masawat, J.M. Slater, *Sens. Actuators B* 124 (2007) 127.
- [13] W. Reybroeck, S. Ooghe, H.D. Brabander, E. Daeseleire, *J. Agric. Food Chem.* 55 (2007) 8359.
- [14] Y. Pang, H. Cui, H. Zheng, G. Wan, L. Liu, X. Yu, *Luminescence* 20 (2005) 8.
- [15] H. Nakazawa, S. Ino, K. Kato, T. Watanabe, Y. Ito, H. Oka, *J. Chromatogr. B* 732 (1999) 55.
- [16] S. Huq, M. Garriques, K.K.M.R. Kallury, *J. Chromatogr. A* 1135 (2006) 12.
- [17] N. Pastor-Navarro, S. Morais, Á. Maqueira, R. Puchades, *Anal. Chim. Acta* 594 (2007) 211.
- [18] H. Oka, Y. Ito, Y. Ikai, T. Kagami, K. Harada, *J. Chromatogr. A* 812 (1998) 309.
- [19] M.C.V. Mamani, J.A. Farfán, F.G.R. Reyes, S. Rath, *Talanta* 70 (2006) 236.
- [20] X. Wei, Z. Liu, S. Liu, *Anal. Biochem.* 346 (2005) 330.
- [21] M. Yang, Y. Xu, J.H. Wang, *Anal. Chem.* 78 (2006) 5900.
- [22] C.R. Anderson, H.S. Rupp, W. Wu, *J. Chromatogr. A* 1075 (2005) 23.
- [23] A.V. Pereira, Q.B. Cass, *J. Chromatogr. B* 826 (2005) 139.
- [24] R.V. Oliveira, A.C.D. Pietro, Q.B. Cass, *Talanta* 71 (2007) 1233.
- [25] L. Oliferova, M. Statkus, G. Tsysin, Y. Zolotov, *Talanta* 72 (2007) 1386.
- [26] E. Yamamoto, S. Takakuwa, T. Kato, N. Asakawa, *J. Chromatogr. B* 846 (2007) 132.
- [27] L. Tasso, T.D. Costa, *J. Pharm. Biomed. Anal.* 44 (2007) 205.
- [28] H.B. Bo, C.H. Liu, H.L. Zhang, Y.M. Li, L.R. Chen, *Chinese J. Anal. Chem.* 33 (2005) 515.
- [29] U. Koesukwiwat, S. Jayanta, N. Leepipatpiboon, *J. Chromatogr. A* 1149 (2007) 102.
- [30] H. Oka, Y. Ito, H. Matsumoto, *J. Chromatogr. A* 882 (2000) 109.
- [31] N.V. Eeckhout, J.C. Perez, J. Claereboudt, R. Vandeputte, C.V. Peteghem, *Rapid Commun. Mass Spectrom.* 14 (2000) 280.
- [32] D.S. Age, S. O'Connor, S. Ensley, J.O. Payero, D. Snow, D. Tarkalson, *J. Agric. Food Chem.* 53 (2005) 7165.
- [33] L. Chen, L. Ding, H. Jin, D. Song, H. Zhang, J. Li, K. Zhang, Y. Wang, H. Zhang, *Anal. Chim. Acta* 589 (2007) 239.

Immunonanogold-catalytic resonance scattering spectral assay of trace human chorionic gonadotrophin

Aihui Liang^a, Mingjing Zou^b, Zhiliang Jiang^{a,b,*}

^a Key Laboratory of New Processing Technology for Nonferrous Metals and Materials of Education Ministry, Guilin University of Technology, Guilin 541004, China

^b Guangxi Key Laboratory of Environmental Engineering, Protection and Assessment, Guangxi Normal University, Guilin 541004, China

Received 12 October 2007; received in revised form 7 January 2008; accepted 9 January 2008

Available online 18 January 2008

Abstract

Gold nanoparticles in diameter of 10 nm were used to label rabbit anti-human chorionic gonadotrophin (RhCG) antiserum to obtain a resonance scattering spectral probe (AuRhCG) for human chorionic gonadotrophin (hCG). The immunoreaction between AuRhCG and hCG take place to form hCG–AuRhCG immunocomplex in pH 5.0 citric acid–Na₂HPO₄ buffer solution. The immunocomplex solutions were centrifuged to obtain the supernatant solution. The AuRhCG in the supernatant solution exhibited strong catalytic effect on the particle reaction between Ag⁺ and hydroquinone to produce gold–silver composite particles in pH 3.4 citric acid–trisodium citrate buffer solution. There is a stronger resonance scattering (RS) peak at 423 nm for the particles. With the addition of hCG, the AuRhCG in the supernatant solution decreased, and the RS intensity at 423 nm decreased. The decreased RS intensity $\Delta I_{423\text{ nm}}$ was proportional to the concentration of hCG in the range of 2.5–208.3 mIU/mL with a detection limit of 0.83 mIU/mL. This method has been applied to the determination of hCG in urine samples, with satisfactory results. © 2008 Elsevier B.V. All rights reserved.

Keywords: Human chorionic gonadotrophin; Immunonanogold-catalytic silver-enhancement; Silver–gold composite particles; Resonance scattering spectral assay

1. Introduction

Gold nanoparticles have novel chemical and physical properties, high electron density and good biocompatibility [1–4]. It was applied to analytical chemistry and cytobiology as a good label for some macromolecules such as immunoglobulins [5], enzymes [6], lectins [7], and for cells [8]. Recently, the catalytic effect of immunonanogold on the Ag⁺-hydroquinone particle reaction was studied spectrophotometrically and electrochemically, and was utilized to develop some sensitive bioassays [9–11]. Resonance scattering (RS) analysis is a sensitive and simple technique [12–17]. To improve their selectivity, specific immunoreaction was combined with RS detection to assay some antigen, with good results [18]. It is necessary to enhance the sensitivity of immune RS assay, using nanocatalysis. However, there is no report using RS technique as detection to monitor

the immunonanogold-Ag(I)-hydroquinone nanocatalytic reaction, and combining RS effect of gold–silver composite particle and nanogold-labeled immunoreaction.

Human chorionic gonadotrophin (hCG) is an important hormone that is excreted by embryo and trophoblast. The secretion of hCG is proportional to the amount of trophoblast cells, so hCG assay is an important diagnostic target of all pregnancy tests and trophoblastic diseases such as chorionic carcinoma, invasive and non-invasive hydatidiform moles [19,20]. At present, several methods for hCG have been reported, including radioimmunoassay [21,22], electrochemical immunoassays [23–26], chemiluminescence immunoassay [27,28], fluorescence immunoassays [29,30], and colloidal gold-labeled spectrophotometry [31]. The radioimmunoassay with isotope ¹²⁵I-labeled anti-hCG was often used to assay hCG. However, its incubation lasts for a long time [21], while there were several disadvantages such as the narrow measuring range, poor sensitivity and the specially equipped laboratories [22]. A 0–2000 mIU/mL hCG was detected by an electrochemical immunoassay, but its assay course was also long [23]. Lately, a label-free electrochemical detection was

* Corresponding author. Tel.: +86 773 5846141; fax: +86 773 5846201.
E-mail addresses: zljjiang@mailbox.gxnu.edu.cn, zljjiang@glite.edu.cn (Z. Jiang).

reported, with a detection limit of about 20 mIU/mL hCG in human urine [24]. Horseradish peroxidase-labeled hCG antiserum and nanogold were used to fabricate an immunosensor for hCG, with a measuring range of 0.5–30.0 mIU/mL and a detection limit of 0.3 mIU/mL [26]. A micro-plate magnetic chemiluminescence enzyme immunoassay was based on alkaline phosphatase (ALP)-labeled anti-hCG for the determination of 0.15–500 mIU/mL hCG, its sensitivity was 13 times higher than that of the spectrophotometry. However, it also spent a comparatively long time to accelerate the incubation [28]. A fluorescence immunoassay with fluorescein isothiocyanate (FITC) label was used to determine 25–1500 mIU/mL hCG, but the regeneration of the capillary column was time-consuming and affected the activity of the antibody easily [29]. Europium and Samarium chelates were also used for label, 0.007–0.525 $\mu\text{g/mL}$ hCG was detected by time-resolved fluorometry, but the shortage is time-consuming [30]. Colloidal gold particles coated with rabbit anti-hCG were used in a spectrophotometric sandwich assay for the determination of 30–250 mIU/mL hCG [31]. However, the sensitivity is not high. Here, a sensitive and selective immunonangold-catalytic RS assay for hCG was proposed, coupling the catalytic effect of immunonangold on the reaction between Ag(I) and hydroquinone, and the RS effect of silver–gold composite nanoparticles.

2. Experimental

2.1. Reagents and apparatus

HAuCl_4 was obtained from the National Pharmaceutical Group Chemical Reagents Company and diluted to 1.0%. A 1000 IU/mL hCG purified was purchased from Lizhu Company. A 9.0 mg/mL Rabbit anti-human chorionic gonadotrophin (RhCG) purified by $(\text{NH}_4)_2\text{SO}_4$ was purchased from Zhongke Shenglongda Biological Reagents Limited Company and diluted to 0.45 mg/mL as labeling solution. A 0.2 mol/L NaH_2PO_4 and 0.1 mol/L citrate acid were used to prepare pH 3.8–7.2 buffer according to a certain volume ratio. A 0.1 mol/L trisodium citrate and citrate acid were used to prepare pH 3.0–6.6 buffer. A 0.1 mol/L HCl, 0.1 mol/L K_2CO_3 , 10.0% KCl and 1.0% trisodium citrate were also used. 1.1 mg/mL silver acetate (AgAc) and 10.0 mg/mL hydroquinone were prepared freshly. All reagents were of analytical grade and doubly distilled water was used.

A Cary Eclipse Spectrofluorometer (Varian) and RF-540 Spectrofluorometer (Shimadzu) were used to record the RS Spectrum and measure the RS intensity. A H-600 transmission electron microscope (TEM) (Electronic Stock Limited Company) was used to observe the appearance of gold and gold–silver composite nanoparticles. A 79-1 magnetic heat beater (Zhongda Instrumental Plant), a SK8200LH ultrasonic reactor (Kedao Ultrasonic Instrument Limited Company), a YGL-16G centrifugal machine (Anting Science Instrumental Plant) and a SYZ-550 Quartz Sub-boiling machine (Jingbo Instrument plant) were also used.

2.2. Preparation and identification of gold nanoparticles

Gold nanoparticles were prepared by the improved trisodium citrate-reduced procedure as follows [32]. 250 mL of double distilled water and 15.0 mL of 1.0% trisodium citrate were added in a conical flask and boiled for 5 min, and then 2.50 mL of 1.0% HAuCl_4 solution was added into boiling solution while stirring. The mixed solution was boiling for another 15 min, cooled, diluted to 250 mL and stored. Three methods identify the suitable gold nanoparticles for our work. First, the diameter and the appearance of gold particles were observed by transmission electron microscope. An average diameter was controlled less than 10 nm, the distribution and diameter should be homogeneous. Second, λ_{max} was controlled at about 516 nm [33]. Third, the RS intensity at 580 nm ($I_{580\text{nm}}$) increased with the diameter of gold nanoparticles, the intensity of 19.3 $\mu\text{g/mL}$ colloidal gold solution was controlled at 7.0 ± 2 .

2.3. Preparation of immunogold probe

The labeling pH was adjusted and tested by RS method. The successful conjugation of colloidal gold and RhCG depends on pH condition. We tested the effect of different pH on conjugation by RS method. We adjusted 1.0 mL of 57.96 $\mu\text{g/mL}$ colloidal gold solutions to different pH by adding 0.10 mol/L K_2CO_3 or 0.10 mol/L HCl, and then 20 μL of 0.45 mg/mL RhCG was added respectively. After 5 min, 0.10 mL of 10% KCl solution was added. Two hours later, the solution was diluted to 3.0 mL and $I_{580\text{nm}}$ was determined. When the pH is less than 5.5, $I_{580\text{nm}}$ enhanced since colloidal gold solution aggregated. When the pH is more than 5.5, gold nanoparticles were not aggregate by KCl solution. The intensity lowered and stabilized. A pH 6.5 was chosen in this assay.

The amount of RhCG was selected. We adjusted 1.0 mL of colloidal gold solution to pH 6.5 by adding about 15.0 μL of 0.1 mol/L K_2CO_3 , and different volumes (0, 5.0, 10.0, 15.0, 20.0, 25.0, 30.0, 35.0, 40.0, 45.0 and 50.0 μL) of RhCG were added respectively. Five minutes later, we added 0.10 mL of 10.0% KCl solution, mixed well and stored for 2 h, and then diluted it to 3.0 mL, respectively. $I_{580\text{nm}}$ was recorded. The results showed stronger RS intensities for the tubes with 0–10.0 μL of RhCG than those in the tubes with 15.0–50.0 μL of it. To ensure the accurate labeling amount, we chose 10.0, 15.0 and 20.0 μL of RhCG for labeling, respectively. We used 10.0 μL of RhCG as the minimum amount, the gold nanoparticles were not coated by RhCG completely, the blank signals were strong. For the 15.0 μL of RhCG, we obtained a good working curve between the RS intensities and the concentration of hCG. For the 20.0 μL of RhCG, redundant antiserum left, the linear relation became bad or disappeared. A 15.0 μL of RhCG as the minimum use level was chosen to stabilize 1.0 mL of colloidal gold.

The AuRhCG was prepared. A 100 mL of colloidal gold solution was adjusted to pH 6.5. During the magnetic stirring, 1.50 mL of RhCG was added slowly, and stirred for 10 min. Then we added 1.63 mL of 3.0% PEG20000 as stabilizer and

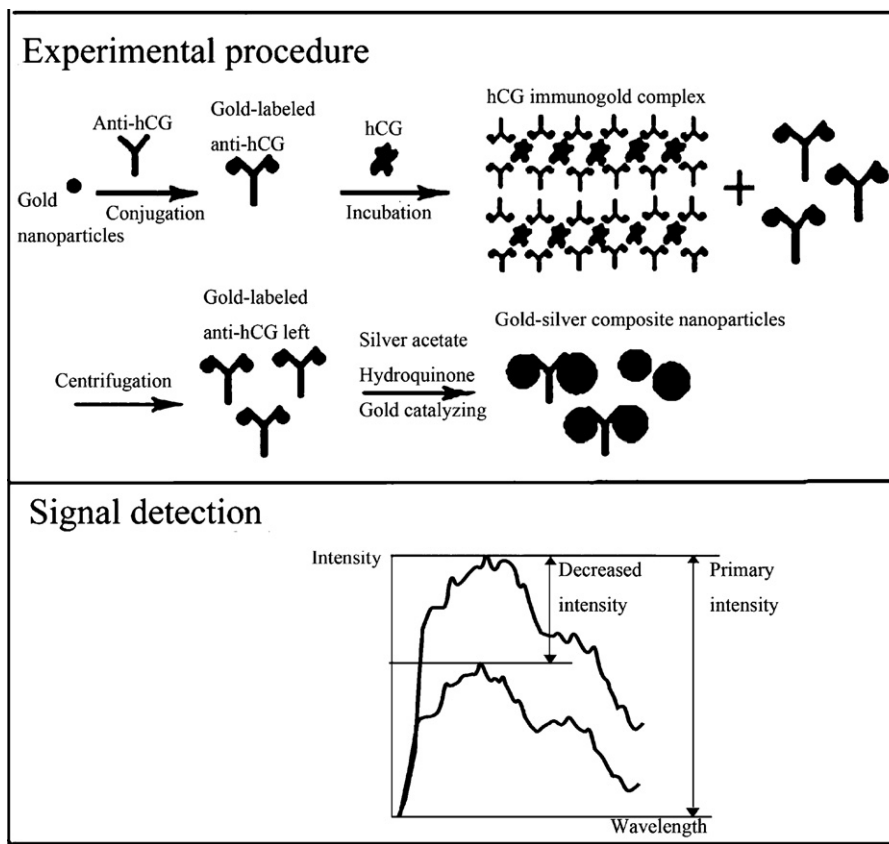


Fig. 1. Resonance scattering spectral detection principle.

kept its last concentration at 0.05%. Later, the solution containing 6.45 $\mu\text{g}/\text{mL}$ AuRhCG was stirred for another 30 min and stored at 4 °C. The results of unpurified AuRhCG were consistent with those for purified AuRhCG. We used the unpurified AuRhCG.

2.4. Procedure

A 1.0 mL of pH 5.0 citrate acid– Na_2HPO_4 buffer, 1.0 mL of 6.45 $\mu\text{g}/\text{mL}$ AuRhCG, certain quantity of hCG were successively added, diluted to 3.0 mL, mixed thoroughly and incubated in a ultrasonic reactor (59 kHz) for 20 min at 20 °C. And then the immunogold complex solution was centrifuged for 40 min at the speed of 13,000 rpm, certain volume of the supernatant solution was taken out and stored.

In a 10-mL mark tubes, 0.60 mL of pH 3.4 trisodium citrate–citrate acid buffer, 1.0 mL of the supernatant, 60.0 μL of 1.1 mg/mL silver acetate were orderly added, mixed thoroughly and reacted in a ultrasonic reactor (59 kHz) for 10 min at 28 °C. Later, 40.0 μL of 10.0 mg/mL hydroquinone was added and irradiated for 5 min at 28 °C, and then diluted to 3.0 mL. Working voltage of 400 V, the excited slit and emission slit of 5 nm were chosen, the synchronous scattering spectrum was recorded by means of the synchronous scanning under the condition of the excited wavelength λ_{ex} and emission wavelength λ_{em} ($\lambda_{\text{ex}} - \lambda_{\text{em}} = \Delta\lambda = 0$), the $I_{423 \text{ nm}}$ and $(I_{423 \text{ nm}})_b$ of the blank were measured. Then, $\Delta I_{423 \text{ nm}} = (I_{423 \text{ nm}})_b - I_{423 \text{ nm}}$ was calculated.

3. Results and discussion

Under the suitable conditions, the hCG–AuRhCG immunocomplex can be removed by centrifuging, as shown in Fig. 1. The free AuRhCG in supernatant solution strongly catalyzed the reduction of Ag^+ to Ag on the surface of the immunogold to produce gold–silver composite nanoparticles in big size. The composite nanoparticles exhibited a stronger RS peak at 423 nm. The left amount of AuRhCG in the supernatant solution decreased, their catalyzing effect diminished and the RS intensity at 423 nm decreased with hCG quantity increasing. The decreased RS intensity at 423 nm $\Delta I_{423 \text{ nm}}$ was linear to the hCG concentration.

3.1. Transmission electron microscope

Fig. 2 shows transmission electron microscope images of hCG immunogold complex and silver–gold composite nanoparticles. An average diameter of 10 nm was found for the spherical gold nanoparticles, the distribution and diameter are homogeneous. When the gold-labeled antiserum was prepared, nanoparticles dispersed and kept their original diameter. When 2.15 $\mu\text{g}/\text{mL}$ AuRhCG was incubated with 750.0 mIU/mL hCG and the immunogold complex formed, gold nanoparticles also kept their original diameter and dispersed (Fig. 2a). After the catalytic silver-enhancements, there are composite nanoparticles in different sizes and aggregations (Fig. 2b).

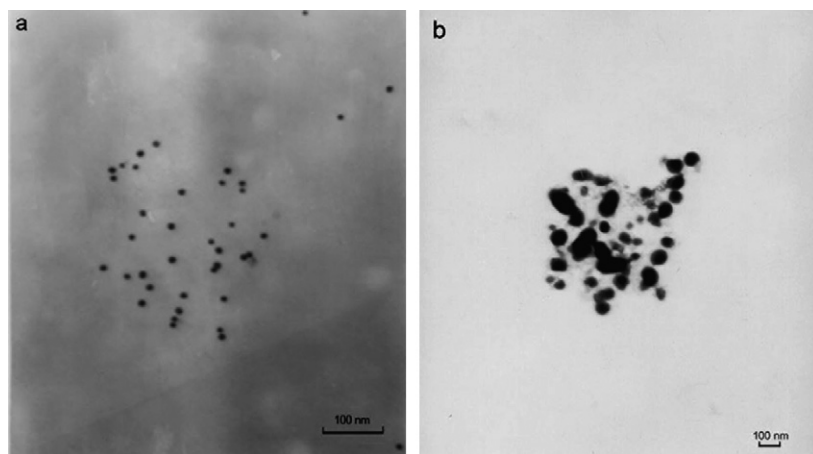


Fig. 2. Transmission electron microscopy: (a). pH 5.0 NaH_2PO_4 –citrate acid buffer– $2.15 \mu\text{g/mL}$ AuRhCG– 750.0 mIU/mL hCG; (b) silver–gold composite nanoparticles–pH 3.4 trisodium citrate–citrate acid buffer $22.0 \mu\text{g/mL}$ AgAc– $133.3 \mu\text{g/mL}$ hydroquinone– $0.717 \mu\text{g/mL}$ AuRhCG– 250.0 mIU/mL hCG.

3.2. Resonance scattering spectrum

The scattering signals of RhCG, hCG and its immunocomplex are very weak. The immunogold probe (AuRhCG) almost kept the same shape as the RS spectrum of gold nanoparticles, and its scattering signals enhanced a little. Used the supernatant solution as catalyst, the formed composite nanoparticles exhibited five synchronous scattering peaks at 360, 423, 465, 488 and 570 nm, the $I_{423 \text{ nm}}$ enhanced evidently (Fig. 3).

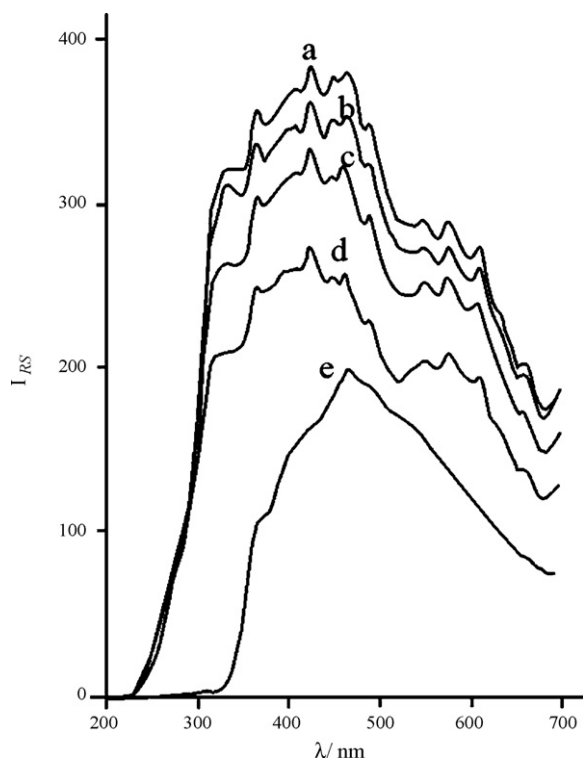


Fig. 3. RS spectrum of the gold–silver composite nanoparticles: pH 3.4 trisodium citrate–citrate acid buffer– $22.0 \mu\text{g/mL}$ silver acetate $133.3 \mu\text{g/mL}$ hydroquinone– $0.717 \mu\text{g/mL}$ AuRhCG: (a) blank; (b) 41.7 mIU/mL hCG; (c) 83.3 mIU/mL hCG; (d) 166.7 mIU/mL hCG; (e) the emission intensity distribution of lamp source on Cary Eclipse Spectrofluorometer.

The synchronous scattering spectrum of liquid-phase inorganic nanoparticles indicates that three factors, including lamp source, free molecular absorption and the RS effect of nanoparticles, produce the synchronous scattering peaks. According to the reference [34], using the principle of planar mirror, we place a baffle in diameter of 3 cm in the front of emission slit and got the distribution of emission intensity by means of synchronous scanning, the strongest emission peak of the apparatus at 465 nm is proved. Owing to the apparatus peak at 465 nm, a synchronous scattering peak at 465 nm appears. The molecular absorption of citrate acid and hydroquinone in visible region was weak, and the effect can be neglected. Besides the peak at 465 nm, the other synchronous scattering peaks are RS peaks. A wavelength of 423 nm was chosen for assay.

3.3. Optimization of the immunoreaction conditions

Used 83.3 mIU/mL hCG as a example, the optimal conditions were considered. Firstly, we tested the effect of citric acid– Na_2HPO_4 (pH 3.8–7.2) buffer solution on $\Delta I_{423 \text{ nm}}$. The $\Delta I_{423 \text{ nm}}$ increased considerably in pH 4.8–5.6 buffer, the optimum $\Delta I_{423 \text{ nm}}$ occurred in 1.0 mL of pH 5.0 buffer. Secondly, we found $\Delta I_{423 \text{ nm}}$ increased in the range of 0 – $0.717 \mu\text{g/mL}$ AuRhCG, we chosen $0.717 \mu\text{g/mL}$ AuRhCG. Thirdly, the effect of ultrasonic irradiation was tested. The incubation in the ultrasonic irradiation was relatively quick and $\Delta I_{423 \text{ nm}}$ kept stable after 15 min (Fig. 4). The incubation in 37°C water completed and $\Delta I_{423 \text{ nm}}$ stabilized after 40 min while it ended at room temperature of 28°C after 60 min. Thus, a 20 min ultrasonic irradiation at 28°C was chosen.

3.4. Optimization of immunogold catalyzing condition

The optimum catalyzing conditions were examined. The $\Delta I_{423 \text{ nm}}$ kept stabilizing and changed little in the range of $12,000$ – $14,000 \text{ rpm}$. The $\Delta I_{423 \text{ nm}}$ increased in 0 – 40 min and stabilized in 30 – 55 min . Later, the $\Delta I_{423 \text{ nm}}$ decreased evidently. Thus, centrifuging at the speed of $13,000 \text{ rpm}$ for 40 min was chosen for use. The optimum $\Delta I_{423 \text{ nm}}$ occurred in 0.60 mL of pH

Table 1
The influence of coexistent substance

Coexistent substance	Tolerance ($\mu\text{g/mL}$)	Relative error (%)	Coexistent substance	Tolerance ($\mu\text{g/mL}$)	Relative error (%)
Dextrose	1300	8.0	DL-Tryptophan	18	-1.9
L-Arginine	18	6.0	Cane sugar	1300	7.8
Glycine	18	5.2	L-Aspartate	40	6.7
HSA	105	-7.2	BSA	13	-6.2
IgG	13	-8.2	L-Tyrosine	89	4.7
IgA	5	-8.3	IgM	2	-8.0
Urea	133	-9.3	Dodecyl benzene Sulfonate	6	8.2
Vitamin B ₂	2	-0.1	Vitamin C	44	-9.6
Quinine sulfate	27	-6.4	L-Glutamate	40	-5.1
Vitamin K	53	-2.9	Niacin	40	4.9
Vitamin B ₁	89	-0.4	Alexin C ₃	3	-8.0
L-Cystine	13	-5.8	L-Lysine	27	-6.4
Alexin C ₄	0.4	-8.0	Ni ²⁺	39	-9.3
Folic acid	1	-9.5	Mg ²⁺	32	6.7
DL-Methionine	40	-2.2	Mn ²⁺	10	9.5

3.4 citric acid–trisodium citrate buffer solutions. The $\Delta I_{423 \text{ nm}}$ increased linearly with the increasing amount of supernatant solution in the range of 0–1.0 mL, the linear regression equation was $\Delta I_{423 \text{ nm}} = 53.5 V + 5.0$, the correlation coefficient was 0.989. The $\Delta I_{423 \text{ nm}}$ decreased beyond 1.0 mL. The maximum $\Delta I_{423 \text{ nm}}$ took place when 1.0 mL of the supernatant solution was added. The $\Delta I_{423 \text{ nm}}$ increased with the addition of silver acetate in the range of 0–14.7 $\mu\text{g/mL}$. When silver acetate was added over 14.7 $\mu\text{g/mL}$, the $\Delta I_{423 \text{ nm}}$ increased slowly. The $\Delta I_{423 \text{ nm}}$ reached the maximum at 22.0 $\mu\text{g/mL}$ silver acetate solution. When the added hydroquinone was more than 100.0 $\mu\text{g/mL}$, the $\Delta I_{423 \text{ nm}}$ was bigger. A maximum $\Delta I_{423 \text{ nm}}$ got at 133.3 $\mu\text{g/mL}$ hydroquinone (Fig. 5). Besides, the effect of immunonanogold catalyzing time was tested. At room temperature of 28 °C, silver acetate was added in the supernatant solution, deposited for 15 min, and then hydroquinone was added. After 30 min, $\Delta I_{423 \text{ nm}}$ was maximum, later, with the time going, $\Delta I_{423 \text{ nm}}$ dropped slowly. In the ultrasonic irradiation at 28 °C, silver acetate was added and irradiated for 10 min, and then hydro-

quinone was added, reacted for another 5 min, $\Delta I_{423 \text{ nm}}$ reached the maximum, after 10 min, $\Delta I_{423 \text{ nm}}$ lowered evidently in irradiation. We chose the latter for use.

3.5. Selectivity

The influence of coexistent substance such as proteins, amino acids and inorganic ions on the determining 83.3 mIU/mL hCG was examined. The tolerance limit was taken as the maximum concentration of the coexistent substance that resulted in approximately $\pm 10\%$ relative error in the determination. As shown in Table 1, the examined coexistent substances did not significantly interfere in the analysis, thus it has a good selectivity.

3.6. Working curve

The different hCG concentrations and their corresponding intensities $I_{423 \text{ nm}}$ were recorded to obtain the working curve. hCG concentrations C_{hCG} in range of 2.5–208.3 mIU/mL is lin-

Table 2
Results for hCG

Sample	hCG content ($n = 7$, IU/mL)	R.S.D. (%)	IS results (IU/mL)	hCG added (mIU)	hCG found (mIU)	Recovery (%)
1	35.69 \pm 1.89	5.3	40.50	200	196.8	98.4
2	33.32 \pm 1.55	4.6	30.60	200	194	97.0
3	25.98 \pm 1.16	4.5	26.22	100	106.7	106.7
4	31.01 \pm 1.61	5.2	32.25	100	97.0	97.0
5	13.16 \pm 1.10	8.4	13.10	100	19.5	97.5
6	16.29 \pm 0.99	6.0	15.80	100	105	105
7	36.22 \pm 1.19	3.3	36.20	200	202	101
8	12.31 \pm 0.76	6.1	13.70	100	97.0	97.0
9	9.57 \pm 0.92	9.6	8.30	100	96.0	96.0
10	10.40 \pm 0.75	7.3	14.1	100	99.0	99.0
11	27.57 \pm 1.20	4.3	30.50	100	102	102
12	16.20 \pm 0.99	6.1	16.10	100	95.0	95.0
13	28.35 \pm 0.76	2.7	29.40	100	105	105
14	31.31 \pm 0.93	3.0	30.62	200	204.4	102.2
15	37.10 \pm 0.88	2.4	39.60	200	206	103
16	0.154 \pm 0.024	5.2	0.171	100	105	105
17	0.241 \pm 0.033	4.2	238	100	101.5	101.5
18	0.266 \pm 0.036	5.6	0.270	100	102	102

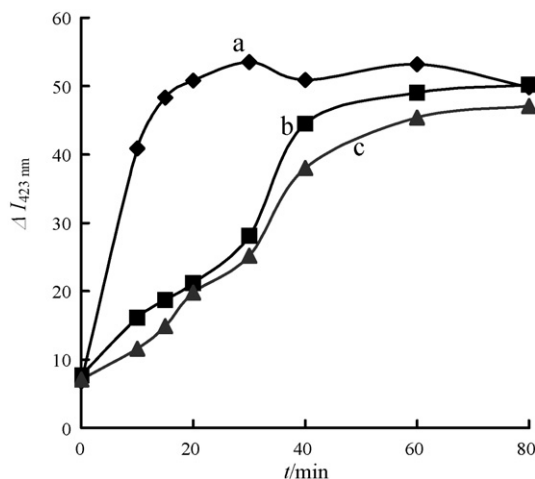


Fig. 4. Effect of incubation time on $\Delta I_{423\text{ nm}}$: (a) pH 3.4–22.0 $\mu\text{g/mL}$ AgAc–133.3 $\mu\text{g/mL}$ hydroquinone–0.717 $\mu\text{g/mL}$ AuRhCG–83.3 mIU/mL hCG–ultrasonic irradiation 28 °C; (b) pH 3.4–22.0 $\mu\text{g/mL}$ AgAc–133.3 $\mu\text{g/mL}$ hydroquinone–0.717 $\mu\text{g/mL}$ AuRhCG–83.3 mIU/mL hCG–37 °C; (c) pH 3.4–22.0 $\mu\text{g/mL}$ AgAc–133.3 $\mu\text{g/mL}$ hydroquinone–0.717 $\mu\text{g/mL}$ AuRhCG–83.3 mIU/mL hCG–28 °C.

ear to the decreased intensity $\Delta I_{423\text{ nm}}$. The linear regression equation, correlation coefficient and detection limit [35] for hCG are $\Delta I_{423\text{ nm}} = 0.678 C_{\text{hCG}} + 0.17$, 0.9982 and 0.83 mIU/mL. Compared with the reported assay for hCG [23–28,36,37], the assay has high-sensitivity, good-selectivity and simplicity, with the wider linear range.

3.7. Analysis of samples

Urine samples for women were offered by No.5 Hospital of Guilin City, China. Samples were pre-treated by centrifuging at 3500 rpm for 30 min and diluted to suitable concentration. Following operations were according to the procedure, the results were showed in Table 2, and were agreement with that of the immunospectrophotometry (IS) [36]. The recovery was in the range of 95.0–106.7%.

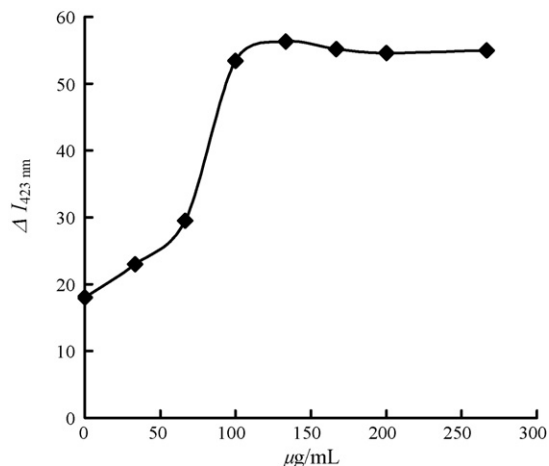


Fig. 5. Effect of hydroquinone concentration on $\Delta I_{423\text{ nm}}$: pH 3.4–22.0 $\mu\text{g/mL}$ AgAc–0.717 $\mu\text{g/mL}$ AuRhCG–83.3 mIU/mL hCG.

4. Conclusion

Combining the nanogold-labeled technique and RS detection technique with immunonanogold catalytic effect, a new immunonanogold-catalytic silver-enhancement RS assay for hCG was developed. This assay was applied to detect hCG in real samples, with high sensitivity, good selectivity, wide linear range, and less used amount of sample. In further work, this new idea could be extended to other immunoprotein assay to improve their sensitivity.

Acknowledgements

This work was supported by the National Natural Science Foundation of China (Grant Nos. 20365001 and 20667001), Guangxi Science Foundation (Grants No. 0728213), and the Foundation of New Century Ten-Hundred-Thousand Talents of Guangxi.

References

- [1] H.C. Chu, C.H. Kuo, M.H. Huang, *Inorg. Chem.* 45 (2006) 808.
- [2] J.H. Huang, J.H. Lv, H.J. An, X.D. Zhang, Z.Z. Zhou, C.H. Fan, J. Hu, *Angew. Chem. Int. Ed.* 44 (2005) 5100.
- [3] K. Sato, K. Hosokawa, M. Maeda, *J. Am. Chem. Soc.* 125 (2003) 8102.
- [4] A. Henglein, D. Meisel, *Langmuir* 14 (1998) 7392.
- [5] C. Zhang, Z.Y. Zhang, B.B. Yu, J.J. Shi, X.R. Zhang, *Anal. Chem.* 74 (2002) 96.
- [6] R. Kumar, A.N. Maitra, P.K. Patanjali, S. Parvesh, *Biomaterials* 26 (2005) 6743.
- [7] D.C. Hone, A.H. Haines, D.A. Russell, *Langmuir* 19 (2003) 7141.
- [8] S. Takae, Y. Akiyama, H. Otsuka, T. Nakamura, Y. Nagasaki, *Biomacromolecules* 6 (2005) 818.
- [9] Z.F. Zhang, H. Cui, M.J. Shi, *Phys. Chem. Chem. Phys.* 8 (2006) 10176.
- [10] Y.Y. Chen, J.S. Qiu, X.K. Wang, J.H. Xiu, *J. Catal.* 242 (2006) 227.
- [11] X. Chu, X. Fu, K. Chen, G.L. Shen, R.Q. Yu, *Biosens. Bioelectron.* 20 (2005) 1805.
- [12] S.P. Liu, H.Q. Luo, N.B. Li, Z.F. Liu, W.X. Zheng, *Anal. Chem.* 73 (2001) 3907.
- [13] Z.L. Jiang, S.M. Zhou, A.H. Liang, C.Y. Kang, X.C. He, *Environ. Sci. Technol.* 40 (2006) 4286.
- [14] R.P. Jia, H.L. Zhai, Y. Shen, X.G. Chen, Z.D. Hu, *Talanta* 64 (2004) 355.
- [15] H. Zhong, J.J. Xu, H.Y. Chen, *Talanta* 67 (2005) 749.
- [16] C.Z. Huang, Y.F. Li, *Talanta* 70 (2006) 609.
- [17] Z.P. Li, X.R. Duan, C.H. Liu, B.A. Du, *Anal. Biochem.* 351 (2006) 18.
- [18] Z.L. Jiang, S.J. Sun, A.H. Liang, W.X. Huang, A.M. Qin, *Clin. Chem.* 52 (2006) 1389.
- [19] K. Mann, H.J. Karl, *Cancer* 52 (1983) 654.
- [20] M.M. Elliott, A. Kardana, J.W. Lustbader, L.A. Cole, *Endocrine* 7 (1997) 15.
- [21] A. Banerjee, N.S. Srilatha, G.S. Murthy, *Biochim. Biophys. Acta* 1569 (2002) 21.
- [22] S. Madersbacher, P. Berger, *Methods* 21 (2000) 41.
- [23] T.K. Lim, T. Matsunaga, *Biosens. Bioelectron.* (2001) 1063 (16).
- [24] K. Kerman, N. Nagatani, M. Chikae, T. Yuhi, Y. Takamura, E. Tamiya, *Anal. Chem.* 78 (2006) 5612–5616.
- [25] J. Chen, F. Yan, Z. Dai, H.X. Ju, *Biosens. Bioelectron.* 21 (2005) 330.
- [26] J. Chen, J.H. Tang, F. Yan, H.X. Ju, *Biomaterials* 27 (2006) 2313.
- [27] H. Sasamoto, M. Maeda, A. Tsuji, H. Manita, *Anal. Chim. Acta* 309 (1995) 221.
- [28] L.X. Zhao, J.M. Lin, F. Qu, *Acta Chim. Sin.* 62 (2004) 71.

- [29] N. Nakamura, T.K. Lim, J.M. Jeong, T. Matsunaga, *Anal. Chim. Acta* 439 (2001) 125.
- [30] Q.P. Qin, M. Christiansen, T. Lovgren, B. Norgaard-Pedersen, K. Pettersson, *J. Immunol. Methods* 205 (1997) 169.
- [31] J.H.W. Leuvering, P.J.H.M. Thal, A.H.W.M. Schuurs, *J. Immunol. Methods* 62 (1983) 175.
- [32] Z.L. Jiang, M.J. Zou, A.H. Liang, *Clin. Chim. Acta* 387 (2008) 24.
- [33] Z.L. Jiang, Z.W. Feng, T.S. Li, F. Li, F.X. Zhong, J.Y. Xie, X.H. Yi, *Sci. China Ser. B* 31 (2001) 183.
- [34] Z.L. Jiang, S.P. Liu, S. Chen, *Spectrochim. Acta A* 58 (2002) 3121.
- [35] Z.G. Chen, J.B. Liu, Y.L. Han, *Talanta* 71 (2007) 1246.
- [36] J. Guo, S.K. Lv, *J. Clin. Lab. Sci.* 4 (1986) 114.
- [37] P.V. Lode, J. Rainaho, K. Pettersson, *Clin. Chem.* 50 (2004) 1026.

Application of microwave heating for the fast extraction of fat content from the poultry feeds

S.A. Mahesar^a, S.T.H. Sherazi^{a,*}, Kamran Abro^a, Aftab Kandhro^a,
M.I. Bhangar^a, F.R. van de Voort^b, J. Sedman^b

^a National Center of Excellence in Analytical Chemistry, University of Sindh, Jamshoro 76080, Pakistan

^b McGill IR Group, McGill University, Montreal, Quebec, Canada

Received 8 October 2007; received in revised form 11 January 2008; accepted 11 January 2008

Available online 1 February 2008

Abstract

A rapid method has been developed to extract and quantitatively measure the total oil content in poultry feeds using a domestic microwave oven. The optimized extraction procedure involves the replicate (6×) extraction of 5 g of ground feed with 12 ml of hexane for 20 s in a 900 W oven. Each replicate involves the collection of the resulting miscella and its replacement with fresh solvent for re-extraction. The collected extracts were centrifuged and transferred to a vial. The solvent was evaporated to a constant weight and the residual lipid weighed. In comparison to conventional Soxhlet extraction method, lipid contents obtained using the optimized microwave procedure was not significantly different. However, FTIR analysis indicated that the microwave procedure was superior in minimizing the formation of free fatty acids (FFA) relative to the Soxhlet procedure if the temperature of the sample was kept within the range of 45–50 °C. This simple, sequential extraction procedure is rapid, highly efficient and provides a simple mean of quantitating the lipid content of poultry feed in less than 40 min without the need for specialized microwave oven.

© 2008 Elsevier B.V. All rights reserved.

Keywords: Poultry feed; Oil content; Microwave extraction; FFA; FTIR

1. Introduction

Poultry feed generally consists of agro-based industrial byproducts containing lipid, protein, as well as supplemental vitamins, minerals and antibiotics. A wide range of commodity byproducts such as maize, sorghum, broken rice, or meals of various types (fish, meat, bone, blood, etc.) [1–3] are commonly used in manufactured poultry feeds. Feed composition plays an important role in feed intake, growth and the development of bird abdominal fat and breast muscle, including its fatty acid composition [4,5]. The lipid content in particular as well as compositions are also nutritionally important in poultry feed nutrition, specifically in increasing the energy value of the ration to levels unattainable with other ingredients. Direct lipid supplementation with fats is often the most economical means of increasing available energy, leading to

enhanced growth rates and shorter production times while permitting the inclusion of other lower-energy, lower-cost ingredients. With some FA being essential, fats are a means by which these FA can be provided [6,7] as well as increasing palatability, reducing the dust associated with compounded feeds and improving the operating efficiency of palletizing machines by reducing the wear on pellet dies. Dietary fats vary appreciably in composition, their energy and FA contributions, with their digestibility varying widely, depending on the type of fat, its level of saturation, age of bird, level of fat inclusion in the diet and presence of other dietary components [8]. Ultimately, the energy value of lipids depends largely upon the lipid quality, its efficient hydrolysis and absorption of the resultant fatty acids [9].

With the lipid content of feed formulations being critical, the accurate assessment of total extractable lipid is a key indicator of the energy content of the feed, however, conventional Soxhlet solvent extraction technique to assess this parameter are both tedious and time consuming. Microwaves (MW) are composed of an electric and magnetic field and thus represent electromag-

* Corresponding author. Tel.: +92 22771379; fax: +92 22771560.
E-mail address: tufail.sherazi@yahoo.com (S.T.H. Sherazi).

netic energy. The spectral frequency of MW ranges from 300 to 300,000 MHz [10]. Microwave energy acts as a nonionising radiation that causes rotation of the dipoles, but does not affect molecular structure. Domestic microwave oven is very common electrical device used for heating the food. Generally it comprises a source of microwave radiation such as a magnetron, and a chamber which serves as a multi-mode microwave cavity. Normally domestic microwave oven operates at a fixed frequency of 2.45 GHz. Microwave energy is precisely controllable and can be turned on and off instantly, eliminating the need for warm-up and cool-down. Therefore, the periodic heating and cooling produces thermal stresses in the substrate and hence causing the substrate to dissolve in the solvent [11]. Microwave dielectric heating depends on the ability of materials to absorb MW energy and convert it to heat. The mechanism of energy transfer by means of a microwave field is greatly different from the well-established modes (radiation, conduction, and convection) of heat transfer [12].

Recently, microwave-assisted extraction (MAE) has engrossed increasing interest as it allows fast extractions of solutes from plant material, with extraction efficiency similar to that of the classical techniques. There are many applications of MAE which deal with the extraction of oils from herbs and spices [13–16]. The MAE is rapidly replacing other extraction methods such as Soxhlet, sonication, supercritical fluid extraction [17,18]. Furthermore, it considerably reduces extraction time, energy consumption, enhances the efficiency of the extraction and is environment friendly technique [19–21]. Microwave systems specifically designed for assisting extraction processes are commercially available, however, they are priced several magnitudes higher than conventional domestic microwave ovens. In a recent study [22], we have reported the use of a domestic microwave oven to extract a portion of oil for qualitative point of view from the poultry feeds and free fatty acid (FFA) content of the feed lipid was determined by single bounce attenuated total reflectance (SB-ATR) Fourier transform infrared (FTIR) spectroscopy. The time savings and simplicity of using MAE to obtain lipid samples for analysis led us to consider examining this procedure from a *quantitative* standpoint. The objective of this study was to determine whether microwave extraction using a domestic microwave oven could serve as a rapid procedure to determine the total lipid content of poultry feed in comparison to sonication and conventional Soxhlet extraction.

2. Experimental

2.1. Reagents and samples

All reagents used were of analytical grade. Oleic acid (99%) and sodium hydroxide were purchased from Fluka Chemie GmbH (Buchs, Switzerland). Hexane was obtained from Fisher Scientific U.K. Ltd., and propanol was purchased from Merck (Darmstadt, Germany). Refined, bleached, and deodorized (RBD) canola oil was obtained locally and poultry feed samples collected from industry suppliers.

2.2. Preparation and extraction

2.2.1. Soxhlet and sonication

Poultry feed samples were ground using a Mammonlex super blender mill grater 3 (No: 4AO-0018, Type JW-1001, Taiwan), sifted through 1.0 mm mesh screen to obtain a uniform particle size and kept in plastic bags until required for extraction. Four procedures were used to extract oil from all the poultry feed samples; Soxhlet extraction (SE), sonication (SO), single microwave-assisted extraction (SiMAE) and sequential microwave assisted extraction (SeMAE). Soxhlet extraction (AOAC 920.39) [23] involved the extraction of 5 g of feed for 6 h in a 250 ml Soxhlet extractor using 150 ml hexane. At the end of the extraction, the solvent was recovered by distillation using rotary evaporator and the residual oil was oven-dried at 75 °C for 1 h. The oil was then transferred to a desiccator and allowed to cool before being weighed. The drying, cooling and weighing was repeated until a constant dry weight within 0.01 g was obtained. Ultrasonic extraction involved placing 5 g of feed and 100 ml of solvent in an Erlenmeyer flask and sonicating in an ultrasonic bath (Sonicor, SC-121 TH, Copiague, NY, USA) for 60 min at 40 kHz and 40 °C [24]. At the end of the extraction cycle, the miscella was centrifuged to remove the any fines, the solvent was recovered and the residual oil dried and weighed as per the Soxhlet procedure. Microwave extraction was carried out using a Pell-PM 023 domestic microwave oven (Japan) with adjustable power settings ranging from 100 to 900 W. For the SiMAE procedure, 5 g of ground poultry feed was placed in a 30 ml screw capped vial containing 12 ml hexane and subjected to 900 W of microwave energy for 20 s. At this point, the vial was taken out of the oven and shaken vigorously and replaced in the oven. This procedure was repeated until a cumulative 10 min of microwave exposure had been reached, the miscella centrifuged, solvent removed and the residual oil dried and weighed. In SeMAE the same basic procedure was followed, except that after reaching 2 min of cumulative microwave extraction time the miscella was collected and replaced with fresh solvent. This process was repeated four more times to attain a total of 10 min of microwave exposure. Poultry feed residues left over from the microwave extractions were re-extracted using the Soxhlet procedure to determine whether any residual extractable lipid was present in these samples.

2.2.2. FTIR free fatty analysis (FFA) analysis

The oils extracted from the poultry feed samples obtained by all extraction procedures were analyzed for FFAs by FTIR using a ZnSe SB-ATR accessory [22]. All infrared spectra were acquired using a Thermo Nicolet Avatar 330 FTIR spectrometer equipped with a deuterated triglycine sulfate (DTGS) detector and KBr optics and controlled by OMNIC software (Thermo Nicolet Analytical Instruments, Madison, WI) with spectra collected by co-addition of 32 scans at a resolution of 8 cm⁻¹. The spectrum of each sample was rationed against a fresh background spectrum recorded from the bare ATR crystal cleaned with propanol to remove any residues of the previous sample and the residual solvent evaporated using a stream of nitrogen gas.

3. Result and discussion

3.1. Time effects on oil extraction and FFA content

For the microwave extraction procedure, various parameters including the hexane to sample ratio, time of microwave heating in relation to the temperature attained and solvent replacement were evaluated and optimized. In contrast to microwave heating of moist biological systems (e.g., foodstuffs), microwave coupling in dried products occurs largely as a result of the dipole provided by the ester linkage of the lipid component as non-polar hexane has little microwave energy absorption capacity. With contrast to conductive heating, microwave heats the whole sample volume simultaneously. It interrupts weak hydrogen bonds by promoting the rotation of molecular dipoles, an effect that is opposed by the viscosity of the medium. The rotation of the dipoles in an alternating field causes friction, which produces heat [25].

Therefore, MW heating can have different nature than conventional heating techniques, depending on the absorbing properties of the solvent and reactants. When only the solvent or the solvent and reactant absorb microwaves equally, then nominal differences between MW and conventional heating techniques are expected. If the bulk solvent does not absorb MW, but the reactants do, then direct energy transfer and heating of the reactant molecules will occur to the acceptable depth of penetration. The whole solvent will in turn be heated by conduction from the reactants. Although homogeneous reaction conditions can be established with thorough mixing, the temperature of the reactants will always be higher than that of the solvent, as long as the solvent continues to lose heat through the vessel wall to the environment [26]. MW heating has been already successfully used for the extraction of natural oils [27] and focused microwave-assisted Soxhlet extraction (FMASE) of fatty acids from solid samples [28,29].

Thus when lipid is present heating will occur and in the initial extraction, poultry feed samples can readily couple microwave energy to an extent that causes both bumping and boiling indicating localized heating. Under these conditions it was found that microwave extraction was very efficient, but SB-ATR analysis of the lipid samples indicated that the FFA content of the oil extracts increased with the increase of microwave exposure time as shown in Fig. 1. However, keeping the microwave exposure to 20 s at 900 W eliminated this effect. In Soxhlet extraction,

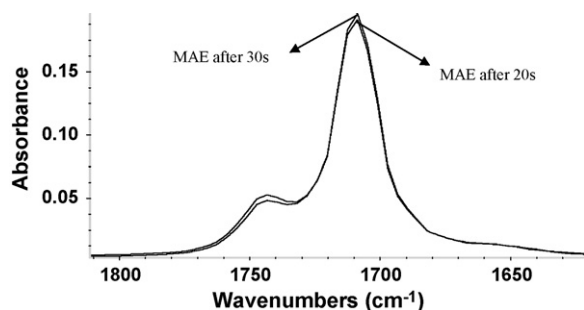


Fig. 1. ATR-FTIR spectra of the effect of increasing the extraction time (temperature) on FFA content of poultry feed sample.

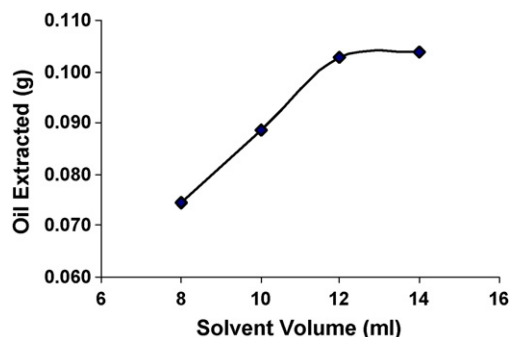


Fig. 2. Response of solvent volume used for first 2 min microwave extraction relative to the amount of oil extracted from poultry feed sample (values presented in the graph are mean value of triplicate analysis, S.D. is <5%).

temperatures attained are limited to that of the solvent boiling point, while in microwave extraction, *in situ* localized heating is probably the reason some lipolysis can occur. On average, 20 s of heating at 900 W was found to produce temperatures of $\sim 45\text{--}50^\circ\text{C}$ in the initial sample extract based on measuring the temperature immediately after taking the samples out.

3.2. Solvent volume optimization

Four volumes of hexane, ranging from 8 to 14 ml, in 2 ml increments, were assessed to determine the extraction efficiency of oil from poultry feeds in the first 2 min extraction of the six extraction cycles. The first extraction results, Fig. 2 indicate that the amount of oil extracted increases with added hexane, but that it reaches a plateau after 12 ml of hexane, the later two extracts representing $\sim 71\%$ of the total oil present in the poultry feed. Since there was no significant difference between 12 and 14 ml to carry out the extraction, 12 ml of hexane was used in first 2 min extraction and for remaining four sequential extractions 8 ml was used.

3.3. Microwave fractional extraction

The effect of sequential use of fresh solvent on oil recovery was examined relative to a single extraction using 12 ml of hexane for 20 s, with a cumulative microwave time of 10 min. In the sequential extraction, the 12 ml of hexane was collected and 8 ml of fresh hexane added. In the single accumulated extraction, $\sim 70\%$ of the total oil (relative to the Soxhlet) was extracted, while in the sequential extraction process an asymptotic extraction was obtained as indicated in Fig. 3, but the total amount extracted was very similar to that obtained using the Soxhlet (100%). Fig. 4 summarizes the results obtained for sequential microwave extraction, single microwave extraction, sonication and the Soxhlet extraction. Sonication on its own is clearly inferior as is a single microwave extraction; however, the results for sequential microwave extractions are quite similar.

SB-ATR FTIR was also used to determine the FFA [22] of extracted oil obtained by each of these extraction methods. The sequential microwave extraction resulted in up to 4% less FFA being present relative to the Soxhlet extraction procedure (Fig. 5), however, the poor extraction efficiency of the sonica-

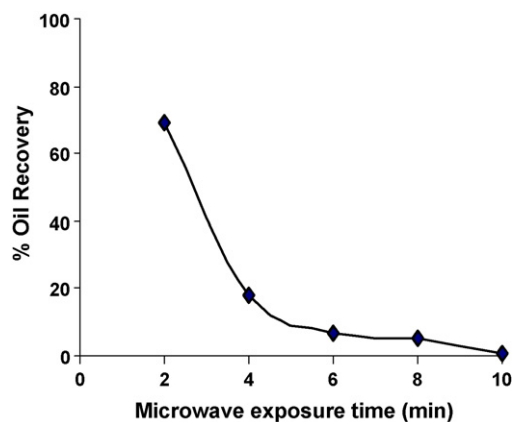


Fig. 3. Effect of extraction cycles (2 min each) on % recovery of total oil content in poultry feed sample during sequential microwave extraction (values presented in the graph are mean value of triplicate analysis, S.D. is <5%).

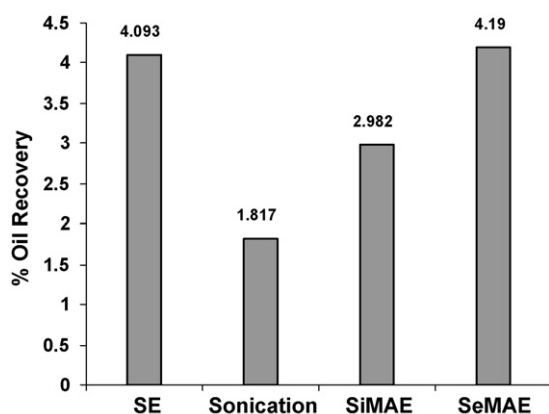


Fig. 4. Comparison of the four extraction procedures on a typical poultry feed sample (values presented in the graph are mean value of triplicate analysis, S.D. is <5%).

tion procedure disqualifies it as being a competitive procedure. Table 1 compares the microwave sequential extraction procedure results to the Soxhlet extraction procedure for 12 commercial poultry feed samples analyzed. These results indicate that the two procedures are in very good agreement, with the sequential microwave extraction procedure giving a slightly better oil recovery. However, on the basis of FFA analysis by FTIR, the FFA content of the Soxhlet extraction tends to be higher, indi-

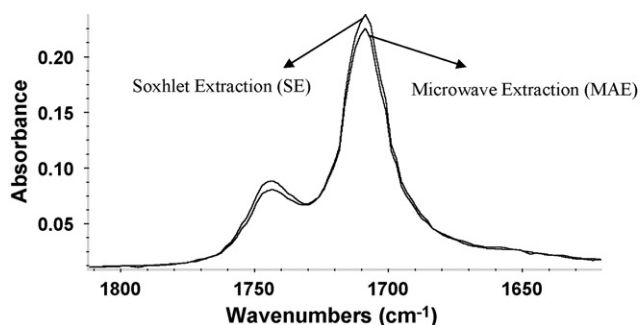


Fig. 5. Spectral comparison of the FFA content of microwave sequential extraction and Soxhlet extracted oils in a poultry feed sample.

Table 1

Hexane extractable lipid obtained from triplicate analysis of 12 commercial poultry feeds by sequential microwave and Soxhlet extractions

Sample	Microwave extraction	Soxhlet extraction
PF-1	3.210 ± 0.034	3.127 ± 0.087
PF-2	2.869 ± 0.048	2.770 ± 0.079
PF-3	2.239 ± 0.059	2.190 ± 0.057
PF-4	3.073 ± 0.044	3.006 ± 0.076
PF-5	3.091 ± 0.045	2.985 ± 0.079
PF-6	5.080 ± 0.061	4.985 ± 0.101
PF-7	5.296 ± 0.054	5.208 ± 0.125
PF-8	4.190 ± 0.049	4.093 ± 0.080
PF-9	2.897 ± 0.067	2.824 ± 0.065
PF-10	3.188 ± 0.068	3.120 ± 0.077
PF-11	2.556 ± 0.035	2.452 ± 0.050
PF-12	3.860 ± 0.065	3.769 ± 0.069
Mean	3.46241	3.37741
S.D.	0.957	0.951

cating that there is a reduced hydrolytic effect associated with the MAE as it carried out only for 20 s intervals @ 900 W to avoid localized heating.

4. Conclusion

Although sophisticated commercial microwave extraction systems are available, it has been demonstrated that a simple, rapid, sequential microwave extraction procedure can be used to quantitatively determine the lipid content of dry poultry feeds using a conventional microwave oven. The microwave extraction method provides a substantial shortening of the extraction time (from 6 h to <40 min) relative to the AOAC 920.39. The other advantages of proposed method using microwave oven are much more environment friendly in terms of energy and solvent (hexane) use in comparison to the conventional Soxhlet method. Furthermore, it also reduces any lipolysis while retaining quantitation.

Acknowledgements

The National Centre of Excellence in Analytical Chemistry, University of Sindh, Jamshoro, Pakistan is gratefully acknowledged for the financial support. The authors also would like to thank Higher Education Commission (HEC), Pakistan and McGill IR Group, McGill University, Canada.

References

- [1] M.K. Ambula, G.W. Oduho, J.K. Tuitoeck, *Trop. Anim. Health Prod.* 35 (2003) 285.
- [2] V. Ravindran, R. Blair, *World Poultry Sci.* 48 (1992) 205.
- [3] N.M. Dale, H.L. Fuller, *Poultry Sci.* 58 (1979) 1529.
- [4] S. Leeson, L. Caston, J.D. Summers, *Poultry Sci.* 75 (1996) 529.
- [5] M. Sanz, A. Flores, C.J. Lopez-Bote, *Poultry Sci.* 78 (1999) 378.
- [6] G. Cherian, J.S. Sim, *Poultry Sci.* 70 (1991) 917.
- [7] E. Ketels, G. De Groote, *Poultry Sci.* 68 (1989) 1506.
- [8] J. Wiseman, *Fats in Animal Nutrition*, Butterworths, London, 1984, 227 pp.
- [9] Z. Nir Nitsan, M. Mahagna, *Br. Poultry Sci.* (1993) 3453.

- [10] D. Keyson, D.P. Volanti, L.S. Cavalcante, A.Z. Simoes, I.A. Souza, J.S. Vasconcelos, J.A. Varela, E. Longo, J. Mater. Process. Technol. 189 (2007) 316.
- [11] S.J. James, A.M. Foster, I.C. Phillips, T.J. Wilkins, M.J. Swain, D. Burfoot, Microwave Science Series Report No. 11, MAFF Publications, London, 1994.
- [12] F. Priego-Capote, J. Ruiz-Jiménez, M.D. Luque de Castro, Food Chem. 100 (2006) 859.
- [13] M.E. Lucchesi Chemat, J. Smadja, L. Faretto, G. Colnaghi, F. Visinoni, Anal. Chim. Acta 555 (2006) 157.
- [14] F.M. Lanas, M.E.C. Queiroz, I.C.E. da Silva, Chromatographia 39 (1994) 687.
- [15] J.M. Snyder, J.W. King, M.A. Jackson, J. Am. Oil Chem. Soc. 74 (1997) 585.
- [16] D.F.G. Walker, K.D. Bartle, A.A. Clifford, Analyst 119 (1994) 1471.
- [17] G. Flamini, M. Tebano, P.L. Cioni, L. Ceccarini, A.S. Ricci, I. Longo, J. Chromatogr. A 1143 (2007) 36.
- [18] A. Longarese-Patron, M.P. Canizares-Macias, Talanta 69 (2006) 882.
- [19] A. Loupy, A. Petit, J. Hamelin, F. Texier-Boullet, P. Jacquault, D. Mathe, Synthesis 9 (1998) 1213.
- [20] A.M. Ferhat, B.Y. Meklati, J. Smadja, F. Chemat, J. Chromatogr. A 1112 (2006) 121.
- [21] F. Priego-Capote, M.D. Luque de Castro, Talanta 65 (2005) 81.
- [22] S.T.H. Sherazi, S.A. Mahesar, M.I. Bhangar, F.R. van de Voort, J. Sedman, J. Agric. Food Chem. 55 (2007) 4928.
- [23] W. Horowitz, Official Methods of Analysis of the Association of Official Analytical Chemists, AOAC Inc., Washington, DC, USA, 1984.
- [24] I.T. Stainisavljevic, M.L. Lazic, V.B. Veljkovic, J. Ultrasonics Sonochem. 14 (2007) 646.
- [25] A. Lagha, S. Chemat, P.V. Bartels, F. Chemat, Analysis 27 (1999) 452.
- [26] B.L. Foster, M.E. Cournoyer, Chem. Health Safety 12 (2005) 27.
- [27] A. Zlotorzynski, Crit. Rev. Anal. Chem. 25 (1995) 43.
- [28] B. Kaufmann, P. Christen, Phytochem. Anal. 13 (2002) 105.
- [29] J.A. Perez-Serradilla, M.C. Ortiz, L. Sarabia, M.D. Luque de Castro, Anal. Bioanal. Chem. 388 (2007) 451.

Electrocatalytic oxidation of NADH at gold nanoparticles loaded poly(3,4-ethylenedioxythiophene)–poly(styrene sulfonic acid) film modified electrode and integration of alcohol dehydrogenase for alcohol sensing

K.M. Manesh^a, P. Santhosh^a, A. Gopalan^{a,b}, K.P. Lee^{a,b,*}

^a Department of Chemistry Graduate School, Kyungpook National University, Daegu 702-701, South Korea

^b Nano Practical Application Center, Daegu 704-230, South Korea

Received 28 October 2007; received in revised form 20 January 2008; accepted 21 January 2008

Available online 2 February 2008

Abstract

A new modified electrode is fabricated by dispersing gold nanoparticles onto the matrix of poly(3,4-ethylenedioxythiophene)–poly(styrene sulfonic acid), PEDOT–PSS. The electrocatalytic activity of the PEDOT–PSS–Au_{nano} electrode towards the oxidation of β -nicotinamide adenine dinucleotide (NADH) is investigated. A substantial decrease in the overpotential (>0.7 V) has been observed for the oxidation of NADH at the PEDOT–PSS–Au_{nano} electrode in comparison to the potential at PEDOT–PSS electrode. The Au nanoparticles dispersed in the PEDOT–PSS matrix prevents the fouling of electrode surface by the oxidation products of NADH and augments the oxidation of NADH at a less positive potential (+0.04 V vs. SCE). The electrode shows high sensitivity to the electrocatalytic oxidation of NADH. Further, the presence of ascorbic acid and uric acid does not interfere during the detection of NADH. Important practical advantages such as stability of the electrode (retains $\sim 95\%$ of its original activity after 20 days), reproducibility of the measurements (R.S.D.: 2.8%; $n=5$), selectivity and wide linear dynamic range (1–80 μM ; $R^2 = 0.996$) are achieved at PEDOT–PSS–Au_{nano} electrode. The ability of PEDOT–PSS–Au_{nano} electrode to promote the electron transfer between NADH and the electrode makes us to fabricate a biocompatible dehydrogenase-based biosensor for the measurement of ethanol. The biosensor showed high sensitivity to ethanol with rapid detection, good reproducibility and excellent stability.

© 2008 Elsevier B.V. All rights reserved.

Keywords: Gold nanoparticles; PEDOT–PSS; NADH oxidation; Modified electrode; Ethanol biosensor

1. Introduction

The electrochemical detection of β -nicotinamide adenine dinucleotide (NADH) is of considerable interest since a number of dehydrogenases require NADH as a cofactor for the enzymatic reaction. NADH is the terminal electron donor moiety in the mitochondrial electron transport chain [1]. However, direct electrochemical oxidation of NADH at a bare platinum electrode requires a high (>1 V) overpotential. The high overpotential for the oxidation of NADH results in interferences from easily oxidizable species present in the real samples. The overpotential for

NADH oxidation could be reduced by using a mediator. Also, electrode fouling is one of the main concerns as radical intermediates are generated during the one-electron oxidation of NADH. The subsequent polymerization products also foul the electrode [2]. Hence, considerable efforts have been devoted to modify the electrode surface with an adequate material to diminish the overpotential for the oxidation of NADH and to minimize the surface passivation effects.

Various methodologies have been adopted to immobilize the mediator on the surface of electrode [3–6]. Different types of modification were performed on the surface of the electrode to maintain satisfactory operational time for the mediator in the electrode [7]. The electrodes modified with carbon nanotubes were used for the oxidation of NADH [8–13]. For instance, a hybrid thin film from multi-wall carbon nanotubes dispersed in nafion with electrochemically generated redox mediator was

* Corresponding author at: Department of Chemistry Graduate School, Kyungpook National University, Daegu 702-701, South Korea.

Tel.: +82 53 950 5901; fax: +82 53 95 28104.

E-mail address: kplee@knu.ac.kr (K.P. Lee).

developed for the sensitive detection of NADH [14]. However, the stability of the modifications limits the reproducibility and the operational lifetime of such modified electrodes. On the other hand, modified electrodes were also fabricated with CdS nanoparticles [15], nanostructured TiO₂ [16], boron-doped diamond [17], exfoliated graphite [18], single crystal gold [19] and conducting polymer nanotubules [20] for the electrochemical detection of NADH. However, the selective electrochemical detection of NADH is still a challenging task.

Gold nanoparticles display unparalleled catalytic activity for a number of reactions [21–24] that include oxidation of carbon monoxide [25]. Au nanoparticles have also been widely used to construct biosensors due to their excellent ability to immobilize biomolecules and at the same time retain the biocatalytic activities of those biomolecules. Recently, electrodes based on Au nanoparticles self-assembled on a thiol-terminated, sol–gel-derived silicate network from 3-(mercaptopropyl) trimethoxysilane were developed for the selective and sensitive detection of NADH [26], glucose [27] and L-lactate [28]. Many kinds of biosensors, such as enzyme sensor [29–31], immunosensor [32] and DNA sensor [33] were developed based on Au nanoparticles to obtain better analytical performances.

Poly(3,4-ethylenedioxythiophene), PEDOT doped with an excess of poly(styrene sulfonic acid) (PSS) has been attracting interest due to its film forming properties, high stability in water as well as in air and high conductivity. PSS plays the dual role of charge balancing and stabilizing the aqueous dispersion. The matrix of PEDOT–PSS is highly porous that facilitates the electrochemical redox reactions [34]. Further, the solubility of PEDOT–PSS in organic solvent is adequate enough to form thin films by many kinds of conventional techniques, such as solvent-casting, spin-casting and dip-coating methods. The presence of negatively charged electrolyte ions in PEDOT–PSS provides good redox activity even in neutral medium. This is attributed to the effective doping (protonation) of PEDOT by the trapped polyelectrolyte ions over a broad range of pHs.

In the present investigation, an electrocatalytic electrode was fabricated by dispersing Au nanoparticles onto PEDOT–PSS coated indium-doped tin oxide glass (ITO) plate and used for the detection of NADH. The PEDOT–PSS–Au_{nano} electrode exhibited excellent electrocatalytic activity towards the oxidation of NADH at a low potential in the phosphate buffer, PBS (pH 7.2). Further, an ethanol biosensor was developed by immobilizing alcohol dehydrogenase enzyme into the PEDOT–PSS–Au_{nano} matrix. The results are presented herein and discussed.

2. Experimental

2.1. Chemicals

PEDOT–PSS was obtained from Sigma–Aldrich (1.3 wt.% suspension in water; a composition of 0.5 wt.% PEDOT and 0.8 wt.% PSS). Sulfuric acid, auric acid, ascorbic acid and uric acid of analytical grade from Aldrich were used as received. Baker's yeast alcohol dehydrogenase (alcohol: NAD⁺ oxidoreductase, E. C. 1.1.1.1) (ADH), β -nicotinamide adenine

dinucleotide (NADH) and β -nicotinamide adenine dinucleotide (reduced form, NAD⁺) were obtained from Sigma chemicals. Double-distilled water was used throughout the experiments. Aqueous solutions of NADH were prepared in PBS (pH 7.2), afresh at the time of experiments.

2.2. Fabrication of PEDOT–PSS–Au_{nano} electrode

PEDOT–PSS matrix electrode was prepared by spin coating (2000 rpm for 1 min) on ITO substrate using SPIN-1200, MIDAS spin coater system. A very thin film of PEDOT–PSS was casted over a cleaned ITO electrode (1.0 sq. cm). Conductivity of the PEDOT–PSS coated ITO was found to be 5 mS cm⁻¹ and the average particle size was ~200 nm. Before each experiment, ITO coated glass was cleaned in an ultrasonic bath using double distilled water and acetone, then dried with a dry nitrogen flow.

Au particles were electrochemically deposited onto spin casted PEDOT–PSS electrode from 0.5 M H₂SO₄ solution of HAuCl₄ (2.0 × 10⁻⁴ M) by employing a repetitive potential scan from 1.1 to 0.0 V (vs. SCE) at a scan rate of 50 mV s⁻¹ and thus, the PEDOT–PSS–Au_{nano} modified electrode was fabricated. Before subjecting to electrochemical experiments, the PEDOT–PSS–Au_{nano} modified electrode was washed extensively with distilled water.

2.3. Electrochemical measurements

Electrochemical measurements were done with EG & G PAR Electrochemical Analyzer in a standard 10 mL cell containing the modified electrode, a SCE reference electrode and a Pt wire auxiliary electrode. Prior to all electrochemical measurements, the solutions were purged with nitrogen for 10 min. The amperometric response of PEDOT–PSS–Au_{nano} electrode was recorded under steady-state conditions in the PBS (pH 7.2) by applying a constant potential (+0.04 V) to the working electrode. The background response at PEDOT–PSS–Au_{nano} electrode was allowed to decay to a steady-state under stirring. When the background current became stable, the aliquot amount of the analyte was injected into the electrolytic cell, and its response was measured. In the case of square wave voltammetry, a 10 mL aliquot of buffer solution with NADH of a definite concentration was placed in the voltammetric cell and the solution was purged with nitrogen for 10 min. Then, a potential scan was initiated at a scan rate of 10 mV s⁻¹ and the resulting voltammogram was recorded. Optimum conditions (pulse amplitude, frequency, step potential and quiet time) were established by measuring the peak currents in dependence on all parameters. The electrochemical sensing of ethanol was carried out in PBS (pH 7.2) in the presence of NAD⁺ (0.2 mM) with ADH (7 U mL⁻¹) using the PEDOT–PSS–Au_{nano} electrode.

2.4. Characterization

The surface topography of PEDOT–PSS–Au_{nano} electrode was examined using atomic force microscopy, AFM (Digital Instruments; Nanoscope Multimode) in the tapping mode with silicon nitride tip (tip height: 4 μ m and the tip radius is of 15 nm).

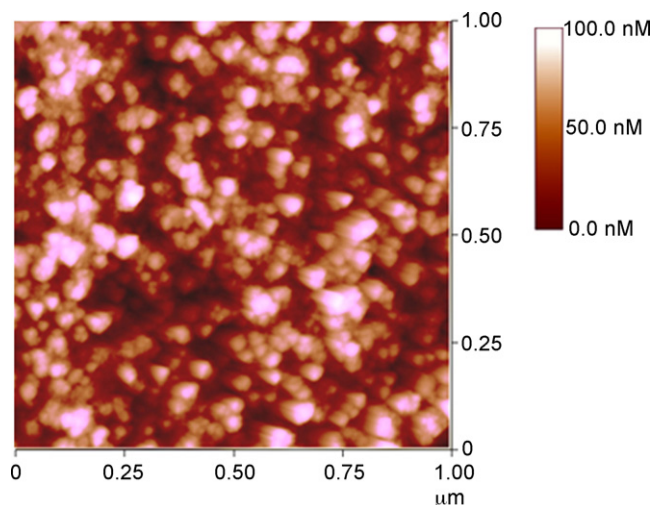


Fig. 1. AFM image of Au nanoparticles deposited on PEDOT–PSS spin coated ITO glass plate.

X-ray diffraction pattern of the sample was collected by employing a D8-Advanced Bruker AXS diffractometer using Cu $K\alpha$ radiation.

3. Results and discussion

3.1. Fabrication and morphology of PEDOT–PSS–Au_{nano} modified electrode

The PEDOT–PSS–Au_{nano} modified electrode was fabricated by two steps. Firstly, film of PEDOT–PSS was formed on the surface of ITO glass plate through spin coating. Subsequently, Au nanoparticles were deposited by the reduction of H₂AuCl₄ from an electrolyte solution consisting of H₂AuCl₄. In the typical fabrication of modified electrode, Au nanoparticles were deposited onto PEDOT–PSS coated ITO electrode from 0.5 M H₂SO₄ solution containing H₂AuCl₄ (2.0×10^{-4} M) by applying a repetitive potential scan from 1.1 to 0.0 V (vs. SCE) at a scan rate of 50 mV s^{-1} as described in the literature [25]. Cyclic voltammogram (CV) shows two cathodic peaks at ~ 0.75 and ~ 0.53 V (vs. SCE). The peak at 0.53 V represents the reduction of solution bound Au^{III} to Au⁰ and the wave at 0.75 V is attributed to the reduction of adsorbed AuCl₄[−] ions to Au⁰ [25].

The surface topography of PEDOT–PSS–Au_{nano} electrode was analyzed through atomic force microscope (AFM). Fig. 1 shows the AFM image of PEDOT–PSS–Au_{nano} electrode. A relatively high-coverage of ordered monolayer of Au nanoparticles without agglomeration was found on the surface of PEDOT–PSS with an average size of Au as 10–15 nm. Further, it can be seen that Au nanoparticles were homogeneously distributed onto the surface of the modified electrode. PEDOT–PSS with its network structure acts as a three-dimensional, random and electronically conducting background (micro-reactor) and provides the matrix for the distribution of Au nanoparticles [35].

Crystalline structure and size of the Au nanoparticles present in PEDOT–PSS–Au_{nano} were examined by XRD analysis (Fig. 2). Peaks observed around 38.0° , 47.9° , 64.1° and 76.1°

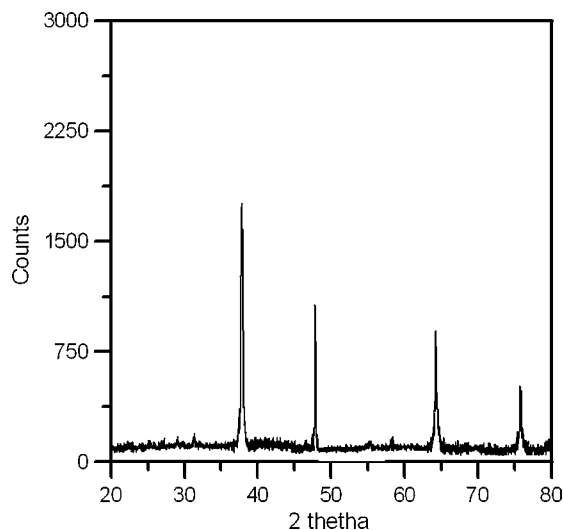


Fig. 2. XRD spectrum of PEDOT–PSS–Au_{nano}.

are attributed to (1 1 1), (2 0 0), (2 2 0) and (3 1 1) facets of the fcc crystal structure of Au [20]. From the full width measured at the half-maximum of the peak at $2\theta = 38^\circ$, the average crystallite size of the Au particles was evaluated to be ~ 10 nm using Scherer's equation [36].

Real surface area, rugosity factor, specific surface area and the amount of Au nanoparticles deposited on the PEDOT–PSS–Au_{nano} were determined. Fig. 3 shows the CV recorded at PEDOT–PSS–Au_{nano} in aq. 1 M H₂SO₄ solution at a scan rate of 50 mV s^{-1} . A clear oxidation peak around 1.48 V and a sharp reduction peak at 1.0 V are observed, due to the reduction of the surface oxide monolayer on Au nanoparticles [37]. The specific surface area, S ($\text{cm}^2 \mu\text{g}^{-1}$) of the catalyst particles was calculated by using the relation,

$$S = \frac{100A_{\text{rsa}}}{WA_{\text{gsa}}}$$

where A_{rsa} is the real surface area (as estimated from the charge consumed for the reduction process of the surface oxide monolayer (the peak at ~ 1.0 V in Fig. 3 and using a reported value of $400 \mu\text{C cm}^{-2}$ [38–40], A_{gsa} is the geometric surface area ($A_{\text{gsa}} = 0.0707 \text{ cm}^2$) and W (in $\mu\text{g cm}^{-2}$) is the amount of Au loading. The real and specific surface areas were estimated to

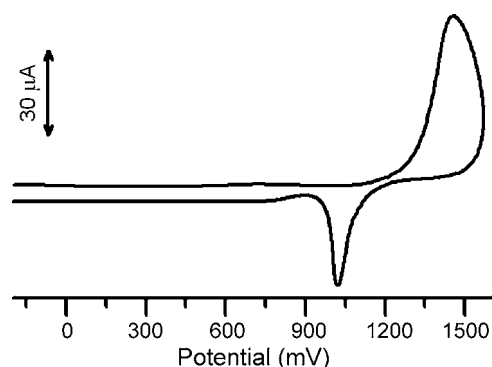


Fig. 3. CV of PEDOT–PSS–Au_{nano} in aq. 1 M H₂SO₄ solution; scan rate: 50 mV s^{-1} .

be 1.52 cm^{-2} and $28.23 \text{ cm}^2 \mu\text{g}^{-1}$, respectively. The rugosity factor is the ratio of A_{rsa} to A_{gsa} , assuming spherical particles of similar radius and found to be 19.56. The amount of Au nanoparticles deposited onto the PEDOT–PSS–Au_{nano} was determined [41] by using the charge (Q_{dep}) (obtained through graphical integration of cyclic voltammetric curves) utilized for the deposition of Au nanoparticles and was found to be $88 \mu\text{g cm}^{-2}$.

3.2. Voltammetric studies on NADH oxidation

3.2.1. Cyclic voltammetry

Fig. 4 compares the CVs for 1 mM NADH in PBS (pH 7.2) recorded at ITO/PEDOT–PSS and ITO/PEDOT–PSS–Au_{nano} electrodes, respectively, at a scan rate of 50 mV s^{-1} . Oxidation of NADH (1 mM) occurs at PEDOT–PSS and PEDOT–PSS–

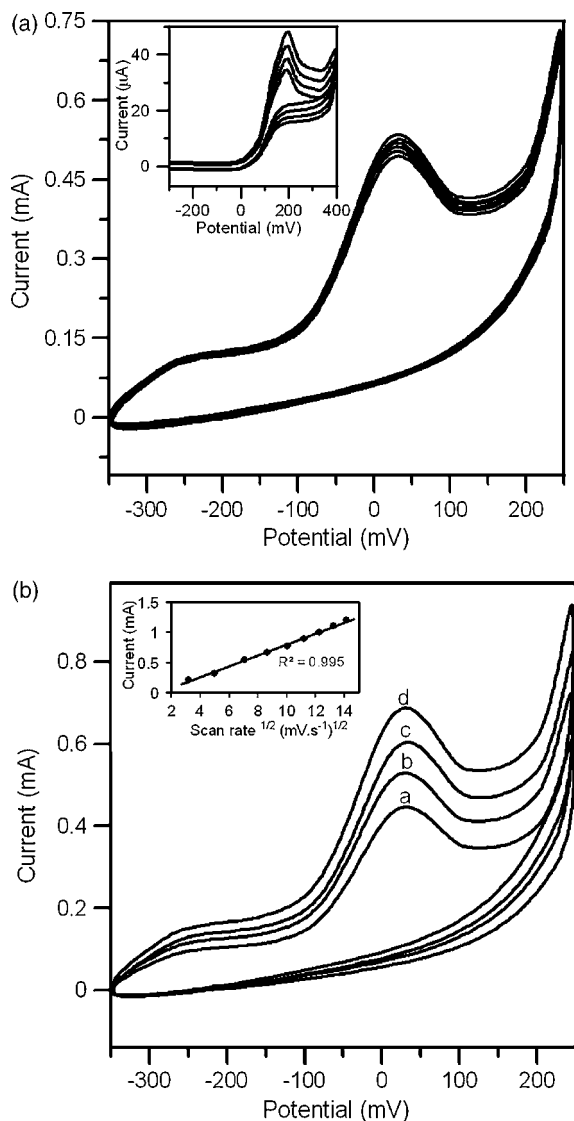


Fig. 4. (a) CVs recorded at PEDOT–PSS–Au_{nano} and PEDOT–PSS (inset) electrodes in the presence of 1 mM NADH in PBS (pH 7.2); scan rate: 50 mV s^{-1} (b) CVs of PEDOT–PSS–Au_{nano} electrode in the presence 0.8 (a), 1.0 (b), 1.2 (c) and 1.4 (d) mM NADH in PBS (pH 7.2); scan rate: 50 mV s^{-1} . Inset shows the plot of scan rate with peak current.

Au_{nano} electrodes with an oxidation peak current at 0.2 V (Fig. 4a-inset) and 0.04 V (Fig. 4a) (vs. SCE), respectively. A large negative shift in the oxidation potential was noticed at PEDOT–PSS–Au_{nano} electrode. Unlike at the PEDOT–PSS modified ITO electrode (Fig. 4a-inset), a stable oxidation peak, without change in position in the subsequent sweep of potentials was noticed for PEDOT–PSS–Au_{nano} electrode (Fig. 4a). This observation informs that the electrode is not influenced by fouling effect of the oxidation products. The large decrease in the overpotential for the oxidation of NADH at a PEDOT–PSS–Au_{nano} electrode is ascribed to the high specific surface area provided by the Au nanoparticles and the synergistic effects between the dispersed Au nanoparticles and the PEDOT–PSS matrix, which facilitates direct electron transfer between NADH and the electrode surface. Furthermore, a higher current was noticed at the PEDOT–PSS–Au_{nano} electrode in comparison to PEDOT–PSS modified electrode. The magnitude of the oxidation peak current is proportional to the concentration of NADH (Fig. 4b)—a factor which is important for the development of a biosensor. The interesting aspect is that oxidation of NADH at PEDOT–PSS–Au_{nano} electrode occurs with a low positive potential without having an additional redox mediator.

In general, the formal potential of the NADH/NAD⁺ couple in neutral pH at 25 °C is estimated to be -0.56 V vs. SCE, and an over potential of $>1.0 \text{ V}$ is often required for the direct oxidation of NADH at the bare electrode. However, in the present study, oxidation of NADH occurs with a large decrease in the overpotential ($>0.70 \text{ V}$) at PEDOT–PSS–Au_{nano} electrode. On comparative literature, oxidation potential of $\sim 0.075 \text{ V}$ for NADH was reported at an electrode modified with polyaniline-doped mercaptosuccinic-acid-capped Au nanoparticles [42]. In another study, oxidation of NADH has been reported around 0.07 V at the Au nanoparticles self-assembled 3-mercaptopropyltrimethoxy silane modified gold electrode [43].

The scan rate dependence of the voltammetric response at the PEDOT–PSS–Au_{nano} electrode was explored. The peak current for the oxidation of NADH increases linearly ($R^2 = 0.995$) with the square root of scan rate between 10 and 200 mV s^{-1} (Fig. 4b-inset), suggesting that the overall oxidation of NADH at the electrode is controlled by the diffusion of NADH in solution. Further, the oxidation peak potential shifts towards positive potentials with increasing scan rates informing the electrochemical irreversibility of the electrochemical process. The diffusion coefficient (D) was determined by the equation;

$$I = (2.99 \times 10^5) AC_0 D^{1/2} \nu^{1/2} n(\alpha n_a)^{1/2}$$

where n is the number of electrons involved for the oxidation of NADH, which is 2 (as determined from Tafel slope), C_0 is the bulk concentration, A is the electrode area, ν is the scan rate, with values for α and n_a which are 0.48 and 1, respectively. The D value was found to be $2.98 \times 10^{-6} \text{ cm}^2 \text{ s}^{-1}$.

3.2.2. Square wave voltammetry

The voltammetric response of NADH at the PEDOT–PSS–Au_{nano} electrode was studied by square wave voltammetry since this technique could provide a better resolution and signal-to-noise ratio. The influence of square wave voltammetric

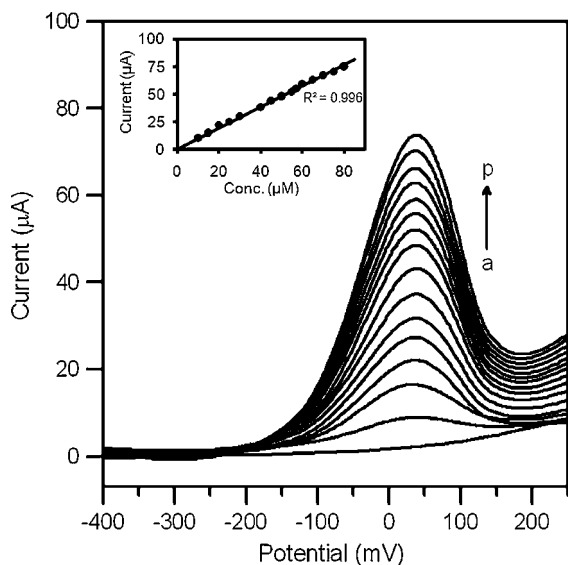


Fig. 5. SWVs of NADH on PEDOT-PSS-Au_{nano} electrode at different concentrations of NADH: (a) 0, (b) 10, (c) 15, (d) 20, (e) 25, (f) 30, (g) 40, (h) 45, (i) 50, (j) 55, (k) 57.5, (l) 60, (m) 65, (n) 70, (o) 75 and (p) 80 μM in PBS (pH 7.2).

parameters on the analytical signal was monitored to understand the kinetics of NADH oxidation, as well as to optimize the parameters for analytical application. Square wave voltammograms (SWVs) were recorded by changing the pulse amplitude (ΔU), frequency (f) and step potential in the range 10–100 mV, 10–100 Hz and 1–10 mV, respectively. Conditions such as 1.0 μM , pH 7.2, $t = 3$ s, step potential = 3 mV gave optimized response to oxidation of NADH. SWVs of PEDOT-PSS-Au_{nano} electrode (condition: $t = 3$ s, step potential = 3 mV, $f = 90$ Hz, and $\Delta U = 50$ mV) recorded for different concentration of NADH and the SWVs are shown in Fig. 5. A peak corresponding to the oxidation of NADH was observed at 0.04 V and the peak intensity was found to increase with concentration of NADH. Fig. 5 (inset) depicts the typical calibration curve by plotting the peak current, I_{cat} at 0.04 V, with the concentration of NADH. The I_{cat} linearly increases with concentration of NADH in the range of 1–80 μM (Fig. 5-inset). The linear regression equation is $y = 0.958x$, with a correlation coefficient of 0.996. A detection limit of 0.1 μM was calculated as the NADH concentration from the signal to the blank signal y_B (intercept) for three standard deviations of y -residuals $s_{y/x}$ [44]. The experimentally determined detection limit is in close agreement with the calculated detection limit.

3.3. Constant potential amperometry

The voltammetric results detailed above suggest that the PEDOT-PSS-Au_{nano} electrode facilitates a stable and low potential amperometric detection of NADH. Further, the sensitivity was examined by recording the amperometric response of oxidation of NADH at PEDOT-PSS-Au_{nano} electrode in a stirred solution, but with smaller addition of NADH over the concentration range of 0.1 to 2.2 μM . Fig. 6 shows an amperometric trace recorded at the PEDOT-PSS-Au_{nano} electrode ($E = +0.04$ V) during the successive addition of NADH aliquots into a stirred PBS (pH 7.2). The PEDOT-PSS-Au_{nano} electrode

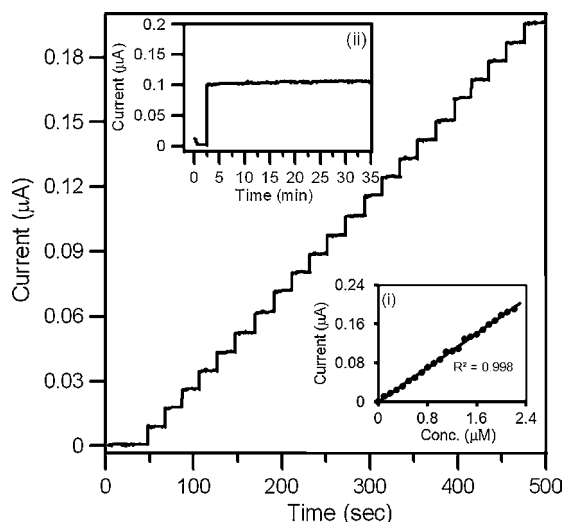


Fig. 6. Amperometric response of PEDOT-PSS-Au_{nano} electrode for the oxidation of NADH at +0.04 V in PBS (pH 7.2). Each addition increased the concentration of NADH by 0.1 μM . (i) Plot of [NADH] vs. catalytic peak current; (ii) Stability of the current response of 1 μM NADH at PEDOT-PSS-Au_{nano} electrode at the applied potential of +0.04 V in PBS (pH 7.2).

responds effectively to the NADH spikes, yielding steady-state signals within 2 s. Fig. 6(i) shows a calibration curve for the NADH. The calibration plot over the concentration range of 0.1–2.2 μM has a slope of $88 \pm 2 \text{ mA M}^{-1} \text{ cm}^{-2}$ with a correlation coefficient $R^2 = 0.9981$. The electrocatalytic behavior was highly reproducible, as reflected by a relative standard deviation of 1.2% estimated from the slopes of the calibration plots for six freshly prepared samples at PEDOT-PSS-Au_{nano} electrode.

Besides good sensitivity and linearity for the detection of NADH, an extremely attractive feature of the PEDOT-PSS-Au_{nano} electrode is the stable amperometric NADH response. Fig. 6(ii) shows the amperometric responses of 1 μM NADH at PEDOT-PSS-Au_{nano} electrode recorded over a continuous period of 35 min, when the potential was held at +0.04 V. It is clear that the current response to NADH oxidation at PEDOT-PSS-Au_{nano} electrode is stable over the entire period. However, it must be noted that a decaying of current signal up to 58.2% was observed at PEDOT-PSS modified electrode (figure not shown). For the PEDOT-PSS modified electrode, surface passivation by the radical intermediates may limit the stability and cause the loss of analytical sensitivity and reproducibility over the operational time. On the other hand, the formation of radical intermediates and subsequent reaction at PEDOT-PSS-Au_{nano} electrode are minimum, probably due to the lower oxidation potential (0.04 V). Hence, PEDOT-PSS-Au_{nano} electrode is free from the fouling effect by the oxidation products. These results demonstrated that PEDOT-PSS-Au_{nano} electrode greatly minimizes the surface passivation effects which generally give hindrance to amperometric detection of NADH.

3.4. Influence of interferences

Ascorbic acid (AA) and uric acid (UA) generally interference with the electrochemical determination of NADH, since

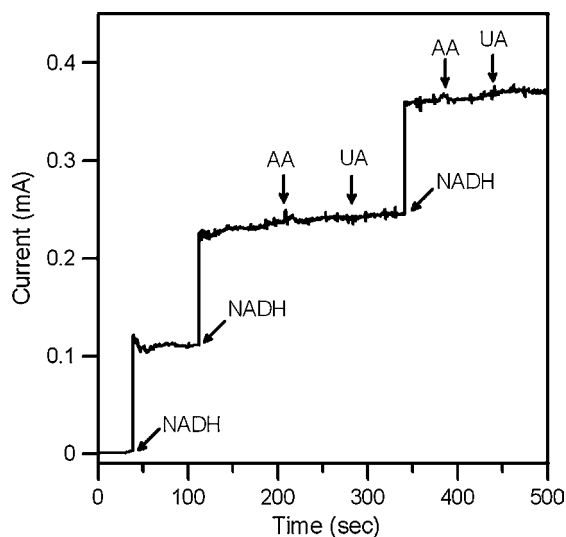


Fig. 7. Amperometric responses of PEDOT-PSS-Au_{nano} electrode to NADH, UA and AA (each of 1 mM concentration) at +0.04 V in PBS (pH 7.2).

AA and/or UA are/is commonly oxidized at potentials nearer to oxidation potential of NADH. Hence, cyclic voltammetry experiments were performed to examine the influence of UA and AA on the oxidation of NADH at PEDOT-PSS-Au_{nano} electrode. A broad anodic peak at 0.185 V and a shoulder around 0.04 V were observed for the oxidation of AA and NADH, respectively. On the other hand, two well defined oxidation peaks, one at 0.038 V and another at 0.256 V, due to the oxidation of NADH and UA, respectively, were observed at PEDOT-PSS-Au_{nano} in the PBS (pH 7.2) containing NADH and UA of equal concentration. In order to authenticate the influence of AA or UA on the oxidation of NADH, amperometric measurements were made at the PEDOT-PSS-Au_{nano} electrode with the intermittent addition of NADH, AA and UA at equal concentrations. Fig. 7 represents the

amperometric response for NADH, AA and UA of 1 mM concentration at the PEDOT-PSS-Au_{nano} electrode in PBS (pH 7.2). A well-defined NADH response was observed at the potential of +0.04 V. The subsequent injection of AA and UA did not show any additional signal or disturb the current response indicating the absence of interference in the signal.

3.5. Development of ethanol biosensor

To validate the usefulness of the described electrocatalytic system, an ethanol biosensor was developed. The biosensor was prepared by incorporating a model enzyme, alcohol dehydrogenase (ADH), into the PEDOT-PSS-Au_{nano} electrode. Au nanoparticles are convenient scaffold for enzyme immobilization and have been used previously for the immobilization of other dehydrogenases in enzymatic reactors [26,45]. In general, dehydrogenase requires NAD⁺ as a cofactor for enzymatic reaction due to the fact that NAD⁺ can be reduced to NADH simultaneously with oxidation of analyte. In the present study, alcohol dehydrogenase enzyme catalyzes the oxidation of ethanol, and simultaneously the cofactor NAD⁺ gets reduced to NADH. The enzymatically formed NADH undergoes electrochemical oxidation to NAD⁺ at the PEDOT-PSS-Au_{nano} electrode. Thus, NADH produced at the PEDOT-PSS-Au_{nano} electrode can be quantitatively correlated to the amount of ethanol.

It is known that in the dehydrogenase-based amperometric biosensor, pH, concentration of the enzyme and cofactor influence the response of biosensor. Hence, experiments were performed in order to study the influence of pH, ADH (enzyme) and NAD⁺ (cofactor) concentration on the current response at PEDOT-PSS-Au_{nano} electrode. The study of pH influence was conducted in the range of 6.0–9.0 (Fig. 8(i)). The current response increased almost linearly from 6.0 to 7.2 and at pH 7.2, the largest response was observed and the current response

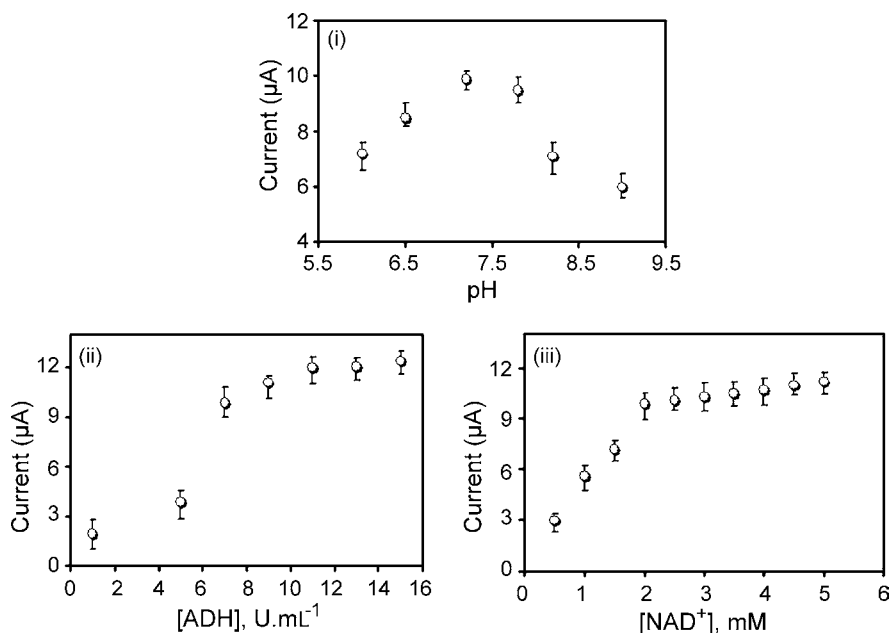


Fig. 8. Current responses at PEDOT-PSS-Au_{nano} electrode as a function of pH (i), ADH (ii) and NAD⁺ (iii); potential: +0.04 V, [ethanol]: 10 µM.

decreases appreciably in the alkaline pHs. The unstable nature of NAD^+ in alkaline solution is the reason for the decrease in current response. Hence, pH 7.2 buffer was used in all experiments.

The current response of the PEDOT–PSS– Au_{nano} electrode was studied by varying the amount of ADH used for the fabrication of modified electrode. Seven electrodes were prepared with different amount of ADH in the range between 1 and 15 U mL^{-1} , while the amount of other components were kept constant. It can be seen from Fig. 8(ii) that the current response at PEDOT–PSS– Au_{nano} electrode was dependent on the amount of enzyme incorporated into the electrode. An increase in the current was observed up to 7 U mL^{-1} , while no significant increase in the response current was observed for higher loading of the enzyme. Experiments were also performed to study the influence of NAD^+ concentration. Fig. 8(iii) shows the current response vs. concentration of NAD^+ recorded at the PEDOT–PSS– Au_{nano} electrode in PBS (pH 7.2) containing $10 \mu\text{M}$ ethanol. A largest response current was observed at PEDOT–PSS– Au_{nano} electrode with the $[\text{NAD}^+] = 0.2 \text{ mM}$ (Fig. 8(iii)). As the concentration kept increasing, the current response increases faintly. The increase in response is due to the higher conversion efficiency with higher concentration of NAD^+ in the enzyme-catalyzed reaction. Nevertheless, by considering the high cost of cofactor, NAD^+ , 0.2 mM was kept as optimum.

After being optimized the conditions, square wave voltammograms were recorded ($t = 3 \text{ s}$, step potential = 3 mV , $f = 90 \text{ Hz}$, and $\Delta U = 50 \text{ mV}$) for the different concentration of ethanol at PEDOT–PSS– Au_{nano} electrode (Fig. 9a). A voltammetric peak at 0.04 V was observed upon the addition of ethanol and the peak corresponds to the oxidation of NADH at the PEDOT–PSS– Au_{nano} electrode. It is to be noted that the peak 0.04 V did not appear in the absence of either ethanol or the co-factor, NAD^+ . This observation clearly supports that the peak observed at 0.04 V is due to the oxidation of enzymatically produced NADH . Fig. 9a also informs that the peak current at 0.04 V increases with increasing the concentration of ethanol.

A steady-state amperometric response of the PEDOT–PSS– Au_{nano} electrode to the addition of ethanol aliquots to a stirred PBS (pH 7.2) is shown in Fig. 9b. Upon addition of an aliquot of ethanol, the current increased steeply to 97% of the stable value within 5 s, indicating a fast response at the electrode. A calibration plot was drawn between the response current and the concentration of ethanol ($1\text{--}100 \mu\text{M}$) (Fig. 9b-bottom inset). The calibration plot is found to be linear ($R^2 = 0.9995$). It is interesting to note that the sensitivity toward ethanol ($97 \text{ mA M}^{-1} \text{ cm}^{-2}$) is comparable to the sensitivity to NADH ($95 \text{ mA M}^{-1} \text{ cm}^{-2}$), and this is an indication of efficient signal transduction at the PEDOT–PSS– Au_{nano} biosensor. A plateau current was observed while increasing the concentration of ethanol beyond $75 \mu\text{M}$ showing the characteristics of the Michaelis–Menten kinetics [46]. The apparent Michaelis–Menten constant (K_M) was estimated from the slope and intercept values of the plot of the reciprocals of the steady-state current vs. ethanol concentration (Fig. 9b-top inset) and a value of $K_M = 13 \text{ mM L}^{-1}$ was obtained.

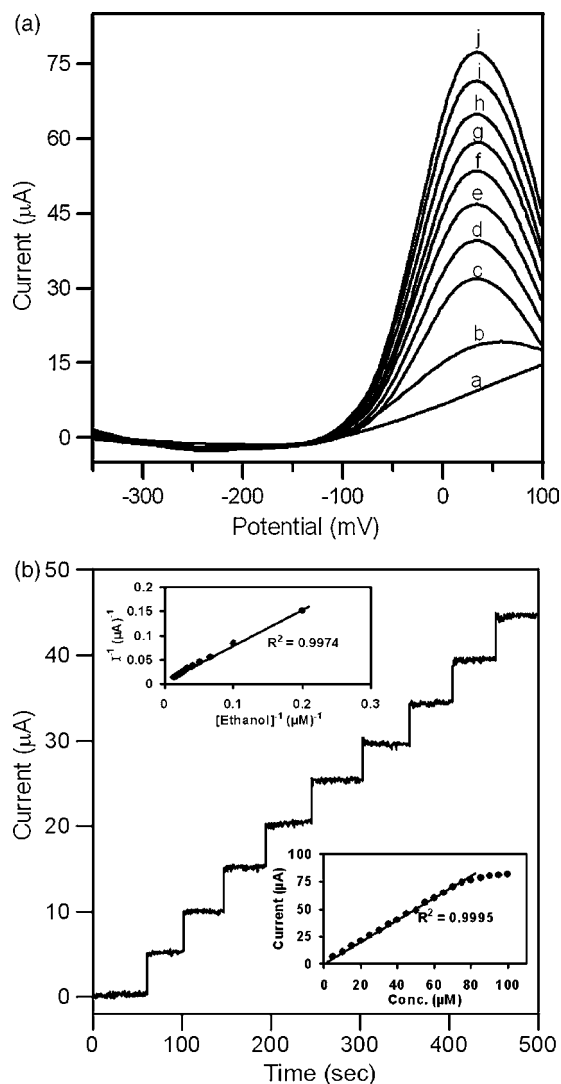


Fig. 9. (a) SWVs recorded at PEDOT–PSS– Au_{nano} electrode in PBS (pH 7.2) for the different concentration of ethanol in the presence of NAD^+ (0.2 mM), [ethanol]: (a) 10, (b) 20, (c) 30, (d) 40, (e) 50, (f) 55, (g) 60, (h) 65, (i) 70 and (j) $75 \mu\text{M}$ (b) Amperometric responses of PEDOT–PSS– Au_{nano} electrode to successive additions of $5 \mu\text{M}$ ethanol in PBS (pH 7.2) at $+0.04 \text{ V}$. Inset (bottom) shows the calibration plot of the concentration of ethanol with current at PEDOT–PSS– Au_{nano} electrode ($1\text{--}100 \mu\text{M}$); Inset (top) shows the Lineweaver–Burk plot.

3.6. Stability and reproducibility of PEDOT–PSS– Au_{nano}

The stability of the PEDOT–PSS– Au_{nano} electrode was determined for a period of operation. The performance of PEDOT–PSS– Au_{nano} electrode for the detection of NADH was tested in PBS (pH 7.2) for a period of 20 days. The first 2 days, a 2.3% decrease of the initial over a response current signal was noticed. After 15 days, the current response decreased by 4.8% of initial current. After 20 days, the decrease in current signal was 6.2% of the initial value. PEDOT–PSS– Au_{nano} electrode retains $\sim 94\%$ of its original activity after 20 days and continued to exhibit excellent response to NADH .

The repeatability of the current response of the PEDOT–PSS– Au_{nano} electrode was examined in the presence of $1 \mu\text{M}$ NADH in PBS (pH 7.2). R.S.D. was found to be 2.3% for ten succes-

sive assays. The electrode-to-electrode reproducibility was also determined in the presence of 1 μ M NADH in PBS (pH 7.2) by comparing the performance of five freshly prepared electrodes. The reproducibility is revealed with a R.S.D. of 2.8%. The good reproducibility might be due to the homogenous distribution of Au nanoparticles throughout the PEDOT–PSS matrix.

The experimental results show that Au nanoparticles dispersed in the PEDOT–PSS matrix have larger specific surface area and good biocompatibility and suited for immobilization of biomolecules or enzymes. PEDOT–PSS matrix provides an efficient electron-conducting tunnel for NADH oxidation. It is well documented in the present study that the PEDOT–PSS–Au_{nano} electrode is an excellent electrocatalytic material for the preparation of sensitive, reproducible and stable electrochemical biosensors for dehydrogenase substrates.

4. Conclusions

Au nanoparticles are uniformly dispersed into PEDOT–PSS matrix and an electrocatalyst electrode was fabricated for the detection of NADH. PEDOT–PSS–Au_{nano} electrode provides an enhanced electrocatalytic response to the oxidation of NADH. The response time for NADH detection is low and the performance of the electrode is stable. Stability of the electrode, reproducibility of the measurements, selectivity and wide linear response for NADH are in favor of fabricating an enzymatic sensor for the determination of ethanol at PEDOT–PSS–Au_{nano} electrode. A biosensor has thus been successfully assembled by immobilizing alcohol dehydrogenase enzyme into the PEDOT–PSS–Au_{nano} matrix and the functioning of sensor electrode is satisfactory. The present study forms a platform for the development of modified electrodes suited for the combined usage of electrocatalysis and electrochemical biosensing.

Acknowledgments

This work was supported by the Korean Research Foundation Grant ((KRF-2006-J02402). The authors acknowledge the Korea Basic Science Institute (Daegu) and Kyungpook National University Center for Scientific Instrument.

References

- [1] M. Dixon, E.C. Webb, *Enzymes*, Longman, London, 1979.
- [2] W.J. Blaedel, R.A. Jenkins, *Anal. Chem.* 47 (1975) 1337.
- [3] A.V. Bogachev, Y.V. Bertsova, B. Barquera, M.I. Verkhovskiy, *Biochem.* 40 (2001) 7318.
- [4] Y. Zu, R.J. Shannon, J. Hirst, *J. Am. Chem. Soc.* 125 (2003) 6020.
- [5] A.A. Karyakin, Y.N. Ivanova, K.V. Revunova, E.E. Karyakina, *Anal. Chem.* 76 (2004) 2004.
- [6] B.P. Simon, J. Macanas, M. Munoz, E. Fabregas, *Talanta* 71 (2007) 2102.
- [7] N. de-los-Santos-Alvarez, M.J. Lobo-Castanon, A.J. Miranda-Ordieres, P.T. Blanco, H.D. Abruna, *Anal. Chem.* 77 (2005) 2624.
- [8] L. Zhu, J. Zhai, R. Yang, C. Tian, L. Guo, *Biosens. Bioelectron.* 22 (2007) 2768.
- [9] R. Antiochia, I. Lavagnini, F. Magno, *Anal. Bioanal. Chem.* 381 (2005) 1355.
- [10] M. Zhang, A. Smith, W. Gorski, *Anal. Chem.* 76 (2004) 5045.
- [11] M. Musameh, J. Wang, A. Merkoci, Y. Lin, *Electrochem. Commun.* 4 (2002) 743.
- [12] C.E. Banks, R.G. Compton, *Analyst* 9 (2005) 1232.
- [13] S. Chakraborty, C.R. Raj, *Electrochem. Commun.* 9 (2007) 1323.
- [14] C.R. Raj, S. Chakraborty, *Biosens. Bioelectron.* 22 (2006) 700.
- [15] W. Vastarella, R. Nicastri, *Talanta* 66 (2005) 627.
- [16] A. Curulli, F. Valentini, G. Padeletti, M. Viticoli, D. Caschera, G. Palleschi, *Sens. Actuators B* 111–112 (2005) 441.
- [17] T.N. Rao, I. Yagi, T. Miwa, D.A. Tryk, A. Fujishima, *Anal. Chem.* 71 (1999) 2506.
- [18] P. Ramesh, S. Sampath, *Anal. Chem.* 72 (2000) 3369.
- [19] X. Xing, X. Shao, M. Liu, C. Chiun, *J. Electroanal. Chem.* 406 (1996) 83.
- [20] F. Valentini, A. Salis, A. Curulli, G. Palleschi, *Anal. Chem.* 76 (2004) 3244.
- [21] K.M. Manesh, J.H. Kim, P. Santhosh, A.I. Gopalan, K.P. Lee, H.D. Kang, *J. Nanosci. Nanotech.* 7 (2007) 3365.
- [22] A.I. Gopalan, K.P. Lee, K.M. Manesh, P. Santhosh, J.H. Kim, J.S. Kang, *Talanta* 71 (2007) 1774.
- [23] A.I. Gopalan, K.P. Lee, K.M. Manesh, P. Santhosh, J.H. Kim, *J. Mol. Catal. A* 256 (2006) 335.
- [24] K.P. Lee, A.I. Gopalan, P. Santhosh, K.M. Manesh, K.H. Kim, K.S. Kim, *J. Nanosci. Nanotech.* 6 (2006) 1575.
- [25] P. Santhosh, A. Gopalan, K.P. Lee, *J. Catal.* 238 (2006) 177.
- [26] B.K. Jena, C.R. Raj, *Anal. Chem.* 78 (2006) 6332.
- [27] B.K. Jena, C.R. Raj, *Chem. Eur. J.* 12 (2006) 2702.
- [28] B.K. Jena, C.R. Raj, *Electroanal.* 19 (2007) 816.
- [29] A. Gole, C. Dash, V. Ramakrishnan, S.R. Sainkar, A.B. Mandale, M. Rao, M. Sastry, *Langmuir* 17 (2001) 1674.
- [30] Y. Xiao, H.X. Ju, H.Y. Chen, *Anal. Chim. Acta* 391 (1999) 73.
- [31] J. Jia, B. Wang, A. Wu, G. Cheng, Z. Li, S. Dong, *Anal. Chem.* 74 (2002) 2217.
- [32] Y. Zhou, R. Yuan, Y. Chai, D. Tang, Y. Zhang, N. Wang, X. Li, Q. Zhu, *Electrochem. Commun.* 7 (2005) 355.
- [33] T. Niazov, V. Pavlov, Y. Xiao, R. Gill, I. Willner, *Nano. Lett.* 4 (2004) 1683.
- [34] S. Ghosh, O. Inganäs, *Adv. Mater.* 11 (1999) 1214.
- [35] S.S. Kumar, C. Sivakumar, J. Mathiyarasu, K.L. Phani, *Langmuir* 23 (2007) 3401.
- [36] L.V. Azaroff, *Elements of X-ray Crystallography*, McGraw-Hill, New York, 1968, pp. 549.
- [37] F.N. Crespilho, V. Zucolotto, C.M.A. Brett, O.N. Oliveira, F.C. Nart, *J. Phys. Chem. B* 110 (2006) 17478.
- [38] A.A. Michri, A.G. Pshchenichikov, K.R. Burshtein, *Sov. Electrochem.* 8 (1972) 351.
- [39] S. Trasatti, O.A. Petrii, *Pure Appl. Chem.* 63 (1991) 711.
- [40] H.A. Kozłowska, B.E. Conway, A. Hamelin, L. Stoicovicu, *J. Electroanal. Chem.* 228 (1987) 429.
- [41] L.M. Huang, H.Z. Lin, T.C. Wen, A. Gopalan, *Electrochim. Acta* 52 (2006) 1058.
- [42] S. Tian, J. Liu, T. Zhu, W. Knoll, *Chem. Commun.* 21 (2003) 2738.
- [43] C.R. Raj, B.K. Jena, *Chem. Commun.* 15 (2005) 2005.
- [44] J.C. Miller, J.N. Miller, *Statistics for Analytical Chemistry*, Ellis Horwood Series, PTR Prentice Hall, New York, London, 1993, pp. 119.
- [45] J. Wang, *Analyst* 4 (2005) 421.
- [46] K.M. Manesh, H.T. Kim, P. Santhosh, A.I. Gopalan, K.P. Lee, *Biosens. Bioelectron.* 23 (2008) 771.

Determination of PASHs by various analytical techniques based on gas chromatography–mass spectrometry Application to a biodesulfurization process

Milagros Mezcua^{a,*}, Amadeo R. Fernández-Alba^b, Karina Boltes^a,
Raul Alonso Del Aguila^a, Pedro Leton^a, Antonio Rodríguez^a, Eloy García-Calvo^a

^a Department of Chemical Engineering and Analytical Chemistry, University
of Alcalá, 28871 Madrid, Spain

^b Pesticide Residue Research Group,
University of Almería, 04120 Almería, Spain

Received 26 July 2007; received in revised form 24 December 2007; accepted 8 January 2008

Available online 21 January 2008

Abstract

Polycyclic aromatic sulphur heterocyclic (PASH) compounds, such as dibenzothiophene (DBT) and alkylated derivatives are used as model compounds in biodesulfurization processes. The development of these processes is focused on the reduction of the concentration of sulphur in gasoline and gas–oil [D.J. Monticello, *Curr. Opin. Biotechnol.* 11 (2000) 540], in order to meet European Union and United States directives.

The evaluation of biodesulfurization processes requires the development of adequate analytical techniques, allowing the identification of any transformation products generated. The identification of intermediates and final products permits the evaluation of the degradation process.

In this work, seven sulfurated compounds and one non-sulfurated compound have been selected to develop an extraction method and to compare the sensitivity and identification capabilities of three different gas chromatography ionization modes. The selected compounds are: dibenzothiophene (DBT), 4-methyl-dibenzothiophene (4-m-DBT), 4,6-dimethyl-dibenzothiophene (4,6-dm-DBT) and 4,6 diethyl-dibenzothiophene (4,6 de-DBT), all of which can be used as model compounds in biodesulfurization processes; as well as dibenzothiophene sulfoxide (DBTO₂), dibenzothiophene sulfone (DBTO) and 2-(2-hydroxybiphenyl)-benzenesulfinate (HBPS), which are intermediate products in biodesulfurization processes of DBT [A. Alcon, V.E. Santos, A.B. Martín, P. Yustos, F. García-Ochoa, *Biochem. Eng. J.* 26 (2005) 168]. Furthermore, a non-sulfurated compound, 2-hydroxybiphenyl (2-HBP), has also been selected as it is the final product in the biodesulfurization process of DBT [A. Alcon, V.E. Santos, A.B. Martín, P. Yustos, F. García-Ochoa, *Biochem. Eng. J.* 26 (2005) 168].

Since, typically, biodesulfurization reactions take place in a biphasic medium, two extraction methods have been developed: a liquid–liquid extraction method for the watery phase and a solid phase extraction method for the organic phase. Recoveries of the selected compound in both media were studied. They were in the range of 80–100% for the watery and in the range of 40–60% for the organic phase, respectively.

Gas chromatography coupled to mass spectrometry (GC–MS) has been employed for the identification of these selected compounds. Three different ionization modes were applied: conventional electron impact (EI); positive chemical ionization (PCI), using methane as the reagent gas; and a recently developed ionization mode known as hybrid chemical ionization (HCI), using perfluorotri-*n*-butylamine as the reagent gas. Limits of detection and identification capabilities have been compared between the three analytical techniques.

The sensitivity of the three analytical techniques was studied and LOD between 0.05 and 1, between 0.09 and 2 and between 0.001 and 0.043 were achieved for PCI, EI and HCI, respectively.

The developed method was applied in samples from a biodesulfurization process. The biodesulfurization reactions were conducted in resting cell operation mode, using Erlenmeyer flasks or an agitated tank bioreactor. The microorganism employed was *Pseudomonas putida* CECT 5279. The reaction was performed under controlled air flow, stirring and temperature conditions.

© 2008 Elsevier B.V. All rights reserved.

Keywords: Biodesulfurization; Dibenzothiophene; Gas chromatography mass spectrometry (GC–MS); Hybrid chemical ionization (HCI); Alkylated dibenzothiophenes

* Corresponding author. Fax: +34 950015483.

E-mail address: mmezcu@ual.es (M. Mezcua).

1. Introduction

Crude oil and its distillates contain significant amounts of low-molecular-mass organosulphur compounds such as alkyl- and cycloalkyl-thiols, alkyl- and arylthioethers and aromatic heterocycles based on thiophene. This last group of polycyclic aromatic sulfurated hydrocarbons (PASHs) includes thiophene itself, benzothiophene, dibenzothiophene and their alkylated derivatives. These compounds have been of concern for decades because they constitute a major class of ubiquitous environmental contaminants found in both air and sea areas [3–5]. In order to mitigate the consequences of this contamination, such as acid rain [6,1] and air pollution, caused by sulphur dioxide released from the combustion of oils, more and more regulations on sulphur content in petroleum are being established. The current specification in Europe and USA calls for a maximum sulphur content of 50 ppm in gasoline and diesel oil by 2005 and this level should be reduced to below 10 ppm by the year 2010 [7]. The current industrial method used for the removal of sulphur from fuels is hydrodesulfurization (HDS), which requires high temperature and high pressure. Thus biodesulfurization (BDS) [2], which operates under room temperature and pressure conditions, is expected to be complementary as well as promising possible alternative to HDS.

Biocatalytic desulfurization can proceed via two different biochemical pathways, named Kodama [8] and 4S route [9]. However, the carbon skeleton of aromatic sulphur compounds only remains intact via the 4S pathway, and consequently fuel value is not lost.

When biodesulfurization is conducted via the 4S pathway, sulphur is eliminated from DBT in four consecutive reactions—catalyzed by different enzymes. In such processes the identification of intermediate products is crucial for any kinetic study.

Furthermore, in biodesulfurization reactions an immiscible organic phase (model organic solvent or fuel) is mixed with a water fraction necessary for microorganisms. PASHs like DBT and their alkylated derivatives are very hydrophobic compounds, but some of the intermediate degradation products can be more hydrophilic. This situation implies the necessary measurement of each compound in both liquid fractions.

The organic phase used is normally a long chain hydrocarbon, such as dodecane, tetradecane, hexadecane, or oil if the biodesulfurization is performed in a real matrix. As the watery phase, different buffers are used (phosphate buffer or *N*-[2-hydroxyethyl]piperazine-*N'*-[2-ethane-sulfonic acid (HEPES) buffer) in resting cell operation mode. In the cases of biodesulfurization by growing cells, the water fraction consists, in the culture medium, with the carbon source and other nutrients necessary for the microorganisms [10–15].

Preconcentration steps after a degradation process are very important when intermediate products have to be determined: since normally the concentration of unknowns is very low. The extraction procedure is typically optimized for the compounds that will be degraded and for some others which are expected to be formed, provided that analytical standards

are available [16–18]. Then, the application of the method is performed in order to detect all of the transformation products generated in the degradation process. Even when a preconcentration is not necessary, a change of the solvent is normally required, before injection in the gas chromatography equipment.

These two phases involved in biodesulfurization processes should be separated and analyzed in a different way. The organic phase can be directly analyzed by gas chromatography (GC) or liquid chromatography (LC), or can be extracted by solid phase extraction. The watery phase can be directly analyzed by LC or can be extracted by liquid–liquid extraction if GC analysis is required.

Solid phase extraction sorbents are normally chosen by the nature of their primary interaction or retention mechanisms with the analyte in question. In that case, non-polar or moderately polar compounds should be extracted from a non-polar organic solvent. Sorbents like silica, aminopropyl, cyanopropyl are especially indicated in the extraction of compounds with functional groups, such as hydroxyls, amines and heteroatoms (S, O, N) from non-polar matrices.

In fact, the solid phase extraction methods used for the extraction of biodesulfurization compounds (pattern compounds or degradation products) developed by various authors, involve the use of silica packing for the separation and concentration of DBT, 2-HBP, 2,2'-biphenylol and DBT-sulfone [19], alkylated dibenzothiophenes and its transformation products [20,21].

Different solvents have been used to perform liquid–liquid extraction such as ethyl acetate [22–28], *n*-hexane [29] and methylene chloride [30]. The culture broth is normally acidified before liquid–liquid extraction takes place at pH 2 [27,28].

However, detailed recovery studies of these extraction procedures are not usually reported in the literature. Only Onaka et al. [20] performed a study of solid phase extraction applied to biodesulfurization processes.

Several papers have been published concerning the analysis of PASHs in environmental matrices [31,32] and in biodesulfurization processes [33].

Different analytical techniques have been used for studying degradation of organic compounds under different conditions. As examples: GC–MS; GC atomic emission detector (GC-AED) or LC time of flight mass spectrometry (LC-ToF-MS) techniques have been used in the determination of the transformation products of imidacloprid (a pesticide), methyl *tert*-butyl ether (an additive of gasoline) and bisphenol A (an industrial chemical) in degradation processes such as advanced oxidation processes or sunlight photo-alteration [16–18,34,35].

However, in biodesulfurization, high-performance LC coupled to an ultra violet detector (HPLC-UV) [22,27,28,30,36] and GC coupled to a flame ionization detector (GC-FID) [20,23,26,29,37,38] are used by most of the authors to follow degradation processes and to quantify the pattern compound as well as the final product. GC–MS [22–25,30,38] is normally used to identify intermediates.

The sensitivity of analytical techniques traditionally used in biodesulfurization processes seems to be enough (although no data on the limits of detection are reported by any authors) to detect the initial compound and final products, but in some cases these techniques are not adequate in the detection of intermediate products [30].

Very simple and accessible analytical techniques, such as HPLC-UV and GC-FID, are enough to monitor a global biodesulfurization process. In contrast, it is not always possible to confirm the identification of degradation products extensively: that can represent a very important factor in the process evaluation [36].

Electron impact ionization mode in mass spectrometry is the method widely employed for the identification of intermediates in biodesulfurization processes [22–25,30,38].

However, to the best of our knowledge, chemical ionization mass spectrometry has never been used to identify PASHs involved in biodesulfurization processes. It is a widely used analytical technique, which is recognized for the improved selectivity and sensitivity that can be achieved in the detection of several compounds [39,40].

Hybrid chemical ionization (HCI), a new and useful alternative to conventional chemical ionization mass spectrometry [41], has been applied to the analysis of the selected compounds. This technique takes advantage of the high versatility of ion trap (IT) spectrometers combined with external ionization sources. In hybrid configuration, reagent ions are generated in the external source through electron impact ionization (EI) of a reagent gas.

The aim of this work has been to develop a method able to monitor a biodesulfurization reaction. The method involves a solid phase extraction procedure for the organic phase and a liquid–liquid extraction procedure for the watery phase. The analytical determination was performed by GC. The limits of detection and identification capabilities of electron impact ionization (EI), positive chemical ionization (PCI) and HCI have been compared.

Finally these methods were applied to determine the selected compounds in samples from a biodesulfurization process and in a sample of gasoline.

2. Experimental

2.1. Chemicals

The following compounds were supplied by Sigma–Aldrich (Steinheim, Germany): HEPES buffer, dibenzothiophene, dibenzothiophene sulfone (DBTO), DBTO₂, 2-hydroxibiphenyl, 4-methyl-dibenzothiophene and tetracycline (TC) 4-methyl-dibenzothiophene and 4,6-dimethyl-dibenzothiophene. L-Glutamic acid, glycerine and other nutrients for basalt salt medium formulation were from Panreac (Barcelona, Spain). Deionized water was used to prepare all media and stock solutions except where otherwise indicated.

Hexane, dichloromethane and methanol HPLC grade were delivered by Merck (Darmstadt, Germany).

2.2. Experimental procedure for microorganism growth

The bacterium used was *Pseudomonas putida* CECT 5279, a GMO supplied by Centro de Investigaciones Biológicas, Consejo Superior de Investigaciones Científicas (CSIC), Madrid, Spain [42]. This microorganism was maintained in a concentrated stock solution with glycerol in saline serum (50%) at -80°C .

The biocatalyst production was conducted following a standardized procedure reported in Ref. [43]. This procedure includes inoculum buildup in two growth steps using a complex medium, and the final fermentation in a 15-l agitation tank bioreactor (Biostat C—Braun). In the last case, the medium used was composed of a basalt salt medium with L-glutamic acid as the carbon source. Operational conditions were 30°C , 250 rpm and 1 l/min of aeration. Growth was stopped in stationary growth phase, and biomass was collected by centrifugation. The collected cells were re-suspended in glycerol–saline serum (50%) and maintained at -18°C until use.

2.3. Biodesulfurization assays

The biodesulfurization reactions were made in resting cell operation mode, using a 2-l agitated tank reactor (Biostat B—Braun), with 500 ml of total reaction volume and 50% oil volume of a model oil containing 4-m-DBT. It was added into the reaction broth, dissolving directly in hexadecane (the organic solvent selected as model oil). The organic phase was always prepared to contain an initial concentration of 50 mg/l of 4-m-DBT in hexadecane. The aqueous phase was HEPES buffer (pH 8). Air flow was adjusted to 1 l/min and the agitation speed and temperature was controlled at 250 rpm and 30°C . Tween 85 and ethanol were added as surfactant and co-solvent in 1 and 0.5% volume proportions, respectively for the bioavailability enhancement of 4-m-DBT. The biocatalyst concentration used was 4 g/l in watery phase.

The samples collected at different time intervals were decanted over a 2-h period. After that, organic and watery phases were separated and finally each phase was centrifuged (7000 rpm, 22°C , 10 min) to obtain the organic and aqueous fraction as well as the biomass pellet.

2.4. Sample treatment

The solid phase extraction method developed for the extraction of selected compounds from the organic phase was performed as follows.

A packed silica cartridge (500 mg, 3 ml) from Waters (Milford, MA, USA) was used, the cartridge was first conditioned with 5 ml of *n*-hexane. After that, 10 ml of sample was loaded, then the cartridge washed with 1 ml of *n*-hexane. Finally, compounds were eluted from the solid phase with two 6 ml portions of dichloromethane. The extract was evaporated until dryness under nitrogen stream and then recomposed in 1 ml of ethyl acetate and injected into the GC–MS system.

The liquid–liquid extraction method for the extraction of the selected compounds from the watery phase was performed as

follow: 4 ml of sample was adjusted to pH 2 with chlorine acid 2N, the sample was extracted with 2 ml of ethyl acetate, and the extraction was made by stirring in a test tube. The ethyl acetate phase was separated from the water and directly injected into the GC–MS system.

2.5. GC mass spectrometry methods

Two different chromatographic systems were used in this work, a gas chromatograph coupled to a mass spectrometer with a quadrupole as analyzer (GC-q-MS) and a gas chromatograph coupled to a mass spectrometer with an IT as analyzer (GC-IT-MS).

2.5.1. GC-q-MS methods

Gas chromatography–mass spectrometry (GC–MS) analyses were run on a HP 6890 series gas chromatograph (Hewlett-Packard, Palo Alto, CA) interfaced to a HP 5973 mass-selective detector. Data acquisition, processing and instrumental control were performed by the HP MSD Chem-Station software. Analytes were separated in a Hewlett-Packard HP-5MS capillary column (5% biphenyl/95% dimethylsiloxane), 30 m × 0.25 mm i.d., 0.25 μm film thickness. A split/splitless injector was used in the pulse splitless mode. An empty liner was filled with 0.5 cm Carbofrit (Restek, Bellefonte, CA) placed 3.6 cm from the upper part of the liner. The injector operating conditions were as follows: injection volume 10 μl; injector temperature 250 °C; initial pulse pressure 30 psi (1.5 min). The helium carrier gas flow was maintained at 1 ml/min.

The oven temperature programme was 1.0 min at 70 °C then it was increased at 10 °C min⁻¹ until reaching 250 °C. It was kept at this temperature for 2 min, the total run time being 21 min. The transfer line temperature was set at 280 °C.

In this system two ionization modes were employed, electron impact ionization and PCI. The specific conditions for each are detailed below.

2.5.1.1. Electron impact ionization mode. Electron impact (EI) mass spectra in full scan mode were obtained at 70 eV, the monitoring was from *m/z* 50 to 400. The ion source and quadrupole analyzer temperatures were fixed at 230 °C and 106 °C, respectively.

2.5.1.2. Positive chemical ionization mode. Positive chemical ionization (PCI) mass spectra in full scan mode were obtained using methane as the reagent gas at 40 ml/min. The ion source and quadrupole analyzer temperatures were fixed at 250 °C and 106 °C, respectively.

2.5.2. GC-IT-MS method

The experiments were performed on a Varian 4000 GC/MS/MS system equipped with an external ionization source. Automatic injections (1 μl) were performed in a split/splitless injector at 250 °C, working in splitless mode with a splitless time of 1 min. Separations were performed in a crosslinked 5%-phenyl-95%-dimethylpolysiloxane Varian FactorFour (VF-5 ms, Varian, Middelburg, The Netherlands) capillary column

(30 m, 0.25 mm, 0.25 μm), using the same oven program as in GC-q-MS methods. The helium carrier gas flow was maintained at the constant value of 1 ml/min. The GC–MS interface and the IT temperature were set at 250 and 200 °C, respectively. Data acquisition, processing and instrumental control were performed by the Varian MS Workstation Version 6.42. Typical IT–MS operating conditions were optimized by the software at the following values: electron multiplier at 1125 V, trap offset at 7 V, lens 1 at 35 V, lens 3 at 23 V and gate lens at –108 V. The external ion source worked in CI mode at a temperature of 200 °C.

2.5.2.1. Hybrid chemical ionization. Hybrid chemical ionization mass spectra were obtained using perfluorotri-*n*-butylamine (FC 43) as the reagent gas, which is a reagent commonly used as a calibration compound in electron ionization mass spectrometry. The spectrum obtained under EI shows the characteristic fragment ions at *m/z* 69 [CF₃]⁺, 131 [C₃F₅]⁺, 264 [C₅F₁₀N]⁺, 414 [C₈F₁₆N]⁺ and 614 [C₁₂F₂₄N]⁺ used for routine calibration purposes.

HCI mass spectrum for the sample ions is acquired after three steps: ionization of the reagent gas (the ionization time is determined by a prescan), then the selected reagent ions are stored in the IT. After that, reagent ions react with sample molecules to form sample ions (the reaction time is determined by a prescan) and finally the reagent ions are ejected.

The selected ion chosen to react with the sample ions was 131 [C₃F₅]⁺, the ejection amplitude was 40 V, the maximum reaction time and the reaction storage level were 100 ms and 80 *m/z*, respectively.

3. Results and discussion

3.1. Extraction methods

Recoveries of the two extraction methods were evaluated; 50 ml of C16 and 10 ml of HEPES buffer were spiked with 1 mg/l and 5 mg/l, respectively of all the compounds.

Three aliquots of fortified C16 and HEPES buffer were extracted by solid phase extraction and liquid–liquid extraction, respectively following the protocol explained in the experimental part. The concentration of the compounds in the extracts was compared with the concentration of the compounds in a standard solution containing 10 mg/l of all the compounds. The recoveries of both extraction methods were evaluated and are shown in Table 1.

Very good recoveries, between 88 and 120% were obtained in the watery phase for all the compounds. Recoveries in the organic phase were between 70 and 83% for DBT, 4-m-DBT, 4,6-dm-DBT and 4,6 de-DBT and between 40 and 67% for 2-HBP, HBPS, DBTO, DBTO₂. Very good precision in the extraction was achieved for all the compounds in both methods with R.S.D. values below 10%.

3.2. Comparison between the three analytical techniques

Linearity and inter/intra-day precision were investigated in the three analytical techniques, similar and good results were

Table 1
Retention time, recoveries in watery and organic phases and limits of detection of the selected compounds, obtained by the use of the different techniques

	Retention time (min), GC-q-MS	Retention time (min), GC-IT-MS	Recoveries (R.S.D. %) (N = 6)		Limits of detection in full scan mode (mg/l)		
			LLE	SPE	EI	PCI	HCI
2-HBP	11.6	12.45	100 (7)	67 (3)	1.40	1.00	0.043
DBT	14.4	15.29	90 (5)	78 (4)	0.50	0.10	0.005
4-m-DBT	15.5	16.34	100 (4)	83 (4)	0.40	0.10	0.002
4,6-dm-DBT	16.52	17.31	100 (10)	70 (6)	0.40	0.10	0.001
HBPS	17.14	17.90	110 (9)	40 (3)	1.80	1.00	0.003
DBTO	18.11	19.06	100 (6)	60 (8)	2.00	1.00	0.021
DBTO ₂	18.17	18.90	100 (4)	64 (2)	1.70	1.00	0.005
4,6 de-DBT	18.17	18.89	80 (8)	70 (5)	0.09	0.05	0.002

obtained for all the investigated compounds in the three techniques. Results are not included in this paper as it is only focused on the sensitivity and identification capabilities of the investigated analytical techniques.

A practical limit of determination was calculated experimentally in the three ionization modes by the injection of spiked extract and calculated using a signal-to-noise ratio of 10. The limits of determination are shown in Table 1. Similar values were achieved in PCI and EI for all the compounds; they are ranged from 0.05 mg/l to 2 mg/l. However, the limits of determination in HCI are at least two orders of magnitude lower than in PCI and EI in all the cases. The low limits of detection achieved for degradation products such as HBPS (see Table 1), which some authors are not able to detect in biodesulfurization processes by using GC-MS (EI) are of special interest [30]. For the above-mentioned compound, the limits of determination in EI and PCI, are 1.8 mg/l and 1 mg/l, respectively, while in HCI the limit of determination is 0.003 mg/l which allows the determination of this degradation product at very low concentrations.

GC-EI-MS, GC-PCI-MS and GC-HCI-MS were used to identify the group of selected PASHs investigated in this work, chromatograms obtained by the injection of a spiked extract at a concentration of 0.5 mg/l under the conditions explained in the experimental part were acquired applying each of the techniques and are shown in Fig. 1. Good chromatographic separation was obtained for most of the compounds except for DBTO₂ and 4,6 de-DBT, where a coelution at the end of the chromatogram was not resolved.

Identification capabilities of the three ionization modes were compared by the acquisition of mass spectra in full scan mode of all the compounds. In Table 2, the main ions obtained for all the PASHs investigated in the three techniques are shown, to construct this table each compound was injected individually.

The mass spectrum of dibenzothiophene under electron impact ionization shows as base peak the ion at m/z 184 corresponding with the molecular ion, m/z 139 and 152, which, correspond to the loss of the sulphur atom.

2-Hydroxybiphenyl, 4-m-dibenzothiophene and 3,4-dm-dibenzothiophene and dibenzothiophene sulfoxide show the molecular ion $[M]^+$ as base peak, m/z 170, 198, 212 and 216, respectively. These compounds present little fragmentation in GC-EI-MS and the ions show a relative abundance lower than 40% in most of the cases (see Table 2). HBPS does not show

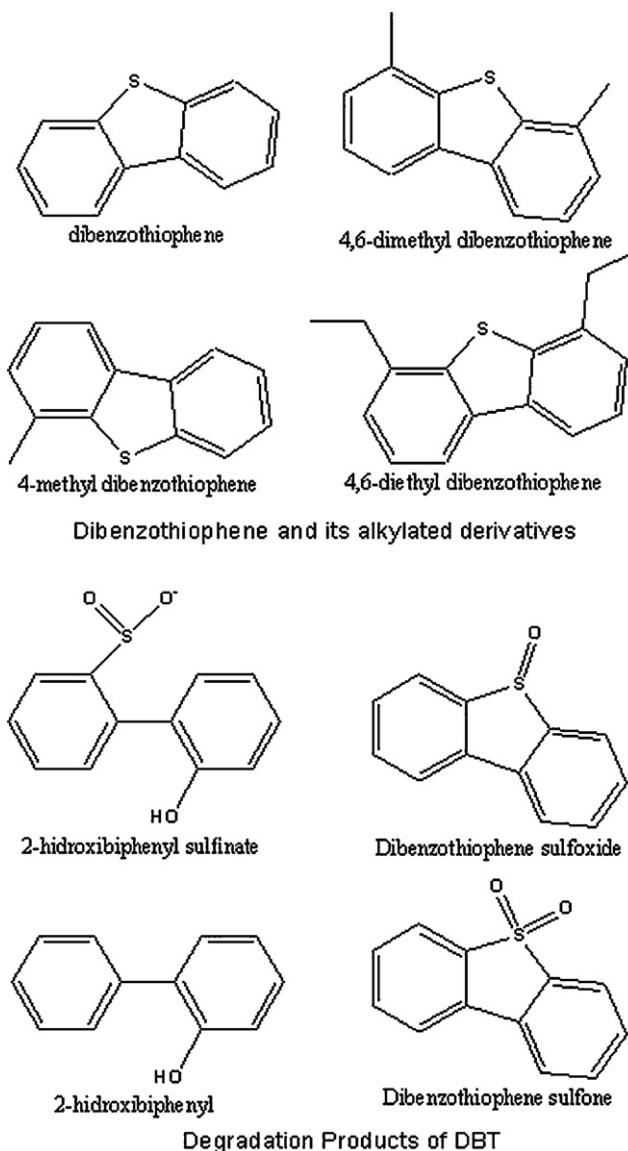


Fig. 1. Selected compounds for the study, including dibenzothiophene and three alkylated derivatives of dibenzothiophene and four degradation products of dibenzothiophene.

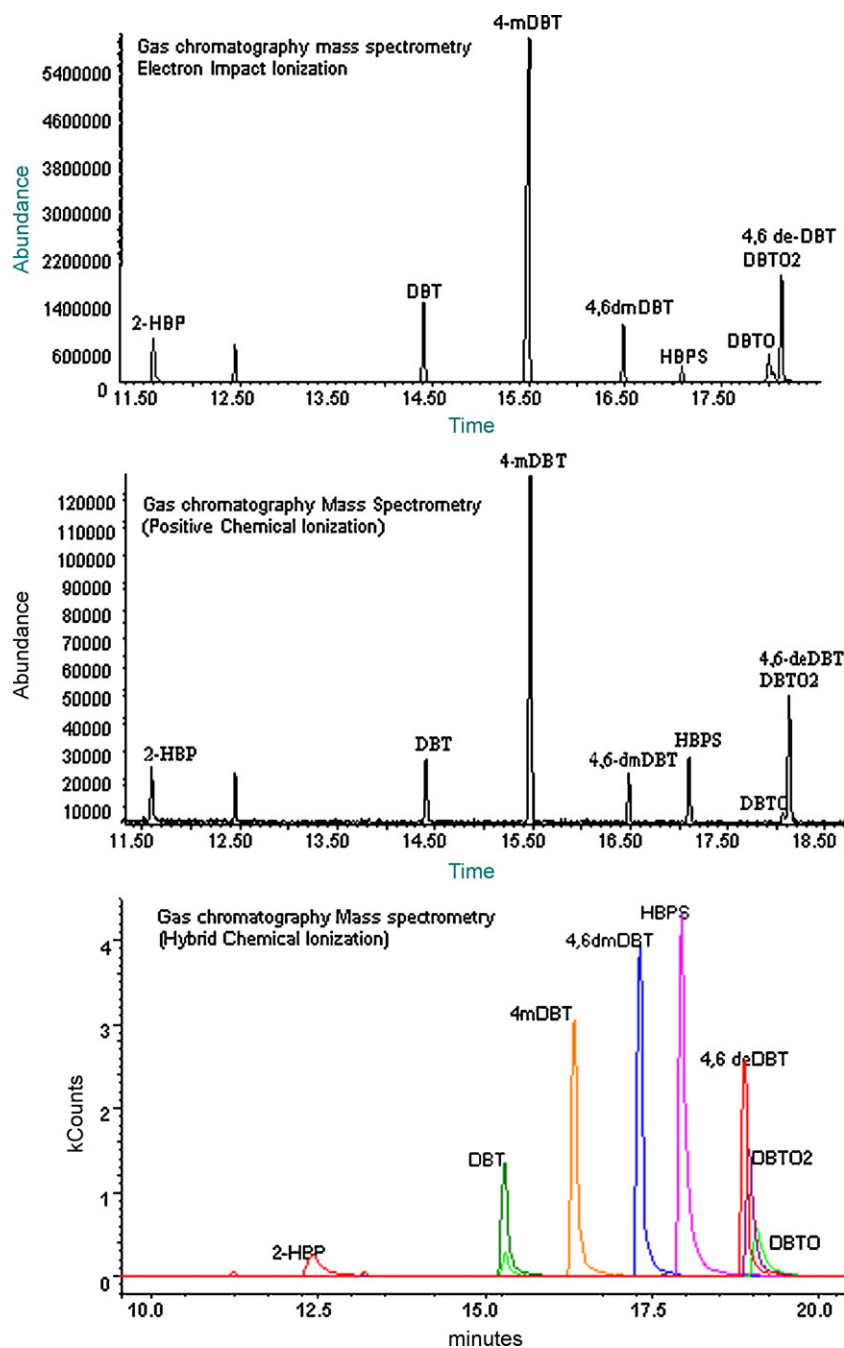


Fig. 2. Chromatograms obtained under GC-EI-MS, GC-PCI-MS and GC-HCI-MS of a mixture of the studied compounds at a concentration of 0.5 mg/l.

Table 2

Molecular weight and main ions of the selected compounds in the three ionization modes

	Mw	Main ions in full scan mode (% relative abundance)		
		EI	PCI	HCI
2-HBP	170	170 (100), 141 (40), 115 (30)	171 (100), 199 (30), 211 (15)	261 (100), 281 (77), 199 (50), 301 (40), 170 (20)
DBT	184	184 (100), 139 (25), 152 (15)	185 (100), 213 (30), 225 (15)	315 (100), 184 (80)
4-m-DBT	198	198 (100), 165 (15),	199 (100), 227 (30), 239 (15)	329 (100), 198 (98)
4,6-dm-DBT	212	212 (100)	213 (100), 241 (30), 253 (15)	343 (100), 212 (100)
HBPS	233	216 (100), 187 (75), 168 (50), 139 (48)	217 (100), 201 (30), 185 (20)	347 (100)
DBTO	200	184 (100), 171 (50), 200 (50)	185 (100), 213 (40)	184 (100), 331 (<15)
DBTO ₂	216	216 (100), 187 (40), 168 (40), 139 (40)	217 (100)	347 (100), 216
4,6 de-DBT	240	225 (100), 240 (95), 210 (30)	241 (100)	240 (100), 371 (98)

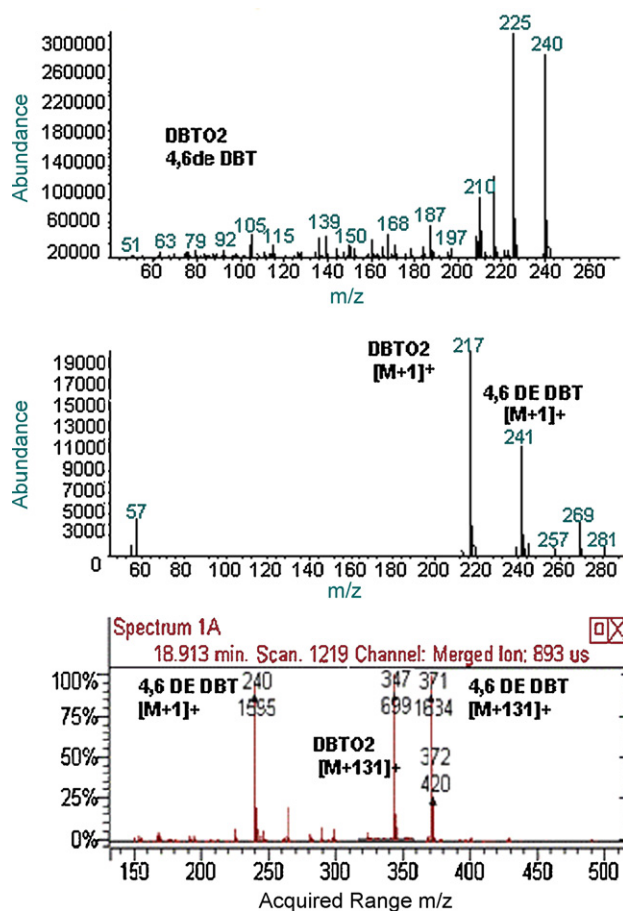


Fig. 3. Mass spectra of DBTO2 and 4,6 de-DBT in an unresolved peak, obtained under GC-EI-MS, GC-PCI-MS and GC-HCI-MS.

the molecular ion in its spectra, the base peak m/z 216 corresponds to the loss of the hydroxyl group. 4,6 de-DBT presents the ion m/z 225 as base peak which corresponds to the loss of a methyl group, the molecular ions m/z 240 and 210 (loss of two methyl groups) are present as well in the mass spectrum (see Table 2). Dibenzothiophene sulphone presents the ion m/z 184 as base peak, which corresponds to the loss of an oxygen atom, the molecular ion m/z 200 is present in the mass spectrum with a relative abundance lower than 30%.

Electron impact ionization is the most popular technique since its spectra are highly reproducible, which means that mass spectral libraries can be used for the identification of unknowns. Compound identification is currently performed by comparing an unknown electron ionization MS spectrum with collections of reference spectra. The identification process is based on search algorithms which compare the obtained spectra with those of a library, and which are generally implemented in the GC-MS instrument. A spectral match and fit factor defines the certainty of the identification. Although library searches are a powerful tool for the identification of unknowns, for this purpose, a series of conditions must be met: the compound must be included in the library; the MS conditions at which both spectra have been obtained must be similar; and finally, the GC separation must be sufficiently efficient to obtain a clean mass spectrum.

Applying PCI, using methane as the reagent gas, the $[M+H]^+$ of all the compounds are obtained except for HBPS and DBTO, which present the $[M-OH+H]^+$, m/z 217 and the $[M-O+H]^+$, m/z 185, respectively.

The HCl mode requires the use of an external ionization source in which the ionization of the reactive gas takes place by electron ionization (EI). From the reagent ions generated,

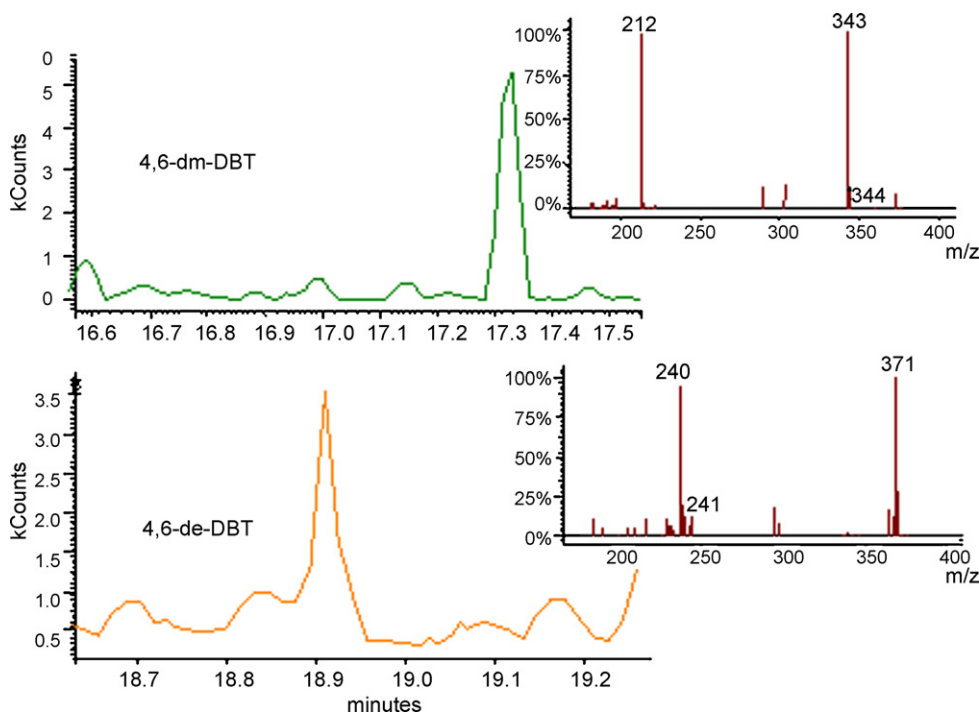


Fig. 4. Chromatographic peak and mass spectra of the identified compounds (4,6 deDBT, 4,6-dm-DBT) in a sample of gasoline hydrodesulfurated extracted by the proposed solid phase extraction method and analyzed by GC-HCI-MS.

only those which are selected are stored in the IT. These trapped reagent ions are allowed to react with sample molecules, which enter the IT directly from the GC column through the transfer line, forming CI products ions. This approach has a number of potential advantages, including avoiding ion-molecule reactions with neutral reagent and avoiding losses of negative ions that occur when they move from the external source to the trap. On the other hand, the adequate selection of a specific reagent gas ion allows improvement in the selectivity of the analytical method, especially in highly complex matrices.

When HCl is applied for the identification of the selected group of PASHs, the $[M+C_3F_5]^+$ ion is observed for all the compounds except for HBPS which presents the $[M-OH+C_3F_5]^+$ ion. In addition to these adduct most of the compounds show in their mass spectra the molecular ion $[M]^+$.

Under GC-EI-MS, most of the compounds investigated in this work can be identified by using the library, but as can be seen in the chromatogram obtained (Fig. 2), a coelution in the last part is not resolved (last peak in the chromatograms). In Fig. 3, we show the mass spectra of this peak obtained by using the three analytical techniques, the unresolved peak corresponds with DBTO₂ and 4,6-dm-DBT, the mass spectra show ions from the two compounds. The EI spectra show many ions, the ions with higher relative abundances are at m/z 225 and 240 and they are results of the fragmentation of 4,6 de-DBT. The ions which give the fragmentation of DBTO₂ (at m/z 216, 187, 168, 139) are present in the spectra with a relative abundance lower than 40%.

In contrast, the PCI spectra show only two main ions, m/z 217 as base peak, and m/z 241 with a relative abundance of 60%, they correspond with the $[M+H]^+$ of DBTO₂ and 4,6 de-DBT, respectively. While in EI, the ions corresponding to DBTO₂ are minorities in comparison with the ions corresponding to 4,6 de-DBT, in PCI. This compound presents a better analytical response.

The HCl spectra show three main ions at m/z 347, 240 and 371, corresponding to the $[M+C_3F_5]^+$ of DBTO₂ $[M+C_3F_5]^+$ of 4,6 de-DBT and $[M]^+$ of 4,6 de-DBT, respectively.

When two compounds are coeluting, the mass spectra obtained by chemical ionization is simpler than when EI is applied. These techniques can be used as complementary techniques for identification purposes.

4. Application to real samples

As we outlined in Section 1, the PASHs selected in this work are frequently involved in biodesulfurization experiments. DBT and alkylated derivatives are used as model compounds for biodesulfurization, and the other compounds selected are intermediates that can be found during a biodesulfurization reaction or as final products in these degradation processes. These biodesulfurization reactions are normally developed for a further application in the biodesulfurization of crude oils, which is a very complicated matrix and in which the identification of compounds can be complicated.

A sample of hydrodesulfurated diesel extracted by the SPE procedure optimized in this work was analyzed by GC-EI-MS,

GC-PCI-MS and GC-HCl-MS. Under PCI and EI, no compounds were identified, however under HCl, two alkylated DBTs were identified, namely 4,6 de-DBT and 4,6-dm-DBT. Chromatogram and mass spectra of these compounds are shown in Fig. 4. These two compounds were identified by the presence of the molecular ion and the $[M+C_3F_5]^+$.

GC-PCI-MS method was applied in a biodesulfurization reaction which was performed under the conditions explained in the experimental part. The biodesulfurization reaction was performed with an initial concentration of 4-m-DBT (50 mg/l) as model compound, the analysis by GC-PCI-MS revealed that a similar concentration of 4-m-DBT is present in the initial and in the final sample, and no transformation products were generated. However, a low quantity of DBT was detected in the initial sample and 2-HBP, a transformation product of DBT, was detected in the final sample. Initial and final samples of the biodesulfurization reaction were analyzed under HCl and electron impact ionization-based techniques proposed in this work (HCl-MS and GC-EI-MS) and no additional compounds were identified.

5. Conclusions

The extraction procedures and the analytical methods developed can be applied in the determination of PASHs in samples from a degradation process.

The method typically employed in the identification of degradation products in biodesulfurization process is GC-EI-MS [33]. This technique is very useful since libraries can be employed but, in many cases, the technique is not able to identify degradation products. Consequently, more selective techniques based on chemical ionization must be used in the identification of degradation products.

An improvement in sensitivity is achieved by the use of GC-HCl-MS, compared to GC-EI-MS and GC-PCI-MS, which is required in the detection of some degradation products.

Acknowledgements

Milagros Mezcua acknowledges the “Juan de la Cierva” research contract from The Spanish Ministry of Science and Technology.

The work has been supported by the Spanish Ministry of Science and Technology Project number CTQ2004/06553-C02-02: Biodesulfuración de fracciones petrolíferas: Condiciones y formas de operación.

The authors wish to acknowledge the help given by Simon Turner in revising the text.

References

- [1] D.J. Monticello, *Curr. Opin. Biotechnol.* 11 (2000) 540.
- [2] A. Alcon, V.E. Santos, A.B. Martín, P. Yustos, F. García-Ochoa, *Biochem. Eng. J.* 26 (2005) 168.
- [3] M. Blumer, W. Youngblood, *Science* 188 (1975) 53.
- [4] G. Grimmer, J. Jacob, K.W. Naujak, *Fresenius Anal. Chem.* 314 (1983) 29.
- [5] F. Berthou, V. Vignier, *Int. J. Environ. Anal. Chem.* 27 (1986) 81.
- [6] J.J. Kilbane, *Trends Biotechnol.* 7 (1989) 97.
- [7] European standard for gasoline EN 228/1999 and for diesel EN 590/1999.

- [8] K. Kodama, K. Umehara, K. Shimizu, S. Nakatani, Y. Minoda, K. Yamada, *Agric. Biol. Chem.* 37 (1973) 45.
- [9] Y. Izumi, T. Ohshiro, H. Ogino, Y. Hine, M. Shimao, *Environ. Microbiol.* 60 (1994) 223.
- [10] J. Xiaoqiang, W. Jianping, S. Zhipeng, C. Qinggele, X. Shuangping, *Chem. Eng. Sci.* 61 (2006) 1987.
- [11] I. Bagus, W. Gunam, Y. Yaku, M. Hirano, K. Yamamura, F. Tomita, T. Sone, K. Asano, *J. Biosci. Bioeng.* 101 (2006) 322.
- [12] C.Q. Ma, J.H. Feng, Y.Y. Zeng, X.F. Cai, B.P. Sun, Z.B. Zhang, H.D. Blankespoor, P. Xu, *Chemosphere* 65 (2006) 165.
- [13] F. Li, Z. Zhang, J. Feng, X. Cai, P. Xu, *J. Biotechnol.* 127 (2007) 222.
- [14] A. Caro, K. Boltes, P. Letón, E. García-Calvo, *Biochem. Eng. J.* 35 (2007) 191.
- [15] G. Mohebbali, A.S. Ball, B. Rasekh, A. Kaytash, *Enzyme Microb. Technol.* 40 (2007) 578.
- [16] S. Malato, J. Cáceres, A. Agüera, M. Mezcua, D. Hernando, J. Vial, A.R. Fernández-Alba, *Sci. Technol.* 35 (2001) 4359.
- [17] M. Mezcua, M.J. Gómez, I. Ferrer, A. Agüera, M.D. Hernando, A.R. Fernández-Alba, *Anal. Chim. Acta* 524 (2004) 241.
- [18] I. Ferrer, M. Mezcua, M.J. Gómez, E.M. Thurman, A. Agüera, M.D. Hernando, A.R. Fernández-Alba, *Rapid Commun. Mass Spectrom.* 18 (2004) 443.
- [19] T. Onaka, K. Okamura, M. Suzuki, *J. Chromatogr. Sci.* 35 (1997) 417.
- [20] T. Onaka, M. Kobayashi, Y. Ishii, K. Okumura, M. Suzuki, *J. Chromatogr. A* 903 (2000) 193.
- [21] T. Onaka, M. Kobayashi, Y. Ishii, J. Konishi, K. Maruhashi, *J. Biosci. Bioeng.* 92 (2001) 80.
- [22] K. Kirimura, T. Furuya, R. Sato, Y. Ishii, K. Kino, S. Usami, *Appl. Environ. Microbiol.* (2002) 3867.
- [23] Y. Ishii, S. Kozaki, T. Furuya, K. Kino, K. Kirimura, *Curr. Microbiol.* 50 (2005) 63.
- [24] W. Li, Y. Zhang, M.D. Wang, Y. Shi, *FEMS Microbiol. Lett.* 247 (2005) 45.
- [25] F. Li, P. Xu, J. Feng, L. Meng, Y. Zheng, L. Luo, C. Ma, *Appl. Environ. Microbiol.* (2005) 276.
- [26] N. Nomura, M. Takada, H. Okada, Y. Shinohara, T. Nakajima, K. Tadaatsu, N. Hiroo, *J. Biosci. Bioeng.* 100 (2005) 398.
- [27] S. Maghsoudi, M. Vossoughi, A. Kheirilomoon, E. Tanaka, S. Katoh, *Biochem. Eng. J.* 8 (2001) 151.
- [28] S. Maghsoudi, A. Kheirilomoon, M. Vossoughi, E. Tanaka, S. Katoh, *Biochem. Eng. J.* 5 (2000) 11.
- [29] Y. Hou, Y. Kong, J. Yang, J. Zhang, D. Shi, W. Xin, *Fuel* 84 (2005) 1975.
- [30] S. Abbad-Andaloussi, C. Lagnel, M. Warzywoda, F. Monot, *Enzyme Microb. Technol.* 32 (2003) 446.
- [31] J.T. Anderson, A.H. Hegazi, B. Roberz, *Anal. Bioanal. Chem.* 386 (2006) 891.
- [32] J.T. Anderson, in: W. Kleiböhmer (Ed.), *Environmental Analysis (Handbook of Analytical Separations, vol. 3)*, Elsevier, Amsterdam, 2001.
- [33] M. Mezcua, A.R. Fernández-Alba, A. Rodríguez, K. Boltes, P. Letón, E. García-Calvo, *Talanta* 73 (2007) 103.
- [34] A. Agüera, M. Mezcua, D. Hernando, S. Malato, J. Cáceres, A.R. Fernández-Alba, *Int. J. Environ. Anal. Chem.* 84 (2004) 149.
- [35] M. Mezcua, I. Ferrer, M.D. Hernando, A.R. Fernández-Alba, *Food Addit. Contam.* 23 (2006) 1242, 2006.
- [36] M.F. Luo, J.M. Xing, Z.X. Gou, S. Li, H.Z. Liu, J.Y. Chen, *Biochem. Eng. J.* 13 (2003) 1.
- [37] K.I. Noda, K. Watanabe, K. Maruhashi, *J. Biosci. Bioeng.* 95 (2003) 354.
- [38] K.I. Noda, K. Watanabe, K. Maruhashi, *J. Biosci. Bioeng.* 95 (2003) 504.
- [39] M.A. Huestes, *J. Chromatogr. B* 833 (2006) 210.
- [40] D. Carrizo, J.O. Grimalt, *J. Chromatogr. A* 1118 (2006) 271.
- [41] A. Agüera, *J. Chromatogr. A* 1133 (2006) 287–292.
- [42] B. Galan, E. Diaz, A. Fernandez, M.A. Prieto, J.L. Garcia, F. Garcia-Ochoa, E. Garcia-Calvo, *International Patent* (2001) Wo 01/70996 AL.
- [43] A.B. Martin, A. Alcon, V.E. Santos, F. Garcia-Ochoa, *Energy Fuels* 18 (2004) 851.

Controlled synthesis of ZnO from nanospheres to micro-rods and its gas sensing studies

Shalaka C. Navale^{a,b}, S.W. Gosavi^b, I.S. Mulla^{a,*}

^a *Physical and Materials Chemistry Division, National Chemical Laboratory,
Dr. Homi Bhabha Road, Pashan, Pune 411008, India*

^b *DST Unit on Nanoscience, Department of Physics, University of Pune, Pune 411008, India*

Received 17 December 2007; received in revised form 21 January 2008; accepted 22 January 2008

Available online 13 February 2008

Abstract

1D ZnO rods are synthesized using less explored hydrazine method. Here we find, besides being combustible hydrazine can also be used as a structure-directing agent. The ratio of zinc nitrate (ZN) to hydrazine is found to control the morphology of ZnO. At lower concentration of ZN as compared with hydrazine the morphology of ZnO is found to be spherical. As we increase the hydrazine content the morphology changes from spherical (diameter ~ 100 nm) to the elongated structures including shapes like Y, T as well dumbbell (diameter ~ 40 nm and length ~ 150 nm). Interestingly for more than 50% of hydrazine ZnO micro-rods are formed. Such rods are of diameter ~ 120 nm having length of about 1 μm for ZN to hydrazine ratio of 1:9, isolated as well as bundle of rods are seen in scanning electron microscopy (SEM). The X-ray diffraction (XRD) reveals the phase formation with average particle size of 37 nm as calculated using Scherrer's formula. The high-resolution transmission electron microscopy (HRTEM) is also done to confirm the d-spacing in ZnO. Gas sensing study for these samples shows high efficiency and selectivity towards LPG at all operating temperatures. Photoluminescence (PL) study for these samples is performed at room temperature to find potential application as photoelectric material.

© 2008 Elsevier B.V. All rights reserved.

Keywords: Nanostructures; Hydrazine; ZnO; Photoluminescence; LPG sensor

1. Introduction

Controlled synthesis of semiconductor nanostructures in terms of size and shape has been strongly motivated and novel applications can be investigated dependent on their structural properties [1–4]. Among various semiconductor nanostructures, variety of nanostructures of ZnO has been investigated presenting it as richest family of nanostructures. It crystallizes in a wurtzite structure and exhibits n-type electrical conductivity [5]. ZnO nanomaterial with one-dimensional (1D) structure, such as nanowires or nanorods, are especially attractive due to their tunable electronic and opto-electronic properties, and the potential applications in the nanoscale electronic and opto-electronic devices [6].

Zinc oxide has proven itself as one of the competitive and promising candidates to replace expensive materials like CdS, TiO₂, GaN, SnO₂, and In₂O₃ for applications such as solar cells [7], photocatalysis [8], ultraviolet laser [9,10], transparent conductive oxides [11], spintronics [12], and gas sensors [13]. For gas sensor application, SnO₂ has been the most investigated material. However, ZnO is particularly applicable to gas sensors because of its typical properties such as resistivity control over the range 10⁻³ to 10⁻⁵ cm, high electrochemical stability, absence of toxicity, and abundance in nature [14]. ZnO gas sensors have been fabricated in the form of powders, pellets, thick and thin films.

The most important aspect for an ideal sensor is to have 3 'S', i.e. sensitivity, selectivity, and stability. Many reviews on current research status of sensors based on various new types of nanostructured materials such as nanotubes, nanorods, nanobelts, and nanowires are available [15,16]. These nanostructure-based sensors represent a powerful detection platform for a broad range including biological sensors, electrochemical sensors,

* Corresponding author. Tel.: +91 20 25902276; fax: +91 20 25902636.
E-mail address: is.mulla@ncl.res.in (I.S. Mulla).

gas sensors, optical sensors, pH sensors, orientation sensors, etc. The sensing devices include individual nanostructured sensors, multi-nanostructured sensors, MOSFET-based sensors, and nanostructured film sensors. These nanosensor devices have number of advantages such as high sensitivity, selectivity, fast response, and recovery time which sets them apart from other sensors available today [17]. Furthermore, development of gas sensors to monitor combustible gases is imperative due to the concern for safety requirements in homes and for industries, particularly for detection of LPG, which is one of extensively used but potentially hazardous gases, because explosion accident may be caused when it leaks out accidentally or by mistake. So the detection of LPG is necessary for domestic appliances. Many researchers world wide are tailoring ZnO either in doped or undoped form to be used as gas sensor, few to be mentioned here are as NO₂ [18], NH₃ [19], CO [20], and LPG [21] sensors.

Pal and Santiago [22] reported the synthesis of different morphologies ZnO nanostructures using hydrothermal technique by controlling the content of ethylenediamine (soft surfactant) and the pH of the reaction mixture. Yang and co-workers [23] reported the synthesis of flower-like ZnO nanostructures by

cetyltrimethylammonium bromide (CTAB)-assisted hydrothermal process. However, the morphological control and crystal evolution of flower-like ZnO nanostructures remain challenging to material scientists.

Herein we report tailoring of various morphological changes from nanosphere to nanorods in various shapes and to micron rods using controlled hydrazine as surface directing agent. Their gas sensing study has also been carried out at various operating temperatures and is found to be good reducing gas sensor. The luminescent property of ZnO rods has been investigated extensively for their potential use as photoelectric material.

2. Experimental

Various morphologies of ZnO were synthesized by wet chemical method. Hydrazine, a combustible agent is used in this synthesis. Not much synthesis is done by this method. All chemicals used herein are of Loba Chem, India (AR Grade). A known quantity of zinc nitrate (ZN) was added in double distilled water of 500 ml. A white precipitate was formed on addition of hydrazine. The concentration ratios of ZN to hydrazine were

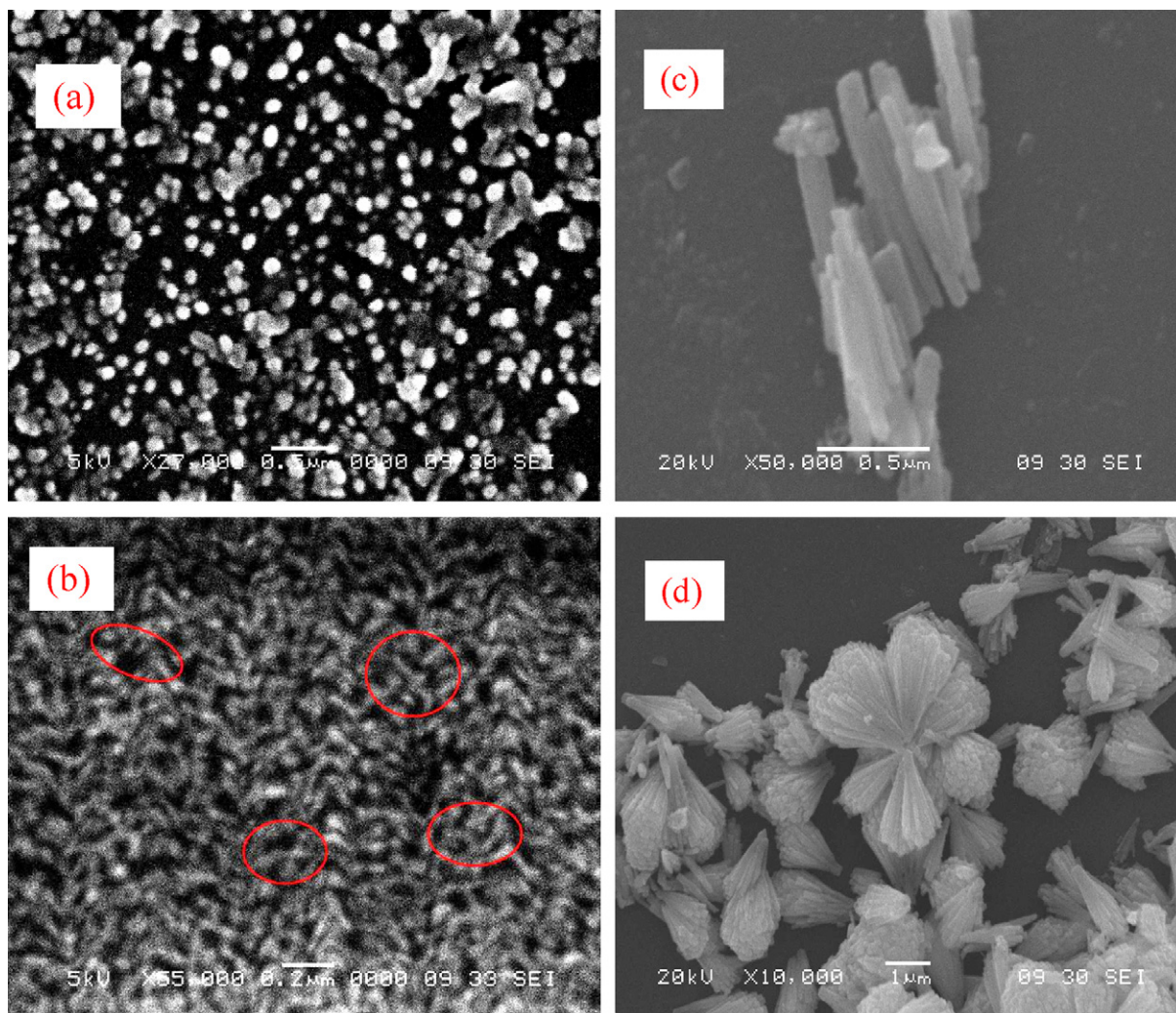


Fig. 1. SEM images for various concentration of ZN:hydrazine: (a) 1:2, (b) 1:4, (c) 1:9, and (d) 1:9.

varied as follows: (a) 1:2, (b) 1:4, and (c) 1:9. These solutions were continuously stirred for 30 min and kept for aging for 10 days. Later these were filtered and dried at room temperature for 24 h and then calcined in the furnace at 300 °C for 5 h to remove the organic volatiles and white ZnO powder is formed.

The structural and particle size determination was done by XRD using copper K α line with an accelerating voltage of 40 kV. PANalytical X'Pert PRO machine was used for the same. The SEM images were observed using Leica Cambridge 440 microscope while HRTEM was done using JEOL 2010. Gas sensing and PL studies were carried to explore the possible applications for these samples. The gas sensing study was performed for ZnO micro-rods by making them as pellets. The pellets of diameter 6 mm and thickness 2 mm were made using hydraulic press. These were then sintered for 2 h at 275 °C so as to have mechanical strength. For electrical measurements, silver paste contacts were used to form ohmic contacts on the ZnO pellets. The experimental details for gas sensing study are described by Navale et al. [18]. The powder sample was sonicated in iso-propanal and the emission spectrum was recorded using PerkinElemer LS-55 of Xenon source with 325 nm.

3. Results and discussions

The possible reaction occurring in the solution is as follows:

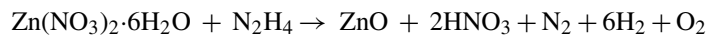


Fig. 1a–c shows the SEM images of ZnO with various morphologies. In Fig. 1a distinct spheres of average diameter ~100 nm are seen. Fig. 1b shows 1D rods in various forms like Y, T, as well as dumbbell shapes. The rods here are of diameter 40–50 nm and length ~150 nm. It is interesting to note that in Fig. 1a there is no other morphology except spheres while Fig. 1b does not show any spheroidal form. Fig. 1c shows uniform 1D rods of diameter ~120 nm and length ~1 μm , while Fig. 1d shows flower- and bud-like structures. It can be seen that for lower concentration of hydrazine the ZnO is in the nanoform without any aggregation. While for high concentration of hydrazine (1:9), ZnO takes the form of micro-rods without any nanostructures. The lower hydrazine contents allow isolated nucleation while higher hydrazine concentration brings the entire nucleating centre together to facilitate aggregation and develop into microstructures. Thus we conclude that the ratio of ZN to hydrazine plays an important role in controlling the morphology of our powders. In the present study we observe that hydrazine being combustible is also acting as a structure-directing agent. Fig. 1c shows isolated nanorods as well as cluster of rods bundled together to form flower-like structure as seen in Fig. 1d for 1:9 Zn to hydrazine ratio. It is observed that only the spindles or the typical flower-like structure with the bundles of zinc oxide rods emerge from single nucleus. The absence of the long rods suggests that the growth of zinc oxide rods triggers from the nucleus very systematically in the pulses giving rise to flower-like structure. This might be facilitating due to the variations in the stirring speed during synthesis. In general, it can be stated that the morphology of the zinc oxide can be

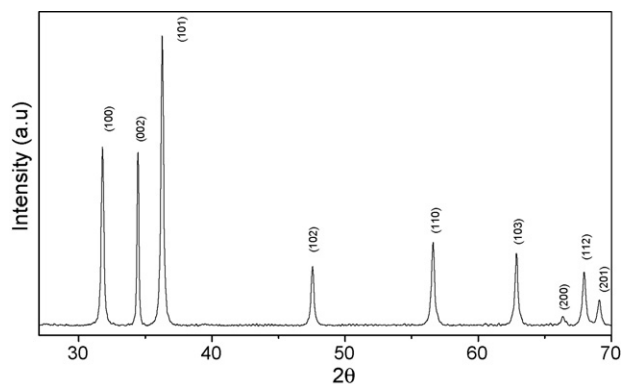


Fig. 2. XRD pattern for ZnO nanorods.

tailor made by controlling mainly the ratio of ZN to hydrazine and stirring parameter.

The XRD diffraction pattern shown in Fig. 2 for micro-rods is found to match with that mentioned in JCPDS 36-1451. The average crystallite size was calculated using Scherrer's formula, $t = 0.9\lambda/\beta \cos \theta$ and was found to be ~37 nm. The lattice parameters calculated for hexagonal phase of ZnO using

$$\frac{1}{d^2} = \frac{4/3(h^2 + hk + k^2)}{a^2} + \frac{l^2}{c^2}$$

has been calculated to be $a = 3.238 \text{ \AA}$ and $c = 5.189 \text{ \AA}$ which are in close agreement with the reported JCPDS 36-1451. The HRTEM image in Fig. 3 indicates the d-spacing along the (1 0 0) plane to be 2.804 \AA and is found to match with that reported in literature [JCPDS].

The gas sensing studies for the pellets (for sample with 1:9) are in temperature range of 250–350 °C. It was found that only reducing gases were sensed. The reducing gases used were H₂, ethanol, H₂S, NH₃, and LPG. The response time is of several minutes at 250 °C while a large improvement was observed at higher operating temperatures. The response time is explained in literature [18]. The samples show high efficient response and

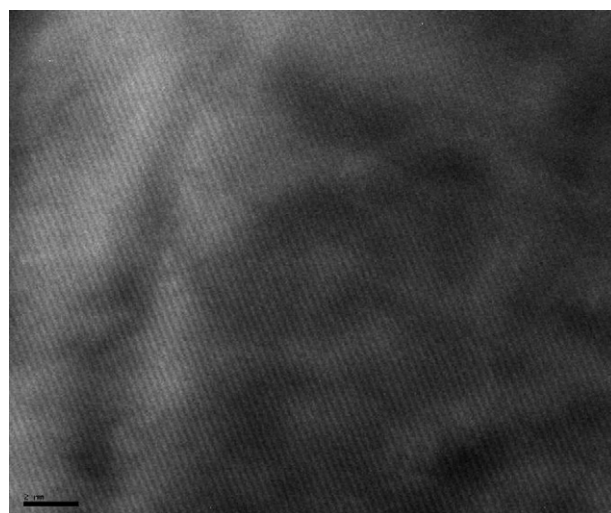


Fig. 3. HRTEM image along the (1 0 0) plane.

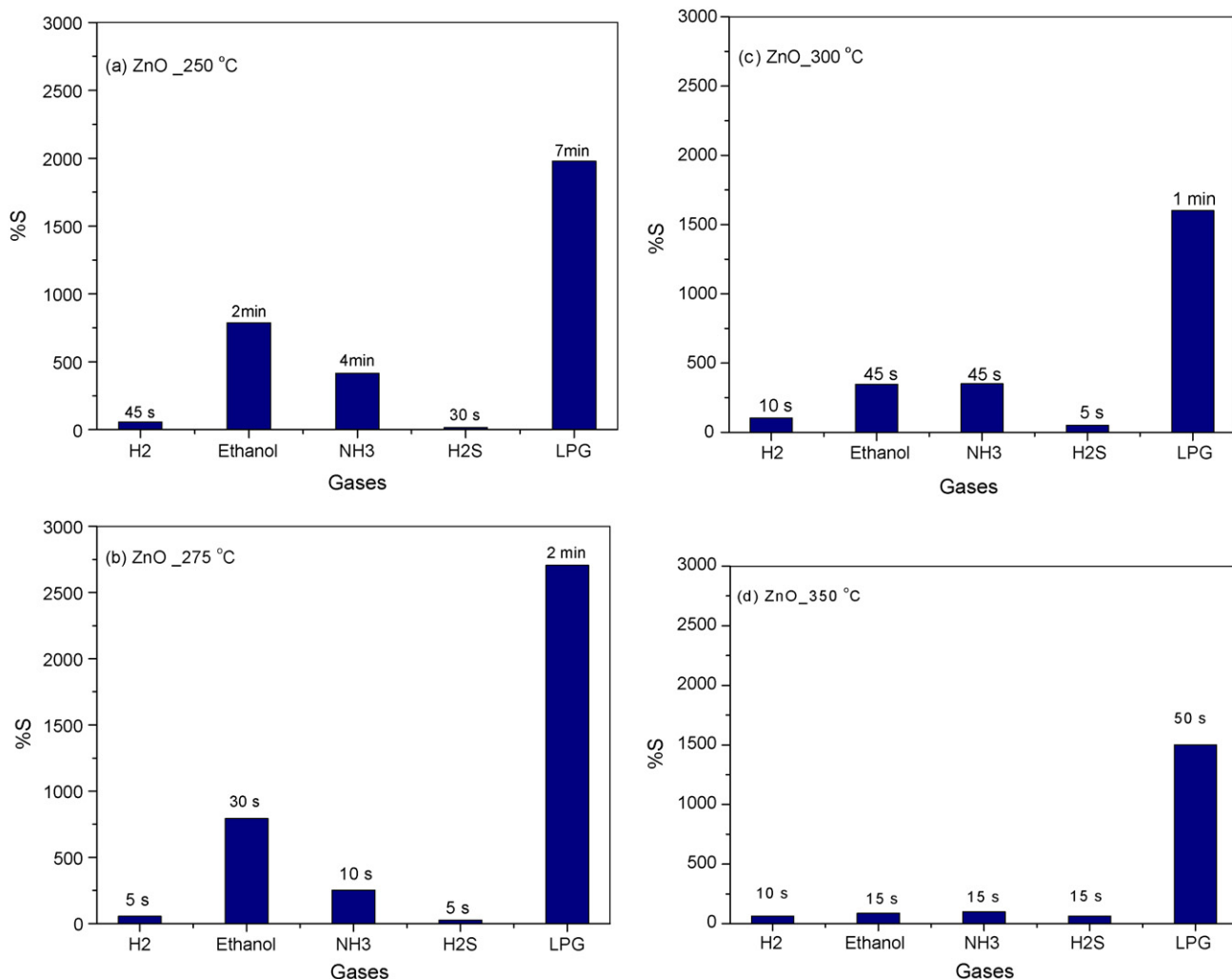


Fig. 4. Gas response (%S) against various reducing gas at operating temperatures: (a) 250 °C, (b) 275 °C, (c) 300 °C, and (d) 350 °C.

high selectivity towards LPG (200 ppm) as compared with other gases.

The change in electrical resistance was used as a measure for gas response study at various temperatures. The gas response (%S) is calculated as follows:

$$\%S = \frac{(R_a - R_g) \times 100}{R_a}$$

where R_a is resistance of the sample in air; R_g is resistance of the sample when exposed to gas.

The %S against various reducing gases is shown in Fig. 4. At lower operating temperature samples take longer time to sense the gas while for higher operating temperatures the sensing is fast. On the bar graph is shown the time required for sensing. Fig. 5 shows sensing response (%S) at various operating temperatures. It is seen that for temperatures lower and higher than 275 °C, the gas response is less (%S) indicating 275 °C to be an optimum temperature to have high sensing response at the cost of sensing time. While for higher operating temperatures the sensing period is short but response is less. The response for our samples is found to be better than that reported in literature [21].

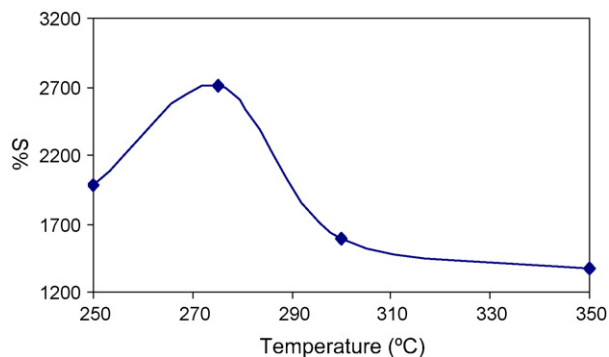


Fig. 5. Gas response (%S) against operating temperatures (°C).

However independent of temperature it shows high selectivity for LPG.

The PL study done for 1:9 composition at room temperature using excitation wavelength of 325 nm. The emission spectrum (Fig. 6) matches to that reported in literature [24]. Three emission peaks accompanied with weak shoulder peaks

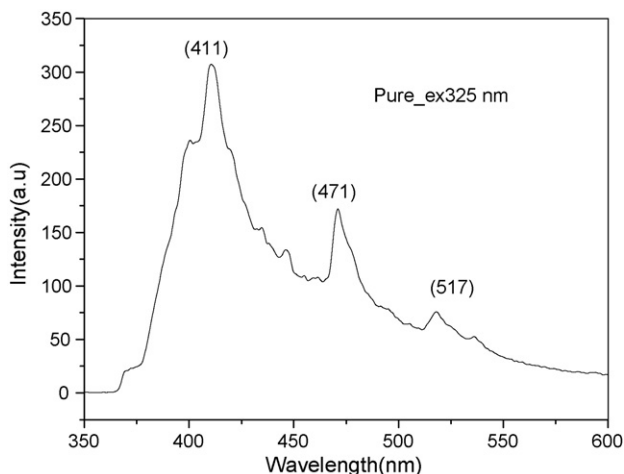


Fig. 6. PL observed at room temperature.

were observed. The intense peaks 411, 471, and 517 nm can be assigned to violet, weak blue and green regions, respectively. The strong violet emission corresponds to near band edge emission of the wide band gap of ZnO due to annihilation of excitons [25]. The weak blue implies that there are few surface defects in ZnO. The green band emission corresponds to the singly ionized oxygen vacancy in ZnO and results from the recombination of photogenerated hole with the single ionized charge state of this defect [26].

4. Conclusions

1D ZnO rods were synthesized using less explored hydrazine as a structure-directing agent. Controlled ratio of Zn to hydrazine is found to give various morphologies of ZnO. We also report high sensitivity as well as selectivity towards LPG. The optimum operating temperature we found for our sample is 275 °C. The emission spectrum shows intense peaks for violet, weak blue and green regions which can be attributed to annihilation of excitons, surface defects and ionized oxygen vacancy, respectively.

Acknowledgment

S.C. Navale acknowledges CSIR, New Delhi, for awarding senior research fellowship.

References

- [1] A.P. Alivisatos, *Science* 271 (1996) 933.
- [2] W.J.E. Beek, M.M. Wienk, R.A.J. Janssen, *Adv. Mater.* 16 (2004) 1009.
- [3] W.J.E. Beek, M.M. Wienk, M.K. Emerink, X. Yang, R.A.J. Janssen, *J. Phys. Chem. B* 109 (2005) 9505.
- [4] Y. Xia, P. Yang, Y. Sun, Y. Wu, B. Mare, B. Gates, Y. Yin, F. Kim, H. Yan, *Adv. Mater.* 15 (2003) 323.
- [5] Z.M. Jarzebski, *Oxide Semiconductors*, Pergamon press, Oxford, 1973, p. 150.
- [6] M.H. Huang, Y. Wu, H. Feick, N. Tran, E. Weber, P. Yang, *Adv. Mater.* 13 (2001) 113.
- [7] A. Ennaoui, M. Weber, R. Scheer, H.J. Lewerenz, *Sol. Energy Mater. Sol. Cells* 54 (1998) 277.
- [8] J. Liqiang, W. Baiq, X. Baifu, L. Shudan, S. Keying, C. Weimin, F. Honggang, *J. Solid State Chem.* 177 (2004) 4221.
- [9] M.H. Huang, S. Mao, H. Feick, H. Yan, Y. Wu, H. Kind, E. Weber, R. Russo, P. Yang, *Science* 292 (2001) 1897.
- [10] D.C. Reynolds, D.C. Look, B. Jogai, *Solid State Commun.* 99 (1996) 873.
- [11] R. Das, S. Ray, *J. Phys. D: Appl. Phys.* 36 (2003) 152.
- [12] H. Ohno, *Science* 281 (1998) 951.
- [13] G.S.T. Rao, D.T. Rao, *Sens. Actuator B* 55 (1999) 166.
- [14] B. Ismail, M.A. Abaab, B. Rezig, *Thin Solid Films* 383 (2001) 92.
- [15] G. Eranna, B.C. Joshi, D.P. Runthala, R.P. Gupta, *Crit. Rev. Solid State Mater. Sci.* 29 (2004) 111.
- [16] Z.L. Wang, *J. Phys. Condens. Matter* 16 (2004) R829.
- [17] X.-J. Huang, Y.-K. Choi, *Sens. Actuator B* 122 (2007) 659.
- [18] S.C. Navale, V. Ravi, I.S. Mulla, S.W. Gosavi, S.K. Kulkarni, *Sens. Actuator B* 126 (2) (2007) 382.
- [19] G. Sarala Devi, V. Bala Subrahmanyam, S.C. Gadkari, S.K. Gupta, *Anal. Chem. Acta* 568 (2006) 41.
- [20] H. Gong, J.Q. Hua, J.H. Wang, C.H. Onga, F.R. Zhu, *Sens. Actuator B* 115 (2006) 247.
- [21] V.R. Shinde, T.P. Gujar, C.D. Lokhande, *Sens. Actuator B* 120 (2) (2007) 551.
- [22] U. Pal, P. Santiago, *J. Phys. Chem. B* 109 (2005) 15317.
- [23] H. Zhang, D. Yang, Y.J. Ji, X.Y. Ma, J. Xu, D.L. Que, *J. Phys. Chem. B* 108 (2004) 13.
- [24] J. Wang, L. Gao, *Solid State Commun.* 132 (2004) 269.
- [25] K. Vanheusden, W.L. Warren, C.H. Seager, *J. Appl. Phys.* 79 (1996) 7983.
- [26] S. Monticone, R. Tufeu, V. Kanaev, *J. Phys. Chem. B* 102 (1998) 2854.

Simultaneous determination of 6-methylcoumarin and 7-methoxycoumarin in cosmetics using three-dimensional excitation–emission matrix fluorescence coupled with second-order calibration methods

Jin-Fang Nie, Hai-Long Wu^{*}, Shao-Hua Zhu, Qing-Juan Han, Hai-Yan Fu, Shu-Fang Li, Ru-Qin Yu

State Key Laboratory of Chemo/Biosensing and Chemometrics, College of Chemistry and Chemical Engineering, Hunan University, Changsha 410082, China

Received 1 November 2007; received in revised form 12 January 2008; accepted 15 January 2008

Available online 20 January 2008

Abstract

This paper reports a simple, rapid, and effective method for quantitative analysis of 6-methylcoumarin (6-MC) and 7-methoxycoumarin (7-MOC) in cosmetics using excitation–emission matrix (EEM) fluorescence coupled with second-order calibration. After simple pretreatments, the adopted calibration algorithms exploiting the second-order advantage, *i.e.*, parallel factor analysis (PARAFAC) and self-weighted alternating tri-linear decomposition (SWATLD), could allow the individual concentrations of the analytes of interest to be predicted even in the presence of uncalibrated interferences. In the analysis of facial spray, with the external calibration method, the average recoveries attained from PARAFAC and SWATLD with the factor number of 3 ($N=3$) were 101.4 ± 5.5 and $97.5 \pm 4.1\%$ for 6-MC, and 103.3 ± 1.7 and $101.7 \pm 1.8\%$ for 7-MOC, respectively. Moreover, in the analysis of oil control nourishing toner, the standard addition method (SAM) was suggested to overcome the partial fluorescence quenching of 6-MC induced by the analyte–background interaction, which also yielded satisfactory prediction results. In addition, the accuracy of the two algorithms was also evaluated through elliptical joint confidence region (EJCR) tests as well as figures of merit (FOM), including sensitivity (SEN), selectivity (SEL) and limit of detection (LOD). It was found that both algorithms could give accurate results, only the performance of SWATLD was slightly better than that of PARAFAC in the cases suffering from matrix effects. The method proposed lights a new avenue to determine quantitatively 6-MC and 7-MOC in cosmetics, and may hold great potential to be extended as a promising alternative for more practical applications in cosmetic quality control, due to its advantages of easy sample pretreatment, non-toxic and non-destructive analysis, and accurate spectral resolution and concentration prediction.

© 2008 Elsevier B.V. All rights reserved.

Keywords: 6-Methylcoumarin; 7-Methoxycoumarin; Cosmetics; Excitation–emission matrix fluorescence; PARAFAC; SWATLD

1. Introduction

The coumarin derivatives, 6-methylcoumarin (6-MC) and 7-methoxycoumarin (7-MOC), have been widely used as fragrance enhancers in many cosmetic products [1]. However, in terms of toxicological experiments [2,3], both 6-MC and 7-MOC have been validated to be potent photo-contact sensitizers which may cause serious skin and systemic disorders in some consumers on

contact in the presence of sunlight. Therefore, China Standards has announced the use of 6-MC in cosmetic products with a maximum concentration of 0.003% (30 mg kg^{-1}) [4]. Recently, the European Commission stipulates that the use of 7-MOC as a fragrance ingredient in cosmetics should be prohibited [5]. In order to protect consumer's health, it is therefore important to establish an effective routine method for quantifying the two fragrance ingredients in cosmetic products.

A series of analytical techniques [4,6–17] have been developed for the determination of coumarins in different matrices, including gas chromatography (GC) with mass spectrometric detection [6,7,17], high-performance liquid chromatography

^{*} Corresponding author. Tel.: +86 731 8821818; fax: +86 731 8821818.
E-mail address: hluwu@hnu.cn (H.-L. Wu).

(HPLC) with ultraviolet [4,8,16], fluorescence [9] or mass spectrometric detection [10], thin-layer chromatography (TLC) with ultraviolet detection [11], capillary electrophoresis with ultraviolet [12,13] or laser-induced fluorescence detection [14] and supercritical-fluid chromatography (SFC) [15]. Among these conventional techniques, HPLC [4,16] and GC [17] are the primary ones for the routine determinations of 6-MC and 7-MOC in cosmetic products. Unfortunately, both HPLC and GC may inherently suffer from the main disadvantages associated with the need of large amounts of hazardous organic solvents, large sample volumes and/or tedious and time-consuming pretreatment procedures. Moreover, since the interferences depend on the source of the sample, it may be troublesome to optimize the separation conditions for each particular analyte of interest and every unknown interferent. On the other hand, the spectrofluorimetry methods have proved capable of providing high sensitivity and clean spectrum acquisition, and are considered to be suitable for quantitative analysis of the analytes of interest that possess natural fluorescence, e.g., 6-MC and 7-MOC. However, quantification of 6-MC and 7-MOC in cosmetics is still difficult to be achieved without thorough previous separation procedures. This is due to the facts that the serious overlapping between the fluorescence spectra of 6-MC and 7-MOC occurs, and the natural interferences in the complicated backgrounds of cosmetic products remarkably affect the fluorescence signals of the analytes. To the extent of our literature search, the simultaneous determination of 6-MC and 7-MOC in cosmetic products using a spectrofluorimetric method has not been reported so far.

Increasing interest in rapid development and extensive applications of various second-order calibration methods which utilize “mathematical separation” instead of “physical or chemical separation” of background interferences has been recently kindled to achieve simple experimentation, and direct concentration determination as well as spectral profiles of the analytes of interest in complex matrices. A great variety of second-order calibration algorithms have been proposed, such as generalized rank annihilation method (GRAM) [18], parallel factor analysis (PARAFAC) [19], bilinear least squares (BLLS) [20], alternating tri-linear decomposition (ATLD) [21] and self-weighted alternating tri-linear decomposition (SWATLD) [22]. In contrast to other traditional measurement techniques, these methods allow for direct concentration determination of single analyte or the simultaneous concentration determination of multiple analytes even in the presence of uncalibrated interferences, which has been called the “second-order advantage”. With the application of the property, numerous second-order calibration methods have proved wide practical applications, mainly including drugs analysis [23], environment monitoring [24], quality control and food analysis [25]. Furthermore, it was also reported recently that the combination of PARAFAC and excitation–emission matrix (EEM) fluorescence spectroscopy can be used for the monitoring of bioprocesses [26], and characterization of natural organic material [27]. Nevertheless, there is no attempt to introduce the second-order calibration methods into cosmetic analysis to date.

In the present study, a simple, rapid, and effective method for the direct quantitative analysis of 6-MC and 7-MOC in cos-

metics was proposed, by combining excitation–emission matrix fluorescence with second-order calibration strategies based on both PARAFAC and SWATLD algorithms. Herein, the external calibration method was employed to simultaneously determine 6-MC and 7-MOC in facial spray samples which only existing spectral overlapping, and the standard addition method (SAM) was utilized for the quantification of 6-MC in oil control nourishing toner samples in order to overcome the fluorescence quenching problem arose from matrix effects. Moreover, the figures of merit (FOM) involving sensitivity (SEN), selectivity (SEL) and limit of detection (LOD) were investigated, and the accuracy of the proposed method was also estimated by using the elliptical joint confidence region (EJCR) test.

2. Theory

2.1. PARAFAC and SWATLD

The rapid development of modern hyphenated instruments capable of generating second-order data has led to a resurgence of interest in the development of second-order calibration-based analytical methodologies. Recently, a review of the benefits and applications of these methods was reported by Escandar et al. [28]. Since the decomposition of a three-way data array stacked with a serial of response matrices measured for each sample is often mathematically unique, the second-order calibration methods can overcome the well-known rotational freedom problem present in bilinear matrix decomposition methods [29] and give rise to physical and chemical solutions. In other words, the principal advantage the second-order calibration methods over the bilinear methods is that quantitative analysis of analytes of interest using the former methods can be performed even in the presence of uncalibrated interferences or in cases when there are compounds which are not present in all samples, only maintaining the species of interest the same in both the calibration standard(s) and the sample(s) to be analyzed.

Fluorescence excitation–emission matrices are the most acceptable instances due to their perfect tri-linear property, and several available second-order calibration algorithms have been developed and applied to enhance the wealth of information offered by this kind of data. Especially useful are PARAFAC [19] and SWATLD [22], which yielded better results in most cases according with the literatures and our own experience. Both of them implemented to EEMs can provide access to extract reliably the spectral profiles and estimate accurately the concentrations of analytes of interest even in the presence of unknown interferents and uncalibrated spectral interferences. The PARAFAC and SWATLD algorithms are applied to a three-way array by stacking K response matrices, $\underline{\mathbf{X}}$, with dimensions $I \times J \times K$ (I is the number of excitation wavelengths, J the number of emission wavelengths and K the number of samples), and decompose it based on the tri-linear component model as follow.

$$x_{ijk} = \sum_{n=1}^N a_{in} b_{jn} c_{kn} + e_{ijk} \quad (i = 1, 2, \dots, I; j = 1, 2, \dots, J; k = 1, 2, \dots, K), \quad (1)$$

where x_{ijk} is the fluorescent intensity of sample k at excitation wavelength i and emission wavelength j , and N denotes the number of factors, which should be considered as the total number of fluorescing species, consisting of the components of interest and the background as well as uncalibrated interferences. a_{in} is the element (i, n) of an $I \times N$ matrix \mathbf{A} with relative excitation spectra of the N species; b_{jn} is the element (j, n) of a $J \times N$ matrix \mathbf{B} with relative emission spectra of the N species; c_{kn} is the element (k, n) of a $K \times N$ matrix \mathbf{C} with relative concentrations of the N species in K samples; and e_{ijk} represents the element of an $I \times J \times K$ three-way residual array, \mathbf{E} . For PARAFAC, an alternating least squares approach is employed to solve the tri-linear component model by successively assuming the loading matrices in two modes known and estimating the unknown parameters in the last mode, which minimizes the sum of squares of the residuals e_{ijk} . However, SWATLD solves the tri-linear component model by alternatively minimizes three objective functions with intrinsic relationship. For more detailed information on these two algorithms, the reader is referred to the original literature [19,22]. Thus, after finishing the simultaneously decomposition of the standard and unknown spectra, one can resort to the aid of the resolved excitation and emission profiles, \mathbf{A} and \mathbf{B} , for verification of the association of each of the N columns in the relative concentrations, \mathbf{C} , with particular species profiles. The final concentration estimation in the unknown samples can be obtained by regression of the appropriate column of \mathbf{C} that corresponds to the analyte of interest against its standard concentrations.

The traditional PARAFAC algorithm [19] is sensitive to the estimated component number in a system, and either over-estimation or under-estimation of the underlying factors will result in erroneous results. Hence, the core consistency diagnostic (CORCONDIA) test [30] is used to determine the number of components in the present work. The goal of this strategy is to check the rationality of the structural model based on the data, and find the number of latent components in terms of the internal parameter known as core consistency, which indicates how well the given model is in concert with the distribution of superdiagonal and off-superdiagonal elements of the Tucker3 core. The core consistency is calculated as a function of a trial number of components. When the core consistency drops from a high value, above approximately 60%, to a low value, this indicates that an appropriately number of components has been attained. Unlike the PARAFAC algorithm, SWATLD is insensitive to the excess on the factor number and a rough estimation can theoretically guarantee the correctness of results.

2.2. Second-order standard addition method (SOSAM)

Matrix effects often occur and the instrument responses of the analyte sometimes change in scale or shape because of chemical interactions between the analyte and the interfering species. In these cases, the external calibration methods are no longer effective, and the standard addition method [31] as a means of overcoming matrix or background effects is recommended to ensure accurate results. In contrast to

external standard calibration, standard addition has the disadvantage of being more time-consuming as a function of various standard additions. However, it is an alternative in situations where the external calibration is not feasible. In particular, the second-order standard addition method [32] with the “second-order advantage”, an extension of SAM to second-order data, can be utilized to circumvent this drawback induced by matrix effects and simultaneously determine several components in the presence of unexpected interferences. In this paper, the SOSAMs based on both PARAFAC and SWATLD algorithms were applied to excitation–emission matrix fluorescence data. In a typical SOSAM [33] analysis, there are three major steps: (i) with an appropriate number of factors, PARAFAC or SWATLD algorithms are applied to decompose the three-way data array \mathbf{X} which gathers the second-order response data of the sample and of each successive addition; (ii) through comparing the loadings of the spectral modes with the spectrum of pure analyte, one can identify the column corresponding to the analyte of interest in the relative concentration matrix; and (iii) the estimated concentration of each analyte can be found through the regression of the values of the identified column against the standard addition concentrations, in the same way as in univariate standard addition.

2.3. Figures of merit

The determination of figures of merit is an important requisite for method comparison, such as SEN, SEL and LOD. In second-order calibration, the evaluation of FOM is closely relative to the calculation of net analyte signal (NAS), which is defined as the part of the signal that relates uniquely to the analyte of interest. The calculation of NAS can be accomplished as described elsewhere [34], the following equations can be obtained to estimate the SEN and SEL in this present work.

$$\text{SEN} = \lambda \{[(\mathbf{A}^T \mathbf{A})^{-1}] * [(\mathbf{B}^T \mathbf{B})^{-1}]\}_{nn}^{-1/2}, \quad (2)$$

$$\text{SEL} = \{[(\mathbf{A}^T \mathbf{A})^{-1}] * [(\mathbf{B}^T \mathbf{B})^{-1}]\}_{nn}^{-1/2}, \quad (3)$$

where nn designates the (n, n) element of matrix $[(\mathbf{A}^T \mathbf{A})^{-1}] * [(\mathbf{B}^T \mathbf{B})^{-1}]$, λ is the total signal for component n at unit concentration, which is also the parameter converting scores to concentrations, and the symbol $*$ indicates the Hadamard product. Notice that when the second-order advantage is employed, Eqs. (2) and (3) imply that SEN and SEL are sample-specific and cannot be defined for the multivariate method as a whole. In such cases, average values for a set of samples can be estimated and reported.

The LOD is estimated according to Eq. (4) [35,36].

$$\text{LOD} = 3.3s(0) \quad (4)$$

where $s(0)$ is the standard deviation in the predicted concentration for three different background blank samples, in the PARAFAC and SWATLD.

3. Experimental

3.1. Reagents and chemicals

All reagents and chemicals used were of analytical reagent grade. Two coumarins, 6-MC and 7-MOC, were purchased from Sigma–Aldrich Corporation (USA) and National Institute for Control of Pharmaceutical and Biological Products (Changsha, China), respectively. Stock solutions of 6-MC (0.586 mg ml^{-1}) and 7-MOC (0.085 mg ml^{-1}) were prepared in a 100 ml brown volumetric flask by dissolving in ethanol and then stored at 4°C in a refrigerator, remaining stable for at least 3 months. The working solutions of 6-MC and 7-MOC were daily prepared by diluting the stock solutions with doubly distilled water. Phosphate buffered saline solutions (PBS) were prepared by using $0.067 \text{ mol l}^{-1} \text{ Na}_2\text{HPO}_4$ and $0.067 \text{ mol l}^{-1} \text{ K}_2\text{H}_2\text{PO}_4$ with different pH values. Doubly distilled water was used throughout the experiments.

The illegal addition of either or both of 6-MC and 7-MOC used as fragrance ingredients may be mainly introduced in liquid cosmetic products, few in solid or emulsified ones which must be converted into a liquid form with some necessary pretreatments [4]. Hence, in our paper two kinds of liquid cosmetic products bought from commercial market in Changsha (China), *i.e.*, transparent face spray and semitransparent oil control nourishing toner, were chosen in recovery analytical experiments. Both of 6-MC and 7-MOC were demonstrated to be absent in these cosmetic products. Owing to the use of 95% ethanol as the solvent in most liquid cosmetic products, the face spray was used without any pretreatments, but the oil control nourishing toner should be ultrasonically treated for 15 min and then centrifuged at $8000 \times g$ for 10 min for further use.

3.2. Apparatus

All of the fluorometric measurements were performed on an F-4500 fluorescence spectrophotometer (Hitachi, Japan) equipped with a continuous xenon lamp. In all cases, a 1.00 cm quartz cell was used. All computer programs were written in Matlab, and all calculations were carried out on a personal computer under the Windows XP operating system. All glassware were previously soaked in chromate lotion overnight, and then rinsed with doubly distilled water before use.

3.3. Analytical methodology

Prior to analysis, the linear analytical ranges and the influence of pH on the fluorescence spectra were investigated for both 6-MC and 7-MOC, respectively. It was found that by linear regression between different concentrations and relative fluorescence intensity, a linear concentration range of $3.520\text{--}11.720 \text{ }\mu\text{g ml}^{-1}$ of 6-MC and a linear concentration range of $0.000\text{--}4.080 \text{ }\mu\text{g ml}^{-1}$ of 7-MOC were realized. Moreover, the pH in the range of 4.5–9.2 showed slight effect on the fluorescence intensity of both 6-MC and 7-MOC, but the base hydrolysis of the two fragrance ingredients took place when pH was further increased. The fluorescence intensity of the two

Table 1
6-MC and 7-MOC concentrations in the calibration and test sets

Sample	6-MC ($\mu\text{g ml}^{-1}$)	7-MOC ($\times 10^{-3} \mu\text{g ml}^{-1}$)
C1	4.102	40.800
C2	4.688	34.000
C3	5.274	30.600
C4	5.860	27.200
C5	6.446	20.400
C6	7.032	13.600
C7	8.204	6.800
C8	8.790	0.000
T1	3.516	20.400
T2	4.688	19.040
T3	5.860	16.320
T4	6.446	13.600
T5	7.618	12.240
T6	8.556	10.200

fragrance ingredients peaked at pH 7.0, suggesting a recommended value for the experiments. So in order to confirm the effectiveness of the method proposed, all samples were prepared according to the linear range of the analytes and adjusted pH value to 7.0 with 2 ml phosphate buffered saline solutions.

3.3.1. Simultaneous determination of 6-MC and 7-MOC in facial spray

Twenty-two samples were prepared for the simultaneous determination of 6-MC and 7-MOC in facial spray. The first eight samples (C1–C8) were built as a calibration set. The concentration levels correspond to values in the range $4.102\text{--}8.790 \text{ }\mu\text{g ml}^{-1}$ for 6-MC and $0.000\text{--}40.800 \text{ ng ml}^{-1}$ for 7-MOC. In addition, six samples (T1–T6) containing only 6-MC and 7-MOC with the concentrations within their corresponding calibration ranges as a test set were prepared to validate the quality of the chemometric algorithms. Table 1 lists the concentrations of the two analytes in both calibration and test samples. Eight prediction samples (P1–P8) were constructed by spiking facial spray with the two fragrance ingredients yielding concentrations in the range $4.102\text{--}8.556 \text{ }\mu\text{g ml}^{-1}$ for 6-MC and $7.480\text{--}37.400 \text{ ng ml}^{-1}$ for 7-MOC, respectively (Table 2). Duplicate analysis was performed for each sample. The spectra of PBS blank solution and facial spray blank solution with 10 times dilution were recorded in triplicate experiments during the whole analysis procedure.

3.3.2. Quantification of 6-MC and 7-MOC in oil control nourishing toner

The quantification of 7-MOC in oil control nourishing toner in the presence of 6-MC was done following a similar procedure to that described for the simultaneous determination of 6-MC and 7-MOC in facial spray. Table 2 lists the concentrations of the samples. 6-MC was not added in the calibration set but it was added in both test set and prediction set acting as an interferent.

To determine 6-MC in oil control nourishing toner, toner samples were spiked with appropriate amounts of standard solutions, obtaining concentration levels between 26.370 and $38.090 \text{ }\mu\text{g ml}^{-1}$. One milliliter of spiked toner samples and 2 ml

Table 2
Added and predicted concentrations for 6-MC and 7-MOC in spiked facial spray and oil control nourishing toner samples

Sample	Added concentration		Predicted concentration (recovery %)					
	6-MC ($\mu\text{g ml}^{-1}$)	7-MOC ($\times 10^{-3} \mu\text{g ml}^{-1}$)	Facial spray			Oil control nourishing toner		
			6-MC	7-MOC	Average	6-MC	7-MOC	Average
P1	4.102	37.400	PARAFAC	SWATLD	PARAFAC	SWATLD	PARAFAC	SWATLD
P2	4.922	32.640	4.303 [104.9]	3.937 [96.0]	38.915 [104.1]	39.124 [104.6]	37.105 [99.2]	37.742 [100.9]
P3	5.860	27.880	5.536 [112.5]	5.189 [105.4]	33.636 [103.1]	33.674 [103.2]	31.762 [97.3]	32.286 [98.9]
P4	6.680	23.120	6.273 [107.0]	5.985 [102.1]	28.284 [101.4]	28.142 [100.9]	27.474 [98.5]	27.698 [99.4]
P5	7.501	18.360	6.877 [102.9]	6.778 [101.5]	23.377 [101.1]	23.051 [99.7]	22.895 [99.0]	23.017 [99.6]
P6	7.970	13.600	7.378 [98.4]	7.205 [96.1]	18.650 [101.6]	18.345 [99.9]	18.483 [100.7]	18.423 [100.3]
P7	8.204	10.200	7.625 [95.7]	7.520 [94.4]	14.051 [103.3]	13.645 [100.4]	13.746 [101.1]	13.718 [100.9]
P8	8.556	7.480	7.777 [94.8]	7.573 [92.3]	10.965 [107.5]	10.657 [104.5]	10.737 [105.3]	10.697 [104.9]
Average recovery (%)			101.4 \pm 5.5	97.5 \pm 4.1	103.3 \pm 1.7	101.7 \pm 1.8	101.3 \pm 3.0	101.8 \pm 2.7

PBS were added into 10 ml volumetric flasks. For each concentration, five successive additions of 50 μl working solutions were performed and the flasks were completed to the mark with doubly distilled water. All measurements were carried out in duplicate. The spectra of PBS blank solution and oil control nourishing toner blank solution were recorded in triplicate during the whole analysis procedure.

3.4. Measurements

All of the spectral surfaces were recorded at excitation wavelengths varying from 265 to 350 nm in 3 nm steps, and emission wavelengths varying from 365 to 450 nm in 3 nm steps with a scanning rate of 1200 nm min^{-1} . The slit width was 5.0/5.0 nm.

4. Results and discussion

Fig. 1 shows the three-dimensional EEMs plots of pure 6-MC and 7-MOC in standard samples in the well-chosen excitation and emission wavelength ranges which avoid Rayleigh and Raman scatterings. As shown in Fig. 1a, 6-MC presented a broad emission band with a peak value at 410 nm and two excitation maxima at 285 and 325 nm. Moreover, 7-MOC exhibited strong fluorescence, and the maximal excitation and emission peaks were found to be at 330 and 390 nm, respectively (Fig. 1b). Obviously, the spectroscopy peaks of 7-MOC will be much more intense than that of 6-MC when they possess the same concentrations.

In order to avoid the decomposition dominated by the 7-MOC peaks, the appropriate dilution was carried out in the experiment according to the China Standards and European Commission. Even after the reasonable dilution, however, a serious overlapping between the EEMs of 6-MC and 7-MOC was experimentally observed, which consequently made the quantitative analysis of the two analytes using traditional fluorescent methodologies impossible. In such instances, first-order calibration methods can be chosen to predict the concentration of the components of interest without tedious separation steps, even in the lack of spectrum selectivity. Unfortunately, however, these methods may be restricted when they are used for simultaneously analyzing 6-MC and 7-MOC in complex cosmetic matrices, *i.e.*, facial spray and oil control nourishing toner. This may be in agreement with the fact that the complex cosmetics either exhibit overlapped emission fluorescence spectroscopy with 6-MC and 7-MOC (Fig. 1c and d), or interact with the two analytes resulting in the changes of spectra signals in scale. Accordingly, the first-order calibration methods, which require all the detectable species including analytes and interferences to be present in both calibration and prediction samples, are practically impossible to be utilized in these cases.

Alternatively, one can resort to the second-order calibration methods that allow for unique decomposition of tri-linear data and only require that the species of interest in both calibration standards and the samples are the same. In this paper, PARAFAC and SWATLD algorithms were recommended to assay the contents of 6-MC and 7-MOC in facial spray and oil control nourishing toner, which fully exploit the “second-

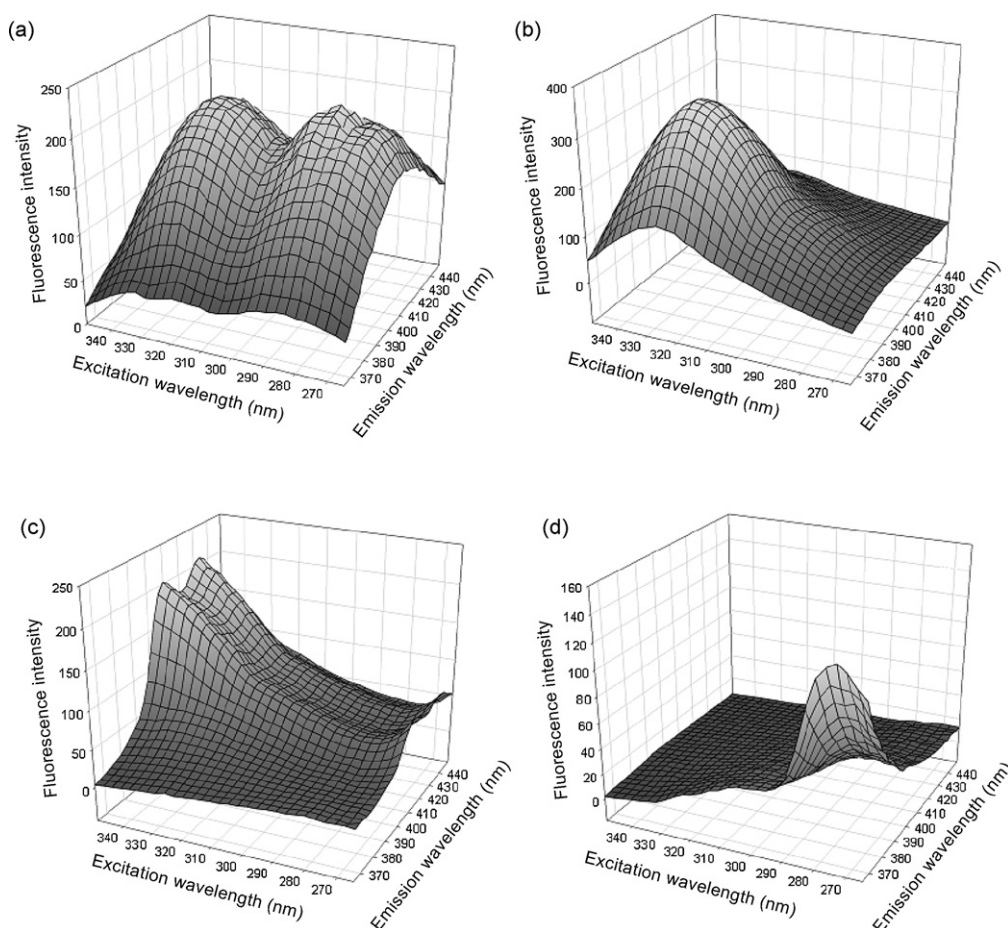


Fig. 1. Three-dimensional plots of the excitation–emission matrix fluorescence spectra: (a) for $8.790 \mu\text{g ml}^{-1}$ of pure 6-methylcoumarin; (b) for $27.200 \text{ ng ml}^{-1}$ of pure 7-methoxycoumarin; (c) for facial spray and (d) for oil control nourishing toner, with 10 times dilution.

order advantage” to accomplish reliable resolution of spectra and accurate quantification of individual components of interest.

4.1. Simultaneous determination of 6-MC and 7-MOC in facial spray

Prior to analysis, the reliability of the calibration models was validated by investigating a test set of six samples (T1–T6) without interferences. Subsequently, both PARAFAC and SWATLD algorithms were applied for the decomposition of the three-way array formed by stacking the excitation–emission fluorescence matrices for the six test samples and other eight calibration samples (C1–C8). The predicted recoveries of 6-MC and 7-MOC in the six test samples by using both PARAFAC and SWATLD algorithms were found to be 101.6 and 102.9% for PARAFAC and 103.3 and 101.5% for SWATLD, respectively. The results clearly indicate that the chemometric algorithms chosen are reliable for the simultaneous quantification of 6-MC and 7-MOC in facial spray. The specific implementation as well as the study of facial spray samples will be discussed in details below.

Eight prediction samples (P1–P8) were prepared with the concentrations of 6-MC and 7-MOC shown in Table 2. The value of core consistency parameter was first analyzed using PARAFAC or SWATLD to estimate the optimal component

number N for each facial spray sample. The analysis using the core consistency diagnostic test indicates that three factors are necessary, because there is sharp decrease in core consistency when more factors are utilized, denoting a recommended factor number of three consisting of two target analytes and one natural interferent from the facial spray background.

Fig. 2 shows the actual spectral profiles and the loadings from the decomposition of the excitation–emission matrix fluorescence data array obtained for both the calibration and predicted samples by using PARAFAC (Fig. 2a1 and b1) and SWATLD (Fig. 2a2 and b2) with the factor number of three ($N=3$). The loadings associated with the excitation mode were shown in Fig. 2a and the loadings associated with the emission mode were shown in Fig. 2b. These excitation and emission spectral profiles were collected into the matrices **A** and **B**, respectively. In Fig. 2, the solid lines and dash dotted lines represented the loadings of 6-MC and 7-MOC, respectively, and the long dashed lines represented the loadings for an inherent interference deriving from the facial spray background. Moreover, the dotted solid lines denoted the actual spectral profiles of the two analytes. It was found that not only the loadings in the excitation and emission modes of 6-MC and 7-MOC were quite similar to their actual ones, but also the structures of the excitation and emission modes of the interesting analytes were not affected by the variety of the

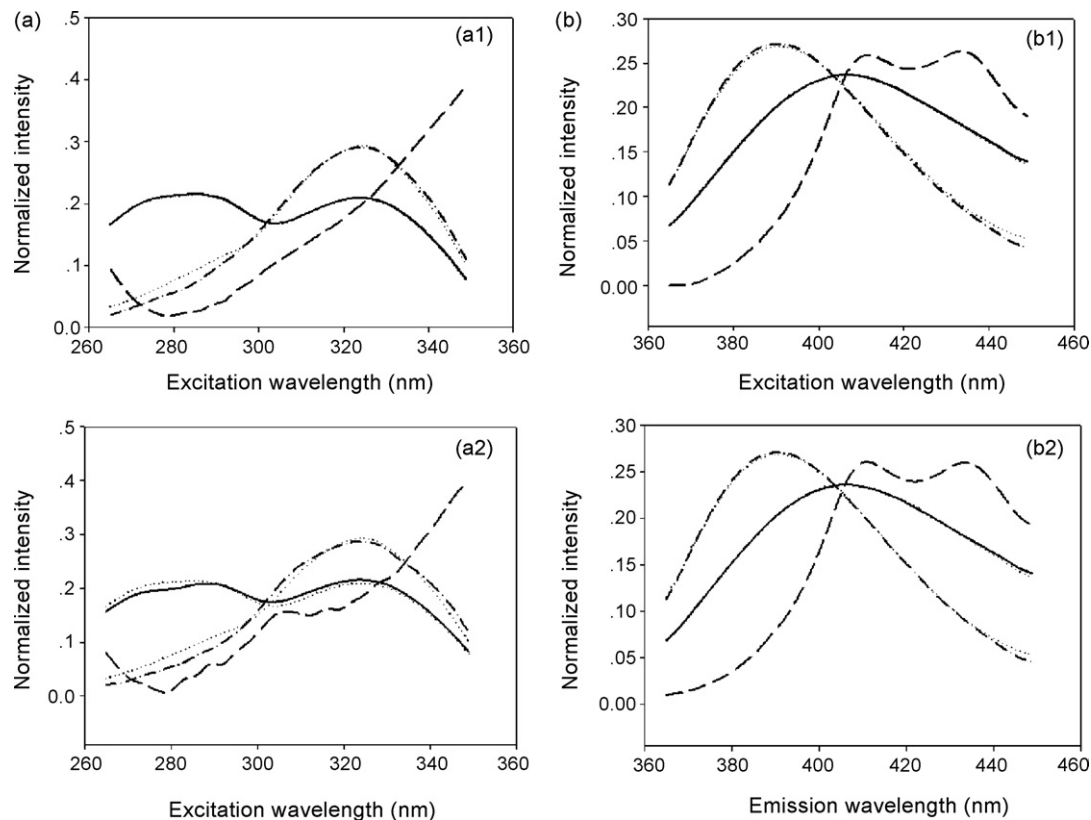


Fig. 2. Loadings, normalized to unit length, obtained from both PARAFAC and SWATLD with $N=3$ for the facial spray samples and the actual spectral profiles: (a) excitation and (b) emission.

algorithms chosen, which implies the good reliability and stability of the decomposition based on the second-order methods, as corresponding to tri-linear data.

With the aid of the spectral profiles extracted by these algorithms, the corresponding column in absolute concentration modes to the analyte as a function with its standard concentrations can be found to evaluate the actual concentrations in facial spray samples through a linear regression, similar to a calibration curve plot. The prediction results using both PARAFAC and SWATLD algorithms with $N=3$ were summarized in Table 2. For 6-MC, the average predicted recoveries gained from PARAFAC and SWATLD are 101.4 ± 5.5 and $97.5 \pm 4.1\%$, respectively. For 7-MOC, the predicted recoveries gained from PARAFAC and SWATLD are 103.3 ± 1.7 and $101.7 \pm 1.8\%$, respectively. These results show that both second-order calibration algorithms allow for the satisfactory prediction capacity of simultaneous determination of 6-MC and 7-MOC in complex facial spray matrix.

4.2. Quantification of 6-MC and 7-MOC in oil control nourishing toner

With a similar experimental scheme in the analysis of facial spray samples, both PARAFAC and SWATLD methods were also utilized to quantify the 6-MC and 7-MOC in oil control nourishing toner samples with $N=3$ suggested by the core consistency test. The loading profiles related to excitation and emission modes together with the actual ones were

shown in Fig. 3. Obviously, the resolved spectra of 6-MC and 7-MOC are similar to those obtained from the individual excitation–emission matrix analysis and previously discussed in Section 4.1. These results further confirm that the proposed second-order methods in this paper allow the spectral profiles of analytes of interest to be extract reliably and accurately even in different complex matrices, mainly due to the characteristic of tri-linear data.

The scores related to sample mode were used for calibration through a linear regression with the prediction results of 7-MOC shown in Table 2. The average recoveries of 7-MOC in oil control nourishing toner samples using PARAFAC and SWATLD were found to be 101.3 ± 3.0 and $101.8 \pm 2.7\%$, respectively. However, it should be noted that obvious deviations in prediction of 6-MC in oil control nourishing toner samples occurred (data not shown). This might be attributed to partial fluorescence quenching of 6-MC in the cosmetic samples. Fig. 4 demonstrates the specific quenching behavior obtained from PARAFAC (Fig. 4a) and SWATLD (Fig. 4b) with $N=3$, where the squares and stars represent the ideal and the practical scores, respectively. As can be seen from Fig. 4, the practical values are gradually biased against the ideal ones and the extension of these deviations rises as the concentration of 6-MC increases. It could be explained that the matrix effects induced by the interaction between the analyte and this cosmetic might affect the fluorescence spectrum of 6-MC in scale, especially in cases of high concentrations of 6-MC, which in turn hindered the application of external calibration methods.

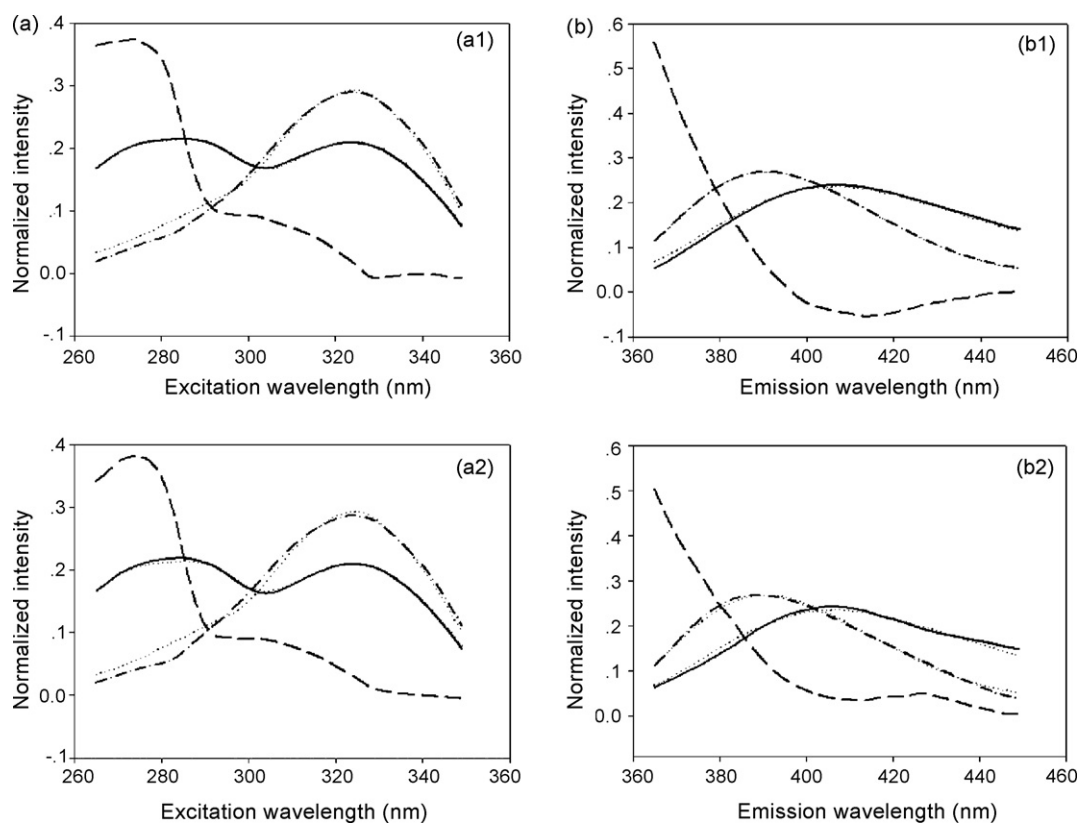


Fig. 3. Loadings, normalized to unit length, obtained from both PARAFAC and SWATLD with $N=3$ for the oil control nourishing toner samples and the actual spectral profiles: (a) excitation and (b) emission.

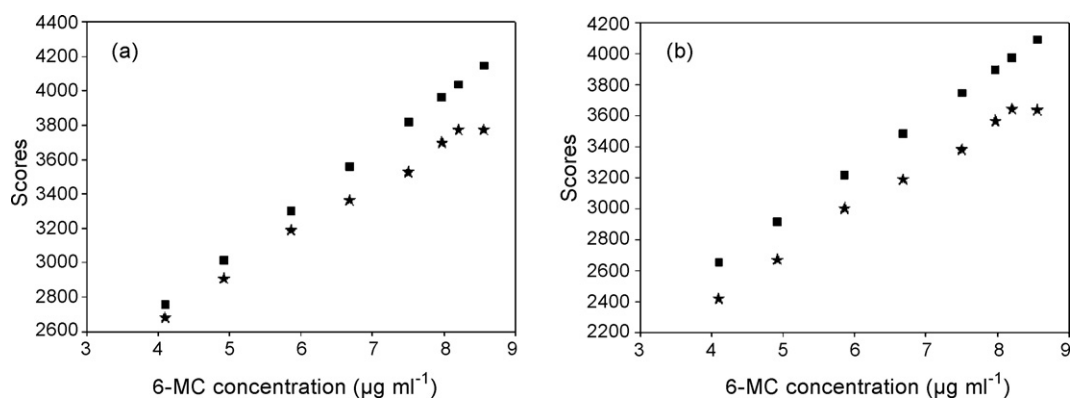


Fig. 4. Scores contained in matrix **C** resolved by PARAFAC (a) and SWATLD (b) with $N=3$. The squares and stars represent the ideal and the practical scores, respectively.

Table 3
Results for 6-MC in spiked oil control nourishing toner obtained when employing second-order standard addition method

Sample	Added concentration ($\mu\text{g ml}^{-1}$)	Predicted concentration ($\mu\text{g ml}^{-1}$)		Recovery (%)	
		PARAFAC	SWATLD	PARAFAC	SWATLD
M1	4.688	4.687	4.559	100.0	97.2
M2	5.274	5.520	5.433	104.7	103.0
M3	5.860	5.915	5.852	100.9	99.9
M4	6.446	6.707	6.612	104.0	102.6
M5	7.032	7.045	7.062	100.2	100.4
M6	7.618	8.020	7.964	105.3	104.5
Average recovery (%)				102.5 \pm 2.1	101.3 \pm 2.1

In order to resolve such problem, the second-order calibration methods were combined with the standard addition strategy in this paper to significantly improve the accuracy of prediction for 6-MC in the presence of matrix effects. A three-way data array with the size of $29 \times 29 \times 6$ were obtained under the same initial conditions for each concentration level, where 6 denoted the measurement times containing the original samples plus five standard additions. A specific strategy based on PARAFAC or SWATLD was built for each sample and the number of factors was estimated to be three ($N=3$) by the core consistency analysis. The loadings for 6-MC obtained through the utilization of PARAFAC and SWATLD algorithms are equivalent to the filtered signal free of interferences and similar to the corresponding ones shown in Figs. 2 and 3. The prediction results of 6-MC in oil control nourishing toner were shown in Table 3. The correlation coefficients of the standard addition lines based on SWATLD ($N=3$) were between 0.9973 and 0.9998, and the recovery was between 97.2 and 104.5%. Similar results were also obtained by using the PARAFAC algorithm.

4.3. Figures of merit

The root-mean-square error of prediction (RMSEP) can be calculated in terms of the formula as $RMSEP = \left[\frac{1}{I-1} \sum_{i=1}^I (c_{act} - c_{pred})^2 \right]^{1/2}$, where I is the number of prediction samples, c_{act} and c_{pred} are the actual and predicted concentrations of the analytes, respectively. The RMSEP results and the figures of merit, including SEN, SEL and LOD, for direct determinations of 6-MC and 7-MOC with different concentration magnitudes in facial spray or oil control nourishing toner using both PARAFAC and SWATLD were shown in Table 4. One can find that the proposed second-order calibration method based on either PARAFAC or SWATLD can yield satisfactory predictive capacity for quantitative analysis of 6-MC and 7-MOC in the two complex cosmetics.

Moreover, a linear-regression analysis of the actual versus the predicted concentration was applied to further investigate

Table 4
Statistical parameters and figures of merit in both of facial spray and oil control nourishing toner using PARAFAC and SWATLD

	Spray		Toner	
	6-MC ^a	7-MOC ^b	6-MC ^a	7-MOC ^b
PARAFAC				
RMSEP	0.404	0.800	0.242	0.520
SEN	183.610	77.550	225.600	78.870
SEL	0.572	0.610	0.696	0.620
LOD	0.155	0.150	0.030	0.020
SWATLD				
RMSEP	0.422	0.780	0.195	0.390
SEN	168.380	78.140	226.500	78.230
SEL	0.588	0.620	0.674	0.610
LOD	0.103	0.090	0.025	0.040

^a Value calculated with the concentration expressed as ($\mu\text{g ml}^{-1}$).

^b Value calculated with the concentration expressed as (ng ml^{-1}).

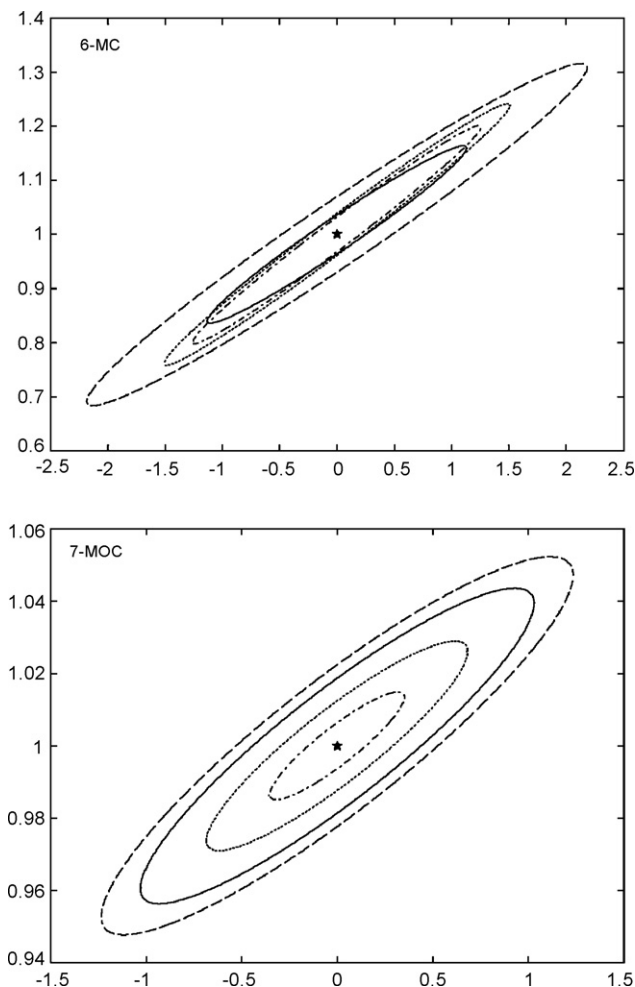


Fig. 5. EJCRs for 6-MC and 7-MOC applying PARAFAC and SWATLD with $N=3$. The solid lines and dotted lines correspond to the EJCRs in facial spray and oil control nourishing toner by applying PARAFAC, respectively. The dashed lines and dash-dotted lines correspond to the EJCRs in facial spray and oil control nourishing toner applying SWATLD, respectively. The pentacle (*) indicates the ideal points (0, 1).

the accuracy of the two proposed algorithms of PARAFAC and SWATLD [37]. The calculated intercept and slope were compared with their ideal values of 0 and 1, based on the EJCR test. If the point (0, 1) lies inside the EJCR, then bias are absent and consequently, the recovery may be taken as unity (or 100% in percentile scale). More details about EJCR are described in the original literature [38]. Fig. 5 gives the results of EJCRs for both PARAFAC and SWATLD algorithms. It showed that the ideal point (0, 1) labeled with a pentacle (*) lay in all EJCRs. In the analysis of facial spray, the elliptic size corresponding to the PARAFAC algorithm was smaller than that related to the SWATLD algorithm for both 6-MC and 7-MOC; on the contrary, the elliptic size corresponding to the SWATLD algorithm was smaller than that related to the PARAFAC algorithm in the analysis of oil control nourishing toner. These results proved again that both algorithms could allow for accurate quantitative determinations of 6-MC and 7-MOC in complex cosmetics, but the SWATLD was specially recommended in the systems suffering from serious matrix effects.

5. Conclusions

In the present study, a simple, rapid, and effective method has been successfully developed to determine 6-methylcoumarin and 7-methoxycoumarin in complicated cosmetics, based on the second-order calibration of excitation–emission matrix fluorescence data using both PARAFAC and SWATLD algorithms. The proposed quantitative method proved to be capable of performing the simultaneous determination of 6-MC and 7-MOC in facial spray or direct determination of 6-MC or 7-MOC in oil control nourishing toner with simple pretreatment step, even in the presence of serious natural fluorescent interferences or partial fluorescence quenching of the analyte of interest. Herein, the second-order advantage was adequately exploited in both experimental modes. Furthermore, the figures of merit and the EPCR tests indicated that both algorithms could give accurate results as an alternative to each other, only the performance of SWATLD was slightly better than that of PARAFAC in the cases suffering from matrix effects. Such a chemometrics-based protocol shows several advantages over the traditional methods, such as simple sample pretreatment, non-toxic and non-destructive analysis, and accurate spectral resolution and concentration prediction, and may possess great potential to be further tailored as a general and promising alternative for more practical applications in cosmetic quality control, of which some research works are now underway in our group.

Acknowledgements

The authors would like to acknowledge financial supports by The National Natural Science Foundation of China (Grant Nos. 20775025 and 20435010) and The National Basic Research Program (No. 2007CB216404).

References

- [1] S.P. Felter, J.D. Vassallo, B.D. Carlton, G.P. Daston, *Food Chem. Toxicol.* 44 (2006) 462.
- [2] S. Kato, T. Seki, Y. Katsumura, T. Kobayashi, K. Komatsu, S. Fukushima, *Toxicol. Appl. Pharmacol.* 81 (1985) 295.
- [3] S. Ruepp, F. Boess, L. Suter, M.C. de Vera, G. Steiner, T. Steele, T. Weiser, S. Albertini, *Toxicol. Appl. Pharmacol.* 207 (2005) 161.
- [4] J. Li, C. Wang, T. Wu, N. Li, *China Surfact. Deterg. Cosmet.* 36 (2006) 257.
- [5] Cosmetics Unmasked Homepage, New Restrictions Proposed for Fragrance Chemicals. <http://www.gina.antczak.btinternet.co.uk/CU/PERF.HTM#top>.
- [6] D.R. Boyd, N.D. Sharma, P.L. Loke, J.F. Malone, W.C. McRoberts, J.T.G. Hamilton, *Chem. Commun.* 24 (2002) 3070.
- [7] I. Meineke, H. Desel, R. Kahl, G.F. Kahl, U. Gundert-Remy, *J. Pharm. Biomed. Anal.* 17 (1998) 487.
- [8] I. Kazuhisa, F. Miwako, A. Takayuki, M. Yasuharu, *J. Chromatogr. B* 753 (2001) 309.
- [9] R. Gatti, V. Andrisano, A.M.D. Pietra, V. Cavrini, *J. Pharm. Biomed. Anal.* 13 (1995) 589.
- [10] X.Y. Sun, S.M. Xing, M.H. Li, L.Q. Wang, J. Wan, J. Shengyang, *J. Shengyang Pharmaceut. Univ.* 17 (2000) 110.
- [11] J.Q. Liu, H.Q. Zhuang, L.E. Mo, Q.N. Li, *J. Instrum. Anal.* 18 (1999) 26.
- [12] H.Y. Zhang, Q.F. Li, Z.H. Shi, Z.D. Hu, R. Wang, *Talanta* 52 (2000) 607.
- [13] R.J. Ochocka, D. Rajzer, P. Kowalski, H. Lamparcayk, *J. Chromatogr. A* 709 (1995) 197.
- [14] W.P. Wang, J.H. Tang, S.M. Wang, L. Zhou, Z.D. Hu, *J. Chromatogr. A* 1148 (2007) 108.
- [15] F. Lu, L.L. Liu, L. Li, Y.T. Wu, *Acta Pharmaceut. Sin.* 35 (2000) 832.
- [16] A. Bettero, C.A. Benassi, *J. Pharm. Biomed. Anal.* 1 (1983) 229.
- [17] J. Li, C. Wang, T. Wu, N. Li, *Life Sci. Instrum.* 4 (2006) 33.
- [18] E. Sanchez, B.R. Kowalski, *Anal. Chem.* 58 (1986) 499.
- [19] R. Bro, *Chemometr. Intell. Lab. Syst.* 38 (1997) 149.
- [20] M. Linder, R. Sundberg, *Chemometr. Intell. Lab. Syst.* 42 (1998) 159.
- [21] H.L. Wu, M. Shibukawa, K. Oguma, *J. Chemometr.* 12 (1998) 1.
- [22] Z.P. Chen, H.L. Wu, J.H. Jiang, Y. Li, R.Q. Yu, *Chemometr. Intell. Lab. Syst.* 52 (2000) 75.
- [23] D.M. Fang, H.L. Wu, Y.J. Ding, L.Q. Hu, A.L. Xia, R.Q. Yu, *Talanta* 70 (2006) 58.
- [24] M.L. Nahorniak, K.S. Booksh, *J. Chemometr.* 17 (2003) 608.
- [25] C.M. Andersen, M. Vishart, V.K. Holm, *J. Agric. Food Chem.* 53 (2005) 9985.
- [26] M.B. Haack, A. Eliasson, L. Olsson, *J. Biotechnol.* 114 (2004) 119.
- [27] R.D. Holbrook, J.H. Yen, T.J. Grizzard, *Sci. Total Environ.* 361 (2006) 249.
- [28] G.M. Escandar, N.M. Faber, H.C. Goicoechea, A.M. de la Peña, A.C. Olivieri, R.J. Poppi, *Trends Anal. Chem.* 26 (2007) 752.
- [29] H.L. Wu, R.Q. Yu, K. Oguma, *Anal. Sci.* 17 (2001) 1483.
- [30] R. Bro, H.A.L. Kiers, *J. Chemometr.* 17 (2003) 274.
- [31] D.A. Skoog, D.M. West, *Analytical Chemistry, An Introduction*, 4th ed., Saunders College Publishing, Philadelphia, 1986.
- [32] K. Booksh, J.M. Henshaw, L.M. Burgess, B.R. Kowalski, *J. Chemometr.* 9 (1995) 263.
- [33] H.L. Wu, R.Q. Yu, M. Shibukawa, K. Oguma, *Anal. Sci.* 16 (2000) 217.
- [34] P.C. Damiani, A.J. Nepote, M. Bearzotti, A.C. Olivieri, *Anal. Chem.* 76 (2004) 2798.
- [35] A.C. Olivieri, N.M. Faber, *Chemometr. Intell. Lab. Syst.* 70 (2004) 75.
- [36] K. Faber, B.R. Kowalski, *Anal. Chem.* 69 (1997) 1620.
- [37] J.A. Arancibia, G.M. Escandar, *Talanta* 60 (2003) 1113.
- [38] A.G. González, M.A. Herrador, A.G. Asuero, *Talanta* 48 (1999) 729.

Determination of textile dyes by means of non-aqueous capillary electrophoresis with electrochemical detection

Alejandra-Alicia Peláez-Cid^{a,b}, Sonia Blasco-Sancho^a, Frank-Michael Matysik^{a,*}

^a *Institute of Analytical Chemistry, University of Leipzig, Linnéstr. 3, D-04103 Leipzig, Germany*

^b *Centro de Química, Instituto de Ciencias, Universidad Autónoma de Puebla, Complejo de Ciencias Edificio 192 CU, 72570 Puebla, Mexico*

Received 6 August 2007; received in revised form 15 January 2008; accepted 24 January 2008

Available online 2 February 2008

Abstract

Eight textile dye compounds including five cationic dyes, namely, basic blue 41, basic blue 9, basic green 4, basic violet 16 and basic violet 3, and three anionic dyes, acid green 25, acid red 1 and acid blue 324, were separated and detected by non-aqueous capillary electrophoresis (NACE) with electrochemical detection. Simultaneous separations of acid and basic dyes were performed using an acetonitrile-based buffer. Particular attention was paid to the determination of basic textile dyes. The optimized electrophoresis buffer for the separation of basic dyes was a solvent mixture of acetonitrile/methanol (75:25, v/v) containing 1 M acetic acid and 10 mM sodium acetate. The limits of detection for the basic dyes were in the range of 0.1–0.7 $\mu\text{g mL}^{-1}$. An appropriate solid-phase extraction procedure was developed for the pre-treatment of aqueous samples with different matrices. This analytical approach was successfully applied to various water samples including river and lake water which were spiked with textile dyes.

© 2008 Elsevier B.V. All rights reserved.

Keywords: Textile dyes; Non-aqueous capillary electrophoresis; Electrochemical detection; Environmental analysis; Solid-phase extraction

1. Introduction

Dyes represent an important class of compounds produced worldwide in large quantities of more than 7×10^8 kg per annum [1] and are used in many industries such as nutritional, cosmetics, paper, pharmaceutical, printing inks, textile, tannery, and others. Among these industrial applications textile industry consumes 50% of the overall dye production. Some dyes, like malachite green (basic green 4), have found applications as fungicide and antiseptic in aquaculture [2,3]. Dye compounds can be classified into cationic, non-ionic, and anionic subgroups. Anionic dyes can further be divided into direct, acid, and reactive type while cationic dyes represent the basic ones. Non-ionic dyes refer to disperse dyes because they do not form ions in an aqueous medium.

A number of dyes, in particular azo dyes and their metabolites, are known to have toxic and even carcinogenic character [4]. The environmental risk posed by a dye compound can be

defined in both its inherent ecotoxicology and the concentrations found in the environmental compartments. Thus, reliable analytical methods are needed to detect critical concentrations of dyestuff in the environment.

A variety of analytical approaches for the determination of dye compounds has been reported in the literature. These methods include thin-layer chromatography [5], HPLC [2,3,6–8], pyrolysis gas chromatography [9], capillary electrophoresis in aqueous [5,10–15], and in non-aqueous media [16–19]. Common detection techniques are UV [8,11–13] and diode array detection [5–7,10], fluorescence [15], mass spectrometry [2,3,9,14], and electrochemical detection (ED) [16–20]. Capillary electrophoresis (CE) techniques are particularly suited to achieve highly efficient separations of ionic dye species. For example an aqueous CE method with diode array detection enabled the determination of eight food colorants in milk beverages [10] with detection limits lower than $0.5 \mu\text{g mL}^{-1}$. In addition, the attractive performance of CE separations in the context of ink analysis was demonstrated by Vogt et al. [21] and reviewed by Zlotnick and Smith [22]. However, in aqueous systems various dye compounds can form hydrophobic interactions with the capillary wall which results in poor

* Corresponding author. Tel.: +49 341 97 36 107; fax: +49 341 97 36 115.
E-mail address: matysik@rz.uni-leipzig.de (F.-M. Matysik).

peak shapes. Non-aqueous capillary electrophoresis (NACE) is an attractive alternative which can diminish these problems. In NACE organic solvent systems are used instead of conventional aqueous buffers. In particular, the manipulation of selectivity by varying the organic solvents choices and ratios can help to solve complicated separation problems. This forms the basis for interesting possibilities to adjust performance characteristics like selectivity, resolution, and analysis time. Among the solvents that can be used for NACE acetonitrile exhibits the largest ratio of dielectric constant to viscosity which leads to a high electro-osmotic velocity and fast separations. It has been demonstrated that electrochemical methods are well suited for analyte detection in conjunction with NACE [23]. In acetonitrile-based buffers electrochemical detection exhibits a very good stability of the detection response within an extended accessible potential range and low limits of detection (LOD) can be achieved [18].

The aim of this work was to investigate the applicability of NACE–ED to the determination of cationic and anionic textile dyes which represent common dye classes in textile effluents. Particular attention was paid to the adaptation of the analytical approach to the necessary matrix change from an aqueous sample to the NACE buffer system.

2. Experimental

2.1. Electrophoretic and electrochemical equipment

A high-voltage supply (Model HCN 7E-35000, F.u.G. Elektronik, Rosenheim–Langenfunzen, Germany) was used for measurements in conjunction with a home-made CE system. Care was taken to ensure that the hydrostatic levels of the input and output reservoirs were identical. Sample injection was done by elevating the sample vial up to a difference in height of 10 cm above the detector cell electrolyte level for a duration of 10 s. A commercial CE system PrinCE model 255 (Prince Technologies, Emmen, The Netherlands) equipped with a UV–vis detector (Bischoff model lambda 1010, Leonberg, Germany) operated at 200 nm, was used for comparative measurements with UV detection.

In case of electrochemical detection the implementation of an isolating transformer ensured galvanic separation between the high-voltage supply and the potentiostat. The electrochemical detector cell was placed in a Faraday cage so as to minimize interference from external noise. All electrochemical measurements were performed in the three-electrode mode with the aid of a voltammetric analyzer Model Autolab PGSTAT10 (Eco Chemie, Utrecht, The Netherlands) equipped with a low current amplifier module ECD system. The current signal was filtered through a third-order Sallen–Key filter having a time constant of 100 ms. The interval time of the current measurements for amperometric recordings of the electropherograms was 0.3 s when the analysis time was shorter than 1000 s and when the analysis time was longer, it was 0.5 s. Before running a new electropherogram, a working electrode potential of 3.0 V was applied for 5 s followed by -1.0 V for 5 s to ensure long-term stability of the detector response.

2.2. Detector configuration and capillary specifications

The electrochemical detector cell used for the present work has been described in detail elsewhere [24]. Briefly, the detector cell consists of an inert PTFE cell body with two stainless steel tubes which guide the separation capillary and the working electrode to the right axial position. The working electrode was a 25- μm platinum microdisk electrode. Fused-silica capillaries with an i.d. of 75 μm and an o.d. of 360 μm (Polymicro Technologies, Phoenix, AZ, USA) were used throughout this work. Before initial use, new capillaries were washed with 0.1 M NaOH for 10 min, with distilled water for 5 min, for 15 min with pure acetonitrile and for 25 min with the buffer used. After use, the capillaries were flushed with pure acetonitrile. The capillary and working electrode are kept in place by PTFE adapters fitted to the stainless steel tubes. The capillary-to-electrode distance of 75 ± 5 μm was adjusted under a stereomicroscope by carefully pushing the separation capillary towards the tip of the working electrode. One of the stainless steel tubes served as counter electrode and high-voltage ground. The cell was ready for operation after filling it with 1.5 mL of the separation buffer and placing a PTFE cap with an attached silver/silver chloride reference electrode on top of it. As internal solution of the reference electrode a non-aqueous acetonitrile-based buffer containing 1 M acetic acid and 10 mM sodium acetate was used which ensured that the drift of the reference electrode potential was less than 1 mV h^{-1} . All potentials given in this work were measured with respect to this reference system. In the presence of a high voltage of 20 kV a shift of the working electrode potential of about 300 mV towards more negative potentials occurred [25] that had to be taken into consideration for a suitable potential setting.

2.3. Chemicals

Acetonitrile (99.9% HPLC grade, water <0.02%) and acetic acid (99.99%) were obtained from Sigma–Aldrich (Steinheim, Germany), methanol (LiChrosolv) and sodium acetate (Suprapur) were purchased from Merck (Darmstadt, Germany). Ferrocene was from Riedel-de-Haën AG (Seelze–Hannover, Germany) and was purified by sublimation. For solid-phase extraction (SPE), the cartridges ENVI-Chrom P (0.25 and 0.50 g—6 ml) and ENVI-18 (0.50 g—6 ml) were purchased from Supelco (Bellefonte, PA, USA). The chemicals used for SPE were of analytical-reagent grade and were used as received.

The following textile dyes were used in this work: Sandocryl blue (basic blue 41), sandocryl red (basic violet 16), sandocryl green (basic green 4), sandolan green (acid green 25), sandolan red (acid red 1) and nylosan blue (acid blue 324) which were kindly provided by Clariant (México). The dye compounds crystal violet (basic violet 3) and methylene blue (basic blue 9) were analytical-reagent grade and were obtained from Feinchemie K.-H., Kallies KG (Sebnitz, Germany) and Riedel-de-Haën (Seelze, Germany), respectively. All dye substances were used as received without further purification. Table 1 summarizes specifications of the dye compounds used.

Sample pre-treatment for aqueous solutions was based on SPE using ENVI-Chrom P cartridges. The SPE cartridges were

Table 1
Overview of basic and acid dyes used in this work

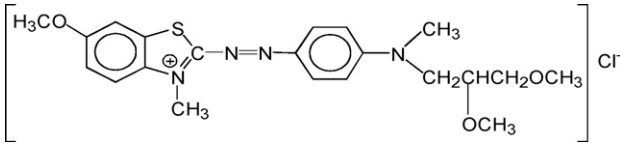
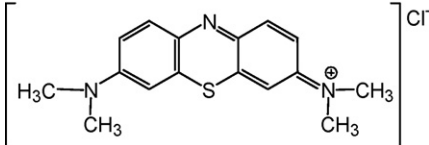
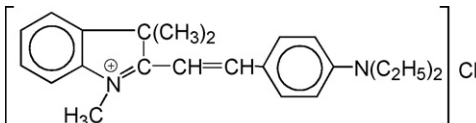
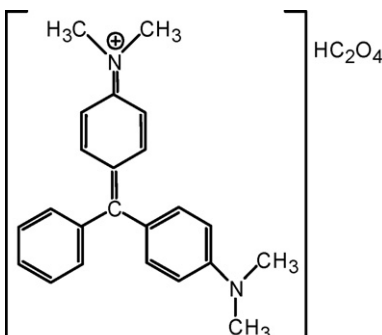
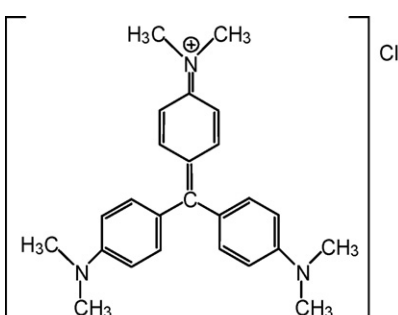
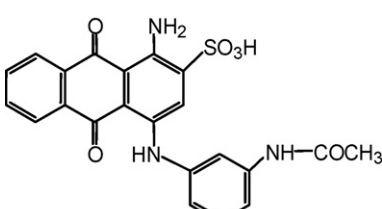
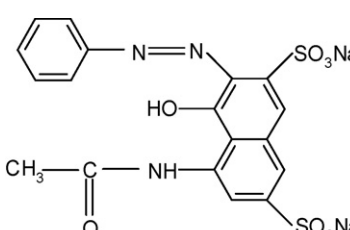
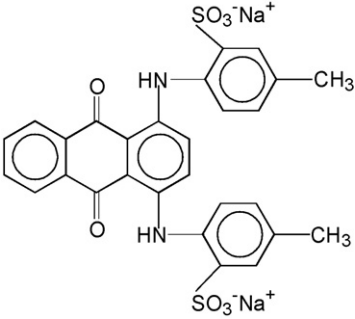
Name	Color index (code)	Chemical structure	Chemical classification
Sandocryl blue	CI. 11105 basic blue 41 (BB41)		Monoazo
Methylene blue	CI. 52015 basic blue 9 (BB9)		Thiazine
Sandocryl red	CI. 48013 basic violet 16 (BV16)		Methine
Sandocryl green	CI. 42000 basic green 4 (BG4)		Triarylmethane
Crystal violet	CI. 42555 basic violet 3 (BV3)		Triarylmethane
Nyosan blue	Acid blue 324 (AB324)		Anthraquinone
Sandolan red	CI. 18050 acid red 1 (AR1)		Monoazo

Table 1 (Continued)

Name	Color index (code)	Chemical structure	Chemical classification
Sandolan green	CI. 61570 acid green 25 (AG25)		Anthraquinone

activated immediately prior to use by passing through 3 ml methanol followed by 6 ml of distilled water. The sample was applied to the cartridge and drawn through at a flow-rate of 3 mL min^{-1} . The cartridges were then rinsed with 12 mL of distilled water and 2 mL of pure acetonitrile. Thereafter the dyes were eluted with 3–5 mL of acetonitrile/tetrahydrofuran (2:1, v/v) solution at a flow-rate of 1 mL min^{-1} and investigated by NACE–ED by injecting directly the extracted solution.

3. Results and discussion

3.1. Voltammetric behaviour of textile dyes in non-aqueous solutions

In order to investigate the applicability of ED in non-aqueous media for the determination of textile dyes the voltammetric behaviour of the individual dye compounds was studied. Fig. 1

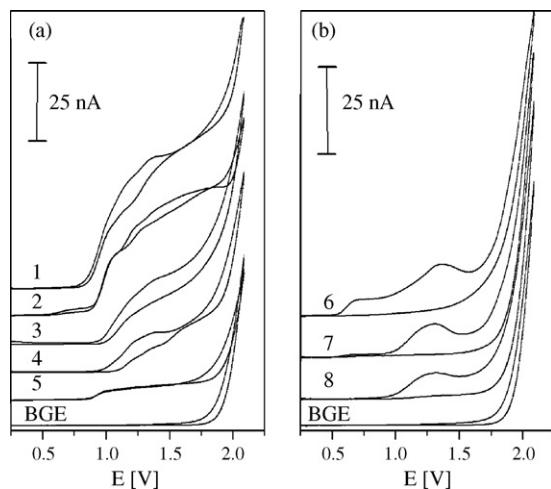


Fig. 1. (a) Cyclic voltammograms of basic dyes: 1, basic violet 3 ($408 \mu\text{g mL}^{-1}$); 2, basic green 4 ($418.5 \mu\text{g mL}^{-1}$); 3, basic blue 9 ($320 \mu\text{g mL}^{-1}$); 4, basic blue 41 ($451 \mu\text{g mL}^{-1}$); 5, basic violet 16 ($369 \mu\text{g mL}^{-1}$) and acetonitrile-based background electrolyte (BGE) containing 1 M acetic acid and 10 mM sodium acetate. (b) Cyclic voltammograms of saturated solutions of acid dyes 6, acid blue 324; 7, acid green 25; 8, acid red 1 and acetonitrile-based background electrolyte containing 1 M acetic acid and 10 mM sodium acetate. A $25\text{-}\mu\text{m}$ platinum microdisk electrode was used as working electrode and the scan rate was 25 mV/s .

shows the cyclic voltammograms for the basic and acid dyes in acetonitrile solution. All target analytes can be oxidized within the accessible potential range. However, the oxidation mechanisms are rather complex involving typically more than one oxidation step and following reactions. In the context of this work no further efforts were undertaken to investigate details of the oxidation processes. All dye compounds allow the recording of mass transport controlled detection signals within the potential window from 1.5 to 1.7 V. In order to obtain information regarding problems due to electrode fouling five consecutive cyclic voltammograms were recorded for the respective dye compounds. Without an electrochemical pre-treatment between the successive recordings decreasing and changing signals were typically obtained. This indicates the presence of reaction products on the electrode surface causing changes in the electrode response. However, an electrochemical activation procedure which applied an anodic pulse of 3.0 V for 5 s and a cathodic pulse of -1.0 V for 5 s was sufficient to restore the initial electrode behaviour. Fig. 2 exemplifies this situation for basic blue 9 illustrating the positive effect of an electrochemical pre-

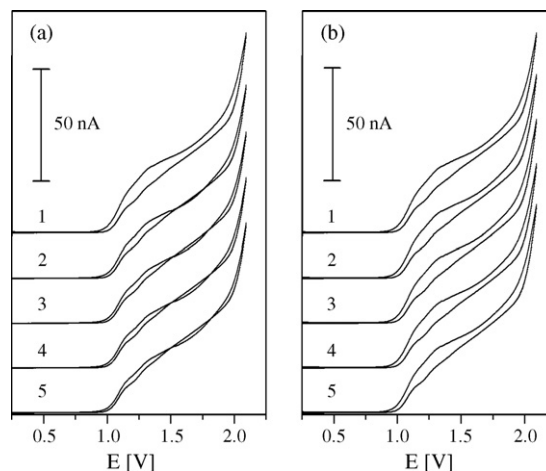


Fig. 2. Repetitive cyclic voltammograms of basic blue 9 ($320 \mu\text{g mL}^{-1}$) in acetonitrile containing 1 M acetic acid and 10 mM sodium acetate (a) without pre-treatment between successive runs and (b) with an electrochemical pre-treatment (3 V and -1 V for 5 s) between successive runs. Other conditions were as in Fig. 1.

treatment between the runs. It should be noted that the effects of deactivation of the sensing electrode is much smaller for typical concentrations ($\mu\text{g mL}^{-1}$) used in the NACE experiments. In addition, in contrast to cyclic voltammetry experiments in NACE the electrode is just a short period of time in contact with the analyte zones.

As a conclusion of the above voltammetric studies and taking into account the shift of the signal due to the presence a high voltage during NACE separations [25], the detection potential of 1.8 V was selected for NACE–ED determinations combined with an electrochemical pre-treatment between consecutive electropherograms.

3.2. Non-aqueous capillary electrophoresis studies

The electrolyte system used for NACE–ED determinations of textile dye compounds consisted of 1 M acetic acid and 10 mM sodium acetate in acetonitrile which was previously proofed to yield very reliable NACE–ED results [16]. Basic dye compounds form cationic species in this buffer medium and acid dyes migrate as anionic species. Consequently, the migration times for basic dyes were shorter than that of an electro-osmotic flow (EOF) marker (ferrocene) and acid dyes showed longer migration times than ferrocene. The acid dye compounds were only slightly soluble in the electrolyte system used. Therefore, stock solutions of known concentration were prepared in methanol and diluted with the buffer used for NACE separations. For some of the dye substances, in particular acid green 25 and acid red 1, more than one component were found in the NACE–ED recordings. This observation reflected the limited purity of the respective dye substances. All concentrations given in this study refer to the total amount of the respective dye preparations. The actual concentrations of the main dye components are correspondingly lower in these cases. Fig. 3 illustrates a simultaneous separation of acid and basic textile dyes present in a mixture. Obviously, the basic dyes exhibit similar migration behaviour and some of them co-migrate (basic violet 3 and basic blue 41) or are not completely resolved from other signals (basic violet 16). On the other hand a good separation performance was achieved for the acid dyes and some of their impurities.

The following studies were focused on the separation and detection of basic dyes because they were available as pure substances and the reliability of the ED response is better if the analytes migrate before the EOF. The latter result can be attributed to water transported by the EOF and corresponding oxidation reactions at the platinum sensing electrode leading to changes of the electrode response characteristics. However, a well-defined detection response could be restored by the electrochemical pre-treatment protocol described under Section 3.1 which was applied between consecutive electrophoretic runs. In order to improve the separation of basic dyes methanol was added to the separation buffer. It was found that an increasing content of methanol led to an improved resolution for the separation of basic dyes, however, the peak width for basic blue 9 increased slightly. A methanol content of 25% resulted in well-separated signals for all dye compounds. In particular, for the signals of basic violet 3 (peak 4) and basic blue 41 (peak 5) a

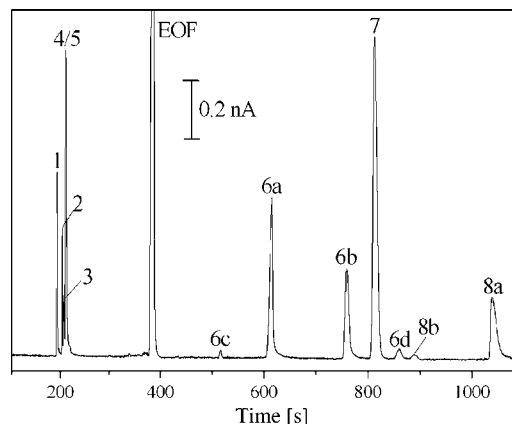


Fig. 3. Non-aqueous capillary electrophoretic separations with electrochemical detection (NACE–ED) for a mixture of acid and basic textile dyes: 1, basic blue 9 ($3.2 \mu\text{g mL}^{-1}$); 2, basic green 4 ($4.2 \mu\text{g mL}^{-1}$); 3, basic violet 16 ($3.7 \mu\text{g mL}^{-1}$); 4, basic violet 3 ($4.1 \mu\text{g mL}^{-1}$); 5, basic blue 41 ($4.5 \mu\text{g mL}^{-1}$); 6, acid green 25 ($31 \mu\text{g mL}^{-1}$); 7, acid blue 324 ($25 \mu\text{g mL}^{-1}$); 8, acid red 1 ($28 \mu\text{g mL}^{-1}$). The letters a–d represent several separated species present in the respective dye sample, EOF corresponds to the electro-osmotic flow. Experimental conditions: capillary dimensions, 60 cm \times 75 μm i.d.; running electrolyte, 1 M acetic acid and 10 mM of sodium acetate in acetonitrile; hydrodynamic injection, 10 s at a height difference of 10 cm; separation voltage of 20 kV; sensing electrode, 25- μm diameter platinum microdisk electrode; detection potential, 1.8 V.

baseline separation could be established. Fig. 4 illustrates these results in detail. The composition of the electrophoresis buffer used in Fig. 4(b) was chosen for all subsequent studies of basic textile dyes.

The precision of migration times and peak heights was very good as specified in Table 2. Comparative measurements were made using a commercial CE system equipped with a UV detector. The limits of detection obtained with ED and UV detection were compared. The results are summarized in Table 2. In all cases ED led to lower LODs than UV detection.

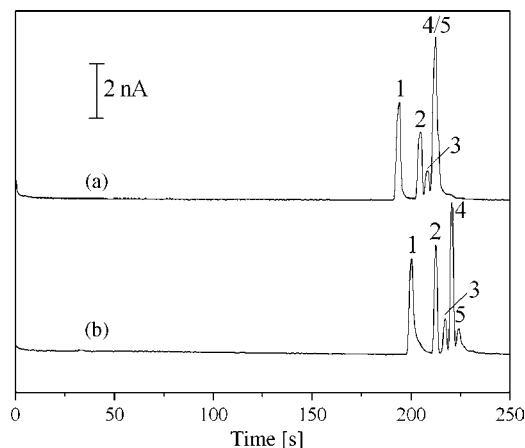


Fig. 4. NACE–ED for a mixture of five basic dyes: 1, basic blue 9 ($16 \mu\text{g mL}^{-1}$); 2, basic green 4 ($21 \mu\text{g mL}^{-1}$); 3, basic violet 16 ($18 \mu\text{g mL}^{-1}$); 4, basic violet 3 ($20 \mu\text{g mL}^{-1}$); 5, basic blue 41 ($23 \mu\text{g mL}^{-1}$) (a) in acetonitrile containing 1 M acetic acid and 10 mM sodium acetate and (b) in acetonitrile–methanol (75:25, v/v) containing 1 M acetic acid and 10 mM of sodium acetate. Experimental conditions were as in Fig. 3.

Table 2

Analytical characteristics of determinations of basic textile dyes by means of non-aqueous capillary electrophoresis with electrochemical detection (ED)/ultraviolet detection (UV)

Compound	Concentration ($\mu\text{g mL}^{-1}$)	Migration time (s) (RSD ^a , %)	Peak height (nA) (RSD ^a , %)	LOD ^b (ED) ($\mu\text{g mL}^{-1}$)	LOD ^b (UV ^c) ($\mu\text{g mL}^{-1}$)
BB9	16	201.5 (0.43)	3.80 (2.55)	0.13	1.70
BG4	21	213.8 (0.41)	4.07 (0.88)	0.16	0.86
BV16	18	218.5 (0.45)	1.28 (2.30)	0.43	2.39
BV3	20	222.1 (0.45)	5.64 (1.68)	0.11	0.68
BB41	23	225.5 (0.42)	0.98 (4.02)	0.72	2.16

Experimental conditions were as in Fig. 4.

^a Relative standard deviation (number of measurements, 6).

^b The limits of detection (LOD) were calculated on the basis of the peak-to-peak noise and a signal-to-noise ratio of 2.

^c Detection wavelength, 200 nm; capillary dimensions, 85 cm \times 75 μm i.d. (65-cm effective length); separation voltage, 25 kV.

3.3. Studies of aqueous sample solutions

The above results demonstrate the attractive performance of NACE–ED for mixtures of cationic textile dyes prepared in non-aqueous media. However, for the determination of cationic dyes in real aqueous samples additional challenges have to be considered. The main problem is the necessity of matrix change from the aqueous to the non-aqueous medium. Initial attempts were made to inject aqueous samples directly into the NACE–ED system. In this case noisy signals and distorted peak shapes were obtained. In addition, precipitation of inorganic salts could complicate the determination. Therefore, sample pre-treatment methods such as liquid–liquid extraction (LLE) and solid-phase extraction were tested. A LLE protocol was adapted from a report by Pandit and Basu [26]. However, this approach was only applicable for spiked samples prepared from distilled water but failed in case of more complex aqueous matrices. Consequently, experiments based on SPE were conducted using various SPE cartridges and elution procedures. Finally, a SPE protocol was elaborated which is based on ENVI-Chrom P cartridges and described in Section 2. The recoveries of extractions of cationic textile dyes were determined for different aqueous sample matrices including distilled, river and lake water. Table 3 summarizes the recoveries obtained for various dye components in different aqueous samples. In general, the recoveries were reduced in more complex aqueous matrices.

Fig. 5 illustrates results of NACE–ED measurements after SPE of lake water (5a) and lake water spiked with textile dyes (5b). No interfering substances were found which suggests that this analytical approach has the potential to be applied to a wide range of real samples. According to literature reports typical dyestuff concentrations found in textile effluents range between

Table 3

Recoveries of solid-phase extraction experiments of basic textile dyes based on ENVI-ChromP cartridges (see Section 2 for details)

Type of water	Recovery (%)			
	Basic blue 9	Basic green 4	Basic violet 16	Basic violet 3
Distilled	93	81	Not determined	98
River	87	84	85	82
Lake	62	48	83	43

Determinations were done by NACE–ED.

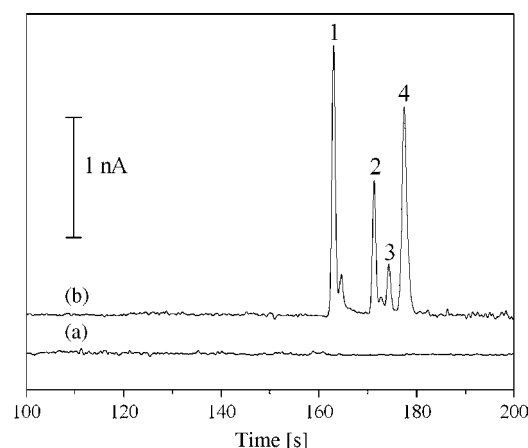


Fig. 5. NACE–ED of (a) a lake water sample after solid-phase extraction and (b) of a lake water sample spiked with a mixture of four basic dyes: 1, basic blue 9 ($0.013 \mu\text{g mL}^{-1}$); 2, basic green 4 ($0.017 \mu\text{g mL}^{-1}$); 3, basic violet 16 ($0.015 \mu\text{g mL}^{-1}$); 4, basic violet 3 ($0.016 \mu\text{g mL}^{-1}$) after SPE. Experimental conditions were as in Fig. 3.

10 and $7000 \mu\text{g mL}^{-1}$ [27–30] to which the above protocol could easily be adapted. For environmental samples with considerably lower concentrations of the target analytes the sensitivity can further be increased by the application of large sample volumes to the SPE extraction cartridges.

4. Conclusions

This work demonstrated the applicability of NACE–ED for the determination of acid and basic textile dyes. A compromise between separation and detection aspects was found using a mixed acetonitrile/methanol (75:25, v/v) solvent system containing 1 M acetic acid and 10 mM sodium acetate. In this medium baseline separations could be achieved for all dye compounds studied with limits of detection between 0.1 and $0.7 \mu\text{g mL}^{-1}$ which were clearly lower than obtained with UV detection.

Based on solid-phase extraction an effective sample pre-treatment protocol could be established to investigate aqueous dye samples for which a matrix change from the aqueous to the non-aqueous medium has to be carried out. The application of the elaborated analytical approach enables determinations of textile dyes in real samples such as river or lake water.

Acknowledgements

A.A. Peláez-Cid is grateful for the Alban scholarship no. E04E044054MX within the European Union Programme of High Level Scholarships for Latin America. The authors wish to thank M.P. Elizalde-González for support and discussion.

References

- [1] T. Robinson, G. McMullan, R. Marchant, P. Nigam, *Bioresour. Technol.* 77 (2001) 247.
- [2] P. Scherpenisse, A.A. Bergwerff, *Anal. Chim. Acta* 529 (2005) 173.
- [3] D.R. Doerge, M.I. Churchwell, T.A. Gehring, Y.M. Pu, S.M. Plakas, *Rapid Commun. Mass Spectrom.* 12 (1998) 1625.
- [4] M. Inoue, F. Okada, A. Sakurai, M. Sakakibara, *Ultrason. Sonochem.* 13 (2006) 313.
- [5] T. Goldmann, F. Taroni, P. Margot, *J. Forensic Sci.* 49 (2004) 716.
- [6] M.P. Elizalde-González, A.A. Peláez-Cid, *Environ. Technol.* 24 (2003) 821.
- [7] M.M. Dávila-Jiménez, M.P. Elizalde-González, A.A. Peláez-Cid, *Colloids Surf. A* 254 (2005) 107.
- [8] L.-H. Ahlström, E. Björklund, L. Mathiasson, *Anal. Bional. Chem.* 382 (2005) 1320.
- [9] A. Plum, W. Engewald, A. Rehorek, *Chromatographia* 57 (2003) S-243.
- [10] H.-Y. Huang, Y.-C. Shih, Y.-C. Chen, *J. Chromatogr. A* 959 (2002) 317.
- [11] P. Blatny, C.-H. Fischer, E. Kenndler, *Fresenius J. Anal. Chem.* 352 (1995) 712.
- [12] P. Blatny, C.-H. Fischer, A. Rizzi, E. Kenndler, *J. Chromatogr. A* 717 (1995) 157.
- [13] S. Hamai, K. Sato, *Dyes Pigments* 57 (2003) 15.
- [14] E.D. Lee, W. Müick, J.D. Henion, T.R. Covey, *Med. Environ. Mass Spectrom.* 18 (1989) 253.
- [15] P.K. Dasgupta, Z. Genfa, J. Li, C.B. Boring, S. Jambunathan, R. Al-Horr, *Anal. Chem.* 71 (1999) 1400.
- [16] F.-M. Matysik, *J. Chromatogr. A* 802 (1998) 349.
- [17] F.-M. Matysik, *Electrochim. Acta* 43 (1998) 3475.
- [18] F.-M. Matysik, *Electroanalysis* 11 (1999) 1017.
- [19] A.R. Fakhari, M.C. Breadmore, M. Macka, P.R. Haddad, *Anal. Chim. Acta* 580 (2006) 188.
- [20] N. Dossi, E. Piccin, G. Bontempelli, E. Carrilho, J. Wang, *Electrophoresis* 28 (2007) 4240.
- [21] E. Rohde, A.C. Mcmanus, C. Vogt, W.R. Heinemann, *J. Forensic Sci.* 42 (1997) 1004.
- [22] J.A. Zlotnick, F.P. Smith, *J. Chromatogr. B* 733 (1999) 265.
- [23] F.-M. Matysik, *Electrophoresis* 23 (2002) 3711.
- [24] F.-M. Matysik, *J. Chromatogr. A* 853 (1999) 27.
- [25] F.-M. Matysik, *Anal. Chem.* 72 (2000) 2581.
- [26] P. Pandit, S. Basu, *J. Colloid Interface Sci.* 245 (2002) 208.
- [27] I.G. Laing, *Rev. Prog. Coloration* 21 (1991) 56.
- [28] C. O'Neill, F.R. Hawkes, D.L. Hawkes, N.D. Laurencio, H.M. Pinheiro, W. Delée, *J. Chem. Technol. Biotechnol.* 74 (1999) 1009.
- [29] P.C. Vandevivere, R. Bianchi, W. Verstraete, *J. Technol. Biotechnol.* 72 (1998) 289.
- [30] O.J. Hao, H. Kim, P.-C. Chiang, *Crit. Rev. Environ. Sci. Technol.* 30 (1999) 449.

The use of FT-NIR for API content assay in organic solvent media: A single calibration for multiple downstream processing streams

Licinia O. Rodrigues^{a,*}, Joaquim P. Cardoso^b, José C. Menezes^a

^a *IBB, Centre for Biological and Chemical Engineering, IST, Technical University of Lisbon,
Avenue Rovisco Pais, P-1049-001 Lisbon, Portugal*

^b *CIPAN S.A. Vala do Carregado, P-2601-906 Alenquer, Portugal*

Received 22 September 2007; received in revised form 7 January 2008; accepted 9 January 2008

Available online 17 January 2008

Abstract

The use of near infrared spectroscopy (NIRS) in downstream solvent based processing steps of an active pharmaceutical ingredient (API) is reported. A single quantitative method was developed for API content assessment in the organic phase of a liquid–liquid extraction process and in multiple process streams of subsequent concentration and deuration steps. A new methodology based in spectra combinations and variable selection by genetic algorithm was used with an effective improvement in calibration model prediction ability. Root mean standard error of prediction (RMSEP) of 0.05 in the range of 0.20–3.00% (w/w) was achieved. With this method, it is possible to balance the calibration data set with spectra of desired concentrations, whenever acquisition of new spectra is no longer possible or improvements in model's accuracy for a specific selected range are necessary. The inclusion of artificial spectra prior to genetic algorithms use improved RMSEP by 10%. This method gave a relative RMSEP improvement of 46% compared with a standard PLS of full spectral length.

© 2008 Elsevier B.V. All rights reserved.

Keywords: Near infrared; Downstream processing; Organic media; Multivariate calibration

1. Introduction

Lab based methods used by the pharmaceutical industry are often time consuming and add to the manufacturing cycle time. NIR spectroscopy offers one possible option for process based analytical measurements and has a significant advantage over some other technologies as it allows fast analytical measurements with simple sample preparation. However, the main feature of NIR of being sensitive to both chemical and physical effects can sometimes be a challenge when one is dealing with large sample matrix variations and very low analyte concentrations. These two conditions, which are a commonplace inside the pharmaceutical manufacturing, hinder not only the development of robust calibrations but also the application of the same models in more than one point of the process.

To overcome this problem in the present study, a new methodology was applied to build one robust calibration model capable

of accurately predicting active pharmaceutical ingredient (API) content in solvent samples independently of their origin. The model robustness is based on spectral selectivity for the analyte of interest and careful wavenumbers selection.

To the best of our knowledge, the use of the same calibration for measuring streams from different points of consecutive downstream processing steps has not yet been reported.

1.1. Process overview

An API purification process includes a series of steps: at the end of the API fermentation, the culture media is first clarified by filtration or centrifugation and the biomass discarded. After the clarification and concentration steps, the active compound is extracted from the aqueous media to an organic phase, by liquid–liquid extraction. The extraction phase is then concentrated by evaporation. At this point, it has a cloudy orange appearance given by the degradation products. Next, to remove these non-desired products, the solution is submitted to purifying steps, where it loses most impurities but the water content increases.

* Corresponding author. Tel.: +351 21 841 9838; fax: +351 21 841 9197.
E-mail address: bsel@ist.utl.pt (L.O. Rodrigues).

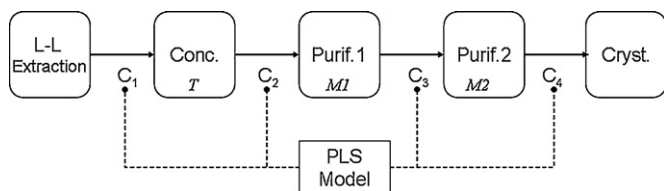


Fig. 1. Process description. The use of one single calibration model along the process is proposed.

A schematic representation of the process is presented in Fig. 1. The use of a single model along the process is proposed for assessment of concentrations C1, C2, C3 and C4.

2. Methods

2.1. Feature selection for partial least squares modelling

Partial least squares [1] is used in spectroscopy to extract relevant information from complex spectra containing overlapping absorption peaks, interferences from light scatter and noise. PLS was first considered as being almost insensitive to noise, and therefore, no feature selection was required [2]. In the last years, it has been widely recognised that variable selection can improve the prediction ability [3].

In near infrared spectroscopy (NIRS) the number of measured variables is very large and in most cases not all of them contain useful information. Theoretically, the regression coefficient for such variables will be close to zero and the inclusion of these variables should not affect negatively the calibration. However, there are significant improvements in the prediction accuracy of a calibration when a proper selection of variables is made. Moreover, the variable selection usually leads to a reduction of latent variables in the model and improve the stability of the calibration by the reduction of multicollinearity between variables [4].

Genetic algorithms (GA) have been successfully used as a method to select the most informative variables [5–7]. GAs are based upon the principle of natural evolution and selection: reproduction, mutation and selection based on fitness. The main risk of the application of GA is overfitting [5]. Meaningless variables can be selected due to the presence of non-causal correlations [8]. As such, it is necessary that the model defined neither over-fits nor under-fits the data. The selection criteria can be based on root mean squared error of cross validation (RMSECV) or on root mean squared error for prediction of an external data set (RMSEP) defined as follows:

$$\text{RMSECV} = \sqrt{\frac{\sum_{i=1}^n (Y_{i(\text{cv})} - Y_{i(\text{ref})})^2}{n}} \quad (1)$$

$$\text{RMSEP} = \sqrt{\frac{\sum_{i=1}^n (Y_{i(\text{pred})} - Y_{i(\text{ref})})^2}{n}} \quad (2)$$

where n stands for the number of prediction samples, $Y_{i(\text{cv})}$ and $Y_{i(\text{pred})}$ for predicted values for cross validation and external validation, respectively, and $Y_{i(\text{ref})}$ for reference value of sample i .

2.2. Combined spectra method (CSM)

The proposed methodology combines the spectra of two samples of different concentrations and assumes that the concentration of the averaged spectrum is also the average of the original concentration values (Fig. 2). This assumption pretends to reveal the most linearly correlated wavenumbers, assuming Beer's Law for transmission, which states that observed absorbance at a given wavelength for a mixture of different components is additive and the individual contributions are linear.

It is thus expected that proportional relations between the new spectra and the new concentrations will only be achieved for the variables truly linearly correlated with the analyte, enhancing the “good” and the “bad” spectral ranges.

Combined spectra method was performed with the following steps:

- (1) Find the optimum number of latent variables and the best pre-processing method for a full PLS model with the raw calibration set (Data Set 1).
- (2) Perform the spectra combination in the unprocessed spectra, for the desired concentration range. Use the Matlab function code below to create the new spectra, in which X represents the spectral matrix and Y the corresponding concentration vector, taken from Data Set 1:


```
function [xc,yc] = combspec(X,
Y, ncomb)
mix = zeros(1, size(x,2)+1);
for i = [1:10]
sx = shuffle([x y]);
mx = meanspc(sx, ncomb); mix = [mix; mx];
end
mix(1, :) = [];
yc = mix(:, end); xc = mix(:, 1:end-1);
```
- (3) Add the resulting spectra to the original data set and pre-process it again to build Data Set 2.
- (4) Run the GA in Data Set 2.
- (5) Cut Data Set 2 according to GA best fit results to obtain Data Set 3.
- (6) Build the PLS model with Data Set 3 and predict an independent data set for validation.
- (7) Compare resulting RMSEP with the previously RMSEP calculated in step one. If no significant improvement is reached, the algorithm should return to step 2 and new set of spectra combinations should be added to the previous one.

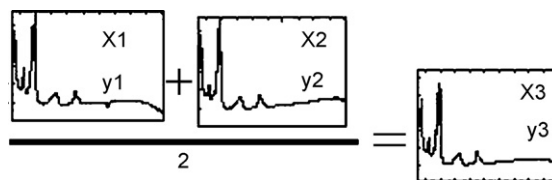


Fig. 2. Combined spectra method. It combines the spectra of two (or more) samples of different concentrations and produces an averaged spectrum and its virtual concentration.

3. Experimental

3.1. Samples

Data set was built with samples collected from four streams of the process. The samples were divided into a training set (118 samples), on which the GA is run and the PLS model is built, and an independent evaluation set (68 samples), on which the models are tested.

As mentioned previously, samples were collected in four different process streams (see Fig. 1). Stream 1 results from a liquid–liquid extraction with ethyl acetate. It has a low API concentration, water is present in its saturation levels (approximately 8%) and acetone is present (approximately 3%). Stream 2 is the condensate of an evaporative process. API concentration is 10 times higher, acetone was removed, and new impurity products, related with API degradation during the concentration step, are present. Streams 3 and 4 result from consecutive purification steps through activated charcoal filters. The water content slightly increases and impurities are removed.

3.2. Reference method

All samples were analysed for API content through spectrophotometry by reaction with imidazol reagent and the results used as reference values. The method has a precision of $\pm 0.065\%$ (w/w), at 95% confidence level.

3.3. Equipment and software

NIR absorbance spectra were measured with a BOMEM MB-160 FT-NIR spectrometer with an indium-arsenide (InAs) detector; a Vial Holder for 8 mm cells and a temperature controller. Spectra were acquired using GramsAI-7 (Thermo, USA) and for spectra pre-treatment and calibration development, Matlab (Mathworks Inc., USA) with PLS toolbox v.3 (Eigenvector Inc., USA), were used.

3.4. Spectra acquisition

Each sample was measured in duplicate in transmittance mode. The spectra were collected in the wavenumber range of $4000\text{--}12,000\text{ cm}^{-1}$ ($833\text{--}2500\text{ nm}$), based on 32 scans with 16 cm^{-1} step (resolution). The reference spectrum was taken with an empty cell and the analysis was carried at controlled temperature of $25\text{ }^\circ\text{C}$.

4. Results and discussion

4.1. Pre-processing selection

As a consequence of their different origin in the process, samples have different compositions and matrices (e.g. degradation products, other residual organic solvents and moisture content). Batch-to-batch variations are expected as well, arising from the composition of the fresh solvent, mainly from residual solvent and water. As such, the first step in model development

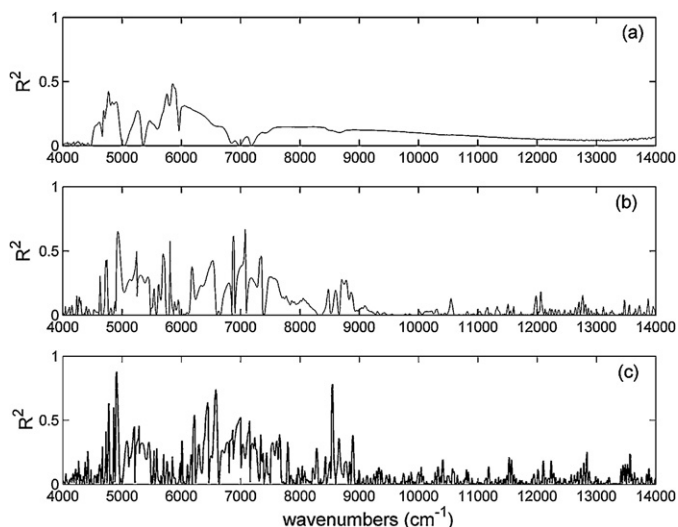


Fig. 3. Squared correlation coefficients, R^2 , vs. wavenumber for different pre-processing methods. (a) Auto-scaled data; (b) Savitsky-Golay first derivative; (c) Savitsky-Golay second derivative. Maximum coefficient obtained in each case was 0.48, 0.67 and 0.88, respectively.

was to investigate the most adequate pre-processing method for suppressing this variability. For each pre-processing method, the squared correlation coefficient, R^2 , between each variable and the analyte was computed. The highest coefficients were obtained with the second-derivative method (see Fig. 3), with which an R^2 maximum value of 0.88 was obtained.

The highest values obtained using first derivative or auto-scaling processing were significantly lower, 0.67 and 0.48, respectively. The second derivative was, therefore, used as pre-processing method from this point on. A second-order polynomial adjusted to an 11-points window gave the best results for Savitsky-Golay method (evidence not shown).

Standard normal variate (SNV) and multiplicative scatter correction (MSC) transformations were also tested in the full range spectra, giving a maximum R^2 of 0.25. This poor results were already expected since the transmission spectra were not significantly affected by scatter.

The optimum dimension was determined by the minimum RMSECV for the calibration samples. Samples were divided into 10 segments randomly and leave-one segment out was used as cross-validation method. Eight (8) latent variables (LVs) were necessary to retain a significant variance in the data and to avoid overfitting. An R^2 of 0.993 and a RMSECV of 0.063% was obtained.

4.2. Combined spectra method and variable selection

The distribution of the concentration values among the original calibration set was evaluated. The histogram shows a lack of samples in the higher concentration range (Fig. 4). As so, the combined spectra method was only performed with raw spectra from samples with analyte concentration from 1.5 to 3.0%, in order to increase the model sensibility for this range. Seventy pairs of (spectra/concentration) were added to the original data and submitted to a GA.

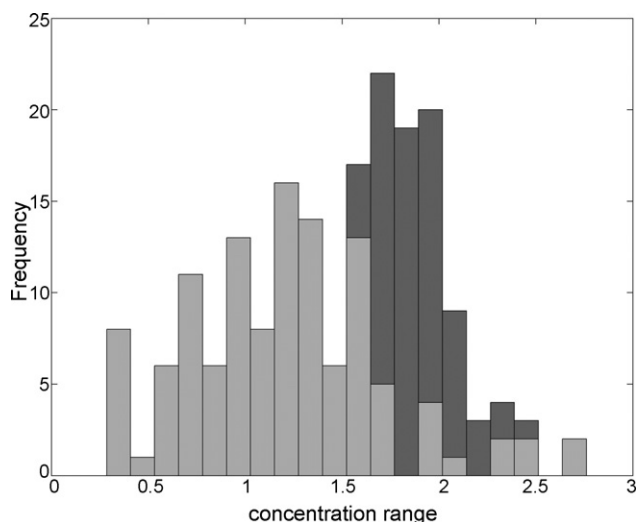


Fig. 4. Frequency histogram for samples' concentrations. Original (light grey) calibration data set; data (dark grey) produced by combined spectra method.

GA was performed using a PLS regression method. Details on the algorithm used can be found in Table 1. The maximum number of factors was imposed regarding the number of components (eight) determined by cross validation on the preliminary model. Intervals of 10 variables were selected rather than individual variables to prevent the selection of possible random correlated variables. The selected variables are highlighted in Fig. 5. Samples' matrix is made up of a complex mixture of solvents, water, API and API degradation products. The API itself is a molecule that is expected to have absorbance contributions in several regions of the NIR spectrum. The degradation products are also very similar to the API in chemical structure. After spectral pre-processing, the physical features like light scattering, temperature, density or viscosity are not present or non-significant. As such, the selected wavenumbers are not expected to correspond to any spectral features that could be related to any physical phenomenon.

4.3. PLS model

The augmented data set (118 real samples plus 70 from CS method) and the variables selected by GA (shown in Fig. 5) were used to build the final PLS model. Fig. 6 shows a compar-

Table 1
Parameters of the GA used

Parameter	Value
Population size	64
Window width	10
Initial terms	30
Maximum generations	100
Mutation rate	0.005
Crossover	Double
Regression	PLS
Maximum LV	8
Cross validation	Contiguous

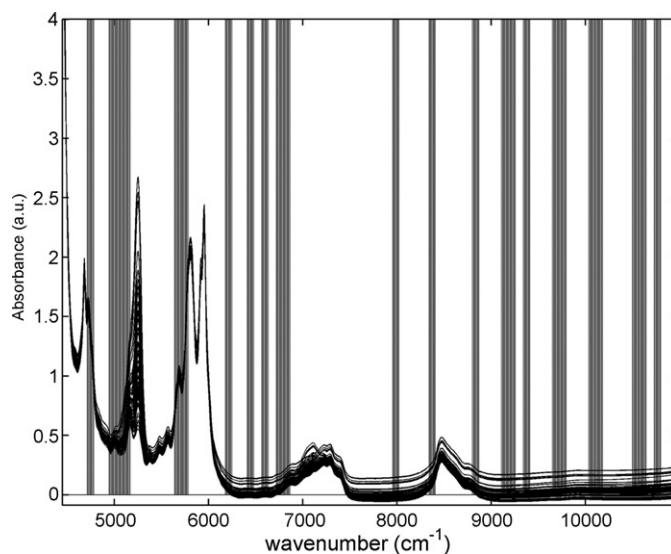


Fig. 5. Overview of the best variable selection obtained with GA. Wavenumbers included are marked in shaded areas.

ison obtained between final and full spectra models' results. As expected, the use of PLS without a preliminary variable selection results in a poor prediction capacity with larger prediction residuals (Fig. 6a).

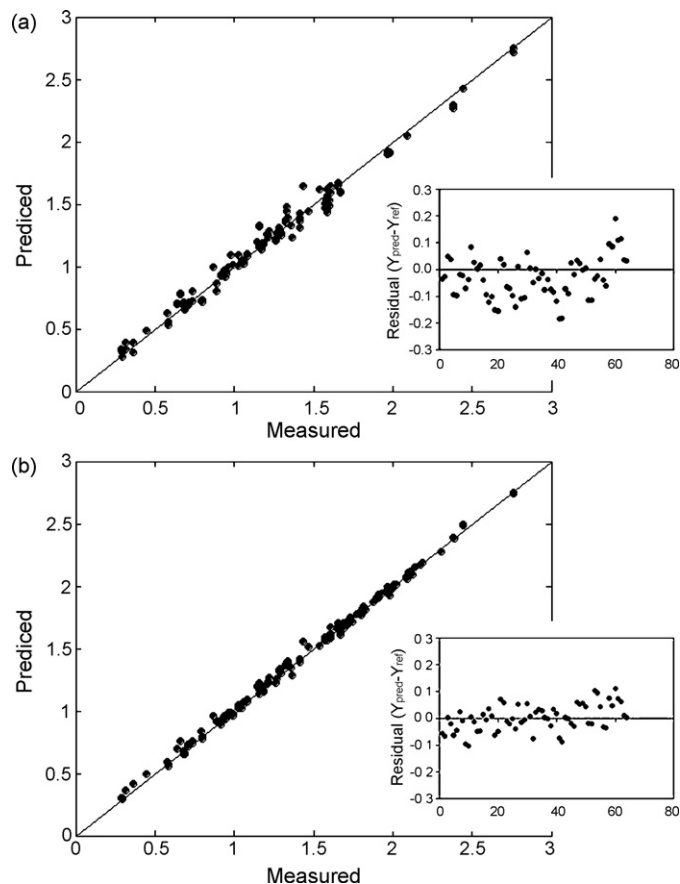


Fig. 6. Comparison between models and their cross-validation residuals. (a) Full spectrum PLS model, $R^2 = 0.993$, RMSECV = 0.063, RMSEP = 0.091; (b) PLS with variable selection by GA on augmented data set, $R^2 = 0.999$, RMSECV = 0.029, REMSEP = 0.049.

Table 2

Figures of merit of the PLS models' predicting performance for the independent validation data set

Model	Selection method	Data set (variable selection)	Data set (model building)	RMSECV	RMSEP	Accuracy improvement (%)
Full spectrum	None	Original	Original	0.063	0.091	Reference
A	Correlation	Original	Original	0.043	0.065	29
B	GA	Original	Original	0.043	0.061	33
C	GA-CSM	Augmented	Original	0.038	0.054	41
Final	GA-CSM	Augmented	Augmented	0.029	0.049	46

Best results are achieved when GA algorithm is applied in the data set containing the combined spectra.

The effect of using 70 combined spectra can be noticed in the predicted versus measured plot (Fig. 6b), where a linear correlation coefficient of 0.999 is achieved. However, it is relevant to stress that figures of merit like R^2 , RMSEC or RMSECV cannot be directly used for comparison because the effect of the combined spectra might not be entirely eliminated from the cross-validation procedure. For this reason, the performance of different models was evaluated in terms of their accuracy (as RMSEP) in predicting a new independent test set of 34 samples collected from the different process streams (see Fig. 1).

In order to compare the benefits of the proposed methodology, three other models were built and validation results were compared. The validation results are presented in Table 2. Model A uses wavenumbers selected by univariate correlation. In Model B, only the original data set was used for wavenumber selection and model building. In Model C, the augmented data set by CMS was used for wavenumber selection but the model was built with the original data. The final model uses the augmented data set for both wavenumber selection and model building.

Using the full model as reference, the variable selection by univariate correlation (Model A), in which only the most correlated variables are used, improved the RMSEP in 29%. The standard use of GA on the original data (Model B) showed a similar improvement, 33%. Finally, Model C, built without adding the combined spectra to the calibration set, although better than the previous ones underperformed when compared with the final model. Using the augmented data set, a 46% reduction in the prediction error is achieved, leading to the best RMSEP found of 0.049%, which is considered to be acceptable for production plant monitoring for all the process streams.

A precision test was performed with spectra replicates from the independent test set. The full spectrum PLS model showed a precision of 0.02 and the final model (built with the proposed method showed) a precision of 0.01. The improvement of 50% in analytical precision is a strong indicator that the proposed method enhances the selectivity towards the analyte, resulting in a more robust model.

5. Conclusion

The content of a certain active pharmaceutical ingredient (large molecule anti-bioactive) in different organic solutions can be analysed by NIR spectroscopy with an accuracy of 0.05% (w/w) within the process concentration range of 0.10–3.00% (w/w).

A single calibration model was used to monitor the API content in several points across consecutive steps of downstream

processing. The effects of sample matrix variability among the process streams were attenuated by selecting intervals of variables from spectroscopic data by genetic algorithms. The proposed methodology of adding artificially created data (generated by combining spectra of samples of different concentrations) to the original data set was found to improve the genetic algorithm's performance for the selection of the most informative wavenumbers. A 40% reduction in the RMSEP (0.06%) was achieved when compared with a full spectrum prediction (0.09%). Moreover, a more significant improvement, 46%, in prediction ability was obtained when the same artificial data was also used in the PLS regression step, reducing the RMSEP to 0.05%.

The methodology proposed here is simple, yields lower prediction errors than classical methodologies and might be valuable to use whenever a calibration model is required to accurately interpolate a concentration range that, for operational reasons, might be difficult to populate. Also it is less arbitrary than weight calibration methods, although it assumes that linearity and additivity of Beer's Law hold for the studied case. The use of one single model for multiple critical to quality monitoring points across a multi-stage process, simplifies the routine analysis procedure and its implementation as a new analytical method (e.g. documentation), and has obvious advantages in calibration development and maintenance over time.

Acknowledgements

L.R. gratefully acknowledges the financial support from the Portuguese Foundation for Science and Technologies (grant no. BDE/15514/2004). The authors also thank Companhia Industrial Produtora de Antibióticos S.A. (CIPAN) in Portugal for providing the best conditions to carry out this work in the downstream plant and for authorising its publication.

References

- [1] P. Geladi, B.R. Kowalski, *Anal. Chim. Acta* 185 (1986) 1–17.
- [2] E.V. Thomas, D.M. Haaland, *Anal. Chem.* 62 (1990) 1091–1099.
- [3] E.V. Thomas, *Anal. Chem.* 66 (1994) 795a.
- [4] T. Næs, T. Isaksson, T. Fearn, T. Davies, *A User Friendly Guide to Multivariate Calibration and Classification*, NIR Publications, 2002.
- [5] R. Leardi, Application of genetic algorithm-PLS for feature selection in spectral data sets, *J. Chemom.* 14 (2000) 643–655.
- [6] M. Khanmohammadi, M.A. Karimi, K. Ghasemi, M. Jabbari, A. Garmarudi, *Talanta* 72 (2007) 620–625.
- [7] C. Abrahamsson, J. Johansson, A. Sparén, F. Lindgren, *Chemom. Intell. Lab. Syst.* 69 (2003) 3–12.
- [8] D. Jouan-Rimbaud, D.L. Massart, O.E. Noord, *Chemom. Intell. Lab. Syst.* 35 (1996) 213–220.

The use of NIR as a multi-parametric in situ monitoring technique in filamentous fermentation systems

Licinia O. Rodrigues^{b,*}, Luís Vieira^a, Joaquim P. Cardoso^a, José C. Menezes^b

^a CIPAN S.A., Vala do Carregado, P-2601-906 Alenquer, Portugal

^b Institute of Biotechnology & Bioengineering, IST, Centre for Biological and Chemical Engineering, Technical University of Lisbon, Av. Rovisco Pais, P-1049-001 Lisbon, Portugal

Received 5 August 2007; received in revised form 18 January 2008; accepted 24 January 2008

Available online 2 February 2008

Abstract

The use of Fourier transform near infrared (FT-NIR) spectroscopy for simultaneous determination of multiple properties in an active pharmaceutical ingredient (API) fermentation process is described, together with procedures for developing accurate NIR calibrations with a performance independent of scale and the specific bioreactor used. Measurements were made in situ, by insertion of transfection probes into pilot and industrial bioreactors providing direct contact with the fermentation culture media. The ultimate goal was to establish methods for real time process monitoring aimed at enhanced process supervision, fault detection diagnosis and control of bioreactors. The in situ acquired spectra were related to lab results of samples taken from the reactors during the course of the manufacturing process. Suitable spectral wavenumber regions were selected and calibration models based on partial least squares (PLS) were developed. The root mean square errors of prediction for API content, viscosity, nitrogen source and carbon source concentration were all within acceptable ranges as compared to the off-line lab measurements, respectively, 0.03% (w/w), 150 cp, 0.01% (w/w), and 0.4% (w/w).

© 2008 Elsevier B.V. All rights reserved.

Keywords: Fermentation; In situ; NIR; Transfection; Antibiotic

1. Introduction

Fermentation processes are usually controlled based on concentration values of the main carbon and nitrogen substrates present, main metabolites produced – active pharmaceutical ingredients (APIs) – biomass concentration and even some other important substances such as precursors, inducers, and promoters. These parameters are usually obtained by laborious off-line techniques that take from 30 min to 4 h long. As such, for the purpose of real time process supervision and diagnosis, off-line measurements should be replaced by on-line automatic and preferably multi-parametric techniques.

The application of near infrared spectroscopy (NIRS) in fermentation processes has seen a renewed interest in recent years, after some years of neglect, as chemometrics has

matured into a science and better and more robust instrumentation became available (probes). The NIR potential to be simultaneously calibrated for the most important chemical compounds (substrates, API, precursors) and physical parameters like viscosity can now be explored. The antibiotic production by fermentation, however, revealed to be a significant challenge to NIRS in situ measurements [1]: aerobic fermentation process's inherent conditions such as vigorous stirring and gas bubbles; the growing of antibiotic producers filamentous bacteria as branched structures resulting in high viscosities in liquid phase; culture media non-Newtonian behaviour; and complex production medium containing meals (fish, soya, etc.), oils, and other water-soluble ingredients. Furthermore, the rheological properties of culture liquids vary along cultivation time, from batch-to-batch and with reactor scale [2].

Developments were reported using NIR in antibiotic production are related with at-line reflection analysis [3–7] and with ex situ use of flow cells or fiber optic probes (reflectance) placed on the glass window of the fermentor [8]. In this work the

* Corresponding author. Tel.: +351 21 841 9838; fax: +351 21 841 9197.
E-mail address: bsel@ist.utl.pt (L.O. Rodrigues).

goal was to establish if NIR spectroscopy could be used reliably for extended periods in pilot and industrial bioreactors in cultivations with complex media.

2. Methods and materials

2.1. Process description

The bioprocess studied is an industrial scale process for the production of, an API, at CIPAN S.A. (Portugal). The API is clavulanic acid, a beta-lactamase inhibitor. It is produced by *Streptomyces clavuligerus* microorganisms in a fed batch process that lasts about 100 h. This work uses data acquired from 3 pilot bioreactors (geometric volume of 500 L) and 3 industrial reactors (20 m³ and 40 m³). The cultivation is carried out using a medium containing soybean meal, a defined carbon source, nitrogen source, inorganic oils, and an anti-foam. The operating conditions are typically of those employed in industrial processes for aerobic submerged cultivations at high cell densities.

2.2. Sampling and reference methods

Samples were collected from the fermentors at regular intervals (approximately 8 h) and characterised by the conventional analytical methods currently established. These at-line values were used as reference for model building.

The concentration of the API was determined by HPLC. The apparent viscosity was measured by a Brookfield concentric cylinder viscometer (Model LVT, Wilmington, USA). Readings were taken using 500 ml samples at 25 °C, 60 rpm and spindle number 3. The nitrogen source was determined by the Kjeldahl method with a Tecator Digestion System. The concentration of the carbon source compound was determined by a spectrophotometric method after reaction with an adequate compound.

2.3. Equipment

Near infrared spectra over the wavenumber range 4000–11,000 cm⁻¹ were recorded in transfection mode by a Yokogawa NR800 FT-NIR (Fourier transform near infrared) analyser equipped with an InGaAs (indium, gallium, arsenide) photodiode. The analyser with a beam splitter at the interferometer allows the connection of two transfection probes to measure two fermentors simultaneously. The mechanical path length of the transfection probes was adjusted to 0.5 mm (1 mm of optical path length). Reference spectra were taken from air and probes were inserted into the fermentors through standard DN25 ports. A total of 600 averaged spectra (128 scans each) were recorded for each individual batch at 1 averaged spectra/10 min. The exact time of sample collection from the bioreactor was recorded and the correspondent acquired spectra were selected for model building data sets.

2.4. Software

Data collection was made in automatic mode by the NR800 analyser software every 10 min. Download and storage of the acquired spectra were made by Yokogawa's SPECTLAND2 software through ethernet communication to a separate process PC for calibration development or for trending of predicted parameters. Data handling and analysis, partial least squares regression, genetic algorithms (GA), and interval PLS (iPLS) were performed by MATLAB v6.5 (Mathworks Inc., USA) and PLS toolbox v.3 from Eigenvector Inc. (USA). All final models were transferred to NR800 after being reproduced in and exported through Unscrambler v.9.1.2.a (Camo) to the analyser memory.

3. Multivariate modelling

3.1. Data pre-treatment

Slight differences in bioreactor design (e.g., sparger and baffles size and/or orientation, design and/or number of turbines, etc.) affect the spectra through changes in physic-chemical properties of cultivation media. As the biomass grows, not only it changes the chemical composition of the matrix but it also affects physical properties like colour, density and viscosity of the cultivation media. The same type of spectral changes is observed along a batch during cultivation time (Fig. 1). The most evident changes are the baseline shifts that are related to changes in physical properties (particulate matter, air bubbles) originating light scattering. Aeration, stirring speed, temperature, pH, and feeding flows also cause smaller alterations in the spectra.

There are several spectral pre-processing algorithms which one can use to remove disturbances or to enhance their information content (e.g., the signal to noise ratio or the selectivity of some of its features for chemical or physical sample attributes). For convenience we can classify the algorithms into scaling, filtering, baseline correction and derivatives [9]. Since each

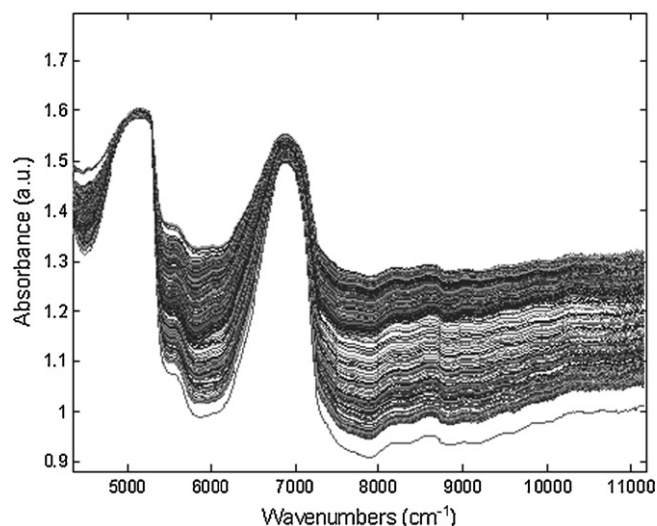


Fig. 1. Evolution of the transfection spectra collected throughout an industrial fermentation batch.

algorithm has some parameters that can be adjusted, and since several of them can be applied to the same data set in consecutive order, there are many possible combinations of the above algorithms and their tuning parameters. Some of these combinations normally lead to comparable results while others consistently under-perform.

In this study all spectra were mean centred, and several combinations of methods of each of the above categories were tested for each property to be calibrated. The best results were consistently obtained with standard normal variate scaling (SNV) and Savitsky–Golay (SG) 1st derivative. The application of SNV corrects the multiplicative interferences effects of light scatter, while SG filtering followed by a 1st derivative removes baseline shifts and enhances the main features in the spectra. With SNV method the scattering is removed by normalizing each spectrum by the standard deviation of the responses across the entire spectral range, like auto-scaling the transposed spectrum.

3.2. Wavenumber selection

After pre-processing, it is important to remove non-significant wavenumbers (non-informative spectral ranges) in order to achieve better, more stable and robust models. Different approaches were tested in this study for wavenumber selection such as univariate correlation, iPLS [10] and GAs [11].

3.3. Data set and PLS models

Six batches (pilot and industrial) were monitored in situ and data were used as calibration set. The models were validated using an independent test set from two production scale batches.

The calibration models were built by leave-one-out cross-validation and their predictive ability was assessed in terms of the root mean squared error of prediction first for samples set aside during cross-validation (RMSECV) and then for external validation batches (RMSEP) by comparing predictions with reference values

$$\text{RMSEP} = \sqrt{\frac{\sum_{i=1}^{n_p} (Y_{i(\text{pred})} - Y_{i(\text{ref})})^2}{n_p}} \quad (1)$$

where n_p denotes the size of the validation set, and $Y_{i(\text{pred})}$ and $Y_{i(\text{ref})}$ are the predicted and reference values for sample i , respectively.

4. Results and discussion

The predominant changes in the spectra collected along a batch are baseline shifts related to scattering due to an increasing cell population along the cultivation (see Fig. 1). Therefore, pre-processing is essential to enhance the chemical information present in the spectra and to remove the biomass effect. Using principal component analysis (PCA) on spectra collected during the six calibration batches, after pre-processing with SNV, relevant differences were found between pilot and production scales (Fig. 2). In particular, the batch-to-batch variability in the industrial runs (Fig. 2b) is higher because data was col-

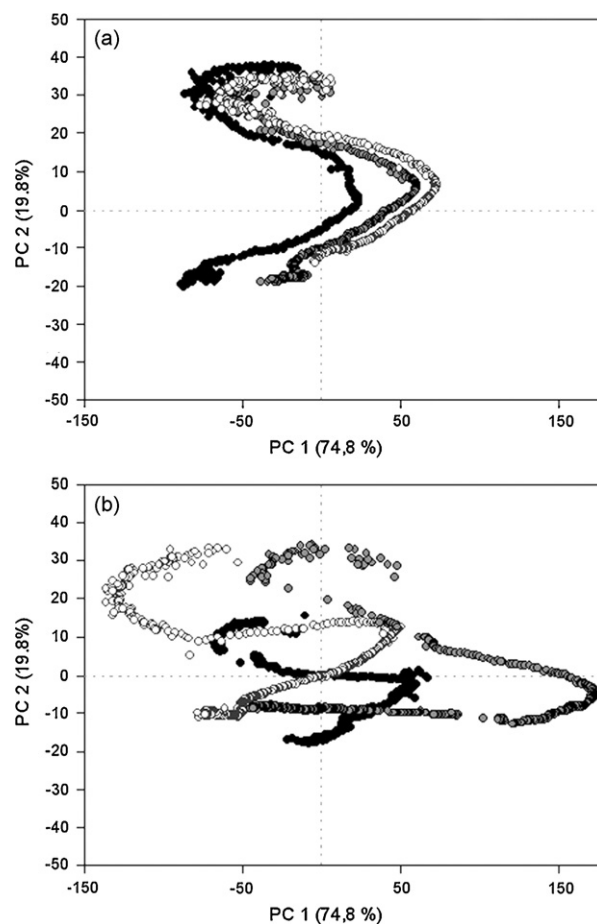


Fig. 2. PCA score plots from fermentation calibration batches. Each point represents a spectra and different colours stand for different batches.

lected from different scales. This clearly shows that scale must be included in model development as a source of variability, if a scale-independent calibration is to be used across different scales and different bioreactors of particular design characteristics.

4.1. PLS models development

In order to achieve the best prediction performance, several spectral pre-treatments were investigated followed by variable selection made by different methods. The best combination of methods is described in Table 1 for the API content prediction.

First, using the iPLS method, the spectral range was split into 20 intervals, PLS models were calculated for each interval and RMSECV calculated using up to 10 latent variables (LVs). This procedure was repeated for each spectral treatment (Fig. 3). The best RMSECV (0.08) was achieved applying SNV processing and using the entire variable range for a PLS model with 5 LVs. However, this accuracy in API content was not acceptable for process control purposes. As such, a wavenumber selection was made in the mean centred SNV pre-treated spectra using a GA that was performed with a PLS regression method. Details on the algorithm used can be found in Table 2. The maximum number of PLS factors was imposed regarding the number of factors (10) used on the iPLS method. Intervals of 10 variables were

Table 1
Figures of merit of the models built for API content prediction

Result no.	Pre-processing	Wavenumbers selection method	No. of wavenumbers	R^2	LVs	RMSECV
1	Autoscale	iPLS	92	0.723	6	0.13
2	1st derivative	iPLS	92	0.584	5	0.12
3	2nd derivative	iPLS	91	0.294	2	0.14
4	SNV	iPLS	1750	0.895	5	0.08
5	SNV	None	1750	0.909	5	0.07
6	SNV	GA	240	0.984	9	0.09
7	SNV	GA + uncertainty test	132	0.978	6	0.03

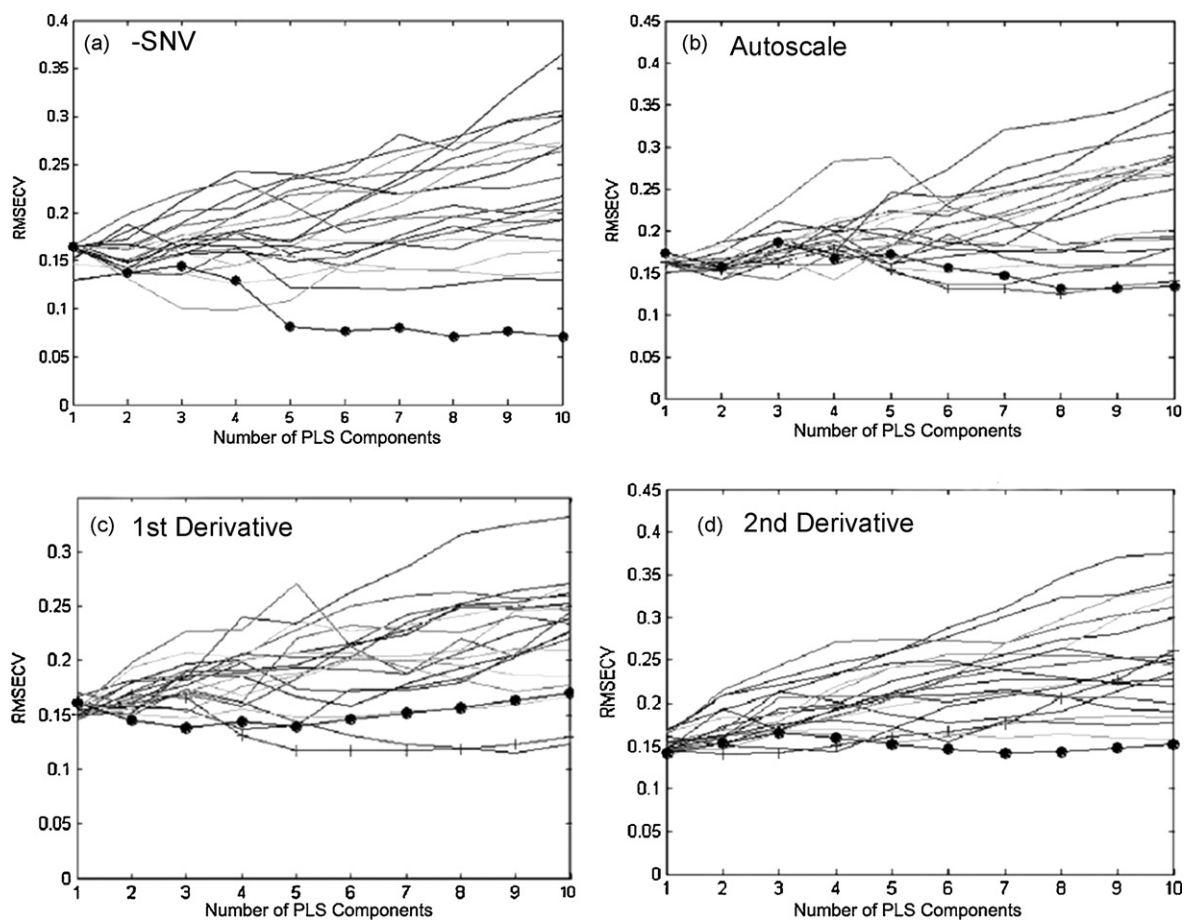


Fig. 3. Variable selection results with iPLS method for different pre-processing: (a) SNV; (b) autoscale; (c) 1st derivative; (d) 2nd derivative; each line represents the RMSECV of one spectral interval. Lines with black circular marks represent the global model built with all variables.

Table 2
Parameters used in the genetic algorithm's routine

Parameter	Value
Population size	64
Window width	10
Initial terms	30
Max. generations	100
Mutation rate	0.005
Crossover	Double
Regression	PLS
Max. LV	9
Cross-validation	Contiguous

selected rather than individual variables to prevent the selection of possible random correlated variables. The best model achieved an RMSECV of 0.09, which is similar to the reference method precision and therefore, considered acceptable. However, this model was built with 9 LVs, and there is a risk of data over-fitting, meaning therefore, that the relationship found between the data and the target values or dependent variables may not hold for subsequent predictions. To minimize the possibility of over-fitting, the variables (wavenumbers) were tested by an uncertainty test that makes a comparison between model leverages and prediction leverages in order to eliminate non-significant variables. With this procedure, a final model for API

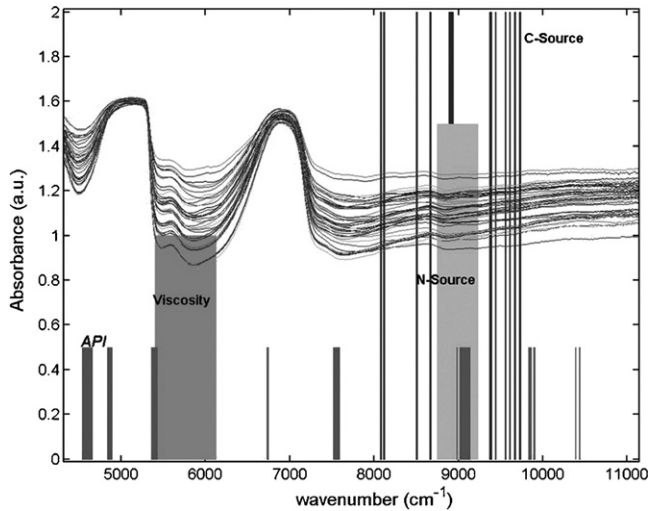


Fig. 4. Wavenumbers selected by genetic algorithm (grey areas) that were used for PLS models development. Each grey shade highlights the range used for each analyte.

content was built with 132 variables and 6 LVs with RMSECV of 0.03.

The variables selection strategy for other properties studied was identical to the one described for API model development. The different wavenumbers ranges used by the models of each property are identified in Fig. 4. The ranges used have a minimum overlap between them, which gives a good robustness indicator for the models.

The NIR calibration results for the prediction of viscosity, N-source and C-source are presented in Table 3. Viscosity is modelled best with just mean centred spectra without any further treatments, as the modelling captures baseline shifts related to biomass growth and the cultivation broth's physical changes.

For N-source and C-source compounds, a 1st Savitsky–Golay derivative was needed to enhance the chemical properties of the broth by reducing the global baseline variations. The model for N-source compound has a low correlation coefficient (0.716) when compared with the other ones. Still, regarding the narrow calibration range from 0.03 to 0.08%, the achieved RMSECV of 0.01% is the better one in absolute values. The C-source model has a RMSECV of 0.4% that represents a relative error of 13%.

4.2. Real time validation

The transflection probe was placed into a production plant bioreactor not used during the model development stage. The

Table 3
Calibration models details for the four analytes. All models built with mean centered data

Property	Calibration range	Pre-processing	R^2	RMSEP	LVs
API content	0.10–0.50%	SNV	0.978	0.03%	6
Viscosity	50–1500 cp	mncn	0.898	150	2
N-source	0.03–0.08%	1st derivative	0.716	0.01	1
C-source	0.7–3.6%	1st derivative	0.900	0.4%	1

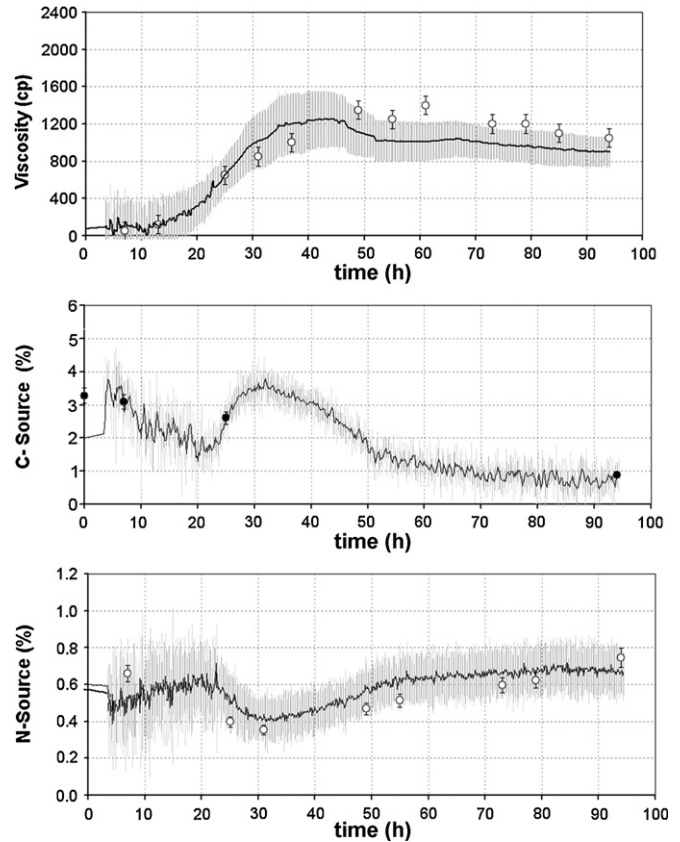


Fig. 5. Predicted profiles of a validation batch at production scale. In situ NIR predictions (lines); reference values (circles). Grey areas represent the confidence intervals for each prediction based on a 95% confidence interval.

predicted properties profiles simultaneously produced by each of the validated models are shown in Fig. 5 for C-source, N-source, and viscosity, as well as the corresponding analytical values obtained by standard reference methods. In Fig. 5 the grey areas represent the confidence intervals for each prediction, based on a 95% confidence interval around the predicted Y-value that is computed as a function of the sample's lever-

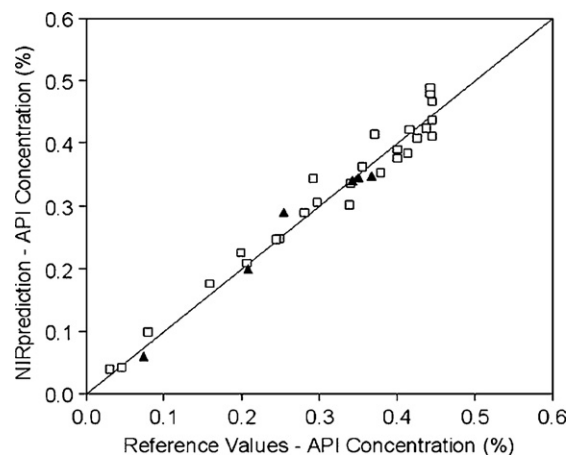


Fig. 6. API model cross-validation results for model development and prediction results for real time validation. NIR predicted values vs. reference values. (□) Cross-validation results, $y = 0.9947x + 0.0025$; RMSECV = 0.03; (▲) validation results, RMSEP = 0.03.

age and its X -residual variance [12]. The viscosity profile may be influenced by the differences between the fluid conditions inside and outside the bioreactor for the at-line reference analysis (aeration, temperature). Both N-source and C-source profiles are in good agreement with reference values and show variations that are not visible by the low frequency conventional sampling scheme.

The API profile is undisclosed as biosynthetic patterns would be revealed. However, real time prediction results can be seen in Fig. 6 where the reference values are plotted against the real time predicted values. The scale and specific reactor used did not affect the model's prediction performance.

5. Conclusion

The main objective of the present study was to develop a multi-parametric technique for process monitoring and supervision of several bioreactors of different scales and slightly different designs.

A NIR method was developed based on a transfection steam-sterilizable probe immersed into the fermentation cultivation media, to monitor key bioprocess analytes in real time. This fiber optics technique can be an alternative to other methods based on sample collection and off-line analysis. The measurements were made under real industrial conditions such as high temperatures, humidity, and floor vibrations.

Quantitative results obtained were considered satisfactory both for process understanding and process control, emphasizing that the models were valid when applied to variable matrices, scales, volumes, temperatures, aeration, and stirring conditions. This method enables to simultaneously monitor multiple fermentation reactors giving multi-parametric analyses of the fermentation media, with satisfactory accuracy.

The models built can be used both in pilot and production scale and as such are a valuable tool for process optimization at pilot scale and for variability control in industrial production.

Acknowledgments

The authors are grateful to CIPAN S.A. For the support and permission to publish the above results, and to the Portuguese Foundation for Science and Technology for the financial support to L.O. Rodrigues (grant no. BDE/15514/2004).

References

- [1] M. Scarff, S.A. Arnold, L.M. Harvey, B. McNeil, *Crit. Rev. Biotechnol.* 26 (2006) 17–39.
- [2] E.S. Bylinkina, *Chem. Petrol. Eng.* 20 (May (5)) (1984).
- [3] A.P. Ferreira, T.P. Alves, J.C. Menezes, *Biotechnol. Bioeng.* 91 (2005) 474–481.
- [4] S. Vaidyanathan, S.A. Arnold, L. Matheson, P. Mohan, G. Macaloney, B. McNeil, L.M. Harvey, *Biotechnol. Prog.* 16 (8) (2000) 1098–1105.
- [5] S. Vaidyanathan, S.A. Arnold, L. Matheson, P. Mohan, B. McNeil, L.M. Harvey, *Biotechnol. Bioeng.* 74 (5) (2001) 376–388.
- [6] S.A. Arnold, J. Crowley, S. Vaidyanathan, L. Matheson, P. Mohan, J.W. Hall, L.M. Harvey, B. McNeil, *Enzyme Microb. Technol.* 27 (2000) 691–697.
- [7] S.A. Arnold, L. Matheson, L.M. Harvey, B. McNeil, *Biotechnol. Lett.* 23 (2001) 143–147.
- [8] I.K. Brookes, B.N. Gedge, S.V. Hammond, in: Davies, Williams (Eds.), *Near Infrared Spectroscopy: The Future Waves*, NIR Publications, Chichester, UK, 1996, pp. 259–267.
- [9] T. Næs, T. Isaksson, T. Fearn, T. Davies, *A User Friendly Guide to Multivariate Calibration and Classification*, NIR Publications, 2002.
- [10] L. Nørgaard, A. Saudland, J. Wagner, J.P. Nielsen, L. Munck, S.B. Engelsen, *Appl. Spectrosc.* 54 (2000) 413–419.
- [11] R. Leardi, R. Boggia, M. Terrile, *J. Chemometr.* 6 (5) (1992) 267–281.
- [12] S. De Vries, J.F. Ter Braak Cajo, *Chem. Intell. Lab. Syst.* 30 (1993) 239–245.

Ultrasound-assisted dynamic extraction of valuable compounds from aromatic plants and flowers as compared with steam distillation and superheated liquid extraction

Jannat M. Roldán-Gutiérrez, J. Ruiz-Jiménez, M.D. Luque de Castro*

Department of Analytical Chemistry, University of Córdoba, Campus of Rabanales Annex C-3, 14071 Córdoba, Spain

Received 10 September 2007; received in revised form 15 January 2008; accepted 24 January 2008

Available online 6 February 2008

Abstract

A method for the extraction of valuable compounds from plants and flowers (*viz.* laurel, rosemary, thyme, oregano and tuberose) is proposed. The dynamic approach allows go-and-backward circulation of the extractant (ethanol) through the solid sample subjected to the action of an ultrasound probe (thus reducing sample amount and avoiding overpressure). A multivariate optimisation study and application of the optimum values of the variables to kinetics studies show that 10 min is sufficient to obtain extraction efficiencies that greatly surpass those provided by steam distillation for essential oils or superheated liquid extraction for these oils and other valuable compounds, with lower costs and higher quality of the extract. The extraction time of the proposed method is 176–165 min shorter than steam distillation and 31–20 min shorter than superheated liquid extraction, depending on the target compound.

© 2008 Elsevier B.V. All rights reserved.

Keywords: Solid–liquid extraction; Ultrasound; Steam distillation; Superheated liquid extraction; Laurel; Rosemary; Thyme; Oregano; Tuberose; Aromatic plants; Ultrasound-assisted extraction; Dynamic extraction; HPLC–MS identification; GC–MS

1. Introduction

Essential oils are aromatic substances widely used in the perfume industry, pharmaceutical sector, food and human nutrition field. They are mixtures of volatile compounds mainly constituted by monoterpenes and sesquiterpenes and their oxygenated derivatives, together with aliphatic aldehydes, alcohols and esters—90–95% of the whole oil. A large percentage of the volatile fraction is composed by terpenes, which make little contribution to the flavour or fragrance of the oil, and are decomposed by heat, light and oxygen – owing to their unsaturated groups – to produce undesirable compounds which can give off-flavour and off-aromas. The oxygenated fraction is highly odoriferous and mainly responsible for the characteristic flavour [1].

Conventional methods for essential oils isolation are hydrodistillation or steam distillation. In the former the plant material is inserted into water, subjected to heating and the

vapor, which contains the volatile compounds, is passed through a cooler for condensation with subsequent collection. In steam distillation a steam from boiling water is passed through the raw material for times ranging between 60 min and several hours, which drives out most of its volatile fragrant compounds. The condensate, which contains both water and the aromatics, is settled in a flask. Steam distillation is commonly used for fresh plant materials such as flowers, leaves, and stems. Essential oils from citrus used in the food and perfume industries are commonly isolated by cold pressing, in which a pressure is applied to the sample in contact with the solvent without increasing the temperature. Conventional methods based on solid–liquid extraction [1–3] provide extracts containing the volatile fraction together with a non-volatile fraction, the nature of which strongly depends on the method used. In this case the raw material is plunged in a solvent able to dissolve the target compounds and then agitated to favour mass transfer. Solvents for this maceration/solvent extraction process include hexane, dimethyl ether, methanol and ethanol [4–7].

All conventional methods to isolate valuable compounds from aromatic plants have important drawbacks, such as low yields, formation of by-products – owing to degradation of

* Corresponding author. Tel.: +34 957 218615; fax: +34 957 218615.
E-mail address: qa1lucam@uco.es (M.D. Luque de Castro).

thermally unstable and unsaturated compounds by temperature or hydrolytic effects, respectively – large extraction times and the presence of the extractant, usually a toxic organic solvent [4–6]. These drawbacks have led to searching for alternative extraction techniques. Supercritical fluid extraction (SFE) – particularly with CO₂ as extractant – has recognised advantages [8–11] over other extraction techniques such as the possibility to work at relatively low temperatures and its non-toxic character and chemical inertness [12], which makes SFE an excellent choice for the isolation of valuable compounds from aromatic plants [13–15], despite the drawbacks linked to the use of CO₂-SFE as are the necessity of high purity CO₂ – owing to contamination of the extracted species with CO₂ impurities – the exclusive affinity of the supercritical CO₂ to low-polar and non-polar compounds in the sample and the relatively high acquisition cost [1]. Microwave-assisted extraction (MAE) and superheated liquid extraction (SLE) are relatively recent alternatives for the isolation of valuable compounds from aromatic plants. Their yields are better than those provided by conventional methods but they also have the shortcoming of sample subjection to high temperatures with formation of undesirable compounds and frequent use of toxic organic solvents [1].

Ultrasound-assisted extraction (USAE) is a more recent approach to obtain valuable compounds from plants [16], which circumvents some of the drawbacks of conventional techniques, such as losses and degradation of volatile and thermolabile compounds, thanks to its working temperatures, most times at (or close to) ambient conditions. In many situations, USAE is faster and more efficient than conventional extraction and provides high efficiencies with modest consumption of extractant, which does not require to be polar as is the case with MAE. The main advantages of USAE *versus* other techniques – such as MAE, SLE and SFE – are lower costs, thanks to the simplicity of the equipment needed, and the similar or better yields obtained most times [17]. The main shortcoming of USAE is potential formation of free radicals during sonolysis of the solvent, which can produce degradation of some labile compounds by oxidation [18].

The aim of this research was to develop a rapid, efficient and inexpensive method for the extraction of valuable compounds from aromatic plants and flowers. The extract thus obtained was subject to liquid–liquid extraction coupled to either gas chromatography–flame ionization detection (GC–FID) or gas chromatography–mass spectrometry (GC–MS) for detection and identification of the extracted compounds, respectively.

2. Experimental

2.1. Instruments and apparatus

Ultrasound-assisted extraction was performed using an extractor consisting of a stainless steel cylindrical extraction chamber (100 mm × 10 mm i.d.) that is closed with screw-caps at either end and permits the circulation of the leaching fluid through it. The screw-caps also contained cotton filters to ensure that the sample remained in the extraction chamber. A four-

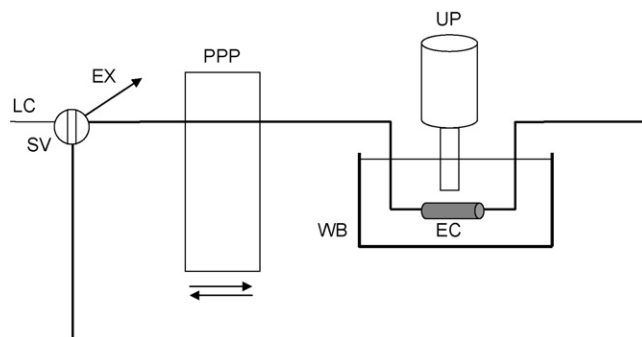


Fig. 1. Experimental set-up for the dynamic ultrasound-assisted extraction of essential oils from aromatic plants and flowers. LC, leaching carrier; EX, extract; SV, switching valve; PPP, programmable peristaltic pump; UP, ultrasonic probe; EC, extraction chamber; WB, thermostatic water bath.

channel Gilson Minipuls-3 low-pressure peristaltic pump, PTFE tubing of 0.8 mm i.d. and an injection valve – acting as a selection valve – were used to build the flow manifold shown in Fig. 1. The peristaltic pump was programmed for changing the rotation direction at preset intervals and three glass balls were placed with the sample in the extraction chamber, thus avoiding increased sample compactness and increased pressure in the dynamic system as a result.

Ultrasonic irradiation was applied by means of a Branson 450 digital sonifier (20 kHz, 450 W) equipped with a cylindrical titanium alloy probe (12.70 mm in diameter) and immersed into a water bath in which the extraction chamber was placed.

A simple laboratory Quickfit apparatus consisting of a 2000-ml steam generator flask, a condenser and a receiving vessel was used to perform steam distillation.

Superheated water extraction (SWE) was performed using the assembly described by Fernández-Pérez et al. [4].

Identification of the compounds in the extracts was performed by using a Varian CP 3800 gas chromatograph coupled to a Saturn 2200 ion trap mass spectrometer (Sugar Land, TX, USA) and a Varian (Palo Alto, CA, USA) Star 3400 gas chromatograph was used for optimisation and quantification. Both chromatographs were equipped with Factor Four Capillary columns (VF-5ms 30 m × 0.25 mm) i.d. DF = 0.25).

2.2. Reagents and samples

Ethanol and hexane of HPLC-grade were both from Scharlau (Barcelona, Spain). Eighteen microohms deionised water from a Millipore Milli-Q water purification system was used to prepare the water–ethanol extractant mixtures. A stock standard of 6600 µg/ml of nonane (Sigma, St. Louis, MO, USA) was prepared in HPLC-grade hexane and used as internal standard. Anhydrous Na₂SO₄ from Merck (Darmstadt, Germany) was used as drying agent in the liquid–liquid extraction step.

Leaves of laurel (*Laurus nobilis* L.), rosemary (*Rosmarinus officinalis* L.), thyme (*Thymus vulgaris* L.) and oregano (*Oreganum majorana*) were collected in the South of Spain (Montilla, Córdoba). Tuberoses were from a local flower shop.

2.3. Sample preparation

Leaves were collected from five different plants and, in each case, mixed, dried in an oven at 40 °C for 24 h, milled and kept at 4 °C in dark until use. Flower samples (tuberose) were not dried to protect labile compounds and could not be milled at the same size as the other samples owing to formation of a paste which blocked the extraction chamber.

2.4. Extraction procedures

2.4.1. Ultrasound-assisted extraction

One gram of milled leaves was placed in the extraction chamber, which was assembled to the dynamic system, as shown in Fig. 1, and filled with the extractant (ethanol) propelled by the peristaltic pump with the extraction chamber immersed into a water bath at 25 °C. The extractant was then circulated through the solid sample for a 10-min preset time under ultrasonic irradiation (duty cycle 0.3 s, output amplitude 10% of the converter, applied power 450 W with the probe placed at the minimal distance to the top surface of the extraction cell, but without contacting it). During extraction the direction of the leaching carrier (at a flow-rate of 4 ml min⁻¹) was changed each 120 s, thus minimising increased compactness of the sample in the extraction cell that could cause overpressure in the system.

2.4.2. Steam distillation

The steam generator flask was filled with Milli-Q purified water and heated with a heating mantle. As the water vaporised, the steam passed to the distillation flask containing 3.0 g of plant and, then, through the cooled tube where it was condensed. The distillate (520 ml) was collected in the receiving flask after 3 h distillation.

2.4.3. Superheated water extraction

The cell was filled with 3.0 g of leaves and glass-wool plugs were inserted at both ends of the cell to prevent the frit from being plugged. After assembling the extraction cell to the dynamic manifold, locating the cell in the oven and filling the cell with the extractant (water), the oven was brought up to the working temperature (150 °C) and pressurised with ~10 bar by the pump; then, the pump was stopped and static extraction was developed for 15 min, after which, the outlet valve was opened and the extract, pumped at a flow-rate of 2 ml min⁻¹, was collected in a vial [19].

2.5. Extract preparation–individual separation–detection

After USAE, the extract was subject to liquid–liquid extraction using a small hexane volume for preconcentration and solvent exchange for subsequent insertion into the gas chromatograph. The variables affecting this step – *i.e.* volume of extractant and number of extraction cycles – had been studied in previous research so, 1 ml of hexane and only one extraction cycle were used [20–21]. Six μ l nonane stock standard solution was added to the extract before liquid–liquid extraction. The USAE extract containing the nonane standard solution was put

into contact with 1 ml hexane, shaken for 5 min and centrifuged; then, the ethanolic phase was removed and Na₂SO₄ was added to the organic phase as drying agent to eliminate water traces. The higher volume of the steam distillation extract made necessary 25 ml hexane and 150 μ l nonane stock standard for the liquid–liquid extraction step.

Aliquots – 1 μ l – of the hexane phase were injected into a Factor Four Capillary Column (VF-5ms 30 m \times 0.25 mm, i.d. DF=0.25). The carrier gas (helium) was delivered into the column head at a constant pressure of 20 psi. The temperature of the FID was 300 °C and the oven temperature 40 °C for 2 min, then increased to 250 °C at 4 °C min⁻¹. The chromatograph worked in the splitless mode and the analysis took 69 min.

Identification of the different volatile components in the extract was obtained by injecting 1 μ l hexane extract into the GC column and using a Saturn 2200 ion trap mass spectrometer as detector. The chromatographic conditions were as in GC–FID.

3. Results and discussion

The main objectives of the research were identification of the compounds extracted from the different raw materials and comparison of the performance of the different extraction approaches. A mass-spectrometry library was used instead of individual standards for the identification of the different compounds. The criteria used to assign a proposed compound as a component of the essential oil were similar to those used in previous publications [4,9,10]: the Fit, RFit and average values should be higher than 950. For the comparison of the different extraction approaches a nonane stock standard solution was added to the sample and the ratio between the areas obtained by the target analytes and that provided by nonane, which is not present in the extracts, was used as response variable. The nonane solution was also used for correction of the effect of differences in the amounts of sample used in the different extraction methods.

3.1. Optimisation of the extraction variables

The aromatic plant selected for the optimisation study was laurel; then, the optimal working conditions were applied to the extraction of valuable compounds from other plants and their similar behaviour checked. The response variable for the optimisation of the extraction procedure was the ratio between the area obtained by the nonane standard solution and those provided by the target compounds. An increase of this ratio can be related to an enhancement of the extraction efficiency; a decreased value should be associated to degradation.

Eight variables were considered for multivariate *optimisation of the extraction step* in the dynamic manifold, namely: the probe position, percent of ultrasound exposure duty cycle, ultrasound radiation amplitude, irradiation time, water bath temperature, extractant flow-rate, extractant composition and volume of the dynamic system (extractant volume). A Plackett–Burman design type III resolution allowing three degrees of freedom and involving 12 randomised runs plus three centre points was built for a

Table 1
Optimisation of the ultrasound-assisted extraction of valuable compounds from laurel

Variable	Tested range		Optimum value
	First design	Second design	
Radiation amplitude (%)	10–50	10	10
Duty cycle (%)	30–70	30	30
Irradiation time (min)	1–5	5–10	10
Extractant flow-rate (ml min ⁻¹)	1–4	4	4
Ethanol (%)	25–75	50–100	100
Probe position (cm)	0.1–4	0.1	0.1
Temperature (°C)	25–40	25	25
Extractant volume (ml)	8.5–10	8.5	8.5

screening study of these eight factors. The upper and lower values of each variable were selected from a preliminary study. The tested and the optimum values obtained for each variable are shown in Table 1. The results of this screening study, which are shown in Fig. 2A, were that the probe position, percent of ultrasound exposure duty cycle, ultrasound radiation amplitude, extractant flow-rate, volume of the dynamic system and bath temperature were not statistically significant factors within the ranges of the study; however, the results showed higher extraction efficiencies with the upper values of extractant flow-rate and probe position and the lower values of the other four variables;

thus, 10% radiation amplitude, 25% of duty cycle, 4 ml min⁻¹, 0.1 cm position probe, 8.5 ml volume of the dynamic system and 25 °C water bath temperature were selected for subsequent experiments. The extractant composition and irradiation time were the variables statistically significant, and gave better global extraction efficiencies with the highest values used in this study; so higher concentrations of ethanol in the extractant and longer irradiation times were tested in a multivariate study. The results of this study, as can be seen in Fig. 2B, show that both variables were statistically significant and gave higher extraction efficiencies with the upper values; so, the extractant composition was fixed at 100% ethanol and a kinetics study, discussed later, was made to optimise the irradiation time.

The optimisation of the *chromatographic separation–detection step* was performed in a previous study [21] where the variables of the chromatographic system – split ratio, flow-rate of the carrier gas and temperature program – were studied. The optimum values were checked for application in the present method.

3.2. Evaluation of the precision of the USAE–GC method

In order to know the precision of the proposed method, within-laboratory reproducibility and repeatability studies were evaluated in a single experimental set-up with duplicates [22]. The experiments were carried out using 1 g of milled laurel leaves and the optimum working conditions. Two measurements per day were made in 7 days. The repeatability, expressed as relative standard deviation, was from 2.93 to 7.58%; meanwhile within-laboratory reproducibility ranged from 5.99 to 10.45%, as listed in Table 2.

3.3. Scope of USAE: kinetics studies

To assess the scope of the ultrasound-assisted method to extract valuable compounds from plants, it was applied to other plants such as rosemary, thyme, oregano and flowers such as tuberose. Kinetics studies of the extraction were aimed at both to obtain the optimum irradiation time for maximum or complete extraction from each sample and know if degradation of some compounds takes place under ultrasound action. The behaviour of the target analytes is quite different; thus, maximum extraction of phellandrene, terpinene, pinene and linalyl acetate is obtained after ultrasound irradiation for 2 min, and their concentrations in the extract remain constant for longer irradiation times; all the others are extracted within 8 min US-irradiation, except elemicin and isoelemicin, which require 10 min, and eucalyptol and linalool, which behave as shown in Fig. 3 (*viz.* maximum extraction for 10 min, after which the concentration in the extract declines, probably as a consequence of degradation at longer irradiation times). The behaviour of the aromatic compounds was independent of the plant material. In the case of tuberose, an extraction time of 4 min was optimum; longer times result in significant degradation.

The results provided by the USAE method for extraction of the valuable compounds in the raw materials were compared

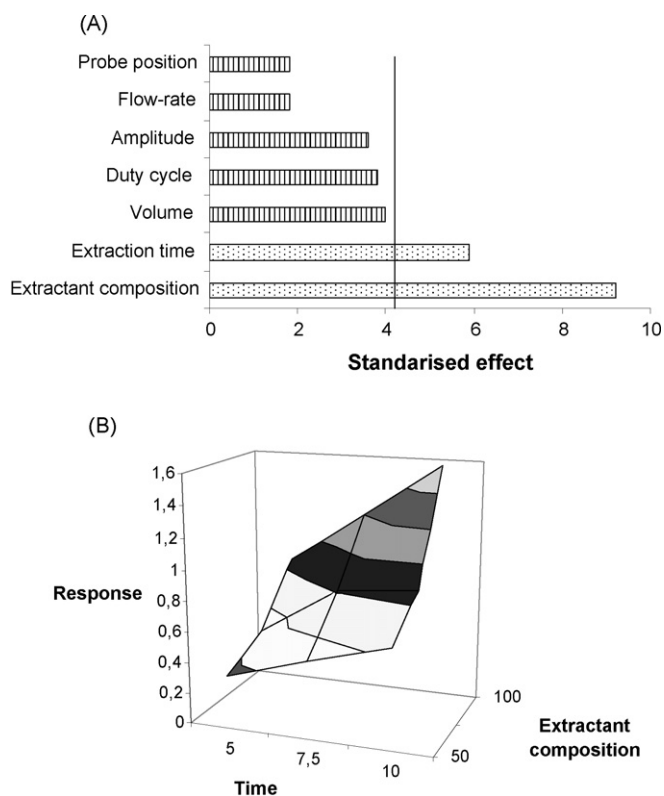


Fig. 2. Results obtained by the optimisation of the extraction variables for phellandrene (similar results were obtained for the rest of the compounds). (A) Plackett Burman design. (B) Second multivariate design.

Table 2

Results obtained from the evaluation of the precision of the proposed USAE method in terms of repeatability relative standard deviation (s_r) and within-laboratory reproducibility relative standard deviation (s_{WR}) for each analyte (traditional nomenclature in brackets)

Compound	s_r (%)	s_{WR} (%)
5-Isopropyl-2-methyl-1,3-cyclohexadiene (Phellandrene)	5.29	9.50
1-Isopropyl-4-methyl-1,3-cyclohexadiene (Terpinene)	4.77	6.20
2,6,6-Trimethylbicyclo[3.1.1]hept-2-ene (Pinene)	7.31	10.46
3,7-Dimethyl-1,6-octadien-3-yl acetate (Linalyl acetate)	5.47	6.34
4-Isopropenyl-1-methyl-1-cyclohexene (Limonene)	4.10	6.68
1,3,3-Trimethyl-2-oxabicyclo[2.2.2]octane (Eucalyptol)	4.81	6.33
3,7-Dimethyl-1,6-octadien-3-ol (Linalool)	4.74	9.40
1,7,7-Trimethylbicyclo[2.2.1]heptan-2-ol (Borneol)	6.58	9.05
<i>p</i> -Menthane-1,2-diyl diacetate (Terpin diacetate)	6.02	6.95
1-Isopropyl-4-methyl-3-cyclohexen-1-ol (Terpinen-4-ol)	4.18	7.42
2-(4-Methyl-3-cyclohexenyl)isopropanol (Terpineol)	5.14	7.40
2-(4-Methyl-3-cyclohexenyl)isopropyl acetate (Terpinyl acetate)	7.59	9.05
2-Methoxy-4-propenylphenol (Isoeugenol)	6.35	9.45
4-Allyl-1,2-dimethoxybenzene (Methyleugenol)	4.90	9.21
2-Methoxy-4-(2-propenyl)phenol (Eugenol)	4.35	8.55
3,4,5-Trimethoxyallylbenzene (Elemicin)	5.79	6.43
1,2,3-Trimethoxy-allylbenzene (Isoelemicin)	2.93	6.00

with those obtained by steam distillation for 3 h, which are usually taken as complete extraction of essential oils. Table 3 shows that the amounts of the oils obtained by USAE are similar to (higher or much higher than) those from steam distillation, which point out either an incomplete extraction or loss of these volatile analytes occurring by application of the latter method. Also SWE provides poorer results than the proposed method, as can be seen in Table 3, where the results were provided by extracts obtained under the optimum SWE working conditions found in the literature [19,20] for all plants but not for tuberose, which was completely degraded (the peaks of the target compounds disappear in the chromatogram of the extracts obtained by SWE for 5 min). As shown in the table, most of the extracted compounds

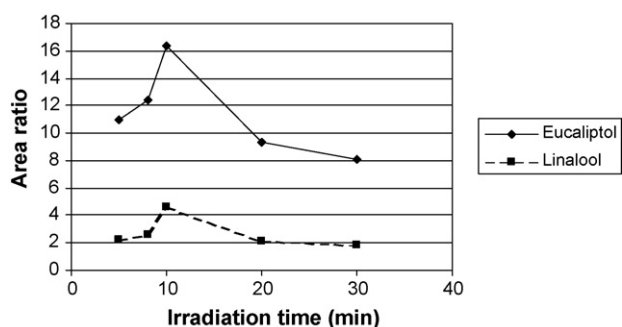


Fig. 3. Effect of the irradiation time on the main components of essential oil from laurel.

Table 3

Comparison of target compound-internal standard peak area ratio of extracts obtained by steam distillation, SWE and USAE under the optimum working conditions for each type of sample

Compound	USAE	Steam distillation	SWE
Laurel			
α -Phellandrene	1.57	0.00	0.43
α -Terpinene	4.35	0.00	0.57
α -Pinene	1.71	0.00	0.41
Linalyl acetate	0.46	0.00	0.12
Limonene	0.09	0.00	0.25
Eucalyptol	16.32	0.22	5.21
Linalool	4.63	0.19	6.91
Borneol	0.12	0.01	0.14
Terpin diacetate	0.05	0.00	0.06
Terpinen-4-ol	0.95	0.04	1.02
α -Terpineol	1.16	0.08	1.34
Terpinenyl acetate	9.37	0.04	1.63
Isoeugenol	0.92	0.20	0.97
Methyleugenol	2.03	0.40	1.60
Eugenol	0.14	0.03	0.04
Elemicin	0.26	0.02	0.03
Isoelemicin	0.51	0.04	0.01
Rosemary			
α -Pinene	4.72	0.00	1.29
Camphene	1.26	0.00	0.31
α -Terpinene	0.29	0.00	0.30
Cymene	0.95	0.00	0.30
Terpinolene	9.56	0.57	3.05
Linalool	0.49	0.00	0.58
Camphor	1.66	0.26	1.78
Borneol	3.56	1.27	4.69
Terpinen-4-ol	3.59	0.00	4.61
α -Terpineol	0.58	0.08	1.40
Verbenone	6.25	1.88	4.81
Carvacrol	2.70	0.41	3.93
Thymol	0.90	0.00	0.71
Thyme			
α -Phellandrene	0.12	0.00	0.00
α -Pinene	1.30	0.00	0.36
Camphene	0.26	0.00	0.06
β -Pinene	0.44	0.00	0.11
α -Terpinene	0.12	0.00	0.18
Cymene	5.17	0.05	1.65
Eucalyptol	0.96	0.00	1.29
Camphor	1.27	0.04	1.59
Borneol	1.33	0.07	1.47
Terpinen-4-ol	1.11	0.00	1.34
α -Terpineol	0.07	0.00	0.09
Verbenone	1.16	0.00	0.46
Thymol	3.47	0.00	0.28
Oregano			
α -Phellandrene	1.84	0.00	0.50
α -Pinene	2.01	0.00	0.49
β -Phellandrene	1.07	0.00	0.14
β -Pinene	1.13	0.00	0.27
Cymene	9.73	0.20	2.52
Limonene	1.70	0.00	1.90
Sabinene	1.71	0.00	1.94
Eucalyptol	2.18	0.00	0.70
Carene	0.06	0.00	0.00
Terpinolene	0.53	0.49	0.00
α -Terpineol	0.78	0.15	0.00
Thymol	0.80	0.00	0.00
Carvacrol	0.82	0.07	0.00
Tuberose			
Linalool	0.01	0.01	
Camphor	0.02	0.02	
Borneol	0.14	0.12	
Terpinen-4-ol	0.14	0.13	
α -Terpineol	0.08	0.07	
Verbenone	0.20	0.14	
Carvacrol	2.64	2.28	
Thymol	6.76	6.52	

are more concentrated in the extracts obtained by USAE. A very significant degradation of these compounds was observed when the SWE time increased from the optimum value of 30–40 min (as observed by decrease of the peaks in the chromatograms from the corresponding extracts).

3.4. Comparison of methods

The proposed USAE method was compared with other alternatives such as steam distillation and SWE in terms of cost, rapidity, quality of the extract and efficiency for the samples under study, shown in Table 3. For aromatic plants, USAE was compared with steam distillation and SWE, but in the case of tuberoso samples, USAE was only compared with steam distillation owing to inability of SWE to extract the target compounds in this matrix without degradation.

3.4.1. Costs

The extraction costs of the proposed method are clearly advantageous. The energy cost required for water evaporation in steam distillation, and for reaching superheated conditions (>5 bar and 150 °C) surpassed that required in USAE. Also, the volume of extract is lower in USAE. These aspects are of paramount importance for potential future implementation of the method at an industrial scale.

3.4.2. Rapidity

USAE requires a total extraction time between 4 and 10 min. The time required for steam distillation was 3 h, and 35 min was needed for SWE; thus, the extraction time for the proposed method is from 176 to 165 min shorter than for steam distillation – from 45 to 12 times faster – and from 31 to 20 min shorter than SWE – from 9 to 2 times faster.

3.4.3. Efficiency

The proposed method provides richer and more concentrated extracts than steam distillation for all the samples and compounds, more than SWE for the more oxygenated fraction and similar to it for terpenes and other less volatile compounds. This assertion can be inferred by comparison of the peak area ratio obtained from the methods under optimum conditions, as shown in Table 3.

3.4.4. Quality of the extracts

The amount of very volatile compounds – usually oxygenated compounds – constitutes a measure of extract quality as these compounds are more valuable than the less volatile fraction. The extract obtained by USAE contains higher amounts of more volatile compounds—which appear at shorter retention times in the chromatogram; therefore, this extract possesses an aroma more similar to the natural aroma of laurel, rosemary, thyme or oregano.

4. Conclusions

The proposed USAE – combined with GC–FID and GC–MS for the determination and identification, respectively, of the com-

pounds of interest – is faster than steam distillation or SWE – 18 and 2.5 times faster, respectively – and allows substantial savings of both energy and investment cost.

USAE is more effective than steam distillation and SWE and gives extracts more valuable than those provided by other well established extraction alternatives thanks to the more efficient extraction of the most volatile fraction, which gives rise to an aroma more similar to the natural aroma of the target plants. Furthermore, the use of ethanol as extractant facilitates industrial application for human uses thanks to its low toxicity.

The proposed USAE approach is a good alternative to conventional extraction techniques as it solves most of their drawbacks, namely: long extraction times, high energy and acquisition costs, low yields and presence of toxic organic extractant residues in the extracts. It can be used for the extraction of valuable compounds from a large number of aromatic plants which are widely used in food, pharmaceutical and cosmetic industries and also it proven to be effective for the extraction of valuable compounds from some flowers.

Acknowledgements

The Spanish Comisión Interministerial de Ciencia y Tecnología (CICYT) is gratefully acknowledged for financial support (Project No. CTQ2006-01614).

References

- [1] A. Basile, M.M. Jiménez-Carmona, A.A. Clifford, J. Agric. Food Chem. 46 (1998) 5205.
- [2] J.C. Chalchat, R.P. Garry, A. Michet, Flavour Frag. J. 6 (1991) 189.
- [3] H.L. De-Pooter, E.A. Aboutabl, A.O. El-Shabrawy, Flavour Frag. J. 10 (1995) 63.
- [4] V. Fernández-Pérez, M.M. Jiménez-Carmona, M.D. Luque de Castro, Analyst 125 (2000) 481.
- [5] M.D. Guillén, N. Cabo, J. Burillo, J. Sci. Food Agric. 70 (1996) 359.
- [6] S.B. Hawthorne, M.S. Krieger, D.J. Miller, Anal. Chem. 60 (1998) 472.
- [7] www.essentialoils.co.za/extraction-methods.htm.
- [8] S.B. Hawthorne, M.L. Riekkola, K. Serenius, Y. Holm, R. Hiltunen, K. Hartonen, J. Chromatogr. 634 (1993) 297.
- [9] M.M. Jiménez-Carmona, M.D. Luque de Castro, Chromatographia 50 (1999) 578.
- [10] M.M. Jiménez-Carmona, J.L. Ubera, M.D. Luque de Castro, J. Chromatogr. A 885 (1999) 625.
- [11] M.D. Luque de Castro, M.M. Jiménez-Carmona, Trends Anal. Chem. 17 (1998) 441.
- [12] M.D. Luque de Castro, M.M. Jiménez-Carmona, V. Fernández-Pérez, Trends Anal. Chem. 18 (1999) 708.
- [13] M.D. Luque de Castro, F. Priego-Capote, Analytical Uses of Ultrasound, Elsevier, Amsterdam, 2006.
- [14] D.L. Massart, B.G.M. Vandeginste, L.M.C. Buydens, S. De Jong, P.J. Lewi, J. Smeyers-Verbeke, Handbook of Chemometrics and Qualimetrics, Part A, Elsevier, Amsterdam, 1997.
- [15] P. Pallado, G. Tassinato, M. D'Alpaos, P. Traldi, Rapid Commun. Mass Spectrom. 11 (1997) 1335.
- [16] R. Japón-Luján, J.M. Luque-Rodríguez, M.D. Luque de Castro, J. Chromatogr. A 1108 (2006) 76.
- [17] E. Reverchon, F. Senatore, J. Agric. Food Chem. 42 (1994) 154.
- [18] M.D. Luque de Castro, F. Priego-Capote, Analytical Applications of Ultrasound, Elsevier, Amsterdam, 2007.

- [19] M. Taverna, A.E. Baillet, D. Baylocq, *J. Assoc. Anal. Chem.* 73 (1990) 206.
- [20] M.T. Tena, P.J. Hidalgo, J.L. Ubera, M. Varcárcel, *Anal. Chem.* 69 (1997) 521.
- [21] R.K. Verma, G.C. Uniyal, M.M. Gupta, *Indian J. Pharm. Sci.* 52 (1990) 276.
- [22] H. Vuorela, Y. Holm, R. Hiltunen, T. Harvala, A. Laitinen, *Flavour Frag. J.* 5 (1990) 81.

Determination of trace amounts of vanadium by UV–vis spectrophotometric after separation and preconcentration with modified natural clinoptilolite as a new sorbent

Leila Rostampour*, Mohammad Ali Taher

Department of Chemistry, Shahid Bahonar University of Kerman, Kerman, Iran

Received 11 September 2007; received in revised form 15 January 2008; accepted 16 January 2008

Available online 2 February 2008

Abstract

Natural clinoptilolite was used as a sorbent material for solid phase extraction and preconcentration of vanadium. The clinoptilolite was first saturated with a cation such as nickel(II) and then modified with benzyldimethyltetradecyleammonium chloride (BDTA) for increasing sorption of 4-(2-pyridylazo)resorcinol (PAR). Vanadium–PAR complex was quantitatively retained on the sorbent by the column method at the pH range 6.2–7.0 at a flow rate of 1 mL min⁻¹. It was removed from the column with 5.0 mL of dimethylformamide solution at a flow rate of 0.8 mL min⁻¹ and determined by UV–vis spectrophotometry at $\lambda_{\text{max}} = 550$ nm. 0.031 μg of vanadium can be concentrated from 450 mL of aqueous sample (where detection limit as 0.07 ng mL⁻¹ with preconcentration factor of 90). Relative standard deviation for eight replicate determination of 5.0 μg of vanadium in final solution is 2.1%. The interference of number of anions and cations has been studied in detail to optimize the conditions and method was successfully applied for determination of all vanadium as V(IV) form in standard samples.

© 2008 Elsevier B.V. All rights reserved.

Keywords: Separation and preconcentration of vanadium; Natural zeolite; Clinoptilolite

1. Introduction

The determination of vanadium has received extensive attention because of its increasing importance in biological and environmental studies. This metal is widely distributed in the earth's crust but in low abundance and their presence in the atmosphere is mainly due to the combustion of fossil fuels, which have important vanadium contents [1]. Vanadium at trace amounts represents an essential element for normal cell growth, but can be toxic when present at higher concentration [2].

The content of vanadium in natural samples such as soils and plants is very low in the range of a few $\mu\text{g L}^{-1}$, hence powerful analytical methods are required. Several analytical techniques have been reported for the determination of vanadium, which includes voltammetry [3], atomic absorption spectrometry [4,5], spectrofluorimetry [6], atomic emission spectrometry [7], high performance liquid chromatography [8,9] and ion chromatogra-

phy inductively coupled plasma-optical emission spectrometry [10]. These techniques suffers from several disadvantages such as few techniques are expensive (ICP-OES), few other having poor sensitivity (AAS) and few others require specific electrodes (voltammetry) for the determination of vanadium. Spectrophotometry is a common technique used for the determination of vanadium owing to its simplicity and low-cost instrumentation. Most of the direct spectrophotometric methods for determination of vanadium in environmental samples lack the necessary sensitivity and/or selectivity without sample pretreatment [11]. Preconcentration/separation procedures based on sorption are considered to be superior to the liquid–liquid extraction due to their simplicity and ability to obtain high enrichment factors. Application of sorbents obtained by immobilization of chelating agents on solid supports has the advantage of controlling the capacity and selectivity of metal sorption by the appropriate choice of loading organic agents, thus controlling the efficiency of the process. Chelating resins [12–14], activated carbon [15] and various modified polymers [16–18] have been applied for the pretreatment of vanadium. Zeolites are naturally occurring hydrated aluminosilicate minerals, and belong to the class of

* Corresponding author.

E-mail address: eli_rostampour@yahoo.com (L. Rostampour).

minerals known as “tectosilicates”. Most common natural zeolites are formed by alternation of glass-rich volcanic rocks (tuff) with fresh or saline water in playa lakes or by seawater [19]. The structure of zeolites is formed by $[\text{SiO}_4]^{4-}$ and $[\text{AlO}_4]^{4-}$ tetrahedral units. An oxygen bridge joins Si and Al atoms. Neutralization of an overall negative surface charge requires counter ions (e.g., Na^+ , Ca^{2+} , K^+ and Mg^{2+}). Due to the charged nature of the framework and its ability to form Bronsted acid sites, zeolites are useful for many applications [20]. Natural zeolites have been intensively studied because of their applicability in removing trace quantities of heavy metal ions from aqueous solutions by utilizing the ion-exchange phenomenon [21–24]. Clinoptilolite is the most abundant natural zeolite and its typical unit cell formula is given either as $\text{Na}_6[(\text{AlO}_2)_6(\text{SiO}_2)_{30}] \cdot 24\text{H}_2\text{O}$ or $(\text{Na}_2, \text{K}_2, \text{Ca}, \text{Mg})_3[(\text{AlO}_2)_6(\text{SiO}_2)_{30}] \cdot 24\text{H}_2\text{O}$ [25,26]. The sorption on zeolitic particles is a complex process because of their porous structure, inner and outer charged surfaces, mineralogical, existence of crystal edges, broken bands and other imperfections of the surface [27]. The reason for selecting zeolite as an adsorbent is its relatively moderate surface area, high and selective ion-exchange capacity, low cost and relative simplicity of application and operation. It is believed that the ability of zeolite as an adsorbent for organic compounds and metal ions from adsorption of surfactants onto zeolites [28].

The aim of this research was to investigate analytical applicability of natural clinoptilolite zeolite as a new sorbent for preconcentration of vanadium traces. In this method vanadium(IV)–PAR complex was adsorbed onto modified clinoptilolite zeolite and then was recovered by 5.0 mL of dimethylformamide. After this steps vanadium was determined with UV–vis spectrophotometry. It was found that this method is simple, highly sensitive, fast and economical.

2. Experimental

2.1. Apparatus and reagents

Spectrophotometric vanadium determinations with PAR were performed by use of a single beam Varian Cary-50 UV–vis spectrophotometer equipped with 1.0 cm quartz cell. A metrohm 713 pH meter connected to a glass electrode was used for pH measurements. A funnel-tipped glass tube (100 mm \times 5 mm) was used as the column for preconcentration. All glassware and columns were washed with concentrated nitric acid before use. All reagents used were of analytical grade. Vanadium(IV) stock standard solution (100 $\mu\text{g mL}^{-1}$) was prepared by dissolving 0.5180 g of $\text{VOSO}_4 \cdot 5\text{H}_2\text{O}$ (Merck) in 5 mL of concentrated H_2SO_4 and dilution to 1000 mL with water in standard flask. Fresh working standard solutions of VO^{2+} were prepared daily by dilution of the stock solution. A solutions of 4-(2-pyridylazo) resorcinol (99%, Merck) $10^{-3} \text{ mol L}^{-1}$ was prepared by dissolution in distilled water. Benzyltrimethylammonium chloride (BDTA) solution (0.1 mol L^{-1}) was prepared by dissolving 20.6120 g of (98%, Merck) in 500 mL of distilled water. Phosphate buffer solution was prepared by dissolving 1.2 g of NaH_2PO_4 in 90 mL of distilled water and titration to pH 6.5 with NaOH solution. Make up

volume to 100 mL with distilled water. Nickel(II) standard solution (200 $\mu\text{g mL}^{-1}$) was prepared by dissolving 0.1021 g of nitrate nickel (Merck) in 100 mL of distilled water. Cadmium(II) standard solution (200 $\mu\text{g mL}^{-1}$) was prepared by dissolving 0.5544 g of nitrate cadmium (Merck) in 1000 mL of distilled water. Zinc(II) standard solution (200 $\mu\text{g mL}^{-1}$) was prepared by dissolving 0.6185 g of zinc nitrate (Merck) in 1000 mL of distilled water. Solution of alkali metal salts and various metal salts were used for studying of anionic and cationic interferences, respectively. Natural clinoptilolite zeolite was obtained from Semnan region in the centre of Iran.

2.2. Zeolite modification

The zeolite raw mineral was ground and sieved in order to obtain a sample with particle size class 0.110–0.125 mm. The ammonium form of clinoptilolite ($\text{NH}_4^+\text{-Z}$) was obtained from the zeolite by treatment with 1.0 mol L^{-1} ammonium nitrate solutions in solid/liquid ratio of 1 g/10 mL. This mixture was shaken mechanically for 72 h at room temperature. The NH_4NO_3 solution was replaced three times. After the shaking period, the solid was filtered and washed with distilled water, then was dried in an oven at 100 °C. In order to remove (evaporation) NH_3 and formation of H-form of clinoptilolite ($\text{H}^+\text{-Z}$), it was put in furnace at 380 °C for 2 h. This form of zeolite had much higher ion-exchange capacity than $\text{NH}_4^+\text{-Z}$.

Clinoptilolite was saturated with nickel (or cadmium or zinc) by shaking 10 g of clinoptilolite with 100 mL of 200 mg L^{-1} nickel (or cadmium or zinc) solution for 2 h. These metals seem to reach saturation, which means that the metal had filled possible available sites and further adsorption could take place only at new surfaces. After the treatment, the resulting zeolite phase was subjected to washing with nitric acid 4 mol L^{-1} in order to eliminate excess of Ni^{2+} (or Cd^{2+} or Zn^{2+}) ions and then was washed with distilled water to remove excess of acid.

The modification of zeolite was performed as follows: 100 mL of BDTA solution (0.1 mmol mL^{-1}) was added to 10 g of clinoptilolite and the mixture was shaken at room temperature for 24 h. The BDTA-modified zeolite was filtered and washed with distilled water, then was dried in an oven at 100 °C.

2.3. General procedure

0.3 g of the adsorbent (BDTA-modified clinoptilolite) was added to a A funnel-tipped glass tube. An aliquot of vanadium solution containing 0.05–15.0 μg was taken into a beaker. 1 mL of 0.2% ascorbic acid solution was added for convert of all vanadium forms to V(IV), if exists. Then 1 mL of 0.001 mol L^{-1} solution of PAR, 2 mL phosphate buffer (pH 6.5) were added and the resulting solution was diluted to 50 mL with distilled water. All mixtures were flushed with pure nitrogen and kept at low temperature for a few minutes, then this solution was passed through the column at a flow rate 1.0 mL min^{-1} . The adsorbed complex on the column was eluted with 5.0 mL of DMF at a flow rate 0.8 mL min^{-1} and the absorbance measured at 550 nm against blank prepared in the same way but without vanadium.

Table 1
Analysis of vanadium in standard alloys

Sample	Composition (%)	Found ^a
NKK no. 1021; Al Si, Cu, Zn alloy	Mg, 0.29; Pb, 0.18; Zn, 1.76; Si, 5.56; Sn, 0.10; Ti, 0.04; Mn, 0.20; Cu, 2.72; Cr, 0.03; Fe, 0.99; Bi, 0.01; Ni, 0.14; Zr, 0.01; Sb, 0.01; Ca, 0.004; V, 0.007	0.0068 ± 0.0002
NKK no. 920; aluminum alloy	Si, 0.78; Fe, 0.729; Mg, 0.46; Cr, 0.27; Zn, 0.8; Ti, 0.15; Bi, 0.06; Ga, 0.05; Ca, 0.03; Co, 0.10; Ni, 0.29; Cu, 0.71; Mn, 0.20; V, 0.15	0.148 ± 0.002

Conditions were same as Fig. 2.

^a Mean of four determination ± standard deviation.

2.4. Analysis of vanadium in standard alloys

The method was applied to the determination of vanadium in Nippon Keikinzoku Kogyo (NKK) no 920 aluminum alloy, NKK no 1021 Al, Si, Ca, Zn alloy. A 0.1-g sample of the standard alloy was completely dissolved in 10 mL of hydrochloric acid (1:1) by heating on a water-bath. The 0.2% ascorbic acid solution was used for convert of all vanadium forms to V(IV). The solution was filtered and diluted to 100 mL with distilled water in a standard flask. An aliquot of this sample was taken and analyzed by the general procedure. The results obtained are given in Table 1. These results are in agreement with certified values.

2.5. Analysis of vanadium in synthetic samples

A synthetic sample containing vanadium was prepared in 10 ml of concentrated hydrochloric acid. The 0.2% ascorbic acid solution was used for convert of all vanadium forms to V(IV). The solution was filtered if needed, and the volume was made to 100 ml in a standard flask. An aliquot of the sample solution was analyzed by the general procedure and the results are given in Table 2.

3. Results and discussion

3.1. Effect of the surfactant

The clinoptilolite zeolite without modification was not suitable for separation and preconcentration of vanadium. Therefore, benzyldimethyltetradecylammonium chloride was added to zeolite. Zeolite cannot adsorb ligand molecules because of its smaller pore size than the ligand molecules. In addition to this, natural zeolite has a negative charge in the entire range

pH. Therefore, anionic ligand groups will be repelled from the negatively charged zeolite surface. This induces a relatively low adsorption capacity. For this reason, in order to increase the adsorption capacity, the surface of natural zeolite was modified with a surfactant to generate a surface with hydrophobic properties and partially neutralize the negative charges [29]. A series of experiments were carried out to find the optimum time to reach equilibrium. The conditioning (mixing) time of 24 h was found to be sufficient for reaching equilibrium.

3.2. Absorption spectra

The stability of the VO²⁺ ion depends on the prevailing conditions. In acidic solution and at low temperature, VO²⁺ species can be kept for quite a long time. In alkaline solution, VO²⁺ species can be stored for about 4 days at room temperature. V(IV) is readily oxidized by oxygen in air in neutral or high pH media and the oxidation rate increases with increasing pH and temperature. V(IV) can be stabilised by complexation with a variety of ligands, because of the high affinity of V(IV) for most oxygen, nitrogen and sulfur containing ligands [10]. In addition to ascorbic acid [30] and (NH₄)₂S [10] can be used as a reducing agent. PAR reacts with vanadium(IV) in solution to give red–violet complex with an absorption maximum at 550 nm with stoichiometric ratio 1:1 as determined using the molar ratio and continuous variation methods [31]. Between pH 6.2 and 7.0, this complex is sorbed on modified zeolite and desorbed from the zeolite with DMF, then was measured at 300–650 nm against blank. The absorbance of the blank was measured at the same wavelengths. The blank absorbance results from the reagent fixed on the zeolite. The net absorbance, A_{NC}, for the complex was obtained from the following equation [32]:

$$A_{NC} = A_{\text{complex}} - A_{\text{blank}}$$

Table 2
Analysis of vanadium in synthetic samples

Composition of synthetic sample (µg g)	Concentration of vanadium (µg g)	
	Certified value	Found ^a
As, 4.0; Cd, 3.0; Cu, 0.60; Ca, 150; Fe, 6.0; Ni, 6.5; Mn, 10.0; Hg, 8.0; Mg, 100; Pb, 25; Zn, 3.5; Tl, 1.5; Pd, 7.5; Rh, 0.85; Ir, 5.5	6.5	6.4 ± 0.2
Mn, 3.5; Pb, 2.0; Sb, 1.5; Ni, 6.0; Mo, 4.5; Mg, 75; Ca, 74; Cd, 7.5; Hg, 2.5; Bi, 8.0; Zn, 12; Al, 2.5; Pd, 7.5; Rh, 18.0; Ir, 15.0	25.0	24.8 ± 0.6
Ni, 15; Fe, 3.5; Zn, 6.5; Ca, 120; Mg, 65; Mn, 25; As, 3.5; Bi, 16; Mo, 6.5; Sb, 7.5; Hg, 15.0; Pd, 3.5; Rh, 17.5; Ir, 25.5	48.0	47.6 ± 0.8

^a Average of five determinations, ± standard deviation.

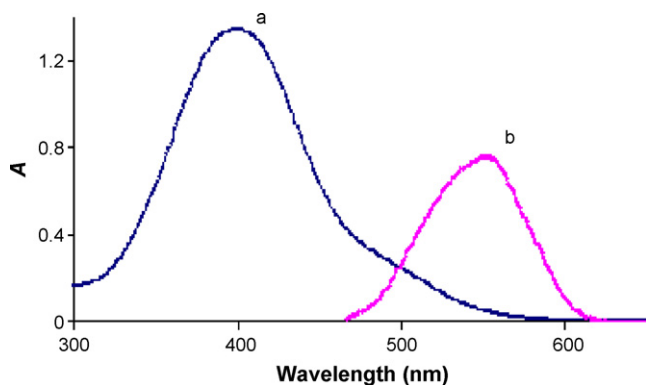


Fig. 1. Absorption spectra of the PAR and its V(IV) complex: spectrum (a) PAR blank against dimethylformamide; spectrum (b) PAR–V(IV) complex against reagent blank. Conditions: V(IV), 5.0 μg ; pH, 6.5; flow rate of sample, 1.0 mL min^{-1} ; PAR, 0.001 mmol; eluent, 5.0 mL DMF with flow rate 0.8 mL min^{-1} .

The spectra of the complex and blank are shown in Fig. 1.

3.3. Choice of solvent

A number of solvents were examined to dissolve the metal complex along with the zeolite. It is essential to select a solvent which the complex is highly soluble, stable and also allows sensitive UV–vis spectrophotometric measurements. With mineral acids, complex was broken, so these were not suitable. The complex is insoluble in organic solvents such as toluene, *n*-hexane, chloroform, dioxan and nitrobenzene but it is soluble in dimethylformamide (DMF). It was found that 5.0 mL of DMF was sufficient to dissolve the complex. In order to eliminate the water retained in the column, it was necessary to aspirate the column for 2–3 min.

3.4. pH dependence

The optimum pH for the formation and fixation of the complex falls in the range 6.2–7.0 (Fig. 2). At pH values below 6.2, concentration of hydronium ion is high then vanadium(IV) cannot adsorb on the active sites in ligand and the complex was not fixed on the exchanger. At pH values above 7.0, VO^{2+} cations can convert to dimer, other oligomers and polymers, therefore absorbance of the V(IV)–PAR decreased. We chose pH 6.5 as

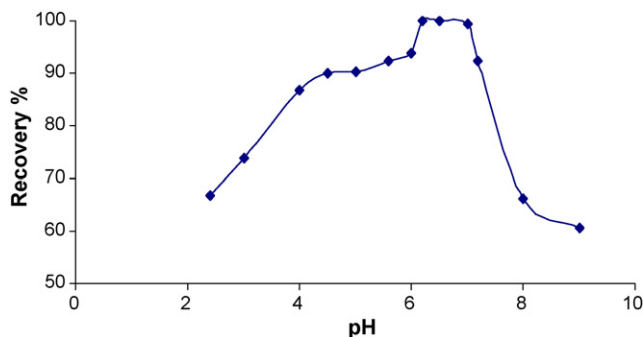


Fig. 2. Effect of pH on adsorption of V(IV)–PAR. Absorbance measured at 550 nm. Conditions were same as Fig. 1.

the best pH value for the standard procedures. The phosphate buffer was found to yield the best results.

3.5. Other experimental conditions

The reaction conditions were investigated with 5.0 μg of vanadium(IV). The flow rate of sample solution was varied from 0.1 to 2.0 mL min^{-1} did not affect adsorption. A flow rate of 1.0 mL min^{-1} was recommended in all experiments.

Under optimum conditions, the volume of the aqueous phase was varied in the range 50–600 mL under optimum conditions. It was observed that the absorption was almost constant to 450 mL (preconcentration factor of 90), however for convenience, all the experiments were carried out with 50 mL of aqueous phase.

3.6. Analytical data

It is possible to retain 0.031 μg of vanadium from 450 mL of solution passing through the column (where detection limit is 0.069 ng mL^{-1}). Analytical curve is linear in the 0.11–3.0 $\times 10^3$ ng mL^{-1} in initial solution or 0.01–3.0 $\mu\text{g mL}^{-1}$ in final solution with correlation factor of 0.997. Eight replicate determination of 5.0 μg of vanadium in final solution gave a mean absorbance of 0.7732 with a relative standard deviation of 2.1%.

3.7. Effect of diverse ions

Various salts and metal ions were added individually to a solution containing of 5.0 μg vanadium and general procedure was applied. The tolerance limit was set, as the diverse ion amount

Table 3
Effect of diverse salts and metal ions

Salt or ion	Tolerance limit (μg)
CO_3^{2-} (Na_2CO_3)	7,000
CH_3COO^- (CH_3COONa)	80,000
Br^- (NaBr), NO_3^- (NaNO_3), F^- (NaF)	4,000
Cl^- (NaCl), CN^- (NaCN)	5,000
HCO_3^- (NaHCO_3)	8,000
SO_4^{2-} (Na_2SO_4)	16,000
$\text{S}_2\text{O}_3^{2-}$ ($\text{Na}_2\text{S}_2\text{O}_3$)	9,000
EDTA (NaSalt)	1,400
Mo^{6+}	3,300
NH_4^+	8,000
Cu^{2+} , Co^{2+}	3,300 ^a
Y^{3+}	5,500 ^b
Ca^{2+}	2,000
Sr^{2+} , K^+	1,000
Al^{3+}	2,000
Mg^{2+} , As^{3+}	3,000
Sn^{2+}	500
Zr^{4+}	10,300 ^b
Zn^{2+}	3,400 ^c
Ru^{3+}	5,400 ^c

Conditions were same as Fig. 2.

^a After masked with 0.5 mL of 0.1% solution of EDTA.

^b After masked with 1 mL of 0.4% sodium fluoride.

^c After masked with 1 mL of 0.5% sodium cyanide.

Table 4
Comparative data from some recent studied on preconcentration of vanadium

Technique	Ligand	Sorbent	DL ($\mu\text{g L}$)	R.S.D.%	Linear range	Reference
SPS	Eriochrome cyanine R	Dextran-type exchanger	0.6	2.2	0.6–25.0 ng mL^{-1}	[33]
SPE-spectrophotometry	PAR	Amberlite XAD-2	1.6	1.6		[34]
SPE-GFAAS	PAN	Naphthalene	1.25	1.2	5.0–625 ng mL^{-1}	[35]
SPS	PAR	Anion-exchanger Dowex 1-X8	0.06	1.5	0.1–2.4 ng mL^{-1}	[36]
SPE-DPP	Morpholine-4-carbodithioates	Microcrystalline naphthalene	200	1.4	0.5–6.5 $\mu\text{g mL}^{-1}$	[37]
SPE-spectrophotometry	QADEAP	C ₁₈ cartridge	0.04	1.68	0.01–0.6 $\mu\text{g mL}^{-1}$	[38]
Catalytic adsorptive stripping voltammetric	Chloranilic Acid		0.2	3.1	5.0–25.0 ng mL^{-1}	[39]
First derivative spectrophotometry	PAR		300	0.8	4.0–16.0 $\mu\text{g mL}^{-1}$	[40]
SPE-spectrophotometry	PAR	Zeolite clinoptilolite	0.07	2.1	0.11–3000 ng mL^{-1}	Present method

SPS, solid phase spectrophotometry; QADEAP, 2-(2-quinolyazo)-5-diethylaminophenol; PAN, 1-(2-pyridylazo)-2-naphthol.

require causing $\pm 3\%$ error in the determination of vanadium. The results are given in Table 3.

3.8. Comparison to other methods

The present method was successfully applied to the extraction, preconcentration and determination of the vanadium ion by UV–vis spectrophotometry. A comparison of the proposed system with some recent studied procedures is given in Table 4. Detection limit obtained is 0.07 $\mu\text{g L}$. Thus, it is comparable to those presented by other methods described in the literature. High range of linear concentration, high sensitivity, low relative standard deviation and high tolerance to interferences from matrix ions allows the application of the new proposed sorbent for determination of all vanadium as V(IV) form, extraction and preconcentration in complex samples. The good features of the proposed method show that it is a convenient and low-cost one.

4. Conclusion

The fixation of the V(IV)–PAR complex on clinoptilolite zeolite is discussed. The application of this method has produced a higher sensitivity and lower detection limit than is given by the solution methods for the determination of all vanadium as V(IV) form at microgram per liter levels. Although, some of metal–PAR complexes absorb at similar wavelengths, however, with control of pH and using common masking agents this problem has been solved easily for vanadium as demonstrated from its application satisfactory to the analyses of standard alloys. The main advantage of this procedure are: (a) natural clinoptilolite is very cheap and abundant; (b) a good preconcentration factor (90) can be achieved; (c) the preparation of the extractor system is simple and fast. Therefore, clinoptilolite zeolite can be used as a good sorbent for preconcentration and determination of vanadium at trace levels.

References

- [1] D.H.K. Lee, *Metallic Contaminants and Human Health*, Academic Press, New York, 1972.
- [2] K. Pyrzynska, T. Wierzbicki, *Anal. Chim. Acta* 540 (2005) 91.
- [3] A. Ensafi, B. Naderi, *Fresenius J. Anal. Chem.* 358 (1997) 480.
- [4] R. Chakraborty, K. Das, *Fresenius J. Anal. Chem.* 349 (1994) 774.
- [5] M. Yaman, S. Gucer, *Fresenius J. Anal. Chem.* 350 (1994) 504.
- [6] S. Kawakubo, K. Ogihara, M. Iwatsuki, *Analyst* 120 (1995) 2719.
- [7] V. Dupont, Y. Auger, C. Jeandel, *M. Water, Anal. Chem.* 63 (1991) 520.
- [8] H. De Beer, P.P. Coetzee, *Fresenius Anal. Chem.* 348 (1994) 806.
- [9] J.H. Miura, *Anal. Chim. Acta* 62 (1990) 1424.
- [10] P.P. Coetzee, J.L. Fischer, H. Mingsong, *Water SA* 28 (2002) 37.
- [11] K. Pyrzynska, T. Wierzbicki, *Talanta* 64 (2004) 823.
- [12] D. Banerjee, B.C. Mondal, D. Das, A.K. Das, *Microchim. Acta* 141 (2003) 107.
- [13] C. Ekinci, U. Koklu, *Spectrochim. Acta Part B* 55 (2000) 1491.
- [14] K. Pyrzynska, T. Wierzbicki, *Mikrochim. Acta* 147 (2004) 59.
- [15] S.L.C. Ferreira, A.S. Queiroz, M.S. Fernandes, H.C. Dos Santos, *Spectrochim. Acta Part B* 57 (2003) 1939.
- [16] R.G. Wuilloud, J.C. Wuilloud, R.A. Olsina, L.D. Martinez, *Analyst* 126 (2001) 715.
- [17] G. Abbasse, B. Ouddane, J.C. Fischer, *Anal. Bioanal. Chem.* 374 (2002) 873.
- [18] K. Hirayama, S. Kegeyama, N. Unohara, *Analyst* 117 (1992) 13.
- [19] V. Badillo-Almaraz, P. Trocellier, I. Davila-Rangel, *Nucl. Instrum. Methods Phys. Res. Part B* 210 (2003) 424.
- [20] Y.P. Pena, W. Lopez, J.L. Burguera, M. Burguera, M. Gallignani, R. Brunetto, P. Carrero, C. Rondon, R. Imbert, *Anal. Chim. Acta* 403 (2000) 249.
- [21] A. Shanableh, A. Kharabsheh, *J. Hazard. Mater.* 45 (1996) 207.
- [22] E. Erdem, N. Karapinar, R. Donat, *J. Colloid Interface Sci.* 280 (2004) 309.
- [23] A. Gunay, E. Arslankaya, I. Tosun, *J. Hazard. Mater.* 146 (2007) 362.
- [24] M. Sprynskyy, B. Buszewski, A.P. Terzyk, J. Namiesnik, *J. Colloid Interface Sci.* 304 (2006) 21.
- [25] D.W. Breck, *Zeolite Molecular Sieves*, Wiley, New York, 1974.
- [26] G.M. Haggerty, R.S. Bowman, *Environ. Sci. Technol.* 28 (1994) 452.
- [27] O. Altin, H.O. Ozbelge, T. Dogu, *J. Colloid Interface Sci.* 198 (1998) 130.
- [28] H. Van Bekkum, E.M. Flanigen, J.C. Jansen, *Introduction to Zeolite Science and Practice. Studies in Surface Sciences and Catalysis*, vol. 58, Elsevier, Amsterdam, 1991.
- [29] B. Armagan, M. Turan, M. Celik, *Desalination* 170 (2004) 33.
- [30] J. Poledniok, F. Buhl, *Talanta* 59 (2003) 1.
- [31] S.P. Mushran, J.R. Om Prakash, Verma, *Bulletin of the Chemical Society Japan* 45 (1972) 1709.
- [32] A. Molina-Diaz, J.M. Herrador-Mariscal, M.I. Pascual-Reguera, L.F. Capitan-Vallvey, *Talanta* 40 (1993) 1059.
- [33] B.S. Boundra, J.M. Bosque-Sendra, M.C. Valencia, *Talanta* 42 (1995) 1525.
- [34] H. Filik, K.I. Berker, N. Balkis, *Anal. Chim. Acta* 518 (2004) 173.
- [35] M.A. Taher, S. Puri, A. Bhalotra, B. Krishan Puri, *Quim. Anal.* 18 (1999) 181.
- [36] M.L. Fernandez-de Cordova, A. Molina-Diaz, *Talanta* 42 (1995) 1057.
- [37] S. Puri, R.K. Dubey, M.K. Gupta, B.K. Puri, *Talanta* 46 (1998) 655.
- [38] Q. Hu, G. Yang, *Bull. Korean Chem. Soc.* 25 (2) (2004) 263.
- [39] J. Wang, D. Lu, S. Thongamdee, Y. Lin, O.A. Sadik, *Talanta* 69 (2006) 914.
- [40] M.N. Abbas, A.M. Homoda, G.A.E. Mostafa, *Anal. Chim. Acta* 436 (2001) 223.

Erratum

Erratum to “Preconcentration and solid-phase extraction of beryllium, lead, nickel, and bismuth from various water samples using 2-propylpiperidine-1-carbodithioate with flame atomic absorption spectrometry (FAAS)”
[Talanta 68(2) (2006) 735–740]

K. Suvardhan^c, K. Suresh Kumar^c, D. Rekha^c,
B. Jayaraj^a, G. Krishnamurthy Naidu^b, P. Chiranjeevi^{c,*}

^a Department of Mathematics, S.V. University, Tirupati 517502, AP, India

^b Department of Pharmacy, S.V. Govt. Polytechnic, Tirupati 517501, AP, India

^c Environmental Monitoring Laboratory, Department of Chemistry, S.V. University, Tirupati 517502, AP, India

This article has been retracted at the request of the Editors-in-Chief.

Considerable concern was raised about the research purportedly conducted at Sri Venkateswara University, India with the alleged involvement of Professor P. Chiranjeevi.

Questions were raised as to the volume of publications, the actual capacity (equipment, orientation and chemicals) of the laboratory in which Professor Chiranjeevi worked, the validity of certain of the research data identified in the articles, the fact that a number of papers appear to have been plagiarized from other previously published papers, and some aspects of authorship.

Professor Chiranjeevi was given the opportunity to respond to these allegations. Thereafter, a committee was constituted by the University to look into these allegations. Based on the enquiry committee report, we have been informed by the head of the Department of Chemistry at Sri Venkateswara University that the university authorities have taken disciplinary action against Professor Chiranjeevi, as the university considers that there are grounds for such action.

Therefore, based on the results of this investigation, the Editors-in-Chief are retracting this article.

DOI of original article: [10.1016/j.talanta.2005.05.020](https://doi.org/10.1016/j.talanta.2005.05.020).

* Corresponding author. Tel.: +91 877 2250556; fax: +91 877 2261274.

E-mail address: chiranjeevi_sai@yahoo.co.in (P. Chiranjeevi).

RNA-templated single-base mutation detection based on T4 DNA ligase and reverse molecular beacon

Hongxing Tang, Xiaohai Yang, Kemin Wang*, Weihong Tan,
Huimin Li, Lifang He, Bin Liu

*Engineering Center for Biomedicine, State Key Laboratory of Chemo/Biosensing and Chemometrics, College of Chemistry and Chemical Engineering,
Key Laboratory for Bio-Nanotechnology and Molecular Engineering of Hunan Province,
Hunan University, Changsha 410082, PR China*

Received 27 October 2007; received in revised form 22 January 2008; accepted 25 January 2008

Available online 3 February 2008

Abstract

A novel RNA-templated single-base mutation detection method based on T4 DNA ligase and reverse molecular beacon (rMB) has been developed and successfully applied to identification of single-base mutation in codon 273 of the p53 gene. The discrimination was carried out using allele-specific primers, which flanked the variable position in the target RNA and was ligated using T4 DNA ligase only when the primers perfectly matched the RNA template. The allele-specific primers also carried complementary stem structures with end-labels (fluorophore TAMRA, quencher DABCYL), which formed a molecular beacon after RNase H digestion. One-base mismatch can be discriminated by analyzing the change of fluorescence intensity before and after RNase H digestion. This method has several advantages for practical applications, such as direct discrimination of single-base mismatch of the RNA extracted from cell; no requirement of PCR amplification; performance of homogeneous detection; and easily design of detection probes.

© 2008 Elsevier B.V. All rights reserved.

Keywords: Single-base mutation detection; Reverse molecular beacon; T4 DNA ligase; RNA-templated

1. Introduction

Many pathogenic and genetic diseases and cancers are associated with the mutation of particular genes [1]. Among these mutations, single nucleotide polymorphisms are the most abundant genetic variation in individuals [2,3]. A majority of these genetic variations can serve as biomarkers for medical diagnosis at early stage of the diseases [4,5]. Therefore, reliable and rapid methods for single-base mutation detection have considerable significance in the biological research, medical science and clinical diagnosis.

In the past decades, a wide variety of techniques and methods have been developed for mutation detection, such as allele-specific oligonucleotides [6], specific primer extension [7], ligation-mediated methods [8], dynamic allele-specific hybridization [9], iFRET [10], and molecular beacon assay [11].

However, most of these methods are incorporated with PCR amplification and gel-based separation.

Molecular beacons are novel hairpin structure nucleotide probes [11–13]. With proper design, it is possible to discriminate between targets that differ by a single nucleotide [14]. However, in practical application, the choices of the probe sequence are limited by target-specific considerations, and a fraction of molecular beacons will not work without optimization, this increases the cost of this method [15,16]. New strategies which combines ligase detection reaction and reverse molecular beacon (rMB) have been established for single-base mutation identification [17,18], but it still need expensive equipments [17] and washing separation steps [18].

Furthermore, compared with cDNA synthesis, transcripts analysis by direct ligation on RNA templates might more accurately report the relative abundance of the RNA [19,20]. In this paper, a novel RNA-templated single-base mutation detection method was established based on T4 DNA ligase and reverse molecular beacon.

* Corresponding author. Tel.: +86 731 8821566; fax: +86 731 8821566.
E-mail address: kmwang@hnu.cn (K. Wang).

Table 1
Oligonucleotide sequences

Name	Sequence
F-A	5'-(TAMRA)CGCTGCGGACAGGCACAAACACA-3'
F-T	5'-(TAMRA)CGCTGCGGACAGGCACAAACACT-3'
F-C	5'-(TAMRA)CGCTGCGGACAGGCACAAACACC-3'
F-G	5'-(TAMRA)CGCTGCGGACAGGCACAAACACG-3'
Quenching probe ^a	5'-pCACCTCAAAGCGCAGCG(DABCYL)-3'
Template-A ^b	5'-TCTCCCAGGACAGGCACAAACACTCACCTCAAAGCTGTTCCCTATAGTGAGTCGTATTAGG-3' 5'-CCTAATACGACTCACTATAGGAACAGCTTTGAGGTGAGTGTTTGTGCCTGTCTGGGAGA-3'
Template-C ^c	5'-TCTCCCAGGACAGGCACAAACACGCACCTCAAAGCTGTTCCCTATAGTGAGTCGTATTAGG-3' 5'-CCTAATACGACTCACTATAGGAACAGCTTTGAGGTGCGTGTTTGTGCCTGTCTGGGAGA-3'
RT-PCR primers	5'-CTGAGGTTGGCTCTGACTG-3' 5'-GTGCTCGCTTAGTGCTCC-3'

^a 5' end phosphorylation.

^b DNA templates for *in vitro* transcription template-A.

^c DNA templates for *in vitro* transcription template-C.

2. Experimental

2.1. Reagents and instruments

The ligation probes, *in vitro* transcription DNA templates, and RT-PCR primers (shown in Table 1) were synthesized in Takara Biotechnology Co. Ltd. (Dalian, China). The ligation probes were designed according to the sequence around codon 273 on the exon 8 of p53 gene. Quenching probe (Q) was designed to have a six-base arm labeled with DABCYL at 3' terminal and phosphorylated at 5' terminal. Fluorescence probe (F) was designed to have a six-base arm labeled with TAMRA at 5' terminal and a discriminating base at its 3' terminal. The fluorescence probes were named as F-A, F-T, F-C, and F-G, according to their 3' terminal nucleotide which hybridizes to the variable position in the target RNA. Six-base arm at 5' terminal of each fluorescence probe are complementary to the six-base arm at the 3' terminal of the quenching probe but not to the target RNA.

T4 DNA ligase, RNase H, Pyrobest DNA polymerase, DNase I, and dNTPs were purchased from Takara Biotechnology Co. Ltd. Trizol reagent kit for total RNA isolation was purchased from Invitrogen Corporation. RT-PCR reagent kit was purchased from Fermentas Corporation. T7 transcription kit was purchased from Fermentas Corporation. DNA gel extraction kit was purchased from Tiangen Biotech. (Beijing) Co. Ltd.

HeLa (human cervical carcinoma), A549 (human lung carcinoma), and C-33A (human cervical carcinoma) cells were preserved in our lab. RPMI 1640 culture medium and fetal bovine serum were purchased from Gibco. All other chemicals used were of analytical reagent grade without further purification. DEPC-treated purified water was used in experiments.

Instruments: All fluorescence measurements were performed on a Hitachi FL-2500 fluorometer (Japan) equipped with a Thermo Neslab water bath circulators (USA). RNA samples' concentration was detected on DU800 Beckman ultraviolet spectrophotometer (USA). PCR amplification was carried out

on PCR system 2700 (Applied Biosystems, USA). Agarose gel electrophoresis was performed using electrophoresis apparatus and electrophoresis tank (Beijing Liuyi Electrophoresis Instrument Factory).

2.2. RNA synthesis by *in vitro* transcription reaction

RNA templates were synthesized by *in vitro* transcription. The DNA templates for *in vitro* transcription were designed according to the sequence around codon 273 on the exon 8 of p53 gene, and T7 promoter was added at their 5' terminal (Table 1). *In vitro* transcription reactions were performed using T7 transcription kit according to the manufacturer's protocol. The resultant RNA samples were purified and dissolved in nuclease-free H₂O. The samples' concentration was detected on Beckman ultraviolet spectrophotometer.

2.3. Single-base mismatch detection on RNA templates

Ligation reactions on *in vitro* synthesized RNA templates were performed in a buffer containing 10 mM MgCl₂, 10 mM Tris-HCl (pH 7.6), 10 μM ATP, 200 nM fluorescence probes, 240 nM quenching probes and 160 nM purified RNA templates. After incubated at 65 °C for 3 min and cooled to room temperature, 7 U T4 DNA ligase was added to the ligation mixture (100 μL) and incubated at 37 °C for 2 h. Then, the reaction was terminated by incubation at 65 °C for 10 min. In order to identify the base type at the mutation site, four separate experiments were performed using different fluorescence probe (F-A, F-T, F-C, and F-G, respectively) for each RNA template. The ligation products were divided into two equal parts. One of them was added 15 μL 5 × RNA degeneration buffer and 1 μL RNase H and the other was added 15 μL 5 × RNA degeneration buffer only. After incubated at 37 °C for 1 h, the reaction mixture was diluted to 400 μL, and the fluorescence was measured on fluorometer with excitation at 521 nm.

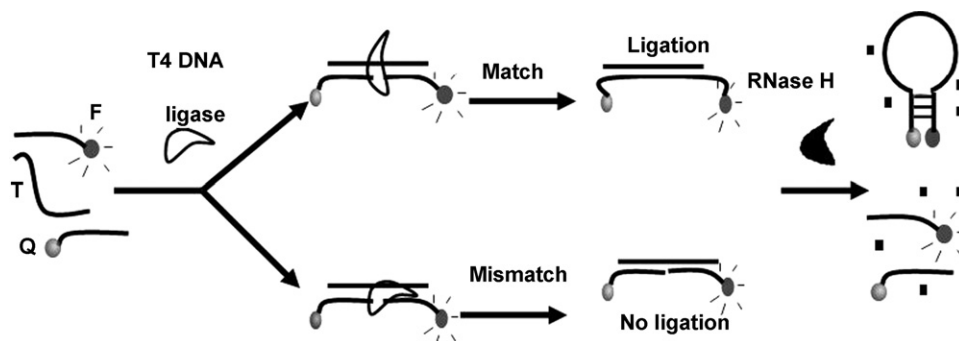


Fig. 1. The scheme of RNA-templated single-base mutation detection. First, the target RNA (T) hybridized with the quenching probe (Q) and fluorescence probe (F). If F and Q perfectly matched to T, the ligation reactions occurred upon adding T4 DNA ligase. After adding RNase H, the target RNA in RNA/DNA duplex was digested and a hairpin structure was formed, causing fluorescence quenching by fluorescence resonance energy transfer. If F and Q not perfectly matched to T, unligated probes could not form a hairpin structure after adding RNase H and could not cause fluorescence quenching. Single-base mutation can be discriminated by analyze the change of fluorescence intensity before and after RNase H digestion.

2.4. Mismatch discrimination based on fluorescence quenching

The change in the fluorescence intensity was measured after 1 h incubation with RNase H. Excitation and emission wavelengths were 521 and 578 nm, respectively. To normalize the difference in different experiments, quenching efficiency (Q_e) was defined as follows: $Q_e = ((F_0 - F_1)/F_0) \times 100\%$. Where F_0 indicates the fluorescence intensity before RNase H digestion and F_1 indicates the fluorescence intensity after RNase H digestion.

2.5. Single-base mismatch detection on total RNA samples

Cells were grown in RPMI 1640 culture medium supplemented with 10% fetal bovine serum, 100 U/mL penicillin, 100 μ g/mL streptomycin at 37 °C, and in atmosphere containing 5% CO₂. Total RNA samples were extracted using Trizol reagent with a standard total RNA isolation protocol from three cell lines, i.e. HeLa, A549, and C-33A. The purified total RNA was dissolved in nuclease-free H₂O, and the samples' concentration was detected on ultraviolet spectrophotometer. Detections were performed refer to the method previously described in this paper (Section 2.3), and modified as follows. Ligation reactions were performed in a 100 μ L buffer containing 10 mM MgCl₂, 10 mM Tris-HCl (pH 7.6), 10 μ M ATP, 50 nM fluorescence probes, 60 nM quenching probes, and 180 μ g total RNA sample. After incubated at 65 °C for 3 min and cooled to room temperature, 7 U T4 DNA ligase was added and incubated at 37 °C for 2 h. Then, the reaction was terminated by incubation at 65 °C for 10 min. The ligation products were divided into two equal parts. One of them was added 15 μ L 5 \times RNA degeneration buffer and 1 μ L RNase H and the other was added 15 μ L 5 \times RNA degeneration buffer only. After incubated at 37 °C for 1 h, the reaction mixtures were all diluted to 100 μ L, and the fluorescence was measured on fluorometer with excitation at 521 nm. In order to identify the base type at the mutation site, four separate experiments were performed using different fluorescence probe (F-A, F-T, F-C, and F-G, respectively) for each total RNA sample.

2.6. RT-PCR and sequencing

Total RNA samples were firstly purified to remove DNA contaminant. Reverse transcription reaction was performed in 20 μ L volumes with 4 μ L 5 \times reverse transcriptase buffer, 3 μ g RNA template, 5 mM dNTPs mixture, 30 U RNase inhibitor, 5 U AMV RTase, and 50 pmole oligo (dT) 18 primer at 42 °C for 1 h. PCR amplification was carried out on PCR system 2700. PCR was performed in 50 μ L of 1 \times Pyrobest buffer, containing 2.0 mM MgCl₂, 200 μ M dNTPs, 400 nM PCR primers, 2.5 U Pyrobest DNA polymerase, and 2 μ L reverse transcription products. The amplification was achieved for 30 cycles at 94 °C for 45 s, 55 °C for 45 s, 72 °C for 1 min, and a final extension at 72 °C for 10 min.

5 μ L PCR products were analyzed on 2% agarose gels containing ethidium bromide. Agarose gels were examined in UV light vision system after electrophoresis. Target DNA samples were recovered and purified using DNA gel extraction kit. Purified PCR products were sent to Takara Biotechnology Co. Ltd. for sequencing.

3. Results and discussion

3.1. Experimental principle

The scheme of this approach is shown in Fig. 1. The detection was carried out by using allele-specific probes, which flanked the point mutation in the target RNA. Quenching probe (Q) was designed to have a six-base arm labeled with DABCYL at 3' terminal and phosphorylated at 5' terminal and fluorescence probe (F) was designed to have a six-base arm labeled with TAMRA at 5' terminal and a discriminating base at its 3' terminal. The arm sequences of the F and Q were complementary to each other but not to the target RNA. After hybridized the target RNA with the F and Q, ligation reaction was carried out in the presence of T4 DNA ligase if the two adjacent probes perfectly matched to the target RNA. Then RNase H was added to cleave the RNA strand in DNA/RNA duplex. The molecular beacon-like hairpin structure (rMB) was formed by the intramolecular hybridization of the complementary arm sequence in the ligation products. This

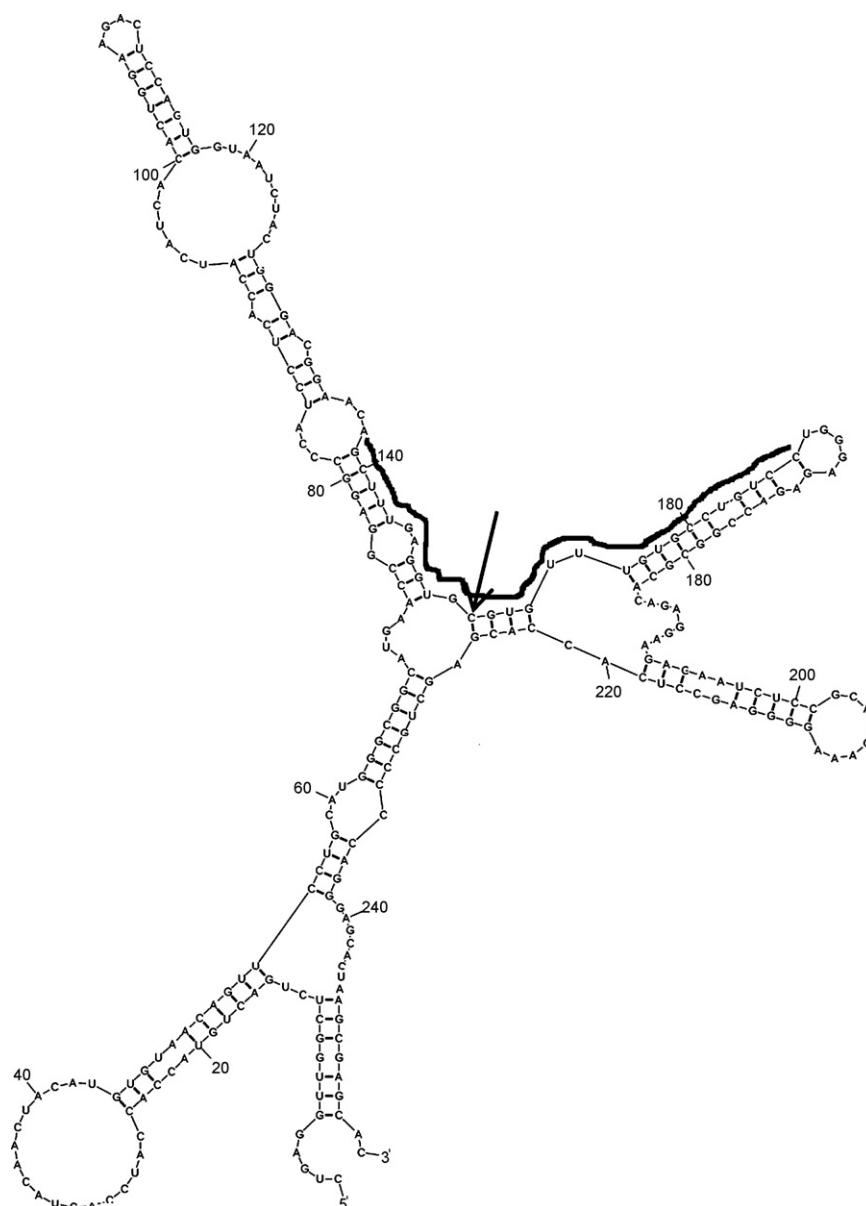


Fig. 2. The most stable secondary structure of partial of p53 mRNA analysis with the Mfold program. The bold line emphasized sequence was chosen for one-base mismatch detection in this paper, and the base variable position was pointed with an arrow.

hairpin structure will keep the fluorophore and quencher in close proximity to each other, causing the fluorescence to be quenched by fluorescence resonance energy transfer. If the two adjacent probes were not perfectly matched to the template, unligated probes could not form a hairpin structure after adding RNase H. One-base mutation can be discriminated by analyzing the change of fluorescence intensity before and after RNase H digestion.

Several computer algorithms such as Mfold [21], primer 5.0, and OligoWalk can be chosen to design the detection primers. The total length comprising the hairpin loop can range between 20 and 35 nucleotides, depending on the target region chosen for probe binding. In order to increase the stability of the DNA/RNA hybridization duplex, the fluorescence probe and quenching probe (not contain the stem sequence) should contain not less than 10 nucleotides. The length of the arm sequences is five or six nucleotides (composed mostly G/C's) to keep the

stable of the intracellular stem loop structure of the molecular beacon-like hairpin structure. Mfold or primer 5.0 can be used to predict the structure of the loop sequence (the sequence in the molecular beacon-like hairpin structure not containing the arm nucleotides) and the molecular beacon; these sequences should not form unexpected secondary structure. The most stable secondary structure of partial of p53 mRNA analysis with the Mfold program is shown in Fig. 2. The bold line emphasized sequence was chosen for one-base mismatch detection in this paper, and the base variable position was pointed with an arrow.

3.2. Discrimination of single-base mismatch on *in vitro* synthesized RNA

To validate our postulated mechanism in Fig. 1, two *in vitro* synthesized RNA templates (named template-A and template-C

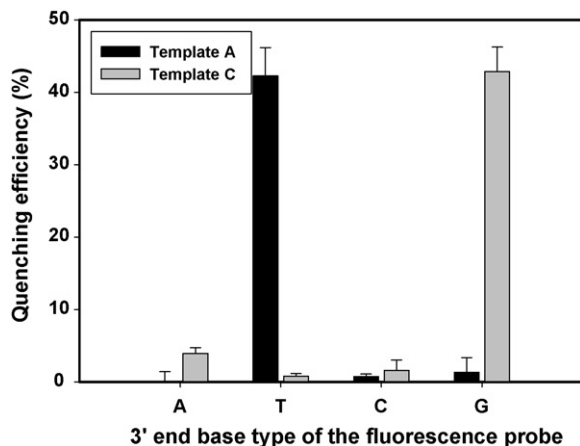


Fig. 3. Single-base mismatch detect of *in vitro* synthesized RNA. The Qe reflected whether the 3' terminal base of fluorescence probe perfectly matched the base at the variable position in the target RNA. Base type at the variable position in the target can be identified by comparing the Qe of relevant fluorescence probes. The concentration of fluorescence probe, quenching probe, and *in vitro* synthesized RNA were 25, 30 and 20 nM, respectively.

according to the base type at the variable position) were used for one-base mismatch detection. The designed probes are shown in Table 1. In order to identify the base type at the mutation site, four separate experiments were performed using different fluorescence probe (F-A, F-T, F-C, and F-G, respectively) for each RNA template.

As shown in Fig. 3, the Qe for template-A were 0.07, 42.24, 0.72, and 1.33% (the corresponding detection probes were F-A, F-T, F-C, and F-G), respectively. The Qe of matched substrate was 31-fold greater than corresponding mismatched substrates. For template-C, the Qe were 3.93, 0.80, 1.60, and 42.8%. The Qe of matched substrate was 10-fold greater than corresponding mismatched substrates. Using this method, we cannot only discriminate one-base mismatch, but also identify the base type at the variable position in the target RNA.

Then, the quantitative relationship between the template RNA concentration and fluorescence quenching efficiency was detected. The perfectly matched fluorescence probe and quench-

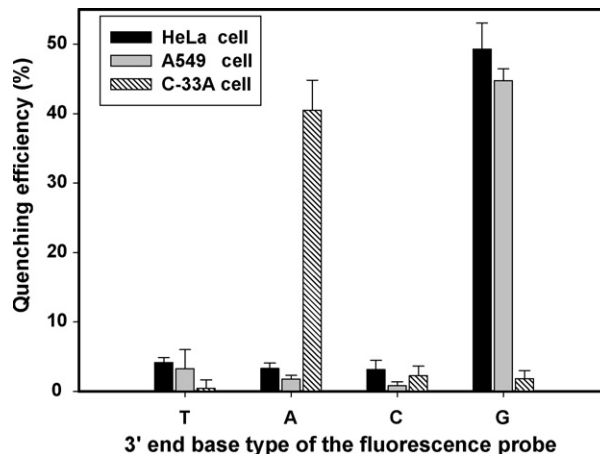


Fig. 4. Single-base mutation detect of extracted total RNA samples. The Qe reflected whether the 3' terminal base of fluorescence probe perfectly matched the base at the variable position in the target RNA. Base type at the variable position in the target can be identified by comparing the Qe of relevant fluorescence probes. The wild-type base at the variable position in the target RNA is C. The concentration of fluorescence probe, quenching probe, and total RNA were 25 nM, 30 nM, and 900 mg L⁻¹, respectively.

ing probe were used in all experiments. The Qe (Y) was linearly correlated to the template-A RNA concentrations (X) in the range of 1.25–24 nM. The regression equation is $Y = 2.241X + 1.068$, $R^2 = 0.9981$. The limit of detection was estimated to be 0.9 nM, defined by three times of standard deviation (σ) over the blank measurement.

3.3. Discrimination of single-base mismatch on total RNA

To investigate whether this approach has the capability of detecting single-base mutation in RNA samples, total RNA samples extracted using Trizol reagent with a standard total RNA isolation protocol from three cell lines, i.e. HeLa, A549, and C-33A. The results were shown in Fig. 4. These results indicated that the base types at the same position of HeLa, A549 and C-33A RNA were C, C, and U, respectively, by comparing the Qe.

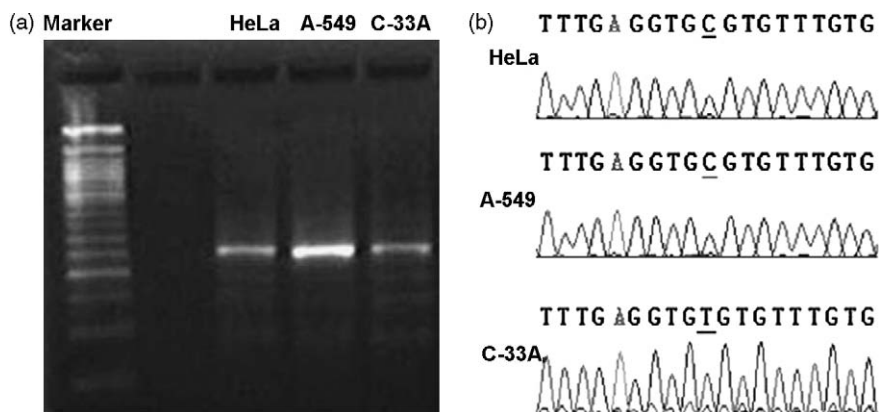


Fig. 5. Sequencing results. (a) The agarose gel electrophoresis image of the RT-PCR productions. (b) The sequencing electropherograms of HeLa, A549, and C-33A cell. The nucleotide at the variable position was indicated with a piece of underline.

3.4. Sequence validation

In order to confirm the detection results, a 255 bp DNA fragment containing the target sequence was amplified specifically from three cell lines utilizing the RT-PCR technique. The sequencing results (shown in Fig. 5) were in accordance with the detection results (Fig. 4). By comparing our experimental results with the database in the global bioresource center ATCC (C-33A has the CGT > TGT transition at codon 273, HeLa and A549 have the wild-type codon CGT at codon 273), we thought this method could detect the single-base mutations directly using total RNA samples.

4. Conclusions

A novel RNA-template single-base mutation detection method based on T4 DNA ligase and reverse molecular beacon has been developed and successfully applied to identification of single-base mutation in codon 273 of the p53 gene. This method has several advantages for practical applications, including (i) direct discrimination of single-base mismatch of the RNA extracted from cell; (ii) no requirement of PCR amplification, reverse transcription PCR, and gel electrophoresis separation; (iii) performance of homogeneous detection; (iv) easily design of detection probes.

For the limitation of the copy number of the target mRNA in the sample cells, the pitfall of this method is high sample consumption. Further systematic studies should be taken to improve the detection sensitivity and minimize sample consumption, such as combination of the ligase chain technology (LCR). The development of this method will make it suitable for the single-base mismatch detection of the clinical sample containing a small number of disease cells, and provide an attractive alternative to traditional RNA analysis tools.

Acknowledgements

This work was partially supported by National Key Basic Research Program of China (2002CB513110), Key

Project of Natural Science Foundation of China (90606003), Major International (Regional) Joint Research Program of Natural Science Foundation of China (20620120107), Key Project of International Technologies Collaboration Program of China (2003DF000039), China National Key Projects (05FK5029).

References

- [1] W.J. Strittmatter, A.M. Saunders, D. Schmechel, M. Pericak-Vance, J. Enghild, G.S. Salvesen, A.D. Roses, Proc. Natl. Acad. Sci. U.S.A. 90 (1993) 1977.
- [2] M.K. Halushka, J.B. Fan, K. Bentley, L. Hsie, N.P. Shen, A. Weder, R. Cooper, R. Lipshutz, A. Chakravarti, Nat. Genet. 22 (1999) 239.
- [3] R. Sachidanandam, D. Weissman, S.C. Schmidt, J.M. Kakol, L.D. Stein, G. Marth, S. Sherry, J.C. Mullikin, B.J. Mortimore, D.L. Willey, Nature 409 (2001) 928.
- [4] A.D. Roses, Nature 405 (2000) 857.
- [5] Y. Michikawa, F. Mazzucchelli, N. Bresolin, G. Scarlato, G. Attardi, Science 286 (1999) 774.
- [6] J.C. Knight, W. McGuire, M.M. Kortok, D. Kwiatkowski, Clin. Chem. 45 (1999) 1860.
- [7] K. Takatsu, T. Yokomaku, S. Kurata, T. Kanagawa, Nucleic Acids Res. 32 (2004) e60.
- [8] U. Landegren, R. Kaiser, J. Sanders, L. Hood, Science 241 (1988) 1077.
- [9] W.M. Howell, M. Jobs, U. Gyllensten, A.J. Brookes, Nat. Biotechnol. 17 (1999) 87.
- [10] W.M. Howell, M. Jobs, A.J. Brookes, Genome Res. 12 (2002) 1401.
- [11] S. Tyagi, D.P. Bratu, F.R. Kramer, Nat. Biotechnol. 16 (1998) 49.
- [12] X.H. Fang, J.J. Li, J. Perlette, W.H. Tan, K.M. Wang, Anal. Chem. 72 (2000) 747.
- [13] S. Tyagi, F.R. Kramer, Nat. Biotechnol. 14 (1996) 303.
- [14] W.H. Tan, K.M. Wang, T.J. Drake, Curr. Opin. Chem. Biol. 8 (2004) 547.
- [15] P. Santangelo, N. Nitin, G. Bao, Ann. Biomed. Eng. 34 (2006) 39–50.
- [16] P.Y. Kwok, Annu. Rev. Genom. Hum. Genet. 2 (2001) 235.
- [17] M.B. Wabuyele, H. Farquar, W. Stryjowski, R.P. Hammer, S.A. Soper, Y.W. Cheng, F. Barany, J. Am. Chem. Soc. 125 (2003) 6937.
- [18] Z.S. Wu, J.H. Jiang, G.L. Shen, R.Q. Yu, Hum. Mutat. 28 (2007) 630.
- [19] M. Nilsson, D.O. Antson, G. Barbany, U. Landegren, Nucleic Acids Res. 29 (2001) 578.
- [20] M. Nilsson, G. Barbany, D.O. Antson, K. Gertow, U. Landegren, Nat. Biotechnol. 18 (2000) 791.
- [21] M. Zuker, Nucleic Acids Res. 31 (2003) 3406.

Separation and determination of amitriptyline and nortriptyline by dispersive liquid–liquid microextraction combined with gas chromatography flame ionization detection

Ali Sarafraz Yazdi^{*}, Nourolhoda Razavi, Samaneh Raouf Yazdinejad

Department of Chemistry, Faculty of Sciences, Ferdowsi University of Mashhad, Iran

Received 19 July 2007; received in revised form 17 January 2008; accepted 18 January 2008

Available online 30 January 2008

Abstract

Dispersive liquid–liquid microextraction (DLLME) coupled with gas chromatography–flame ionization detection (GC–FID) was applied for the determination of two tricyclic antidepressant drugs (TCAs), amitriptyline and nortriptyline, from water samples. This method is a very simple and rapid method for the extraction and preconcentration of these drugs from environmental sample solutions. In this method, the appropriate mixture of extraction solvent (18 μL Carbon tetrachloride) and disperser solvent (1 mL methanol) are injected rapidly into the aqueous sample (5.0 mL) by syringe. Therefore, cloudy solution is formed. In fact, it is consisted of fine particles of extraction solvent which is dispersed entirely into aqueous phase. The mixture was centrifuged and the extraction solvent is sedimented on the bottom of the conical test tube. 2.0 μL of the sedimented phase is injected into the GC for separation and determination of TCAs. Some important parameters, such as kind of extraction and disperser solvent and volume of them, extraction time, pH and ionic strength of the aqueous feed solution were optimized. Under the optimal conditions, the enrichment factors and extraction recoveries were between 740.04–1000.25 and 54.76–74.02%, respectively. The linear range was (0.005–16 $\mu\text{g mL}^{-1}$) and limits of detection were between 0.005 and 0.01 $\mu\text{g mL}^{-1}$ for each of the analytes. The relative standard deviations (R.S.D.) for 4 $\mu\text{g mL}^{-1}$ of TCAs in water were in the range of 5.6–6.4 ($n = 6$). The performance of the proposed technique was evaluated for determination of TCAs in blood plasma. © 2008 Elsevier B.V. All rights reserved.

Keywords: Antidepressant drugs; Dispersive liquid–liquid microextraction; Biological sample; Gas chromatography (GC); Flame ionization detector (FID)

1. Introduction

Amitriptyline is a tricyclic antidepressant (TCA) of the dibenzocycloheptene type and nortriptyline is its active metabolite. They are used for depression treatment, in management of the chronic and also served for neurogenic pains. Some efficiency has also been reported in phobic and panic disorder [1]. These drugs are chemically basic and in the market are in the forms of hydrochloride salts ($\log K_a$ are 9.4 and 9.7 for amitriptyline hydrochloride and nortriptyline hydrochloride, respectively) [2].

Conventional liquid–liquid extraction (LLE) has been widely used as an extraction and sample preparation method for many decades [3,4]. In the last 10 years, some researches are focused on the miniaturizing of analytical LLE, termed liquid phase microextraction (LPME) [5–9] that does not have LLE disad-

vantages and are extremely simple, cheap and virtually solvent free sample preparation technique [10–12].

Recently, Assadi and co-workers developed a novel LPME technique named dispersive liquid–liquid microextraction (DLLME) [13]. It is based on ternary component solvents system that is similar to homogeneous liquid–liquid extraction method (HLLE) [14,15] and also cloud point extraction (CPE) [16]. The advantages of DLLME method are simplicity of operation, rapidity, low cost, high recovery and enrichment factor. In the present work, the method was applied for analysis of amitriptyline and nortriptyline from blood plasma using gas chromatography–flame ionization detection (GC–FID).

2. Experimental

2.1. Chemicals and reagents

The drugs, amitriptyline hydrochloride; 1-propanamine, 3-(10,11-dihydro-5H-dibenzo[*a,d*]cyclohepten-5-ylidene) *N,N*-

^{*} Corresponding author. Tel.: +98 511 8797022; fax: +98 511 8796416.
E-mail address: asyazdi@ferdowsi.um.ac.ir (A.S. Yazdi).

dimethyl-hydrochloride and Nortriptyline hydrochloride; 1-propanamine,3-(10,11-dihydro-5H-dibenzo[*a,d*]cyclohepten-5-ylidene)-*N*-methyl-hydrochloride, were from Daropaksh. Co. (Tehran, Iran).

Organic solvents and analytical reagents: Chloroform, was obtained from Fluka (Buchs, Switzerland) while methanol, dichloromethane, nitrobenzene, tetrachloroethylene, carbon tetrachloride, isopropanol, acetonitrile, sodium chloride were from Merck (Darmstadt, Germany), sodium hydroxide was from Farabi Co. (Iran). Carbon disulfide was obtained from Riedel-de Haen (Hannover, Germany) and acetone was from AnalarR (BDH, England) (all of these reagents were of analytical grade). Doubly distilled water was used for preparation of aqueous solution.

Drug-free human plasma sample was obtained from a healthy male volunteer.

2.2. Instrumentation

Chromatographic analysis was performed on Chrompack CP9001 (Middelburg, The Netherlands) gas chromatography equipped with a split/split-less injector used in split mode and flame ionization detector (FID). Separations were conducted using a CP-Sil 24CB (50% phenyl, 50% dimethylsiloxane) capillary column, WCOT Fused silica, 30 M × 0.32 mm i.d. with

0.25 μm stationary film thickness (Chrompack, Middelburg, The Netherlands).

The carrier gas was ultra pure helium (99.999%, Sabalan Co., Iran) at a flow rate of 1.11 mL min⁻¹ and split ratio 46:1. The GC conditions were as follows: injector temperature 280 °C; initial oven temperature 100 °C for 1 min increased to 240 °C at a rate of 2 °C min⁻¹ and a second ramp to 260 °C at a rate of 2 °C min⁻¹. The total time for one GC run was 18 min.

The FID temperature was maintained at 280 °C. The flow of Zero Air (99.99%, Sabalan Co, Tehran, Iran) for FID was 250 mL min⁻¹ and flow rate of hydrogen was 30 mL min⁻¹.

The Hittich Scientific Centrifuge (model Hittich, UNIVERSAL, USA) was used for centrifuging.

2.3. Dispersive liquid–liquid microextraction procedure

A 5.00 mL of double-distilled water was placed in a 10 mL screw cap glass test tube with conic bottom and spiked at level of 4.00 mg L⁻¹ of TCAs. 1.00 mL of methanol (as a disperser solvent) and 18.0 μL of carbon tetrachloride (as an extraction solvent) were mixed and injected rapidly into the aqueous sample by syringe. The mixture was gently shaken. A cloudy solution (water/methanol/carbon tetrachloride) was formed in the test tube. In this step, the TCAs in water sample were extracted into the fine droplets of carbon tetrachloride. The mix-

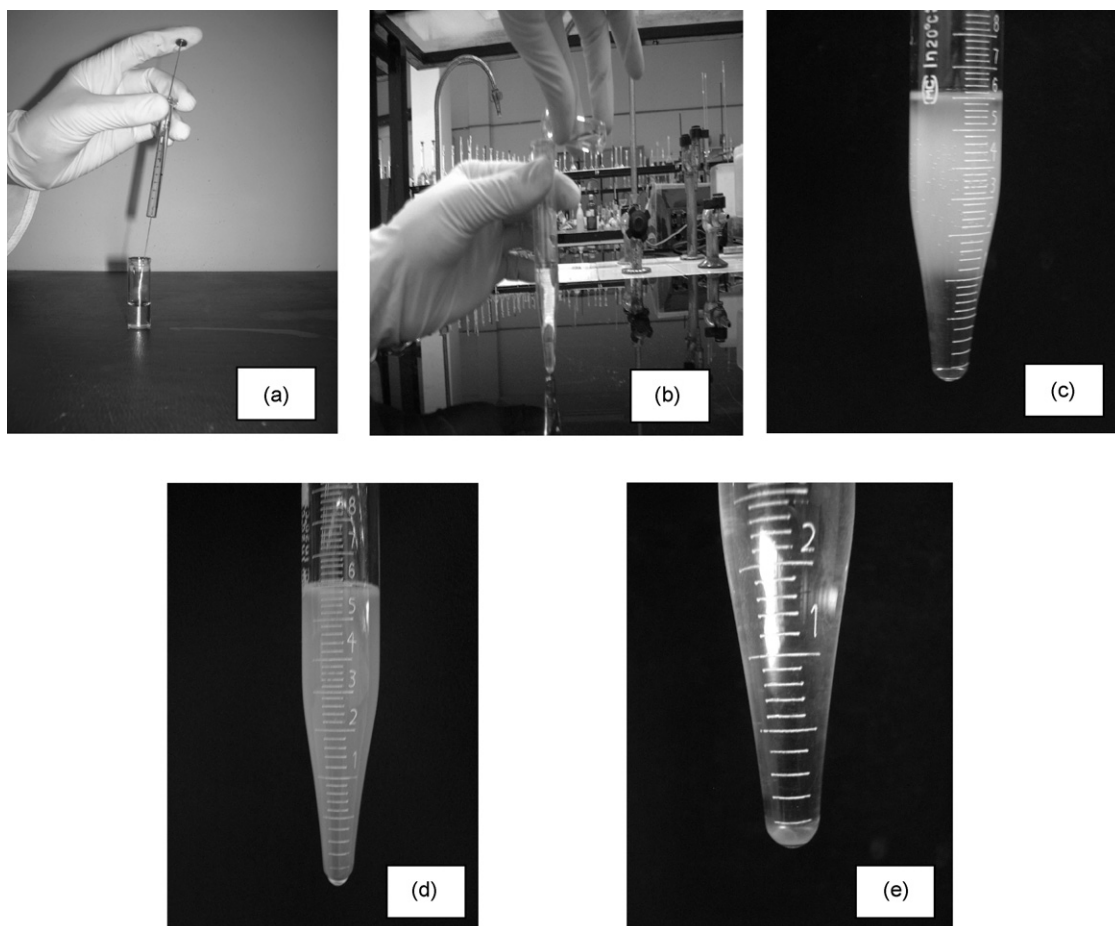


Fig. 1. Photography of different steps in DLLME: (a) before addition of mixture of disperser solvent (methanol) and extraction solvent (CCl₄) into sample solution, (b) starting of addition (c) end of addition (d) after shaking the tube and (e) after centrifuge and enlarged view of sedimented phase ($3.7 \pm 0.2 \mu\text{L}$).

Table 1
Physical properties of extraction solvents

Solvent	Structure and molecular weight	Boiling point (°C)	Density (g mL ⁻¹)	Solubility in 100 g of water
Carbon disulfide	CS ₂ , 76.14	46.26	1.2566	0.29
Carbon tetrachloride	CCl ₄ , 153.82	76.8	1.5842	0.08
Chloroform	CHCl ₃ , 119.38	61.2	1.4799	0.8
Dichloromethane	CH ₂ Cl ₂ , 84.93	39.8	1.25	1.3
Nitrobenzene	C ₆ H ₅ NO ₂ , 123.11	210.8	1.1987	0.19
Tetrachloroethene	C ₂ Cl ₄ , 165.83	121	1.6227	0.015

ture was then centrifuged for 10 min at 1000 rpm. Afterward the dispersed fine droplets of carbon tetrachloride were sedimented on the bottom of test tube. A portion of the sedimented phase (2.0 µL) was removed using 10 µL microsyringe (Hamilton Bonaduz AG, Bonaduz, Switzerland) and injected into GC. The volume of sedimented phase was determined using a 10 µL microsyringe which was about (3.7 ± 0.2 µL). The extraction steps are illustrated in Fig. 1.

2.4. Preparation of standard solutions and plasma sample

Stock solutions of amitriptyline and nortriptyline (100 µg mL⁻¹) were prepared by dissolving calculated amounts of each drug in methanol. They were stored at 4 °C in refrigerator, protected from light. Fresh working solutions (4 µg mL⁻¹) were prepared daily by diluting the stock solution in distilled water. The pH was adjusted to 12 by addition of NaOH (1 M).

2.5. Human plasma

Amitriptyline and nortriptyline are extensively bound to plasma proteins (91–97%) [2], and should be liberated prior to extraction. So, 1.00 mL methanol was added to 0.50 mL plasma. The mixed solution was centrifuged for 15 min at 1000 rpm. A volume of 0.05 mL of supernatant was transferred to test tube and diluted with water to 5.0 mL, the pH was adjusted to 12 with 1 M NaOH.

3. Result and discussion

In this study, DLLME combined with GC–FID was developed for determination of TCAs. There are several factors that affect the extraction process, like, extraction solvent, disperser solvent, volume of extraction solvent, volume of disperser solvent, pH of the aqueous solution, salting effect and extraction

time. The optimization was carried out on water solutions of 4 µg mL⁻¹ for each drug. The chromatographic peak area was used to evaluate the extraction efficiency under different experimental conditions.

3.1. Selection of extraction solvent

Choosing the most suitable extraction solvent is of primary importance for achieving good selectivity of the target compounds. Therefore, some factors should be considered, i.e., the solvent must be immiscible with water, the solubility of the analytes should be higher in the organic phase than the donor phase to promote the extraction of the analytes, good GC behavior and in the case of DLLME, the density of the extraction organic solvent must be higher than water [17,18]. Six solvents, which have these characteristics, were selected and their physical properties are collected in Table 1.

A series of sample solution were studied by using 1.00 mL of acetone and 20.0 µL of different kind of extraction solvents. After the addition of chloroform, carbon disulfide and dichloromethane not only the cloudy state was formed but also there was not sedimented phase on the bottom of the test tube after centrifugation. It was probably due to higher solubility of these solvents in water than the other tested solvents.

With nitrobenzene as an extraction solvent, the cloudy state was formed and remained constant even after centrifugation. In this case the sedimented organic phase was not appeared which may be due to the solvent–solvent interaction of homogeneous distribution throughout the solution. Carbon tetrachloride and tetrachloroethylene formed cloudy state and after centrifuging, the organic solvent separated from sample solution and sedimented on the bottom of test tube.

Three replicate tests were performed for each of these solvents under the same conditions. The results are shown in Table 2.

The extraction efficiency of carbon tetrachloride is higher than tetrachloroethylene (Table 2). Therefore, carbon tetra-

Table 2
Extraction solvent behaviors in DLLME

Analyte	CCl ₄ peak area	C ₂ Cl ₄ peak area	CHCl ₃ , CS ₂ , CH ₂ Cl ₂	C ₆ H ₅ NO ₂
Amitriptyline	360759.67	194929.67	Cloudy state was not formed.	Cloudy state was formed, and remained after centrifuging.
Nortriptyline	235025.33	125615	Extraction solvent was not separated from sample solution, after centrifuging.	

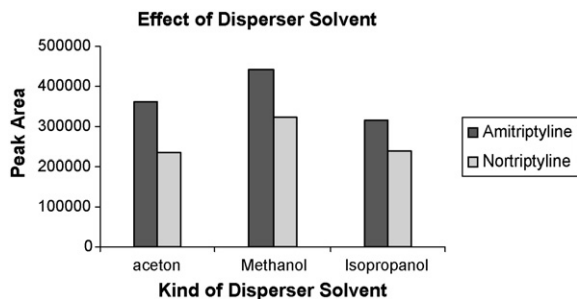


Fig. 2. Effect of disperser solvent on extraction efficiency. Extraction conditions: water sample volume, 5.00 mL; disperser solvent (acetone, isopropanol and methanol) volume, 1.00 mL; extraction solvent (CCl_4) 20.0 μL .

chloride was selected as extraction solvent for subsequent experiments.

3.2. Selection of disperser solvent

The disperser solvent must be miscible in extraction solvent (organic phase) and also sample solution (aqueous phase). Therefore, acetone, methanol and isopropanol were tested. A series of sample solutions were studied using 1.00 mL of each disperser solvent containing 20.0 μL carbon tetrachloride (as an extraction solvent). The effect of disperser solvent on analytical signal was shown in Fig. 2.

The maximum peak area was obtained by using methanol as a disperser solvent. That is due to its higher compatibility of methanol with aqueous solution than the other solvents [19]. Methanol was selected for further experiments.

3.3. Effect of extraction solvent volume

Variations in volumes of both extraction and disperser solvents cause change in the volume of the sedimented phase. For optimization of extraction solvent volume, different volumes of CCl_4 were added to 1.00 mL of methanol and these mixtures were subjected to the same DLLME procedures. Fig. 3 shows that by increasing the volume of CCl_4 , and therefore, sedimented phase volume, the peak area decreases. For the volumes less than 18.0 μL the sedimented phase volume was so little, that means the collection of it was too difficult. Therefore, the volume 18.0 μL was selected as optimal volume.

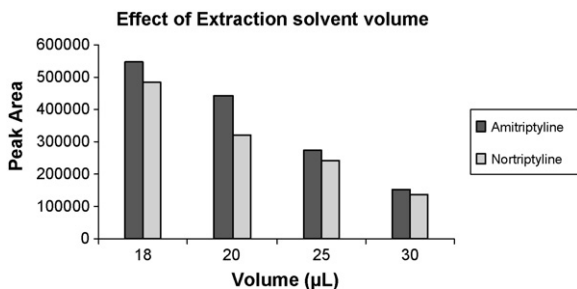


Fig. 3. Effect of the volume of carbon tetrachloride on extraction efficiency. Extraction conditions: water sample volume, 5.00 mL; extraction solvent (CCl_4), disperser solvent 1.00 mL methanol.

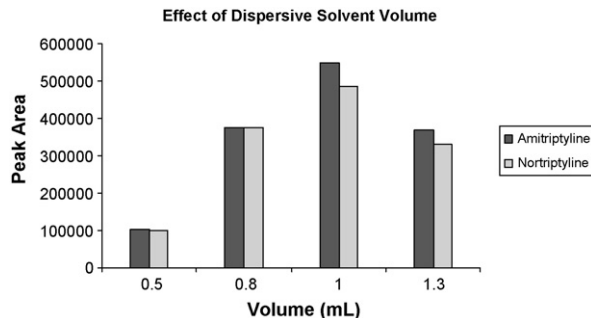


Fig. 4. Effect of volume of methanol on extraction efficiency. Extraction conditions: water sample volume, 5.00 mL; extraction solvent 18.0 μL CCl_4 , disperser solvent methanol.

3.4. Effect of disperser solvent volume

To examine the effect of disperser solvent volume, different volumes of methanol were added to 18.0 μL of CCl_4 . Fig. 4 shows that by increasing the methanol volume, in spite of producing better cloudy state, the sedimented phase volume is decreased. Therefore, up to 1.00 mL addition of methanol, peak area increases, afterward at higher volume of methanol the solubility of analytes in water increase and the extraction efficiency decrease. Therefore, 1.00 mL of methanol was selected as an optimal volume.

3.5. Effect of extraction time

The time of extraction is one of the most important factors in extraction procedures, especially in microextraction methods such as SPME and LPME. Extraction time in DLLME is defined as an interval time between injection of mixture of disperser solvent (methanol) and extraction solvent (CCl_4), and before starting to centrifuge. The time of extraction was examined in the range of 0–30 min with keeping experimental conditions constant [13]. Fig. 5 shows that the time of extraction has no significant effect in extraction efficiency. This is the most important advantage of DLLME technique. It is obvious that the surface area between extraction solvent and sample solution is infinitely large. Therefore, the mass transfer from sample solu-

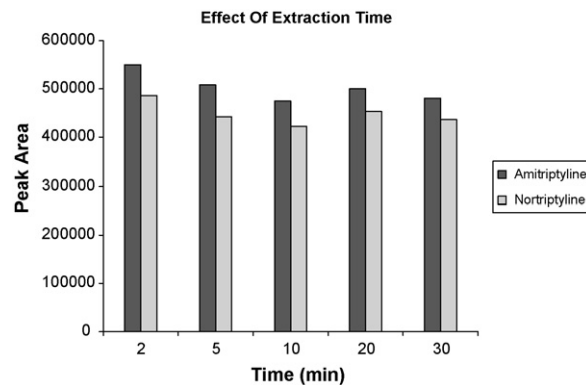


Fig. 5. Effect of extraction time on the peak area of TCAs obtained from DLLME. Extraction conditions: water sample volume, 5.00 mL; extraction solvent 18.0 μL CCl_4 , disperser solvent 1.00 mL methanol.

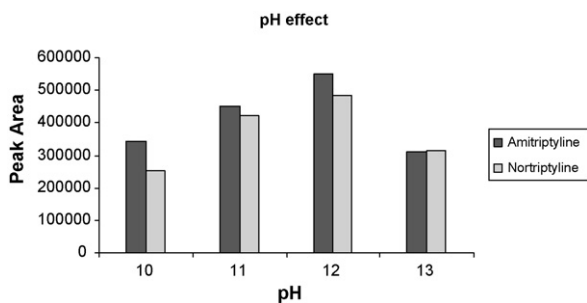


Fig. 6. Effect of aqueous solution pH on the extraction of analytes, peak area.

tion to extraction phase is fast. As a result, equilibrium state is achieved quickly which cause the extraction time to be short.

3.6. Effect of sample pH

The pH of aqueous feed solution which contains acidic or basic drugs should be controlled in the extraction process [20]. Amitriptyline and nortriptyline are basic compounds [2], therefore, the pH of the aqueous feed solution should be higher than the pK_a of the analytes. In this condition analytes are largely neutral and it is obvious that neutral form of organic compound has a greater tendency to extract into the organic solvent compared to the ionized form.

The pH of the sample solutions was changed in the range of 10–13 with addition of NaOH solution (1 M). Fig. 6 shows that, first the peak areas increase and then decrease. It may be explained that at the beginning, the analytes are in the form of amitriptyline and nortriptyline hydrochloride, by the addition of NaOH to the solution ionic forms of analytes will be converted to molecular forms and NaCl salt is also produced. The addition of NaOH (higher than pH 12) causes salting in effect due to spontaneously producing NaCl. This effect reduces the peak area. Therefore, the pH 12 was selected as an optimal pH.

3.7. Salt addition effect

In the extraction methods, the solubility of many analytes in aqueous solutions decreases with increasing ionic strength due to salting out effect [21].

The salt effect on extraction of antidepressant drugs was investigated by adding different amount of sodium chloride in the range of 0–10% w/v. As shown in Fig. 7, by addition of salt, a reverse effect on extraction efficiency is occurred.

The results indicate that by increasing the NaCl, the volume of sedimented phase increases because of the decreasing in solubility of extraction solvent in the presence of salt (salting in effect).

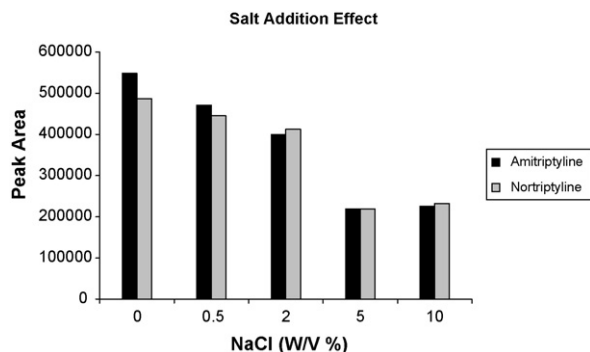


Fig. 7. Effect of addition of NaCl on the peak area. Extraction conditions: water sample volume, 5.00 mL; extraction solvent 18.0 μ L CCl_4 , disperser solvent 1.00 mL methanol; pH 12.

3.8. Validation of the method

3.8.1. Analytical performance

Calibration curves were drawn utilizing 10 spiking levels of drugs in concentrations between (0.004–20 μ g mL^{-1}) with respect to each analyte in distilled water. For each level three replicate extractions at optimal conditions (extraction organic solvent, 18 μ L carbon tetrachloride; disperser solvent, 1.00 mL methanol; and pH 12) were performed and two calibration curves were drawn.

The correlation coefficients (R^2), dynamic linear ranges (DLR) and the limits of detection (LOD) were calculated and shown in Table 3 [22,23]. Limits of detection were calculated as the minimum concentration providing chromatographic signals minimum 3 times higher than background noise. LODs were determined in distilled water [5]. Repeatability (R.S.D.) was evaluated on six replicate experiments at 4 μ g mL^{-1} concentration (Table 3).

Eqs. (1) and (2) were used for calculation of enrichment factor and recovery.

$$E_F = \frac{C_{sed}}{C_0} \quad (1)$$

where E_F , C_{sed} and C_0 are the enrichment factor, concentration of analyte in sedimented phase and initial concentration of analyte in aqueous sample, respectively.

$$R\% = \frac{V_{sed}C_{sed}}{V_{aq}C_0} \times 100 \quad (2)$$

$$R\% = \left(\frac{V_{sed}}{V_{aq}} \right) E_F \times 100 \quad (3)$$

Table 3
Quantitative results of DLLME and GC-FID

Compound	Linearity range (μ g mL^{-1})	Correlation coefficient (R^2)	LODs (μ g mL^{-1}) ($n=6$)	R.S.D. (%)	Enrichment factor (C_{sed}/C_a)	Recovery % ($C_{sed}/C_a \times 100$)
Amitriptyline	0.005–16	0.9960	0.005	5.6	740.04	54.76%
Nortriptyline	0.02–16	0.9972	0.01	6.4	1000.25	74.02%

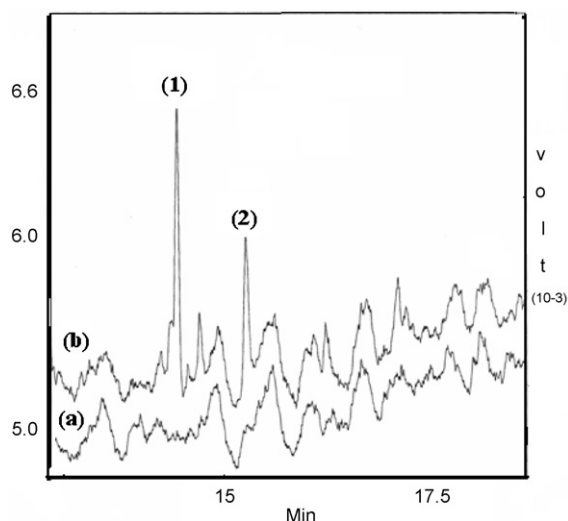


Fig. 8. Chromatogram of drug-free plasma (a), plasma contains $0.067 \mu\text{g mL}^{-1}$ of each analyte (b) 1. amitriptyline, 2. nortriptyline.

where $R\%$, V_{sed} and V_{aq} are the percent of extraction recovery, volume of sedimented phase and volume of aqueous sample, respectively.

In order to examine the enrichment factor of each analyte, three replicate extractions were performed at optimal conditions from aqueous solutions consisting $4 \mu\text{g mL}^{-1}$ amitriptyline and nortriptyline. The enrichment factor was calculated as the ratio of final concentration of analytes in sedimented phase and its concentration in the original solution. The standard solutions of TCAs were prepared in carbon tetrachloride as solvent and the calibration curves were drawn ($4.00\text{--}30.00 \text{ mg L}^{-1}$). Finally, the actual concentration of each analyte in carbon tetrachloride was calculated from this calibration curves and the enrichment factors were determined and summarized in Table 3.

3.8.2. Human plasma

Plasma samples were prepared as mentioned in Section 2.4. Chromatograms of drug-free plasma and a plasma sample containing $0.067 \mu\text{g mL}^{-1}$ of each substance are shown in Fig. 8.

LPME is not exhaustive extraction method, so the relative recovery was determined as the ratio of the concentration founded in real samples and distilled water sample, with both samples spiked at the same concentration level [19,20]. Under the optimized conditions the relative recovery that was obtained for amitriptyline and nortriptyline in plasma sample were 69.17% and 48.23%, respectively. The relative standard deviations (R.S.D.s) ($4 \mu\text{g mL}^{-1}$) in plasma 6.1% for amitriptyline, and 8.4% for nortriptyline. The calibration graphs were linear in the range of ($0.007\text{--}21 \mu\text{g mL}^{-1}$) for amitriptyline and ($0.03\text{--}24 \mu\text{g mL}^{-1}$) for nortriptyline in plasma. LODs (0.007 and $0.02 \mu\text{g mL}^{-1}$) for amitriptyline and nortriptyline, respectively.

4. Conclusion

This method provides high recovery and enrichment factor within a very short time. Solvent consumption was greatly

reduced compared to conventional LLE and low detection limits were achieved. The comparison of the data obtained with this method, with other LPME methods such as SDME in our laboratory, like the enrichment factors show a very good advantage of DLLME. The efficiency factors (EF) with DLLME and SDME methods are (740.04–1000.25) and (89.5–139), respectively. The detection limits of Am. and Nor. are also improved in DLLME ($0.005\text{--}0.01 \mu\text{g mL}^{-1}$) in comparison with single drop microextraction ($0.01\text{--}0.02 \mu\text{g mL}^{-1}$) [24].

Despite of several advantages of DLLME, this method is not well compatible for extraction from biological samples such as urine, plasma and hair. Due to the interaction of matrix components in this kind of samples with organic solvent, it is not possible to produce sedimented phase for injection to GC. To obtain the sedimented phase in this kind of real samples, we have to make several dilutions. This treatment has got two opposite effects. From the first view, this high dilution of the real sample causes changing the inherent property of the matrix. And this is the disadvantage of the method, unless the method uses just for biological samples that were spiked with high concentration level of drugs. From the second view, the method is very good for environmental water samples.

Acknowledgements

This work was financially supported by Ferdowsi University of Mashhad, Iran. The authors are grateful to Dr. Z. Es'haghi for the kind helps.

References

- [1] D. Bose, A. Durgbanshi, A. Matinavarro, M. Capella-Peiro, J. Esteve-Romero, M. Gil-Agusti, J. Pharmacol. Toxicol. Methods 52 (2005) 323.
- [2] A.C. Moffat, Clarks analysis of drugs and poisons in pharmaceuticals body fluids and post mortem material, third edition, Pharmaceutical Press, London, 2004.
- [3] R. Theurillat, W. Thormann, J. Pharm. Biomed. Anal. 18 (1998) 751.
- [4] T. Gunnar, S. Mykkänen, K. Ariniemi, P. Lillsunde, J. Chromatogr. B 806 (2004) 205.
- [5] E.M. Gioti, D.C. Skalkos, Y.C. Fiamegos, C.D. Stalikas, J. Chromatogr. A 1093 (2005) 1.
- [6] C. Deng, N. Li, L. Wang, X. Zhang, J. Chromatogr. A 1131 (2006) 45.
- [7] C. Deng, X. Yang, X. Zhang, Talanta 68 (2005) 6.
- [8] E. Zhao, L. Han, S. Jiang, Q. Wang, Z. Zhou, J. Chromatogr. A 1114 (2006) 269.
- [9] M. Khalili-Zanjani, Y. Yaminia, N. Yazdanfarb, S. Shariatia, Anal. Chim. Acta 606 (2008) 202.
- [10] A. Sarafraz Yazdi, Z. Es'haghi, Talanta 66 (2005) 664.
- [11] H.G. Ugländ, M. Krogh, E. Rasmussen, J. Chromatogr. B 749 (2000) 85.
- [12] A. Sarafraz Yazdi, H. Assadi, Chromatographia 60 (2005) 699.
- [13] M. Rezaee, Y. Assadi, M.-R. Milani Hosseini, E. Aghaee, F. Ahmadi, S. Berijani, J. Chromatogr. A 1116 (2006) 1.
- [14] A.R. Ghiasvand, S. Shadabi, E. Mohagheghzadeh, P. Hashemi, Talanta 66 (2005) 912.
- [15] S. Igarashi, N. Ide, Y. Takagai, Anal. Chim. Acta 424 (2000) 263.
- [16] R. Carabias-Martínez, E. Rodríguez-Gonzalo, B. Moreno-Cordero, J.L. Pérez-Pavon, C. García-Pinto, E. Fernández Laespada, J. Chromatogr. A 902 (2000) 251.
- [17] D.K. Dubey, D. Padasani, J. Chromatogr. A 1107 (2006) 29.

- [18] S. Berijani, Y. Assadi, M. Anbia, M. Milani Hosseini, E. Aghae, *J. Chromatogr. A* 1123 (2006) 1.
- [19] S.C. Sweetman, Martindale, The Complete drug reference 33rd edition 2002, Pharmaceutical Press, Great Britain.
- [20] R. Zhao, S. Chu, X. Xu, *Anal. Sc.* 20 (2004) 663.
- [21] Y. Marcus, Ion Solvation, Wiley, New York, 1985, p. 365.
- [22] C. Basheer, H.K. Lee, J.P. Obbard, *J. Chromatogr. A* 1022 (2004) 161.
- [23] M.B. Melwanki, S. Huang, *Anal. Chim. Acta* 555 (2006) 139.
- [24] A. Sarafraz Yazdi, N.H. Razavi, unpublished work (in press).

Development and application of a capillary electrophoresis–electrochemiluminescent method for the analysis of enrofloxacin and its metabolite ciprofloxacin in milk

Xiaoming Zhou, Da Xing*, Debin Zhu, Yabing Tang, Li Jia

MOE Key Laboratory of Laser Life Science & Institute of Laser Life Science, South China Normal University, Guangzhou 510631, China

Received 18 September 2007; received in revised form 15 January 2008; accepted 18 January 2008

Available online 30 January 2008

Abstract

Enrofloxacin (ENR) is a fluoroquinolone developed exclusively for the use in veterinary practice for the treatment of respiratory and gastrointestinal infections, and ciprofloxacin (CIP) is its main active metabolite. Their contents are regulated by the EU Council Regulation no. 2377/90 in animal edible tissues. We developed a sensitive and rapid method for the determination of ENR and CIP by capillary electrophoresis (CE) with electrochemiluminescence (ECL) detection. The method is based on the detection of aliphatic tertiary or secondary amino moieties in ENR and CIP with end-column tris(2,2-bipyridyl)ruthenium(II) electrochemiluminescence. Parameters that affect separation and detection were optimized. Under the optimized conditions, the calibration functions were linear in the range of 0.03–1 $\mu\text{g ml}^{-1}$ for ENR and 0.05–1.2 $\mu\text{g ml}^{-1}$ for CIP. The detection limits of ENR and CIP were 10 ng ml^{-1} and 15 ng ml^{-1} , respectively, based on the signal-to-noise ratio of 3. The relative standard derivations of the peak height and the migration time for ENR and CIP were less than 4.13%. The developed method was successfully applied to determine ENR and CIP in milk with a solid-phase extraction procedure.

© 2008 Elsevier B.V. All rights reserved.

Keywords: Electrochemiluminescence; Capillary electrophoresis; Enrofloxacin; Ciprofloxacin; Milk

1. Introduction

Quinolones are an important group of synthetic antibiotics with bactericidal action. They are derived from nalidixic acid, a naphthyridine derivative introduced for clinical applications in the livestock and farming industries [1]. Enrofloxacin (ENR) is a fluoroquinolone developed exclusively for the use in veterinary practice for the treatment of respiratory and gastrointestinal infections. It is an extended spectrum antimicrobial drug that has been employed successfully in the treatment of a variety of infections caused by susceptible bacterial pathogens in food animals [2]. The pharmacokinetic properties of ENR have been studied in a number of mammals and aquatic animals, such as cows [3], goats [4], sea bass [5], and juvenile Atlantic salmon [6]; and ENR's active ciprofloxacin (CIP), derived by ENR deethylation,

was investigated in these animals. ENR and CIP are representatives of stimulants that belong to amine species. The molecular structures of ENR and CIP are shown in Fig. 1.

In the recent years, the utilization of antibiotics in food-producing animals has caused public concern due to the transfer of antibiotic-resistant bacteria to man [7]. This is an increasingly prominent problem because antibiotics are used in animals to treat infections and to act as growth promoters, this will lead to the antibiotic-resistant strains can emerge in both healthy and sick animals. This fact would make the antibiotics treatment useless in common human infections. European Community (EC) has fixed a maximum residue limit (MRL) in edible animal products for some quinolones, such as ENR and its metabolite CIP. The MRL values are in the range 100–300 $\mu\text{g kg}^{-1}$ for the sum of ENR and CIP in foodstuffs of animal origin [8]. Therefore, the development of rapid, simple, sensitive, and accurate methods for monitoring their levels in animal-producing foods is of increasing interest. Chromatographic methods such as high-performance liquid chromatography (HPLC) combined with either ultraviolet or fluorescence and mass spectrometry

* Corresponding author. Tel.: +86 20 85210089.

E-mail address: xingda@sclu.edu.cn (D. Xing).

URL: <http://laser.sclu.edu.cn/xingda.htm> (D. Xing).

(MS) detection have been widely studied and were commonly used to analyze quinolone residues in biological samples [9–14]. However, these HPLC-based methods are sometimes limited by poor separation efficiencies, expensive columns, and the consumption of relatively high amounts of buffer solutions and organic solvents. Some non-chromatographic methods, such as luminescence spectroscopy [15,16], immunoassays [17,18], have also been reported for the determination of quinolones including ENR and CIP. Problems encountered by these methods include lack of required selectivity for complex mixtures, or only allow semi-quantitative analysis. Capillary electrophoresis (CE) seems to have potential for the analysis of quinolones. The advantages of CE for quinolones analysis include its speed and cost of analysis, reductions in solvent consumption and disposal, and the possibility of rapid method development. CE combined with ultraviolet (UV) detection [19,20], MS [7,21,22], or laser-induced fluorescence (LIF) [23], amperometric detection (AD) [24,25] for quinolones analysis has been reported. The UV detection is relatively non-specific and the achievable sensitivity is limited. LIF and MS can offer higher detection sensitivity, but the expensive instruments limit extensive application. AD shows high sensitivity and cheap facility. However, the detection of AD is easily affected by the high-voltage (HV) electric field and the adsorption of analytes on the working electrode [26,27]. Electrochemiluminescence (ECL) is a kind of chemiluminescence produced directly or indirectly as a result of electrochemical reactions. ECL detection, emerging as a very sensitive mode of detection, has many advantages including its simplicity, inexpensive instrumentation, low background noise, high sensitivity, good selectivity, and wide dynamic linear range [28–31]. The marriage of CE to ECL is a sensitive and efficient analytical technique and has got excellent performance for the analysis of amino acids [32,33], alkaloids [34,35], drugs [36–38], herbicide [39], and enzyme activities [40,41]. The purpose of this study is to develop a new simple and sensitive CE–ECL method for the analysis of ENR and CIP in milk

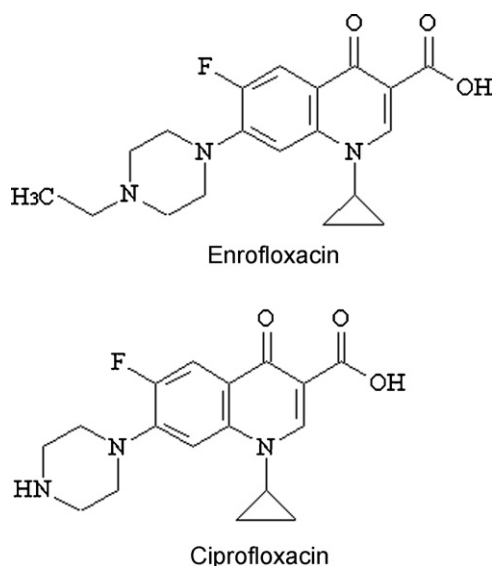
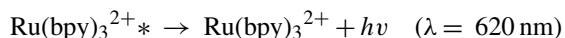
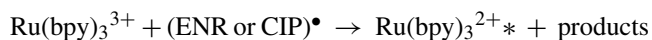
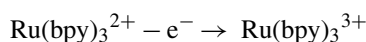


Fig. 1. Molecular structures of ENR and CIP.

samples. The method is based on the capillary electrophoretic separation and the detection of aliphatic tertiary or secondary amino moieties in ENR and CIP with end-column tris(2,2'-bipyridyl)ruthenium(II) electrochemiluminescence. The pathway of this $\text{Ru}(\text{bpy})_3^{2+}/(\text{ENR and CIP})$ system is similar to the reaction of $\text{Ru}(\text{bpy})_3^{2+}$ with alkylamines which was firstly proposed by Noffsinger and Danielson [42]. It can be expressed as follows:



In this study, samples cleanup and further preconcentration were executed by solid-phase extraction (SPE). Some parameters that affect separation and detection conditions were discussed in detail. The detection limits obtained in this work are low enough to determine concentrations below the permissible MRL in milk.

2. Experimental

2.1. Chemicals and materials

Tris(2,2'-bipyridyl)ruthenium(II) chloride ($\text{Ru}(\text{bpy})_3\text{Cl}_2$, 98%) was purchased from Aldrich (Milwaukee, WI, USA). Pure powder of ENR ($\geq 98\%$) and CIP ($\geq 98\%$) was obtained from Sigma (St. Louis, MO, USA). Water ($\geq 18.2 \text{ M}\Omega$) used throughout the experiments was generated by a Milli-Q water purification system (Millipore, Bedford, MA, USA). All other reagents were of analytical grade. All solutions for CE were stored in the refrigerator at 4°C prior to use. The solutions were made up to volume with appropriate buffer. The solutions used throughout the experiments were all passed through $0.22\text{-}\mu\text{m}$ filters before being injected into the CE system. Oasis HLB cartridges (60 mg, Waters, Milford, MA, USA) were used in the procedure of SPE.

2.2. Apparatus and equipments

A programmable high-voltage power supply (0–20 kV, Xi'an Remax Electronics Co. Ltd., Xi'an, China) was applied to perform the electrokinetic sample injection and electrophoretic separation. ECL detection was carried out with a MPI-A capillary electrophoresis ECL detector (Xi'an Remax Electronics Co. Ltd., Xi'an, China), using a three-electrode system consisting of a $300\text{-}\mu\text{m}$ diameter platinum wire as working electrode, Ag/AgCl (KCl saturated) as reference electrode, and a platinum wire as counter electrode. Before use, the working electrode surface was polished with $0.3 \mu\text{m}$ α -alumina powder and washed with water in an ultrasonic cleaner. A $300\text{-}\mu\text{l}$ aliquot of 100 mM pH 8.5 phosphate buffer containing 5 mM $\text{Ru}(\text{bpy})_3^{2+}$ was added to the cell for CE–ECL detection and replaced every 3 h. The photons were captured by PMT which was located in the lower

layer of detection cell. The voltage of PMT was set at 800 V in the process of detection. An uncoated fused-silica capillary with 50 cm length, 50 μm i.d., and 360 μm o.d. was used for separation (Yong Nian Optical Fiber Factory, Hebei, China). The capillary-to-electrode distance was fixed at 120 μm according to the previous optimization [43].

2.3. Electrophoretic procedure

Running buffer solutions were prepared with NaH_2PO_4 and Na_2HPO_4 at different concentrations and pH was adjusted with NaOH and H_3PO_4 . For preconditioning, the capillary was pre-treated by rinsing at high pressure with 1 M NaOH for 10 min, followed by pure water for 10 min, and phosphate electrolyte for 15 min. In order to obtain better reproducibility, between runs, the capillary was rinsed at high pressure with 0.1 M NaOH for 1 min, pure water for 2 min, and buffer for 3 min. The injection was done electrokinetically and CE was executed in room temperature.

2.4. Standard solutions

A standard solution containing ENR and CIP was first dissolved in methanol as a stock solution at concentration of 1 mg ml^{-1} and stored in refrigerator at 4 $^\circ\text{C}$. Working standard solutions were prepared daily with designated concentration by diluting the stocking standard solutions in 0.1% acetic acid.

2.5. Extraction procedure

The extraction procedure of ENR and CIP used here was a modification of the technique reported by Barbosa and coworkers [44]. A 5-g aliquot of milk purchased from a local supermarket was accurately weighed in a 50-ml test tube and spiked with ENR and CIP at different concentration levels. The sample was shaken on a vortex mixer for 30 s and then allowed to stand at 4 $^\circ\text{C}$ in the dark, for at least 20 min, to enable sufficient equilibration with the milk matrix. Then 1.5 ml of 0.1 M phosphate buffer (pH 7.4) and 20 ml of dichloromethane were added to the sample in order to extract the ENR and CIP. After agitating for 10 min the sample was centrifuged for 10 min at 3500 rpm. The organic phase was transferred into a 50 ml heart-shaped flask and the sample was re-extracted with another 10 ml portion of dichloromethane. The organic extracts were combined and 1 ml of 3 M H_3PO_4 was added. Dichloromethane was evaporated under vacuum in a rotary evaporator at room temperature until only aqueous phase remains. The above mixture was defatted with 10 ml of hexane. After centrifugation, the aqueous phase was passed through the HLB cartridge, which was previously conditioned with 2 ml of methanol and 2 ml of water. The cartridge was then washed with 2 ml of water and vacuum-dried. ENR and CIP were eluted from the cartridge with 3 ml of methanol. The eluent was evaporated to dryness at 40 $^\circ\text{C}$ under a stream of nitrogen. The residue was reconstituted in 500 μl of 0.1% acetic acid.

3. Results and discussion

3.1. Optimization of CE–ECL conditions

3.1.1. Effects of detection potential

The ECL intensity is dependent on the rate of the light-emitting chemical reaction, and this reaction rate relies on the detection potential. Therefore, the potential applied to the working electrode directly affected the detection sensitivity. In order to obtain best detection results, optimum potential applied to the working electrode should be selected. In this study, the effect of detection potential from 1.0 V to 1.4 V on the signal intensities of both ENR and CIP was investigated. As can be seen from Fig. 2, the signal intensity of the two analytes exhibited same dependence on the detection potential. Increase in detection potential from 1.0 V to 1.15 V resulted in a strong increase in the signal intensity of ENR and CIP. The reason may be that the relative low oxidation rate of $\text{Ru}(\text{bpy})_3^{2+}$ at the surface of electrode when applied potential was below 1.15 V and reached its maximum oxidation rate at 1.15 V. However, with the increasing detection potential from 1.15 V to 1.4 V, the signal intensity of both ENR and CIP decreased, possibly due to the oxidation of water which has negative effect on the ECL intensity. Thus, 1.15 V was chosen as the detection potential for further determination of the two analytes.

3.1.2. Effects of separation voltage

Both the electroosmotic and electrophoretic velocities are directly proportional to the field strength, so the micro-environment of the outlet of capillary aligned with the working electrode will be affected by the effluent from the capillary when separation voltage was changed. Based on this fact, the effect of separation voltage on and ECL intensity was investigated in the range of 8–20 kV. In these experiments it was found that ECL intensity increased and reached the maximum value at 14 kV for both ENR and CIP. This was also increased due to electroos-

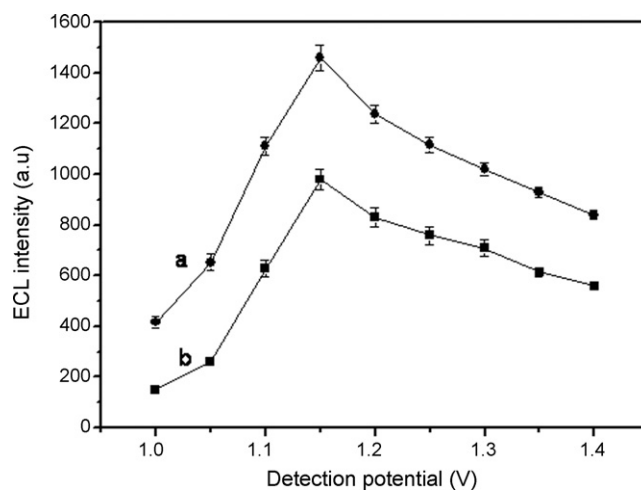


Fig. 2. Effect of detection potential on the ECL intensity ($5 \mu\text{g ml}^{-1}$ standard solutions): (a) ECL intensity of ENR and (b) ECL intensity of CIP. Conditions—electrokinetic injection: 10 s at 10 kV and separation voltage: 14 kV.

mosis and more analytes in the effluent arrived in the diffusion layer of working electrode within a given time [37]. When the separation voltage exceeded 14 kV, the ECL intensity decreased, at the same time the noise of the background increased with the voltage, possibly due to the effect of high joule heat. On the other hand, the strong flow of effluent from the capillary decreased the concentration of $\text{Ru}(\text{bpy})_3^{2+}$ at the working electrode surface, thereby reducing the efficiency of ECL reaction. For this reason, 14 kV was chosen as the optimum in the following experiments.

3.1.3. Effects of running buffer concentration and pH

An investigation of running buffer concentration was performed. Although buffer concentration has various influences on this CE–ECL method, for example, migration time, resolution, and ECL intensity, sensitivity is one of the most important parameters in the trace analysis. So, ECL intensity was carefully examined when the buffer concentration changed from 5 mM to 40 mM. Results have shown that the highest ECL intensity was obtained at a running buffer concentration of 15 mM. Higher buffer concentration had a negative effect on the ECL intensity, perhaps because other ions replace $\text{Ru}(\text{bpy})_3^{2+}$ in the vicinity of the working electrode.

Besides the running buffer concentration, its pH value is also an important parameter because of its effect on the electroosmotic flow (EOF) as well as the net charge of the ENR and CIP. Because both ENR and CIP have two pK values, the pK_1 values of ENR and CIP are 5.86 and 5.88, respectively, and the pK_2 values of ENR and CIP are 8.24 and 7.74, respectively. In acidic running buffer the cationic species should be predominant while the basic pH of the running buffer should have shifted the equilibrium to the right, leaving the anionic species predominant for both the ENR and CIP. Previous reports have indicated that basic pHs provide better separation of quinolones than acidic pHs acidic buffer, possibly due to interactions on the interior capillary wall of the predominantly cationic form of quinolones and lack of an EOF [21]. Barbosa and coworkers have also established the model for predicting the optimum pH range for the separation of ENR and CIP, it is deduced that the best separation is around pH 8 [19]. On the other hand, the ECL response is also pH-dependent because the oxidation of alkylamines occurs only in their deprotonated form and at very low pH values the ENR and CIP radical cations are difficult to deprotonate to form high reducing free radical intermediate which is critical for ECL reaction. For these reasons, acidic buffer could not be assayed in this study. Therefore, the effect of the pH of running buffer on CE separation and ECL intensity was investigated in the pH range of 7.0–9.0 (7.0, 7.5, 8.0, 8.5, and 9.0). As shown in Fig. 3, it was found that the peak of ENR and CIP was completely overlapped at pH 7.0. With the increase of the pH of running buffer, the separation of ENR and CIP was improved gradually. Finally, baseline separation can be reached when background electrolyte was set at pH 8.5. But above this value there was no improvement in the resolution. As was expected, ECL intensity also showed the similar tendency. We noted that the ECL intensity decreased when the buffer pH exceeded 8.5. The reason of the decrease of the ECL intensity can be ascribed to the reduced availability of $\text{Ru}(\text{bpy})_3^{3+}$ due to the competitive reaction with

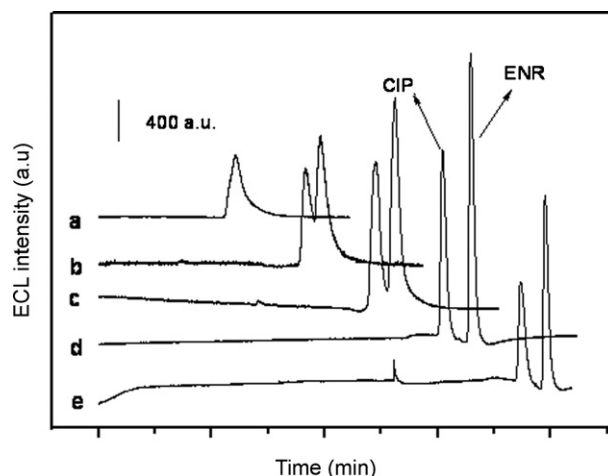


Fig. 3. Electropherograms showing the effect of the running buffer pH on the ECL intensity and separation ($5 \mu\text{g ml}^{-1}$ standard solutions): (a) pH 7, (b) pH 7.5, (c) pH 8, (d) pH 8.5 and (e) pH 9. Conditions—detection potential: 1.15 V, 15 mM phosphate running buffer (pH 8.5), electrokinetic injection: 10 s at 10 kV and separation voltage: 14 kV. Note that the time axes for the electropherograms were shifted horizontally for clarity of presentation.

the OH^- ion which assumes considerable concentration levels at high pHs [45]. For a comprehensive thought, the buffer pH value of 8.5 was chosen to obtain sensitive ECL response and high separation efficiency.

3.1.4. Effect of injection time

In order to avoid excessive heat generation and bubble formation under these high electric field strength conditions, we chose 10 kV as the injection voltage. For injection time optimization, the studied interval was from 5 s to 30 s. The effect of the injection time on resolution was also investigated. The resolution (R_s) between ENR and CIP was calculated with the following equation: $R_s = 2(t_2 - t_1)/(W_{b1} + W_{b2})$, where t_1 and t_2 are migration times of CIP and ENR, respectively, W_{b1} and W_{b2} are the peak widths at half-height of CIP and ENR, respectively. Generally, at larger injection time, more analytes appeared at the working electrode, which produced a higher ECL signal. However, the sample zone may expand in the capillary during its running, which will lead the deterioration of resolution. In our experiments, the ECL intensity of both ENR and CIP increased with the increase of injection time in the range of 5–25 s. When the injection time exceeded 15 s, the resolution got deteriorated gradually (Fig. 4). We noted that the resolution was satisfactory even though the injection time extended as long as 20 s, and attended by a remarkable enhancement of sensitivity. Therefore, we selected 20 s as the injection time for subsequent experiments. The phenomena can be generally referred to as a stacking effect. A rational explanation is that sample injection was performed electrokinetically, and separation was performed using a basic background electrolyte (pH 8.5), 0.1% acetic acid used as samples solvent, which may prompt the protonation of analytes. When high voltage was applied, a discrete pH step was formed and literally stacked charged analytes at the interface of the sample and background electrolyte zones.

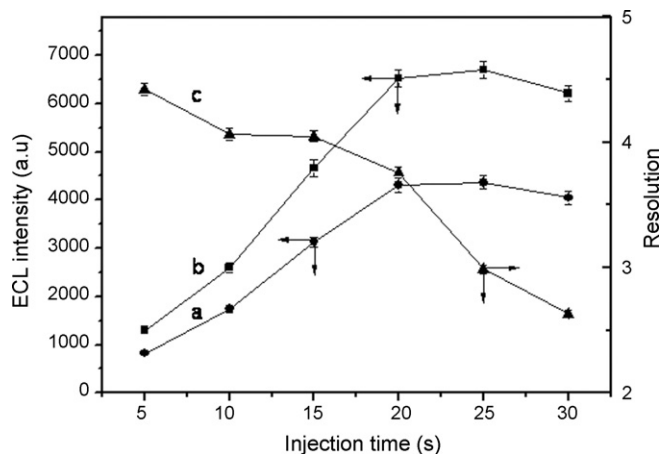


Fig. 4. Effect of injection time on ECL intensity and resolution ($5 \mu\text{g ml}^{-1}$ standard solutions): (a) ECL intensity of CIP, (b) ECL intensity of ENR and (c) resolution between ENR and CIP. Conditions—detection potential: 1.15 V, 15 mM phosphate running buffer (pH 8.5) and separation voltage: 14 kV.

3.2. Linearity, repeatability, detection limit of ENR and CIP

Under optimized experimentation conditions: detection potential 1.15 V, separation voltage 14 kV, 15 mM phosphate running buffer (pH 8.5), injection voltage 10 kV and injection time 20 s, the different concentrations of ENR and CIP were measured from $0.01 \mu\text{g ml}^{-1}$ to $1.5 \mu\text{g ml}^{-1}$. It was found that calibration was linear over concentration ranges of $0.03\text{--}1 \mu\text{g ml}^{-1}$ and $0.05\text{--}1.2 \mu\text{g ml}^{-1}$ for ENR and CIP, respectively. Regression analysis of the calibration data was performed by the use of OriginPro 7.5. The calibration equations and regression coefficients were $y = 1438(\pm 40)x + 32(\pm 13)$ and $R = 0.998$ for ENR, $y = 810(\pm 26)x + 45(\pm 18)$ and $R = 0.997$ for CIP. The calibration graphs of ENR and CIP are shown in Fig. 5. Limits of detection (LOD) were evaluated, by comparing signals from low concentrations of analytes with those from blank samples, and establishing the minimum concentrations at which the analytes could be detected reliably, on the basis of signal-to-noise ratio of

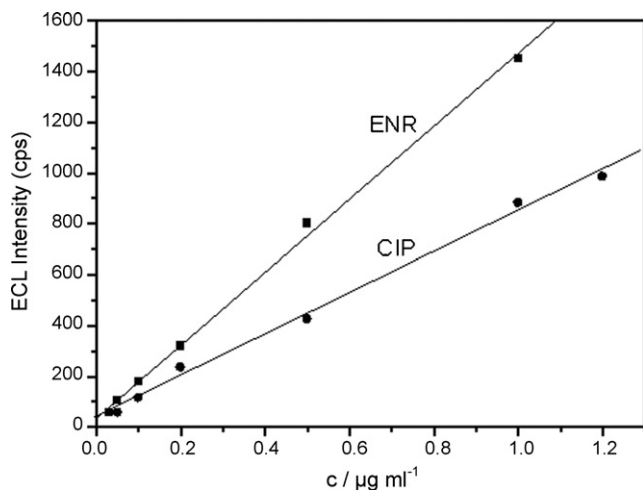


Fig. 5. The calibration graphs of ENR and CIP. Conditions—detection potential: 1.15 V, separation voltage: 14 kV, 15 mM phosphate running buffer (pH 8.5), injection voltage: 10 kV and injection time: 20 s.

3. For ENR and CIP the LOD were 10 ng ml^{-1} and 15 ng ml^{-1} , respectively. The repeatability of the method was studied by six consecutive injections of standard solution of both ENR and CIP at $1 \mu\text{g ml}^{-1}$. Relative standard derivations (R.S.D.s) of the ECL intensity and the migration time were 4.13% and 1.16% for ENR and 3.25% and 0.84% for CIP, respectively.

3.3. Application to milk sample

The developed CE–ECL method in this report was applied to the separation and determination of ENR and CIP in milk samples. On account of the complexity of the milk samples which contain large concentrations of fat and proteins, thus samples need to be pretreated before to perform CE separation. In general, liquid–liquid extraction and SPE are the most frequently used methods to extract quinolones from complex samples. In this study, attempts were initially made to analyze ENR and CIP with a liquid–liquid extraction procedure. However, this proved unsuccessful as numerous interfering peaks appeared in the electropherogram. Therefore, additional sample preparation was required and involved off-line SPE to remove interfering compounds. For SPE procedure, there are different available solid-phase cartridges (for example, ion-exchange cartridge, polymeric phase cartridge, and reversed-phase exchange cartridge) which can be utilized for quinolones (include ENR and CIP) extraction from biological samples. Literature searches have revealed that the highest recoveries can be obtained for both ENR and CIP that was used a polymeric phase HLB cartridge [7,11,44]. Thus, HLB cartridge was chosen for this experiment. The detailed extraction procedure was described in Section 2. Chiefly, proteins and the fat were eliminated by solvent extraction using dichloromethane and hexane. Then the cleaner extracts obtained were used later for a second step using HLB cartridges to eliminate salts and a preconcentration factor 10 was applied. This method was validated using milk samples spiked with several levels of standard ENR and CIP mixture, and subjected to the entire extraction procedure. Recovery studies were determined by comparing the spiked sample peaks with an externally generated calibration curve at three concentration levels. The recoveries data are reported in Table 1. The mean recoveries were 77.4% for CIP and 80.6% for ENR, and R.S.D. was lower than 10% for both ENR and CIP. Calibration parameters in spiked milk samples were determined and were summarized in Table 2. The LOD and

Table 1
Recovery for ENR and CIP at different spiked levels in milk samples

Spiked concentration ($\mu\text{g kg}^{-1}$)	Recovery (%)	R.S.D. (%) ($n = 3$)
CIP		
20	76.3	9.21
40	78.7	8.33
80	77.4	8.12
ENR		
20	79.6	8.48
40	80.8	7.36
80	81.4	7.71

Table 2
Calibration parameters in spiked milk samples

	ENR	CIP
Linearity ($\mu\text{g kg}^{-1}$)	5–400	8–400
Calibration equation ^a	$y = 10.1(\pm 0.4)x + 22.4(\pm 10.4)$, $R = 0.996$	$y = 6.11(\pm 0.2)x + 25.4(\pm 18.1)$, $R = 0.997$
LOQ ($\mu\text{g kg}^{-1}$) ^b	5	8
LOD ($\mu\text{g kg}^{-1}$) ^c	1.5	3

^a y = ECL intensity; x = spiked concentration of the ENR and CIP in $\mu\text{g kg}^{-1}$.

^b Calculated from the peak height based on a signal-to-noise ratio of 10.

^c Calculated from the peak height based on a signal-to-noise ratio of 3.

Table 3
Comparison of the results obtained by the present method with other CE-based assay

	LOQ ($\mu\text{g kg}^{-1}$)		LOD ($\mu\text{g kg}^{-1}$)		Recovery (%)		Extraction procedure
	CIP	ENR	CIP	ENR	CIP	ENR	
CE–ECL	8	5	3	1.5	77.4	80.6	SPE
CE–UV [19]	50	25	25	10	54	74	SPE
CE–MS [7]	17	18	5	5	84	92	Two-step SPE
CE–LIF [23]	20	5	–	–	22	68	Liquid–liquid extraction

limit of quantitation (LOQ) of ENR and CIP were estimated on the basis of the results for two replicates of milk samples spiked at low concentration levels, considering a signal-to-noise ratio of 3 and 10, respectively. For ENR and CIP the LOQ was $5 \mu\text{g kg}^{-1}$ and $8 \mu\text{g kg}^{-1}$ and LOD was $1.5 \mu\text{g kg}^{-1}$ and $3 \mu\text{g kg}^{-1}$, respectively, considering that the MRL established for ENR plus CIP are $100 \mu\text{g kg}^{-1}$, the proposed method is sensible enough for the analysis of ENR and CIP in milk or other biological samples, because the values of LOD and LOQ obtained were below the MRL established for ENR and CIP in the Council Regulation 2377/90 of European Union [8]. The linearity of the response was established from six calibration levels with a start point of the LOQ, covering the range from $5 \mu\text{g kg}^{-1}$ to $400 \mu\text{g kg}^{-1}$ for ENR ($5 \mu\text{g kg}^{-1}$, $10 \mu\text{g kg}^{-1}$,

$50 \mu\text{g kg}^{-1}$, $100 \mu\text{g kg}^{-1}$, $200 \mu\text{g kg}^{-1}$, and $400 \mu\text{g kg}^{-1}$) and from $8 \mu\text{g kg}^{-1}$ to $400 \mu\text{g kg}^{-1}$ for CIP ($8 \mu\text{g kg}^{-1}$, $10 \mu\text{g kg}^{-1}$, $50 \mu\text{g kg}^{-1}$, $100 \mu\text{g kg}^{-1}$, $200 \mu\text{g kg}^{-1}$, and $400 \mu\text{g kg}^{-1}$). Injecting each level in triplicate and intending to establish the MRLs in the middle of the linear calibration range. The studied linearity ranges were considered valuable for analysis since real milk samples with higher content of ENR and CIP only occurs rarely. The calibration curves established for both ENR and CIP present correlation coefficients higher than 0.990. The data of comparing the results obtained by the present method with previously published CE-based assays are given in Table 3. As can be seen, the LOQ and LOD of CIP and ENR, obtained by our method, were lower than that of other CE-based assays. This indicates that the present method is one of the most sensitive methods for the analysis of ENR and CIP using CE to the present.

Fig. 6 shows the typical electropherograms of a blank milk sample and milk sample spiked with $15 \mu\text{g kg}^{-1}$ CIP and ENR, which was threefold lower than of the MRLs established by the European Union. No interferences were found co-migrating with ENR and CIP showing the proper specificity of the proposed method.

4. Conclusions

We have demonstrated that CE–ECL, combined with an effective sample cleanup, is the method of choice for the detection of ENR and its metabolite CIP in milk samples. Relative to other reported CE procedures for ENR and CIP, this approach offers improved detection limits. In addition, the whole method is simple, accurate, selective, and can detect the concentration of ENR and CIP residues in milk below MRLs. This work gives a demonstration of the feasibility of CE and ECL detection for trace analysis of ENR and CIP. However, there may be a much wider range of application of the area of food and other kinds of samples.

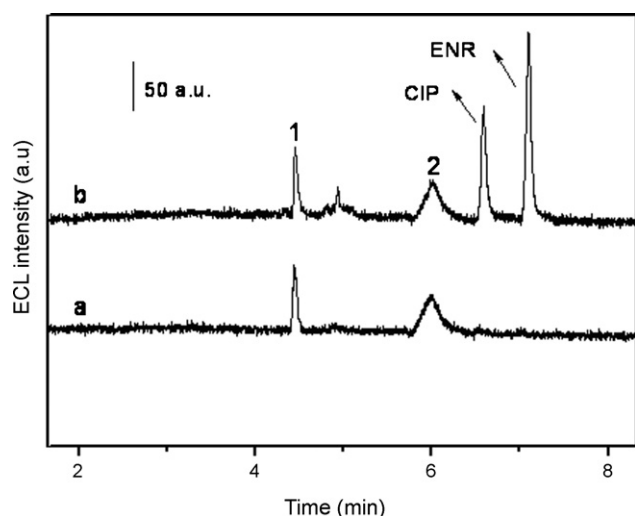


Fig. 6. Electropherograms of (a) blank milk sample and (b) the blank milk sample spiked $15 \mu\text{g kg}^{-1}$ CIP and $15 \mu\text{g kg}^{-1}$ ENR; (1) and (2) are the peaks of unknown compounds in extract. Conditions—detection potential: 1.15 V, 15 mM phosphate running buffer (pH 8.5), electrokinetic injection: 20 s at 10 kV and separation voltage: 14 kV.

Acknowledgments

This research is supported by the National Natural Science Foundation of China (30600128; 30700155) and the National High Technology Research and Development Program of China (863 Program) (2007AA10Z204).

References

- [1] M. Hernández, C. Aguilar, F. Borrull, M. Calull, J. Chromatogr. A 772 (2002) 163.
- [2] T. Backhaus, M. Scholze, L.H. Grimme, *Aquat. Toxicol.* 49 (2000) 49.
- [3] H.K. Verma, G.R. Pangawkar, R.K. Chaudhary, A.K. Srivastava, *Vet. Res. Commun.* 23 (1999) 501.
- [4] G.S. Rao, S. Ramesh, A.H. Ahmad, H.C. Tripathi, L.D. Sharma, J.K. Malik, *Small Rumin. Res.* 44 (2002) 213.
- [5] L. Intorre, S. Cecchini, S. Bertini, A.M. Cognetti Varriale, G. Soldani, G. Mengozzi, *Aquaculture* 182 (2000) 49.
- [6] D.A. Schentag, G.A. Wooster, P.S. Bustos, P.R. Bowser, J.G. Babish, *J. Vet. Pharmacol. Ther.* 20 (1997) 111.
- [7] F.J. Lara, A.M. García-Campaña, F. Alés-Barrero, J.M. Bosque-Sendra, L.E. García-Ayuso, *Anal. Chem.* 78 (2006) 7665.
- [8] The European Agency for the Evaluation of Medicinal Products Report, EMEA/MRL/574/99, <http://www.emea.eu.int>.
- [9] A.L. Cinquina, P. Roberti, L. Giannetti, F. Longo, R. Draisci, A. Fagiolo, N.R. Brizioli, *J. Chromatogr. A* 987 (2003) 221.
- [10] M.D. Marazuela, M.C. Moreno-Bondi, *J. Chromatogr. A* 1034 (2004) 25.
- [11] S. Bañac, O. Ballesteros, E. Jiménez-Lozano, D. Barrón, V. Sanz-Nebot, A. Navalón, J.L. Vílchez, J. Barbosa, *J. Chromatogr. A* 1029 (2004) 145.
- [12] C. González, L. Moreno, J. Small, D.G. Jones, S.F. Sánchez Bruni, *Anal. Chim. Acta* 560 (2006) 227.
- [13] M. Gratacós-Cubarsí, J.A. García-Regueiro, M. Castellari, *Anal. Bioanal. Chem.* 387 (2007) 1991.
- [14] A. Rubies, R. Vaquerizo, F. Centrich, R. Compañó, M. Granados, M.D. Prat, *Talanta* 72 (2007) 269.
- [15] J.A. Hernández-Arteseros, R. Compañó, M.D. Prat, *Analyst* 123 (1998) 2729.
- [16] J.A. Hernández-Arteseros, R. Compañó, R. Ferrer, M.D. Prat, *Analyst* 125 (2000) 1155.
- [17] E. Van Coillie, J. De Block, W. Reybroeck, *J. Agric. Food Chem.* 52 (2004) 4975.
- [18] S. Lu, Y. Zhang, J. Liu, C. Zhou, W. Liu, R. Xi, *J. Agric. Food Chem.* 54 (2006) 6995.
- [19] D. Barrón, E. Jiménez-Lozano, J. Cano, J. Barbosa, *J. Chromatogr. B* 759 (2001) 73.
- [20] J.L. Beltrán, E. Jiménez-Lozano, D. Barrón, J. Barbosa, *Anal. Chim. Acta* 501 (2004) 137.
- [21] J. McCourt, G. Bordin, A.R. Rodríguez, *J. Chromatogr. A* 990 (2003) 259.
- [22] A. Juan-García, G. Font, Y. Picó, *Electrophoresis* 27 (2006) 2240.
- [23] C. Horstkötter, E. Jiménez-Lozano, D. Barrón, J. Barbosa, G. Blaschke, *Electrophoresis* 23 (2002) 3078.
- [24] S.S. Zhang, H.X. Liu, Y.J. Wu, C.L. Yu, *Analyst* 126 (2001) 441.
- [25] L. Wang, X. Wu, Z. Xie, *J. Sep. Sci.* 11 (2005) 1143.
- [26] R.A. Wallingford, A.G. Ewing, *Anal. Chem.* 60 (1988) 258–263.
- [27] X. Huang, N. Zare, *Anal. Chem.* 62 (1990) 440.
- [28] D.B. Zhu, D. Xing, X.Y. Shen, J.F. Liu, *Biochem. Biophys. Res. Commun.* 324 (2004) 964.
- [29] J.F. Liu, D. Xing, X.Y. Shen, D.B. Zhu, *Biosens. Bioelectron.* 20 (2004) 436.
- [30] Y.B. Tang, D. Xing, D.B. Zhu, J.F. Liu, *Anal. Chim. Acta* 582 (2007) 275.
- [31] S.N. Ding, J.J. Xu, W.J. Zhang, H.Y. Chen, *Talanta* 70 (2006) 572.
- [32] M.T. Chiang, C.W. Whang, *J. Chromatogr. A* 934 (2001) 59.
- [33] X.J. Huang, S.L. Wang, Z.L. Fang, *Anal. Chim. Acta* 456 (2002) 167.
- [34] M. Zhou, Y.J. Ma, X.N. Ren, X.Y. Zhou, L. Li, H. Chen, *Anal. Chim. Acta* 587 (2007) 104.
- [35] J.Y. Yin, W.W. Guo, Y. Du, E. Wang, *Electrophoresis* 27 (2006) 4836.
- [36] G.A. Forbes, T.A. Nieman, J.V. Sweedler, *Anal. Chim. Acta* 347 (1997) 289.
- [37] Y.H. Xu, Y. Gao, H. Wei, Y. Du, E. Wang, *J. Chromatogr. A* 1115 (2006) 260.
- [38] J.F. Liu, W.D. Cao, X.R. Yang, E. Wang, *Talanta* 59 (2003) 453.
- [39] S.H. Liu, Y.J. Liu, J. Li, M.L. Guo, W. Pan, S.Z. Yao, *Talanta* 69 (2006) 154.
- [40] T. Li, J.P. Yuan, J.Y. Yin, Z.W. Zhang, E. Wang, *J. Chromatogr. A* 1134 (2006) 311.
- [41] J.P. Yuan, T. Li, X.B. Yin, L. Guo, X.Z. Jiang, W.R. Jin, X.R. Yang, E. Wang, *Anal. Chem.* 78 (2006) 2934.
- [42] J.B. Noffsinger, N.D. Danielson, *Anal. Chem.* 59 (1987) 865.
- [43] W.D. Gao, J.F. Liu, X.R. Yang, E. Wang, *Electrophoresis* 23 (2002) 3683.
- [44] E. Jiménez-Lozano, D. Roy, D. Barrón, J. Barbosa, *Electrophoresis* 25 (2004) 65.
- [45] M. Zorzi, P. Pastore, F.A. Magno, *Anal. Chem.* 72 (2000) 4934.

Ultrasensitive determination of intracellular superoxide in individual HepG2 cells by microfluidic chip electrophoresis

Lanlan Zhu^a, Min Lu^b, Xuefeng Yin^{a,*}

^a Institute of Microanalytical Systems, Department of Chemistry, Zhejiang University, 310027 Hangzhou, China

^b Institute of Biologic Macromolecule and Enzymatic Engineering, College of Life Science, Zhejiang University, Hangzhou, China

Received 2 November 2007; received in revised form 8 January 2008; accepted 9 January 2008

Available online 19 January 2008

Abstract

A microchip electrophoresis method was established for the determination of intracellular superoxide ($O_2^{\bullet-}$) in individual HepG2 cells. Dihydroethidium (DHE) was used as the specific fluorescent probe to react with intracellular $O_2^{\bullet-}$ to form the fluorescent 2-hydroxyethidium. Excellent resolution between 2-hydroxyethidium and ethidium cation (E^+) can be achieved within 20 s. E^+ was reported to be generated from photochemical oxidation of DHE and interfere the determination of $O_2^{\bullet-}$ with fluorescence microscopic technique. An extremely low detection limit of 2.0 amol was achieved owing to the minute sample volume and insignificant dispersion effect during microfluidic chip-based electrophoretic separation. Furthermore, only 2-hydroxyethidium peak was detected with the suggested single-cell analysis method, which indicates the photooxidation of DHE to E^+ could be blocked by isolating either oxygen or light from them.

© 2008 Elsevier B.V. All rights reserved.

Keywords: Superoxide; Dihydroethidium; Single-cell analysis; Microfluidic chip

1. Introduction

In a normal cellular environment, endogenously produced reactive oxygen species (ROS) are essential to life [1]. While in case of overproduction, these reactive species become highly harmful, causing DNA and protein damage, lipid peroxidation [2]. It is of extreme importance to study and understand oxidative stress in diverse diseases, such as cancer, hypertension, atherosclerosis, Alzheimer's disease, lung injury, and aging [3].

ROS, mainly generated from the mitochondrial respiratory chain, include $O_2^{\bullet-}$, hydrogen peroxide (H_2O_2), hydroxyl radical ($\bullet OH$), and hydroperoxyl radical ($HO_2^{\bullet-}$) [4]. It has been considered that each species of them is likely to have a specific role in living cells [5]. The scientific research in the field of ROS associated with biological functions and/or deleterious effects continuously calls for new sensitive and specific techniques that can provide deeper insight on its action mechanisms. However, these reactive species demonstrate unique characteristics, such as high reactivity, low concentration and very short

lifetime, which make the determination of intracellular ROS a challenging task, especially for individual species of ROS.

$O_2^{\bullet-}$ is a free radical, which can form more reactive species via secondary reactions [6]. It has been reported that $O_2^{\bullet-}$ inhibits enzymes including glutathione peroxidase, catalase, and creatine kinase. In vascular cells, excessive production of $O_2^{\bullet-}$ has been suggested to occur in hypertension, hypercholesterolemia, diabetes, and heart failure [7]. $O_2^{\bullet-}$ also serves as a progenitor for other ROS, such as H_2O_2 , peroxynitrite and $\bullet OH$. For example, $O_2^{\bullet-}$ is converted to H_2O_2 spontaneously or by action of superoxide dismutase. $O_2^{\bullet-}$ reacts with NO to form the powerful oxidant peroxynitrite, which can cause many diseases linked to inflammatory processes and autoimmune diabetes [8,9]. Reaction of H_2O_2 and peroxynitrite can give rise to highly reactive $\bullet OH$ [10,11]. Thus, accurate detection and quantification of intracellular $O_2^{\bullet-}$ are critically important in understanding the pathogenesis of various cardiovascular disorders and other noncardiovascular diseases.

Intracellular $O_2^{\bullet-}$ has been measured by fluorescence microscopic technique, such as image-based techniques [12,13] and flow cytometry [14,15]. DHE is one of the most popular fluorescent probes for the measurement of intracellular $O_2^{\bullet-}$ [14,16–18], which is cell permeable and reacts specifically

* Corresponding author. Tel.: +86 571 87991636; fax: +86 571 87952070.
E-mail address: yinxf@zju.edu.cn (X. Yin).

with $O_2^{\bullet-}$ to form a highly fluorescent product. Other reactive oxygen, nitrogen, and halogen species, such as H_2O_2 , $\bullet OH$, peroxyxynitrite and hypochlorous acid failed to oxidize DHE to the same product [19,20]. Recently, Zhao et al. identified the major product formed from the reaction between $O_2^{\bullet-}$ and DHE as 2-hydroxyethidium by using mass spectral and NMR techniques [21]. They also studied the effect of light on the quantitation of $O_2^{\bullet-}$ using DHE. Results indicate that 2-hydroxyethidium stimulates the photooxidation of DHE to E^+ [21,22]. Because of the extensive spectral overlap of 2-hydroxyethidium and E^+ , they suggested that currently popular fluorescence microscopic technique was not suitable for quantitating intracellular $O_2^{\bullet-}$ [21,22] and proposed an improved methodology by using HPLC with fluorescence [21] or electrochemical detection [22]. However, the sensitivity was greatly reduced due to the inevitable dilution effect caused by HPLC eluents as well as solvents used for cell lysate preparation.

The ability of integrated microfluidics to accurately manipulate, handle and analyze very small volumes has opened up new opportunities for analysis of intracellular constituents in individual cells [23]. Wu et al. reported an integrated microfluidic device for analyzing the amino acids in the lysed contents of a single Jurkat cell [24]. To reduce unwanted dilution, the lysis and derivatization of the amino acids of a single Jurkat cell were accomplished in a reaction chamber with a volume of 70 pL by using microfabricated valves. Ramsey and co-workers [25] designed a glass microfluidic device for the high throughput chemical analysis of Jurkat cells, which integrated cell handling, cell lysis, electrophoretic separation and detection of fluorescent cytosolic dyes. Jin and co-workers [26] developed a method for analyzing ascorbic acid in single wheat callus cells in a microfluidic chip with a double-T injector coupled with an end-channel amperometric detector. In our previous articles [27,28], we successfully integrated operational functions for single human erythrocytes introduction, docking, cytolysis, and electrophoretic separation of cellular constituents on a single glass microchip, and detected intracellular reduced glutathione and ROS with laser induced fluorescence detector (LIF). To the best of our knowledge, no work has been reported regarding the analysis of intracellular $O_2^{\bullet-}$ in individual cells by microfluidic chip electrophoresis, in which cell lysis and the reaction of intracellular $O_2^{\bullet-}$ with DHE are carried out in an air-free environment.

Herein, a highly sensitive and selective method for the determination of $O_2^{\bullet-}$ in single HepG2 cells was developed by microfluidic chip electrophoresis combined with LIF detector after examination of the electrophoretic behavior of 2-hydroxyethidium and E^+ . This method can minimize the dilution resulted from sample preparation and HPLC analysis, and achieve a detection limit of 2.0 amol, which is more than three orders of magnitude lower than that obtained by using HPLC-EC [22] and five orders of magnitude lower than that obtained by employing HPLC fluorescence analysis [21,22]. Different from the HPLC analysis results, only 2-hydroxyethidium but not E^+ was detected, indicating that photooxidation of DHE to E^+ was avoided by using the suggested single-cell analysis method.

2. Experimental

2.1. Materials

All chemicals of analytical reagent grade and Millipore purified water were used throughout. PBS, which consisted of 0.9% NaCl, 0.2% Na_2HPO_4 and 0.01% NaH_2PO_4 (pH 7.6), was used for washing and preserving HepG2 cells. Hydroxylpropyl methylcellulose (HPMC) was purchased from Sigma (St. Louis, MO, USA). PBS-HPMC solution (4 mg HPMC was dissolved in 10 mL PBS) was used to make cell suspension to minimize cell assembling, sedimentation and adsorption to microchannels [29]. Potassium superoxide (KO_2) was purchased from Alfa Aesar. DHE and ethidium bromide were purchased from Molecular Probes. The stock solution of DHE was prepared at a concentration of 500 $\mu\text{mol/L}$ in dimethyl sulfoxide (DMSO) and kept in dark at -20°C . Before use, it was diluted to 5.0 $\mu\text{mol/L}$ with PBS solution for cell treatment. The saturated KO_2 in DMSO was prepared immediately prior to use. The standard solution of 10.0 $\mu\text{mol/L}$ 2-hydroxyethidium was prepared daily by adding excess KO_2 -saturated DMSO solution to a 10.0 $\mu\text{mol/L}$ DHE solution and kept in dark at 4°C . Solutions for $O_2^{\bullet-}$ calibration were obtained by diluting the 10.0 $\mu\text{mol/L}$ 2-hydroxyethidium with 10 mmol/L borate buffer (pH 9.2). Five percent (w/v) sulfosalicylic acid (SSA) prepared in 10 mmol/L borate buffer was used to precipitate intracellular protein. Ten millimolar SDS solution was prepared by dissolving the surfactant in 10 mmol/L borate buffer (pH 9.2), which was used as the medium for cell lysis as well as the working electrolyte solution for microfluidic electrophoresis analysis of single cells.

2.2. Apparatus

The schematic diagram of the experimental setup used for single-cell analysis is shown in Fig. 1. It consists of a home-built confocal microscope LIF system coupled with a 4-terminal high voltage power supply. As described previously [27], an air-cooled solid-state laser (473 nm, 10 mW, Optoelectronic Technologies, Changchun, China) was coupled to an inverted microscope (Jiangnan Optics & Electronics, Nanjing, China) with necessary optical components. The laser beam was reflected by a dichroic mirror and focused into a 20 μm spot on the separation channel from the bottom of the chip. The emitted light was collected by the same focusing system, and directed to a pinhole by the optics of the inverted microscope. A photomultiplier tube (PMT, CR 114, Hamamatsu, Beijing; bias: 600 V) was mounted on top of the microscope tube with a cutoff filter to reduce the background noise caused by any scatter and stray light below 520 nm and connected to an amplifier (GD-1, Reike Electronic Equipment, Xi'an, China). Data acquisition and processing were carried out using a N2010 A/D converter (Zheda Instruments, Hangzhou, China) and a computer. A laboratory-built 4-terminal high voltage power supply, variable in the range of 0–1500 V, was used for single-cell sampling and microchip electrophoresis. Laser confocal scanning microscope (LCSM) (LSM 510, Zeiss, Germany) was used to collect the cellular fluorescence.

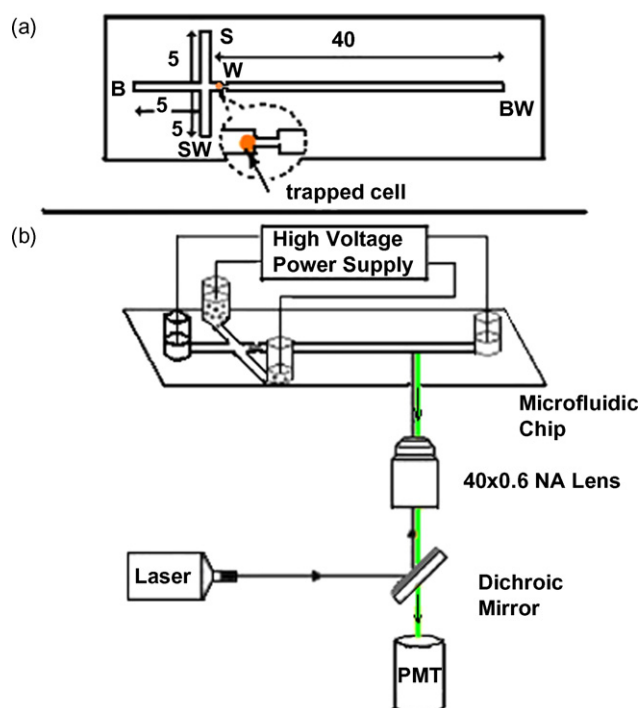


Fig. 1. Schematics of (a) the channel design of the multi-depth microfluidic chip (dimensions are given in mm) and (b) the experimental setup.

2.3. Microfluidic chip fabrication

The schematic diagram of the channel design is shown in Fig. 1a. The channel between sample (S) reservoir and sample waste (SW) reservoir was used for sampling and the channel between buffer (B) reservoir and buffer waste (BW) reservoir was used for separation. To avoid the blockage of the sampling channel by adhered cells, a multi-depth microfluidic chip was fabricated on a glass substrate using conventional lithography and wet etching procedure by controlling the etching time as described previously [30]. Briefly, the line widths of the sampling and separation channel on the photomask were both 20 μm . The separation channel was etched to a depth of 12 μm , while the sampling channel a depth of 37 μm . Owing to the isotropic character of glass in wet etching, the average widths of the sampling channel and the separation channel were about 60 and 40 μm , respectively. A 1-mm long weir (W) was constructed in the separation channel, 100 μm downstream from the channel crossing. The channel at the weir section was 6 μm deep to stop the loaded cell and precisely position it. Access holes were drilled into the etched plate with a 1.2 mm diameter diamond-tipped drill bit at the terminals of the channels. After permanent bonding by a thermal bonding procedure reported before [31], four 4-mm inner diameter and 6-mm tall micropipette tips were epoxyed onto the chip surrounding the access holes, serving as reservoirs.

2.4. Cell culture

HepG2 cells were kindly provided by the Institute of Biological Macromolecule and Enzyme Engineering (College of

Life Science, Zhejiang University, China). Cells were cultured in RPMI-1640 medium (Gibco BRL, Gaithersburg, MD, USA) supplemented with 100 U/mL penicillin, 100 $\mu\text{g}/\text{mL}$ streptomycin, and 10% fetal bovine serum in a humidified atmosphere of 95% air, 5% CO_2 at 37 $^\circ\text{C}$. All cells were grown from the frozen stock and were used for no more than five passages.

2.5. Intracellular labeling $\text{O}_2^{\bullet-}$ with DHE for single-cell analysis

Two microliters of DHE/DMSO stock solution were added to 200 μL of cell suspension and reacted with intracellular $\text{O}_2^{\bullet-}$ in the dark at room temperature for 30 min to form the fluorescent 2-hydroxyethidium. Then the cells were washed with 1 mL of PBS twice to remove any unreacted DHE and extracellular 2-hydroxyethidium formed from DHE autoxidation. Then the cells were resuspended in 0.4% PBS-HPMC to a cell population of 1.2×10^5 cells/mL measured with a hemocytometer (Shanghai Medical Optical Instrument Plant, Shanghai, China).

2.6. Preparation of cell lysate

Two hundred and fifty million of HepG2 cells were treated with 1 mL of 1 mmol/L H_2O_2 for 20 min, subsequently washed with 1 mL of PBS. One milliliter of 5.0 $\mu\text{mol}/\text{L}$ DHE was added to the H_2O_2 -treated HepG2 cells to react with intracellular $\text{O}_2^{\bullet-}$ in the dark for 30 min to avoid photooxidation of DHE [22]. After removing the medium, the cells were washed with 1 mL of PBS twice and lysed with 200 μL of 10 mmol/L SDS borate buffer. Then, 40 μL of 5% (w/v) SSA was added to cell lysate to precipitate intracellular protein [32]. The mixture was centrifuged at $430 \times g$ for 15 min. The supernatant was used for cell lysate analysis.

2.7. Procedures for single-cell analysis

The working electrolyte solution in the volume of 100, 100 and 50 μL were added to the reservoirs B, BW and SW, respectively. Then 150 μL of the DHE-labeled cell suspension (1.2×10^5 cells/mL) were added to the reservoir S. Owing to the difference between the liquid levels of the reservoirs, the cell suspension flowed from S to SW under hydrostatic pressure [27]. When a single cell moved within the cross section of the channels, as monitored under the microscope, a set of electrical potentials was applied to the four reservoirs with B at 1500 V, S and SW both at +1200 V, and BW grounded. The sampled cell was diverted into the separation channel and transported towards the BW reservoir by electroosmotic flow (EOF) and stopped by the weir W. The PBS medium plug surrounding the trapped cell was then replaced quickly with the SDS containing working electrolyte solution to achieve cell lysis [30]. After 5 s, the set of potentials was switched off. Observed under the microscope, the cell lysed completely within 20 s. The chip was then shifted from the channel-crossing viewing position to the detection point. The laser beam was refocused and the set of electrical potentials was resumed. Simultaneously, the data acquisition and processing system was activated to record electropherograms.

2.8. Calibration

One hundred microliters of electrophoresis working electrolyte solution were added to the reservoirs SW, B and BW, respectively. Then 100 μL of standard solution of 2-hydroxyethidium was added to the reservoir S. The chip was operated under either a “sample loading” or “separation” mode. In the sample loading mode, the 2-hydroxyethidium standard solution was electrokinetically injected from S to SW by applying a set of electrical potentials to the four reservoirs for 60 s, with the reservoir S at 500 V, SW grounded, B at 450 V and BW at 480 V. Then, the 4-terminal high voltage power supply was automatically switched to applying another set of electrical potentials to the four reservoirs, with the reservoir B at 1500 V, BW grounded and both S and SW at 1200 V, the pinched sample plug was injected from the channel-crossing into the separation channel and the electrophoresis separation was activated. Simultaneously, the data acquisition and processing system was activated to record electropherograms. Calibration curve was made by plotting the peak areas against the masses of 2-hydroxyethidium injected.

3. Results and discussion

3.1. Electrophoretic behavior of 2-hydroxyethidium and E^+

As $\text{O}_2^{\bullet-}$ is non-fluorescent in its native form, its conversion into fluorescent compound is required for detection with LIF. DHE is a cell permeable fluorescent probe. The LIF detector used in our experiment cannot excite and detect the fluorescence of DHE, whose optimal excitation and emission wavelengths were 370 and 420 nm, respectively. DHE reacts with $\text{O}_2^{\bullet-}$ to form a red fluorescent product 2-hydroxyethidium [21]. $\text{O}_2^{\bullet-}$ can be produced by adding KO_2 -saturated DMSO into aqueous solutions [33]. Thus, the standard solution of 2-hydroxyethidium for $\text{O}_2^{\bullet-}$ calibration was prepared by adding excess KO_2 -saturated DMSO into 10.0 $\mu\text{mol/L}$ DHE aqueous solution. The effect of reaction time on the formation of 2-hydroxyethidium was investigated by monitoring its fluorescent intensity with chip-based electrophoresis. Results showed that initially the fluorescent intensity increased along with the reaction time, then reached to a plateau after 20 min. Therefore, reaction time of 25 min was chosen to prepare the standard solution of 2-hydroxyethidium.

2-hydroxyethidium is amphiprotic. Fig. 2 shows a schematic diagram of the protonation/deprotonation equilibrium of 2-hydroxyethidium. As indicated, two species, abbreviated as 2-OH-E^+ and $2\text{-O}^-\text{-E}^+$, exist in the electrophoretic system.

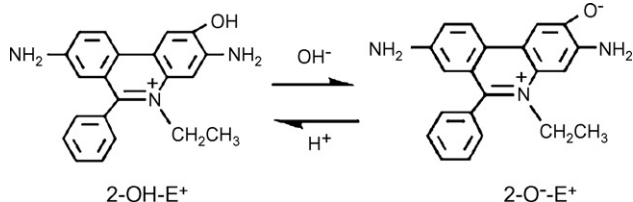


Fig. 2. Schematic diagram of the protonation/deprotonation equilibrium of 2-hydroxyethidium.

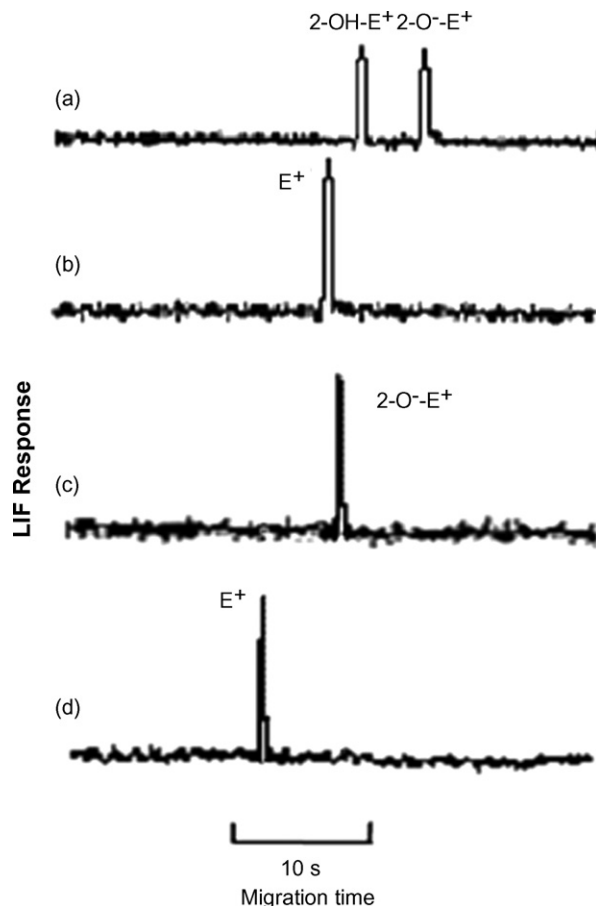


Fig. 3. Electropherograms of E^+ and 2-hydroxyethidium at different pHs. (a) 2.5 $\mu\text{mol/L}$ 2-hydroxyethidium, pH 6.8; (b) 2.5 $\mu\text{mol/L}$ E^+ , pH 6.8; (c) 2.5 $\mu\text{mol/L}$ 2-hydroxyethidium pH 9.2; (d) 2.5 $\mu\text{mol/L}$ E^+ , pH 9.2; field strength 333 V/cm, separation length 2.0 cm.

Therefore, the effect of buffer pH on the electrophoretic behavior of 2-hydroxyethidium was investigated using 10 mmol/L borate buffer at pH 6.8 and pH 9.2, respectively, as working electrolyte solution for chip-based electrophoresis separation. The electropherograms obtained are shown in Fig. 3a and c. Two peaks with migration time of 21.5 s and 27 s can be distinguished in Fig. 3a, indicating that 2-OH-E^+ and $2\text{-O}^-\text{-E}^+$ coexist in the electrophoretic buffer at pH 6.8. The net charge on the zwitterion $2\text{-O}^-\text{-E}^+$ is zero, which migrates much slower than the positively charged 2-OH-E^+ during electrophoretic separation. Therefore, the peak at 21.5 and 27 s can be identified as 2-OH-E^+ and $2\text{-O}^-\text{-E}^+$, respectively. At alkaline pH (pH 9.2), the hydroxyl group in 2-hydroxyethidium acts as an acid and the protonation/deprotonation equilibrium of 2-hydroxyethidium shown in Fig. 2 shifts to the right. Only one peak of $2\text{-O}^-\text{-E}^+$ appears at 20 s in Fig. 3c, implying that the isoelectric point of 2-hydroxyethidium is at pH 9.

The electrophoretic behavior of E^+ was also evaluated at both pHs. The results are shown in Fig. 3b and d. Only one peak was detected at both pHs. The migration times of E^+ were 19 s and 15 s at pH 6.8 and 9.2, respectively. The difference of the migration times of the same species (E^+ or $2\text{-O}^-\text{-E}^+$) at both pHs can be ascribed to the change of electroosmotic flow. Increasing the

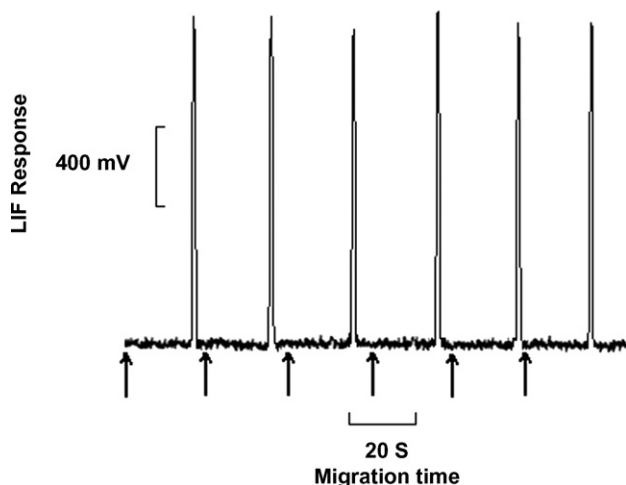


Fig. 4. Recorded electropherograms of 5.0 $\mu\text{mol/L}$ 2-O⁻-E⁺ standard solutions ($n=6$). The arrows corresponding to the starting points of CE separation. Same experiment condition as in Fig. 3c.

pH from 6.8 to 9.2 concomitantly increases EOF, which gives rise to a shorter migration time for the same species. After comparing the electrophoretic behavior of 2-hydroxyethidium and E⁺ at both pHs, 10 mmol/L borate buffer at pH 9.2 was selected as the working electrolyte solution for microfluidic electrophoresis separation in the following experiments. In this pH, only one species 2-O⁻-E⁺ was detected in electropherogram, which implied the higher detection sensitivity for O₂^{•-}.

3.2. Analytical performance

A standard solution of 5.0 $\mu\text{mol/L}$ 2-hydroxyethidium was used to investigate the reproducibility. The results are shown in Fig. 4. The average migration time was 20.0 s with a precision of 0.8% R.S.D. and the peak area reproducibility was 1.9% R.S.D. ($n=6$).

A series of 2-hydroxyethidium standard solutions were used to calibrate O₂^{•-}. A concentration regression equation of $y=2.16 \times 10^2 c$ (c is the concentration in $\mu\text{mol/L}$, y is the peak area in mV s) was obtained for the calibration with regression coefficient γ of 0.99967 and a dynamic range of 0.125–5.0 $\mu\text{mol/L}$. The detection limit for 2-hydroxyethidium was 0.125 $\mu\text{mol/L}$ ($S/N=3$). In single-cell analysis, it is of more significance to determine the mass of analytes rather than the concentration as the cell volume varies. To calculate the mass regression equation for intracellular O₂^{•-} quantitation, the volume of the injected standard sample plug was experimentally measured to be 16 pL by using an inverted fluorescent microscope and a charge-coupled device (CCD) camera as described before [26]. Taking into consideration of the volume of 16 pL, the concentration regression equation can be converted to the mass regression equation of $y=13.5 n$, (n is the mass in amol). Accordingly, the mass detection limit was 2.0 amol in terms of 2-hydroxyethidium, i.e. 0.66 fg, which is more than three orders of magnitude lower than 0.004 ng obtained by employing HPLC-EC [22] and five orders of magnitude lower than 0.2 ng obtained by employing HPLC fluorescence analysis [21,22]. The

drastically improved detection limit was attributed to (1) the minute sample volume, (2) insignificant dispersion effect during microfluidic chip electrophoresis, and (3) the use of highly sensitive LIF detector.

3.3. Determination of intracellular O₂^{•-}

In order to avoid diluting the intracellular O₂^{•-} that is already present at trace levels, an intracellular derivatization method by incubating living cells with a cell membrane-permeable DHE was used to specifically label intracellular O₂^{•-}. The cell itself acted as a reaction chamber. Fluorescent microscopy images of single HepG2 cell before and after incubation with DHE were used to monitor the labeling process. No intracellular fluorescence was observed before the labeling. After incubation with DHE for 30 min, red fluorescence was observed in the cytoplasm of both non-stimulated and 1.0 mmol/L H₂O₂-stimulated HepG2 cells. The fluorescence intensity remained constant for at least another 10 min, indicating that the reaction between intracellular O₂^{•-} and DHE was completed. Therefore, incubation time of 30 min was adopted for intracellular labeling O₂^{•-} with DHE for single-cell analysis.

We used chip-based electrophoresis to determine the background value of O₂^{•-} in individual HepG2 cells and measure the intracellular O₂^{•-} in response to 1.0 mmol/L H₂O₂ stimuli. The electropherograms of a series of single HepG2 cells are shown in Fig. 5a. The average migration time of the peaks (20.3 s) with a reproducibility of 2.1% R.S.D. for five consecutively injected cells, agreed well with that obtained using the 2-hydroxyethidium standard (20.0 s). The O₂^{•-} contents in a single HepG2 cell were 3.1, 2.1, 2.0, 3.5 and 2.5 amol in terms

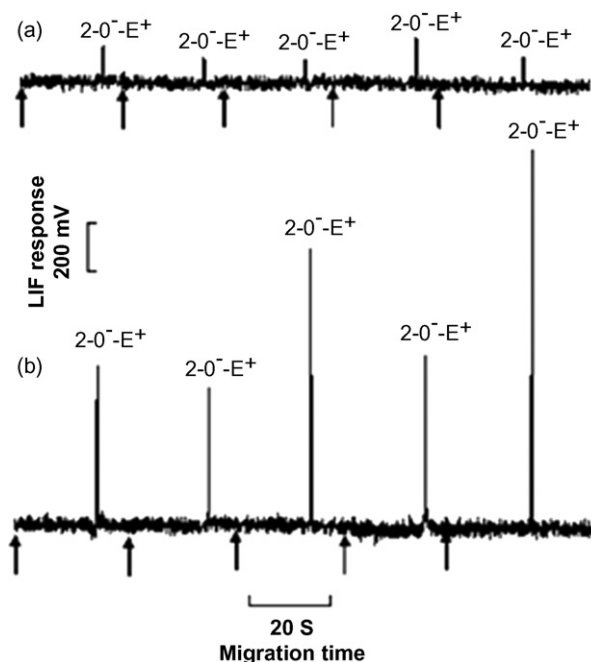


Fig. 5. Electropherograms of five HepG2 cells injected consecutively. (a) Unstimulated and (b) stimulated with 1.0 mmol/L H₂O₂ for 20 min. Field strength 333 V/cm, separation length 2.0 cm. The arrows correspond to the starting points of CE separation.

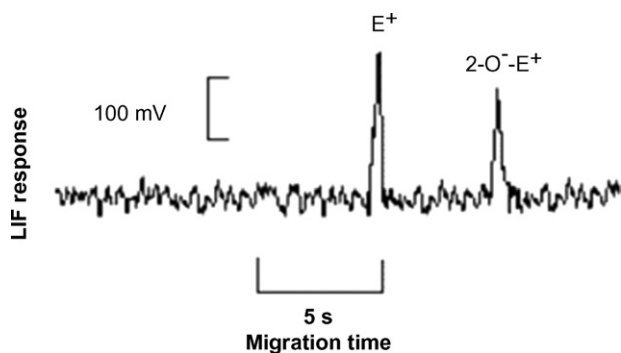


Fig. 6. Recorded electropherogram of cell lysate. Field strength 333 V/cm, separation length 2.0 cm.

of the amount of the generated $2\text{-O}^- \text{-E}^+$, respectively. The duration required for a complete analysis, including cell injection, docking, chip shifting, laser refocusing, cell lysis, separation and detection for each HepG2 cell was less than 3 min. The electropherograms for a series of five HepG2 cells stimulated by 1.0 mmol/L H_2O_2 for 20 min are shown in Fig. 5b. The $\text{O}_2^{\bullet-}$ contents in a single HepG2 cell were equivalent to 14.7, 11.2, 18.1, 11.7 and 21.8 amol in terms of the amount of the generated $2\text{-O}^- \text{-E}^+$, respectively. The result demonstrated the cellular heterogeneity. An average content of 15.5 amol was obtained. Such values were six times higher than those for HepG2 cells absent from H_2O_2 stimulation. Since DHE cannot react with H_2O_2 [13,19,20] to form 2-hydroxyethidium, the escalation of intracellular $\text{O}_2^{\bullet-}$ level in the H_2O_2 -stimulated HepG2 cells may be owing to H_2O_2 overwhelming cellular defense mechanisms and inducing secondarily generated $\text{O}_2^{\bullet-}$ in cells [15].

Different from the HPLC analysis results [21], in which two intracellular fluorescent products corresponding to 2-hydroxyethidium and E^+ were detected in the extract of cells treated by menadione, a redox-cycling quinone known to generate intracellular $\text{O}_2^{\bullet-}$, only one $2\text{-O}^- \text{-E}^+$ peak appeared for the determination of intracellular $\text{O}_2^{\bullet-}$ in individual cells with microfluidic chip electrophoresis as shown in Fig. 5. In our experiment, intact single cells were used as sample. Intracellular contents were isolated from atmospheric oxygen by cell membrane before lysis. After on-chip lysis, intracellular contents was separated and detected in dark within 30 s. While in HPLC analysis, intracellular formed 2-hydroxyethidium stimulated the photooxidation of excess DHE to E^+ during sample lysate preparation. To verify our assumption, cell lysate prepared as described in Section 2 was analyzed by microfluidic electrophoresis after HepG2 cells was stimulated with 1.0 mmol/L H_2O_2 for 20 min. The recorded electropherogram is shown in Fig. 6, in which two peaks corresponding to both $2\text{-O}^- \text{-E}^+$ and E^+ were observed. This indicates that photooxidation of DHE to E^+ can be avoided by the suggested single-cell analysis method.

4. Conclusions

The proposed microfluidic electrophoresis-LIF method provides an ultrasensitive, fast and selective approach for quantitative analysis of trace amount of $\text{O}_2^{\bullet-}$ in individual

HepG2 cells. Extremely low detection limit of 0.66 fg 2-hydroxyethidium as well as the quantification of background intracellular $\text{O}_2^{\bullet-}$ level of individual cells were achieved with the microfluidic chip-based electrophoretic separation. This method demonstrates favorable potentials for studying the pathogenesis of various diseases, basic cellular functions and intra- and intercellular communication associated with $\text{O}_2^{\bullet-}$. With the suggested method, only 2-hydroxyethidium was formed. Thereby, the fluorescent spectral interference of E^+ was avoided. It also implies that currently available image-based technique and flow cytometry can still be applied for intracellular $\text{O}_2^{\bullet-}$ study because cell lysis is not required using these fluorescence-based methods.

Acknowledgements

This work was supported by the National Natural Science Foundation of China under project no. 20775072 and the Zhejiang Provincial Natural Science Foundation of China under project no. Z407029.

References

- [1] A. Gomes, E. Fernandes, J.L.F.C. Lima, J. Biochem. Biophys. Methods 65 (2005) 45.
- [2] D. Ozyurt, B. Demirata, R. Apak, Talanta 71 (2007) 1155.
- [3] J.M. McCord, Methods Enzymol. 349 (2002) 331.
- [4] J. Qin, N. Ye, L. Yu, D. Liu, Y. Fung, W. Wang, X. Ma, B. Lin, Electrophoresis 26 (2005) 1155.
- [5] K. Setsukinai, Y. Urano, K. Kakinuma, H.J. Majima, T. Nagano, J. Biol. Chem. 278 (2003) 3170.
- [6] B. Halliwell, J.M.C. Gutteridge, Biochem. J. 219 (1984) 1.
- [7] H. Cai, D.G. Harrison, Circ. Res. 87 (2000) 840.
- [8] J. Huang, D. Li, J. Diao, J. Hou, J. Yuan, G. Zou, Talanta 72 (2007) 1283.
- [9] H. Wang, R. Cai, Z. Lin, Talanta 69 (2006) 509.
- [10] E. Cadenas, Annu. Rev. Biochem. 58 (1989) 79.
- [11] N. Hogg, M. Darley-Usmar, M.T. Wilson, S. Moncada, Biochem. J. 281 (1992) 419.
- [12] S. Szűcs, G. Vámosi, R. Póka, A. Sárvári, H. Bárdos, M. Balázs, J. Kapelmayer, L. Tóth, J. Szöllősi, R. Adány, Cytometry 33 (1998) 19.
- [13] V. Bindokas, J. Jordán, C. Lee, R. Miller, J. Neurosci. 16 (1996) 1324.
- [14] S. Walrand, S. Valeix, C. Rodriguez, P. Ligot, J. Chassagne, M.P. Vasson, Clin. Chim. Acta 331 (2003) 103.
- [15] W. Carter, P.K. Narayanan, P. Robinson, J. Leukoc. Biol. 55 (1994) 253.
- [16] G. Rothe, G. Valet, J. Leukoc. Biol. 47 (1990) 440.
- [17] S.L. Budd, R.F. Castilho, D.G. Nicholls, FEBS Lett. 415 (1997) 21.
- [18] D. Han, F. Antunes, R. Canali, D. Rettori, E. Cadenas, J. Biol. Chem. 278 (2003) 5557.
- [19] H. Zhao, S. Kalivendi, H. Zhang, J. Joseph, K. Nithipatikom, J. Vázquez-Vivar, B. Kalyanaraman, Free Radic. Biol. Med. 34 (2003) 1359.
- [20] B. Fink, K. Laude, L. McCann, A. Doughan, D.G. Harrison, S. Dikalov, Am. J. Physiol. 287 (2004) C895.
- [21] H.T. Zhao, J. Joseph, H.M. Fales, E.A. Sokoloski, R.L. Levine, J. Vázquez-Vivar, B. Kalyanaraman, Proc. Natl. Acad. Sci. USA 102 (2005) 5727.
- [22] J. Zielonka, J. Vázquez-Vivar, B. Kalyanaraman, Free Radic. Biol. Med. 41 (2006) 1050.
- [23] J. El-Ali, P.K. Sorger, K.F. Jensen, Nature 442 (2006) 403.
- [24] H. Wu, A.R. Wheeler, R.N. Zare, Proc. Natl. Acad. Sci. USA 101 (2004) 12809.
- [25] M.A. McClain, C.T. Culbertson, S.C. Jacobson, N.L. Allbritton, C.E. Sims, J.M. Ramsey, Anal. Chem. 75 (2003) 5646.
- [26] F.Q. Xia, W.R. Jin, X.F. Yin, Z.L. Fang, J. Chromatogr. A 1063 (2005) 227.
- [27] J. Gao, X.F. Yin, Z.L. Fang, Lab Chip 4 (2004) 47.

- [28] Y. Sun, X.F. Yin, *Anal. Bioanal. Chem.* 382 (2005) 1472.
- [29] B. Yao, G.A. Luo, X. Feng, W. Wang, L.X. Chen, Y.M. Wang, *Lab Chip* 4 (2004) 603.
- [30] Y. Sun, X.F. Yin, *J. Chromatogr. A* 1117 (2006) 228.
- [31] J.H. Liu, X.F. Yin, G.M. Xu, Z.L. Fang, H.Z. Chen, *Chem. J. Chin. Univ.* 24 (2003) 232.
- [32] H. Zhang, W.R. Jin, *Electrophoresis* 25 (2004) 480.
- [33] B.R. Lokesh, M.L. Cunningham, *Toxicol. Lett.* 34 (1986) 75.